

Development of Covalent Inhibitors of KDM5B

Miranda Wright

St Hilda's College

Trinity Term 2018

Synthesis for Biology and Medicine Centre for Doctoral Training,

Structural Genomics Consortium,

and Chemistry Research Laboratory

A thesis submitted in partial fulfilment of the requirements of the degree of Doctor of Philosophy

Abstract

Lysine Demethylases (KDMs) represent an interesting drug target as they have been implicated in many diseases including several cancers. Reported inhibitors of KDM5 are commonly metal-chelators which bind in the cosubstrate 2-oxoglutarate (2-OG) binding site. The inhibitors are potent biochemically but suffer from poor selectivity over the closely-related KDM4 and poor cellular potency. An explanation for the large drop off in cellular activity has been attributed to competition from 2-oxoglutarate. In this thesis, I report the development of a covalent inhibitor that is potent and selective for KDM5. The inhibitors were designed with an 8-pyridopyrimidinone-based scaffold and cysteine-selective electrophiles for covalent binding to C480 in KDM5B, a non-conserved residue across the other KDM subfamilies.

The compounds were rationally designed through covalent docking to ensure non-covalent interactions were maintained (Chapter 2). Numerous compounds were synthesised via a common synthetic pathway. Screening of the covalent inhibitors for time-dependent inhibition was performed using an AlphaScreen assay to determine their k_{inact}/K_i values (Chapter 3). AlphaScreen was also used to determine whether covalent binding resulted in less competition from 2-OG and improved selectivity over the other KDM subfamilies. Covalent binding of the inhibitors to KDM5B using MS-labelling experiments was described in Chapter 4. Proof of target engagement of the covalent inhibitors with KDM5B in the cellular environment using pull-down experiments was attempted in Chapter 5.

Chapter 6 describes the development of a bench-stable transfer reagent for the synthesis of trifluoromethyl sulfonimidamides. This work was undertaken while on industrial placement at Janssen Pharmaceuticals who were interested in this interesting bioisosteric replacement in their own drug discovery projects. Current methods require the formation of an unstable sulfonimidoyl

fluoride so it was envisaged that this transfer reagent could be formed on large scale for the synthesis of diverse libraries of CF_3-sulfonimidamides.

The final chapter describes another approach towards a therapeutic for cancer. Ribonucleotide Reductase (RNR) is an enzyme essential for the synthesis of phosphorylated deoxyribonucleotides so a deoxyadenosine-based PROTAC was developed for the targeted degradation of the RRM1 subunit of RNR.

Acknowledgements

I would firstly like to thank the Synthesis for Biology and Medicine Centre for Doctoral Training, for accepting me on the course and giving me the opportunity to learn new concepts at the interface of chemistry and biology. The lab rotation projects gave me experience in different areas of chemistry and therefore allowed me to make an informed decision about my final DPhil project.

I would especially like to thank my supervisor, Paul Brennan, for this interesting and challenging project in which I have gained a wide range of skills that will be useful in my future research career. Paul has been very supportive and has given me the freedom to manage my own project. Thanks also go to my co-supervisor Akane Kawamura for her support and advice on this project. I am also grateful to Jon Hollick, my industrial mentor, who provided me with great suggestions for this project.

I am very grateful to Janssen Pharmaceuticals for giving me the opportunity to broaden my skills while on my industrial placement. My industrial supervisors, Daniel Oehlrich and Brahma Ghosh, and the other team members, Carolina Martinez-Lamenca and Jos Leenaerts, provided valuable support during this experience.

I am also very thankful to those who carried out experiments for my project or offered their expertise. The admin and support staff were also actively involved in ensuring that we had all the equipment necessary for our chemistry.

I am particularly thankful to all my wonderful lab members past and present who have always been willing to offer help when I needed it. They are all great scientists who have taught me a lot during my PhD studies. Saleta, who worked closely with me on this project, has been an amazing team member. She has done a great deal for me through carrying out assays on my compounds and proofreading my thesis chapters and I am very thankful for her hardworking but fun nature. I am very grateful for the friendship of other team members including Moses, Filippo, Tamas, Carmen,

Mark, Rob and Oakley who have made this an enjoyable experience both in the lab and at the many social events.

I am extremely grateful to my friends at the TDI, particularly Darragh, Jennie and Andrew, for welcoming me and making it a fun place to work. I will miss the building socials and pub trips to the Butcher's Arms.

I am also very lucky to have met two of my closest friends, Cynthia and Irene, in the Brennan lab. We have shared many happy moments while working in the lab together and I know that they will continue to be a big part of my life. They have always been available for advice and support when work was getting me down. They are a great encouragement to me and I genuinely could not have done this PhD in Oxford without them. Both have been a huge inspiration to me for their hardworking nature and their determination to not give up.

Outside the lab, my two closest Hildabeast friends, Hannah and Coco, have shared many enjoyable and memorable moments with me. They have also proven to be excellent fitness partners through joining me at Zumba and Salsa classes.

Lastly, I am very grateful for the support of my family who have encouraged me to pursue my ambitions. Despite not understanding the subject, they were always only a phone call away to lift my spirits. My nephews and nieces have provided me with much joy during my PhD and I hope that my hard work on this project will inspire them to pursue their dream career, whether that be in science or not.

Contents

Abstract i
Acknowledgements iii
Contents v
List of Figures ix
List of Tables xii
List of Schemes xii
List of Experiments Contributed by Others xiv
Abbreviations xv
Chapter 1. Introduction 1
1.1. Epigenetics and the Role of Lysine Demethylases 1
1.1.1. Epigenetics and Chromosome Structure 1
1.1.2. Histone Lysine Demethylases 2
1.1.3. KDM Inhibitors in Clinical Development 3
1.1.4. KDM1 Subfamily 4
1.2. JmjC-KDMs 4
1.2.1. Subfamilies and Mechanism 4
1.2.2. JmjC-KDM Histone Substrate Specificities 6
1.2.3. JmjC Domain Architecture 7
1.2.4. 2OG-Binding Site of JmjC Domain 7
1.2.5. KDM5 subfamily: Structure and Biology 11
1.3. KDM5 Inhibitors 12
1.3.1. 2-OG Binding Site Inhibitors: Pyridine Carboxylic Acids 12
1.3.2. 2-OG Binding Site Inhibitors: Pyridopyrimidinones 18
1.3.3. 2-OG Binding Site Inhibitors: Pyridyl Pyrimidine Carboxylic Acids 21
1.3.4. 2-OG Binding Site Inhibitors: Cyanopyrazoles 23
1.3.5. 2-OG Binding Site Inhibitors: 1,7-Naphthyridone 26
1.3.6. 2-OG Binding Site Inhibitors: Pyrrolidine 28
1.3.7. Substrate Competitive KDM5 Inhibitors 29
1.3.8. Conclusion of KDM5 Inhibitors 30
1.4. Covalent Inhibitors 31
1.4.1. Background to Covalent Inhibitors 31
1.4.2. Cysteine-selective Covalent Inhibitors 33
1.4.3. Profiling Covalent Inhibitors 34
1.4.4. Determination of K_i and k_{inact} 35

1.4.5. AlphaScreen Assay for Determination of Time Dependent IC_{50}'s 37
1.5. Project Aims 38
Chapter 2. Design and Synthesis of Covalent Inhibitors 39
2.1. Phenylpiperidine-Based Covalent Inhibitors 39
2.1.1. Synthesis Towards Phenylpiperidine Covalent Inhibitor 41
2.2. Piperazine Covalent Inhibitors 45
2.2.1. Synthesis of Piperazine Covalent Inhibitors 47
2.3. Substituted-Piperazine Covalent Inhibitors 49
2.3.1. Synthesis of Substituted-Piperazine Covalent Inhibitors 52
2.4. Methyl Benzylamine Covalent Inhibitors 54
2.4.1. Synthesis of Methyl Benzylamines Inhibitors 54
2.5. Cyclopentyl Benzylamine Covalent Inhibitors 56
2.5.1. Synthesis of Cyclopentyl Benzylamine Covalent Inhibitors 56
2.6. Tetrahydroisoquinoline Covalent Inhibitors 57
2.6.1. Synthesis of Tetrahydroisoquinoline Covalent Inhibitors 58
2.7. Summary 59
Chapter 3. Screening of Covalent Inhibitors 60
3.1. Piperazine Covalent Inhibitors 60
3.1.1. Time Dependent Inhibition 60
3.1.2. Cell Permeability of Piperazine Covalent Inhibitors 65
3.2. Designed Covalent Inhibitors to Improve Cell Permeability 66
3.2.1. Substituted-Piperazine Covalent Inhibitors 66
3.2.2. Methyl Benzylamine Covalent Inhibitors 68
3.2.3. Cyclopentyl Benzylamine Covalent Inhibitors 69
3.2.4. Tetrahydroisoquinoline Covalent Inhibitors 70
3.2.5. Cell Permeability of Analogues 71
3.3. Determination of Most Potent Covalent Inhibitor Based on Their k_{inact}/K_i values 72
3.4. KDM Selectivity Determined Through AlphaScreen 74
3.5. 2-OG Competition Assay 75
3.6. Cellular Activity by Immunofluorescence Assay 79
3.7. Target engagement of covalent inhibitors with KDM5B using the NanoBRET assay 81
3.8. Cytotoxicity assays of compounds 83
3.9. Quantification of H3K4me3 Levels by ChIP-Seq 84
3.10. Conclusion 86
Chapter 4. Covalent Binding of Inhibitors 88
4.1. Covalent Binding of Piperazine Inhibitors 88

4.2. Kinetics of Covalent Binding of Acrylamide **61** and Chloroacetamide **62** 89
4.3. Mapping of Covalent Modification of KDM5B with **61** and **62** 92
4.4. Covalent Binding of Methyl Benzylamine Inhibitors **77**-**79** 95
4.5. Incubation of Methyl Benzylamines with other KDM proteins 98
4.6. Summary 100
Chapter 5. Activity-Based Protein Profiling (ABPP) 102
5.1. Introduction to Activity-Based Protein Profiling 102
5.2. Design of Clickable Alkyne Analogue 104
5.3. Synthesis of Clickable Analogue 106
5.4. Recombinant KDM5B – In-Gel Fluorescence 111
5.5. Pull Downs in Cell Lysates 113
5.5.1. Cell Lysates - In-Gel Fluorescence 113
5.5.2. Cell Lysates – Biotin Pull-Down 115
5.6. Summary 118
Chapter 6. Bench-Stable Transfer Reagent for the Synthesis of CF_3-Sulfonimidamide 120
6.1. Introduction to Sulfonimidamides and Their Synthesis 120
6.2. Development of Transfer Reagent for CF_3-Sulfonimidamides 123
6.3. Reaction of Transfer Reagent **158** with Amines to Form CF_3-Sulfonimidamides 131
6.4. Removal of Protecting Group from Transfer Reagent and Further functionalisation 132
6.5. Reactivity of Transfer Reagent **158** with C-Nucleophiles 133
6.6. Use of Transfer Reagent to Form CF_3-Sulfonimidamides Using Flow Conditions 135
6.7. Chemical Stability of Transfer Reagent 136
6.8. Summary 136
Chapter 7. Adenine-Based PROTACs for Selective Degradation of Ribonucleotide Reductase 138
7.1. Background – Ribonucleotide Reductase 138
7.2. Background – Use of PROTACs for Protein Degradation 139
7.3. Design of Deoxyadenosine-Based PROTAC 140
7.4. Synthesis of Adenine-Based PROTAC 142
7.5. Degradation of RRM1 with Compound **174** 143
7.6. Synthesis of a C-2 Substituted Deoxyadenosine-Based PROTAC 144
7.7. Summary 149
Chapter 8. Conclusion 151
Experimental - Synthetic Procedures 156
General Experimental Details 156
Synthesis of KDM inhibitors 157
General Procedures for Sulfonimidamides 229

Synthesis of Sulfonimidamides 229
Synthesis of PROTAC compounds 238
Experimental – Assays 250
AlphaScreen KDM5 assay 250
k_{inact}/K_i calculations 251
AlphaScreen KDM selectivity 251
2-OG competition assays 252
RapidFire assays – Kinetics of covalent binding of acrylamide **61** and chloroacetamide **62** 252
RapidFire assays - Incubation of piperazine acrylamide **61** with JARID1C 253
Elastase Digest 253
RapidFire assays – Incubation of methyl benzylamines with KDM5B, KDM5C and KDM4B 254
RapidFire assays – Incubation of clickable alkyne **103** with KDM5B 254
Immunofluorescence-based assay 255
NanoBRET assay 255
Pull-down assays – in-gel fluorescence with KDM5B protein 255
Pull-down assays – in-gel fluorescence in cell lysates 257
Pull-down assays – Biotin pull-down in MCF7 cell lysates 258
Pull-down assays – Western blotting of MCF7 and K562 cell lysates 259
Pull-down assays – Biotin pull-down in k562 cell lysates 259
Docking 260
Bibliography 261
Appendix 1 269

List of Figures

Figure 1.1. Covalent histone modification involved in epigenetic regulation of gene expression. This figure is taken from the literature.[4] 2
Figure 1.2. Structure of GSK2879552 ***1*** *and ORY-1001* ***2****.* 3
Figure 1.3. Mechanism of demethylation with KDM1 class. 4
Figure 1.4. Mechanism of demethylation with JmjC-domain containing KDMs. 5
Figure 1.5. Structure of JmjC-domain of KDMs. (A) Overall structural fold of JmjC-KDMs (Crystal structure of KDM4D in complex with H3K9me3 (yellow) and 2-oxoglutarate (2OG, PDB ID 4HON) with the core DSBH labelled) (B) Cartoon structure of DSBH fold with Fe^{2+} *coordinating motif (yellow hexagons) and the lysine residue that coordinates the carboxylate of 2OG (red diamond) are highlighted.* 7
Figure 1.6. Interactions of JmjC-KDMs with C5-carboxylate of 2-OG (or 2-OG mimetic); (A) Binding mode in KDM3B/C (PDB ID 4C8D, 5FZO); (B) Binding mode of KDM4A, B, C, D, KDM5A, B and C (PDB ID 5TVR, 4LXL, 4XDO, 4HON, 5IVB, 5FUP, 5FWJ); (C) Binding mode of KDM6A, B and C (PDB ID 3AVR, 2XUE, 3ZLI); (D) Binding mode of KDM2A, KDM7A, B and C (PDB IB 4QX7, 3KVA, 3KV4, 3PU8). 10
Figure 1.7. Pan-KDM inhibitors as 2-OG mimics with metal chelation (blue) and charge and hydrogen bonding of carboxylate (red) that led to selective KDM5 inhibitors ***3*** *and* ***4****.* 11
Figure 1.8. Structure of KDM5-C49 ***5*** *and KDM5-C70* ***6****; crystal structure of KDM5-C49* ***5*** *bound to KDM5B.* 13
Figure 1.9. Structure of compound ***7****; crystal structure of compound* ***7*** *bound to KDM5A.* 14
Figure 1.10. Structures of ***8*** *and* ***9****; crystal structure of* ***9*** *bound to KDM4D.* 15
Figure 1.11. Structure of ***10****; crystal structure of* ***10*** *bound to KDM4A.* 16
*Figure 1.12. Structure of (R)-****11*** *and (S)-****11****; crystal structure of (R)-****11*** *bound to KDM5A (purple) and crystal structure of (S)-****11*** *bound in KDM5A (blue).* 17
Figure 1.13. Structure of ***4****; crystal structure of* ***4*** *bound to KDM5B.* 18
Figure 1.14. Structure of compound ***12****; crystal structure of compound* ***12*** *bound to KDM5B.* 19
Figure 1.15. Structure of compounds ***13*** *and* ***14****; crystal structure of compound* ***13*** *bound to KDM4A.* 20
Figure 1.16. Superimposition of QC6352 ***10*** *(Purple) in co-crystal of 2-pyridopyrimidinone* ***12*** *(Blue) in KDM5B.* 21
Figure 1.17. Structures of GSK-J1 ***15****, J2* ***17*** *and J4* ***16*** *(above) and co-crystal of GSK-J1* ***15*** *in KDM5B.* 22
Figure 1.18: Structure of CPI-455 ***18****; crystal structure of CPI-455* ***18*** *bound to KDM5A.* 24
Figure 1.19. Structure of pyrazolo[1,5-a]pyrimidin-7(4H)-one ***3****.* 25
Figure 1.20. Overlay of KDOAM-25 ***4*** *(Purple) bound to KDM5B (Purple) and CPI-455* ***18*** *(Light Blue) bound to KDM5A (Light Blue).* 25
Figure 1.21. Structure of compound ***19****; crystal structure of compound* ***19*** *bound to KDM5A.* 27
Figure 1.22. Structure of compound ***20****; crystal structure of compound* ***20*** *bound to KDM5A.* 28
Figure 1.23. Structure of cyclic peptide CP2 ***21*** *and co-crystal structure of KDM4A with CP2.* 30
Figure 1.24. Structure of covalent inhibitor, Afatinib ***22****, a dual inhibitor of the EGFR and HER2 kinases.* 32
Figure 1.25. Cysteine-reactive electrophiles for covalent protein modification. 34
Figure 1.26. Mechanism of target specific covalent inhibition where E is the enzyme and I is the inhibitor. 34
Figure 1.27. Structure of covalent EGFR inhibitor ***35****.* 36

Figure 1.28. Schematic showing the principle of AlphaScreen, a bead-based assay, used to detect demethylation of histone peptide substrate. 38
*Figure 2.1. Crystal structure of **14** in KDM5B.* 39
*Figure 2.2. Covalent docking of phenylpiperidine acrylamide **36** in KDM5B. Some residues removed for clarity.* 41
Figure 2.3. Designed piperazine covalent inhibitors with cysteine-selective electrophiles. 46
*Figure 2.4. Non-covalent (left) and covalent docking (right) of piperazine acrylamide **61** in KDM5B.* 47
Figure 2.5. Designed covalent inhibitors and their clogD values at pH 7.5. 51
*Figure 2.6. Covalent docking of 3-phenylpiperazine **72** (left) and 2-phenylpiperazine **73** (right) in KDM5B.* 52
*Figure 2.7. Covalent docking of methyl benzylamide acrylamide **77** and of methyl benzylamine chloroacetamide **79** in KDM5B.* 54
*Figure 2.8. Covalent docking of cyclopentyl benzylamine acrylamide **80** in KDM5B.* 56
*Figure 2.9. Covalent docking of tetrahydroisoquinoline acrylamide **83** in KDM5B.* 58
*Figure 3.1. IC_{50} curves of chloroacetamide **62** at the different time point (left) and a graph showing the change in IC_{50} of **62** with time (right).* 61
*Figure 3.2. Change in pIC_{50} for covalent chloroacetamide **62** and non-covalent **99**.* 64
Figure 3.3. Graph comparing the k_{inact} value of the different piperazine electrophiles. 65
Figure 3.4. Comparison of K_i's for different series. 73
Figure 3.5. Comparison of k_{inact}/K_i for all covalent inhibitors. 74
*Figure 3.6**.** 2-OG competition assay with tetrahydroisoquinoline dimethylamino crotonamide **85**.* 76
*Figure 3.7**.** 2-OG competition assay with methyl benzylamine dimethylamino crotonamide **78**.* ... 76
*Figure 3.8**.** 2-OG competition assay with methyl benzylamine chloroacetamide **79**.* 77
*Figure 3.9**.** 2-OG competition assay with methyl benzylamine acrylamide **77**.* 77
*Figure 3.10. 2-OG competition assay with **14**.* 78
*Figure 3.11. Change in IC_{50} with 2-OG concentration for covalent **77** (blue) and non-covalent **14** (orange).* 78
*Figure 3.12. IC_{50}'s of **77**, **78** and **79** in immunofluorescence assay.* 79
Figure 3.13. IC_{50} curves for covalent inhibitors in cellular immunofluorescence assay and cell number count (right). 80
*Figure 3.14. Cell viability assays after incubation of cells with compounds; A) **61**, B) **77**, C) **85**, D) **78**, E) **79**.* 84
Figure 3.15. ChipSeq plots of H3K4me3 marks with input sample (red), 77 (green) and DMSO (purple) after 24 hours (left) and 72 hours (right). 85
*Figure 4.1. Schematic showing covalent modification upon incubation of **61** and **62** with KDM5B.* 88
*Figure 4.2. RapidFire-MS covalent binding of chloroacetamide **62** in KDM5B.* 89
*Figure 4.3. RapidFire-MS covalent binding of acrylamide **61** in KDM5B.* 89
*Figure 4.4. Changes in the % of modified KDM5B after incubation with chloroacetamide **62** over time (mins).* 90
*Figure 4.5. Changes in the % of modified KDM5B after incubation with acrylamide **61** over time (mins).* 90
*Figure 4.6. ln[unmodified E]/[Unmodified E]$_{t=0}$ versus time for **62.*** 91
*Figure 4.7. ln[unmodified E]/[Unmodified E]$_{t=0}$ versus time for **61**.* 91
*Figure 4.8. Sequence of peptides from elastase digest of acrylamide **61** complex with KDM5B.* 92
*Figure 4.9. Sequence of peptides from elastase digest of chloroacetamide **62** complex with KDM5B.* 93
Figure 4.10. MS of native KDM5C. 94

*Figure 4.11. MS of incubation of acrylamide **61** with KDM5C. 94*
*Figure 4.12. Co-crystal structure of **61** bound to KDM5B (PDB ID 6EIN). 95*
*Figure 4.13. Schematic showing covalent modification upon incubation of **77**-**79** with KDM5B. ... 96*
*Figure 4.14. MS showing covalent binding of acrylamide **77** to KDM5B after 120 minutes incubation. 97*
*Figure 4.15. MS showing covalent binding of acrylamide **77** to KDM5B after 150 min incubation. 97*
*Figure 4.16. MS showing covalent binding of **78** to KDM5B after 45 minutes incubation. 98*
*Figure 4.17. MS showing covalent binding of **79** to KDM5B after 120 minutes incubation. 98*
*Figure 4.18. MS of native KDM4B (top) and MS of incubation of **78** with KDM4B (bottom) 99*
*Figure 4.19. MS of native KDM5C and MS of incubation of **78** with KDM5C 100*
Figure 5.1. Design of an activity-based protein profiling probe with reactive group (red), binding group (blue) and reporter tag (pink) and representative examples of reactive group and reporter tag. 102
Figure 5.2. In-gel fluorescence-based protein profiling where probe-labelled enzymes are visualised across proteomes. 103
Figure 5.3. LC/MS-based platforms for ABPP. (a) ABPP and multidimensional protein identification technology. (b) Active-site peptide profiling. 104
*Figure 5.4. Design of clickable alkyne analogue **103**. 105*
*Figure 5.5. Covalent docking of **103** into KDM5B. 105*
Figure 5.6. Time dependent inhibition of clickable analogue by AlphaScreen. 110
*Figure 5.7. MS of the incubation of **103** with KDM5B for 30 minutes at 37 °C. 110*
Figure 5.8. Schematic of protocol for in-gel fluorescence with recombinant KDM5B. 111
*Figure 5.9. In-gel fluorescence of clickable **103** and non-clickable **77** compounds incubated with KDM5B. 112*
Figure 5.10. Coomassie staining of in gel fluorescence with recombinant protein KDM5B. 113
Figure 5.11: Schematic of protocol for in-gel fluorescence with cell lysates. 114
*Figure 5.12. In-gel fluorescence of alkyne **103** with cell lysates. 114*
Figure 5.13. Schematic for biotin pull down in cell lysates. 115
Figure 5.14. Biotin Pull-down with mcf7 cell lysates. 116
Figure 5.15. Western Blot of KDM5B in mcf7 and k562 cell lysates before and after protein precipitation. 117
Figure 5.16. Biotin Pull-down with k562 cell lysates (lysed with RIPA buffer). 118
Figure 6.1. Structure of sulfonamides and tautomers of sulfonimidamides. 120
Figure 6.2. Sulfonimidamides in medicinal chemistry. 121
Figure 6.3 - Trifluoromethyl sulfoximine compounds. 122
Figure 7.1. Regulation of dNTPs production by ribonucleotide diphosphate reductase (RNR). 139
Figure 7.2. Protein degradation using a PROTAC that binds to protein of interest (POI) and recruits E3 ligase for polyubiquitination of the protein. 140
*Figure 7.3. Crystal structure of dATP in the two subunits (blue and pink) of human ribonucleotide reductase R1 (RRM1) (above, PDB ID 2WGH) and structure of designed deoxyadenosine-based PROTAC **174** and triphosphate **175**. 141*
*Figure 7.4. Western blot of RRM1 and RRM2B after incubation of MCF7 and HeLa cells with **174**. 144*
Figure 7.5. Space filling representation of the binding mode (PDB ID 2WGH). 145
*Figure 7.6. Design of a C-2 alkyne deoxyadenosine-based PROTAC **183**. 145*
Figure 8.1. CF_2 and CF-sulfonimidamide transfer reagents. 154

List of Tables

*Table 1.1. Comparison of residues binding to metal centre and substrate selectivity in JmjC-KDMs. * Metal chelating residues are identified from sequence alignments.*[25] 9
*Table 1.2. Comparison of residues interacting with carboxylate in KDM structures on different β strands. * N terminal anti-beta strands.* 10
Table 2.1. Section of Alignment of KDM protein sequences. 40
*Table 3.1. Time-dependent IC_{50}'s against KDM5B and their k_{inact}/K_i values for piperazine analogues **61-69*** 63
*Table 3.2. Cell permeabilities of piperazine acrylamide **61** and chloroacetamide **62** from Caco-2 assay.* 66
*Table 3.3. Time-dependent IC_{50}'s and their k_{inact}/K_i values for substituted piperazines **72**-**76**.* 67
*Table 3.4. Time-dependent IC_{50}'s and their k_{inact}/K_i for methyl benzylamines **77**-**79** and **100**.* 68
*Table 3.5. Time-dependent IC_{50}'s and their k_{inact}/K_i of cyclopentyl benzylamine analogues **80**-**82** and **101**.* 70
*Table 3.6. Time-dependent IC_{50}'s against KDM5B and their k_{inact}/K_i of tetrahydroisoquinoline analogues **83**-**85** and **102**.* 71
*Table 3.7. Cell permeability of analogues **77**, **80** and **83** using Caco-2 assay.* 72
Table 3.8. IC_{50}'s of compounds against other KDM proteins measured by AlphaScreen. 75
Table 3.9. KDM5B nanoBRET IC_{50}'s of covalent inhibitors (average of 2 experiments). 82
*Table 4.1. Percentage of unmodified, singly modified and doubly modified KDM5B after incubation with **77**-**79**.* 96
*Table 6.1. Optimisation of displacement of nitrophenol sulfonimidate **152** with butylamine.* 128
*Table 6.2. Solvent screen of displacement of nitrophenol sulfonimidate **152** with butylamine.* 128
*Table 6.3. Optimisation of preparation of pentafluorophenol sulfonimidate **155**.* 129

List of Schemes

Scheme 2.1. Design of phenylpiperidine covalent inhibitor. 40
*Scheme 2.2. Synthetic route towards amine **40**.* 41
*Scheme 2.3. Synthetic route towards chloro-pyridopyrimidinone **44**.* 42
*Scheme 2.4. Synthetic route towards acrylamide **36**.* 43
*Scheme 2.5. Synthetic route towards amine **57**.* 44
*Scheme 2.6. Synthetic route towards phenylpiperidine acrylamide **36**.* 45
*Scheme 2.7. Synthetic route of piperazine acrylamide **61** and chloroacetamide **62**.* 48
*Scheme 2.8. Synthetic route towards piperazine propiolamide **63**, dimethylamino crotonamide **64** and halonitrobenzenes **65**-**69**.* 49
*Scheme 2.9. Synthetic route towards phenylpiperazine acrylamides **72** and **73**.* 53
*Scheme 2.10. Synthetic route towards benzylpiperazine acrylamides **74**, **75** and **76**.* 53
*Scheme 2.11. Synthetic route towards methyl benzylamine covalent inhibitors **77**-**79**.* 55
*Scheme 2.12. Synthetic route towards cyclopentyl benzylamine covalent inhibitors **80**-**82**.* 57
*Scheme 2.13. Synthetic route towards tetrahydroisoquinoline covalent inhibitors **83**-**85**.* 58
*Scheme 5.1. Attempted synthesis of alkyne benzylamine **107/108** via a nucleophilic aromatic substitution.* 106
*Scheme 5.2. Attempted synthesis of alkyne benzylamine **111** via a nucleophilic aromatic substitution.* 107
*Scheme 5.3. Activation of 7-octyn-1-ol as mesylate **112** and **113**.* 107

*Scheme 5.4. Synthesis of Boc-protected benzylamine **116**. 107*
*Scheme 5.5. Synthesis of TMS-alkyne **120**..... 108*
*Scheme 5.6**.** Synthesis of alkyne acrylamide **103**. 109*
Scheme 6.1. Literature synthetic methodology to access sulfonimidamides. 121
Scheme 6.2. Preparation of trifluoromethyl sulfonimidamides. 123
*Scheme 6.3. Synthesis of imidazole sulfonimidamide **135**. 124*
*Scheme 6.4. Synthesis of imidazole CF_3-sulfonimidamide **139.**..... 124*
Scheme 6.5. Synthesis of imidazole phenyl sulfonimidamide. 125
*Scheme 6.6. Synthesis of activated imidazole sulfonimidamide **145.** 125*
*Scheme 6.7**.** Activation of sulfinamide **134** with pyridine and DMAP. 126*
*Scheme 6.8. Synthesis of nitrophenol sulfonimidate **152**..... 127*
*Scheme 6.9**.** Reaction of pentafluorophenol sulfonimidate **155** with amines..... 130*
*Scheme 6.10. Synthesis of Tetrafluorophenol sulfonimidate **158**. Reaction conditions: (i) NCS (1.1 equiv.), TBAF (1.1 equiv.), AcN, 0°C to rt, 30 min (ii) 2,3,5,6-Tetrafluorophenol (8 equiv.), KO^tBu (1M in THF, 7 equiv.), then **157**, AcN..... 131*
Scheme 6.11. Amine scope with transfer reagent. [a]Reaction Conditions: 2 equiv. amine, DMF, rt, 1 h; [b] 2 equiv. amine, DMF, 50 °C; RSM = Recovered Starting Material. 132
*Scheme 6.12**.** Deprotection of DMPM group and alkylation..... 133*
*Scheme 6.13**.** Attempted reaction of transfer reagent **158** with Grignard reagents. 134*
*Scheme 6.14**.** Attempted reaction of transfer reagent **158** with methyl zinc chloride. 134*
*Scheme 6.15. Synthesis of trifluoromethyl sulfoximine **171**..... 135*
*Scheme 6.16**.** Flow reaction conditions to trifluoromethyl sulfonimidamides. Reaction conditions: **158**, pyrrolidine (2 eq.), AcN, 80 °C, 0.05 mL/min. 135*
*Scheme 6.17. Summary of reactivity of transfer reagent **158** towards N and C nucleophiles. 137*
*Scheme 7.1. Synthesis of carboxylic acid **177**..... 142*
*Scheme 7.2. Synthesis of deoxyadenosine-based PROTAC **174**..... 143*
*Scheme 7.3. Synthesis of 2'-deoxygenated chloroadenosine **191**. 146*
*Scheme 7.4. Attempted synthesis of alkyne deoxyadenosine-based PROTAC **183**. 148*
*Scheme 7.5. Synthesis of C-2 deoxyadenosine PROTAC **183.** 149*

List of Experiments Contributed by Others

Chapter 3:

- Caco-2 assay to test permeability of compounds was carried out by the Institute of Cancer Research.
- 2-OG competition assay of compounds using AlphaScreen was carried out by Saleta Vazquez Rodriguez.
- Immunofluorescence assay of compounds in cells transfected with KDM5B was carried out by John-Paul Bukowski.
- Synthesis of KDM5 tracer for NanoBRET by Saleta Vazquez Rodriguez and NanoBRET assay carried out by Catherine Rodgers.
- Measuring H3K4me3 levels in cells with endogenous KDM5B using ChIPSeq carried out by Saleta Vazquez Rodriguez.
- Cytotoxicity assays of compounds carried out by Catherine Rodgers.

Chapter 4:

- Processing of elastase digest data of **61** and **62** was carried out by Marie-Laetitia Thezenas.
- Co-crystallisation of **61** in KDM5B was carried out by Kannan Velupillai.

Chapter 5:

- Lysis of MCF7 and K562 cells for use in pull-down assays was carried out by Saleta Vazquez Rodriguez.

Chapter 6:

- Chemical stability tests of sulfonimidoyl fluoride **157** and transfer reagent **158** was carried out by Janssen Pharmaceutical Analytical team.

Chapter 7

- Western blot of RRM1 and p53R2 after incubation of MCF7 and HeLa cells with **174** by member of Vincenzo D'Angiolella's lab.

Abbreviations

AcN	Acetonitrile
Boc	*tert*-Butyloxycarbonyl
Caco-2	Colorectal adenocarcinoma cells
CAN	Cerium ammonium nitrate
dATP	Deoxyadenosine triphosphate
CRBN	Cereblon
DBU	1,8-Diazabicyclo[5.4.0]undec-7-ene
DCE	Dichloroethane
DCM	Dichloromethane
DIEA	*N*,*N*-Diisopropylethylamine
DMA	Dimethylacetamide
DMPM	Dimethoxybenzyl
DMAP	4-(Dimethylamino)pyridine
DMF	Dimethylformamide
DMSO	Dimethyl sulfoxide
DNA	Deoxyribonucleic acid
Et_3N	Triethylamine
EtOAc	Ethyl acetate
FAD	Flavin adenine dinucleotide
HATU	*N*-[(Dimethylamino)-1*H*-1,2,3-triazolo-[4,5-*b*]pyridin-1-ylmethylene]-*N*-methylmethanaminium hexafluorophosphate *N*-oxide
H3	Histone 3
HEPES	4-(2-Hydroxyethyl)piperazine-1-ethanesulfonic acid

HFIP	1,1,1,3,3,3-Hexafluoro-2-propanol
IC_{50}	Half maximal inhibitory concentration
JmjC	Jumonji C
KDMs	Lysine demethylases
LiHMDS	Lithium bis(trimethylsilyl)amide
LRMS	Low Resolution Mass Spectroscopy
LDA	Lithium diisopropylamide
MCF7	Michigan Cancer Foundation-7
MDCK	Madin-Darby Canine Kidney cells
MeI	Methyl Iodide
MES	2-(N-Morpholino)ethanesulfonic acid
MS	Mass Spectrum
MsCl	Methanesulfonyl chloride
MW	Molecular Weight
m/z	Mass/charge ratio
NCS	*N*-Chlorosuccinimide
NMM	*N*-Methylmorpholine
NMP	*N*-Methyl-2-pyrrolidone
NOG	*N*-oxalylglycine
PAMPA	Parallel artificial membrane permeability assay
PBS	Phosphate-buffered saline
PDB	Protein Data Bank
PDCA	2,4-Pyridine dicarboxylic acid
PgP	P-glycoprotein
PHD	Plant homeodomain

PK/PD	Pharmacokinetics/pharmacodynamic
PROTAC	Proteolysis-targeting chimera
PS-DIPEA	Polymer supported *N*,*N*-Diisopropylethylamine
RNR	Ribonucleotide diphosphate reductase
SDS	Sodium dodecyl sulfate
SEM	2-(Trimethylsilyl)ethoxymethyl chloride
SM	Starting material
T3P	2,4,6-Tripropyl-1,3,5,2,4,6-trioxatriphosphorinane-2,4,6-trioxide solution
TBAF	Tetrabutylammonium fluoride
TFA	Trifluoroacetic acid
THF	Tetrahydrofuran
TBSCl	*tert*-Butyldimethylsilyl chloride
TMS	Trimethylsilyl
TMSCl	Trimethylsilyl chloride
2-OG	2-oxoglutarate

Chapter 1. Introduction

1.1. Epigenetics and the Role of Lysine Demethylases

1.1.1. Epigenetics and Chromosome Structure

Epigenetics has been defined as the study of heritable changes in gene expression without changes in the underlying DNA sequence. A variety of different biological phenomena can be affected by epigenetic mechanisms. Epigenetic changes are necessary for cell development and differentiation to give different cell types. Normal cell processes such as X-chromosome inactivation in female mammals is controlled by epigenetic changes. However, these epigenetic states can be disrupted by various factors such as ageing, exposure to chemicals and diet which can lead to the development of cancers and other diseases.

Investigation of the molecular basis of epigenetics resulted in a greater understanding of the field. Chromatin is a complex consisting of DNA and histone proteins whose primary function is to enable large amounts of DNA to be packaged in the eukaryotic cell's nucleus (Figure 1.1). Modification of the components of chromatin is necessary for transcriptional regulation and therefore gene expression. The main mechanisms of chromatin remodelling that have been reported include methylation of DNA and methylation, acetylation, ubiquitination and phosphorylation of histone tails. A number of diseases, including cancer and mental disorders, have been associated with these alterations of chromatin structure.[1] Small molecules which bind to enzymes that catalyse the addition and removal of these modifications ('writers' and 'erasers' respectively) are therefore of great interest as therapeutics. DNA methyltransferase inhibitors, such as azacitidine, are already in clinical use, as well as histone deacetylase inhibitors, such as vorinostat and romidepsin, that were both approved as treatments for cutaneous T-cell lymphoma.[2],[3]

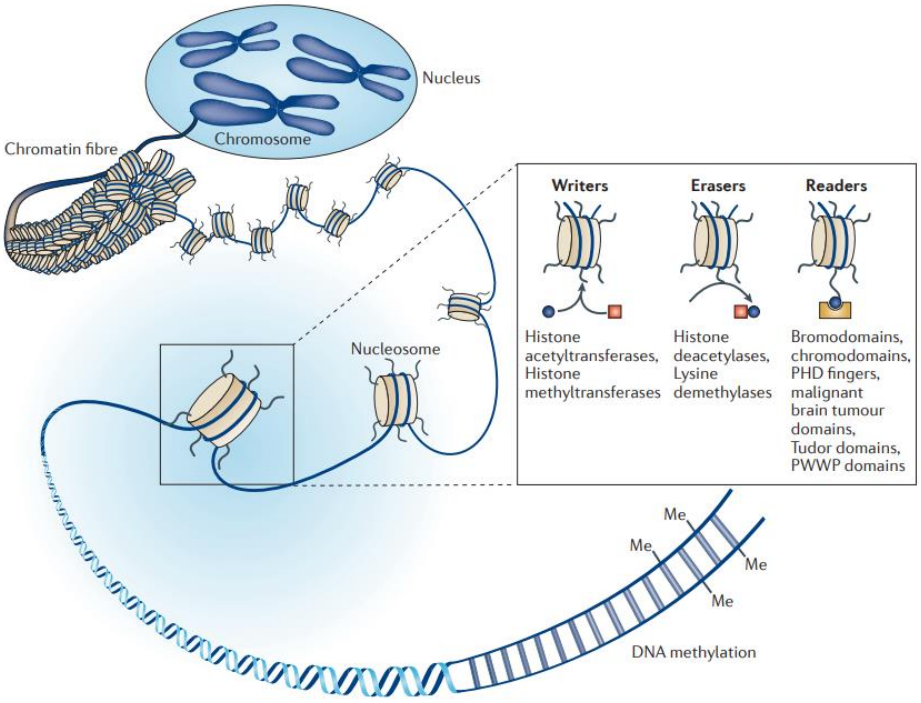


Figure 1.1. Covalent histone modification involved in epigenetic regulation of gene expression. This figure is taken from the literature.[4]

1.1.2. Histone Lysine Demethylases

Histone lysine methylation was first discovered in the 1960s and was initially regarded as an irreversible modification until the discovery of lysine demethylases (KDMs) in 2004.[5,6] Histone *N*-methylation occurs on lysyl and arginyl side chains of histone-3 (H3) and 4 (H4), however, there is some evidence of *N*-methylation on other proteins.[7] *N*-Methylation of histones can lead to transcriptional activation or repression depending on the residue and the extent of histone protein methylation. The regulation of gene expression is also dependent on whether the residues are unmodified, mono-, di-or trimethylated. Histone methylation marks also function cooperatively with other types of histone modifications adding to the complexity of gene regulation.[8]

Lysine demethylases catalyse the removal of methyl modifications on histone tails which regulates gene expression.[9] Over twenty KDMs have been discovered and linked to tumour growth. KDMs

are subdivided into two classes, KDM1 (lysine specific demethylase 1, LSD1) and *Jumonji C* domain containing KDMs (JmjC-KDMs), which differ in their catalytic domains and mechanism of demethylation.

1.1.3. KDM Inhibitors in Clinical Development

There have been successful advances in the development of lysine specific demethylase (LSD1) inhibitors with some compounds progressing to clinical trials. The cyclopropylamine-containing inhibitor, GSK2879552 **1**, is a potent and selective irreversible inhibitor of LSD1 which increases H3K4 methylation and increases expression of tumour-suppressor genes (Figure 1.2).[10] It has potential to prevent cell-growth in LSD1-overexpressing tumour cells. GSK2879552 **1**, was in phase 1 clinical trials for subjects with relapsed/refractory Small Cell Lung Carcinoma but was terminated early due to safety concerns. ORY-1001 **2**, developed by Oryzon Genomics, is another tranylcypromine-based orally bioavailable selective LSD1 inhibitor which is currently in clinical trials for patients with acute myeloid leukemia and solid tumours.[11]

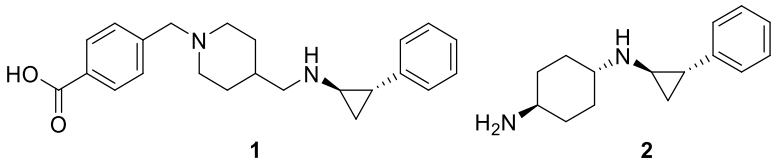


*Figure 1.2. Structure of GSK2879552 **1** and ORY-1001 **2**.*

Many of the reported inhibitors of JmjC-KDMs have failed to show potent cellular activities for progression into *in vivo* studies. However, GS-5801 (acquired by Gilead from Epitherapeutics), a small molecule KDM5 inhibitor, was in phase 1 clinical trials in healthy subjects and in patients with chronic HBV infection but the trial has now been discontinued. The structure of GS-5801 was not been disclosed but it was likely a close analogue of their aminomethyl pyridines.[12]

1.1.4. KDM1 Subfamily

The KDM1 (LSD1) subfamily is related to monoamine oxidases (MAOs) and requires flavin adenine dinucleotide (FAD) as a cosubstrate. Mechanistically, demethylation occurs via hydride transfer from the *N*-methyl group to FAD forming an imine which undergoes hydrolysis (Figure 1.3). FAD is regenerated through oxidation of the reduced FAD ($FADH_2$) by molecular oxygen. Due to the necessity of a nitrogen lone pair in the catalytic mechanism, KDM1 enzymes do not act on trimethylated lysines.[13]

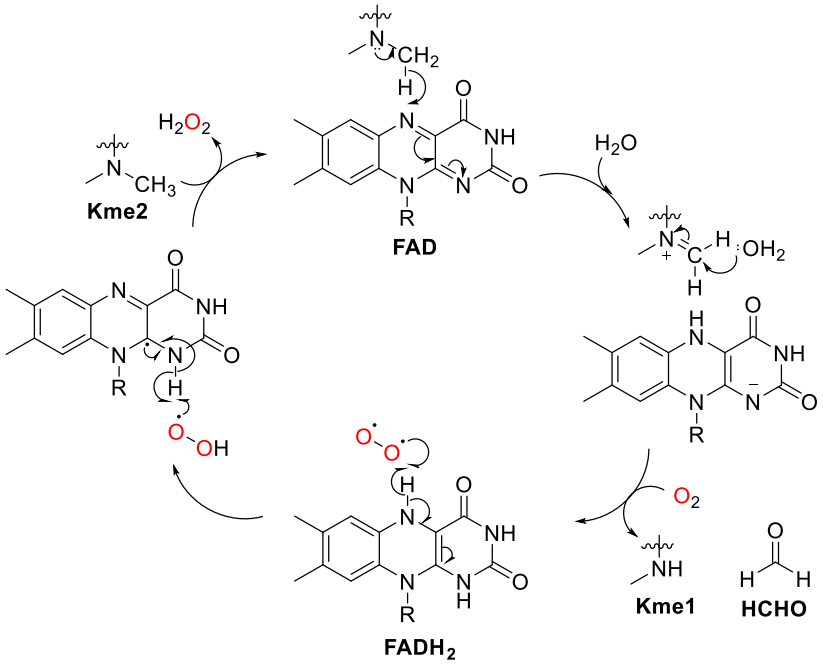


Figure 1.3. Mechanism of demethylation with KDM1 class.

1.2. JmjC-KDMs

1.2.1. Subfamilies and Mechanism

JmjC-KDMs are the larger class of KDMs which are further categorised into KDM2, KDM3, KDM4, KDM5, KDM6 and KDM7 subfamilies based on structural alignments.[14] JmjC-KDMs are part of a larger family of 2-oxoglutarate (2-OG) oxygenases and require 2-OG and dioxygen as cosubstrates and Fe(II) as a cofactor to function.[13] The catalytic mechanism of demethylation for JmjC-KDMs

involves binding of 2-OG to the Fe(II) centre followed by positioning of the histone peptide substrate in the active site (Figure 1.4).[15] Subsequent binding of molecular oxygen and loss of carbon dioxide results in a highly reactive oxo-ferryl (IV) intermediate which oxidises the *N*-methyl group to form an unstable hemiaminal. This can undergo fragmentation to yield formaldehyde and the lysine residue with one less methyl group. Loss of succinate and binding of more water molecules to the Fe(II) regenerates the initial complex which can demethylate the next methylated lysine substrate. The *N*-methylated substrate does not require a lone pair, as observed with the KDM1 mechanism, therefore all possible methyl states including trimethylated lysine residues can be demethylated by JmjC-KDMs.

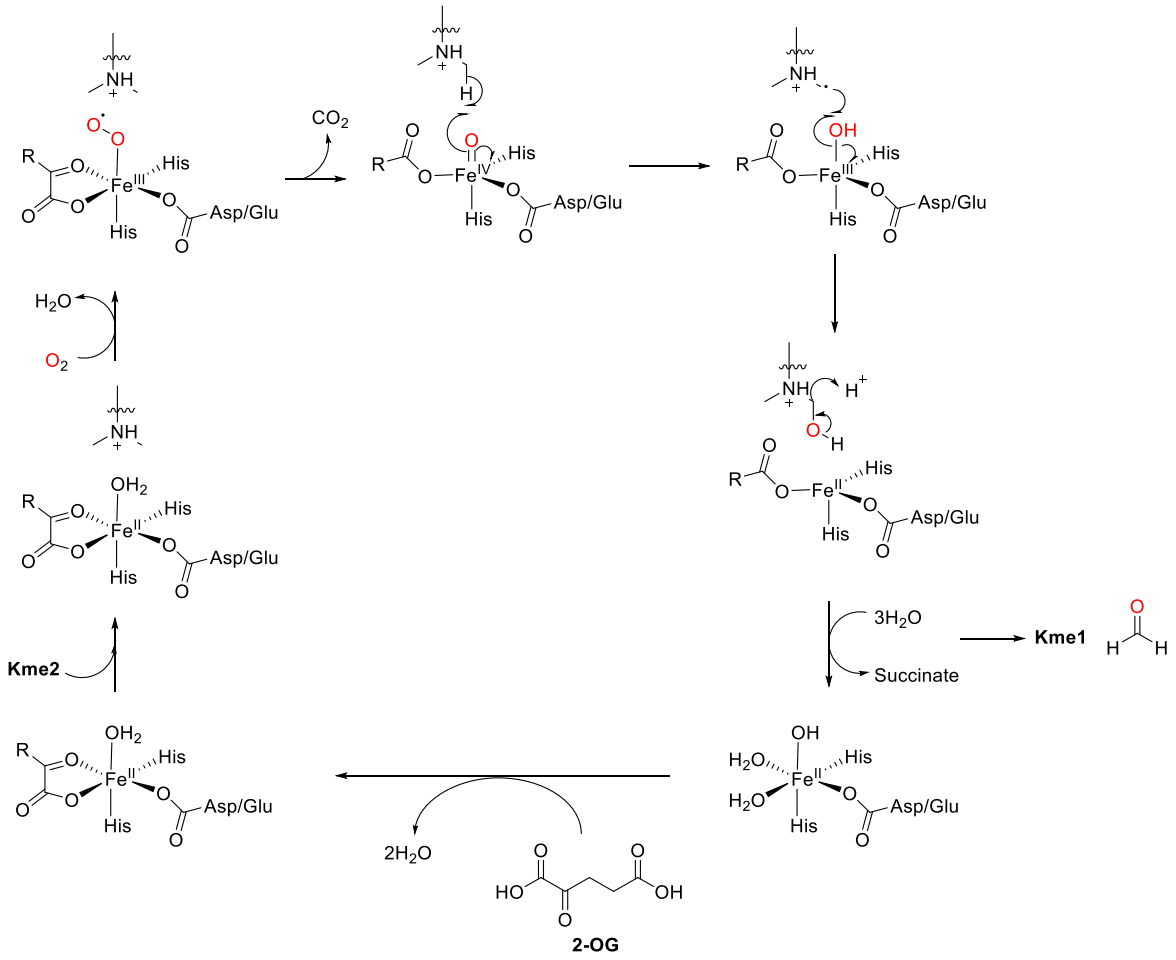


Figure 1.4. Mechanism of demethylation with JmjC-domain containing KDMs.

1.2.2. JmjC-KDM Histone Substrate Specificities

All the JmjC-KDM subfamilies have the same catalytic mechanism of demethylation however they are very distinct in their specificities for the lysine position on the histone tails as well as their methylation state. Di- and mono- *N*ε-methylated lysines can be demethylated by KDM2/KDM3/KDM7 while tri-, di- and in some cases mono-*N*ε-methylated lysines can be demethylated by KDM4/KDM5/KDM6 subfamilies. Lysine 4 of histone H3 (H3K4), H3K27 and H3K36 are specifically demethylated by KDM5,[16–18] KDM6[19,20] and KDM2[21] respectively while H3K9 can be demethylated by KDM3A/B,[22] KDM4 and KDM7 (Table 1.1).[23] There are also differences in the histone substrate specificities within the same subfamily such as KDM4A, B and C which can demethylate both H3K9 and H3K36 while KDM4D and pseudogene KDM4E can only demethylate H3K9.[24–28] Studies have shown that KDM3C does not have enzymatic activity for H3K9 unlike KDM3A/B.[29]

There are around 30 JmjC-domain containing proteins in humans with the majority (approximately 20) showing demethylase activity however some JmjC-proteins are hydroxylase enzymes such as FIH and JMJD4. JmjC-KDMs also have an interesting biological role outside the field of histone lysine modification as they have recently been discovered to demethylate lysines of non-histone proteins and methylated arginines.[30–32]

JmjC-KDMs also contain other domains that are not directly involved in their catalytic activity but are involved in the recognition of histone modification such as reader domains (PHD-finger or Tudor domains) or are DNA-binding domains (CXXC zinc finger domains or AT-rich interacting domains (ARID)).[33] These domains can indirectly affect KDM catalysis and specificity for different substrates.[34,35]

1.2.3. JmjC Domain Architecture

The JmjC domain of KDMs is characterised by a distorted double stranded β-helix (DSBH) core fold which is comprised of eight anti-parallel β-strands named βI-VIII.[36] The asymmetric barrel-like DSBH fold is formed from four long β-strands (βI, VIII, III and VI) on one face and four short β-strands (βII, VII, IV and V) on the other face (Figure 1.5). A N-terminal loop exists in JmjC-KDMs between DSBH and the N-terminal anti-β strands. There is also an extended insertion involved in substrate binding between βIV and V strands.[37]

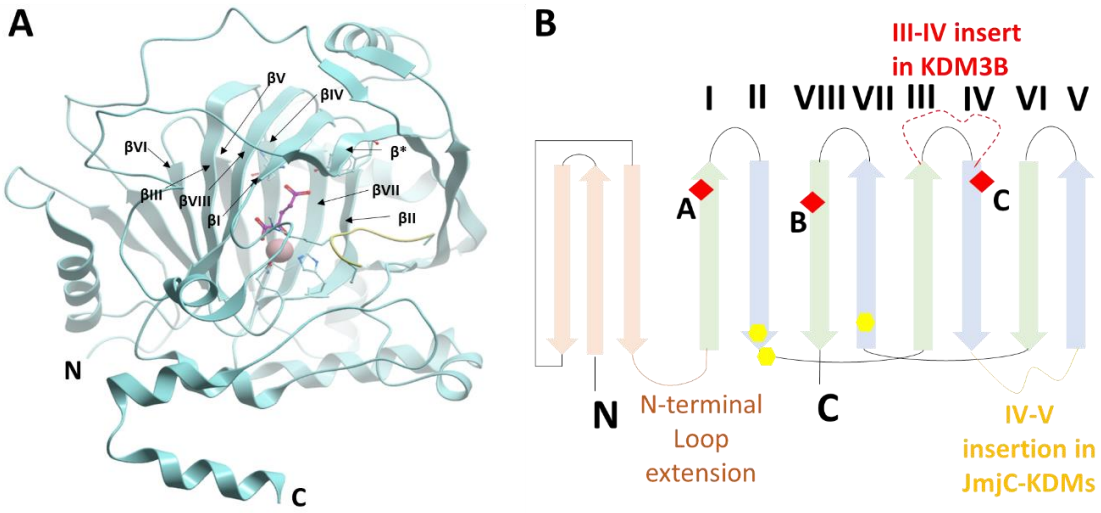


Figure 1.5. Structure of JmjC-domain of KDMs. (A) Overall structural fold of JmjC-KDMs (Crystal structure of KDM4D in complex with H3K9me3 (yellow) and 2-oxoglutarate (2OG, PDB ID 4HON) with the core DSBH labelled) (B) Cartoon structure of DSBH fold with Fe^{2+} coordinating motif (yellow hexagons) and the position of the lysine residue in different KDMs that coordinates the carboxylate of 2OG (red diamond) are highlighted.

1.2.4. 2OG-Binding Site of JmjC Domain

2-oxoglutarate has the same binding mode in the JmjC domain of all KDMs whereby the keto-acid interacts with the metal centre via a bidentate coordination and the C5 carboxylic acid forms a salt bridge with a basic residue.

As shown in the catalytic mechanism, Fe(II) is coordinated by three residues that make up a HxD/E…H motif in which a His (βII) and an Asp/Glu (βII–βIII loop) are separated by one amino acid

while the other His is found on βVII (Figure 1.5). Almost all KDMs have two histidine residues coordinating the metal but differ in the acidic residue of the triad (Table 1.1).[38,39] Aspartic acid coordinates the metal in KDM2A/B, KDM3A/B and KDM7A/B/C while the longer residue, glutamic acid, coordinates the metal in KDM4, KDM5 and KDM6. Alanine mutants have been shown to abolish enzymatic activity proving that these three residues have an essential role in the demethylation mechanism.[40] In KDM7C (PHF2), the His on βVII is replaced with Tyr which could aid in the design of PHF2 selective inhibitors. This anomaly may also convey interesting mechanistic and biological properties.

It is also worthy of note that all KDMs with a coordinating Asp demethylate histone substrates with mono- or di-methylated lysines while the KDMs with a coordinating Glu demethylate histone substrates with di- or trimethylated lysines. Therefore, the addition of a carbon in the acidic residue must convey specificity of the KDMs for the different methylation states of the histone substrates.

Many JmjC-KDM inhibitors have therefore been designed with mono- or bidentate metal coordination as a way of inhibiting the catalytic mechanism of demethylation through competition in the 2-OG binding site.

The C5 carboxylic acid of 2-OG has an important role in binding to JmjC-KDMs via a salt bridge with a basic residue in the KDMs active site. Almost all JmjC-KDMs have a lysine which can engage in an ionic interaction in the 2-OG binding site (Table 1.1). The lysines are found on different strands (Figure 1.6) however the amino group of the lysine overlaps well across the different KDM subfamilies. The lysine is most commonly positioned on βIV strand except for KDM3B and KDM6 in which the lysine is found on βVIII or βI strand respectively.[15,41,42] KDM3C is anomalous with a glutamine as the key binding residue which would change the interaction with 2-OG and notably KDM3C has no reported catalytic activity.[29]

Name	Synonyms	Substrate[+]	Fe(II) metal binding residues		
KDM2A	FBXL11, JHDM1A	H3K36me1/2	H212	D214	H284
KDM2B*	FBXL10, JHDM1B	H3K36me1/2	H211	D213	H283
KDM7A	KIAA1718, JHDM1D	H3K9me1/2			
		H3K27me1/2	H282	D284	H354
KDM7B	PHF8, JHDM1F	H3K9me1/2	H247	D249	H319
KDM7C	PHF2, JHDM1E		H249	D251	Y321
KDM3A*	JMJD1A, JHDM2A	H3K9me1/2	H1120	D1122	H1175
KDM3B	JMJD1B, JHDM2B	H3K9me1/2	H1560	D1562	H1689
KDM3C	JMJD1C, JHDM2C		H2336	E2338	H2466
KDM4A	JMJD2A, JHDM3A	H3K9me2/3 H3K36me2/3	H188	E190	H276
KDM4B	JMJD2B, JHDM3B	H3K9me2/3 H3K36me2/3	H189	E191	H277
KDM4C	JMJD2C, JHDM3C	H3K9me2/3	H190	E192	H278
KDM4D	JMJD2D, JHDM3D	H3K9me2/3	H192	E194	H280
KDM5A	JARID1A, RBP2	H3K4me2/3	H483	E485	H571
KDM5B	JARID1B, PLU1	H3K4me2/3	H499	E501	H587
KDM5C	JARID1C, SMCX	H3K4me2/3	H514	E516	H602
KDM5D*	JARID1D, SMCY	H3K4me2/3	H514	E516	H602
KDM6A	UTX	H3K27me2/3	H1146	E1148	H1226
KDM6B	JMJD3	H3K27me2/3	H1390	E1392	H1470
KDM6C	UTY	H3K27me2/3	H1014	E1016	H1094

*Table 1.1. Comparison of residues binding to metal centre and substrate selectivity in JmjC-KDMs. * Metal chelating residues are identified from sequence alignments.*[25]

Pan-KDM inhibitors such as pyridine dicarboxylic acid (PDCA) and *N*-oxalylglycine (NOG) have been developed that mimic the 2-OG binding mode (Figure 1.7).[43,44] Key features include a bidentate metal chelating group and a carboxylic acid for interaction with the basic lysine residue that is common across the KDMs. More selective inhibitors of the KDM subfamilies have been achieved through interaction with other key residues in the 2-OG binding pocket.

Threonine residues can also hydrogen bond with the 2-OG carboxylate such as in KDM2A, KDM3B and C, and KDM7A, B and C. Both threonine and asparagine in KDM6A, B and C are in hydrogen bonding distance of the carboxylate (Table 1.2).

Both KDM4 and KDM5 have a tyrosine that can interact with the 2-OG carboxylate which has been exploited for the design of dual KDM4/5 inhibitors that are selective over the other KDM subfamilies. KDM4 and KDM5 are closely related JmjC-KDMs so are structurally similar in their direct binding residues to 2-OG. Therefore, the design of KDM5 selective inhibitors has relied on changes

in the conformation of residues in the second coordination sphere which could result in displacements of the primary binding residues. Guided by structural information, selective KDM5 inhibitors, such as cyanopyrazole **3** and pyridine carboxamide **4** (Figure 1.7), have been reported that take advantage of the greater flexibility of the key tyrosine in KDM5 compared to KDM4, creating space for larger groups to bind.

Strands	N- β *	β1	βII	βIII	βIV	βV	βVI	βVII	βVIII
KDM2A			T209		K229				
KDM3B			T1557						K1699
KDM3C			T2333						Q2476
KDM4A	Y132				K206				
KDM4B	Y133				K207				
KDM4C	Y134				K208				
KDM4D	Y136				K210				
KDM5A	Y409				K501				
KDM5B	Y425				K517				
KDM5C	Y440				K532				
KDM6A		K1137	T1143	N1156					
KDM6B		K1381	T1387	N1400					
KDM6C		K1084	T1090	N1103					
KDM7A			T279	Y292	K299				
KDM7B			T244	Y257	K264			T323	
KDM7C			T246	Y259	K266			T323	

*Table 1.2. Comparison of residues interacting with carboxylate of 2-OG in KDM structures on different β strands. * N terminal anti-beta strands.*

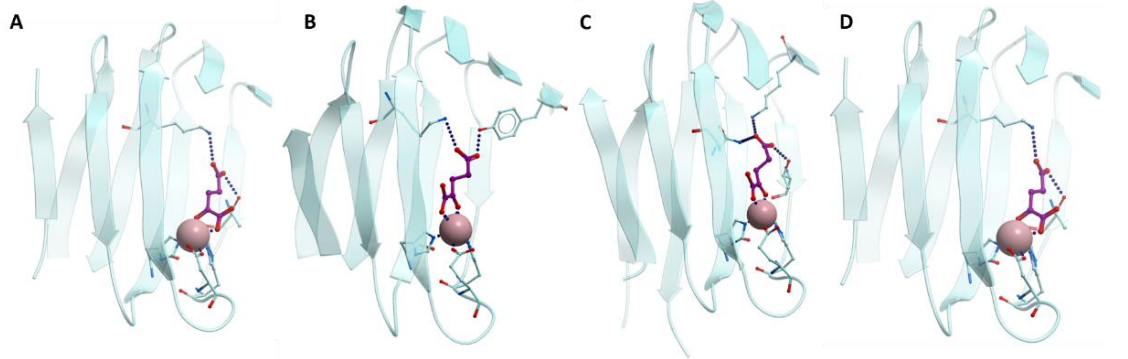


Figure 1.6. Interactions of JmjC-KDMs with C5-carboxylate of 2-OG; (A) Binding mode in KDM3B/C (PDB ID 4C8D, 5FZO); (B) Binding mode of KDM4A, B, C, D, KDM5A, B and C (PDB ID 5TVR, 4LXL, 4XDO, 4HON, 5IVB, 5FUP, 5FWJ); (C) Binding mode of KDM6A, B and C (PDB ID 3AVR, 2XUE, 3ZLI); (D) Binding mode of KDM2A, KDM7A, B and C (PDB IB 4QX7, 3KVA, 3KV4, 3PU8).

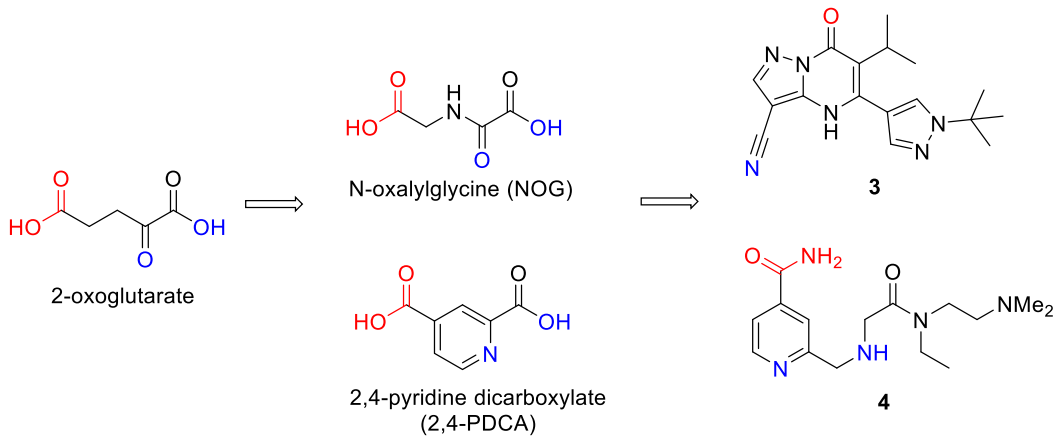


*Figure 1.7. Pan-KDM inhibitors as 2-OG mimics with metal chelation (blue) and charge and hydrogen bonding of carboxylate (red) that led to selective KDM5 inhibitors **3** and **4**.*

1.2.5. KDM5 subfamily: Structure and Biology

Proteins in the KDM5 subfamily are complex proteins composed of JmjC, JmjN, DNA-binding, ARID, C_5HC_2 zinc finger and methyllysine- or methyl-arginine-binding PHD domains.[45],[46] Four genes, KDM5A, KDM5B, KDM5C and KDM5D, are known in this family that are responsible for demethylation of di- and trimethylated lysine 4 of histone 3 (H3K4me2/me3) histone mark which is required for transcriptional activation.

Strong evidence has now shown a link between KDMs and the onset of various cancers. Changes in the expression levels of KDMs can result in activation of oncogene expression, repression of tumour suppressor expression, disruption of chromosomal stability, changes to DNA mismatch repair mechanisms or interaction with hormonal receptors involved in cellular proliferation.[47–49] Overexpression of KDM5A/B has been linked to several cancers such as acute myeloid leukemia,[50] heptatocellular carcinoma,[51] lung,[52] gastric,[53] melanoma,[54] breast,[55] ovarian[56] and testicular cancer.[57]

In particular, upregulation of KDM5B (JARID1B) promotes formation, growth and metastasis in both prostate and gastric cancers.[58],[59] KDM5B has a role in development as it is necessary for the self-renewal of hematopoietic cells.[60] KDM5B has also been associated with glioma due to its

overexpression in cancerous glial cells compared to normal brain tissues.[61] KDM5B is not required for embryonic stem cell self-renewal however it has an essential role in their differentiation.[62]

As a result, KDM5B is an interesting therapeutic target which would benefit from the development of selective small molecule inhibitors that could be used to better understand the role of KDM5B in biology.

1.3. KDM5 Inhibitors

1.3.1. 2-OG Binding Site Inhibitors: Pyridine Carboxylic Acids

2,4-pyridinedicarboxylic acid (PDCA), a micromolar pan-KDM inhibitor, was used as a starting point for the design of more selective KDM5 inhibitors. The para carboxylic acid was retained for key binding interactions with the lysine and tyrosine in KDM5 while the ortho carboxylic acid was replaced with chelating groups. This led to KDM5-C49 **5** claimed by Epitherapeutics in which the carboxylic acid of PDCA was replaced with an aminomethyl group.[63] C49 **5** showed greater potency against the KDM5 subfamily (IC_{50} <15 nM) as well as greater selectivity of ~50-fold over the other KDM subfamilies (KDM2, KDM3 and KDM6) compared to PDCA (Figure 1.8).[64] C49 **5** was less selective over the KDM4 subfamily with an IC_{50} of 210 nM against KDM4C. The requirement for the polar carboxylic acid group resulted in poor cell permeability so the ester pro-drug KDM5-C70 **6** was developed as it was more cell permeable and would be hydrolysed after entering the cell. C70 **6** inhibited the growth of several breast cancer cells and also increased the expression of *MTIF* and *MT1H* genes which has been observed comparably in KDM5B knockdown experiments.[65]

KDM5-C49 **5** retained the same binding mode as 2-OG with the key bidentate metal chelation of the pyridine nitrogen and aminomethyl nitrogen, salt-bridging interaction of the carboxylate with K517 and hydrogen bonding interaction with Y425 in KDM5B (PDB ID 5A3T).[64] The addition of the peptidic chain resulted in a network of polar interactions with Y488 and R98 as well as hydrophobic

interactions with V99, F496 and W486. Co-crystallisation of C49 **5** in KDM4A (PDB ID 5FPV) revealed the same key interactions as there is high structural similarity in their binding pocket which explains the moderate selectivity over KDM4.

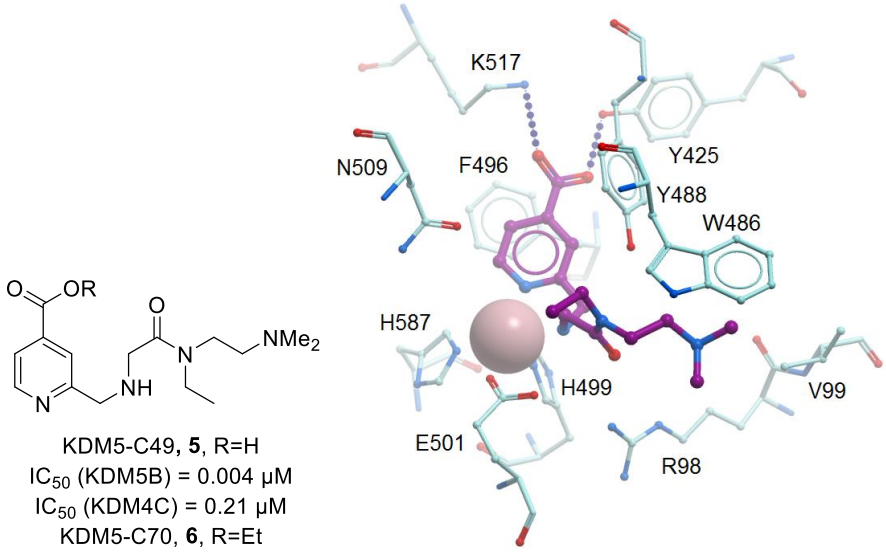
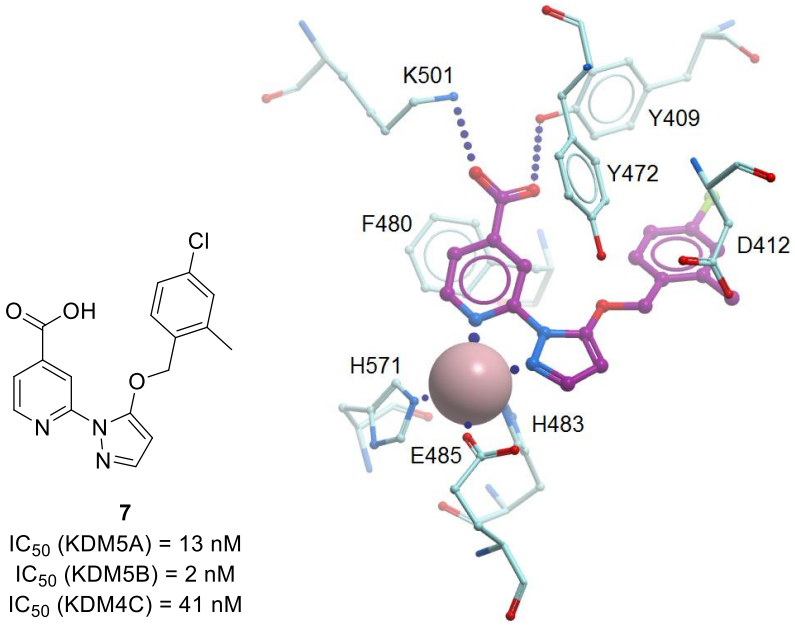


*Figure 1.8. Structure of KDM5-C49 **5** and KDM5-C70 **6**; crystal structure of KDM5-C49 **5** bound to KDM5B (PDB ID 5A3T).*[64]

Further modifications at the 2-position of the isonicotinic inhibitors by Celgene led to pyrazolylpyridine **7** which was a dual KDM4/5 inhibitor with nanomolar IC_{50} and good selectivity over the other KDM subfamilies (Figure 1.9).[66] Some cellular activity was observed in breast cancer cells, ZR-75-1, that were treated with compound **7**, showing an increase in H3K4me3 and an EC_{50} of 90 nM. Similar observations were noted with compound **7** *in vivo*, in a MCF7-breast cancer xenograft PK/PD model.

The planar conformation of the pyridine and pyrazole rings in compound **7** resulted in the same bidentate coordination to the metal when co-crystallised with KDM5A (PDB ID 5IW0).[65] As expected, the carboxylic acid was required for key interactions with the lysine and tyrosine. The addition of the benzyl ether resulted in improved selectivity over the other KDMs through π-stacking interactions with Y409.



7
IC_{50} (KDM5A) = 13 nM
IC_{50} (KDM5B) = 2 nM
IC_{50} (KDM4C) = 41 nM

*Figure 1.9. Structure of compound **7**; crystal structure of compound **7** bound to KDM5A (PDB ID 5IW0).*[65]

Key changes were also made at the 3-position of the pyridine to determine whether bidentate metal chelation was required for potency. This led to 3-amino pyridine carboxylic acids published by GSK such as compound **8** which was a potent KDM4/KDM5 inhibitor with IC_{50}'s <100 nM (Figure 1.10).[67] Compound **8** showed improved selectivity against the other KDM subfamilies with >50-fold selectivity over KDM6B and EGLN3. The presence of the polar carboxylic acid group resulted in poor cell permeability and therefore poor cellular activity for KDM4C (pIC_{50} 5.1) and KDM5C (pIC_{50} 4.2) in osteosarcoma U2OS cells.

The binding mode of the 3-amino pyridine carboxylic acids was determined through a co-crystal of 4-methylthienyl **9** in KDM4D (PDB ID 5FP8). Compound **9** adopted a different metal chelating mode to 2-OG with only monodentate coordination of the pyridine *N* with the metal. However similar salt-bridging/hydrogen bonding interactions as 2-OG were observed between the carboxylic acid and K210 and Y136 while the 4-methylthienyl ring pointed towards Y136, A138 and K245.

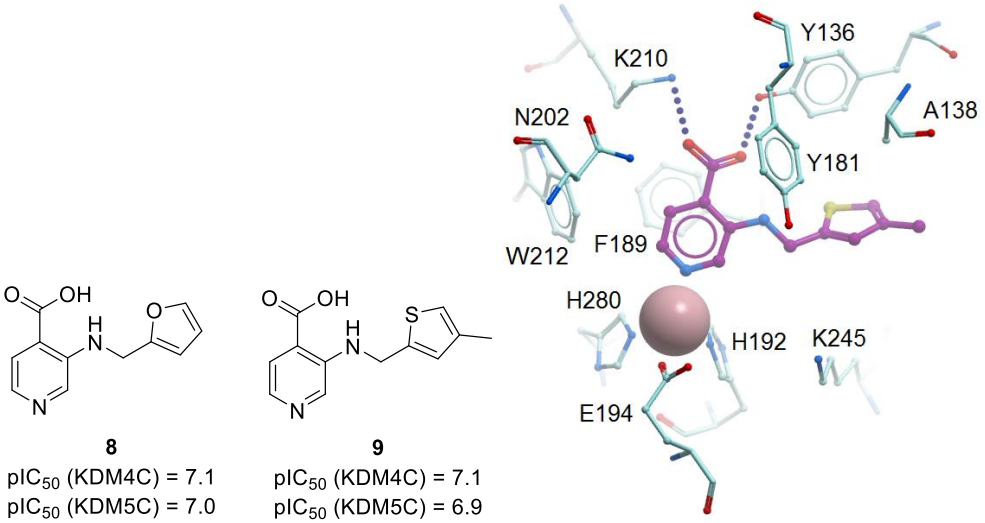


*Figure 1.10. Structures of **8** and **9**; crystal structure of **9** bound to KDM4D (PDB ID 5FP8).*[67]

Similar 3-aminoisonicotinic acid inhibitors were reported by Celgene and Quanticel in which the five-membered heterocycles were replaced with the more lipophilic tetrahydronaphthalene group (Figure 1.11).[68] QC6352 **10** was identified as the most potent in this series in which the (*R*)-enantiomer was active while the (*S*)-enantiomer showed almost no inhibition. QC6352 **10** was more potent against the KDM4 subfamily (IC_{50} (KDM4C) ~ 35 nM) but showed some activity against KDM5B (IC_{50} 750 nM). Excellent selectivity was observed (>1000 fold) over the other KDM families. QC6352 **10** was active against human esophageal squamous cancer KYSE-150 cells (EC_{50} 3.5 nM) and also showed an increase in H3K9me3 and H3K36me3 levels through time-resolved fluorescence and mass spectroscopy detection experiments (H3K36me3 mechanism of action EC_{50} 1.3 nM). As the compound was active against KDM4 and KDM5 biochemically, the cellular activity was likely due to inhibition of both subfamilies. The improved cell potency compared to the other polar pyridine carboxylic acids was likely due to the addition of the lipophilic tetrahydronaphthalene ring with a cLogD of 2.09 which resulted in improved cell permeability (51.2 nm/s (PAMPA)).

The co-crystal of compound **10** in KDM4A (PDB ID 5VGI) revealed that it coordinated to the metal centre through the pyridine *N* as seen with 3-amino isonicotinic acid **9**. The usual binding of the carboxylic acid to Y132 and K206 resulted in the poor selectivity between KDM4 and KDM5. The

additional methyl aniline was projected towards H240 carbonyl and N86 and the phenyl group pointed towards R239 and H240.

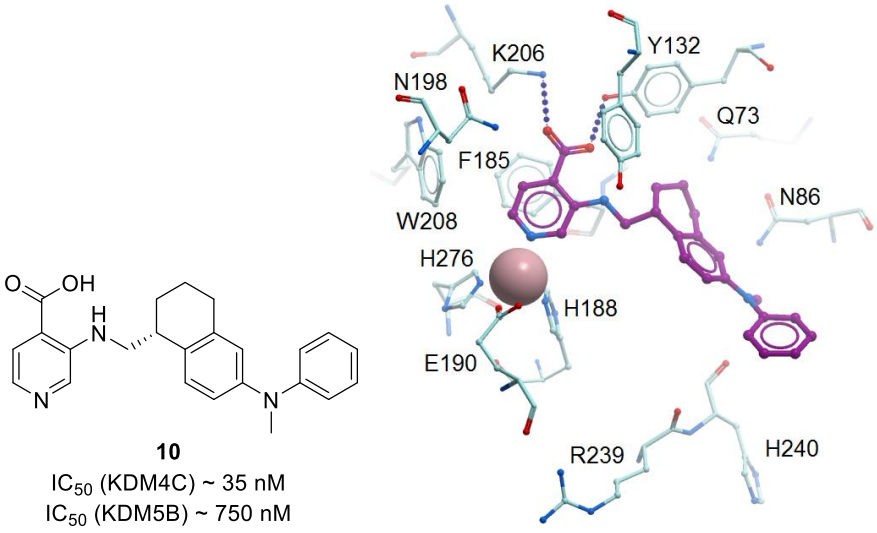


*Figure 1.11. Structure of **10**; crystal structure of **10** bound to KDM4A (PDB ID 5VGI).*[68]

Further changes to the 3-amino isonicotinic acid scaffolds by Celgene Quanticel led to inhibitors in which the aniline-like nitrogen was tied into a pyrrole ring to give chiral enantiomers (*R*)- and (*S*)-2-((2-chlorophenyl)(2-(piperidin-1-yl)ethoxy)methyl)-1*H*-pyrrolo[3,2-*b*]pyridine-7-carboxylic acid **11** (Figure 1.12).[69] Both enantiomers, (*R*)-**11** and (*S*)-**11**, were active against KDM5A with binding affinities of 220 nM and 60 nM with greater than 20-fold selectivity over KDM4A. Low µM cellular potency was not achieved in several breast cancer cells with methyl ester pro-drugs of the racemic compound.

Both enantiomers occupied the 2-OG binding site with monodentate coordination of pyridine *N* and key salt bridging/hydrogen bonding interactions of carboxylic acid with K501, N575 and Y409 in KDM5A ((*R*)-**11** (PDB ID 6BH0) and (*S*)-**11** (PDB ID 6BH1)). There were slight differences in the binding of enantiomers (*R*)-**11** and (*S*)-**11** which were reflected in their potencies. Extensive van der Waals interactions were observed between the chlorine atom in enantiomer (*S*)-**11** and A411, Y409 and Y472. D412 was displaced between the two co-crystal structures which resulted in hydrogen bonding between piperidine *N* in enantiomer (*S*)-**11** and carboxylate of D412 while the piperidine

N in enantiomer (*R*)-**11** hydrogen bonded with Y472. The stronger ionic bonding in compound (*S*)-**11** could explain the slightly greater potency compared to (*R*)-**11**.

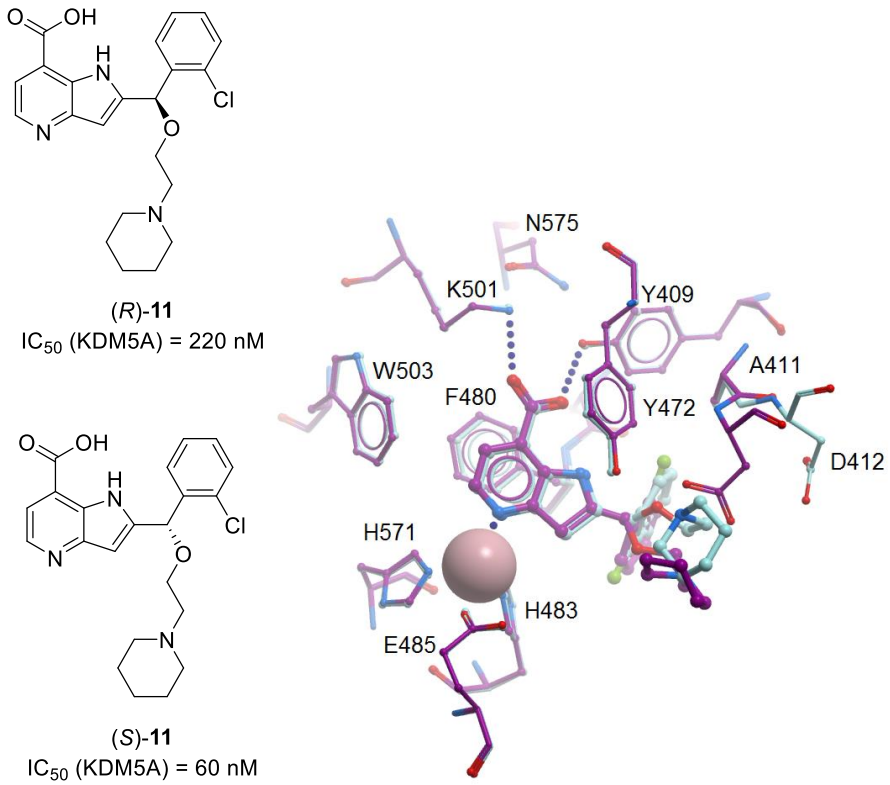


*Figure 1.12. Structure of (R)-**11** and (S)-**11**; crystal structure of (R)-**11** bound to KDM5A (purple – PDB ID 6BH0) and crystal structure of (S)-**11** bound in KDM5A (blue - PDB ID 6BH1).*[69]

The difficulties in achieving cellular activity were partly due to the poor cell permeability of the carboxylic acid so various bioisosteric replacements were attempted. Success was achieved by Tumber *et al*. with carboxamide KDOAM-25 **4**, a structural analogue of KDM5-C49 **5**, which exhibited excellent potency against KDM5B (IC_{50} 19 nM) and was very selective over KDM4C (>1000 fold) unlike the other pyridine carboxylic acids (Figure 1.13).[70] Despite the improved cell permeability to KDM5-C49 **5**, KDOAM-25 **4** showed low cellular activity (~50 µM) in an immunofluorescence assay measuring the increase in H3K4me3 levels in KDM5B-transfected human cervical carcinoma HeLa cells.

The key differences in the co-crystal of KDOAM-25 **4** in KDM5B (PDB ID 5A3N) compared to KDM5-C49 **5** was the displacement of Y425 which became a hydrogen bond acceptor to the carboxamide rather than a hydrogen bond donor. Y425 in KDM5B must be more flexible compared to the

corresponding tyrosine in the KDM4 subfamily which explained the much greater selectivity with the carboxamide.

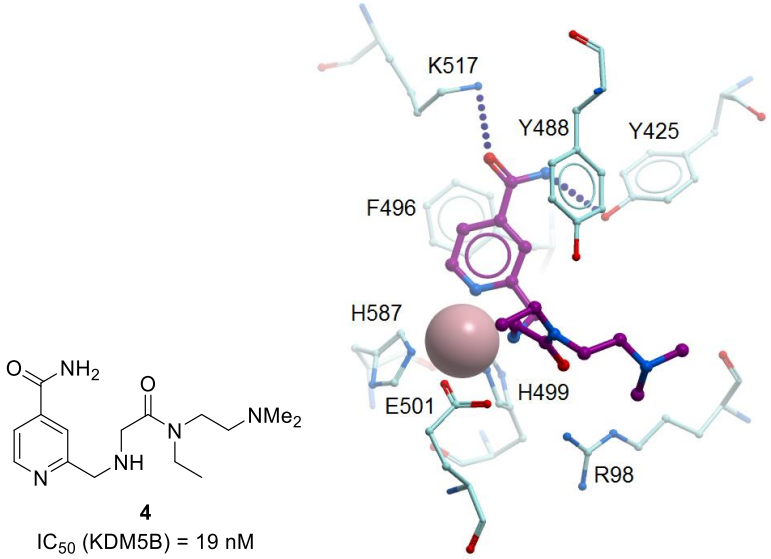


*Figure 1.13. Structure of **4**; crystal structure of **4** bound to KDM5B (PDB ID 5A3N).*[70]

1.3.2. 2-OG Binding Site Inhibitors: Pyridopyrimidinones

To improve the cell permeability while maintaining the key binding interactions, pyrido[3,4-d]pyrimidin-4(3H)-one scaffolds were designed by GSK as bioisosteric analogues of 3-aminoisonicotinic acids (Figure 1.14).[71] Structure activity relationship studies led to a series of pyrazolyloxy analogues in which compound **12** was identified as the most potent against KDM5C (pIC_{50} 7.2). Compound **12** was also active against KDM4C (pIC_{50} 6.3) but showed good selectivity over KDM6B and EGLN3. As previously observed, there was a drop in activity against KDM4C in human osteosarcoma U2OS cells (pIC_{50} 5.3) which was likely explained by competition with a high cellular concentration of physiological 2-OG (~1 mM).[72]

A co-crystal of compound **12** in KDM5B (PDB ID 5FUN)[64] revealed the same binding interactions of the 3-aminoisonicotinic acid series in which the pyridine nitrogen binds to the metal and the amide of the pyridopyrimidinone serves as a weakly acidic isostere (pKa ~ 7.5) and forms a salt bridge with

K517 and a hydrogen bond with N591. The flexibility of Y425 in KDM5B, as discussed with compound **4**, was confirmed with this series as two conformations were observed; one conformation in which Y425 hydrogen bonded to the amide nitrogen and the other conformation where it was displaced to allow space for the phenyl group.

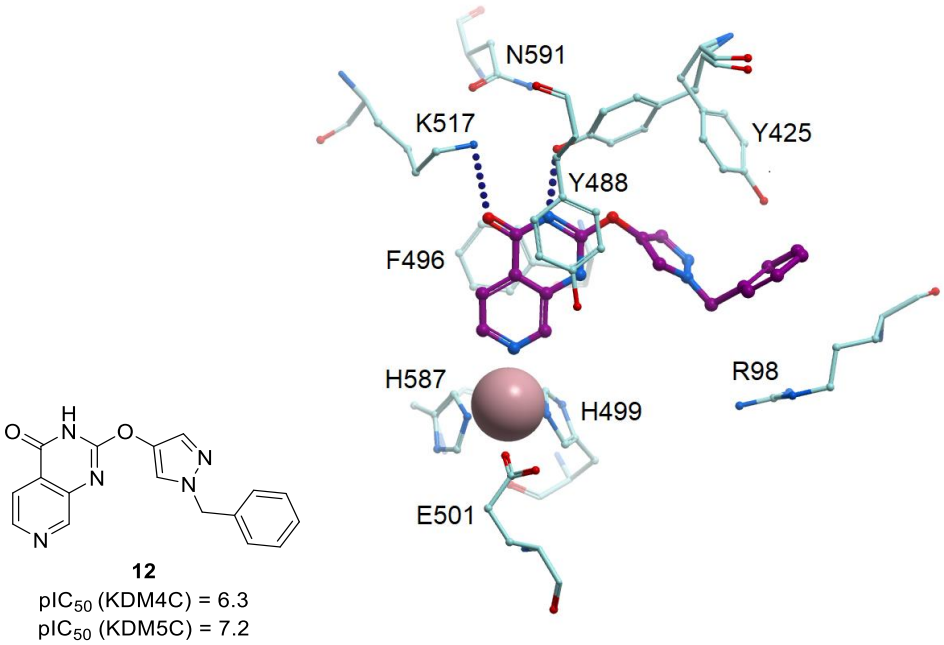


*Figure 1.14. Structure of compound **12**; crystal structure of compound **12** bound to KDM5B (PDB ID 5FUN).*[64]

A series of 8-substituted pyridopyrimidinones were published by the Institute of Cancer Research (ICR) and Structural Genomics Consortium (SGC) as a way of introducing a second metal-chelating nitrogen for improved potency.[73] Dichlorophenyl piperidine **13** and monochlorophenyl piperidine **14** were potent inhibitors with equipotent activity against KDM4 and KDM5 subfamilies (IC_{50} < 50 nM) (Figure 1.15). The 8-pyridopyrimidinone core was less acidic (pKa 8.23) than compound **12** which resulted in a moderate cell permeability for **13** (6.34 x 10^{-6} cm/s (Caco-2)). Some cellular inhibition in an immunofluorescence assay was observed in which levels of H3K9me3 and H3K4Me3 increased upon incubation with increasing compound concentrations, however the cellular IC_{50} (> 50 µM) in transfected human cervical carcinoma HeLa cells dropped off from the *in vitro* value.

Co-crystallisation of compound **13** in KDM4A (PDB ID 5F3I) revealed that the compound bound in the 2-OG binding site and both the pyridine *N* and pyrazole *N*2 coordinated to the metal. The CONH-

group hydrogen bonded to K206 and Y132 and the addition of the phenylpiperidine moiety resulted in new interactions with D135 and Y175 in the histone peptide binding pocket. The piperidine ring was required to rigidify the pyrazole substituents for better selectivity over the other KDM subfamilies (KDM2, KDM3 and KDM6).

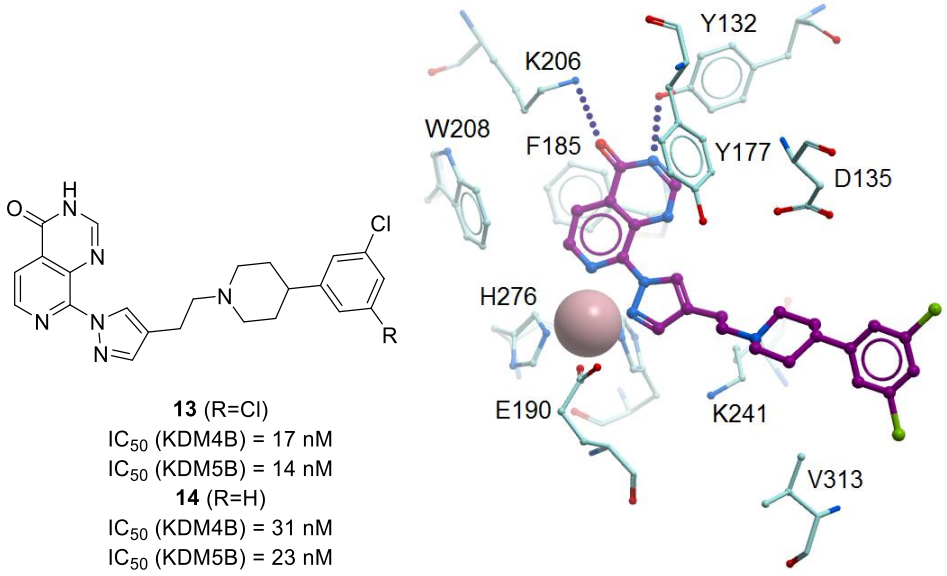


*Figure 1.15. Structure of compounds **13** and **14**; crystal structure of compound **13** bound to KDM4A (PDB ID 5F3I).*[73]

Overlaying 3-aminoisonicotinic acid **10** and 2-pyridopyrimidinone **12** in KDM5B showed that the two scaffolds were positioned in the same plane with good overlap between the pyridine nitrogen, carboxylic acid/amide and the 3-amino nitrogen (Figure 1.16). The hydrogen bonding interaction between the amide and Y425 is not as strong as with the carboxylic acid so Y425 could be displaced out of the binding pocket with 2-pyridopyrimidinone **12**.

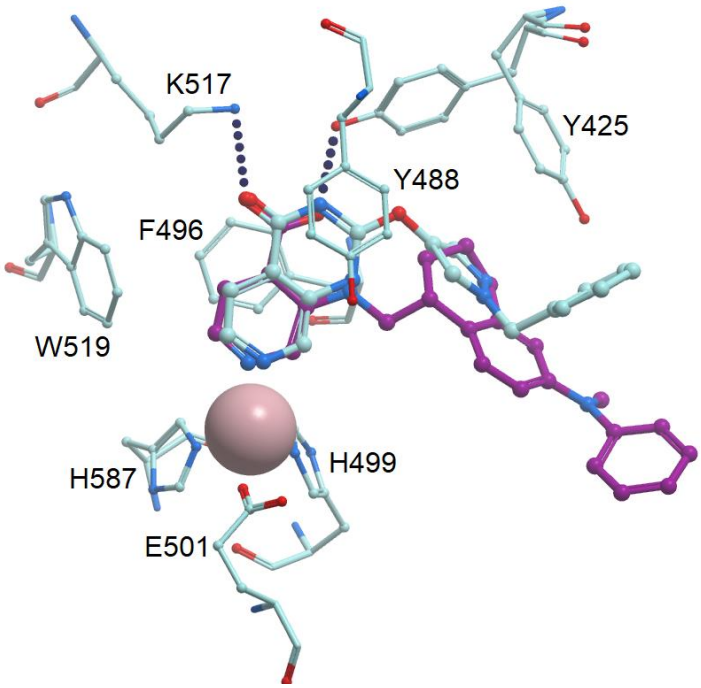


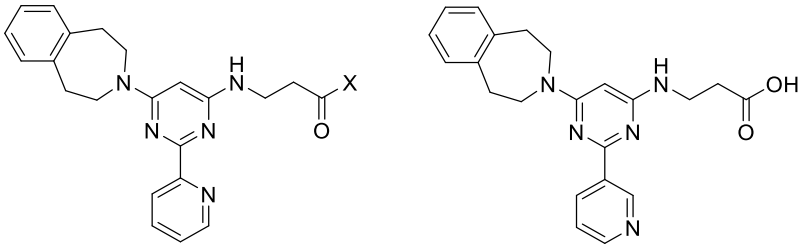
Figure 1.16. Superimposition of QC6352 ***10*** *(Purple) in co-crystal of 2-pyridopyrimidinone* ***12*** *(Blue) in KDM5B (PDB IB 5FUN).*

1.3.3. 2-OG Binding Site Inhibitors: Pyridyl Pyrimidine Carboxylic Acids

Although it was originally reported by GSK as a KDM6B selective inhibitor, GSK-J1 **15** was later discovered to show activity on KDM5 so represented another class of inhibitors (Figure 1.17).[42,74] GSK-J1 **15** was potent against KDM6B (IC_{50} 60 nM) however the highly polar carboxylic acid limited its cellular activity. A previously discussed pro-drug strategy was utilised in which the ester analogue GSK-J4 **16** was cell permeable and was hydrolysed to the active GSK-J1 **15** in the cell. In FLAG-KDM6B-transfected HeLa cells, GSK-J4 **16** inhibited the loss of H3K27me3 by KDM6B. An increase in H3K27me3 was also observed in untransfected cells. GSK-J1 showed good selectivity over KDM4 and other closely related proteins in enzymatic assays however it was only five to ten-fold selective over KDM5B and KDM5C. Incubation of GSK-J4 **16** in cells transfected with KDM6B, KDM4C and KDM5B resulted in similar IC_{50}'s (3-7 μM) for demethylation of the specific substrate so it was likely that inhibition was a combination of activity towards H3K4me2/me3 and H3K27me2/me3.

However, GSK-J1 **15** is the most selective KDM6 inhibitor reported to date and due to its activity against KDM5 could be utilised for the design of KDM5 selective inhibitors.

The binding mode of GSK-J1 **15** in KDM5B was determined through co-crystallisation (PDB ID 5FPU) which revealed a bidentate coordination of the pyridine and pyrimidine nitrogen and the usual salt bridge of the carboxylic acid with K517.[64] GSK-J2 **17**, the pyridine regioisomer, was a suitable inactive control as it showed weaker inhibition (IC_{50} >20 µM (KDM5A)) due to its lack of bidentate coordination. There was no second hydrogen bonding interaction, observed with the other carboxylic acid inhibitors, as Y425 was displaced away from the pocket by the tetrahydrobenzazepine ring. There was also no π-π stacking interaction as the pyrimidine ring was not positioned between F496 and Y488 unlike with pyridine carboxylic acids such as **10** (Figure 1.11)



GSK-J1 **15** (X=OH)
IC_{50} (KDM6B) = 60 nM
GSK-J4 **16** (X=OEt)

GSK-J2 **17**

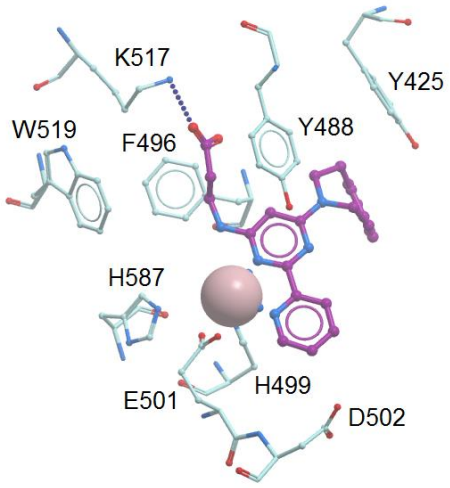


*Figure 1.17. Structures of GSK-J1 **15**, J2 **17** and J4 **16** (above) and co-crystal of GSK-J1 **15** in KDM5B (PDB ID 5FPU).*[64]

1.3.4. 2-OG Binding Site Inhibitors: Cyanopyrazoles

A new chemotype was published by Genentech and Constellation in which there was no iron-coordinating pyridine.[75] Cyanopyrazole, CPI-455 **18**, was potent against the KDM5 subfamily (IC_{50} 10 nM (KDM5A)) and showed 200-fold selectivity over KDM4C, 700-fold selectivity over KDM7B and no activity against KDM2B, KDM3B or KDM6A. Incubation of CPI-455 **18** in human lung adenocarcinoma PC9 cells showed a global increase in levels of H3K4me3 resulting in an EC_{50} of 5.2 μM (Figure 1.18).

CPI-455 **18** was co-crystallised in KDM5A (PDB ID 5CEH) which revealed that the nitrile was the metal-chelating group and the carbonyl oxygen hydrogen bonded to N575. The core of CPI-455 **18** was involved in a π-π stacking interaction with Y472 and F480 and an edge:face interaction with W503. A loss of activity was demonstrated upon alkylation of the 4-nitrogen which confirmed the requirements of an acidic nitrogen for KDM5 inhibition. At physiological pH (7.4), a significant proportion of CPI-455 is in the ionised form as the measured pKa is 6.0. The delocalised negative charge on either *N*1 or carbonyl oxygen was likely interacting with the positively charged K501. Edge-face interactions were observed with the 5-phenyl substituent and Y409 but it was otherwise solvent-exposed. The isopropyl group was positioned in a tight binding pocket comprised of Y409 and S478 in which larger groups were not tolerated.

The isopropyl and phenyl substituents were responsible for the selectivity over KDM6B due to steric collisions with K1381, F1328 and T1387. CPI-455 **18** binds in KDM5A due to flexibility of Y409 which allows space for the isopropyl group to occupy while F1328 in KDM6B projects into the pocket. The selectivity over the KDM4 subfamily was explained through differences in the second sphere of amino acids such as replacements of KDM5A A583 with KDM4C S290 and KDM5A R73 with KDM4C I73 which could result in displacement of Y409 in the primary sphere of binding residues. As with the other 2-OG binding site inhibitors, CPI-455 **18** was 2-OG competitive which could have

contributed to the drop in IC_{50} from enzymatic to cellular assay. CPI-455 **18** also showed no selectivity across the KDM5 subfamily due to limited sequence or structural differences between the isoforms.

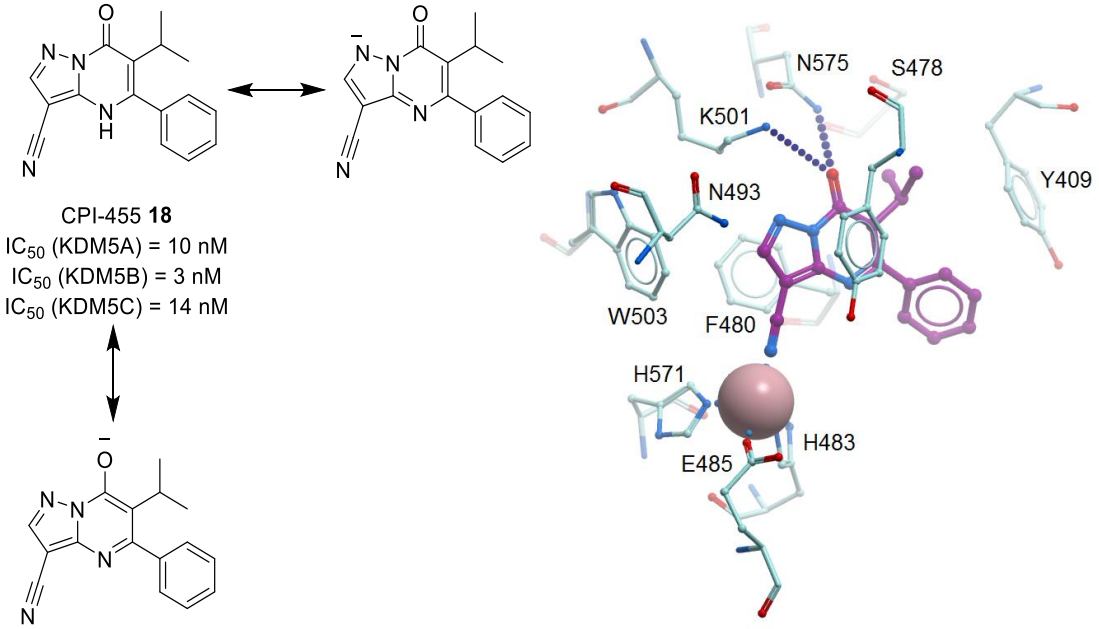
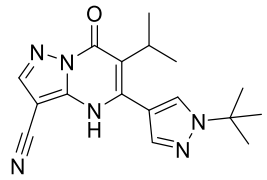


*Figure 1.18: Structure of CPI-455 **18**; crystal structure of CPI-455 **18** bound to KDM5A (PDB ID 5CEH).*[75]

Replacement of the phenyl group with a pyrazole led to the more potent and selective inhibitor **3** (Figure 1.19).[76] Compound **3** showed greater cell potency (PC9 H3K4Me3 EC_{50} = 0.34 µM) compared to CPI-455 **18** by balancing human plasma protein binding (hPPB) of 98.8% and cell permeability of 7.5 x 10^{-6} cm s^{-1} (MDCK P_{app} AB) compared to >99.9% and 17.2 respectively with CPI-455. Compound **3** was tested in various selectivity screens in which it exhibited good selectivity against the other KDM families (KDM1A, 2B, 3B, 4C, 6A, 7B) as well as against 300 kinases (<50% at 10 µM). Due to the good cell activity and pharmacokinetic profile, the compound was a suitable candidate for *in vivo* studies.



3
IC_{50} (KDM5A) = 15.1 nM
IC_{50} (KDM5B) = 4.7 nM
IC_{50} (KDM5C) = 65.5 nM

*Figure 1.19. Structure of pyrazolo[1,5-a]pyrimidin-7(4H)-one **3**.*[76]

Overlay of CPI-455 **18** and KDOAM25 **4** in KDM5A showed that the planes of the cyanopyrazole and the pyridine carboxamide were not aligned (Figure 1.20). The cyanopyrazole core was shifted by the coordination of the nitrile resulting in interactions with N575 as well as greater π-π stacking between Y472 and F480. The pyrazole *N* of compound **18** overlapped with pyrimidinone O of compound **4**. Y409 was displaced out of the binding pocket when CPI-455 **18** was bound which allowed space for the iso-propyl group while Y409 was involved in a key interaction with KDOAM-25 **4**. Overall, the cyanopyrazoles represented a different binding mode to the pyridopyrimidinones and pyridine carboxylates which resulted in improved activities and selectivities.

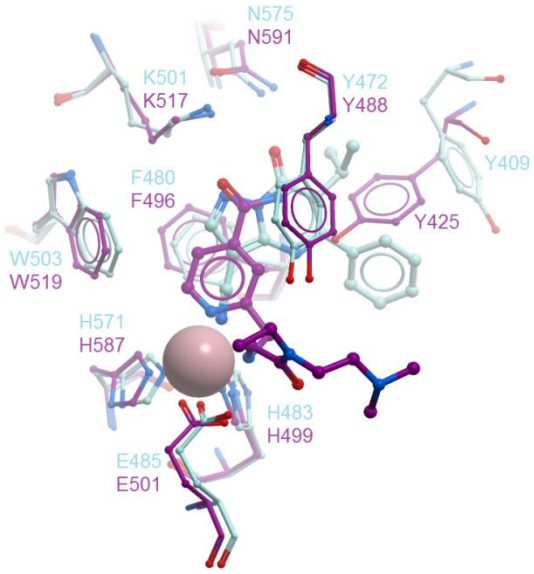
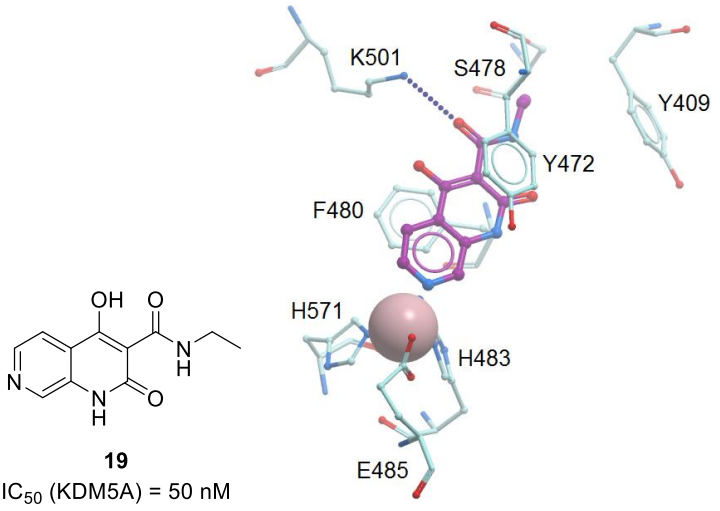


*Figure 1.20. Overlay of KDOAM-25 **4** (Purple) bound to KDM5B (Purple – PDB ID 5A3N) and CPI-455 **18** (Light Blue) bound to KDM5A (Light Blue – PDB IB 5CEH).*

1.3.5. 2-OG Binding Site Inhibitors: 1,7-Naphthyridone

A series of 1,7-naphthyridone compounds such as **19**, hybrids of the pyridopyrimidinone and cyanopyrazole cores, were reported by Genentech as potent KDM5 inhibitors that were selective over KDM4C and KDM2B (Figure 1.21).[77] To extend the compounds into the region occupied by the isopropyl group of the cyanopyrazoles, substitutions were attempted at C-3. Improved potencies were observed with electron withdrawing groups such as carboxamides at C-3 through interactions with K501 and N575. As observed with the isopropyl group of CPI-455, only small alkyl groups were tolerated on the carboxamide due to the tight binding pocket formed by S478 and Y409. These investigations led to compound **19** which was potent against KDM5A (IC_{50} 50 nM) and demonstrated excellent cell permeability in MDCK cells (15.8 x 10^{-6} cm/s) but did not show an increase in H3K4me3 levels up to 30 μM in human lung adenocarcinoma PC9 cells.

Compound **19** was determined to bind in the 2-OG binding site through co-crystallisation of compound **19** with KDM5A (PDB ID 5K4L). As previously observed with pyridopyrimidinones, the pyridine binds to the metal centre through a monodentate coordination and Y472 and F480 engage in π-π stacking interactions with the aromatic core. The carboxamide oxygen hydrogen bonds with K501 while the *N*-ethyl interacts with S478 and Y409 through Van-der-Waals interactions. Alkylation of *N*1 nitrogen was not tolerated as the hydrophobic group was exposed to the solvent front. Y472 is replaced with a leucine in KDM2B so the aromatic stacking interactions were lost resulting in the reduced activity for KDM2B. The selectivity over KDM4 was likely due to the greater ease of displacement of Y409 in KDM5A compared to the corresponding tyrosine in KDM4 to allow space for the ethyl carboxamide.



19

IC_{50} (KDM5A) = 50 nM

*Figure 1.21. Structure of compound **19**; crystal structure of compound **19** bound to KDM5A (PDB ID 5K4L).*[77]

1.3.6. 2-OG Binding Site Inhibitors: Pyrrolidine

Novel KDM5 inhibitors were discovered by Genentech and Constellation through a high-throughput screen which led to pyrazole **20** as a potent inhibitor (IC_{50} 45 nM) with good selectivity over KDM1, 2, 3, 6 and 7 and moderate selectivity (91-fold) over KDM4C (Figure 1.22).[78] Good cellular activity of 960 nM was achieved in a cell-based assay measuring H3K4me3 levels in human lung adenocarcinoma PC9 cells and the pharmacokinetic profile was suitable for further profiling *in vivo*.

The binding mode of compound **20** was determined through co-crystallisation in KDM5A (PDB ID 5V9T) which confirmed that the compound was a metal chelator binding through pyrazole *N*1 and carbonyl oxygen. The pyrazole also engaged in novel hydrogen bonding interactions between *N*2 of pyrazole and E485 while the cyclopropyl carbonyl oxygen retained the key interaction with K501. Compound **20** did not contain a weakly acidic proton, unlike the other scaffolds, so an ionic interaction with K501 was not required for potency. The lack of an acidic proton resulted in improved cell permeability with this series. Compound **20** was positioned primarily in the 2-OG binding site however the isopropyl group occupied part of the histone peptide binding pocket. ^{19}F NMR confirmed that compound **20** was competitive with the histone peptide substrate and therefore this series could be promising for future inhibitor design due to its novel KDM5A inhibition.

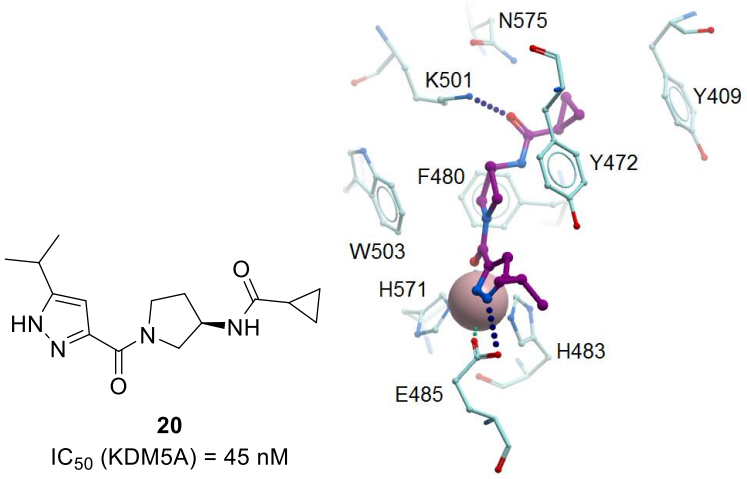
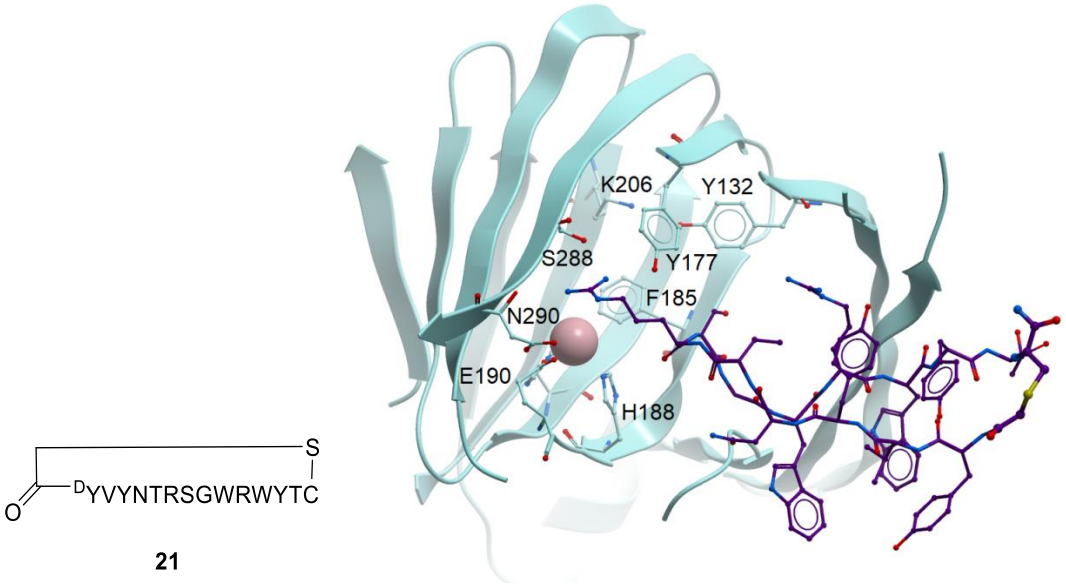


*Figure 1.22. Structure of compound **20**; crystal structure of compound **20** bound to KDM5A (PDB ID 5V9T).*[78]

1.3.7. Substrate Competitive KDM5 Inhibitors

There has been no purely histone substrate competitive KDM5 inhibitors reported to date, however cyclic peptides were published by Kawamura *et al*. as substrate competitive inhibitors of KDM4A-C.[79] The inhibitors were identified through mRNA-display based cyclic peptide library screening which led to cyclic peptide CP2 **21** (IC_{50} 42 nM and K_d 30 nM against KDM4A) (Figure 1.23). CP2 **21** had nanomolar activity against KDM4B and KDM4C and showed >160-fold selectivity over other JmjC-KDMs including KDM2A, KDM3A, KDM5C and KDM6B as well as selectivity within the same subfamily (KDM4D-E). Transfected U2OS cells dosed with cyclic peptide inhibitors showed KDM4A stabilisation (EC_{50} ~ 1 µM) using cellular thermal shift assay (CETSA) however further work is needed to determine the biological effect of these inhibitors against KDM4A in the cell. A co-crystal of CP2 **21** bound in KDM4A was obtained (PDB ID 5LY1) which revealed that CP2 binds in the substrate binding pocket in a different conformation to the histone substrates. CP2 **21** formed a β-sheet with two turns and the Arg pointed towards Fe(II) where the lysine of H3K9me3/H3K36me3 peptides bind. Hydrogen bonding interactions were observed between the positively charged guanidino group of CP2 and Y177, S288 and H290 of KDM4A. Despite the unknown cellular distribution and stability of these cyclic peptides, these potent and selective substrate competitive inhibitors represent a novel approach that could be applied to the development of KDM5 selective inhibitors.



21

Figure 1.23. Structure of cyclic peptide CP2 ***21*** *and co-crystal structure of KDM4A with CP2* ***21*** *(PDB ID 5LY1).*[79]

1.3.8. Conclusion of KDM5 Inhibitors

Although potent and selective inhibitors of KDM5 have been reported such as compound **3** and KDOAM-25 **4**, translation of potency into the cellular assays has generally been poor. This has been explained through a combination of poor cell permeability of the acidic inhibitors and greater competition with the cosubstrate 2-OG in the cellular environment. Selectivity within the KDM5 subfamily has also been difficult to achieve due to identical primary binding residues. It was postulated that a covalent inhibitor could address these issues through specific binding to a non-conserved residue close to the binding site. This could lead to a cell potent and very selective inhibitor as a chemical biology tool to gain a greater understanding of the biological function of the KDM5 family.

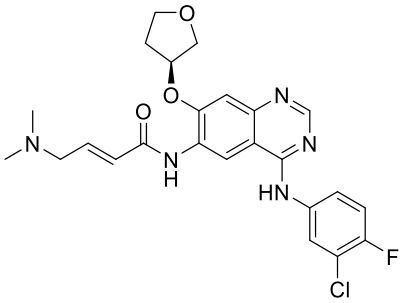
1.4. Covalent Inhibitors

1.4.1. Background to Covalent Inhibitors

Covalent drugs have made a significant impact on human health with several being approved as treatments for a diverse range of therapeutic indications.[80] Clopidogrel, lansoprazole and esomeprazole, covalent inhibitors of their targets, were three of the ten top-selling drugs in the United States in 2009. Many covalent drugs, such as aspirin initially marketed over 100 years ago, were not designed as covalent inhibitors but were determined later through understanding of their mechanism of action.[81] In the 1970s and 1980s, the design of covalent inhibitors was avoided due to concerns over organ toxicity with reactive compounds or compounds that formed reactive metabolites.[82] However, opinion has shifted with the development of 'targeted covalent inhibitors' such as Afatinib **22** (Figure 1.24), a dual irreversible kinase inhibitor of the epidermal growth factor receptor (EGFR) and ErbB-2 (HER2), which was approved as a treatment for non-small cell lung carcinoma.[83,84] Afatinib **22** is active against EGFR mutations such as T790M which are not targeted by first generation tyrosine-kinase inhibitors, erlotinib or gefitinib, therefore it represents a novel mechanism of action.[85,86] Targeted covalent inhibitors optimise the non-covalent interactions of the compound with the desired protein target to ensure selectivity over other cellular proteins prior to the covalent bond formation between the low chemically reactive electrophile and a proximal residue in the active site.

Covalent inhibitors possess several advantages over conventional inhibitors. Covalent inhibitors highly favour the bound form which leads to greater potencies and ligand efficiencies compared to non-covalent inhibitors. Competition with endogenous substrates that lower potencies *in vitro* or *in vivo* can also be reduced using covalent inhibitors. Irreversible binding can result in a longer duration of action and therefore less frequent dosing if the turnover time of the protein is slower than the drug half-life. Pharmacodynamics is no longer tightly coupled to pharmacokinetics as it

relies on protein resynthesis so target inhibition persists even when the drug has been cleared.[87] Covalent inhibitors with high clearance are preferred to minimise off-target interactions. Irreversible inhibitors, such as Afatinib **22**, can also be active in drug-resistant mutations that have been acquired from treatment with reversible inhibitors.[88] These mutations only affect the rate at which the inhibited complex forms so although the mutants react more slowly, complete inhibition will be achieved.



22

*Figure 1.24. Structure of covalent inhibitor, Afatinib **22**, a dual inhibitor of the EGFR and HER2 kinases.*

Greater selectivity between protein families can also be achieved using covalent inhibitors. There are two steps to covalent inhibition; the initial non-covalent binding to the desired protein and the covalent reaction with the specific residue of the protein. For high selectivity, the formation of the non-covalent complex must be sustained for sufficient time to allow the covalent reaction to occur. For optimal covalent bond formation, the electrophile must be positioned in proximity to the desired nucleophilic residue which can be optimised through structure-based drug design and molecular modelling. Selectivity can be difficult to achieve through non-covalent interactions with closely-related protein families that have structurally similar binding sites, however specific covalent binding to a non-conserved residue can lead to greater selectivity. Despite this, there remains concerns over non-selective reactivity of covalent inhibitors with other cellular proteins, so it is important to fine-tune the reactivity of the electrophilic warhead.

1.4.2. Cysteine-selective Covalent Inhibitors

Several potentially nucleophilic amino acids exist such as serine, cysteine, lysine, tyrosine, threonine, aspartate and glutamate. An electrophilic warhead must be carefully chosen to ensure specific reactivity with a desired residue in the binding pocket. The reactivity between nucleophile and electrophile is largely governed by their relative hardness/softness. As cysteines are found in numerous different proteins such as proteases, oxidoreductases and kinases, they are a desirable target residue for the design of covalent inhibitors. Covalent kinase inhibitors commonly target a poorly conserved non-catalytic cysteine residue positioned close to the ATP binding pocket.[89]

Various electrophiles have been identified as selective for cysteine residues (Figure 1.25).[90] Irreversible binding is widely achieved via Michael addition reactions of the cysteine with electrophilic warheads such as acrylamides **23**, dimethylamino crotonamide **24**, propiolic ketones **25** and vinyl sulfonates **26**. Nucleophilic additions and displacements to α-halo ketones **27**, nitriles **28**, alkynes **29**, thiocyanates **30**, epoxides **31** and sulfonyl fluorides **32** have also been explored. Nucleophilic aromatic substitution reactions have been observed with cysteine-reactive halonitrobenzene derivatives of PPARγ inhibitor GW9662 **34** in which covalent modification was observed on β-tubulin.[91] Nitro compounds are commonly avoided in drug development due to toxicity issues including carcinogenicity, mutagenicity, hepatotoxicity and bone-marrow suppression.[92] Despite this, halonitrobenzene electrophiles **33** could be utilised in activity-based protein profiling applications.

The choice of electrophilic warhead is critical for fast kinetics of covalent binding to the desired target protein but slow off-target reactivity leading to toxicological problems. Different electrophiles should therefore be incorporated into the covalent inhibitor to fine-tune the covalent reactivity with the protein of interest.

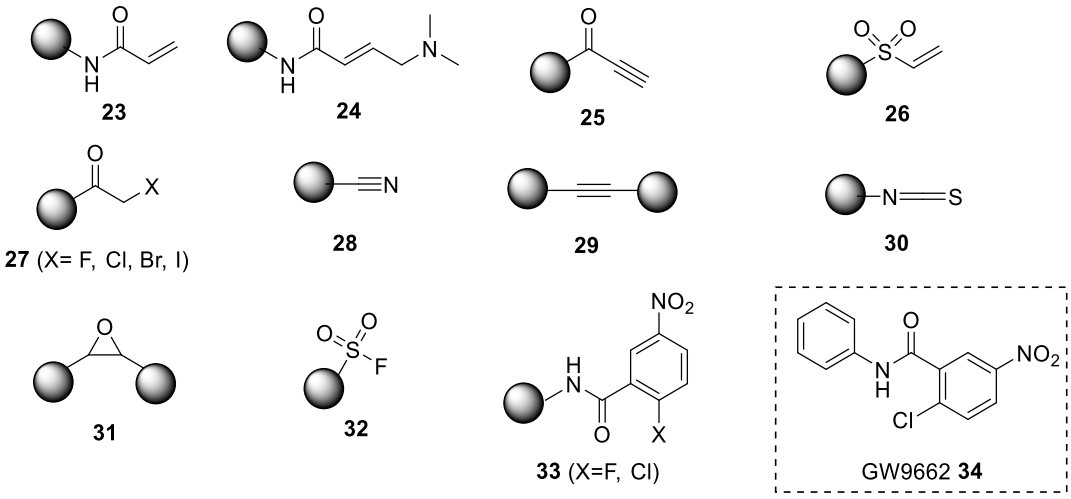


Figure 1.25. Cysteine-reactive electrophiles for covalent protein modification.

1.4.3. Profiling Covalent Inhibitors

Covalent inhibitors bind to the protein through a two-step reaction; first non-covalent binding to the active site of the target protein defined by the equilibrium constant K_i, followed by covalent bond formation between a nearby residue and the electrophile dependent on the rate constant k_2 (Figure 1.26). If they are given sufficient time to react, fully irreversible inhibitors will completely block the target protein from dissociation which results in a negligible value of k_{-2} and their time-dependent inhibition is governed by K_i and k_2 (referred to as k_{inact}).

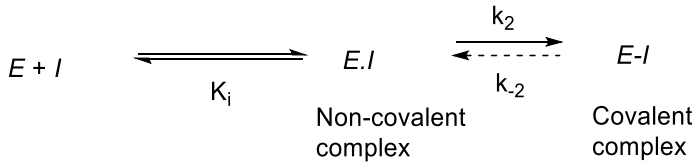


Figure 1.26. Mechanism of target specific covalent inhibition where E is the enzyme and I is the inhibitor.

Due to kinetic considerations, covalent inhibitors must be profiled differently to reversible inhibitors in which IC_{50}'s are used as a measure of activity. If irreversible inhibitors are given sufficient time to fully react, all concentrations of the inhibitor (higher than the protein concentration) will result in complete inhibition so IC_{50}'s cannot be used as a measure of potency.

The parameters, K_i and k_{inact}, determined through time-dependent inhibition are a better way to assess covalent reactivity and therefore rank covalent inhibitors. The potency and selectivity of covalent inhibitors can be modulated either through optimising the non-covalent interactions to the target (K_i) or the rate at which the nucleophilic residue reacts once bound (k_{inact}).

1.4.4. Determination of K_i and k_{inact}

To rank covalent inhibitors based on their potency, IC_{50}'s can be measured at different pre-incubation times using known methods[93] to determine the parameters, k_{inact} and K_i, from the following equations 1 and 2. For mechanism-based inhibition, equations 1 and 2 assume that the amount of substrate and inhibitor do not change significantly during the performance of the assay (as $S >> E_{tot}$) while the amount of catalytically active enzyme does change. Time-dependent IC_{50} values (recorded in µM), $IC_{50}(t)$, are known IC_{50} values at different time points t (recorded in minutes). S and K_M are fixed values where S is substrate concentration and K_M is the Michaelis-Menten constant. The values of a k_{inact} (units of min^{-1}) and K_i (units of µM) are determined through a least-squares fit by fitting the right-hand side to the measured IC_{50} values. The input parameter $\eta_{IC_{50}}$ is also determined based on the measured time-dependent IC_{50}'s. The most potent compounds will have low K_i values, indicating potent non-covalent interactions, and high k_{inact} values, indicating fast covalent binding kinetics. Consequently, covalent inhibitors with the highest k_{inact}/K_i values are the most potent.

$$IC_{50}(t) = K_i\left(1 + \frac{S}{K_M}\right) . \left(\frac{2 - 2e^{-\eta_{IC_{50}} \cdot k_{inact} \cdot t}}{\eta_{IC_{50}} . k_{inact} . t} - 1\right) \quad (1)$$

$$\eta_{IC_{50}} = \frac{IC_{50}(t)}{K_i\left(1 + \frac{S}{K_M}\right) + IC_{50}(t)} \quad (2)$$

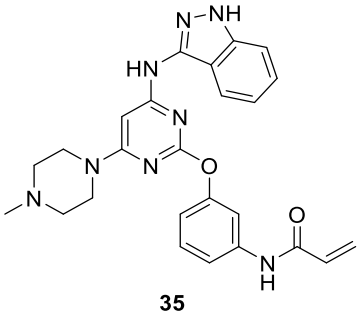
Equation 3, obtained by solving equation 1 for K_i, is analogous to the Cheng-Prusoff equation for competitive inhibition but corrected by a factor C (equation 4) which depends on k_{inact}, time

and $\eta_{IC_{50}}$. For competitive inhibition, k_{inact} is negligible and therefore C=1 which yields the classical Cheng-Prusoff equation.

$$K_i = \left(\frac{K_M}{K_M + S}\right).IC_{50}(t).C\left(k_{inact}, t, \eta_{IC_{50}}\right) \quad (3)$$

$$C\left(k_{inact}, t, \eta_{IC_{50}}\right) = \left(\frac{2 - 2e^{-\eta_{IC_{50}} . k_{inact} . t}}{\eta_{IC_{50}} . k_{inact} . t} - 1\right)^{-1} \quad (4)$$

This method has been used for profiling covalent kinase inhibitors. A paper by *Engel* et al. reported the rational design of novel and irreversible inhibitors of EGFR through selective modification of C797.[94] Optimisation led to compound **35** (Figure 1.27) which was potent against EGFR L858R/T790M and selective over EGFR L858R as well as non-mutated EGFR. K_i and k_{inact}, with respect to mutant variants L858R and T790M/L858R were calculated through measuring IC_{50}'s at different time points using a fluorometric assay and fitting to equation 1 and 2. The value of k_{inact}/K_i for compound **35** toward EFGR L858R/T790M and EGFR L858R mutants was approximately 7 x 10^6 M^{-1} s^{-1} and 4 x 10^3 M^{-1} s^{-1} respectively. Compound **35** exhibited high binding affinity towards EFGR L858R/T790M with a K_i of 0.32 nM while the covalent reactivity was moderate (k_{inact} 2.3 x 10^{-3} s^{-1}). The values of k_{inact} and K_i of compound **35** were comparable to other covalent EGFR inhibitors.[95] As this method has shown promise with covalent kinase inhibitors, it was hoped that it could be applied to the profiling of KDM5 inhibitors.



35

*Figure 1.27. Structure of covalent EGFR inhibitor **35**.*

1.4.5. AlphaScreen Assay for Determination of Time Dependent IC_{50}'s

AlphaScreen (Amplified Luminescent Proximity Homogenous Assay) is an assay that is used for the screening of a broad range of targets.[96] It utilises "Donor" and "Acceptor" beads that are coated with a hydrogel of functional groups for bioconjugation. If the beads are in proximity through a biological interaction between molecules, a series of chemical reactions is initiated resulting in an amplified signal. The Donor bead contains a photosensitiser which is excited by a laser at a long wavelength (680 nm). This results in ambient triplet oxygen being converted to a more excited singlet state which diffuses to react with a chemiluminescer in the Acceptor bead. Fluorophores in the Acceptor bead are activated to emit light at a shorter wavelength (520-620 nm). An inhibitor will disrupt the biological interaction between Donor and Acceptor so the singlet oxygen is undetected by the Acceptor bead leading to a lower fluorescence signal.

AlphaScreen has been applied to the screening of KDM inhibitors using Donor beads coated with streptavidin which binds to a biotinylated histone peptide substrate (Figure 1.28).[97,98] Rubrene-based Acceptor bead is coated with protein A for binding to an antibody that recognises the demethylated lysine product. If the substrate is demethylated by the KDM enzyme, laser excitation will result in emission of luminescent signal typically at 570 nm. The main advantage of this technique is the very low background fluorescence as the wavelength of emission is lower than excitation.

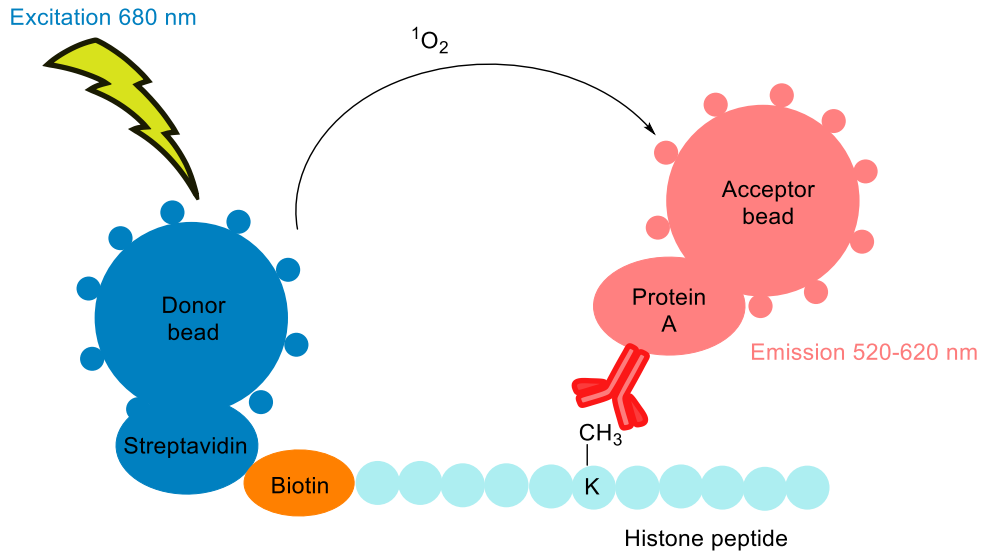


Figure 1.28. Schematic showing the principle of AlphaScreen, a bead-based assay, used to detect demethylation of histone peptide substrate.

1.5. Project Aims

The aim of this project was to develop selective covalent inhibitors of KDM5B to improve cell potency and selectivity over KDM5A, C and D as well as other KDM subfamilies. By incorporating an electrophilic warhead to a 2-OG competitive small molecule inhibitor, it was hypothesised that the irreversibility of the covalent bond formation would result in less competition with the 2-OG cosubstrate. This novel approach could solve the current problems of achieving cellular potency. By targeting a non-conserved cysteine, it would also be possible to improve the selectivity over the other KDM families.

As previously discussed, 8-substituted pyrido[3,4-*d*]pyrimidin-4(3*H*)-one **14** was published as equipotent (IC_{50} < 35 nM) inhibitors of the KDM4 and KDM5 subfamilies in biochemical assays and showed good selectivity over other subfamilies such as KDM2, 3 and 6. This series were highly 2-OG competitive which resulted in poor cellular activity. Selectivity over the KDM4 subfamily has been difficult to achieve with 8-pyridopyrimidinone inhibitors due to similarities in their primary binding residues. This scaffold would therefore be a good starting point for the development of a potent and selective covalent inhibitor of KDM5B that is less competed by 2-OG.

Chapter 2. Design and Synthesis of Covalent Inhibitors

2.1. Phenylpiperidine-Based Covalent Inhibitors

A co-crystal structure of 8-pyridopyrimidinone **14** in KDM5B revealed that the phenylpiperidine group was solvent-exposed but it was positioned in close-proximity to cysteine 480 (C480) so could be utilised for the design of cysteine-selective covalent inhibitors of KDM5B (Figure 2.1).

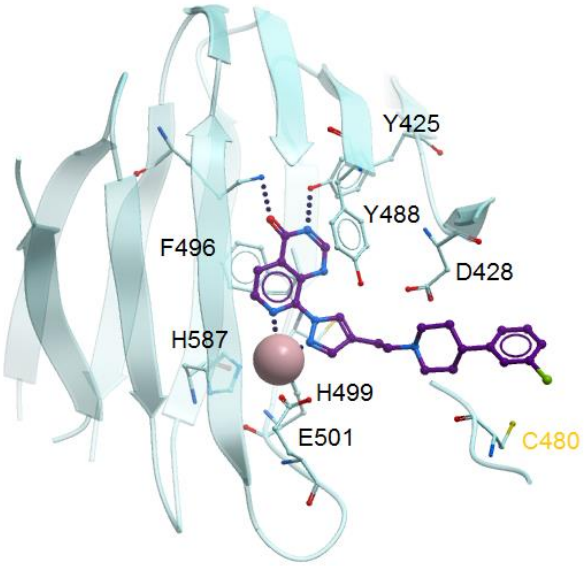


*Figure 2.1. Crystal structure of **14** in KDM5B.*

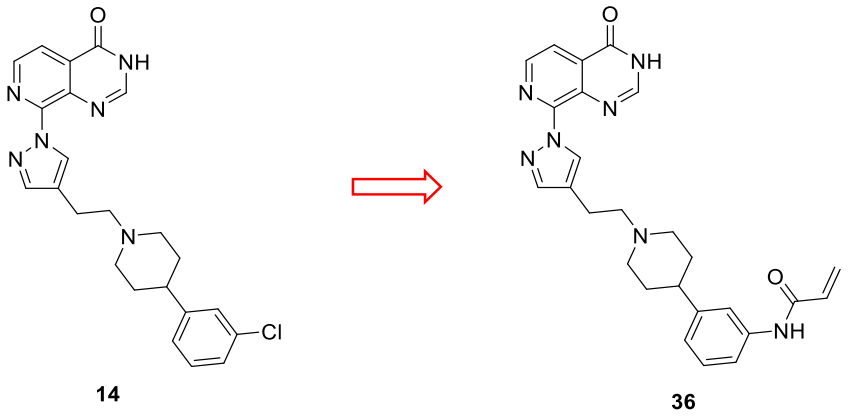
The KDM protein sequences were aligned which identified C480 as a highly unconserved residue across the different subfamilies (Table 2.1). C480 in KDM5B was replaced with a serine in the other members of the KDM5 subfamily. The KDM6 subfamily contains a leucine at this position in the alignment and all the KDM4 proteins contain a glutamic acid. KDM2, KDM3 and KDM7s do not have an overlapping residue at this position so could not covalently bind through a nucleophilic residue. The KDM4 and KDM5 subfamilies have a similar 2-OG binding site which resulted in the pyridopyrimidinone-based inhibitors exhibiting poor selectivity so C480 could be targeted through covalent inhibition to achieve greater selectivity for KDM5B. The addition of cysteine-selective electrophiles to this scaffold could result in selectivity over KDM4 and over the rest of the KDM5

family through covalent binding to KDM5B specifically. The irreversible binding to KDM5B has the potential to reduce competition from the cosubstrate 2-OG and therefore improve the cellular activity of this series.

KDM4A	KDM4B	KDM4C	KDM4D	KDM4E	KDM5A	KDM5B	KDM5C	KDM5D	KDM6A	KDM6B	KDM6C
E169	E170	E171	E173	E170	S464	C480	S485	S495	L1127	L1371	L1074

Table 2.1. Structural alignment of KDMs from overlay of crystal structures at the position of C480 in KDM5B.

Initial design of covalent inhibitor **36** retained the rigid phenylpiperidine moiety which was required for selectivity over other KDM subfamilies. The chlorine at the meta-position of the phenyl ring was replaced with an acrylamide group as a cysteine-selective electrophilic warhead (Scheme 2.1).



Scheme 2.1. Design of phenylpiperidine covalent inhibitor.

Acrylamide **36** was docked covalently into KDM5B to ensure that the covalent bond formation would be favourable in terms of binding energy. **36** adopted the same binding pose as the original compound **14**, maintaining the bidentate coordination to the metal and the key interactions of pyridopyrimidinone CONH with K517/Y425 (Figure 2.2). The covalent bond between the sulfur of C480 and the beta-carbon of acrylamide was possible without changing the binding of the pyridopyrimidinone core, however the sulfur of the cysteine appeared to be repositioned from its normal bond angles.

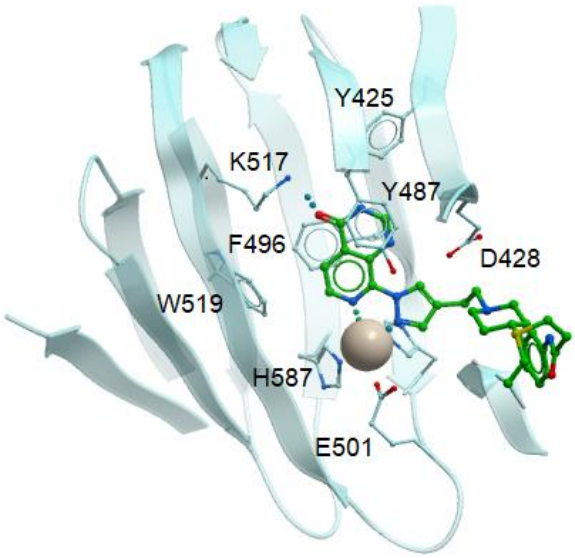
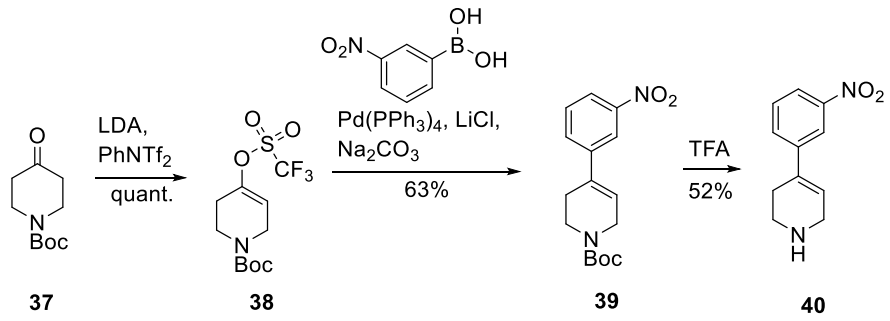


*Figure 2.2. Covalent docking of phenylpiperidine acrylamide **36** in KDM5B. Some residues removed for clarity.*

2.1.1. Synthesis Towards Phenylpiperidine Covalent Inhibitor

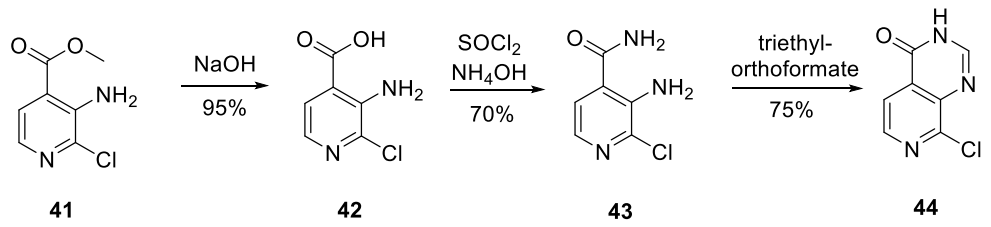
Synthesis of compound **36** began with the formation of vinyl triflate **38** from *N*-Boc-4-piperidone **37** via deprotonation and O-alkylation of the corresponding enolate (Scheme 2.2).[99] Subsequent Suzuki coupling of vinyl triflate **38** with 3-nitrophenyl boronic acid afforded **39**. Boc-deprotection of **39** under acidic conditions gave phenyl tetrahydropyridine **40**.



*Scheme 2.2. Synthetic route towards amine **40**.*

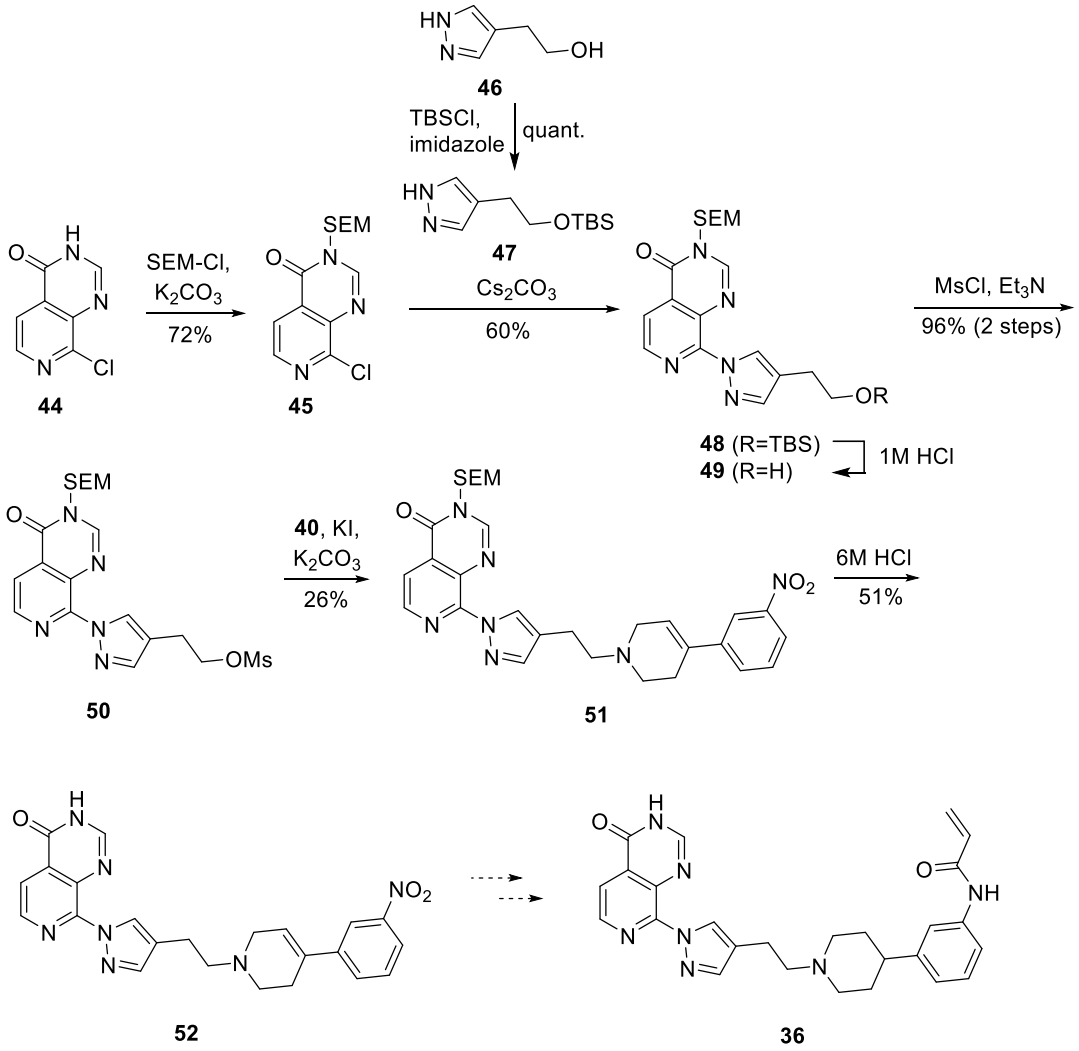
The pyridopyrimidinone core **44** was formed in three steps as previously reported starting from methyl 3-amino-2-chloroisonicotinate **41** in good yield (Scheme 2.3).[73] First steps involved hydrolysis of the methyl ester to give 3-amino-2-chloroisonicotinic acid **42** and amidation via the

acid chloride to give primary amide **43**. The final step to form the chloro-pyridopyrimidinone core **44** was achieved through condensation with triethylorthoformate.



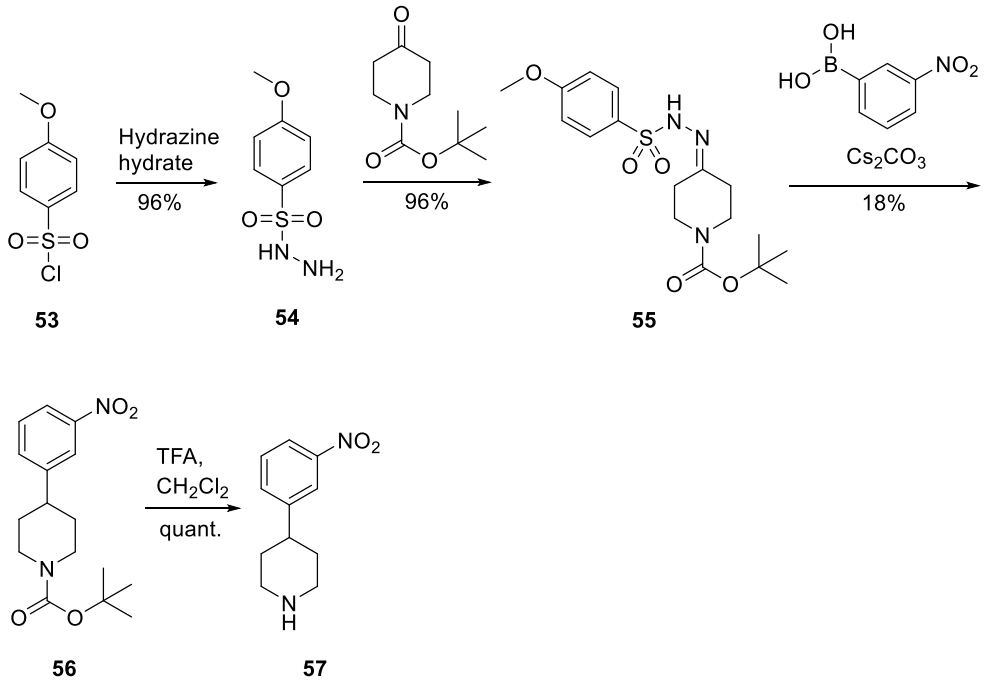
*Scheme 2.3. Synthetic route towards chloro-pyridopyrimidinone **44**.*

It was necessary to protect the amide nitrogen to prevent alkylation in later steps (Scheme 2.4). A trimethylsilylethoxymethyl (SEM) group was utilised as a protecting group as it increases the lipophilicity of subsequent compounds for greater ease of purification. Pyrazole **46** was protected as TBS ether **47** to prevent reactivity of the alcohol. Next step involved displacement of chloride **45** with pyrazole **47** using cesium carbonate as a base to afford compound **48**. The TBS protecting group was removed without loss of the SEM group using mild acidic conditions to afford alcohol **49**. Subsequent activation of the alcohol as mesylate **50** was achieved in 96% yield over two steps. Nucleophilic substitution with phenyl tetrahydropyridine **40** under basic conditions of potassium iodide and potassium carbonate resulted in the formation of compound **51** in low yield due to significant elimination of the starting material to give the alkene byproduct. The SEM group was successfully removed using strong acidic conditions to afford compound **52** however subsequent hydrogenation using palladium on carbon resulted in a very polar compound which did not correspond to the desired hydrogenated product. Reducing the alkene double bond proved to be difficult under normal hydrogenation conditions due to unwanted side reactions of the rest of the compound. It was therefore decided to reduce the alkene to afford nitrophenyl piperidine prior to the substitution step with mesylate **50**.



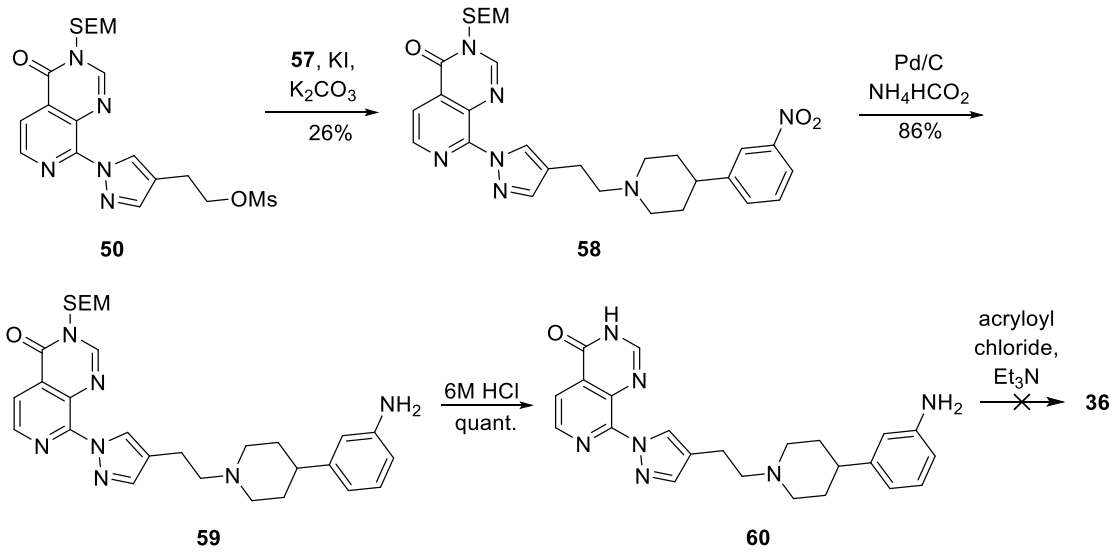
*Scheme 2.4. Synthetic route towards acrylamide **36**.*

A paper from Allwood *et al*. demonstrated the metal-free coupling of boronic acids with tosylhydrazones to prepare 3-nitrophenyl piperidine without the need for a hydrogenation step (Scheme 2.5).[100] Tosylhydrazone **55** was synthesised from sulfonyl chloride **53** via formation of sulfonohydrazide **54** and subsequent reductive amination with Boc-piperidone. Compound **56** was synthesised using tosylhydrazone **55** and 3-nitrophenyl boronic acid under basic conditions. Compound **56** was obtained in low yield as expected with electron deficient aromatics like nitrophenyl boronic acids. Subsequent removal of the Boc group using trifluoroacetic acid afforded 3-nitrophenyl piperidine **57**.



*Scheme 2.5. Synthetic route towards amine **57**.*

Displacement of mesylate **50** with 3-nitrophenyl piperidine **57** was successful using potassium iodide and potassium carbonate to afford compound **58** in low yield due to the competing elimination reaction (Scheme 2.6). As the removal of the SEM group would result in a very polar compound, the nitro group was reduced prior to desilylation. Successful nitro reduction was achieved using palladium on carbon and ammonium formate to give aniline **59** in good yield. SEM deprotection using strong acidic conditions was successful however the final acylation with different electrophiles proved very challenging as the reaction resulted in many products that were difficult to separate. The electrophilic warheads were too unstable for isolation and therefore too reactive as covalent inhibitors.



*Scheme 2.6. Synthetic route towards phenylpiperidine acrylamide **36**.*

2.2. Piperazine Covalent Inhibitors

There was also some concern that C480 was positioned too far from the acrylamide moiety of **36** for covalent binding. As a result, compounds were designed by replacing the original phenylpiperidine with a piperazine ring (Figure 2.3). The piperazine was shorter in length but still possessed the required basic nitrogen. Several cysteine-selective electrophiles could be easily attached to the piperazine nitrogen to give acrylamide **61**, chloroacetamide **62**, propiolamide **63**, dimethylamino crotonamide **64** and halonitrobenzenes **65**-**69**. Overall, these designed compounds were shorter and would be better positioned for covalent binding to C480.

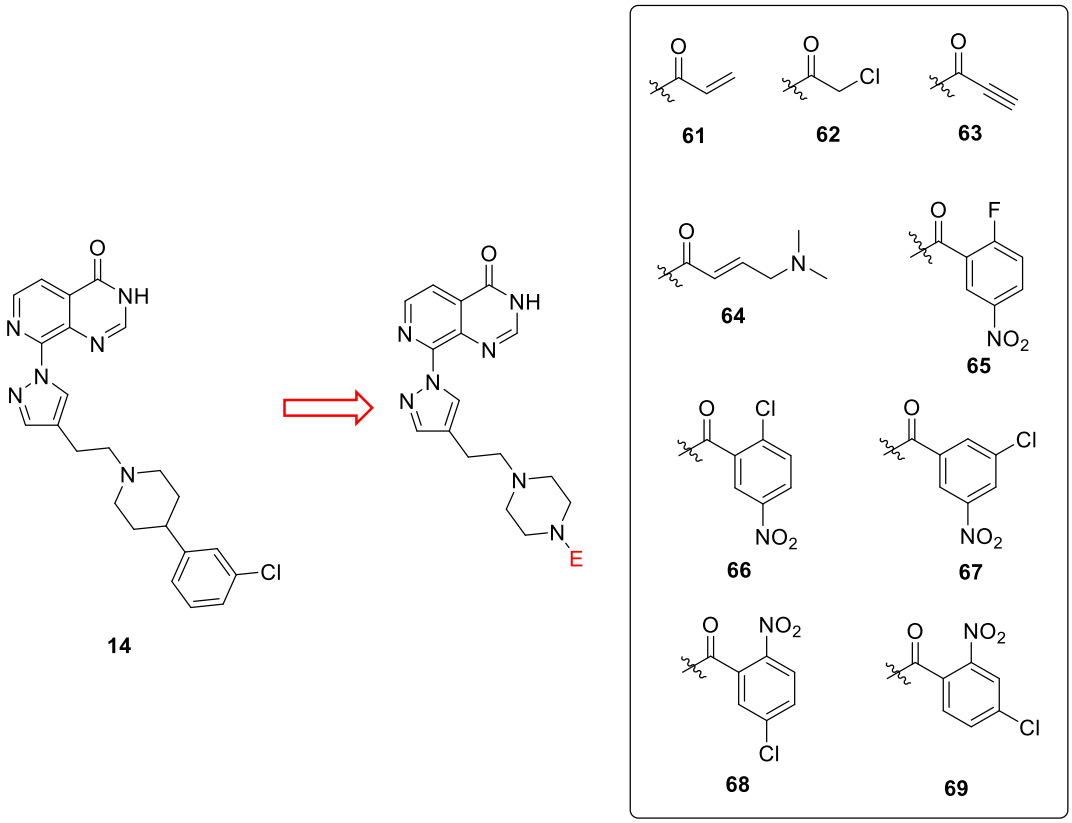


Figure 2.3. Designed piperazine covalent inhibitors with cysteine-selective electrophiles.

Non-covalent docking of acrylamide **61** with KDM5B showed the same binding pose as compound **14** with the usual hydrogen bonding interactions with K517 and Y425 and bidentate coordination to the metal (Figure 2.4). The acrylamide group was projected towards C480 and in proximity for covalent binding. Covalent docking proved that C480 could form a covalent bond with the acrylamide group without distortion of the normal cysteine bond angles. The length of the compound seemed more suitable to ensure correct positioning of the cysteine for covalent bonding without increasing the strain.

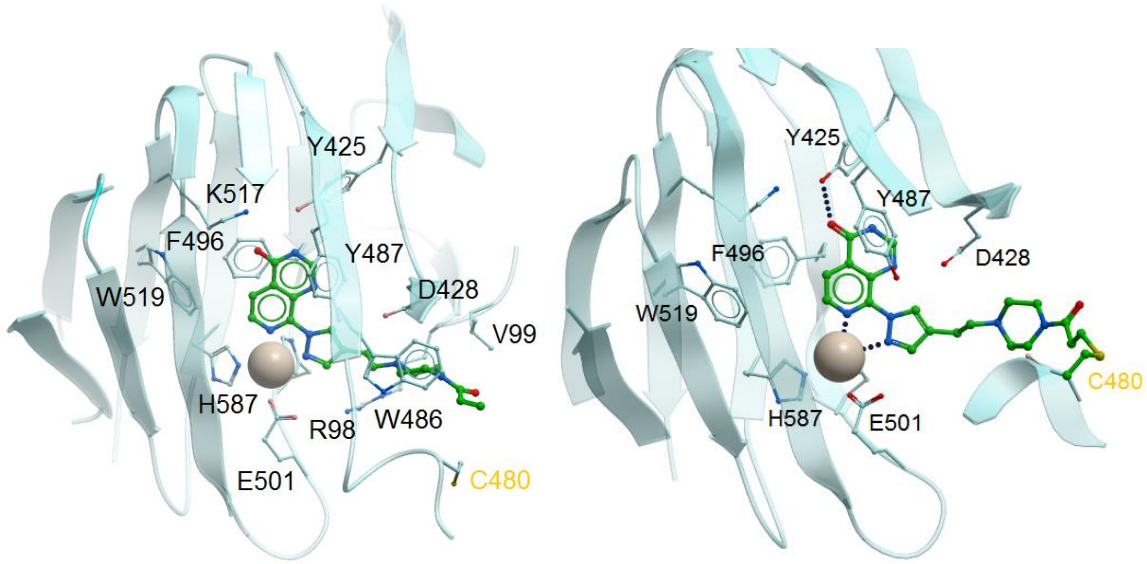


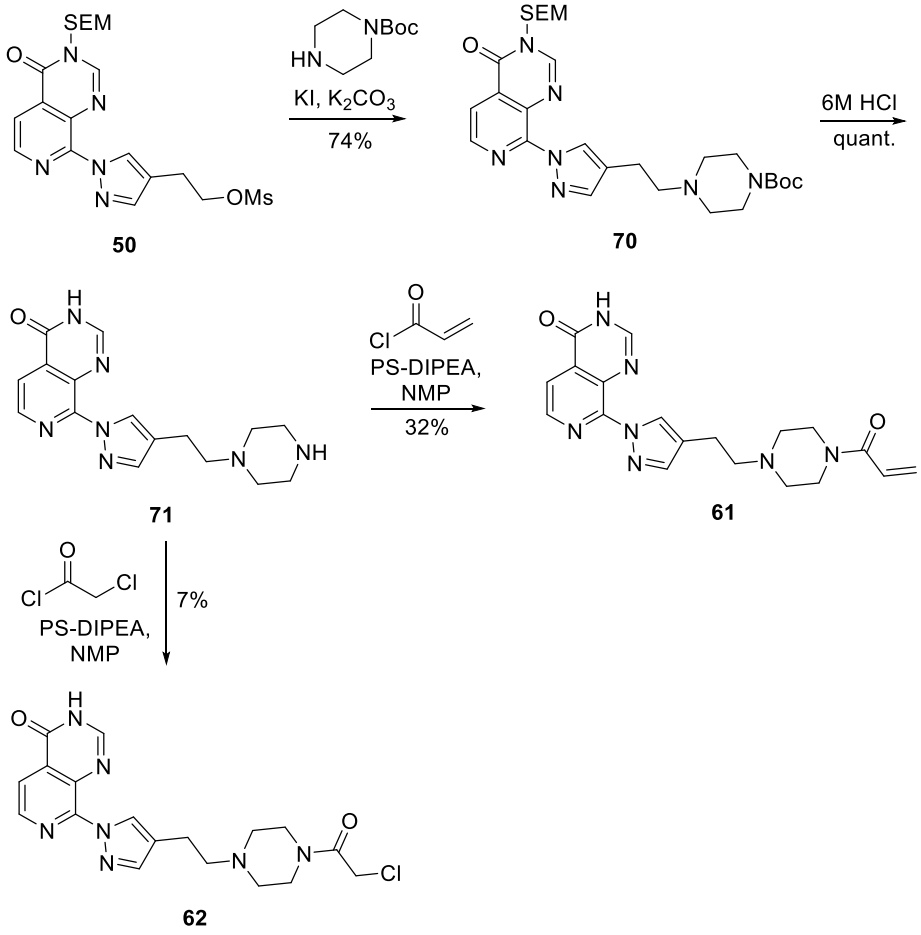
*Figure 2.4. Non-covalent (left) and covalent docking (right) of piperazine acrylamide **61** in KDM5B.*

2.2.1. Synthesis of Piperazine Covalent Inhibitors

Synthesis of the piperazine covalent inhibitors was achieved in 10 linear steps from commercially available **41** via the previously described route to form mesylate **50**. Displacement of mesylate **50** with Boc-piperazine was successful under basic conditions (Scheme 2.7) to afford **70** in good yield. Global deprotection of the SEM and Boc groups using strong acidic conditions resulted in amine **71** which could be reacted with various electrophiles to give the desired covalent inhibitors.

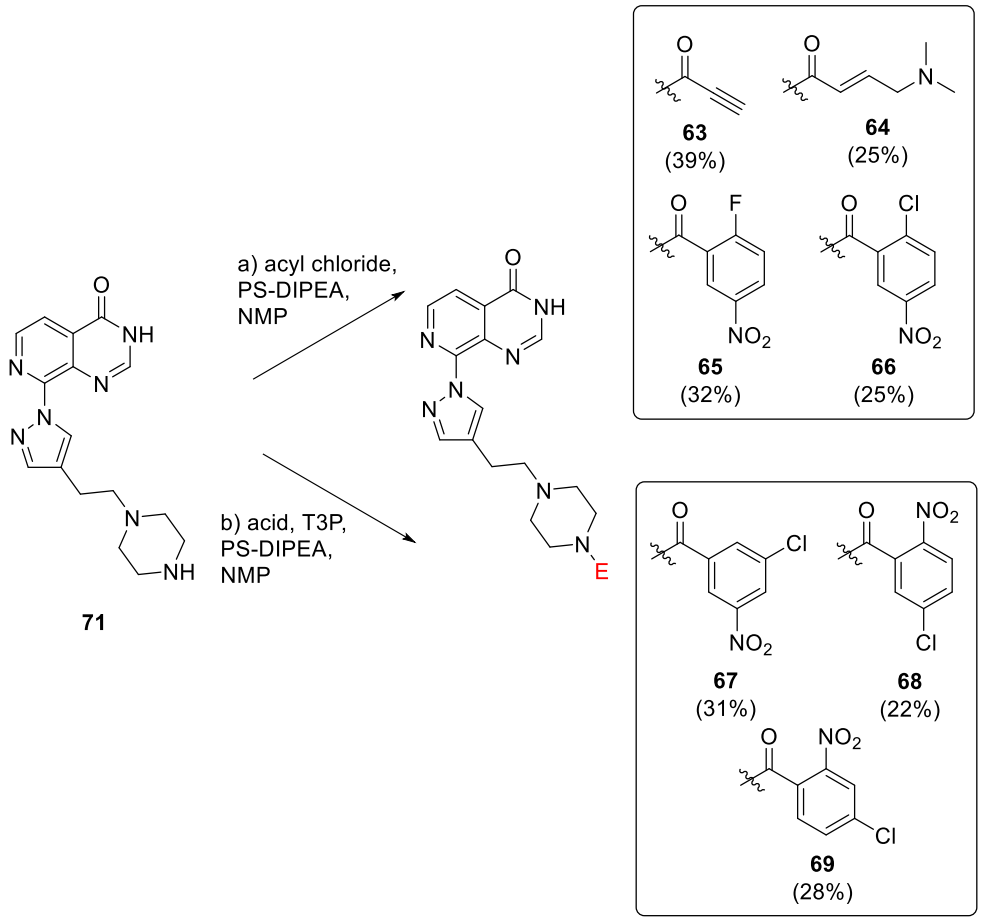
Acylation with acryloyl chloride and triethylamine did not result in the desired acrylamide product but mainly starting material. Different organic bases and solvents were trialled, but they did not result in the formation of the acrylamide. Amide coupling with acrylic acid formed the desired product as well as other side products which were difficult to remove by purification. Polymer-supported bases were also screened in the acylation reaction, but most did not result in any conversion to the product. The use of Amberlyst A26-OH resin did successfully form the acrylamide but other unwanted products also formed. After optimisation of the conditions, acylation with acryloyl chloride and chloroacetyl chloride was achieved using polymer-supported diisopropylethylamine (PS-DIPEA) and *N*-methyl-2-pyrrolidone (NMP) as a polar solvent to afford

acrylamide **61** and chloroacetamide **62** respectively. The poor yields in the final acylation step was likely due to reactivity of the organic bases with the electrophilic warhead.



*Scheme 2.7. Synthetic route of piperazine acrylamide **61** and chloroacetamide **62**.*

Several cysteine-selective electrophiles were attached to the piperazine to tune the covalent reactivity so that the covalent bond formation would be fast enough to react with the desired protein but slow to react with non-specific proteins in the cell. Propiolamide **63**, Dimethylamino crotonamide **64** and halonitrobenzenes **65**-**69** were synthesised through acylation or amide coupling with corresponding acid chloride or carboxylic acid using the polymer-supported base (Scheme 2.8).



*Scheme 2.8. Synthetic route towards piperazine propiolamide **63**, dimethylamino crotonamide **64** and halonitrobenzenes **65**-**69**.*

2.3. Substituted-Piperazine Covalent Inhibitors

The piperazine analogues were discovered to exhibit poor cell permeability (Chapter 3) so several compounds were designed with the aim of improving cell permeability (Figure 2.5). Lipophilic groups such as phenyl and benzyl groups were added to the piperazine ring at different positions to improve the potency of the piperazine analogues as well as improve their cell permeability. Methyl benzylamine, cyclopentyl benzylamine and tetrahydroisoquinoline scaffolds were also designed as they retained the necessary basic nitrogen and were a similar length for covalent binding to C480.

In the substituted piperazine series, compounds were designed with an acrylamide electrophilic warhead as a direct comparison with the parent piperazine inhibitor **61**. In the benzylamine and tetrahydroisoquinoline series, acrylamide, chloroacetamide and dimethylamino crotonamide warheads were incorporated as they were the most commonly used electrophiles in the literature.[101] As all of the compounds contained a basic nitrogen, clogD rather than clogP values were calculated. The addition of phenyl and benzyl groups to the piperazine ring at all positions increased the clogD values. Only a small increase in clogD was observed with 3-phenylpiperazine **72** while 2-phenylpiperazine **73** showed a more desirable clogD of 1.28. As expected, larger clogD values were observed with the addition of the benzyl group compared to phenyl group. Cyclopentyl benzylamines **80**-**82**, such as acrylamide **80**, had optimal clogD values. Methyl benzylamines **77**-**79** had slightly lower clogD's than cyclopentyl benzylamines. Tetrahydroisoquinolines acrylamide **83** and chloroacetamide **84** also had reasonable clogD values of 1.08 and 1.02 respectively. For all the analogues, the dimethylamino crotonamide electrophile had a much lower clogD than the acrylamide and chloroacetamide electrophiles due to the additional polar nitrogen. Although dimethylamino crotonamide inhibitors would likely be less cell permeable, this electrophile may show improved covalent reactivity.

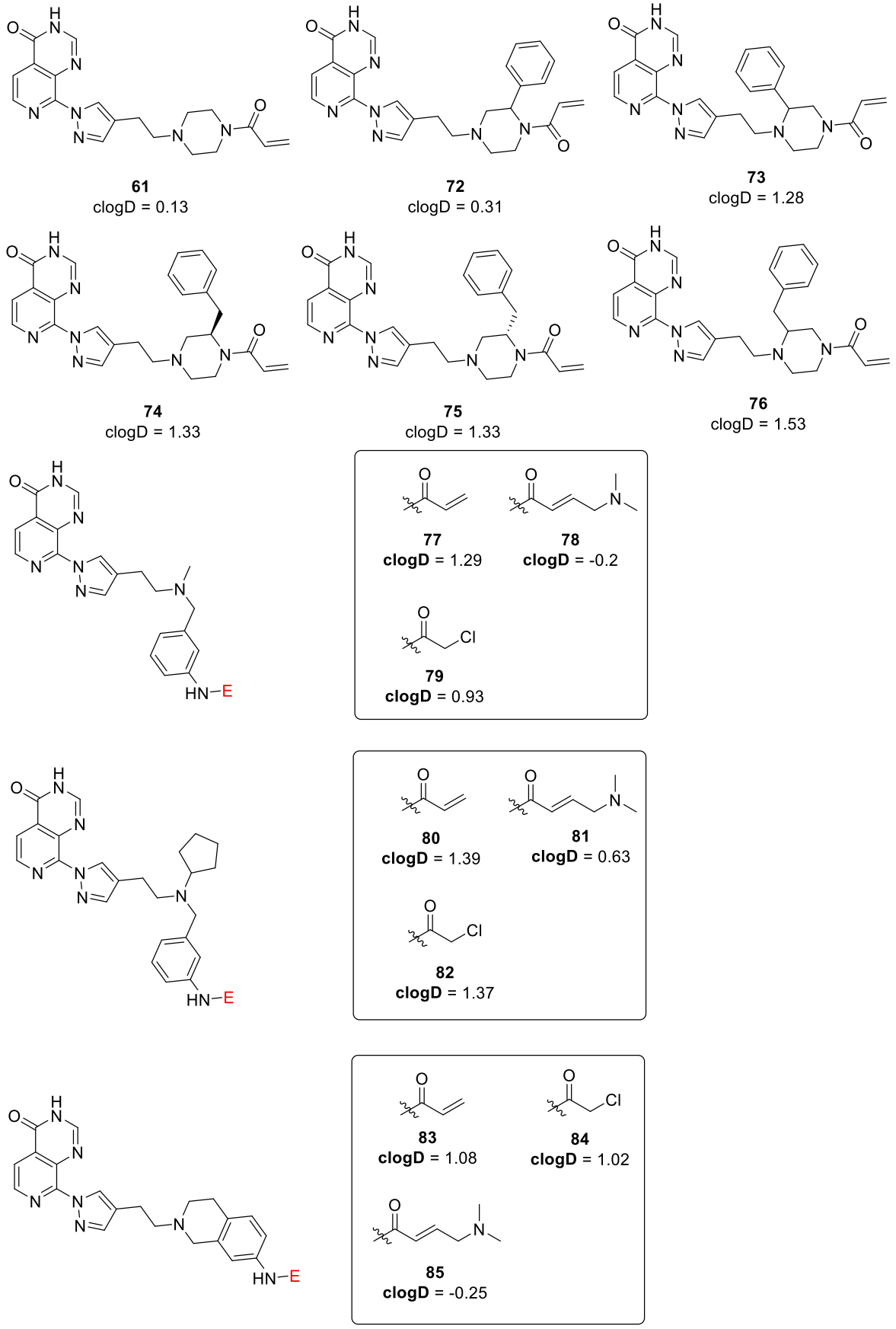


Figure 2.5. Designed covalent inhibitors and their clogD values at pH 7.5.

Covalent docking of 2-phenylpiperazine **73** confirmed that the phenyl ring was solvent exposed and therefore would not hinder binding of the compound to the active site (Figure 2.6). However, the pyridopyrimidinone core was displaced compared to the original ligand and the pyridopyrimidinone and pyrazole ring were twisted from their usual conformation so there was no bidentate coordination to the metal. The carbonyl of the pyridopyrimidinone amide interacted with Y425. Similar binding was observed with the 3-phenylpiperazine **72** but the carbonyl of pyridopyrimidinone could also interact with K517 due to the displacement of the core. Overall, the docking suggested that the addition of phenyl rings to the inhibitor would result in less favourable binding to KDM5B. It was important to synthesise both compounds **72** and **73** for structure-activity relationships to determine whether lipophilic substituents would be tolerated at the 2- or 3-position of the piperazine ring.

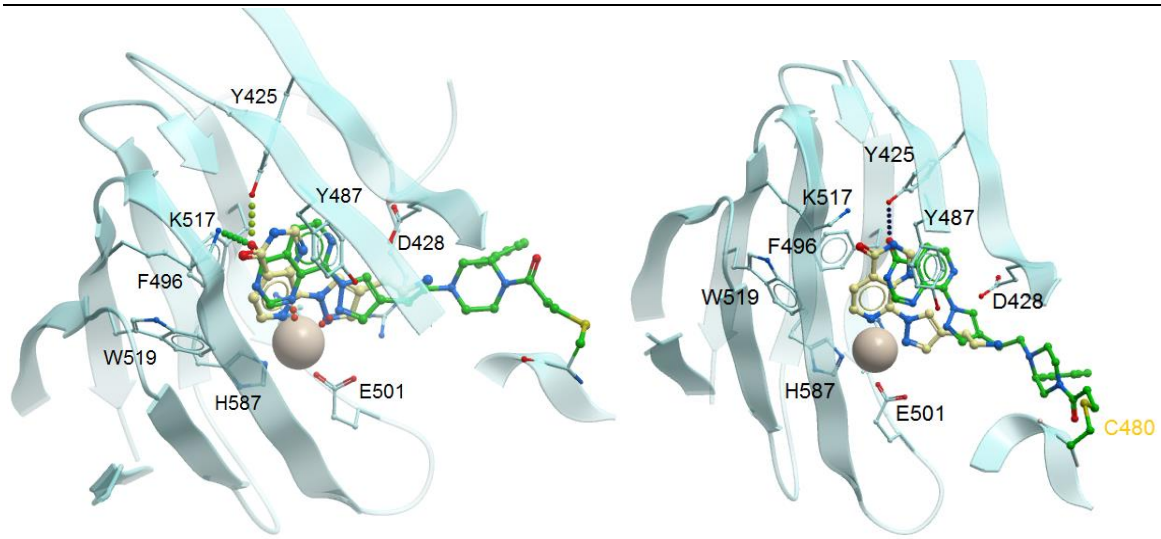
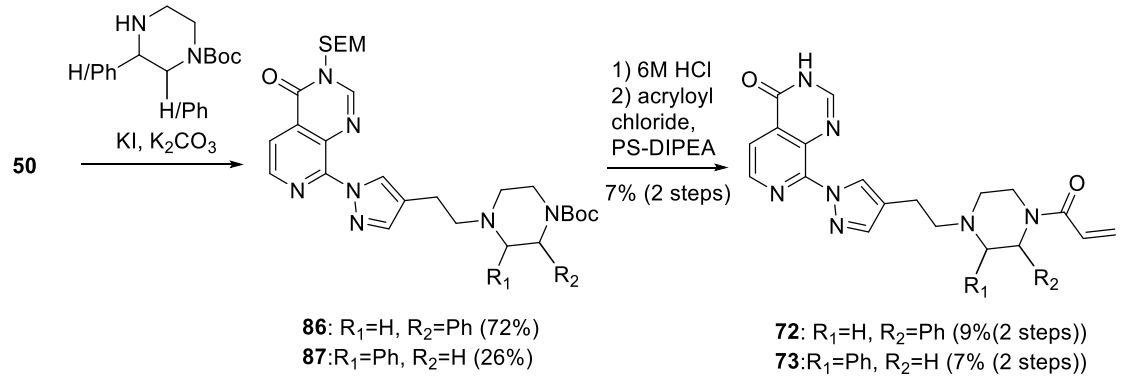


*Figure 2.6. Covalent docking of 3-phenylpiperazine **72** (left) and 2-phenylpiperazine **73** (right) in KDM5B.*

2.3.1. Synthesis of Substituted-Piperazine Covalent Inhibitors

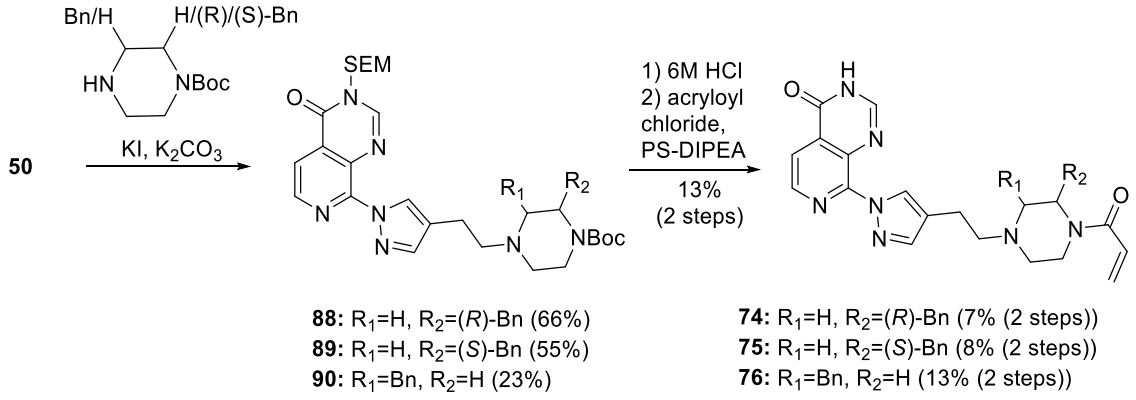
3-Phenylpiperazine acrylamide **72** was synthesized as a racemic mixture via nucleophilic substitution of mesylate **50** with *tert*-butyl 3-phenylpiperazine-1-carboxylate to afford **86**, global deprotection and a final acylation with acryloyl chloride (Scheme 2.9). 2-Phenylpiperazine

acrylamide **73** was synthesised via the same route through displacement of **50** with *tert*-butyl 2-phenylpiperazine-1-carboxylate to give compound **87**; followed by deprotection and acylation.



*Scheme 2.9. Synthetic route towards phenylpiperazine acrylamides **72** and **73**.*

Benzyl groups were added at the 2- and 3- positions of the piperazine ring via the same three step sequence from mesylate **50** (Scheme 2.10). Single enantiomer 3-benzylpiperazine acrylamides **74** and **75** were synthesised through displacement with the optically pure amines to afford **88** and **89** respectively and subsequent deprotection and acylation with acryloyl chloride. Reaction of mesylate **50** with *tert*-butyl 3-benzylpiperazine-1-carboxylate gave **90** which was deprotected and acylated to form 2-benzylpiperazine acrylamide **76** in racemic form.



*Scheme 2.10. Synthetic route towards benzylpiperazine acrylamides **74, 75** and **76**.*

2.4. Methyl Benzylamine Covalent Inhibitors

It was hoped that replacing the piperazine with an aniline (Figure 2.7) would accelerate the kinetics of covalent binding. Methyl benzylamine acrylamide **77** and chloroacetamide **79** were covalently docked in KDM5B to predict whether the compounds would adopt the same pose as the piperazine moiety. The 8-pyridopyrimidinone and pyrazole rings of both compounds were positioned for bidentate coordination with the metal and the key hydrogen bonding interactions of the pyridopyrimidinone amide were observed. Covalent binding was possible with both electrophiles without disrupting the binding pose of the inhibitor. Although the benzylamine could freely rotate, the addition of the covalent bond would rigidify the molecule.

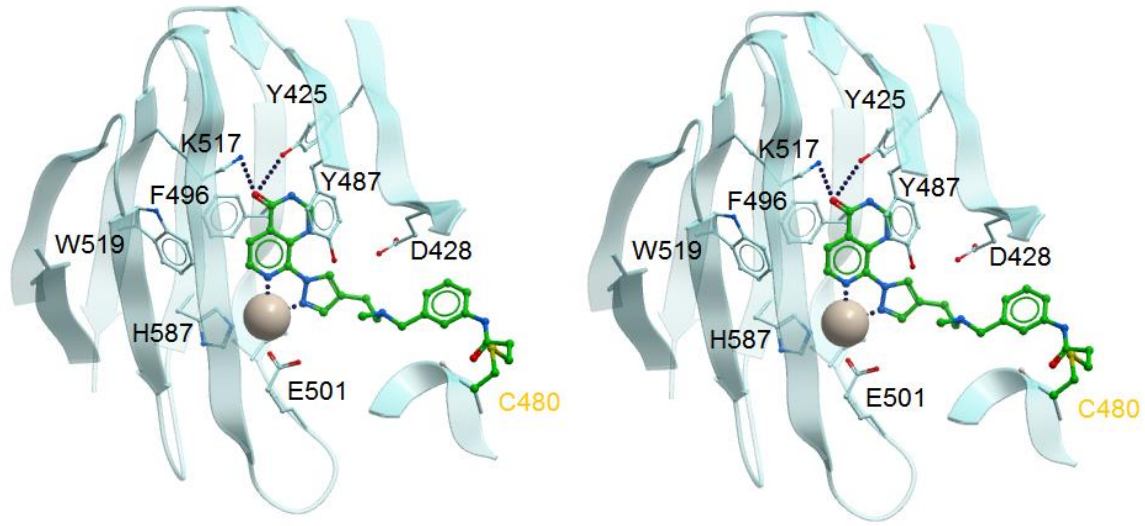
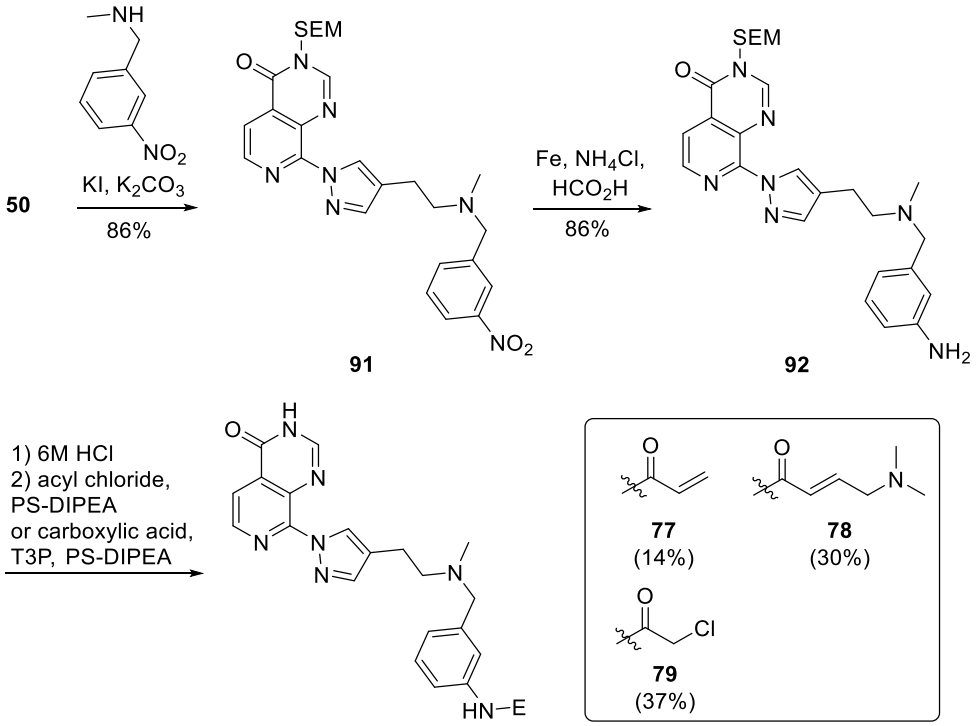


*Figure 2.7. Covalent docking of methyl benzylamide acrylamide **77** and of methyl benzylamine chloroacetamide **79** in KDM5B.*

2.4.1. Synthesis of Methyl Benzylamines Inhibitors

Synthesis of methyl benzylamine covalent inhibitors **77**-**79** required displacement of mesylate **50** with *N*-methyl-1-(3-nitrophenyl)methanamine to give compound **91** (Scheme 2.11). Nitro reduction was achieved using iron, ammonium chloride and formic acid to afford aniline **92**. Final steps to

compounds **77**-**79** involved deprotection of the SEM group and attachment of the electrophilic warheads using the corresponding acid chloride or carboxylic acid.



*Scheme 2.11. Synthetic route towards methyl benzylamine covalent inhibitors **77**-**79**.*

2.5. Cyclopentyl Benzylamine Covalent Inhibitors

Docking of cyclopentyl benzylamine acrylamide **80** into KDM5B confirmed a similar pose to other analogues with the same key interactions in the binding pocket (Figure 2.8). The cyclopentyl group did not clash with any residues so would not impede covalent bonding of C480 with the acrylamide.

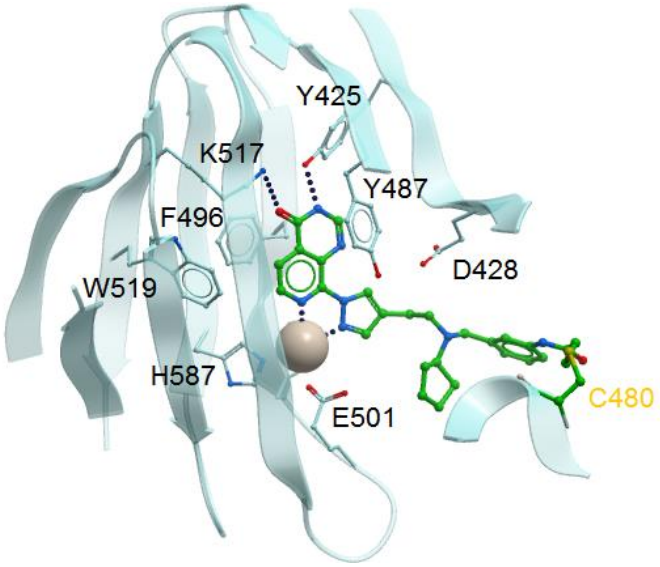
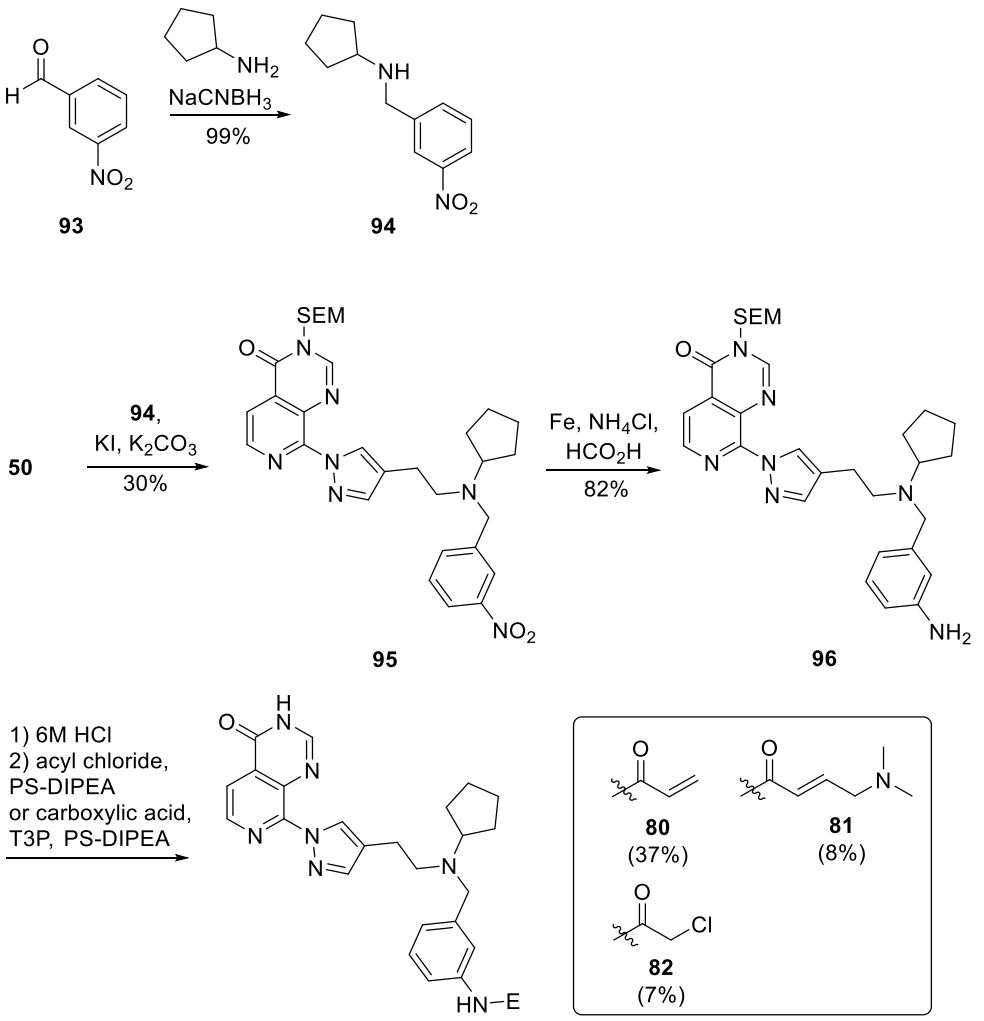


*Figure 2.8. Covalent docking of cyclopentyl benzylamine acrylamide **80** in KDM5B.*

2.5.1. Synthesis of Cyclopentyl Benzylamine Covalent Inhibitors

Cyclopentyl benzylamine inhibitors required the initial formation of amine **94** through reductive amination of 3-nitrobenzaldehyde **93** with cyclopentylamine (Scheme 2.12). Displacement of mesylate **50** with amine **94** gave compound **95** in lower yield than with methyl benzylamine which was likely due to greater steric hindrance of the amine nucleophile **94**. Subsequent nitro reduction gave compound **96** and the final compounds **80**-**82** were synthesised through acylation with acryloyl chloride, chloroacetyl chloride or amide coupling with (*E*)-4-(dimethylamino)but-2-enoic acid.



*Scheme 2.12. Synthetic route towards cyclopentyl benzylamine covalent inhibitors **80**-**82**.*

2.6. Tetrahydroisoquinoline Covalent Inhibitors

To constrain the free rotation of the methyl benzylamine group, the more rigid tetrahydroisoquinoline was incorporated into the covalent inhibitors (Figure 2.9). Tetrahydroisoquinoline acrylamide **83,** docked into KDM5B, showed the same key binding interactions as with other 8-pyridopyrimidinone inhibitors. The tetrahydroisoquinoline ring was positioned favourably to enable covalent binding of C480 to the acrylamide.

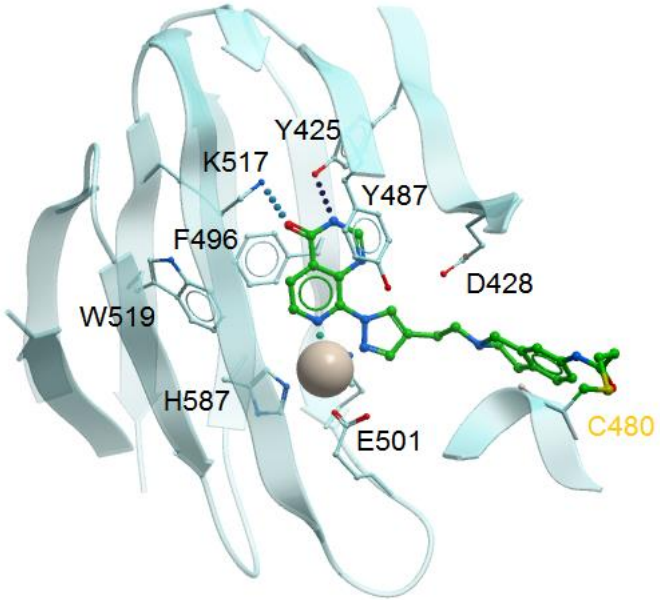
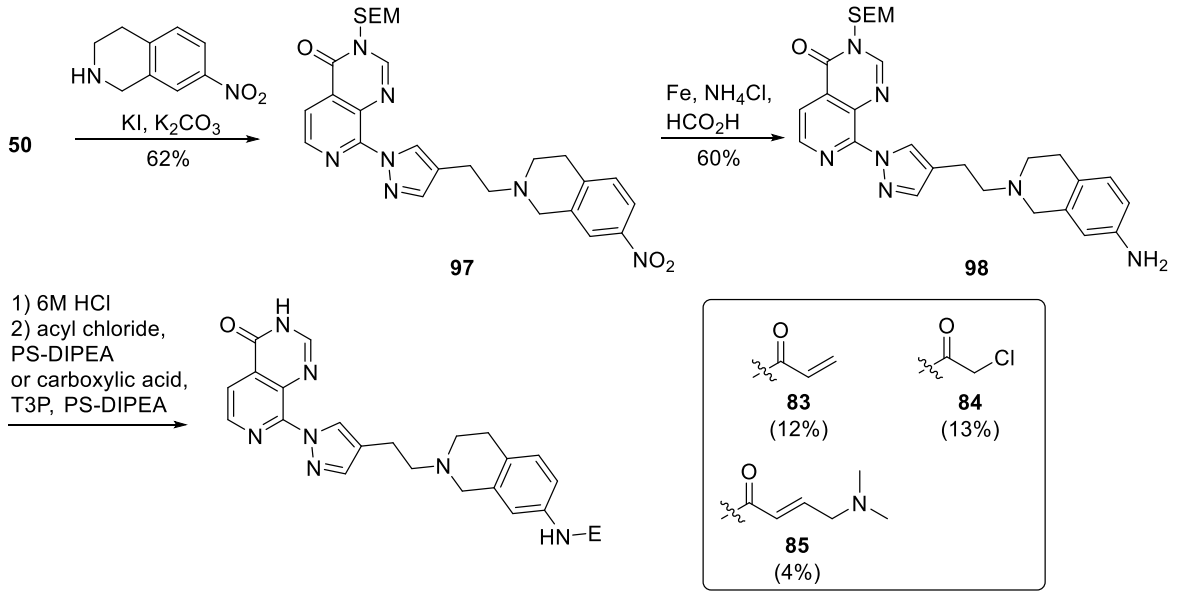


*Figure 2.9. Covalent docking of tetrahydroisoquinoline acrylamide **83** in KDM5B.*

2.6.1. Synthesis of Tetrahydroisoquinoline Covalent Inhibitors

Synthesis of tetrahydroisoquinoline covalent inhibitors **83**-**85** was successful using conditions as described above via nucleophilic substitution to afford compound **97**, nitro reduction to afford compound **98**, removal of the SEM group and acylation (Scheme 2.13).



*Scheme 2.13. Synthetic route towards tetrahydroisoquinoline covalent inhibitors **83**-**85**.*

2.7. Summary

Several 8-pyridopyrimidinone-based compounds with different electrophilic warheads were designed to bind covalently to KDM5B through docking studies. The core 8-pyridopyrimidinone scaffold was maintained but different basic nitrogen scaffolds and electrophilic warheads were incorporated. Phenylpiperidine acrylamide **36**, based on the original published scaffold **14**, was unable to be isolated due to overreactivity however piperazine analogues were less reactive and were a more suitable length for covalent binding to C480. Substitutions of the piperazine ring were explored to increase the calculated clogD for improved cell permeability. Other basic nitrogens such as methyl benzylamines, cyclopentyl benzylamines and tetrahydroisoquinolines were also designed to improve the cell permeability and potency.

The synthesis of the covalent inhibitors was achieved via a multi-step synthetic route through a common intermediate mesylate **50**. 8-chloro pyridopyrimidinone core **44** was synthesised from commercially available ester **41** through hydrolysis, amidation and cyclisation with triethylorthoformate. Subsequent steps involved displacement with pyrazole **47**, removal of TBS group and activation as mesylate **50**. **50** was reacted with various amines to explore structure-activity relationships for optimising non-covalent and covalent interactions with KDM5B. Final steps involved removal of protecting groups and acylation with different electrophiles to give the corresponding covalent inhibitors which would be tested in several assays for biochemical/cellular activity and selectivity for KDM5B as well as for covalent binding to KDM5B.

Chapter 3. Screening of Covalent Inhibitors

3.1. Piperazine Covalent Inhibitors

3.1.1. Time Dependent Inhibition

Piperazine analogues with different covalent electrophiles were synthesised and their potency against KDM5B was tested using an AlphaScreen assay. To rank the different covalent inhibitors based on their potency, IC_{50}'s were measured at different pre-incubation times using a published method[93] to determine their k_{inact} and K_i values from equation 1 and 2 (Chapter 1). S and K_M were fixed values where S was the H3K4me3 substrate concentration of 0.1 µM and K_M was the Michaelis-Menten constant for the substrate of 0.5 µM. The most potent compounds will have low K_i values, indicating potent non-covalent interactions, and high k_{inact} values, indicating fast covalent binding kinetics. Consequently, covalent inhibitors with the highest k_{inact}/K_i values were the most potent.

Chloroacetamide **62** showed a drop in IC_{50} of approximately 7-fold over the 2-hour incubation (Figure 3.1). **62** also showed the largest k_{inact}/K_i of 3.1 x 10^3 M^{-1} s^{-1} (Table 3.1) which was three orders of magnitude lower than the previously discussed EGFR covalent inhibitor **35**. The covalent reactivity was comparable to **35** with a k_{inact} in the order of 10^{-3} s^{-1} however chloroacetamide **62** showed weaker non-covalent binding affinity (K_i = 5.6 x 10^{-7} M) compared to **35** (K_i = 3.2 x 10^{-10} M). Propiolamide **63** was the second most potent electrophile with a k_{inact}/K_i of 2.6 x 10^3 M^{-1} s^{-1}. Dimethylamino crotonamide **64** was slightly more potent than acrylamide **61** with a 7-fold drop in IC_{50} compared to 5-fold and k_{inact}/K_i of 1.7 x 10^3 M^{-1} s^{-1} compared to 1.4 x 10^3 M^{-1} s^{-1}. As expected, non-covalent propanamide **99** showed only a small change in IC_{50} over the incubation times as there is a required pre-incubation time for non-covalent compounds to reach equilibrium.

The piperazine inhibitors with halonitrobenzene electrophilic warheads were also tested for their time-dependent inhibition against KDM5B. Fluoronitrobenzene **65** was expected to show the

greatest covalent inhibition as the rate of nucleophilic substitution of fluorine is faster than chlorine, the nitro group is para to the halogen to stabilise the negative charge and it is further activated by the ortho electron withdrawing amide.[102] Despite this, chloronitrobenzene **66** showed the greatest k_{inact}/K_i of 2.6 x 10^3 M^{-1} s^{-1} with an IC_{50} after 90 minutes incubation of 184 nM. Compound **67** showed the greatest fold change in IC_{50} (4-fold) which was unexpected as it is the least activated towards nucleophilic substitution with the electron withdrawing groups at the meta positions. The chlorine of **67** may have been positioned more favourably within the active site for covalent binding with the desired cysteine than **66** resulting in the unexpected covalent reactivity.

Overall, the halonitrobenzene inhibitors showed less potent IC_{50}'s after the pre-incubation period than other electrophiles. Halonitrobenzene electrophiles are also not widely used as covalent inhibitors so subsequent compounds were synthesised with well-established electrophiles such as acrylamide, dimethylamino crotonamide and chloroacetamide to fine-tune the covalent reactivity.

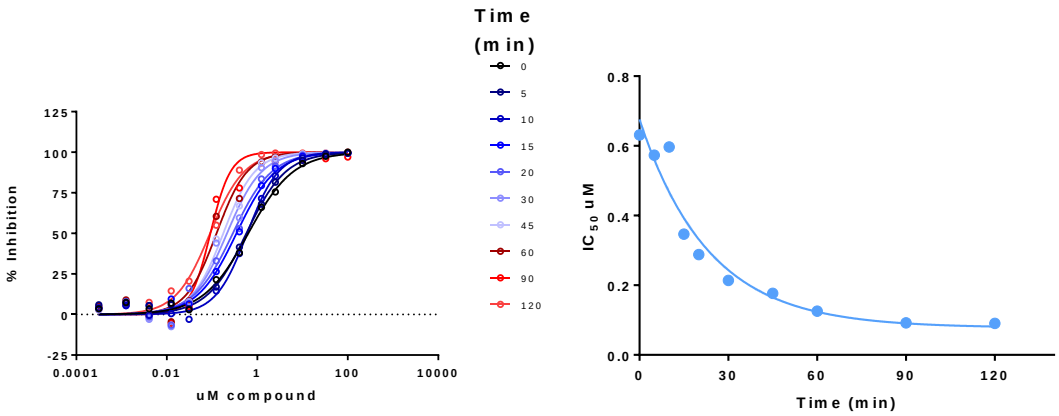
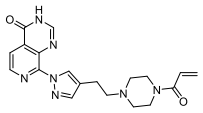
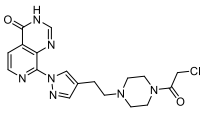
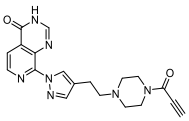
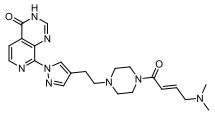
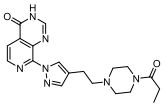


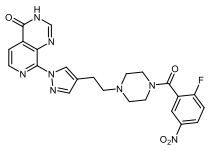
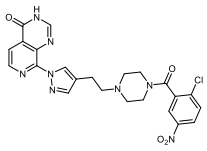
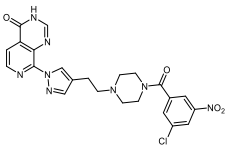
*Figure 3.1. IC_{50} curves of chloroacetamide **62** at the different time points (left) and a graph showing the change in IC_{50} of **62** with time (right).*

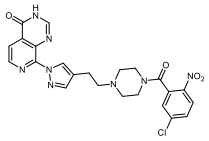
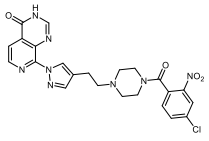
	61		62		63	
Time (min)	**IC_{50} (µM)**	**Standard Deviation (n)**	**IC_{50} (µM)**	**Standard Deviation (n)**	**IC_{50} (µM)**	**Standard Deviation (n)**
0	0.941	± 0.093 (2)	0.632	± 0.032 (2)	0.415	± 0.238 (2)
5	0.895	± 0.143 (2)	0.573	± 0.104 (2)	0.401	± 0.168 (2)
10	0.841	± 0.008 (2)	0.592	± 0.103 (2)	0.371	± 0.028 (2)
15	0.681	± 0.016 (2)	0.347	± 0.023 (2)	0.315	± 0.035 (2)
20	0.519	± 0.046 (2)	0.286	± 0.015 (2)	0.265	± 0.006 (2)
30	0.444	± 0.030 (2)	0.215	± 0.029 (2)	0.222	± 0.007 (2)
45	0.335	± 0.037 (2)	0.179	± 0.049 (2)	0.195	± 0.011 (2)
60	0.294	± 0.030 (2)	0.126	± 0.019 (2)	0.092	± 0.013 (2)
90	0.190	± 0.024 (2)	0.091	± 0.007 (2)	0.108	± 0.021 (2)
120	0.184	± 0.028 (2)	0.090	± 0.013 (2)		
K_i (M)	$8.34 \pm 0.79 \times 10^{-7}$		$5.57 \pm 0.39 \times 10^{-7}$		$3.63 \pm 1.51 \times 10^{-7}$	
k_{inact} (s^{-1})	$1.16 \pm 0.13 \times 10^{-3}$		$1.711 \pm 0.009 \times 10^{-3}$		$1.00 \pm 0.59 \times 10^{-3}$	
k_{inact}/K_i (M^{-1} s^{-1})	**$1.39 \pm 0.02 \times 10^{3}$**		**$3.08 \pm 0.24 \times 10^{3}$**		**$2.62 \pm 0.52 \times 10^{3}$**	

	64		99	
Time (min)	**IC_{50} (µM)**	**Standard Deviation (n)**	**IC_{50} (µM)**	**Standard Deviation (n)**
0	0.977	± 0.089 (2)	2.040	± 0.087 (2)
5	0.933	± 0.029 (2)	1.939	± 0.430 (2)
10	0.737	± 0.036 (2)	1.744	± 0.074 (2)
15	0.623	± 0.060 (2)	1.370	± 0.006 (2)
20	0.542	± 0.052 (2)	1.135	± 0.106 (2)
30	0.441	± 0.027 (2)	1.151	± 0.038 (2)
45	0.367	± 0.015 (2)	1.228	± 0.054 (2)
60	0.230	± 0.019 (2)	1.273	± 0.055 (2)
90	0.133	± 0.004 (2)	0.844	± 0.112 (2)
120	0.136	± 0.003 (2)		
K_i (M)	$8.69 \pm 0.49 \times 10^{-7}$			
k_{inact} (s^{-1})	$1.50 \pm 0.10 \times 10^{-3}$			
k_{inact}/K_I (M^{-1} s^{-1})	**$1.72 \pm 0.02 \times 10^{3}$**			

	65		66		67	
Time (min)	IC_{50} (μM)	Standard Deviation (n)	IC_{50} (μM)	Standard Deviation (n)	IC_{50} (μM)	Standard Deviation (n)
0	1.355	± 0.053 (2)	0.630	± 0.097 (2)	0.812	± 0.160 (2)
5	1.345	± 0.305 (2)	0.549	± 0.047 (2)	0.788	± 0.184 (2)
10	1.184	± 0.021 (2)	0.493	± 0.091 (2)	0.799	± 0.179 (2)
15	1.199	± 0.117 (2)	0.490	± 0.105 (2)	0.759	± 0.195 (2)
20	0.890	± 0.014 (2)	0.247	± 0.045 (2)	0.387	± 0.092 (2)
30	0.361	± 0.028 (2)	0.175	± 0.016 (2)	0.292	± 0.103 (2)
45	0.334	± 0.037 (2)	0.143	± 0.048 (2)	0.213	± 0.056 (2)
60	0.220	± 0.034 (2)	0.073	± 0.014 (2)	0.075	± 0.029 (2)
90	0.405	± 0.052 (2)	0.184	± 0.041 (2)	0.248	± 0.037 (2)
K_i (M)	$1.08 \pm 0.14 \times 10^{-6}$		$4.44 \pm 0.55 \times 10^{-7}$		$5.95 \pm 0.85 \times 10^{-7}$	
k_{inact} (s^{-1})	$1.05 \pm 0.20 \times 10^{-3}$		$1.12 \pm 0.17 \times 10^{-3}$		$8.77 \pm 1.91 \times 10^{-4}$	
k_{inact}/K_I (M^{-1} s^{-1})	**$9.67 \pm 0.63 \times 10^{2}$**		**$2.57 \pm 0.70 \times 10^{3}$**		**$1.51 \pm 0.54 \times 10^{3}$**	

	68		69	
Time (min)	IC_{50} (μM)	Standard Deviation (n)	IC_{50} (μM)	Standard Deviation (n)
0	0.772	± 0.086 (2)	1.082	± 0.228 (2)
5	0.717	± 0.026 (2)	0.868	± 0.059 (2)
10	0.619	± 0.013 (2)	0.947	± 0.263 (2)
15	0.748	± 0.019 (2)	1.655	± 0.083 (2)
20	0.445	± 0.016 (2)	0.589	± 0.043 (2)
30	0.388	± 0.041 (2)	0.425	± 0.004 (2)
45	0.319	± 0.034 (2)	0.453	± 0.004 (2)
60	0.373	± 0.081 (2)	0.479	± 0.045 (2)
90	0.404	± 0.102 (2)	0.394	± 0.042 (2)
K_i (M)	$5.85 \pm 0.62 \times 10^{-7}$		$8.59 \pm 0.10 \times 10^{-7}$	
k_{inact} (s^{-1})	$4.42 \pm 2.87 \times 10^{-4}$		$5.12 \pm 0.15 \times 10^{-4}$	
k_{inact}/K_i (M^{-1} s^{-1})	**$7.34 \pm 4.14 \times 10^{2}$**		**$5.96 \pm 0.11 \times 10^{2}$**	

*Table 3.1. Time-dependent IC_{50}'s against KDM5B and their k_{inact}/K_i values for piperazine analogues **61-69**.*

Chloroacetamide **62** was almost 8 times more potent than non-covalent propanamide **99** after a 2-hour pre-incubation and the increase in pIC_{50} for chloroacetamide **62** over time was more significant than propanamide **99** (Figure 3.2). The small change in pIC_{50} with non-covalent **99** was likely due to the required pre-incubation time in the AlphaScreen assay for non-covalent inhibitors to reach

equilibrium. As the non-covalent interactions between **62** and **99** and the residues in KDM5B are almost identical, the addition of covalent inhibition must have contributed to the improved potencies observed after 2-hour pre-incubation with compounds containing electrophilic warheads.

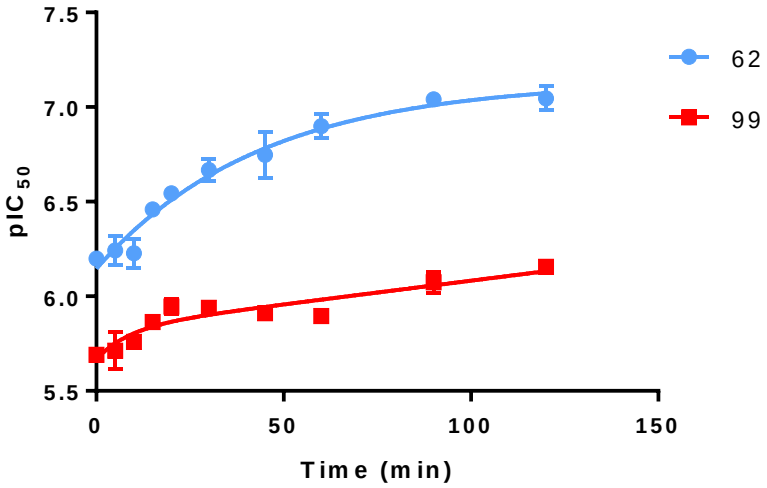


*Figure 3.2. Change in pIC_{50} for covalent chloroacetamide **62** and non-covalent **99**.*

The covalent reactivity of the various electrophilic warheads was compared through plotting the k_{inact}'s of the piperazine series (Figure 3.3). Chloroacetamide **62** showed the highest k_{inact} value of $1.71 \times 10^{-3}\ s^{-1}$ so chloroacetamide was the fastest electrophile for covalent binding. Dimethylamino crotonamide was the second most reactive to covalent binding with a k_{inact} of $1.50 \times 10^{-3}\ s^{-1}$. Acrylamide **61** was less covalently reactive compared to dimethylamino crotonamide **64** (k_{inact} of $1.16 \times 10^{-3}\ s^{-1}$) which suggests that the addition of the dimethylamino group to the alkene accelerated the covalent inhibition. The halonitrobenzene electrophiles were generally slower to bind covalently to KDM5B as they had lower k_{inact} values. Chloronitrobenzene **68** had the lowest k_{inact} of $4.42 \times 10^{-4}\ s^{-1}$ of the different electrophiles so there was likely no significant covalent binding within the pre-incubation time. Overall, the covalent reactivity of the electrophiles was moderate with a k_{inact} in the order of $10^{-3}\ s^{-1}$ which was comparable to known covalent EGFR inhibitors. Tuned covalent reactivity is important to ensure that the inhibitors bind covalently within the timeframe

of the non-covalent complex but are not too reactive that they bind non-specifically to other proteins.

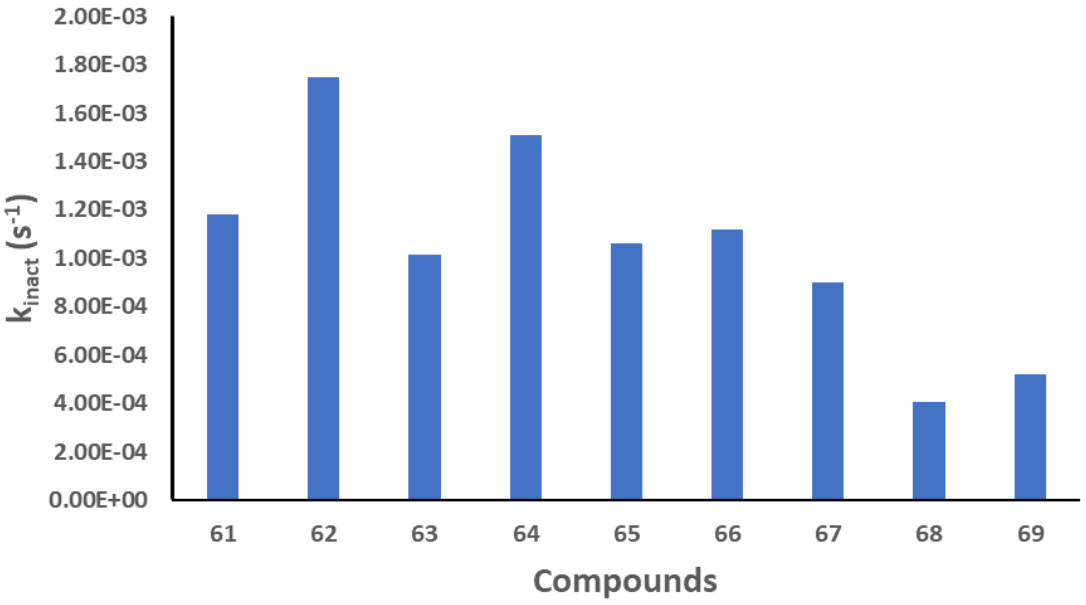


Figure 3.3. Graph comparing the k_{inact} value of the different piperazine electrophiles.

3.1.2. Cell Permeability of Piperazine Covalent Inhibitors

The cell permeability of the piperazine inhibitors was determined using a Caco-2 assay which measures the rate of transport of a compound across the Caco-2 cell line. This cell line resembles intestinal epithelial cells that form a polarised monolayer in which transport can be measured from apical to basolateral (A-B) or basolateral to apical (B-A). Compounds with a cell permeability of 10×10^{-6} cm/s are generally regarded highly cell permeable. The measured A-B permeability for piperazine acrylamide **61** was 0.76×10^{-6} cm/s so it showed poor cell permeability (Table 3.2). Similarly, piperazine chloroacetamide **62** showed very low cell permeability in this assay. The permeability from B to A was much greater than from A to B for acrylamide **61** suggesting that the compound was highly effluxed from the cell. The addition of P-glycoprotein (PgP) inhibitor did not change the permeability from B to A significantly so **61** was unlikely to be a substrate for PgP active transport. Chloroacetamide **62** had a lower permeability from B to A than **61** and there was a more

significant change in permeability (B-A) with the addition of PgP inhibitor so **62** may be a substrate for PgP. Overall, the poor cell permeability of piperazine derivatives **61** and **62** would likely result in poor cellular potency so the addition of lipophilic substituents to the piperazine ring was attempted.

	PE (A-B) ($\times 10^{-6}$ cm/s)	PE (B-A) ($\times 10^{-6}$ cm/s)	PE (B-A) (Added PgP inhibitor) ($\times 10^{-6}$ cm/s)
61	0.76	13.88	9.75
62	0.76	4.7	1.79

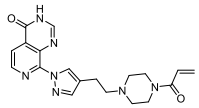
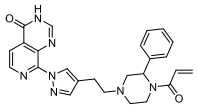
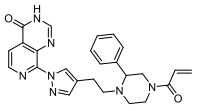
*Table 3.2. Cell permeabilities of piperazine acrylamide **61** and chloroacetamide **62** from Caco-2 assay.*

3.2. Designed Covalent Inhibitors to Improve Cell Permeability

3.2.1. Substituted-Piperazine Covalent Inhibitors

Compounds with phenyl and benzyl substituents on the piperazine ring were synthesised and tested by AlphaScreen against KDM5B (Table 3.3). The parameter (k_{inact}/K_i) was determined for all covalent inhibitors and it was found that additions to the piperazine ring resulted in a loss of potency compared to the original piperazine acrylamide **61**. 3-phenylpiperazine **72** possessed the highest k_{inact}/K_i of 5.58 x 10^2 M^{-1} s^{-1} which was approximately two times less potent than compound **61**. The value of k_{inact} for 3-phenylpiperazine **72** was lower than compound **61** which suggested that the addition of the phenyl ring slowed the rate of covalent binding to the acrylamide. The least potent compound was 2-phenylpiperazine **73** with a value of k_{inact}/K_i of 1.05 x 10^2 M^{-1} s^{-1} which could be explained through reduced non-covalent interaction of the basic nitrogen with D135. As observed in the docking of 3-phenylpiperazine **72** (Figure 2.6, Chapter 2), the addition of the benzene ring may have affected the non-covalent interactions to KDM5B through displacement of the bidentate metal coordination resulting in a less potent K_i. The displacement of the pyridopyrimidinone core was even more pronounced in the docking with 2-phenylpiperidine **73** which correlates well with its poorer IC_{50}'s and higher K_i. The acrylamide electrophile may not have been suitably positioned for covalent binding in compounds **72** and **73** compared to **61** as the k_{inact}

values were also lower. The same trend was observed with the benzyl-substituted piperazines **74**-**76** in which the non-covalent and covalent interactions were hindered resulting in lower activities against KDM5B compared to **61**. The two enantiomers **74** and **75** showed comparable K_i and k_{inact} values so the stereochemistry of the benzyl group did not affect their potency.

						
	61		**72**		**73**	
Time (min)	**IC_{50} (µM)**	**Standard Deviation (n)**	**IC_{50} (µM)**	**Standard Deviation (n)**	**IC_{50} (µM)**	**Standard Deviation (n)**
0	0.941	± 0.093 (2)	1.748	± 0.172 (2)	5.779	± 3.265 (2)
5	0.895	± 0.143 (2)	1.796	± 0.091 (2)	7.733	± 0.641 (2)
10	0.841	± 0.008 (2)	1.891	± 0.209 (2)	8.168	± 0.072 (2)
15	0.681	± 0.016 (2)	1.16	± 0.023 (2)	4.334	± 0.145 (2)
20	0.519	± 0.046 (2)	0.906	± 0.042 (2)	4.321	± 0.504 (2)
30	0.444	± 0.030 (2)	0.925	± 0.143 (2)	3.797	± 0.055 (2)
45	0.335	± 0.037 (2)	0.889	± 0.071 (2)	3.960	± 0.326 (2)
60	0.294	± 0.030 (2)	0.486	± 0.107 (2)	3.037	± 0.026 (2)
90	0.190	± 0.024 (2)	0.544	± 0.015 (2)	2.594	± 0.026 (2)
120	0.184	± 0.028 (2)	0.425	± 0.002 (2)	1.784	± 0.002 (2)
K_i (M)	$8.34 \pm 0.79 \times 10^{-7}$		$1.50 \pm 0.07 \times 10^{-6}$		$5.81 \pm 0.71 \times 10^{-6}$	
k_{inact} (s^{-1})	$1.16 \pm 0.13 \times 10^{-3}$		$8.36 \pm 0.24 \times 10^{-4}$		$6.16 \pm 1.54 \times 10^{-4}$	
k_{inact}/K_i ($M^{-1}s^{-1}$)	**$1.39 \pm 0.02 \times 10^{3}$**		**$5.58 \pm 0.12 \times 10^{2}$**		**$1.05 \pm 0.13 \times 10^{2}$**	

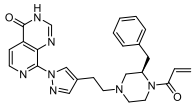
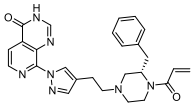
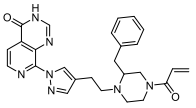
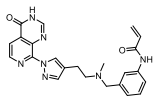
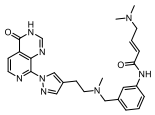
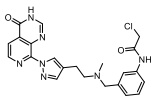
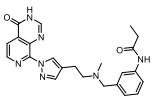
						
	74		**75**		**76**	
Time (min)	**IC_{50} (µM)**	**Standard Deviation (n)**	**IC_{50} (µM)**	**Standard Deviation (n)**	**IC_{50} (µM)**	**Standard Deviation (n)**
0	2.620	± 0.193 (2)	2.897	± 0.045 (2)	2.340	± 0.005 (2)
5	2.655	± 0.057 (2)	2.733	± 0.503 (2)	2.447	± 0.145 (2)
10	2.445	± 0.020 (2)	2.202	± 0.276 (2)	1.865	± 0.071 (2)
15	1.767	± 0.049 (2)	1.899	± 0.103 (2)	1.492	± 0.096 (2)
20	1.478	± 0.111 (2)	1.59	± 0.091 (2)	1.227	± 0.078 (2)
30	1.260	± 0.013 (2)	1.331	± 0.021 (2)	1.095	± 0.028 (2)
45	1.370	± 0.133 (2)	1.524	± 0.069 (2)	1.205	± 0.036 (2)
60	1.143	± 0.032 (2)	1.271	± 0.026 (2)	1.023	± 0.035 (2)
90	0.856	± 0.048 (2)	0.842	± 0.040 (2)	0.673	± 0.028 (2)
120	0.580	± 0.005 (2)	0.662	± 0.007 (2)	0.475	± 0.040 (2)
K_i (M)	$2.19 \pm 0.11 \times 10^{-6}$		$2.26 \pm 0.04 \times 10^{-6}$		$1.908 \pm 0.006 \times 10^{-6}$	
k_{inact} (s^{-1})	$7.49 \pm 0.42 \times 10^{-4}$		$7.04 \pm 0.41 \times 10^{-4}$		$7.94 \pm 0.27 \times 10^{-4}$	
k_{inact}/K_i ($M^{-1}s^{-1}$)	**$3.41 \pm 0.02 \times 10^{2}$**		**$3.12 \pm 0.12 \times 10^{2}$**		**$4.16 \pm 0.15 \times 10^{2}$**	

*Table 3.3. Time-dependent IC_{50}'s and their k_{inact}/K_i values for substituted piperazines **72**-**76**.*

3.2.2. Methyl Benzylamine Covalent Inhibitors

Methyl benzylamines **77**-**79** were synthesised with different covalent electrophiles such as acrylamide, chloroacetamide and dimethylamino crotonamide (Table 3.4). The non-covalent analogue **100** was also synthesised to determine the contribution of covalent binding to their potency. The methyl benzylamine compounds were more potent than the piperazine analogues with higher k_{inact}/K_i values. The most potent compound in this series was chloroacetamide **79** with a k_{inact}/K_i of 4.0 x 10^4 M^{-1} s^{-1} which was 13 times more potent than piperazine chloroacetamide **62**. Chloroacetamide **79** showed improved non-covalent binding to KDM5B with a more potent K_i of 5.4 x 10^{-8} M compared to piperazine chloroacetamide **62** (K_i = 5.6 x 10^{-7} M). Acrylamide **77** was about three times less potent (k_{inact}/K_i of 7.4 x 10^3 M^{-1} s^{-1}) than chloroacetamide **79** followed by dimethylamino crotonamide **78** with a k_{inact}/K_i value of 6.1 x 10^3 M^{-1} s^{-1}. The IC_{50} of acrylamide **77** dropped by 10-fold after incubation for 90 minutes while the IC_{50} of chloroacetamide **79** dropped 6-fold. The value of k_{inact} was also greater for acrylamide **77** and chloroacetamide **79** compared to dimethylamino crotonamide **78** which suggested that the dimethylamino crotonamide electrophile was less covalently reactive. Propanamide **100** did not show a significant change in IC_{50} after the standard pre-incubation time of 15 minutes due to the lack of covalent binding to KDM5B.

	77		**78**		**79**		**100**	
Time (min)	**IC_{50} (µM)**	**Standard Deviation (n)**	**IC_{50} (µM)**	**Standard Deviation (n)**	**IC_{50} (µM)**	**Standard Deviation (n)**	**IC_{50} (µM)**	**Standard Deviation (n)**
0	0.375	± 0.022 (2)	0.170	± 0.014 (2)	0.072	± 0.021 (4)	0.577	± 0.019 (2)
5	0.263	± 0.030 (2)	0.116	± 0.008 (2)	0.044	± 0.009 (4)	0.503	± 0.031 (2)
10	0.165	± 0.018 (2)	0.117	± 0.005 (2)	0.039	± 0.011 (4)	0.298	± 0.161 (2)
15	0.176	± 0.004 (2)	0.121	± 0.029 (2)	0.034	± 0.008 (4)	0.342	± 0.024 (2)
20	0.13	± 0.012 (2)	0.097	± 0.004 (2)	0.023	± 0.011 (4)	0.337	± 0.021 (2)
30	0.113	± 0.0005 (2)	0.082	± 0.006 (2)	0.020	± 0.009 (4)	0.324	± 0.002 (2)
45	0.086	± 0.001 (2)	0.062	± 0.001 (2)	0.016	± 0.007 (4)	0.326	± 0.025 (2)
60	0.064	± 0.004 (2)	0.062	± 0.001 (2)	0.013	± 0.003 (4)	0.335	± 0.025 (2)
90	0.047	± 0.0001 (2)	0.048	± 0.002 (2)	0.010	± 0.005 (4)	0.219	± 0.014 (2)
K_i (M)	2.89 ± 0.30 x 10^{-7}		1.24 ± 0.06 x 10^{-7}		5.36 ± 1.35 x 10^{-8}			
k_{inact} (s^{-1})	2.12 ± 0.21 x 10^{-3}		7.62 ± 0.51 x 10^{-4}		2.03 ± 0.35 x 10^{-3}			
k_{inact}/K_i (M^{-1} s^{-1})	**7.37 ± 0.04 x 10^3**		**6.13 ± 0.12 x 10^3**		**4.00 ± 1.66 x 10^4**			

*Table 3.4. Time-dependent IC_{50}'s and their k_{inact}/K_i for methyl benzylamines **77**-**79** and **100**.*

3.2.3. Cyclopentyl Benzylamine Covalent Inhibitors

A series of cyclopentyl benzylamine compounds with acrylamide, chloroacetamide and dimethylamino crotonamide electrophilic warheads were synthesized to further improve the permeability with the addition of a lipophilic cyclopentyl ring (Table 3.5). Acrylamide **80** had a k_{inact}/K_i of 4.1 x 10^3 M^{-1} s^{-1} so was less potent than corresponding methyl benzylamine acrylamide **77** (k_{inact}/K_i = 7.4 x 10^3 M^{-1} s^{-1}). Similarly, chloroacetamide **82** and dimethylamino crotonamide **81** in this series had lower k_{inact}/K_i's compared to the corresponding methyl benzylamine analogues. The values of K_i were higher in the cyclopentyl benzylamine series compared to the methyl benzylamines which suggests that the cyclopentyl group hindered the initial non-covalent binding to KDM5B despite the favourable docking pose (Figure 2.8, Chapter 2). The trend in potency of the different electrophiles followed that observed in the methyl benzylamine series with chloroacetamide **82** as the most potent electrophile, followed by the acrylamide **80** and subsequently dimethylamino crotonamide **81**. This order of electrophile reactivity correlates well with data reported in the literature.[103] This was reflected in acrylamide **80** and chloroacetamide **82** showing the greatest change in IC_{50} of approximately 10-fold from 0 to 90 minutes while dimethylamino crotonamide dropped by 6-fold. Non-covalent analogue **101** showed strong non-covalent interactions with KDM5B as the IC_{50} after the 2-hour incubation was as potent as the covalent analogues.

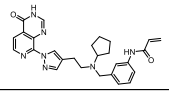
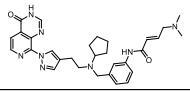
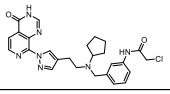
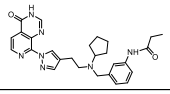
	 80		 81		 82		 101	
Time (min)	**IC_{50} (μM)**	**Standard Deviation (n)**	**IC_{50} (μM)**	**Standard Deviation (n)**	**IC_{50} (μM)**	**Standard Deviation (n)**	**IC_{50} (μM)**	**Standard Deviation (n)**
0	0.619	± 0.026 (2)	0.471	± 0.039 (2)	0.286	± 0.046 (2)	0.141	± 0.017 (2)
5	0.475	± 0.028 (2)	0.324	± 0.034 (2)	0.176	± 0.013 (2)	0.119	± 0.006 (2)
10	0.352	± 0.004 (2)	0.331	± 0.022 (2)	0.175	± 0.003 (2)	0.142	± 0.010 (2)
15	0.329	± 0.009 (2)	0.291	± 0.001 (2)	0.143	± 0.001 (2)	0.152	± 0.002 (2)
20	0.266	± 0.033 (2)	0.254	± 0.004 (2)	0.113	± 0.008 (2)	0.086	± 0.011 (2)
30	0.211	± 0.005 (2)	0.164	± 0.0004 (2)	0.074	± 0.004 (2)	0.105	± 0.007 (2)
45	0.152	± 0.002 (2)	0.131	± 0.011 (2)	0.056	± 0.0004 (2)	0.07	± 0.006 (2)
60	0.111	± 0.008 (2)	0.107	± 0.027 (2)	0.049	± 0.005 (2)	0.099	± 0.014 (2)
90	0.069	± 0.002 (2)	0.081	± 0.009 (2)	0.032	± 0.002 (2)	0.076	± 0.015 (2)
K_i (M)	$5.18 \pm 0.05 \times 10^{-7}$		$3.79 \pm 0.38 \times 10^{-7}$		$2.29 \pm 0.21 \times 10^{-7}$			
k_{inact} (s^{-1})	$2.11 \pm 0.06 \times 10^{-3}$		$1.49 \pm 0.41 \times 10^{-3}$		$2.25 \pm 0.37 \times 10^{-3}$			
k_{inact}/K_i ($M^{-1}s^{-1}$)	**$4.06 \pm 0.08 \times 10^{3}$**		**$3.89 \pm 0.70 \times 10^{3}$**		**$9.81 \pm 0.76 \times 10^{3}$**			

*Table 3.5. Time-dependent IC_{50}'s and their k_{inact}/K_i of cyclopentyl benzylamine analogues **80**-**82** and **101**.*

3.2.4. Tetrahydroisoquinoline Covalent Inhibitors

Tetrahydroisoquinoline analogues **83**-**85** showed good activities against KDM5B in the AlphaScreen assay (Table 3.6). Acrylamide **83** showed greater potency than the corresponding methyl benzylamine acrylamide **77** with a k_{inact}/K_i of 8.3 x 10^3 M^{-1} s^{-1} while chloroacetamide **84** was less potent than corresponding methyl benzylamine **79** with a k_{inact}/K_i of 2.5 x 10^3 M^{-1} s^{-1}. The order of electrophile reactivity was reversed in this series with dimethylamino crotonamide **85** as the most potent electrophile with a k_{inact}/K_i value of 1.1 x 10^4 M^{-1} s^{-1} and chloroacetamide **84** as the least potent electrophile. Despite the greater k_{inact}/K_i for dimethylamino crotonamide **85** compared to acrylamide **83**, the change in IC_{50} after incubation was much lower for dimethylamino crotonamide **85** (~3-fold) compared to acrylamide **83** (~10-fold) and the k_{inact} value was two-fold lower for **85** compared to **83**. This implied that there was a greater contribution to potency from non-covalent interactions compared to covalent interactions for dimethylamino crotonamide **85**. Non-covalent propanamide **102** also showed good potency which must be attributed to strong non-covalent interactions. The greatest contribution to potency for the tetrahydroisoquinoline series was from potent non-covalent interactions rather than fast covalent binding as the IC_{50}'s of the non-covalent **102** and the covalent inhibitors **83**-**85** were comparable.

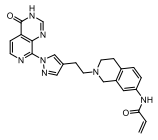
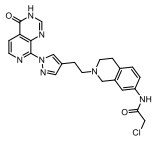
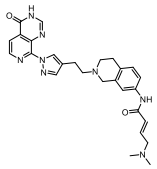
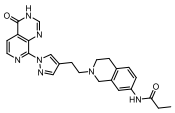
								
	83		**84**		**85**		**102**	
Time (min)	**IC_{50} (μM)**	**Standard Deviation (n)**	**IC_{50} (μM)**	**Standard Deviation (n)**	**IC_{50} (μM)**	**Standard Deviation (n)**	**IC_{50} (μM)**	**Standard Deviation (n)**
0	0.179	± 0.003 (2)	0.560	± 0.035 (2)	0.057	± 0.005 (2)	0.060	± 0.00004 (2)
5	0.150	± 0.010 (2)	0.372	± 0.087 (2)	0.044	± 0.004 (2)	0.063	± 0.001 (2)
10	0.110	± 0.011 (2)	0.394	± 0.030 (2)	0.043	± 0.004 (2)	0.060	± 0.0001 (2)
15	0.111	± 0.005 (2)	0.388	± 0.004 (2)	0.058	± 0.008 (2)	0.062	± 0.00002 (2)
20	0.105	± 0.002 (2)	0.300	± 0.067 (2)	0.035	± 0.005 (2)	0.032	± 0.002 (2)
30	0.084	± 0.001 (2)	0.221	± 0.003 (2)	0.036	± 0.001 (2)	0.035	± 0.001 (2)
45	0.064	± 0.0003 (2)	0.177	± 0.004 (2)	0.028	± 0.0001 (2)	0.027	± 0.003 (2)
60	0.054	± 0.001 (2)	0.169	± 0.002 (2)	0.027	± 0.001 (2)	0.045	± 0.002 (2)
90	0.036	± 0.002 (2)	0.126	± 0.004 (2)	0.020	± 0.002 (2)	0.029	± 0.0006 (2)
K_i (M)	$1.45 \pm 0.07 \times 10^{-7}$		$4.25 \pm 0.58 \times 10^{-7}$		$4.47 \pm 0.57 \times 10^{-8}$			
k_{inact} (s^{-1})	$1.20 \pm 0.05 \times 10^{-3}$		$1.05 \pm 0.20 \times 10^{-3}$		$5.14 \pm 1.31 \times 10^{-4}$			
k_{inact}/K_i ($M^{-1} s^{-1}$)	**$8.28 \pm 0.05 \times 10^{3}$**		**$2.46 \pm 0.13 \times 10^{3}$**		**$1.14 \pm 0.15 \times 10^{4}$**			

*Table 3.6. Time-dependent IC_{50}'s against KDM5B and their k_{inact}/K_i of tetrahydroisoquinoline analogues **83**-**85** and **102**.*

3.2.5. Cell Permeability of Analogues

Methyl benzylamine acrylamide **77** and cyclopentyl benzylamine acrylamide **80** showed a small improvement in cell permeability compared to piperazine acrylamide **61** of 0.76 x 10^{-6} cm/s however the compounds were still poorly cell permeable (Table 3.7). Tetrahydroisoquinoline acrylamide **83** showed a lower cell permeability of 0.76 x 10^{-6} cm/s. As with the piperazine analogue, the permeability of the compounds was greater from B to A resulting in a high efflux ratio. The addition of a PgP inhibitor resulted in an insignificant reduction in permeability from B to A so the compounds were unlikely actively transported by PgP. Cyclopentyl benzylamine **80** and tetrahydroisoquinoline **83** were more highly effluxed than methyl benzylamine **77**.

Overall, there was a very marginal improvement in cell permeability however the compounds were still highly effluxed. It was hoped that enough compound would enter the cell to show cellular activity against KDM5B.

	PE (A-B) (x 10^{-6} cm/s)	PE (B-A) (x 10^{-6} cm/s)	PE (B-A) (Added PgP inhibitor) (x 10^{-6} cm/s)
77	1.52	15.9	11.0
80	1.52	51.9	38.9
83	0.76	21.5	17.9

*Table 3.7. Cell permeability of analogues **77**, **80** and **83** using Caco-2 assay.*

3.3. Determination of Most Potent Covalent Inhibitor Based on Their k_{inact}/K_i values

The different scaffolds including piperazine, methyl benzylamine, cyclopentyl benzylamine and tetrahydroisoquinoline inhibitors were compared in terms of non-covalent interactions with KDM5B (Figure 3.4). Inhibitors with an acrylamide electrophilic warhead in each series were plotted against their K_i values. Piperazine **61** showed the weakest non-covalent inhibition as it had the largest K_i value of 8.3 x 10^{-7} M while tetrahydroisoquinoline **83** showed the most potent non-covalent interactions with the lowest K_i of 1.5 x 10^{-7} M. Cyclopentyl benzylamine **80** had a higher K_i of 5.2 x 10^{-7} M compared to methyl benzylamine **77** with a K_i of 2.9 x 10^{-7} M so the addition of the cyclopentylamine may have been unfavourable for non-covalent binding. Overall, the K_i's of the covalent inhibitors were not as potent as the published covalent EGFR inhibitor however the binding affinities of published non-covalent KDM5 inhibitors are generally less potent than kinase inhibitors. The addition of covalent reactivity should improve the potency of the current KDM5 inhibitors.

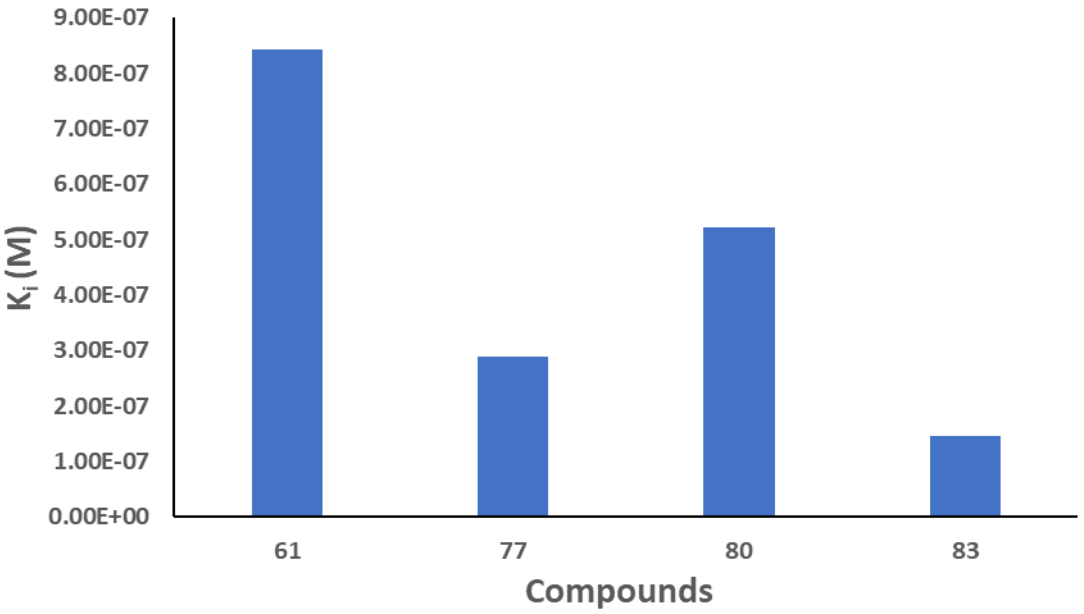


Figure 3.4. Comparison of K_i's for different series.

All the inhibitors were ranked by their combined non-covalent and covalent potency through plotting their k_{inact}/K_i values (Figure 3.5). The most potent compound was methyl benzylamine chloroacetamide **79** with a significantly greater k_{inact}/K_i value of 4.0 x 10^4 M^{-1} s^{-1}. All methyl benzylamine analogues with different electrophilic warheads showed the highest k_{inact}/K_i values, followed by the tetrahydroisoquinoline inhibitors. The cyclopentyl benzylamines **80-82** were all less potent than their corresponding methyl benzylamine. The piperazine analogues **61**-**76** were much less potent compared to the other scaffolds which was likely a combination of less favourable non-covalent and covalent interactions to KDM5B. This correlates with reported experimental methods that show electrophiles directly attached to saturated rings are less covalently reactive than to aromatic rings.[104] The most potent inhibitors were the methyl benzylamines **77-79** and the tetrahydroisoquinoline analogues **83**-**85** which were further profiled for KDM selectivity, 2-OG competition and cellular activity.

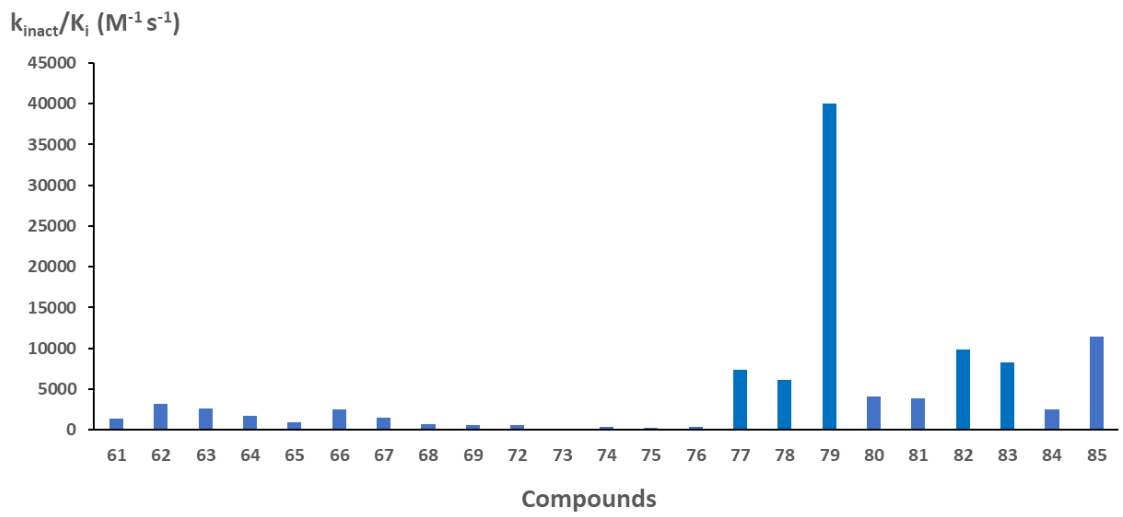


Figure 3.5. Comparison of k_{inact}/K_i for all covalent inhibitors.

3.4. KDM Selectivity Determined Through AlphaScreen

The selected compounds were tested for selectivity over other KDM5 (JARID1) proteins as well as other KDM subfamilies (Table 3.8). IC_{50}'s were measured after pre-incubation of inhibitors with KDM proteins for 2 hours which was the time point at which the IC_{50} values had been shown to plateau. All compounds were >100-fold selective over KDM2A (FBXL11) and KDM3A (JMJD1A) and >10-fold selective over KDM5C. For most compounds, there was insignificant activity on KDM6B (JMJD3) with >1000-fold selectivity. Compounds **79** and **84** showed some activity on KDM6B however both exhibited >30-fold selectivity. The poorer activity for KDM5C was attributed to the lack of covalent binding of the methyl benzylamines (Chapter 4). Methyl benzylamine dimethylamino crotonamide **78** showed >10-fold selectivity over KDM5A and KDM5D unlike the other methyl benzylamines which were almost equipotent. The poor selectivity of acrylamide **77** and chloroacetamide **79** over KDM5A and KDM5D may have been caused by non-specific covalent binding to another cysteine while dimethylamino crotonamide **78** was less reactive. Some activity was observed against the KDM4 subfamily with comparable IC_{50}'s across the different isoforms (KDM4B, KDM4C and KDM4D) in the micromolar range. Most of the inhibitors showed >30-fold

selectivity over KDM4 proteins which was much greater than the published non-covalent 8-pyridopyrimidinone **14**, an equipotent inhibitor of KDM4 and KDM5. Covalent binding to KDM5B contributed to the improved selectivity over KDM4 in the 8-pyridopyrimidinone series which was confirmed through MS-labelling experiments in Chapter 4.

	IC_{50} (μM) (2 hour incubation)									
	KDM5B	**KDM5A**	**KDM5C**	**KDM5D**	**KDM2A**	**KDM3A**	**KDM4A**	**KDM4B**	**KDM4C**	**KDM6B**
77	0.032	0.026	0.780	0.081	3.7	8.2	1.2	1.1	ND	>33
78	0.048	0.656	4.6	0.694	>50	>33	2.4	1.9	2.3	>100
79	0.013	0.030	0.394	0.047	4.4	2.6	0.402	0.631	0.300	0.678
83	0.062	0.050	0.603	0.060	>10	5.9	ND	ND	ND	ND
84	0.126	0.215	2.135	0.304	10.5	11.1	2.4	3.2	1.5	4.8
85	0.021	0.042	0.560	0.072	8.5	5.1	0.829	0.704	0.755	>33

Table 3.8. IC_{50}'s of compounds against other KDM proteins measured by AlphaScreen.

3.5. 2-OG Competition Assay

Published non-covalent KDM5 inhibitors including the pyridopyrimidinone series are highly 2-OG competitive which is thought to be responsible for their poor cellular activity. It was hypothesised that the irreversibility of the covalent inhibitors to KDM5B would reduce competition from the cosubstrate 2-OG compared to the non-covalent inhibitors. The compounds were incubated for 2 hours to ensure complete covalent binding to KDM5B and IC_{50}'s were measured by AlphaScreen with different concentrations of 2-OG from 0.5 μM to 1000 μM (Figure 3.6).

Tetrahydroisoquinoline dimethylamino crotonamide **85** showed an approximately 500-fold drop in IC_{50} from low to high 2-OG concentrations with an IC_{50} in the micromolar range at the highest 2-OG concentration of 1000 μM. Therefore, **85** was significantly 2-OG competitive and would likely exhibit poor cellular activity.

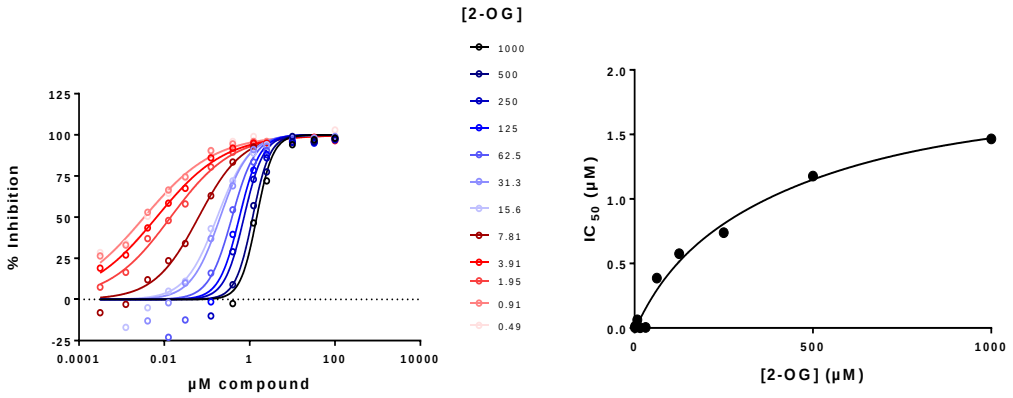


*Figure 3.6. 2-OG competition assay with tetrahydroisoquinoline dimethylamino crotonamide **85**.*

Methyl benzylamine dimethylamino crotonamide **78** showed a 20-fold drop in IC_{50} with increasing 2-OG concentration up to 1000 µM (Figure 3.7). This compound was less 2-OG competitive than with corresponding tetrahydroisoquinoline **85** however the IC_{50} still reached micromolar range at the top 2-OG concentration. As a result, **78** would also likely exhibit poor activity in the cellular assay.

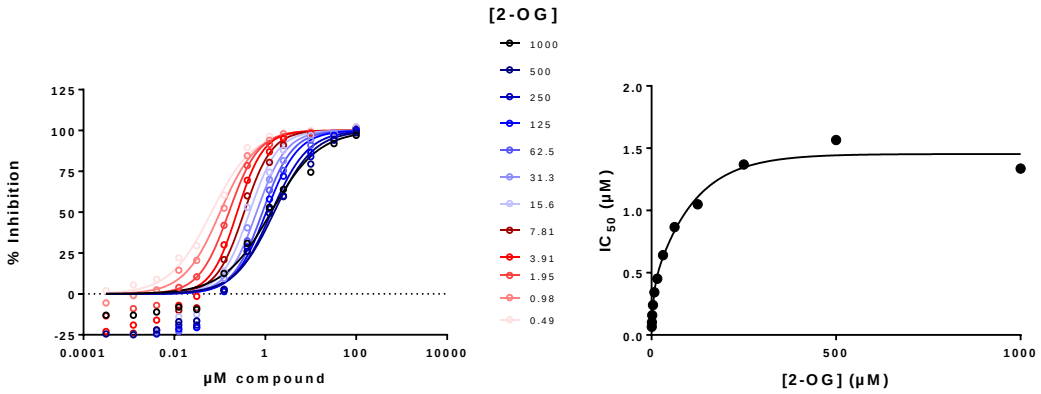


*Figure 3.7. 2-OG competition assay with methyl benzylamine dimethylamino crotonamide **78**.*

Methyl benzylamine chloroacetamide **79** showed a 31-fold drop in potency however a potent IC_{50} of 94 nM was still observed at the top 2-OG concentration of 1000 µM (Figure 3.8). Chloroacetamide **79** was therefore more 2-OG competitive than dimethylamino crotonamide **78** however it showed greater activity at the higher 2-OG concentrations.

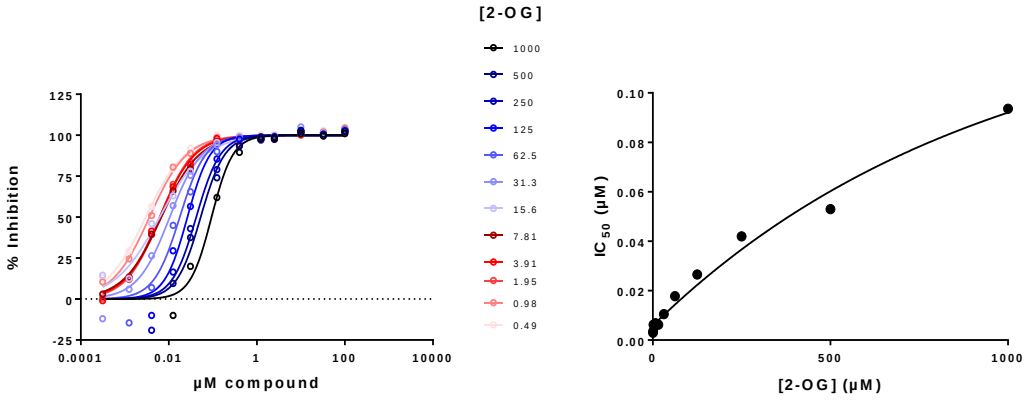


*Figure 3.8. 2-OG competition assay with methyl benzylamine chloroacetamide **79**.*

Similarly, methyl benzylamine acrylamide **77** was also tested for 2-OG competition (Figure 3.9). **77** showed some 2-OG competition with an IC_{50} drop of around 18-fold with a potent IC_{50} of 111 nM at 1000 µM 2-OG concentration. Overall, the methyl benzylamine analogues were less competed by 2-OG than tetrahydroisoquinoline **85** which was likely due to their greater contribution to potency from covalent inhibition. Acrylamide **77** was the best electrophile within the methyl benzylamines showing the least significant drop in IC_{50} with 2-OG concentration of 18-fold.

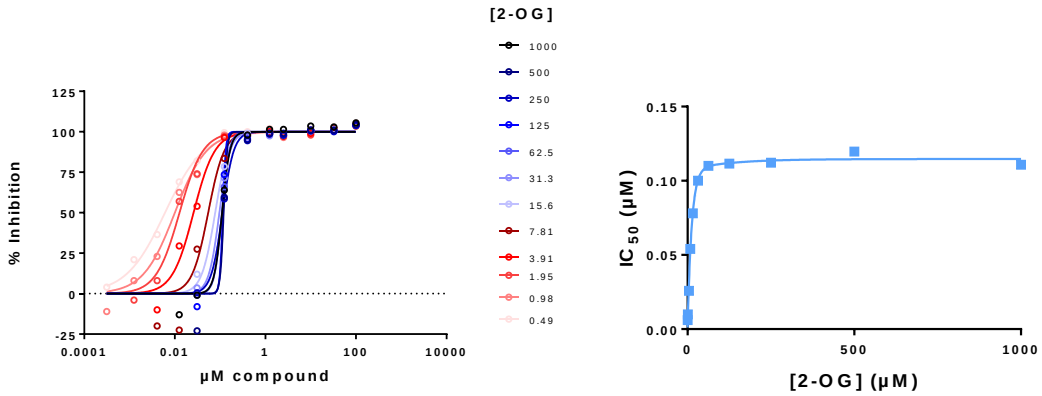


*Figure 3.9. 2-OG competition assay with methyl benzylamine acrylamide **77**.*

The published non-covalent variant **14** was tested in the 2-OG competition assay to compare with the covalent inhibitors (Figure 3.10). There was an approximately 500-fold drop in IC_{50} from 0.5 µM to 1000 µM 2-OG concentration which confirmed that **14** was more significantly competed by 2-OG than the covalent **77**.

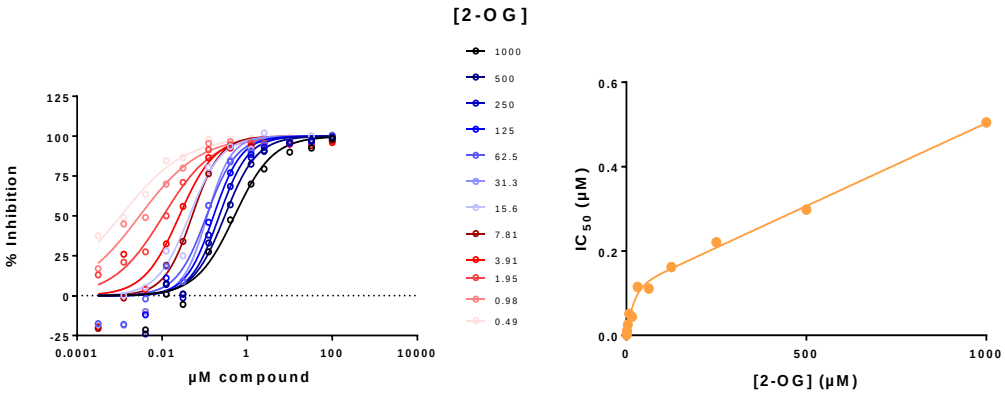


*Figure 3.10. 2-OG competition assay with **14**.*

The graph below compares the change in IC_{50} with 2-OG concentration for acrylamide **77** and the non-covalent variant **14** (Figure 3.11). Non-covalent **14** exhibited significant 2-OG competition with 28 times greater drop in IC_{50} than acrylamide **77**. Covalent inhibitor **77** showed a loss of potency up to 31 μM 2-OG and the IC_{50} remained constant at the higher 2-OG concentrations while non-covalent **14** IC_{50}'s increased linearly at the higher 2-OG concentrations. The graph for **77** levelled off due to reaching equilibrium while **14** remained 2-OG competitive with increasing concentrations of 2-OG. Methyl benzylamine acrylamide **77** was significantly less 2-OG competitive than non-covalent **14** which could translate into greater cellular activities.

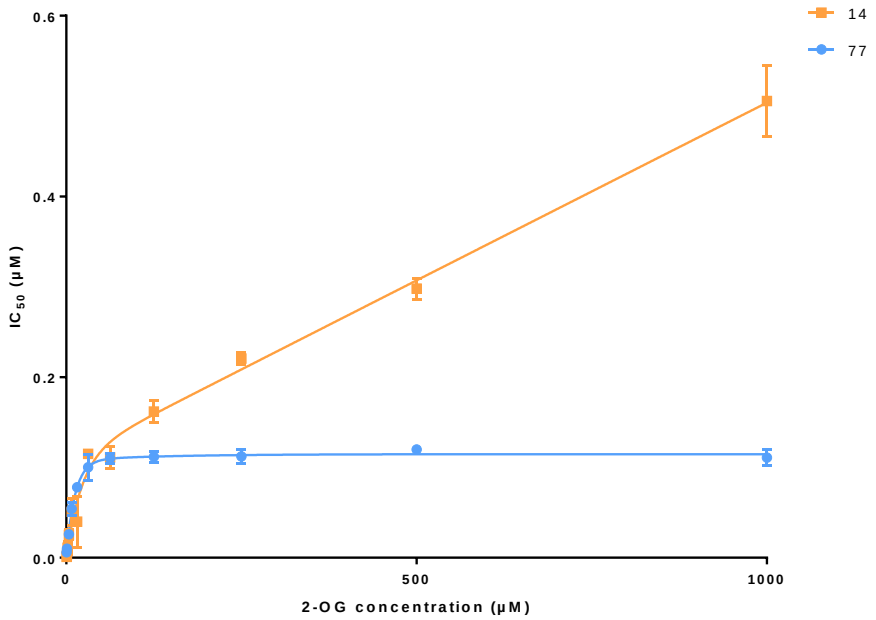


*Figure 3.11. Change in IC_{50} with 2-OG concentration for covalent **77** (blue) and non-covalent **14** (orange).*

3.6. Cellular Activity by Immunofluorescence Assay

The covalent inhibitors were profiled for cellular activity in an immunofluorescence assay which measures the increase in H3K4me3 mark upon incubation of the compounds with human cervical carcinoma HeLa cells transfected with KDM5B (Figure 3.13).[40] The dotted lines represent mutant KDM5B which is an inactive form of KDM5B and cannot demethylate H3K4me3 so the levels of H3K4me3 should remain constant. KDOAM-25 **4**, a known cell-active inhibitor of KDM5B, was included as a positive control. The most potent covalent inhibitor was identified as methyl benzylamine dimethylamino crotonamide **78** with an IC_{50} of 2 µM with no observed cytotoxicity however the levels of H3K4me3 for the wild type do not reach the levels of the mutant so the normalised curve is inconclusive (Figure 3.12, Figure 3.13). Methyl benzylamine chloroacetamide **79** was the second most potent with an IC_{50} of 22 µM with a good normalised curve for inhibition and the compound did not show a significant change in cell number. Methyl benzylamine acrylamide **77** showed cellular activity in the 10-100 µM range with some cytotoxicity at the higher concentration range. The cyclopentyl analogues **80** and **82** were cytotoxic in the concentration range of potency so cellular activity was unlikely due to inhibition of KDM5B. Tetrahydroisoquinoline dimethylamino crotonamide **85** showed some activity in the high concentration range (>100 µM) with a steady cell count at the range of concentrations tested. Although the covalent inhibitors were less 2-OG competitive, there was a considerable loss in potency from the biochemical to the cellular assay. The poor cell permeability of the compounds due to the basic nitrogen could explain the low cellular activity. There was also some concern about the robustness of the immunofluorescence assay as in all cases the mutant KDM5B showed an increase in H3K4me3 which should not be observed.

Compound	IC_{50} (µM)
77	74
78	2
79	22

*Figure 3.12. IC_{50}'s of **77**, **78** and **79** in immunofluorescence assay.*

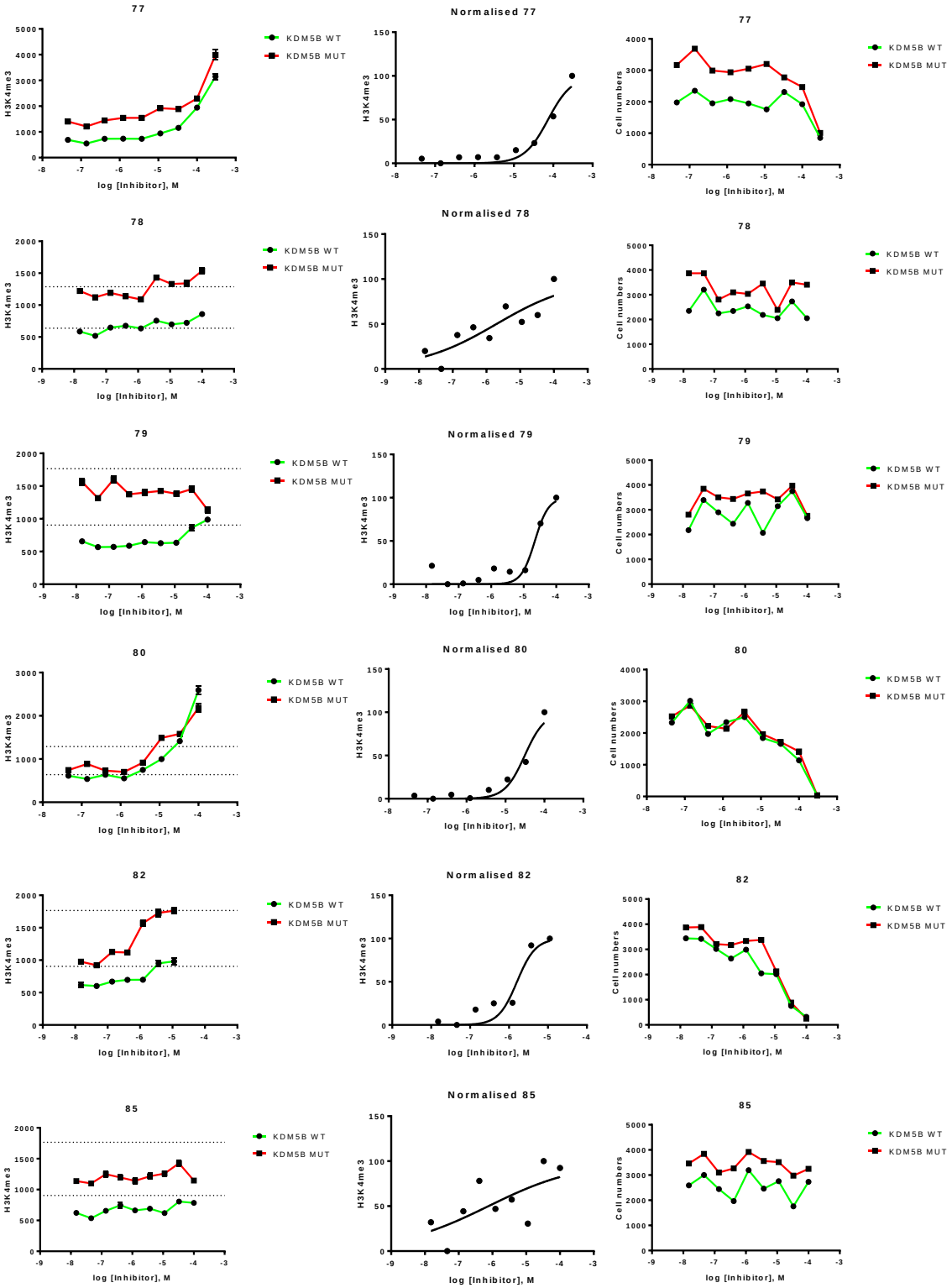


Figure 3.13. IC_{50} curves for covalent inhibitors in cellular immunofluorescence assay and cell number count (right).

3.7. Target engagement of covalent inhibitors with KDM5B using the NanoBRET assay

As the cellular activities measured using the immunofluorescence assay were inconclusive, another assay was attempted to prove target engagement of the covalent inhibitors with KDM5B in the cell. NanoBRET is an assay developed by Promega Corporation to understand the dynamic interaction of proteins in the cell.[105] This assay was adapted from bioluminescence resonance energy transfer (BRET) which is also a proximity-based assay that measures energy transfer from a bioluminescent protein donor to a fluorescent protein acceptor. A NanoLuc Luciferase fusion protein is used as an energy donor. The advantages of NanoBRET over BRET are the greater light intensity and spectral resolution which results in improved detection sensitivity.

NanoBRET has been utilised to quantify the intracellular engagement of inhibitors for HDACs, bromodomains and kinases.[106] In this approach, the target protein is genetically fused with a NanoLuc luciferase and a tool compound is utilised as a cell-permeable fluorescent tracer. Binding of the fluorescence tracer to the intracellular target results in BRET. A compound that can bind and compete with the tracer for the binding site will cause a reduction in BRET.

A cell permeable fluorescent tracer of KDM5 was developed by another group member comprising of the cyanopyrazole scaffold and a fluorescent organic dye NanoBRET$_{590}$® (Figure 3.14). The tracer binds to the KDM5B fused NanoLuc luciferase protein but not to other KDM subfamilies. The covalent inhibitors could then be quantified in terms of their ability to displace the tracer and engage with KDM5B protein fused with NanoLuc luciferase. The tracer (2 µM) was incubated with transfected human embryonic kidney 293 (HEK293) cells followed by serial dilutions of compounds **61**, **77**-**79** and **85** which were incubated for 5 hours and IC$_{50}$'s were determined using the BRET ratio from donor to acceptor.

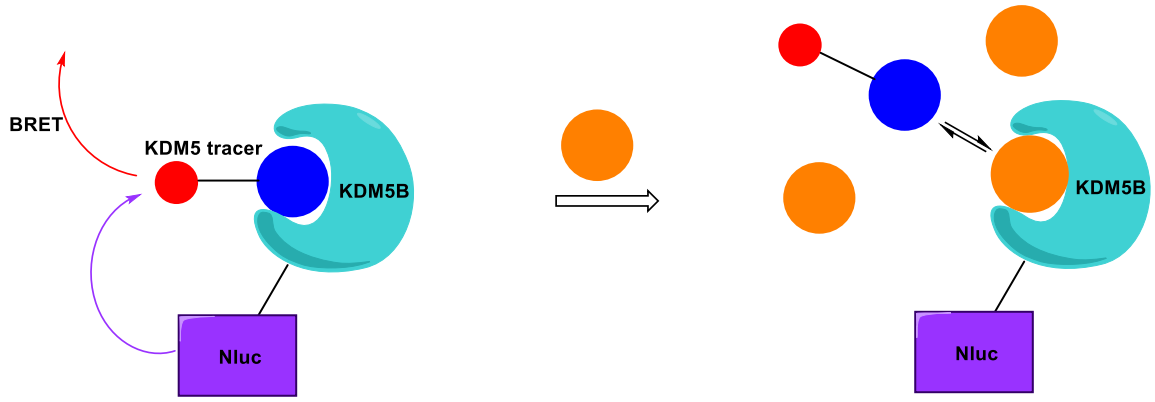


Figure 3.14. Schematic showing NanoBRET intracellular target engagement assay and structure of KDM5 tracer comprising cyanopyrazole core and NanoBRET fluorescent dye.

Methylbenzylamine acrylamide **77** and chloroacetamide **79** were active in the NanoBRET assay with IC_{50}'s of 19.9 µM and 12.8 µM respectively (Table 3.9). Dimethylamino crotonamide **78** was less potent than the other electrophiles with an IC_{50} of 67.1 µM. Despite showing a lower k_{inact}/K_i value compared to the methylbenzylamines in the biochemical assay, piperazine acrylamide **61** showed comparable cellular activity against KDM5B. Tetrahydroisoquinoline dimethylamino crotonamide **85** was among the most potent despite showing poor activity in the immunofluorescence assay.

	IC_{50} (µM)
14	12.3 ± 2.0 (2)
61	21.6
77	19.9 ± 13.4 (2)
78	67.1
79	12.8
85	20.5 ± 23.1 (2)

Table 3.9. KDM5B nanoBRET IC_{50}'s of covalent inhibitors (average of 2 experiments).

Non-covalent inhibitor **14** was also tested in the NanoBRET assay which showed a comparable IC_{50} to acrylamide **77** (Figure 3.15). It was expected that acrylamide **77** would show improved cellular activity as it was less competed by 2-OG than non-covalent **14**. Acrylamide **77** showed much lower cell permeability (1.52 x 10^{-6} cm/s) in the Caco-2 assay than compound **14** (11.8 x 10^{-6} cm/s) which could explain the lack of improved cellular potency.

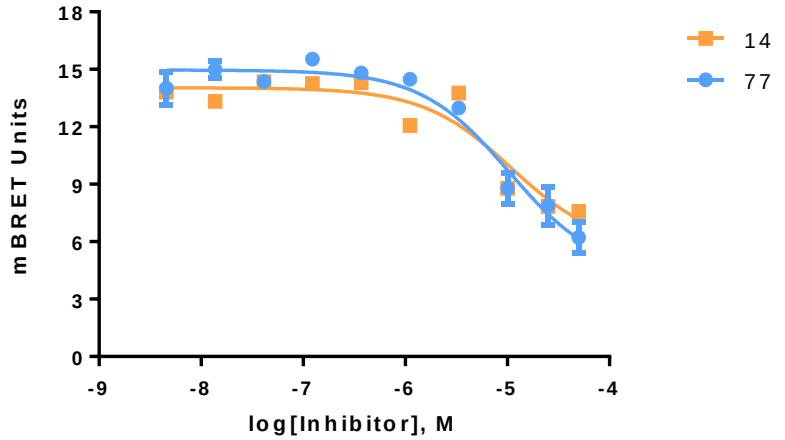


*Figure 3.15. IC_{50} curve of **14** and **77** in KDM5B nanoBRET assay.*

Overall, NanoBRET is a more reliable assay than immunofluorescence-based assay as it reveals the binding characteristics of the compounds in intact cells and is therefore a better proof of target engagement with KDM5.

3.8. Cytotoxicity assays of compounds

Covalent inhibitors, tested in the NanoBRET assay, were incubated at different concentrations with human embryonic kidney HEK293 cells for 72 hours and the cell viability was measured using a CellTiter-Glo® Luminescent assay. This assay quantifies the ATP present as an indicator of metabolically active cells.

In the piperazine series, compound **61** showed no cell death at concentrations up to 50 µM. Tetrahydroisoquinoline **85** also showed no cell death. In the methylbenzylamine series, acrylamide **77** and dimethylamino crotonamide **78** were not cytotoxic while chloroacetamide **79** showed a significant drop in cell count even at low concentrations. Therefore, acrylamide **77** was the optimum covalent inhibitor as it was one of the most potent inhibitors in the cellular assays and was not cytotoxic.

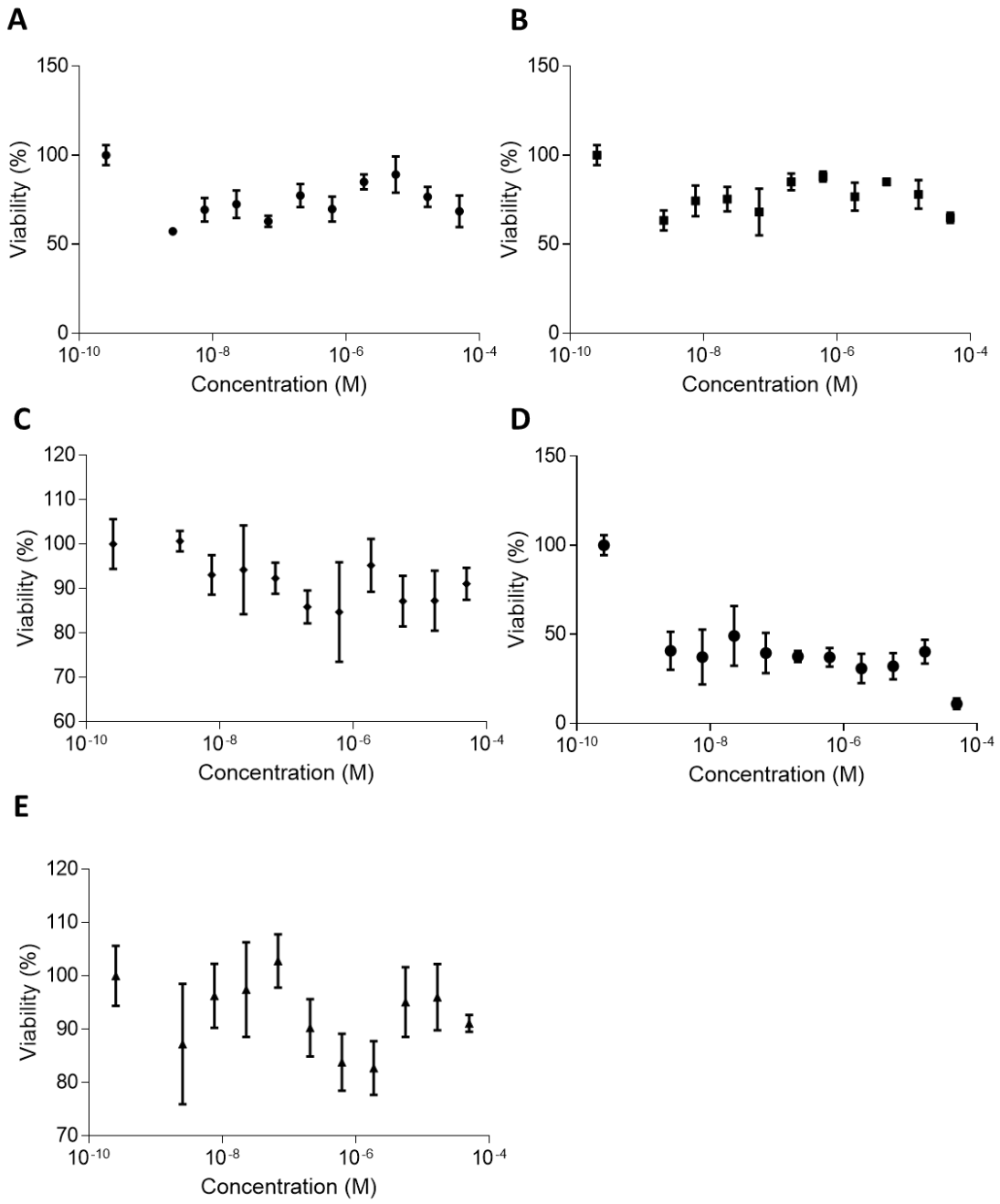


*Figure 3.16. Cell viability assays after incubation of cells with compounds; A) **61**, B) **77**, C) **78**, D) **79**, E) **85**.*

3.9. Quantification of H3K4me3 Levels by ChIP-Seq

Immunofluorescence-based assays are frequently used to detect changes in the levels of H3K4me3 levels as a measure of KDM5 activity however cytotoxicity of compounds can also affect these global changes. Therefore, proof of on-target cellular activity of compounds with endogenous KDM5 was attempted using ChIP-Seq which is a method that combines chromatin

immunoprecipitation (ChIP) with DNA sequencing (Seq). Acrylamide **77** was incubated with human embryonic kidney HEK293 cells at 2 µM for both 24 hours and 72 hours and the global levels of H3K4me3 were measured. A Chip-Rx strategy[107] was used in which SF9 insect cells were spiked in as an internal control prior to the pull-down to reliably quantify the changes in H3K4me3 marks at specific genomic loci. After sequencing and normalisation with the internal control, ChIP-Seq plots were plotted for H3K4me3 marks with both **77** (green) and DMSO control (purple) across the transcriptional start site (TSS) of all genes. (Figure 3.17).

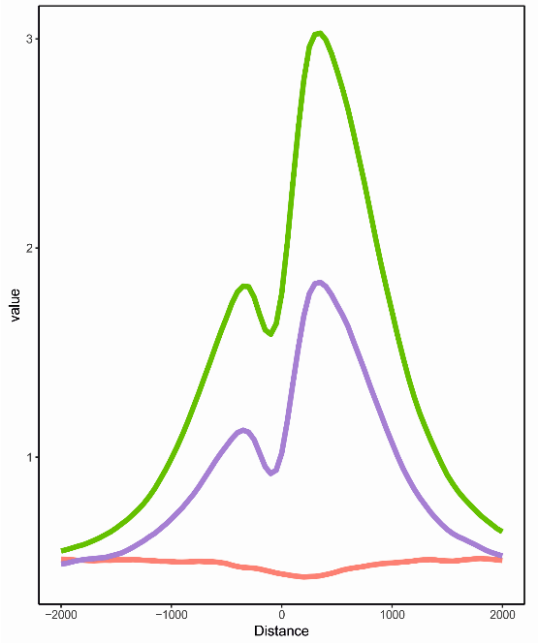


Figure 3.17. ChipSeq plots of H3K4me3 marks with input sample (red), 77 (green) and DMSO (purple) after 72 hours.

After 72 hours, the H3K4me3 levels with **77** were twice that of the control. As increased levels of H3K4me3 is a measure of KDM5 inhibition, covalent inhibitor **77** was likely engaging with and inhibiting the action of KDM5 in the cellular environment.

3.10. Conclusion

In this chapter, piperazine analogues with different electrophilic warheads were tested to determine the best electrophile for covalent reactivity. Acrylamide **61**, chloroacetamide **62**, propiolamide **63** and dimethylamino crotonamide **64** were the most potent covalent electrophiles with the highest k_{inact}/K_i while the halonitrobenzenes were less potent so were slower to react covalently. Piperazine covalent inhibitors showed good potency in the enzymatic assays however the compounds were poorly cell permeable. Compounds with higher clogD values were designed to improve their cell permeability and therefore their cellular potencies. The addition of phenyl and benzyl groups to the piperazine at position 2 and 3 in **72**-**76** was less tolerated than parent piperazine acrylamide **61** resulting in lower k_{inact}/K_i values.

Replacement of the piperazine ring led to methyl benzylamine, cyclopentyl benzylamine and tetrahydroisoquinoline-based inhibitors which were active against KDM5B. The most potent compound, in terms of the kinetic parameter k_{inact}/K_i, was methyl benzylamine chloroacetamide **79** with the highest value of 4.0×10^4 M^{-1} s^{-1}. All the methyl benzylamine inhibitors **77**-**79** were potent in the biochemical assay with high values of k_{inact}/K_i while cyclopentyl inhibitors **80**-**82** were generally less potent than their corresponding methyl benzylamines. Tetrahydroisoquinolines **83**-**85** also showed good activities against KDM5B in the biochemical assay. In terms of selectivity over other KDMs, methyl benzylamines and tetrahydroisoquinolines showed good selectivity over KDM2A, KDM3A and KDM6B. Improved selectivity (>30-fold) was demonstrated over KDM4 family compared to published 8-pyridopyrimidinone inhibitors. Methyl benzylamine dimethylamino crotonamide **78** was the most selective showing some selectivity over different KDM5 isoforms while the other analogues showed comparable selectivity profiles.

Despite showing the greatest covalent binding in biochemical screens, chloroacetamide **79** was cytotoxic so cellular activity was unlikely due to inhibition of KDM5B. Methylbenzylamine acrylamide **77** showed an increase in H3K4me3 levels in the immunofluorescence assay and was

not cytotoxic. Target engagement of covalent inhibitor **77** with KDM5B was confirmed using nanoBRET. Acrylamide **77** showed a comparable IC_{50} to non-covalent **14** which could be explained by its lower cell permeability. The ability of acrylamide **77** to increase global levels of H3K4me3 in cells was demonstrated through ChIP-Seq experiments. Acrylamide **77** was also the least competed by 2-OG within the methyl benzylamine series showing an 18-fold drop in IC_{50} from low (0.5 μM) to high 2-OG (1000 μM) concentrations and was significantly less competed by 2-OG than non-covalent **14**. Considering all the data, methyl benzylamine acrylamide **77** was the best covalent inhibitor as it exhibited moderate cellular activity and reduced competition by 2-OG. A pull-down analogue was designed and synthesised with the methyl benzylamine core scaffold and acrylamide electrophilic warhead to further confirm engagement with KDM5B in the cell.

Chapter 4. Covalent Binding of Inhibitors

To confirm that the inhibitors were binding covalently to KDM5B, MS-labelling experiments were carried out to identify protein peaks relating to the addition of the compound.

4.1. Covalent Binding of Piperazine Inhibitors

10 µM acrylamide **61** and chloroacetamide **62** were incubated with 1 µM KDM5B at 37 °C for 30 minutes and injected into a RapidFire-MS to determine the protein mass (Figure 4.1). If the thiol of a cysteine in KDM5B reacts via Michael addition with acrylamide **61**, the protein mass should increase by the compounds molecular weight (Δm/z = 379). Nucleophilic substitution of a cysteine residue with chloroacetamide **62** should result in an increase in protein mass from the addition of the compounds molecular weight and loss of HCl (Δm/z = 365).

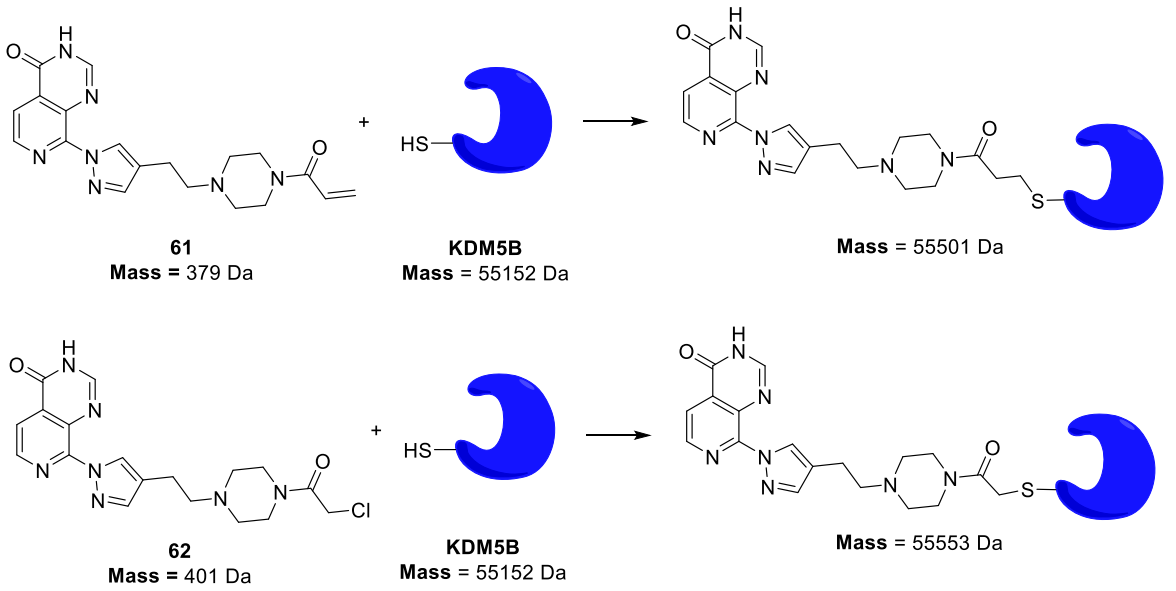


*Figure 4.1. Schematic showing covalent modification upon incubation of **61** and **62** with KDM5B.*

Incubation of chloroacetamide **62** with KDM5B resulted in full modification of the protein with the correct m/z shift (Figure 4.2). The protein was deconvoluted as a cluster of peaks due to different oxidation states and salt adducts. Similarly, incubation of acrylamide **61** with KDM5B resulted in

mainly protein peaks relating to covalent attachment of the compound and a small peak relating to the unmodified protein (Figure 4.3). Both compounds were therefore covalent binders to KDM5B. No protein peaks were observed under these conditions due to the covalent attachment of two molecules of the compounds so were binding specifically to one cysteine residue.

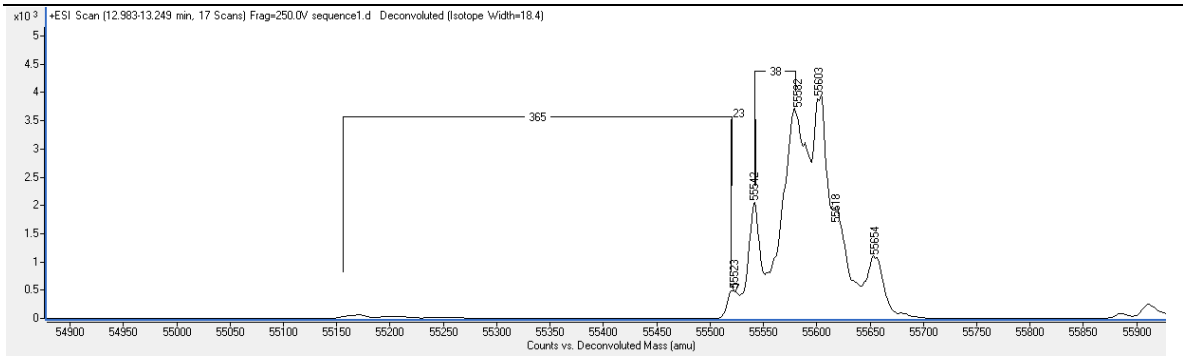


*Figure 4.2. MS showing covalent binding of chloroacetamide **62** in KDM5B*

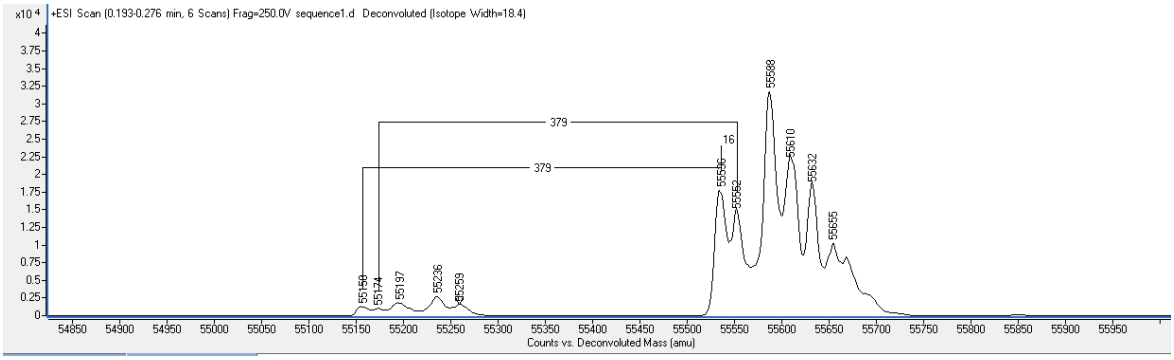


*Figure 4.3. MS showing covalent binding of acrylamide **61** in KDM5B.*

4.2. Kinetics of Covalent Binding of Acrylamide 61 and Chloroacetamide 62

The kinetics of covalent binding is an important parameter for covalent inhibitors as the rate must be fast enough for the covalent bond to form prior to the dissociation of the non-covalent complex but not too reactive resulting in non-specific binding to other proteins. The covalent binding kinetics of **61** and **62** were determined by calculating the degree of modification over time, with compound concentration in large excess (30-100 fold) of protein concentration and incubated at room temperature. As the RapidFire-MS is limited in its rate of injection, the incubation was carried out at room temperature rather than 37 °C as above to slow the rate of covalent binding. The

percentage of modified KDM5B over time was determined through integration of the unmodified and modified KDM5B protein peaks. Incubation of KDM5B with chloroacetamide **62** resulted in full modification after 90 minutes (Figure 4.4). The protein MS revealed single modification as well as some double modification suggesting that the compound was binding non-specifically to another residue. Incubation of KDM5B with acrylamide **61** resulted in maximum modification of 80% after 90 minutes (Figure 4.5). There was only a peak relating to single modification of KDM5B so acrylamide **61** was binding specifically.

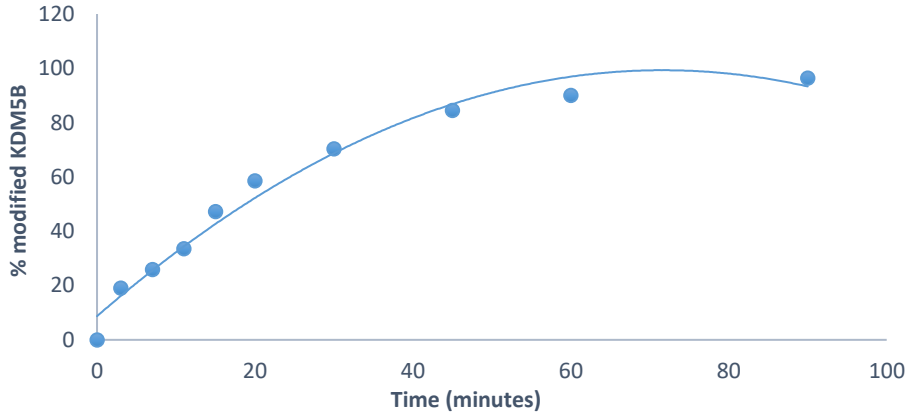


*Figure 4.4. Changes in the percentage of modified KDM5B after incubation with chloroacetamide **62** over time (mins).*

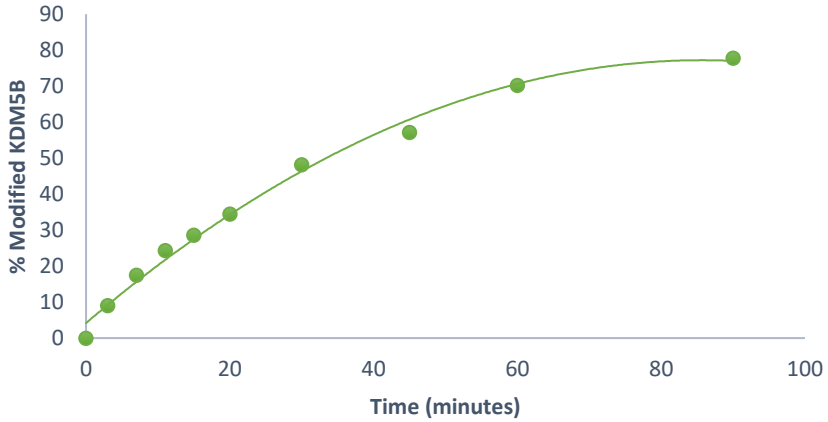


*Figure 4.5. Changes in the percentage of modified KDM5B after incubation with acrylamide **61** over time (mins).*

As the compound was in large excess, the rate equation could be assumed to be first order. By plotting the natural logarithm function of the unmodified protein concentration at a certain time over initial protein concentration, the rate constant can be determined from the gradient. The rate constant was calculated to be 6.03 x 10^{-4} s^{-1} and 4.03 x 10^{-4} s^{-1} for **62** and **61** respectively (Figure 4.6 and Figure 4.7). The half-life for KDM5B under both conditions was approximately 20 minutes. Overall, both compounds showed fast covalent binding kinetics.

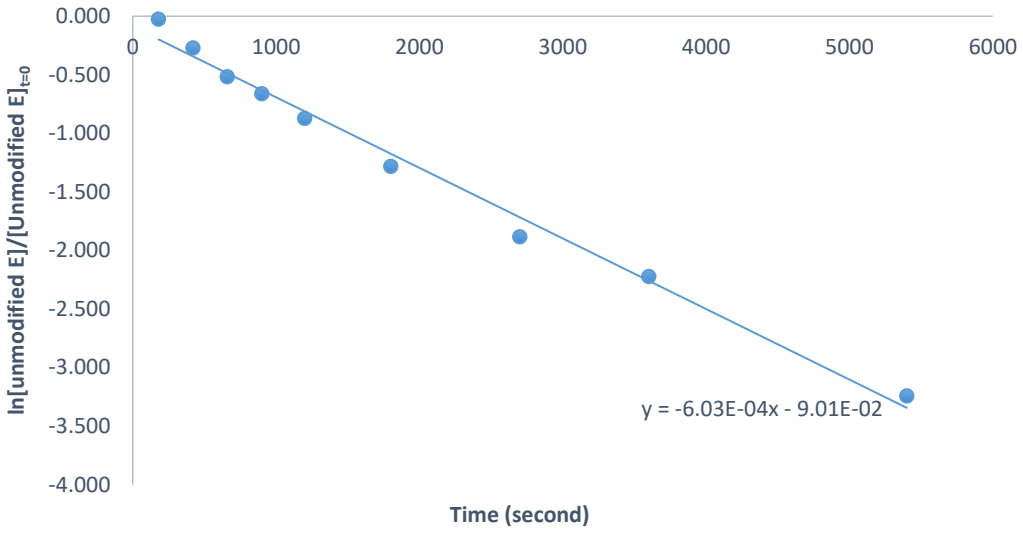


*Figure 4.6. ln[unmodified E]/[Unmodified E]$_{t=0}$ versus time for **62**.*

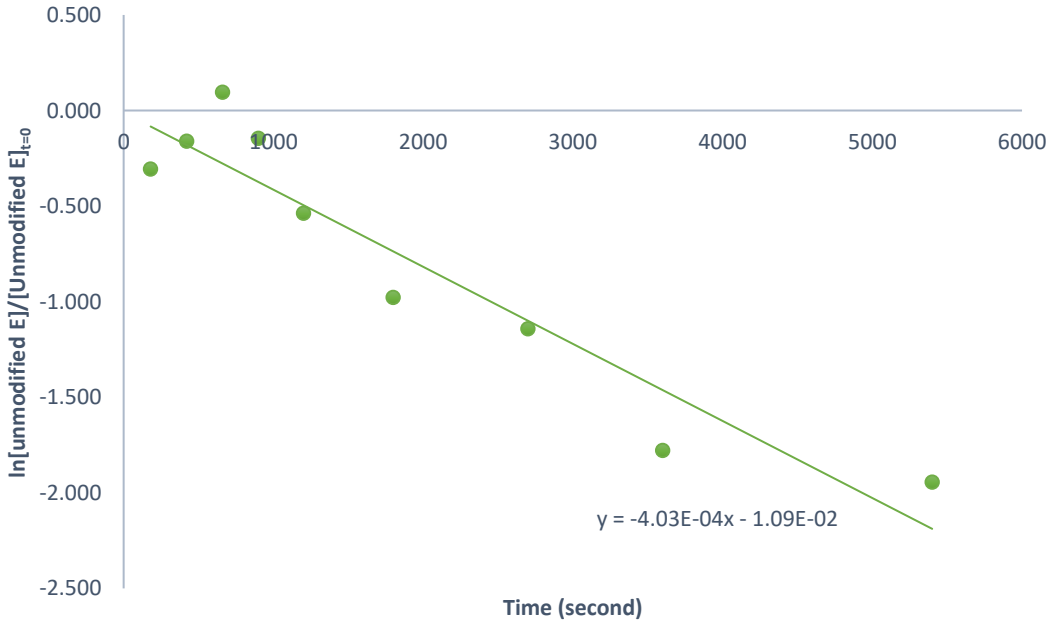


*Figure 4.7. ln[unmodified E]/[Unmodified E]$_{t=0}$ versus time for **61**.*

4.3. Mapping of Covalent Modification of KDM5B with 61 and 62

To determine the site of covalent modification, protein digest experiments were carried out. Acrylamide **61** and chloroacetamide **62** were incubated with KDM5B until full modification was observed, the disulfide bonds were reduced and alkylated with iodoacetamide and subsequently digested with elastase enzyme. This resulted in many fragment peptides that were subjected to LCMS/MS to confirm the site of covalent modification. Acrylamide **61** (purple) was found to bind to the desired C480 (Figure 4.8) exclusively while chloroacetamide **62** (blue) was found to bind non-specifically with several cysteines (Figure 4.9), which is in accordance with the results observed by MS. The red modifications were due to addition of iodoacetamide to the exposed cysteines which would suggest that the protein was not fully modified with the compound or that the reducing agent caused the loss of the covalent inhibitor from the complex.

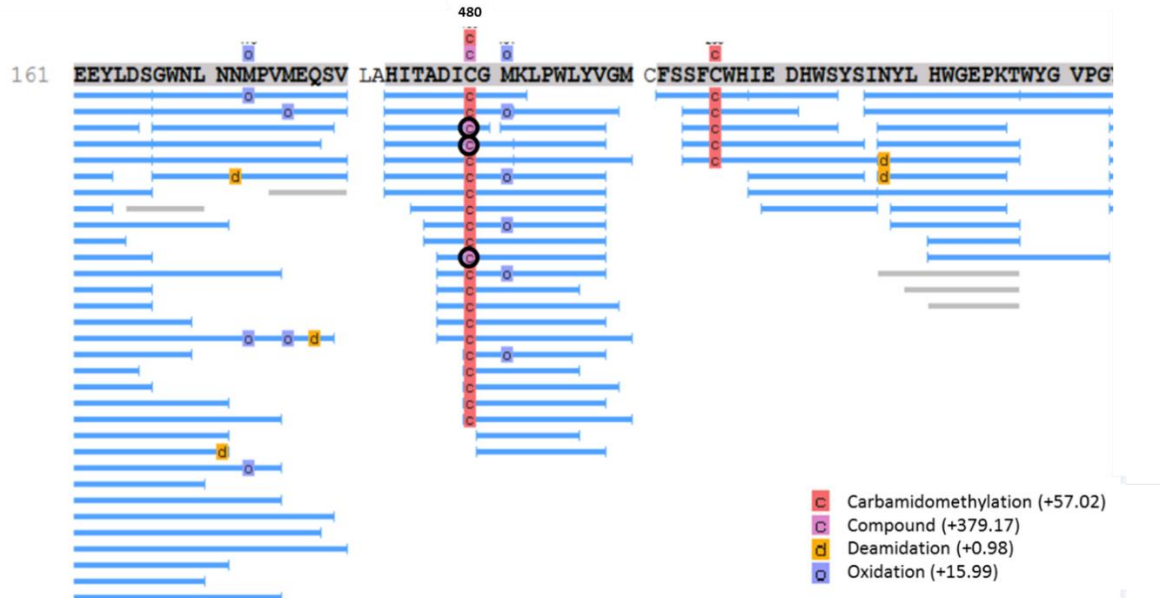


*Figure 4.8. Sequence of peptides from elastase digest of acrylamide **61** complex with KDM5B.*

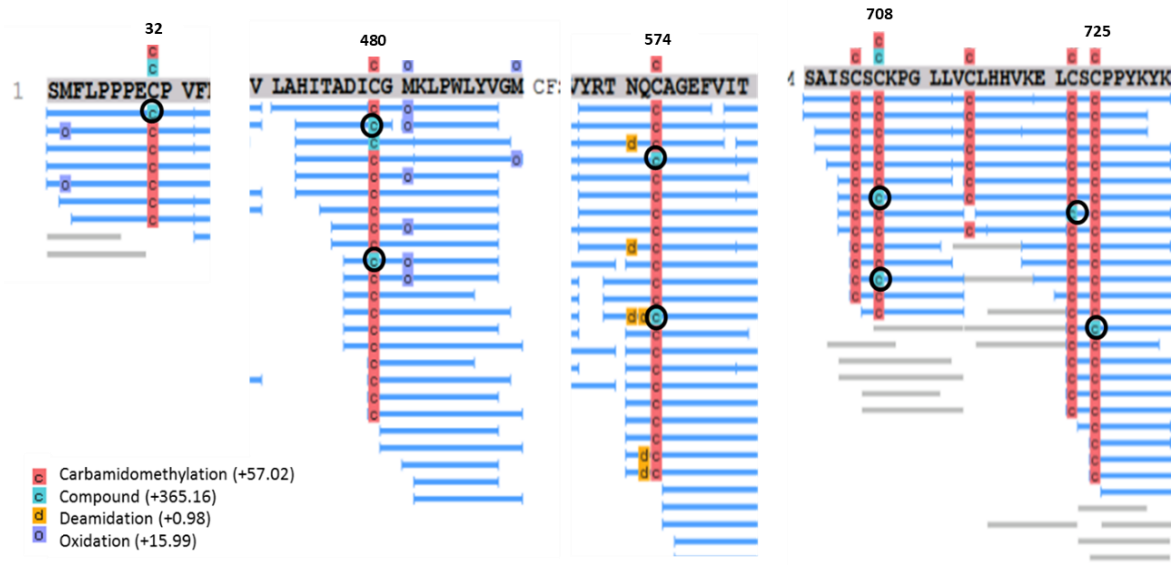


*Figure 4.9. Sequence of peptides from elastase digest of chloroacetamide **62** complex with KDM5B.*

To further confirm specific binding to C480, piperazine acrylamide **61** was incubated with KDM5C. In the KDM alignment, KDM5C was found to contain S485 in place of C480 in KDM5B. As a result, no covalent modification should be observed between KDM5C and the cysteine-selective electrophile of acrylamide **61**. Any observed covalent modification could only be explained through binding to a different cysteine in the protein sequence.

Different concentrations of **61** (6.25-50 µM) were incubated with 1 µM KDM5C for 45 minutes and subsequently injected into the RapidFire-MS. The MS of the protein-compound incubation showed only unmodified protein even at 50 µM (Figure 4.11) which was comparable to the control experiment of 1 µM KDM5C with no compound present (Figure 4.10). The specific covalent modification of **61** with C480 in KDM5B confirms that the compound first binds non-covalently to KDM5B and only when positioned in the binding site does the specific C480 react with the electrophile. As a result, acrylamide **61** was a selective covalent inhibitor of KDM5B.

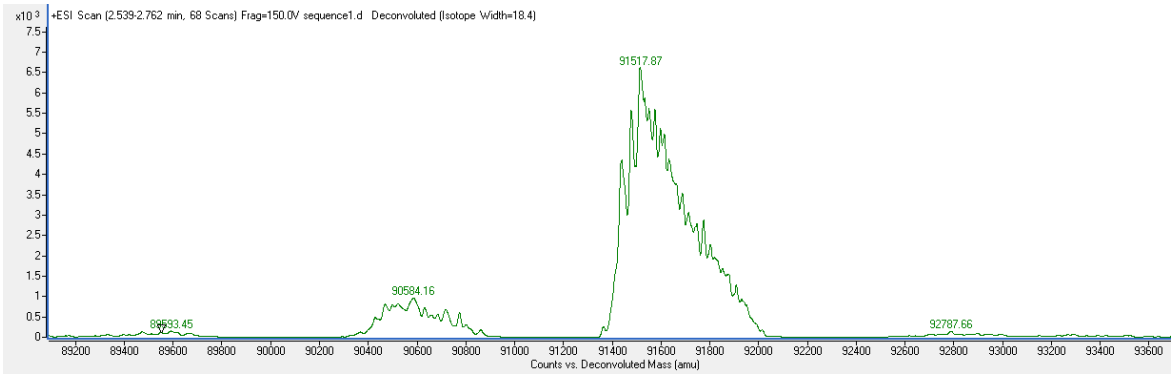


Figure 4.10. MS of native KDM5C

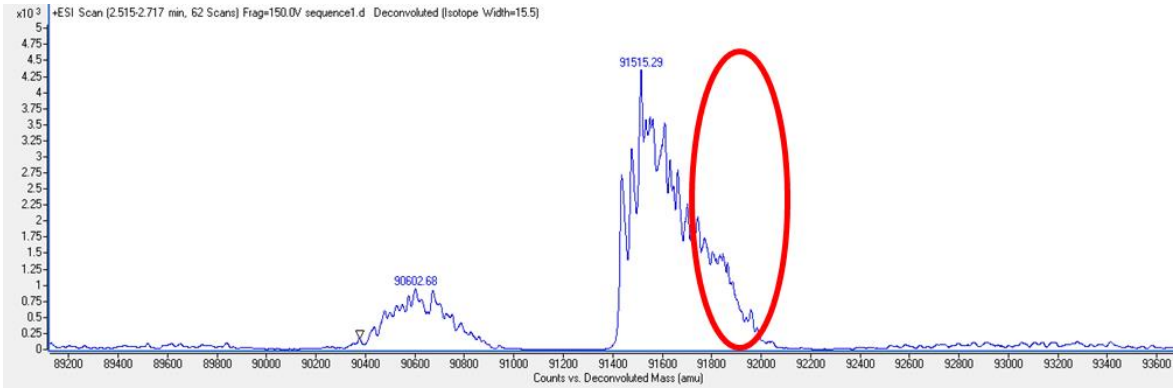


*Figure 4.11. MS of incubation of acrylamide **61** with KDM5C.*

A crystal structure of acrylamide **61** bound to KDM5B was obtained which confirmed the covalent binding with C480 (PDB ID 6EIN) (Figure 4.12). **61** bound in a similar binding mode to the original compound **14** with the bidentate coordination of the pyridine *N* and pyrazole *N*2 to the metal ion. The pyridopyrimidinone CONH group hydrogen bonds to K517/Y425 while the piperazine interacts with W486 and D428 as observed with the phenylpiperidine moiety. A bond was resolved between the sulfur of C480 and the carbon of the acrylamide proving covalent binding to the desired cysteine.

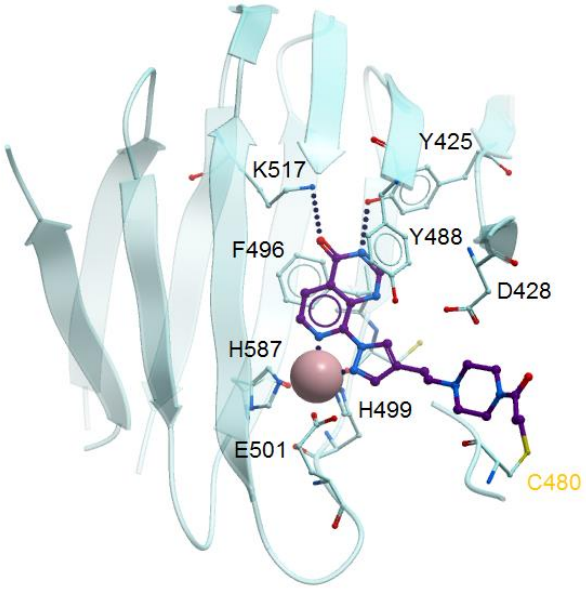


*Figure 4.12. Co-crystal structure of **61** bound to KDM5B (PDB ID 6EIN).*

4.4. Covalent Binding of Methyl Benzylamine Inhibitors 77-79

After biochemical screening of various analogues, it was found that the methyl benzylamine series **77**-**79** were the most potent covalent inhibitors with the highest k_{inact}/K_i value (Figure 3.5). To test that these compounds covalently bind to KDM5B, 10 µM **77**-**79** were incubated with 1 µM KDM5B at room temperature for up to 150 mins to ensure full conversion of the protein (Figure 4.13) and the protein-compound solution was injected into the MS to determine the protein mass.

The percentage of unmodified, singly modified and doubly modified KDM5B, in which one or two molecules of inhibitor respectively bind covalently to the protein, were recorded at each time point after incubation with **77**-**79** (Table 4.1).

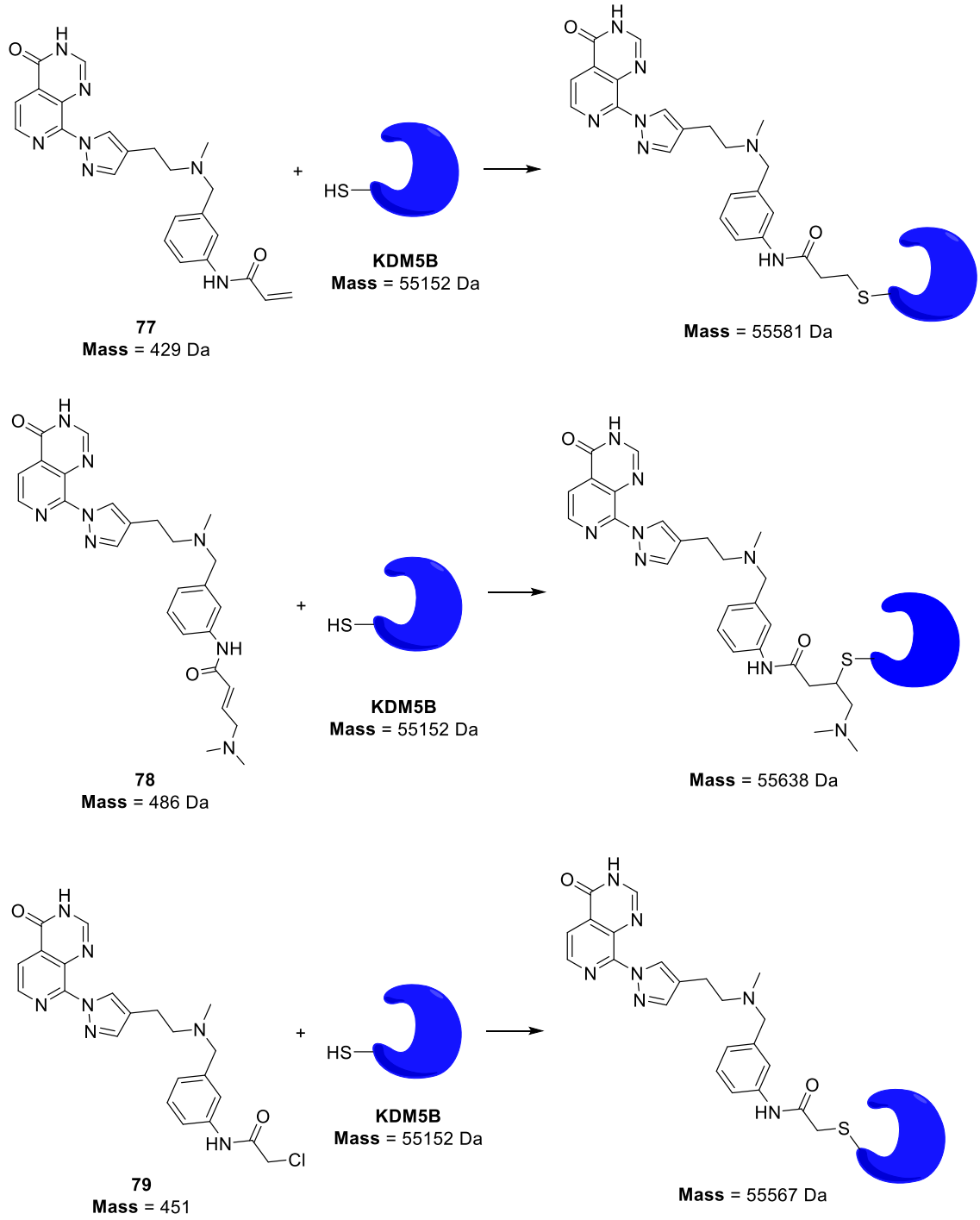


*Figure 4.13. Schematic showing covalent modification upon incubation of **77**-**79** with KDM5B.*

	Acrylamide			Dimethylamino crotonamide			Chloroacetamide		
Time (min)	Unmodified	Singly modified	Doubly modified	Unmodified	Singly modified	Doubly modified	Unmodified	Singly modified	Doubly modified
45	60	38	2	17	83	0	20	80	0
120	7	79	14	0	100	0	0	100	0
150	4	76	20	0	100	0	0	100	0

*Table 4.1. Percentage of unmodified, singly modified and doubly modified KDM5B after incubation with **77**-**79**.*

Acrylamide **77** showed 60% unmodified protein (m/z = 55152 Da), 38% singly-modified protein and a negligible proportion of doubly-modified protein after incubation for 45 minutes (Figure 4.14). The protein peak at m/z of 55585 is due to the addition of the covalent inhibitor as well as other modifications to the protein due to oxidation and salt adducts.

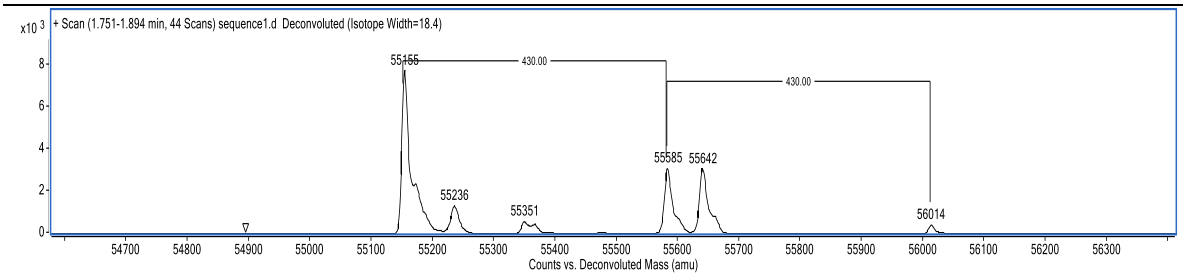


*Figure 4.14. MS showing covalent binding of acrylamide **77** to KDM5B after 45 minutes incubation.*

For complete modification of KDM5B, acrylamide **77** was incubated for 150 minutes. This resulted in negligible quantities of unmodified protein, 76% single modified protein (55585 Da) and 20% doubly modified protein (56013 Da) (Figure 4.15). Although there was full conversion of KDM5B, further incubation time increased the proportion of doubly modified protein.

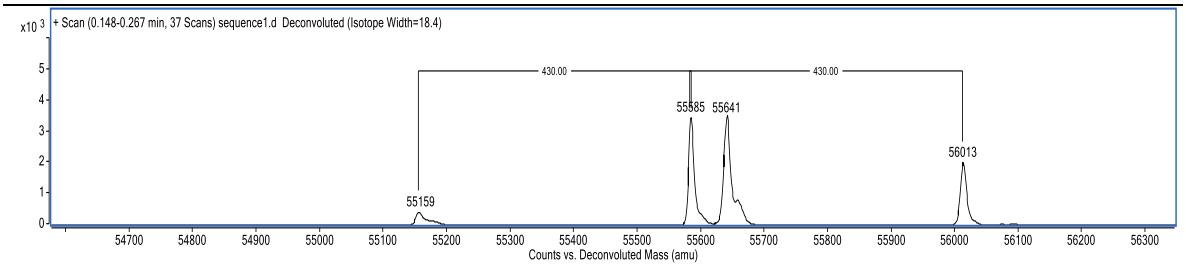


*Figure 4.15. MS showing covalent binding of acrylamide **77** to KDM5B after 150 min incubation.*

Dimethylamino crotonamide **78** showed almost full modification of the protein after 45 minutes incubation with 83% of protein peaks relating to single modification (55642 Da) and 17% of unmodified protein (55157 Da) (Figure 4.16). After 120 minutes incubation, KDM5B was fully modified with the covalent addition of one molecule of **78** to give a protein peak at 55642 Da.

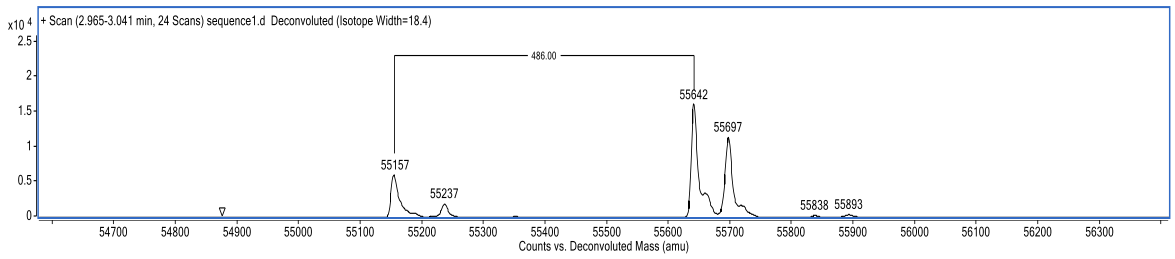


*Figure 4.16. MS showing covalent binding of **78** to KDM5B after 45 minutes incubation.*

Chloroacetamide **79** showed almost full modification of the protein after 45 minutes with 80% of the protein peak area relating to the covalent attachment of **79** and loss of HCl (55570 Da) (Figure 4.17). Incubation with **79** for 120 minutes resulted in full modification of KDM5B and no double covalent modification was observed under these incubation conditions.

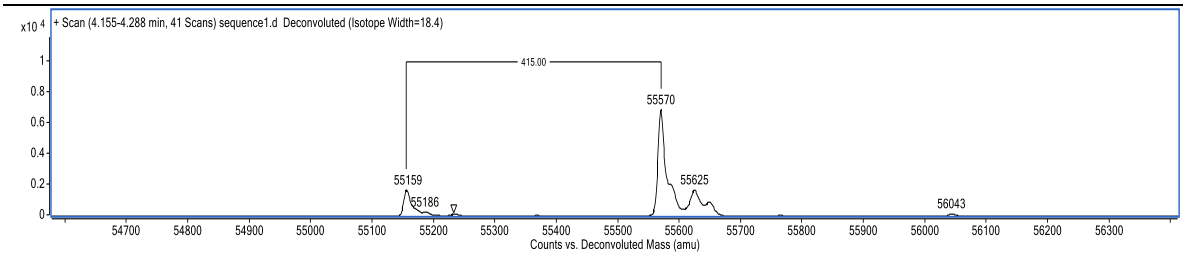


*Figure 4.17. MS showing covalent binding of **79** to KDM5B after 120 minutes incubation.*

Therefore, based on the MS data, acrylamide **77** was the least reactive as KDM5B was largely unmodified after incubation for 45 minutes. There was some non-specific binding to other cysteines as the degree of double modification of KDM5B increased after further incubation with acrylamide **77**. Although double modification was observed under these incubation conditions, more specific reactivity could be achieved if the compound concentration was lowered. Dimethylamino crotonamide **78** and chloroacetamide **79** electrophiles were more reactive towards covalent binding as complete modification of KDM5B was achieved within 2 hours and no double modification was observed so were likely binding to a specific cysteine.

4.5. Incubation of Methyl Benzylamines with other KDM proteins

Incubation of 10 µM of **77**, **78** and **79** with 1 µM KDM4B at room temperature for 2 hours resulted in only unmodified protein peaks which confirmed that there was no covalent binding to KDM4B

(Figure 4.18). The same incubation conditions were used to prove covalent modification with KDM5B so the selectivity over KDM4B in the biochemical assays (Chapter 3) could be attributed to specific covalent binding to KDM5B.

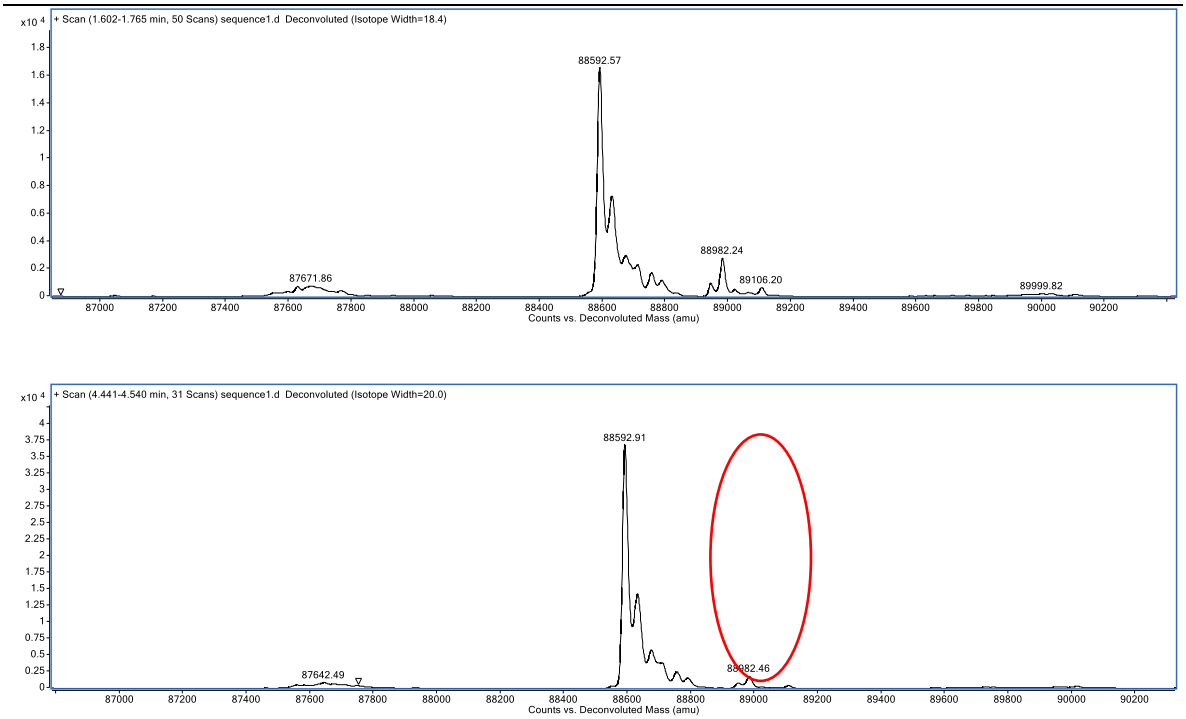


*Figure 4.18. MS of native KDM4B (top) and MS of incubation of **78** with KDM4B (bottom).*

Covalent inhibitors **77-79** were also >20-fold selective over KDM5C. Selectivity over KDM5C was expected as there is a serine at the same position as C480 in KDM5B so no covalent binding should be observed with cysteine-selective electrophilic warheads. This was confirmed using MS-labelling experiments through incubation of 10 µM methyl benzylamines with 1 µM KDM5C for 2 hours (Figure 4.19). This resulted in only unmodified protein peaks and no peaks relating to covalent binding of the compounds to KDM5C.

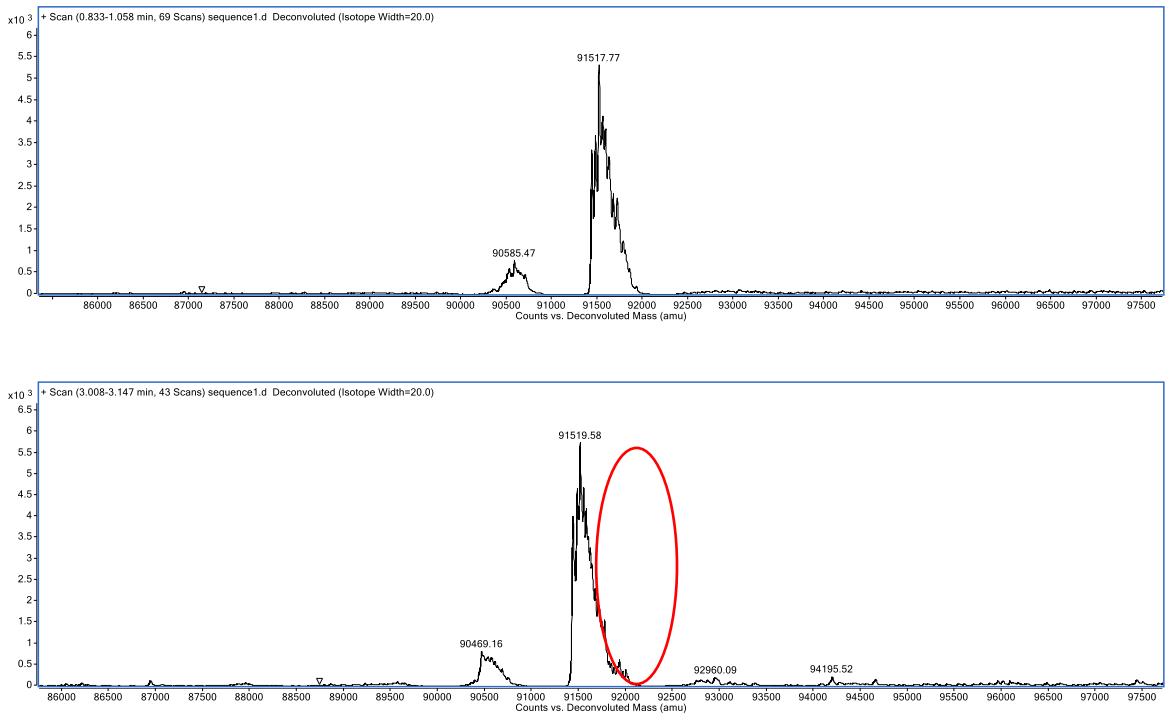


*Figure 4.19. MS of native KDM5C (top) and MS of incubation of **78** with KDM5C (bottom).*

4.6. Summary

Incubation of piperazine acrylamide **61** and piperazine chloroacetamide **62** with KDM5B resulted in full modification of the protein with the addition of the compound. Binding kinetics revealed that the protein was fully modified after 90 minutes incubation of **61** and **62** at room temperature. Covalent attachment of acrylamide **61** to KDM5B was determined to occur at C480 through elastase digestion of the protein-compound complex and analysis of the fragment peptides. A crystal structure of acrylamide **61** was obtained which confirmed the covalent binding to C480. Methyl benzylamine analogues **77-79**, the most potent inhibitors, were also shown to covalently bind to KDM5B through MS labelling experiments. Acrylamide **77** was the slowest to form the covalent complex compared to dimethylamino crotonamide **78** and chloroacetamide **79**. The slow reactivity of acrylamide **77** also resulted in modification of KDM5B from the covalent attachment of two molecules of inhibitor.

No covalent binding was observed after incubation of methyl benzylamines **77**-**79** with KDM5C and KDM4B. The improved selectivity over the KDM4 subfamily and the other KDM5 isoforms compared to the published 8-pyridopyrimidinone compounds could be explained by the contribution from covalent binding to KDM5B.

Chapter 5. Activity-Based Protein Profiling (ABPP)

5.1. Introduction to Activity-Based Protein Profiling

Due to problems with the immunofluorescence assay at measuring cellular activity, activity-based protein profiling (ABPP) seemed an attractive chemical biology tool to prove target engagement of the covalent inhibitors with KDM5B in a cellular environment. ABPP is a functional proteomic technology that uses designed chemical probes to interrogate specific families of enzymes in complex proteomes and quantifies the functional state of specific enzymes within the family.[108–110] The basic unit of ABPP is the probe which consists of two main components; the reactive group (warhead) and a tag (Figure 5.1). Some probes contain a binding group to enhance selectivity for related classes of enzymes and to limit cross-reactivity with other proteins. The reactive group is commonly an electrophile that can covalently bind to a conserved nucleophilic residue in the active site of an enzyme. Photoreactive groups can also be used by labelling proximal residues in the active site upon UV irradiation. The reporter tag can consist of either a fluorophore, biotin or analytic handles such as alkynes and azides, to visualise protein targets after labelling using click-chemistry.[111–113]

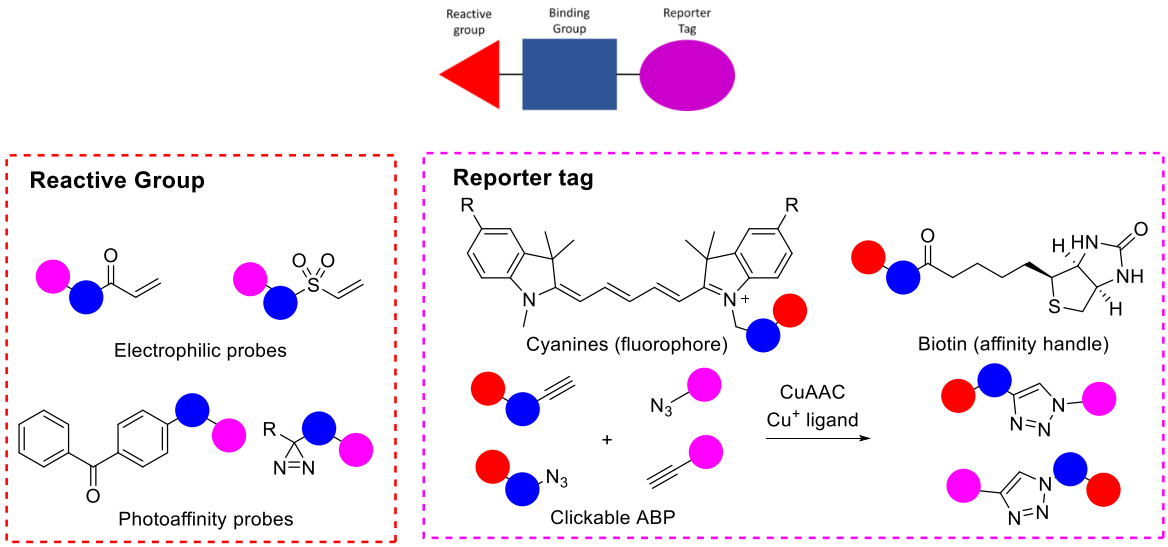


Figure 5.1. Design of an activity-based protein profiling probe with reactive group (red), binding group (blue) and reporter tag (pink) and representative examples of reactive group and reporter tag.

The ABPP probe can be used to determine the protein targets of an inhibitor using various analytical techniques. The first ABPP probes were analysed for enzyme activities using gel-based techniques (Figure 5.2).[114–117] Proteomes are treated with a fluorescent or biotinylated probe and resolved by one or two-dimensional polyacrylamide gel electrophoresis (PAGE). The labelled enzymes are then visualised by either in-gel fluorescence scanning or avidin blotting but commonly a combination of both. Fluorescent probes are useful for rapid screening of proteomes using sodium dodecyl sulfate (SDS)-PAGE. Biotinylated probes can subsequently be utilised to determine probe-labelled enzymes through streptavidin chromatography or streptavidin affinity enrichment, gel separation and subsequent mass-spectrometry. The main advantage of gel-based techniques is the robustness and high throughput of the method.

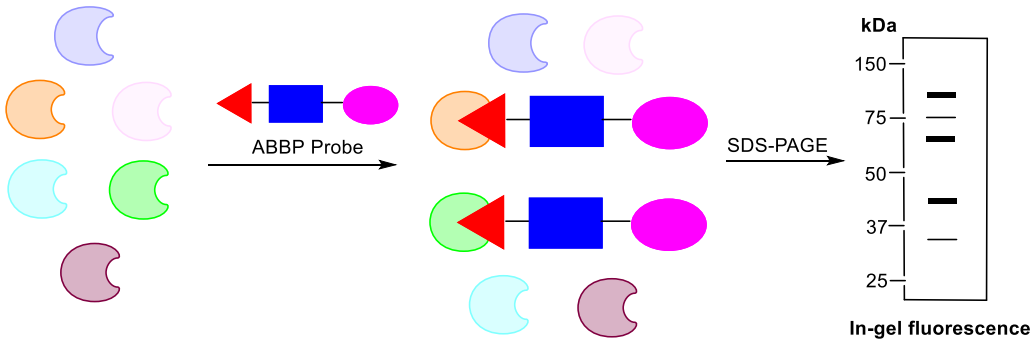


Figure 5.2. In-gel fluorescence-based protein profiling where probe-labelled enzymes are visualised across proteomes.

The introduction of liquid chromatography mass spectrometry (LCMS) greatly improved the resolution of ABPP experiments. The two main LCMS approaches analyse either the protein targets of the probes or the probe-labelled peptides derived from these targets (Figure 5.3). In the first method, biotinylated probes label proteomes and are incubated with streptavidin beads.[118] The enriched proteins are digested on-bead with trypsin and analysed by LCMS/MS. The second method involves treatment of the proteome with the probe and digestion with trypsin to give probe-labelled peptides which are enriched with affinity resin and analysed by LCMS/MS.[119,120] This method is known as active-site peptide profiling which is invaluable for determining whether the probes are targeting the active site of the enzyme.

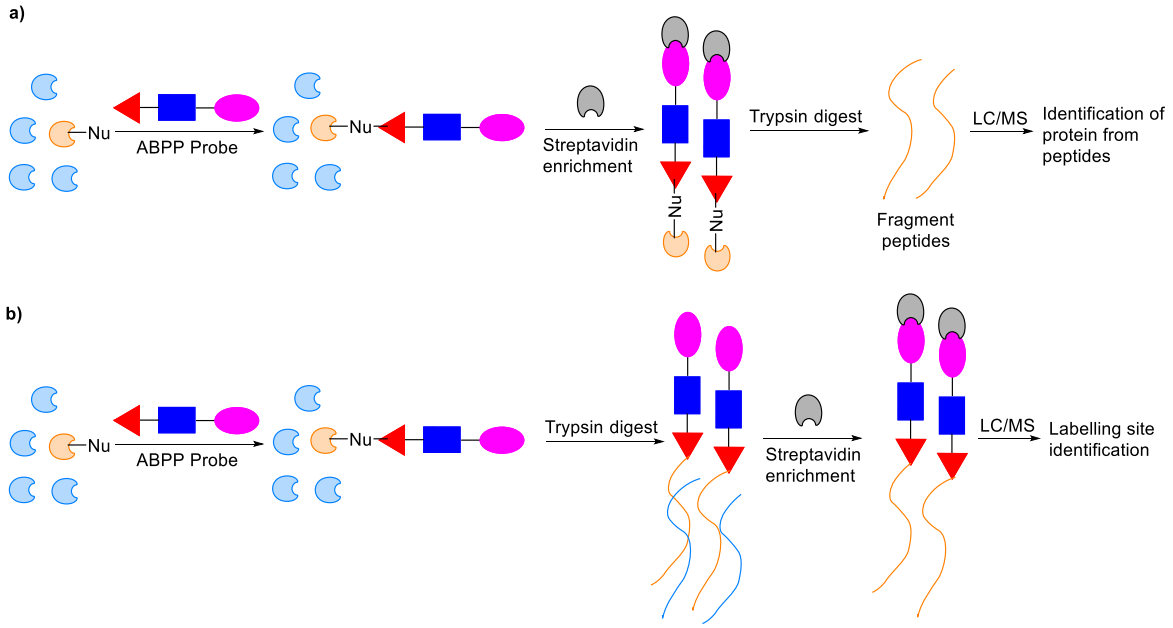


Figure 5.3. LC/MS-based platforms for ABPP. (a) ABPP and multidimensional protein identification technology. (b) Active-site peptide profiling.

A clickable analogue of the best covalent inhibitor would therefore be synthesized as a probe to identify the target proteins in the cellular environment using pull-down experiments.

5.2. Design of Clickable Alkyne Analogue

A clickable analogue **103** of the methyl benzylamine acrylamide **77** was synthesised to prove target engagement with KDM5B in cells using pull-down experiments. The compound was designed to comprise of the 8-pyridopyrimidinone binding group to KDM5B, an acrylamide warhead as the reactive group for covalent binding to C480 and an alkyne as a reporter tag (Figure 5.4). The alkyne was separated by a long carbon chain to position the alkyne outside the protein and ensure reactivity with the biotin azide (or fluorescent tag) in the click reaction. The alkyne chain was positioned meta to the acrylamide on the aniline ring to ensure that there was no loss in covalent reactivity through steric hindrance of the tag.

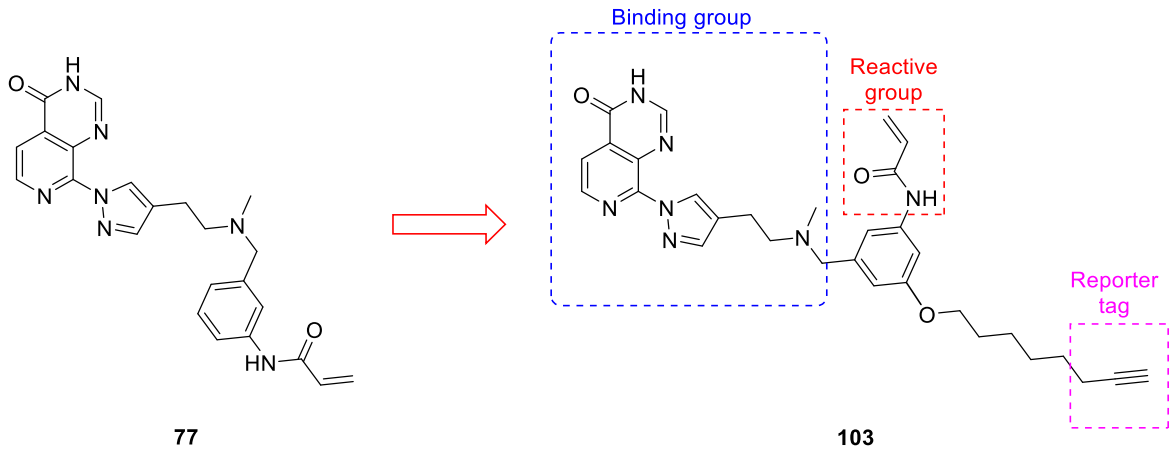


*Figure 5.4. Design of clickable alkyne analogue **103**.*

Clickable compound **103** was docked into KDM5B to ensure that the addition of the oct-7-yn-1-ol group would not hinder the non-covalent and covalent binding to the active site (Figure 5.5). As observed with the non-clickable analogue, pyridine *N* and pyrazole *N*2 coordinated to the metal centre and the acrylamide was positioned in a favourable orientation for covalent binding to C480. The alkyl chain was positioned out of the pocket into a solvent-exposed region which was necessary for the sufficient reactivity of the alkyne in the click reaction of the pull-down experiments.

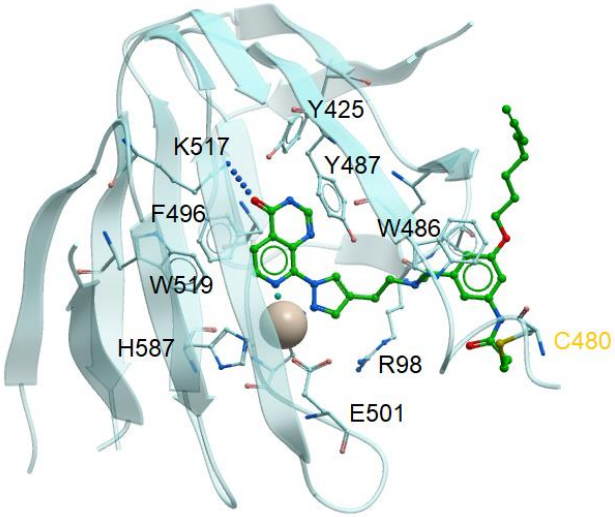
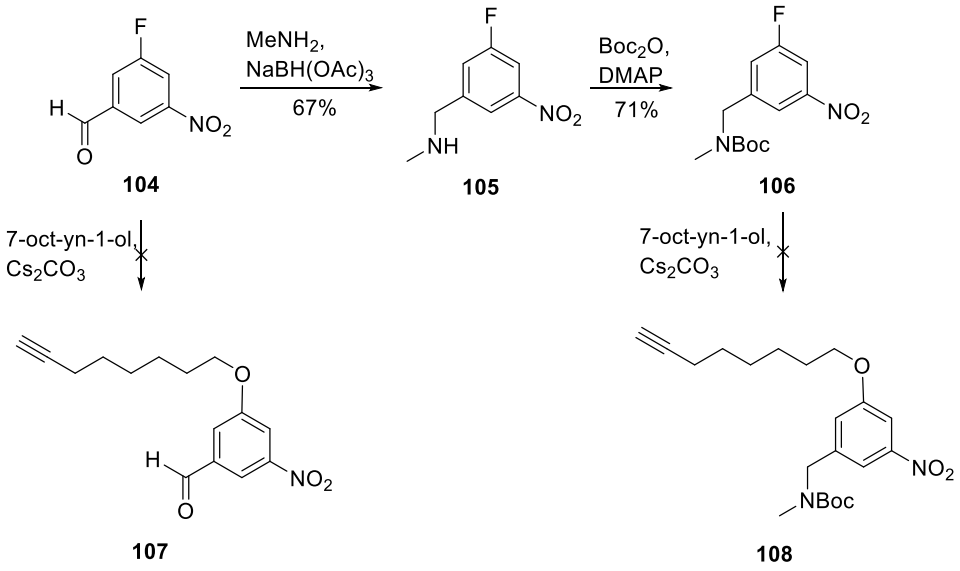


*Figure 5.5. Covalent docking of **103** into KDM5B.*

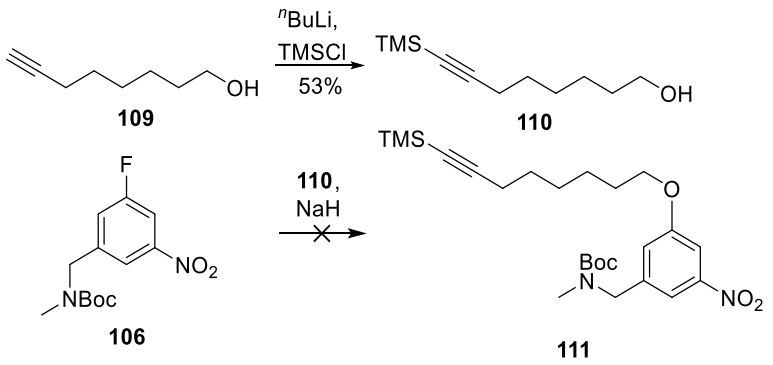
5.3. Synthesis of Clickable Analogue

The preparation of pull-down analogue was originally anticipated through a nucleophilic aromatic substitution reaction (Scheme 5.1). Reductive amination of 3-fluoro-5-nitrobenzaldehyde **104** with methylamine afforded compound **105** and the nitrogen was subsequently protected with a Boc group to give **106**. Attempts at the substitution using 7-octyn-1-ol and cesium carbonate with aldehyde **104** or amine **106** to give compounds **107** and **108** respectively was unsuccessful and only resulted in starting material.



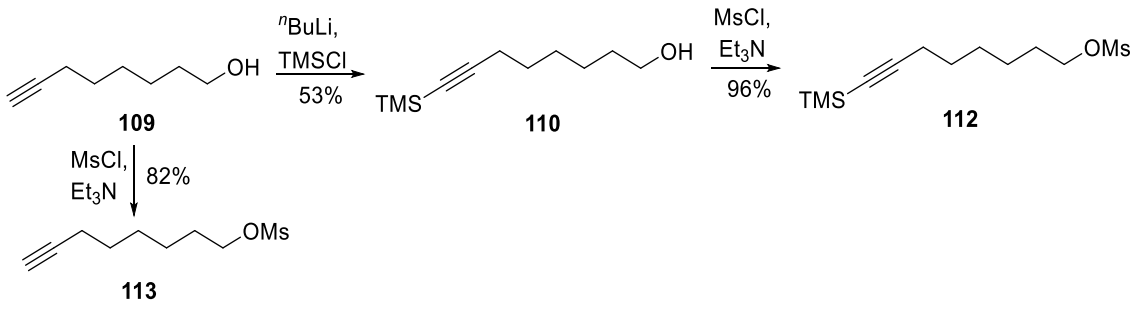
*Scheme 5.1. Attempted synthesis of alkyne benzylamine **107/108** via a nucleophilic aromatic substitution.*

As the use of a stronger base such as sodium hydride could result in deprotonation of the acetylene of 7-octyn-1-ol **109** leading to unwanted side products, it was protected with a TMS group using *n*-butyl lithium to afford compound **110** (Scheme 5.2). Nucleophilic aromatic substitution with compound **106** using sodium hydride and protected alkyne **110** resulted in decomposition products rather than the desired product **111**. Due to difficulties with the use of a nucleophilic aromatic substitution, an alkylation of a phenol was attempted.



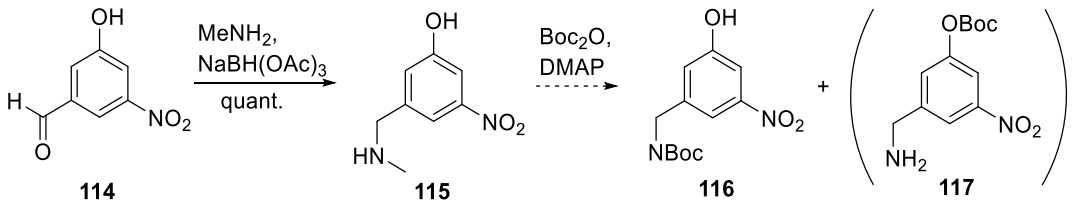
*Scheme 5.2. Attempted synthesis of alkyne benzylamine **111** via a nucleophilic aromatic substitution.*

7-octyn-1-ol **109** was activated as mesylate **113** for subsequent alkylation with a phenol (Scheme 5.3). TMS-protected oct-yn-ol **110** was also activated as mesylate **112** in case there was unwanted side reactions of the acetylene.



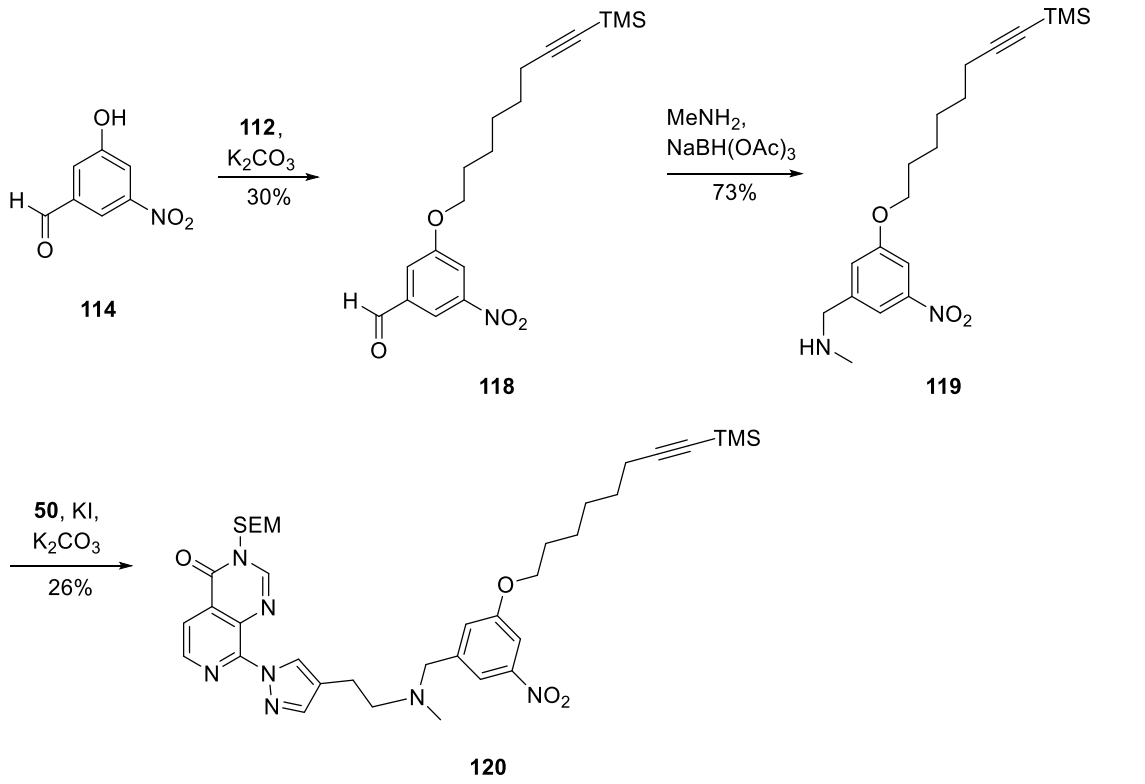
*Scheme 5.3. Activation of 7-octyn-1-ol as mesylate **112** and **113**.*

Initially reductive amination of aldehyde **114** was attempted prior to the alkylation of the phenol. Aldehyde **114** was treated with methylamine and sodium triacetoxyborohydride to yield **115** in quantitative yield (Scheme 5.4). Subsequent Boc protection was unsuccessful due to the formation of a mixture of products relating to protection of nitrogen **116** and oxygen **117**. It was therefore desirable to perform the reductive amination last to avoid a protection step.



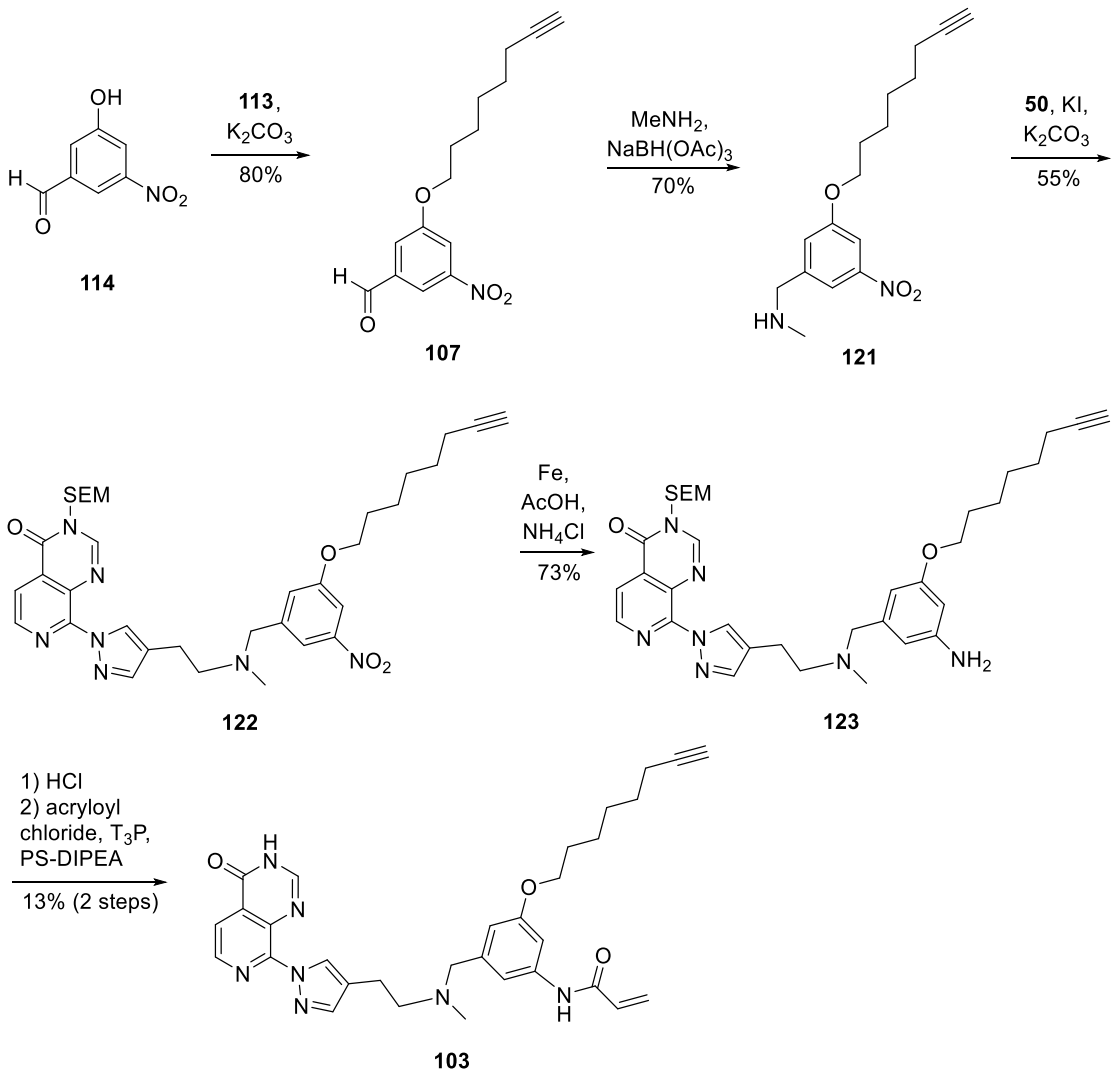
*Scheme 5.4. Synthesis of Boc-protected benzylamine **116**.*

Alkylation of aldehyde **114** with TMS-acetylene mesylate **112** was successful using potassium carbonate as the base to afford **118** followed by reductive amination with methylamine to give amine **119** (Scheme 5.5). Displacement of mesylate **50** with amine **119** gave **120** in poor yield which was likely due to the loss of TMS under basic conditions or elimination to give the alkene as a side product.



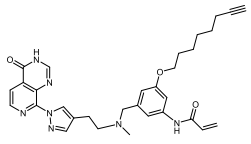
*Scheme 5.5. Synthesis of TMS-alkyne **120**.*

Alkylation of 3-hydroxy-5-nitrobenzaldehyde **114** was therefore attempted on unprotected acetylene mesylate **113** and subsequent reductive amination of **107** with methylamine afforded amine **121** (Scheme 5.6). Nucleophilic substitution with mesylate **50** gave **122** in greater yield than with TMS-acetylene **119** so TMS protection was an unnecessary step. Reaction of **122** with iron, ammonium chloride and acetic acid afforded aniline **123**. Final steps required removal of silyl protecting group under acidic conditions and acetylation with acryloyl chloride to give acrylamide **103**.



*Scheme 5.6. Synthesis of alkyne acrylamide **103**.*

The pull-down derivative alkyne **103** was screened for time-dependent inhibition using the same method as previously described in Chapter 3 (Figure 5.6). Acrylamide alkyne **103** showed an approximately 30-fold drop in IC_{50} from 0 to 120-minute pre-incubation time with a potent IC_{50} of 3 nM after 2 hours incubation. **103** had a k_{inact}/K_i value of 1.2 x 10^5 M^{-1} s^{-1} which was greater than the non-clickable analogue **77**. The k_{inact} was much larger while the K_i value was comparable to the non-clickable methyl benzylamine analogue so the addition of the oct-7-yn-1-ol functionality must improve the covalent reactivity of the acrylamide by changing the electronics of the aniline ring.



103		
Time (min)	**IC_{50} (μM)**	**Standard Deviation (n)**
0	0.094	± 0.015 (2)
5	0.046	± 0.001 (2)
10	0.018	± 0.002 (2)
15	0.014	± 0.001 (2)
20	0.009	± 0.002 (2)
30	0.008	± 0.0002 (2)
45	0.005	± 0.001 (2)
60	0.005	± 0.0002 (2)
90	0.003	± 0.001 (2)
120	0.003	± 0.0001 (2)
K_i (M)	7.11E-08	
k_{inact} (s^{-1})	8.23E-03	
k_{inact}/K_i (M^{-1} s^{-1})	**1.2E+05**	

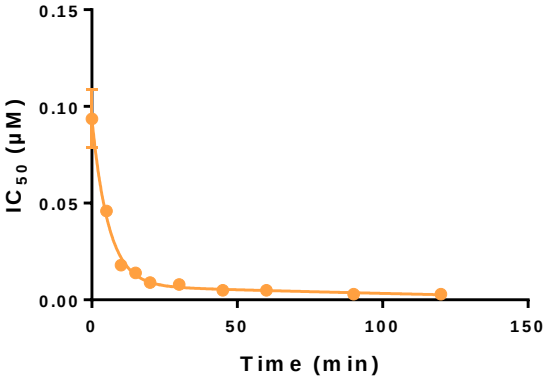


*Figure 5.6. Time dependent inhibition of clickable analogue **103** by AlphaScreen.*

The clickable analogue **103** was incubated with KDM5B to ensure that the protein-compound complex would form in the pull-down assay. It was important that the addition of the oct-7-yn-1-ol to the methyl benzylamine did not hinder the covalent binding. Incubation of **103** with KDM5B at 37 °C for 30 minutes resulted in a peak relating to full modification of KDM5B with the correct m/z change (Δm/z = 553) for the addition of the compound and other protein peaks due to oxidation and the addition of salt adducts (Figure 5.7). Therefore, the cells would be incubated at 37 °C for the pull-down assay to ensure full modification of the protein.

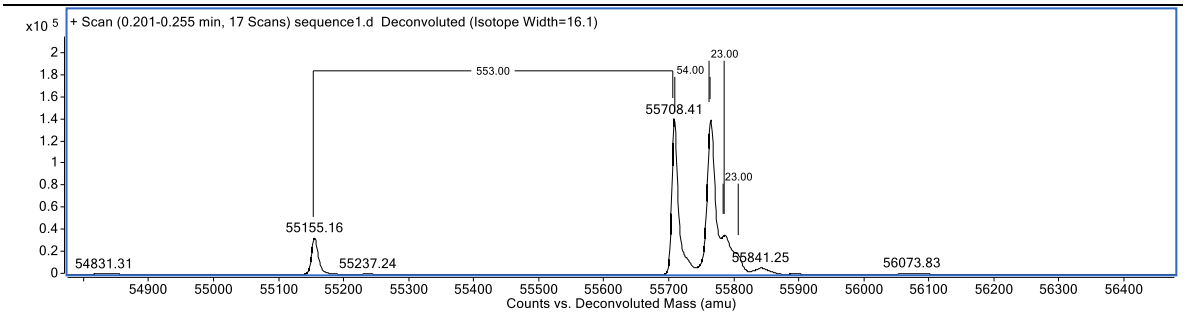


Figure 5.7. MS of the incubation of **103** with KDM5B for 30 minutes at 37 °C.

5.4. Recombinant KDM5B – In-Gel Fluorescence

Prior to testing that the compounds engaged with KDM5B in cells, the click reaction was attempted between the IR fluorescent azide dye (Cyanine 5.5) and the clickable compound bound to KDM5B protein (Figure 5.8). Both clickable **103** and non-clickable **77** compounds were tested to prove that the dye was only reacting under click chemistry conditions with the alkyne of **103** and not with another functionality in the compounds. Different conditions were tested to check the efficiency of the click reaction and the possible cross-reactivity of the fluorescent dye. Samples were incubated with or without 5 µM compound and 1 µM KDM5B for 2 hours at 37 °C to ensure all protein was covalently modified. Subsequent addition of 1% SDS caused the tertiary structure of the protein to unfold and therefore allow Huisgen cycloaddition click reaction between the IR-dye conjugated with an azide and the alkyne. After 1-hour incubation at room temperature with the click reagents, the protein was precipitated to remove excess reagents and the samples were run on a SDS-PAGE gel to visualise the proteins through fluorescence.

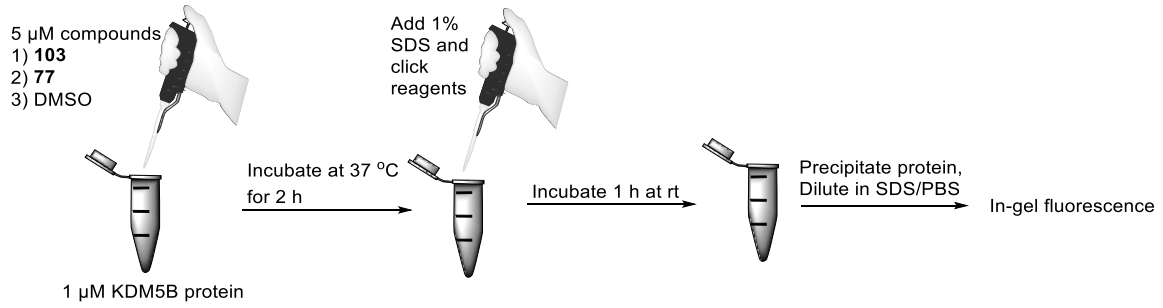


Figure 5.8. Schematic of protocol for in-gel fluorescence with recombinant KDM5B.

Protein bands were only observed in the samples in which the protein was incubated with clickable analogue **103** alone (Sample 4) and incubated with both clickable **103** and non-clickable **77** compounds (Sample 6) (Figure 5.9). Faint bands were also observed with protein alone (Sample 1) and non-clickable **77** incubation controls (Sample 5) due to a small degree of background fluorescence. Non-clickable analogue **77** could compete with the clickable analogue **103** resulting in a slightly less intense band for sample 6, with around 30% reduction in the signal compared to

sample 4. As expected, there were no bands observed in the no protein and no compound control (Sample 2). There were faint bands with samples 1, 3 and 5 which relate to background signal from the click chemistry conditions. Sample 3 showed a less intense band than sample 1 which would suggest that the copper was responsible for the background fluorescence. Incubation of the clickable analogue **103** in absence of KDM5B protein and with the dye only present also showed no band on the gel (Sample 7). The observed protein bands were therefore only specifically formed from the covalent complex of the clickable analogue **103** with recombinant protein followed by a click reaction with IR-dye.

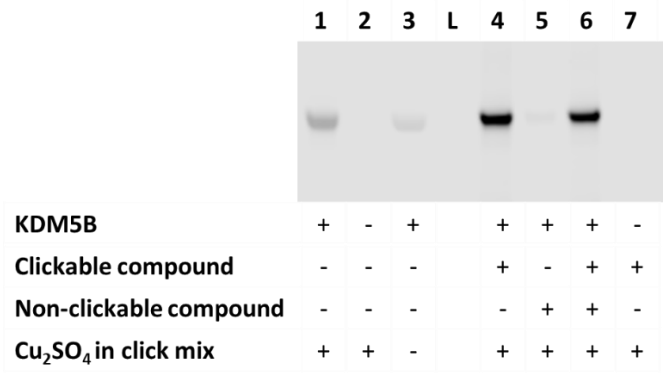


*Figure 5.9. In-gel fluorescence of clickable **103** and non-clickable **77** compounds incubated with KDM5B.*

The ladder was not visible on the gel which may have been due to the strong fluorescence from the samples so the gel was stained with Coomassie to visualise the proteins in the samples as well as the ladder (Figure 5.10). Protein bands were observed at the correct mass of the recombinant KDM5B (~55 kDa) for all protein samples including the control samples (Sample 1 and 3) which confirmed that the conditions of the click reaction did not result in degradation of the protein. Given that in-gel fluorescence was successful with KDM5B protein, it could be attempted in cells or cell lysates to prove that the covalent inhibitor engaged specifically with KDM5B in the cellular environment.

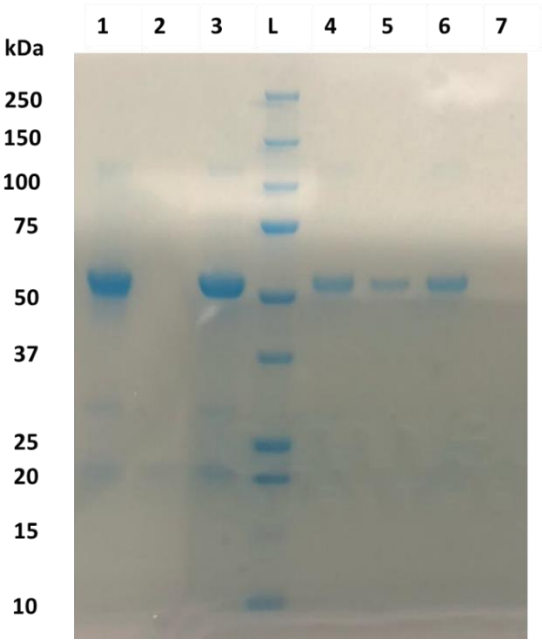


Figure 5.10. Coomassie staining of in gel fluorescence with recombinant protein KDM5B.

5.5. Pull Downs in Cell Lysates

5.5.1. Cell Lysates - In-Gel Fluorescence

As the compounds were poorly cell permeable, it was better to attempt in-gel fluorescence in cell lysates in which the cell components have been released from within the cell membrane. MCF7 cells which highly express KDM5B, were lysed in NP-40 buffer, and protein quantification by the Bradford Protein Assay gave a total protein concentration of 10.3 mg/ml.

Different concentrations of the clickable analogue **103** (0.5 µM – 50 µM) were incubated with 2 mg/mL of cell lysates for 2 hours at 37 °C to ensure complete covalent attachment of the compound with the proteins (Figure 5.11). The lysate was precipitated and resuspended in lysis buffer to remove excess compound which could have interfered in the click reaction. The compound-bound lysate was incubated with an azide conjugated to an IR-dye (Cyanine 5.5) using click reaction conditions. After a protein precipitation and resuspension step, the samples were run on SDS-PAGE to visualise the proteins which engaged with the inhibitor.

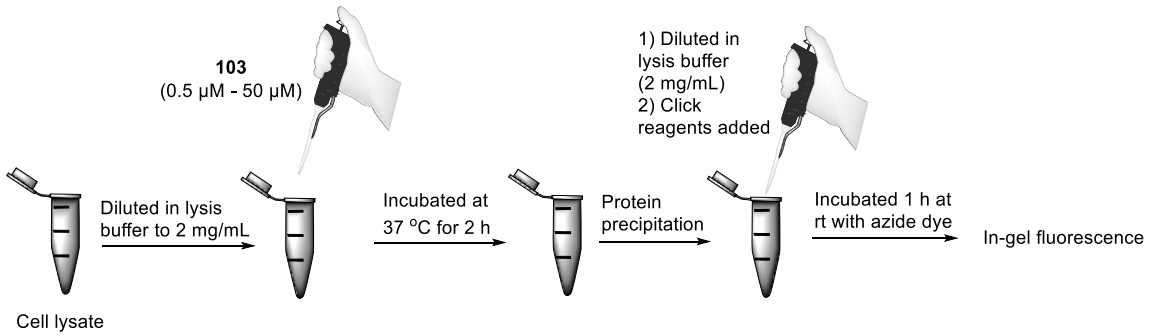


Figure 5.11: Schematic of protocol for in-gel fluorescence with cell lysates.

Both 50 µM and 10 µM of inhibitor **103** showed engagement with several proteins in the cell lysate while lower concentrations showed only faint protein bands (Figure 5.12). No visualization of KDM5B was detected which could have been caused by lower abundance of the protein compared to other cellular proteins. There were around 7 proteins that were not observed in the control with no compound so were likely due to non-specific binding of the compound to other proteins. The high fluorescence signals from the compound samples may have resulted in poor detection of the protein bands of the ladder. Overall, some background fluorescence was observed between the clickable dye and the cellular proteins leading to non-specific protein bands.

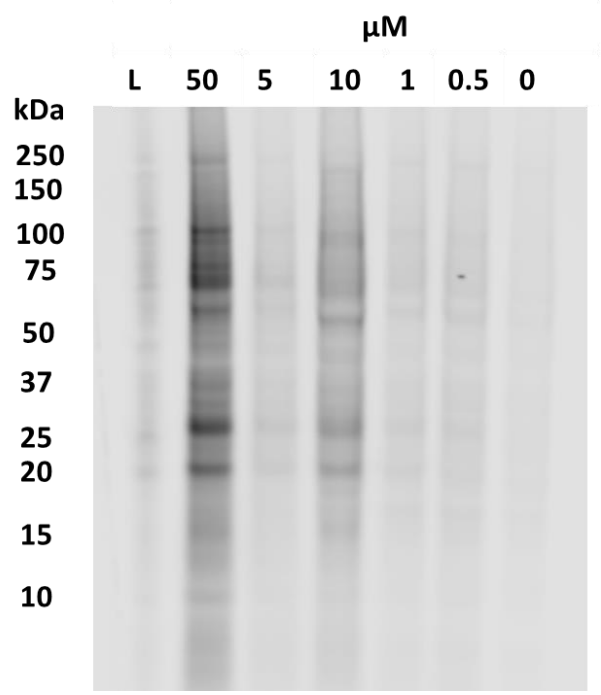


*Figure 5.12. In-gel fluorescence of alkyne **103** with cell lysates.*

5.5.2. Cell Lysates – Biotin Pull-Down

As in-gel fluorescence showed a lot of background signal due to interaction of the dye with the components of the cell lysates, the use of a biotin pull-down experiment would be more specific as the samples are enriched (Figure 5.13). Compound **103** was incubated at different concentrations (0.5-50 µM) with MCF7 in NP-40 cell lysates and conjugated with a biotin azide using click chemistry. The clicked proteins were subsequently incubated with streptavidin beads which bind to the biotinylated proteins and after a few washes, the samples were boiled to elute the enriched proteins from the beads. The supernatant was run on an SDS-PAGE, transferred to a nitrocellulose membrane by Western Blotting and the proteins were imaged through incubation of the membrane with a Streptavidin-IR Dye.

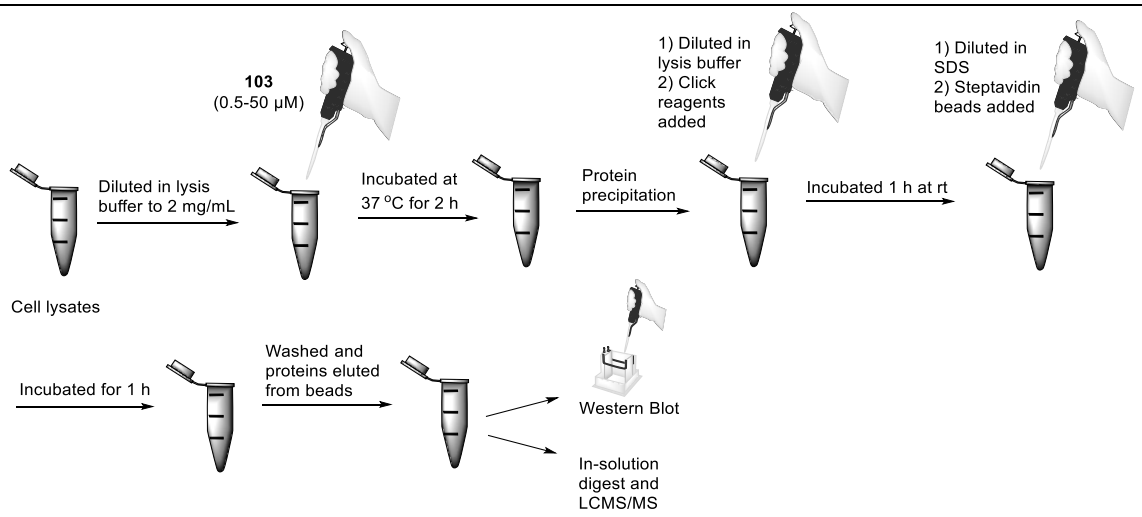


Figure 5.13. Schematic for biotin pull down in cell lysates.

The membrane showed protein bands with a low molecular weight of ~14 kDa that were observed in the boiled bead samples but not in the input samples after the click and bead incubations (Figure 5.14). There were also some faint bands at a molecular weight of ~140 kDa, ~75 kDa and ~30 kDa, in all the samples which does not correlate with KDM5B with a mass of ~180 kDa. All the protein bands were also observed in the no compound control which would suggest that these bands are due to non-specific reactivity between the cellular proteins and the biotin azide.

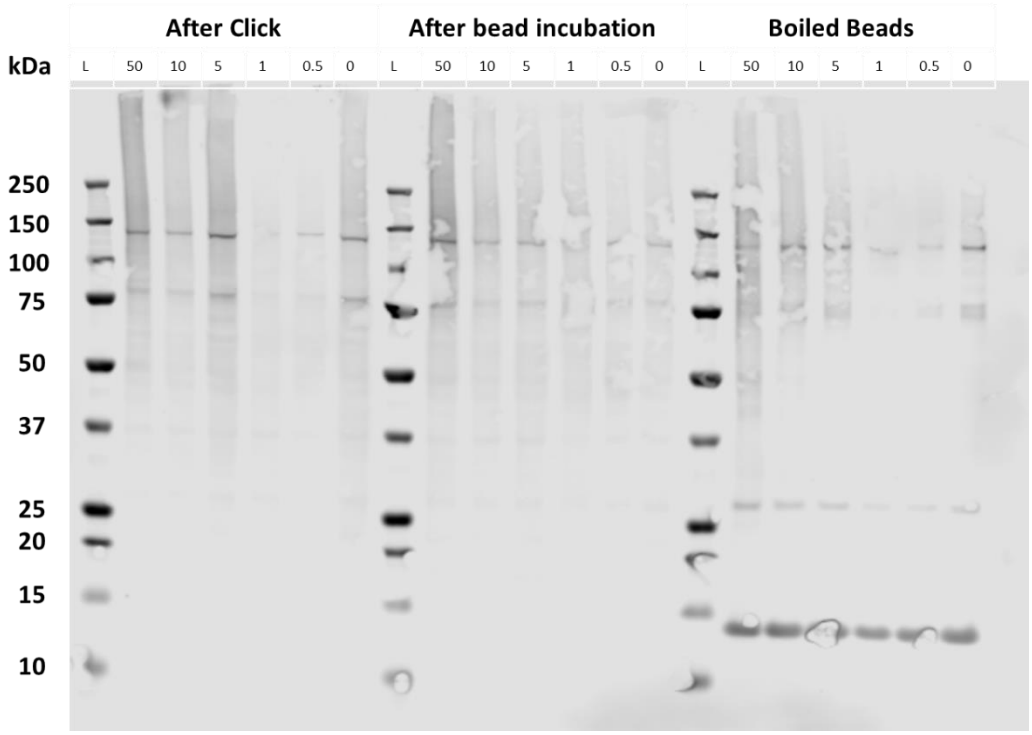


Figure 5.14. Biotin Pull-down with MCF7 cell lysates.

There was some concern that KDM5B had not been released from the nucleus during the cell lysis which could have reduced target engagement with the poor cell-permeable compounds. Two cell lysates had been prepared with different lysis buffers; MCF7 cells were lysed with NP-40 buffer, a mild buffer, while K562 cells were lysed with strongly denaturing RIPA buffer. To determine whether KDM5B was present in the two different cell lysates, both cell lysates were analysed by western blotting (Figure 5.15). MCF7 cell lysates, used in the previous experiments, showed only a faint band for KDM5B with a mass of ~180 kDa while K562 cell lysate showed a much more intense band for KDM5B. As a protein precipitation step had been used previously, the cell lysates were also analysed post precipitation which revealed that no KDM5B was present with MCF7 cell lysates while KDM5B was observed with K562 cells. Overall, the stronger RIPA buffer had sufficiently released KDM5B from the nucleus into the cell lysates unlike with the milder buffer used to lyse MCF7 cells.

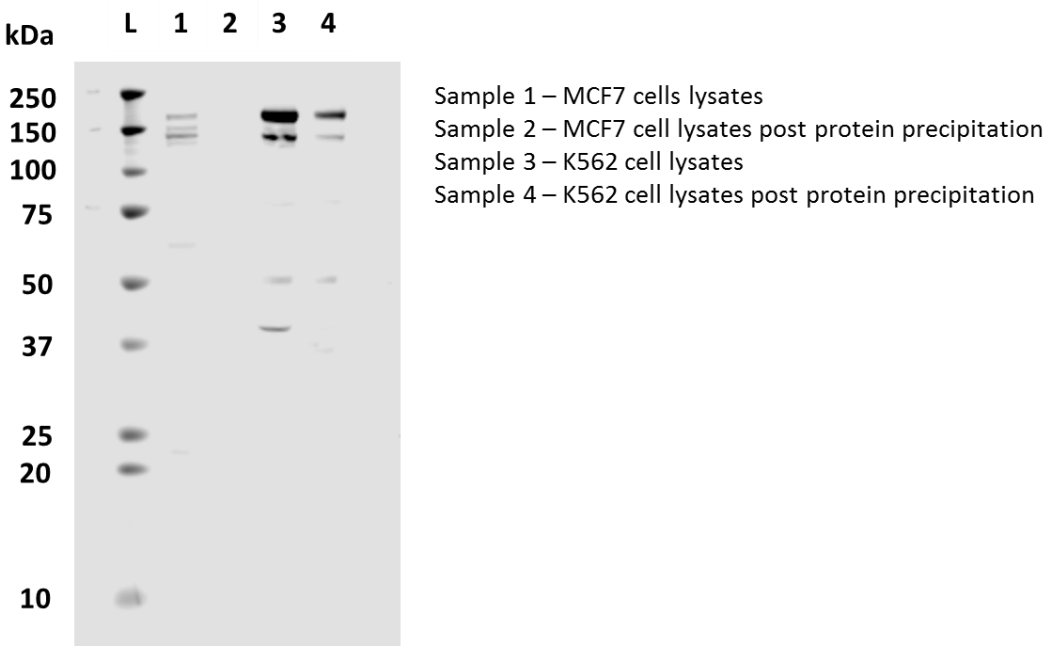


Figure 5.15. Western Blot of KDM5B in MCF7 and K562 cell lysates before and after protein precipitation.

The biotin pull-down was therefore repeated using K562 cells that were lysed with RIPA buffer (Figure 5.16). A single concentration of 5 µM of clickable compound **103** was incubated for 2 hours at 37 °C with 1.8 mg/mL cell lysates and a protein precipitation was performed prior to the click reaction as the RIPA buffer could interfere with the reagents in the click reaction. The protein-compound complex was resuspended in SDS/PBS and subjected to the click conditions with azide-biotin and a second protein precipitation step was necessary to remove excess click reagents and therefore prevent pull-down of non-specific proteins. The biotinylated proteins were attached to Streptavidin beads, eluted from the beads for loading onto the gel and finally transferred to a membrane through western blotting. The protein bands were visualised through incubation of the membrane with a Streptavidin-IR dye. Similar protein bands were observed as with the MCF7 cell lysates with masses of ~140 kDa, ~75 kDa and ~30kDa, however these proteins are also found in the DMSO control. There was a new protein band of ~50 kDa which was enriched in the boiled beads sample (Sample 4) and was not pulled down with the DMSO control. The protein at ~14 kDa was also enriched in Sample 4 which could relate to a histone protein. There was no protein band with a mass relating to KDM5B so either the protein had degraded under the conditions of the pull-

down or the concentration of KDM5B in the cell lysate was too low to be detected in the conditions of the pull-down assay.



Figure 5.16. Biotin Pull-down with K562 cell lysates (lysed with RIPA buffer).

5.6. Summary

103 was designed based on methyl benzylamine acrylamide **77** with the addition of an aliphatic alkyne chain for use in a click reaction in a pull-down experiment. After optimisation of the synthetic route, synthesis of **103** was achieved through preparation of amine **121** which was obtained from alkylation of phenol **114** and reductive amination with methylamine. Final steps to **103** involved displacement of mesylate **50** with amine **121**, nitro reduction and acylation with acryloyl chloride.

103 was potent against KDM5B in the AlphaScreen assay showing good covalent reactivity with a high k_{inact}/K_i value of 1.2 x 10^5 M^{-1} s^{-1}. Covalent binding of **103** to KDM5B was confirmed through MS-labelling experiments in which full modification was observed after incubation at 37 °C for 30 minutes. The addition of the aliphatic alkyne chain did not hinder inhibition or covalent binding to KDM5B.

In-gel fluorescence pull-down with recombinant KDM5B proved that the click reaction was successful between the protein-compound complex and the azide dye. Attempts to prove target engagement of **103** with KDM5B in cell lysates through in-gel fluorescence and biotin experiments did not result in protein bands corresponding to KDM5B. The click reaction may have been unsuccessful, so future work would attempt the click reaction between the compound and the biotin azide prior to incubation with the cell lysates.

Chapter 6. Bench-Stable Transfer Reagent for the Synthesis of CF_3-Sulfonimidamide

This chapter describes research that was published as part of my industrial placement at Janssen Pharmaceuticals which involved optimising chemistry to access trifluoromethyl sulfonimidamides for their drug discovery projects.[121]

6.1. Introduction to Sulfonimidamides and Their Synthesis

Sulfonimidamides, bioisosteric replacements of sulfonamides in which the S=O is replaced with an S=N double bond (Figure 6.1), have become increasingly important since their discovery in the early 1960s[122,123] and have been applied in multiple fields including asymmetric metal catalysis.[124–130] This functionality also possesses unique properties for optimising physiochemical and biological properties. The addition of a basic sp^2-hybridised nitrogen atom results in tautomerism through proton transfer between imine and amide nitrogen of the sulfonimidamide, offering interesting properties in drug design as the imine nitrogen can act as a hydrogen bond donor or acceptor.[131,132] The chirality about the sulfur atom is commonly configurationally stable and could therefore have an important role in the interaction with biomacromolecules.[133] Drug discovery programmes have therefore incorporated the sulfonimidamide functionality as a way of improving drug properties.[134]

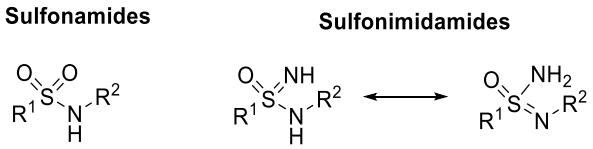


Figure 6.1. Structure of sulfonamides and tautomers of sulfonimidamides.

A potent inhibitor of dipeptidyl peptidase-IV (DPP-4) **124**, featuring a sulfonimidamide dihydropyrrolopyrazole core, was reported by Merck, Sharp and Dohme Corporation as a treatment for type-2 diabetes (Figure 6.2).[135] Six-membered bicyclic sulfonimidamide **125** was published by

Hoffmann-La Roche as a potent inhibitor of β-secretase enzyme (BACE1) for the treatment of Alzheimer's disease.[136] The chirality of the sulfur atom was important for favourable binding in the active site.

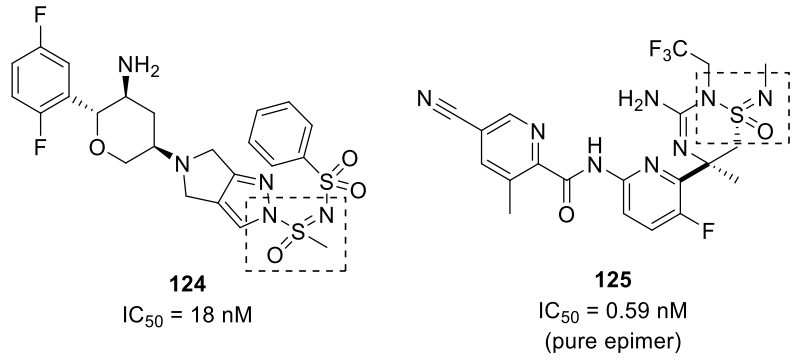
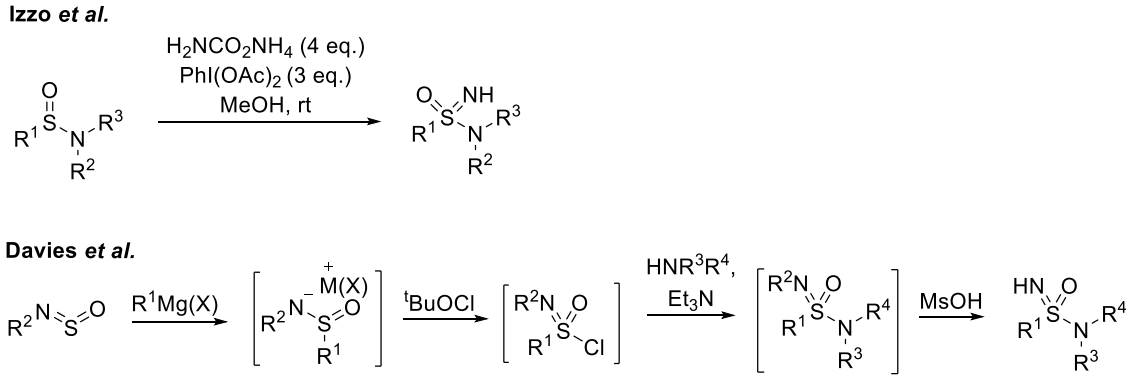


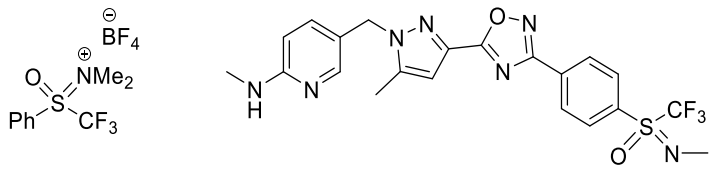
Figure 6.2. Sulfonimidamides in medicinal chemistry.

Several new synthetic methodologies have been published to access the sulfonimidamide moiety for drug discovery programmes. A recent publication by Izzo *et al.* reported the synthesis of unprotected sulfonimidamides through electrophilic NH transfer of tertiary sulfinamides using ammonium carbonate as a nitrogen source and $PhI(OAc)_2$ as an oxidant (Scheme 6.1).[137] Davies *et al.* reported a one-pot three component method using stable *N*-sulfinyltritylamine (TrNSO), organometallic reagents and amines to afford sulfonimidamides.[138] Although this method was applicable to aromatic, vinyl and simple alkyl organometallics, there was no report of its applicability for the synthesis of trifluoromethyl sulfonimidamides.



Scheme 6.1. Literature synthetic methodology to access sulfonimidamides.

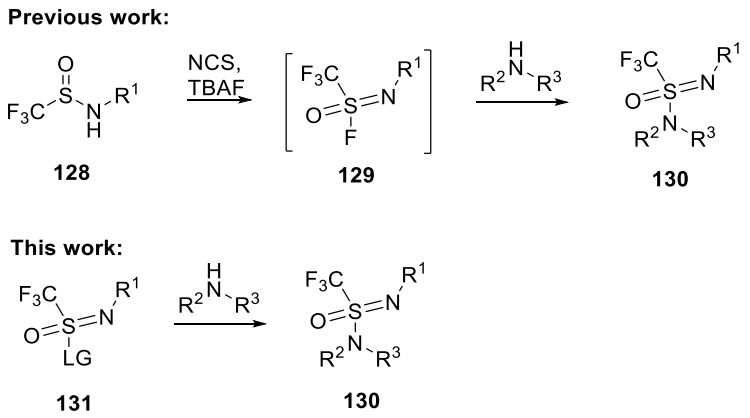
Fluorine atoms have been incorporated into numerous drug compounds as a way of improving properties such as potency, pKa, metabolic stability and membrane permeability.[139] The introduction of the large and strongly electron withdrawing CF_3 group to the sulfonimidamide moiety could provide interesting properties for drug development. CF_3-sulfoximines have found application in organic synthesis and medicinal chemistry. Trifluoromethyl sulfoximine **126** was discovered to be a useful source of the electrophilic trifluoromethyl cation for the transfer to different nucleophiles (Figure 6.3).[140,141] The CF_3-sulfoximine motif has been incorporated into some bioactive compounds including **127**, an inhibitor of HIF to treat hyperproliferative and angiogenesis disorders.



126 **127**, IC_{50} = 0.6 nmol/L

Figure 6.3 - Trifluoromethyl sulfoximine compounds.

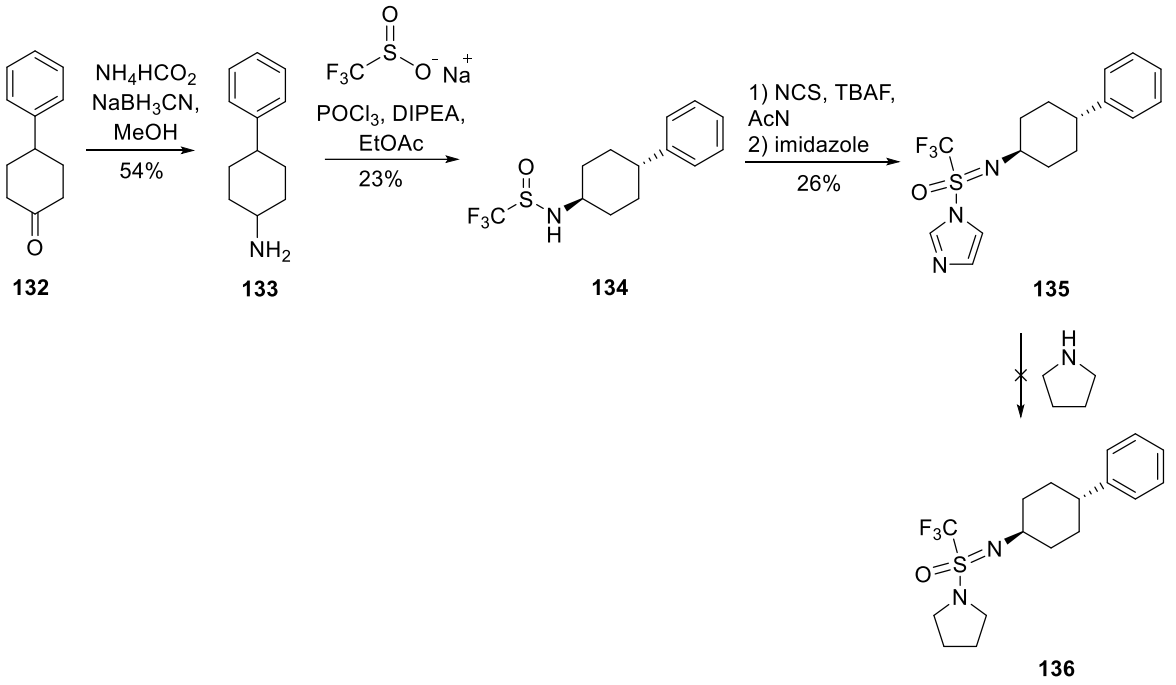
Oehlrich and coworkers published a two-step method for the synthesis of CF_3-sulfonimidamides **130** from sulfinamides **128**.[142] The first step involved oxidative chlorination to give sulfonimidoyl chloride and subsequent fluorination to give the more stable sulfonimidoyl fluoride **129** (Scheme 6.2). The second step involved reaction with various amines to give the corresponding CF_3-sulfonimidamides **130**. A chemically diverse range of CF_3-sulfonimidamides were synthesised in good yield from a wide scope of sulfinamides and amine starting materials. There were some concerns over the long-term stability of the sulfonimidoyl fluoride intermediate which limited its use in the scale up of large libraries of sulfonimidamides. As a result, we wanted to develop a bench-stable transfer reagent **131** bearing a leaving group that would be reactive towards amines for the synthesis of CF_3-sulfonimidamides **130** in one step. This reagent would hopefully be more activated for reaction with poor amine nucleophiles and less susceptible to sulfonamide byproduct formation compared to the sulfonimidoyl fluoride.



Scheme 6.2. Preparation of trifluoromethyl sulfonimidamides.

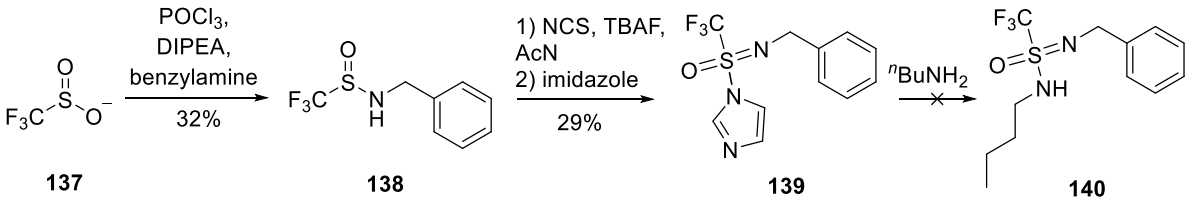
6.2. Development of Transfer Reagent for CF_3-Sulfonimidamides

As imidazole sulfonimidamide **135** was synthesised in previous investigations by Oehlrich and coworkers, it was postulated that **135** could be utilised as a bench-stable transfer reagent for the synthesis of CF_3-sulfonimidamides through displacement of the imidazole with various amines. Synthesis of **135** was achieved in three steps (Scheme 6.3). Reductive amination of phenyl cyclohexanone **132** with ammonium formate and sodium cyanoborohydride afforded **133**. Subsequent reaction with sulfinyl chloride, formed *in situ* from chlorination of sodium trifluoromethanesulfinate, afforded sulfinamide **134** after separation of the diastereoisomers by column chromatography. Sulfinamide **134** was converted to the sulfonimidoyl fluoride using the previously reported conditions of *N*-chlorosuccinimide (NCS) and tetrabutylammonium fluoride (TBAF) and directly reacted with imidazole to give CF_3-sulfonimidamide **135.**[142] Reaction with pyrrolidine was unsuccessful even with microwave heating as only starting material was observed by LCMS. This could be explained through steric hindrance between the incoming secondary amine (pyrrolidine) and sulfonimidamide **135**.



*Scheme 6.3. Synthesis of imidazole sulfonimidamide **135**.*

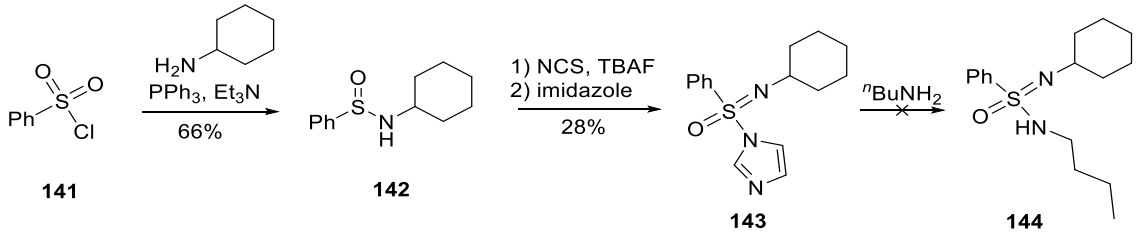
To reduce the steric hindrance around the sulfur atom, the secondary cyclohexyl amine was replaced with primary benzylamine. Primary butylamine was also used as the nucleophile rather than the secondary pyrrolidine to prevent steric effects. Benzylamine CF_3-sulfonimidamide **139** was synthesised through reaction of sodium trifluoromethanesulfinate **137**, phosphoryl chloride, benzylamine and diisopropylethylamine to afford sulfinamide **138** and subsequent two-step reaction via sulfonimidoyl fluoride (Scheme 6.4). Reaction between **139** and butylamine revealed only starting material by LCMS so it was unlikely due to steric hindrance of the incoming nucleophile but rather due to the poor leaving group ability of the imidazole.



*Scheme 6.4. Synthesis of imidazole CF_3-sulfonimidamide **139.***

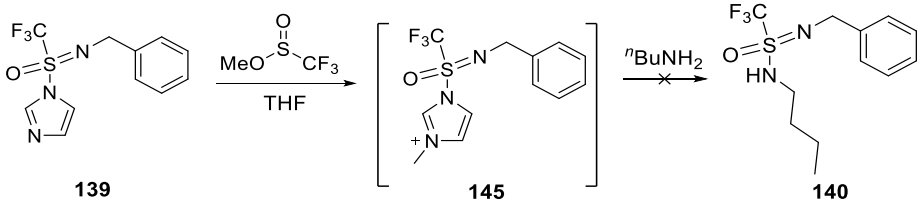
The use of imidazole as a leaving group for a bench-stable transfer reagent for the synthesis of phenyl sulfonimidamide **144** was also attempted. Sulfinamide **142** was synthesised via a different

mechanism through reduction of benzene sulfonyl chloride **141** using triphenylphosphine (Scheme 6.5). Imidazole sulfonimidamide **143** was afforded through the same oxidative chlorination, fluorination and displacement with imidazole. The imidazole could not be displaced by butylamine so the unreactivity of the imidazole sulfonimidamide was likely due to electronic effects.



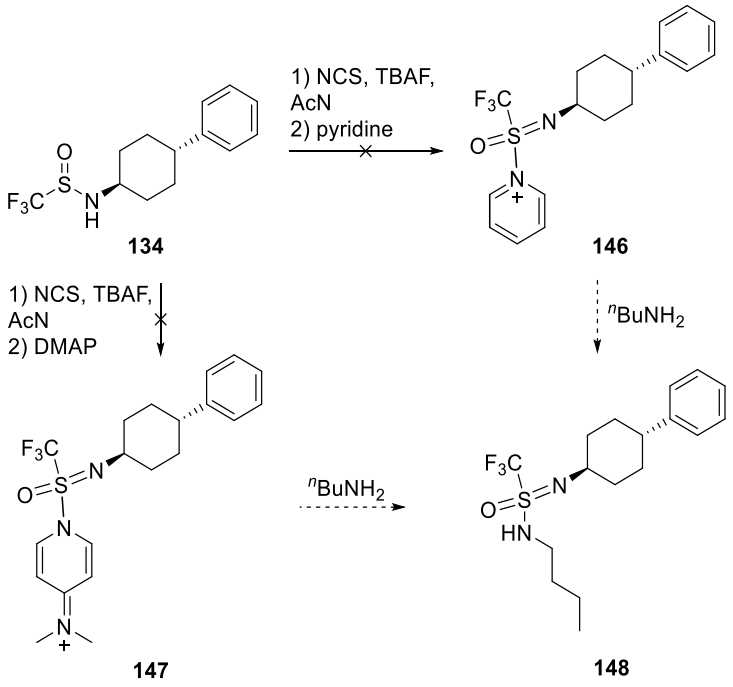
Scheme 6.5. Synthesis of imidazole phenyl sulfonimidamide.

To improve the leaving group ability of sulfonimidamide transfer reagent **139**, the imidazole was activated as the methyl imidazole **145** using methyl trifluoromethylsulfonate however subsequent *in situ* reaction with butylamine resulted in decomposition products (Scheme 6.6).[143]



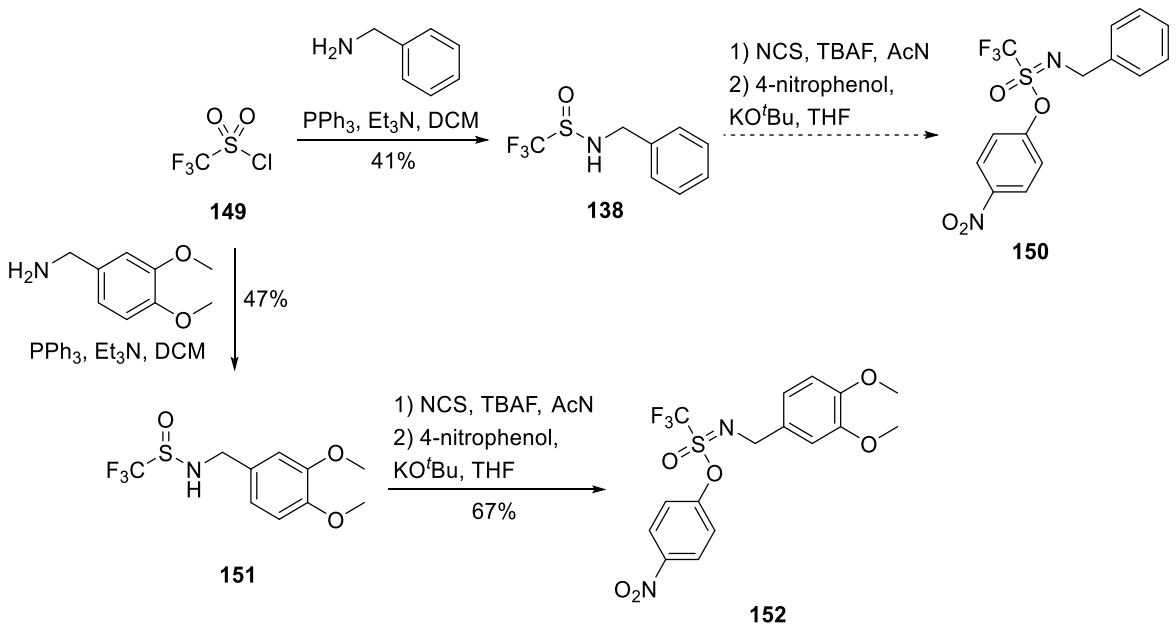
*Scheme 6.6. Synthesis of activated imidazole sulfonimidamide **145.***

As quaternised nitrogens are a good leaving group in other synthetic reactions, pyridine and 4-dimethylaminopyridine were also trialled as leaving groups, however the initial formation of the sulfonimidamides **146** and **147** respectively was not successful (Scheme 6.7). This was likely due to the high activation energy to form quaternised nitrogens.



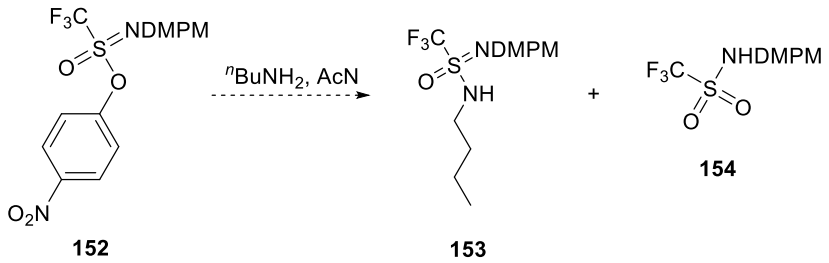
*Scheme 6.7. Activation of sulfinamide **134** with pyridine and DMAP.*

Common leaving groups for the synthesis of sulfonamides include *p*-nitrophenol[144] and pentafluorophenol[145] so these leaving groups were investigated for the synthesis of sulfonimidamides. Synthesis of CF_3-sulfinamide **138** was achieved from commercially available trifluoromethane sulfonyl chloride **149** via careful addition of triphenylphosphine and benzylamine in greater yield than previous chlorination of CF_3-sulfinate **137** (Scheme 6.8). *p*-Nitrophenol sulfonimidamide **150** could only be isolated in trace quantities which was thought to be due to volatility of sulfonimidoyl fluoride intermediate.



*Scheme 6.8. Synthesis of nitrophenol sulfonimidate **152**.*

Sulfinamide **151** bearing a 3,4-dimethoxylbenzyl group (DMPM) was synthesised from **149** to improve its stability compared to **138** and for greater ease of deprotection to enable further functionalisation of the sulfonimidamide. Subsequent formation of activated sulfonimidamide **152** with *p*-nitrophenol was achieved via sulfonimidoyl fluoride in good yield. The reaction of **152** with butylamine was attempted with different equivalents of amine, the addition of co-bases and different temperatures to give sulfonimidamide **153** (Table 6.1). No conversion of the starting material was observed with 10 equivalents of butylamine at room temperature. A small conversion to product was observed after overnight heating at 60 °C. To achieve full conversion of the starting material without long heating times, the reaction was attempted in the microwave, but decomposition of the benzyl group was observed. The addition of triethylamine as a co-base slowed the reaction down while the use of 1,8-diazabicyclo[5.4.0]undec-7-ene (DBU) resulted in a 1:1 ratio of the desired product **153** and sulfonamide byproduct **154**. Lithium bis(trimethylsilyl)amide (LiHMDS) resulted in decomposition of the starting material and minimal product formation.



152 **153** **154**

Amine eq.	Co. base	Temperature (°C)	Time	Conversion of SM (LCMS)
10		rt	4 h	0%
10		60	16 h	15% **153**
10		120 (MW)	30 min	Decomposition
2	2 eq. Et_3N	60	16 h	10% **153**
2	2 eq. DBU	60	24 h	66% (UV)
				1:1 **153**:**154**
2	2 eq. LiHMDS	rt	8 h	Decomposition

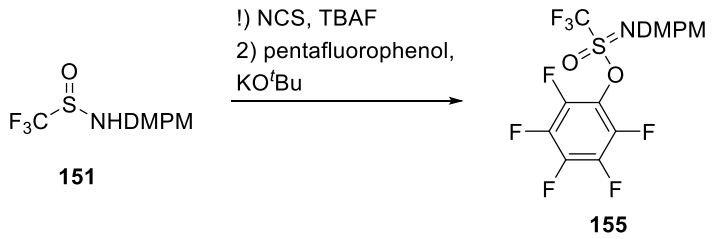
*Table 6.1. Optimisation of displacement of nitrophenol sulfonimidate **152** with butylamine.*

Different solvents were screened to improve conversion of starting material to the product **153** (Table 6.2). Good conversion was achieved in DMA and DMSO at room temperature and the product was obtained in good yield. It was also possible to lower the equivalents of amine using these solvents. However, the reaction time was very long even with a good nucleophilic amine so an elevated temperature of 60 °C was attempted which resulted in formation of the sulphonamide **154** in a 1:1 ratio with product **153**. Sulfonamide formation was also observed using DBU as a co-base. Non-polar solvents such as DCE showed no conversion even when heating at reflux. Heating in DMF also resulted in significant sulfonamide (SA) formation and therefore a lower isolated yield.

Solvent	Amine Eq.	Temperature (°C)	Time	Conversion of SM (LCMS)	Isolated yield
AcN	10	60	20 h	15%	
DMA	2	rt	48 h	66%	
DMSO	4	rt	42 h	80%	57%
DMSO	2	60	1.5 h	100%	
				1:1 **153**:**154**	
DMSO	2	rt	21 h	100%	
	+ 1 eq. DBU			3:2 **153**:**154**	
DCE	2	60	16 h	0%	
DMF	2	60	20 h	100%	23%

*Table 6.2. Solvent screen of displacement of nitrophenol sulfonimidate **152** with butylamine.*

As long reaction times at room temperature were required for good nucleophiles such as butylamine, it was decided that a better leaving group would be needed for displacement with less-nucleophilic amines. Pentafluorophenol was investigated to activate the CF_3-sulfonimidamide. The reaction of sulfonimidoyl fluoride with two equivalents of the potassium salt of pentafluorophenol resulted in 29% conversion to the product (Table 6.3). Increasing the number of equivalents to six improved the conversion to 60%. Some sulfonamide formation was observed which may have been due to small quantities of excess potassium *tert*-butoxide when concentrated *in vacuo* so an excess of phenol was used in further reactions. Purification of the sulfonimidoyl fluoride (SF) by flash chromatography prior to the addition of the phenoxide was trialled to determine whether the presence of TBAF and NCS was slowing down the reaction. The best conversion was observed with 14 equivalents of phenoxide to give a yield of 63%.



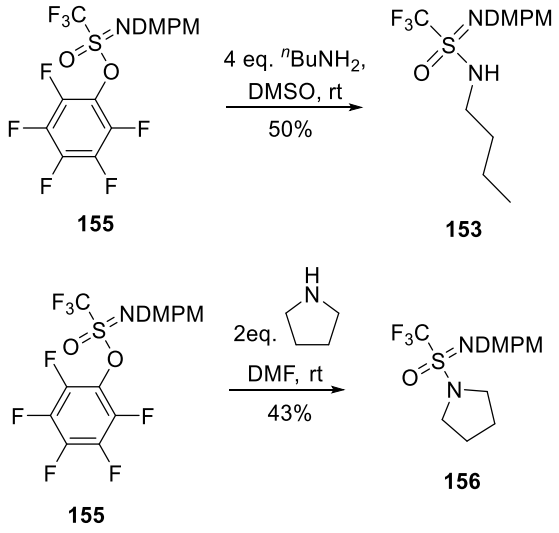
151 **155**

Conditions	Time	Conversion of SM (LCMS)	Isolated yield
2 eq. Phenol, 2 eq. KO^{t}Bu	16 h	29% **155**, 18% **154**, 52% **151**	20%
4 eq. Phenol, 2 eq. KO^{t}Bu	16 h	50% **155**, 13% **154**, 37% **151**	29%
6 eq. Phenol, 6 eq. KO^{t}Bu	20 h	60% **155**, 10% **154**, 30% **151**	
6 eq. Phenol, 6 eq. KO^{t}Bu (with pure SF)	16 h	58% **155**, 25% **154**, 17% **151**	40%
10 eq. Phenol, 9 eq. KO^{t}Bu (with pure SF)	16 h	80% **155**, 20% **151**	67%
15 eq. Phenol, 14 eq. KO^{t}Bu (with pure SF)	16 h	90% **155**, 10% **151**	63%

*Table 6.3. Optimisation of preparation of pentafluorophenol sulfonimidate **155**.*

Pleasingly, attempts to displace sulfonimidamide **155** bearing a pentafluorophenol leaving group with butylamine in DMSO was successful to afford **153** after stirring at room temperature for one hour. Reactivity with other amines such as pyrrolidine was also demonstrated to afford **156**

(Scheme 6.9). Therefore, pentafluorophenol was a better leaving group than imidazole and *p*-nitrophenol and was more reactive to amines under mild conditions to afford CF_3-sulfonimidamides in moderate yield. The reaction with butylamine in acetonitrile did not proceed to full conversion and the reaction was slow resulting in some sulphonamide **154** formation.

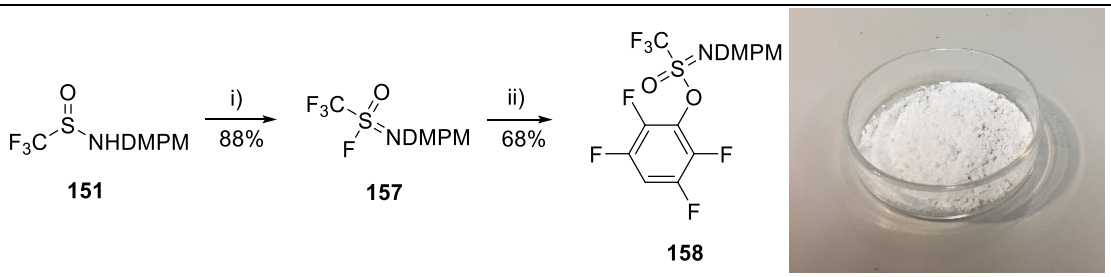


*Scheme 6.9. Reaction of pentafluorophenol sulfonimidate **155** with amines.*

Separation of the sulfonimidoyl fluoride from the pentafluorophenol sulfonimidate **155** by column chromatography proved challenging so the product was isolated as an oil due to small impurities of starting material. The requirement for large equivalents of pentafluorophenol to form the activated reagent **155** was also undesirable. The use of tetrafluorophenol as a leaving group was investigated as it is slightly more nucleophilic and would therefore be a good compromise between ease of formation of activated sulfonimidamide and reactivity with various amines.

Tetrafluorophenol sulfonimidate **158** was synthesised in two steps from sulfinamide **151** (Scheme 6.10). The first step involved formation of sulfonimidoyl fluoride **157** as previously described through oxidative chlorination and subsequent *in situ* fluorination using NCS and TBAF.[142] The isolated sulfonimidoyl fluoride was subjected to an excess of potassium tetrafluorophenoxide at room temperature to afford the desired transfer reagent **158** in good yield (68%) on a 3 g scale. The reaction could be performed in one-pot through concentration of sulfonimidoyl fluorination and *in*

situ reaction with phenoxide but the yield was reduced due to sulfonamide byproduct formation. The transfer reagent was isolated as a white solid which was much easier to handle than the sulfonimidoyl fluoride **157** as a colourless oil.



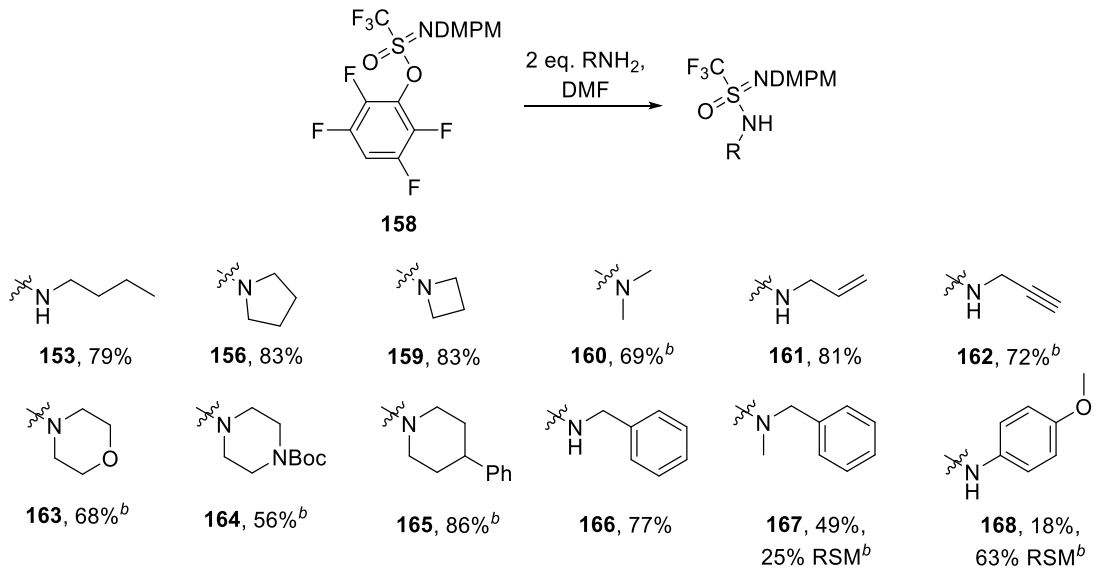
*Scheme 6.10. Synthesis of Tetrafluorophenol sulfonimidate **158**. Reaction conditions: (i) NCS (1.1 equiv.), TBAF (1.1 equiv.), AcN, 0°C to rt, 30 min (ii) 2,3,5,6-Tetrafluorophenol (8 equiv.), KO^{t}Bu (1M in THF, 7 equiv.), then **157**, AcN.*

6.3. Reaction of Transfer Reagent 158 with Amines to Form CF_3-Sulfonimidamides

Excellent reactivity was demonstrated between activated tetrafluorophenol transfer reagent **158** and various amines to afford structurally distinct CF_3-sulfonimidamides (Scheme 6.11). Pyrrolidine and azetidine, simple secondary amines, afforded sulfonimidamides **156** and **159** respectively in good yield through stirring at room temperature for one hour. Heating to 50 °C was required for good conversion of starting material with dimethylamine to give sulfonimidamide **160** in moderate yield. Primary amines, such as butylamine, reacted at room temperature to give sulfonimidamide **153** in good yield. Allylamine and propargylamine, electron deficient primary amines, required only two equivalents to obtain compounds **161** and **162** respectively in good yield unlike previously reported reaction with the sulfonimidoyl fluoride which required more forcing conditions with eight equivalents of amine for good conversion to the product.[142]

Some examples of larger and less nucleophilic amines were also successful at forming the corresponding sulfonimidamides in good to moderate yields. Morpholine, previously unsuccessful with trifluoromethyl sulfonimidoyl fluoride, reacted with transfer reagent **158** to give sulfonimidamide **163**. Pleasingly, reaction with Boc-piperazine afforded compound **164** which could be further functionalised through selective deprotection of the Boc group over the benzyl group.

Similarly, phenylpiperidine was successful under the reaction conditions to afford compound **165** in excellent yield. Benzylamine reacted at room temperature to give sulfonimidamide **166** in good yield while the bulkier secondary amine, *N*-methyl benzylamine, required elevated conditions of heating to 50 °C for moderate conversion to **167** with some recovered starting material. **158** was also reactive towards poor nucleophiles such as *p*-methoxy aniline to give compound **168** in low yield however there was good recovery of starting material. It could be possible to improve the yield with more equivalents of the amine to force conversion of the starting material. Overall, the transfer reagent was more reactive than the sulfonimidoyl fluoride[142] towards a wide range of amines and could therefore be applied to the synthesis of more complex drug compounds.

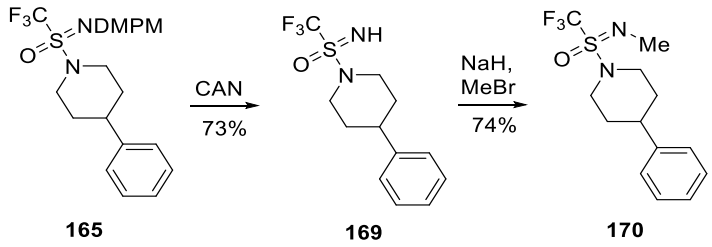


Scheme 6.11. Amine scope with transfer reagent. [a]Reaction Conditions: 2 equiv. amine, DMF, rt, 1 h; [b] 2 equiv. amine, DMF, 50 °C; RSM = Recovered Starting Material.

6.4. Removal of Protecting Group from Transfer Reagent and Further functionalisation

The removal of the dimethoxybenzyl protecting group was attempted to demonstrate the utility of the transfer reagent for the synthesis of unprotected trifluoromethyl sulfonimidamide. Deprotection of **165** was achieved using ceric ammonium nitrate (CAN) as an oxidizing agent to afford compound **169** in good yield (Scheme 6.12). Further functionalisation through alkylation of

the nitrogen with methyl iodide was successful to afford compound **170**. As a result, the transfer reagent has the potential to be useful for the synthesis of pharmaceutical compounds through the easy removal of the protecting group in the later steps and subsequent chemical modification to optimize properties of the imine nitrogen.

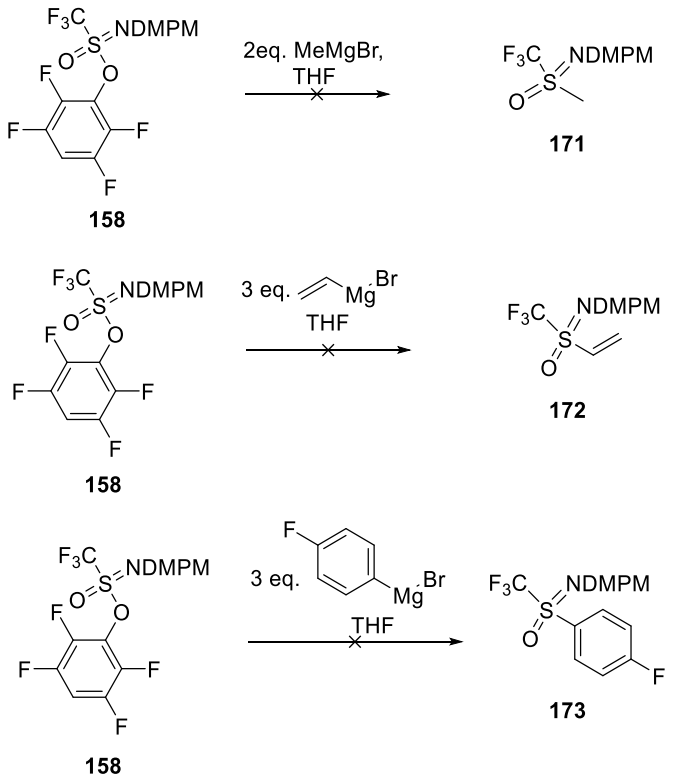


165 **169** **170**

Scheme 6.12. Deprotection of DMPM group and alkylation.

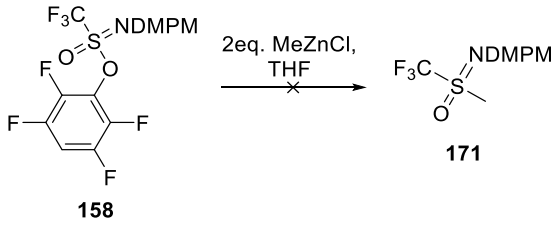
6.5. Reactivity of Transfer Reagent 158 with C-Nucleophiles

As reactivity of CF_3-sulfonimidoyl fluoride with a carbon nucleophile was reported,[142] the applicability of the transfer reagent **158** to the formation of CF_3-sulfoximines was attempted. The reaction of the transfer reagent with methyl magnesium bromide was unsuccessful as only starting material was observed, even upon heating to 50 °C (Scheme 6.13). Other Grignard reagents, such as vinylmagnesium bromide and *p*-fluorophenyl magnesium bromide, were also trialled but only small conversion of starting material was observed at room temperature and decomposition was observed when heated to 50 °C.



*Scheme 6.13. Attempted reaction of transfer reagent **158** with Grignard reagents.*

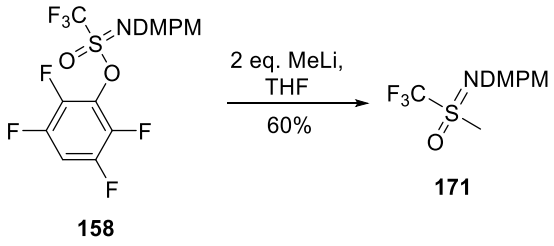
The use of zincates as carbon nucleophiles was also trialled but only small conversion of starting material was observed after heating for 3 days with methyl zinc chloride (Scheme 6.14). Reaction with the simplest zincate was very slow so it would have been difficult to optimise with less reactive, larger nucleophiles.



*Scheme 6.14. Attempted reaction of transfer reagent **158** with methyl zinc chloride.*

Given the poor reactivity with Grignard reagents and zincates, the more reactive methyl lithium was attempted. Gratifyingly, reaction of the transfer reagent **158** with methyl lithium afforded CF_3-sulfoximine **171** in 60% yield with no observed sulfonamide formation unlike using sulfonimidoyl fluoride (Scheme 6.15).[142] Given the greater reactivity and stability under basic conditions

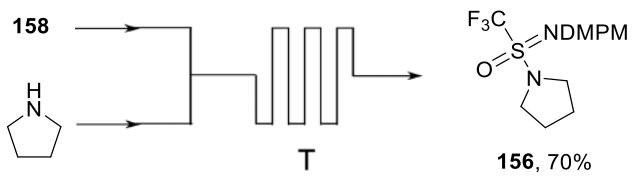
compared to the sulfonimidoyl fluoride, the conditions could be optimised for reaction with other commercially available carbon nucleophiles for the synthesis of structurally-diverse CF_3-sulfoximines.



*Scheme 6.15. Synthesis of trifluoromethyl sulfoximine **171**.*

6.6. Use of Transfer Reagent to Form CF_3-Sulfonimidamides Using Flow Conditions

Flow chemistry is a process of performing chemical reactions in a tube in which the reactive components are pumped together through a mixing junction and flowed down a temperature-controlled tube. There are several advantages of flow chemistry including fast reaction times, fewer unwanted byproducts and safer reactions so it is particularly useful in the scale up of chemical reactions. The synthesis of CF_3-sulfonimidamide **156** was demonstrated using flow conditions in a two-flow chip reactor. **156** was synthesised in 70% yield by mixing solutions of **158** and pyrrolidine in a reactor heated to 80 °C at a flow rate of 0.05 ml/min (Scheme 6.16). A lower yield of **156** was obtained compared to batch conditions due to incomplete conversion of starting material however the efficient mixing of the flow conditions allowed the use of higher temperatures.



*Scheme 6.16. Flow reaction conditions to trifluoromethyl sulfonimidamides. Reaction conditions: **158**, pyrrolidine (2 eq.), AcN, 80 °C, 0.05 mL/min.*

6.7. Chemical Stability of Transfer Reagent

The aim of this work was to develop a bench-stable transfer reagent that could be synthesised in large quantities without degradation with long-term storage. To test their stability sulfonimidoyl fluoride **157** and tetrafluorophenol sulfonimidamide **158** were subjected to various chemical stability tests (Appendix 1). Sulfonimidoyl fluoride **157** degraded to the corresponding sulfonamide **154** under acidic conditions of 0.1 N HCl and pH 4 at both 37 °C and 60 °C. Full conversion to sulfonamide **154** was observed upon heating at 60 °C under neutral conditions of pH 7.4. Basic conditions of 0.1 N NaOH resulted in full conversion to sulfonamide and some degradation was even observed heating in MeOH and DMSO at both temperatures. Transfer reagent **158** was stable to all acidic and neutral pH conditions. As seen during reaction optimisation, some conversion to sulfonamide **154** was observed under strongly basic conditions. Overall, transfer reagent **158** is a bench-stable solid that is easy to handle and is more chemically stable than sulfonimidoyl fluoride **157** for long-term storage.

6.8. Summary

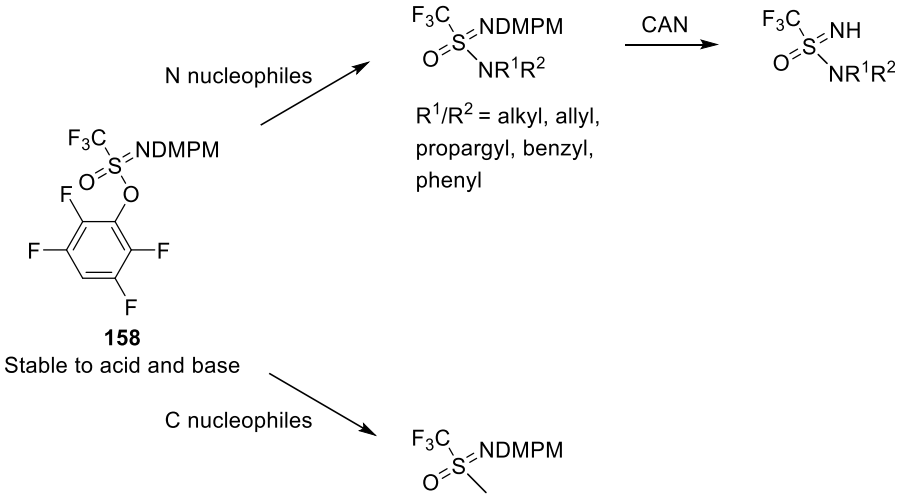
A transfer reagent for the synthesis of trifluoromethyl sulfonimidamides was developed (Scheme 6.17). The reagent comprised of a dimethoxybenzyl protecting group for the imine and a leaving group. Tetrafluorophenol was determined to be the optimum leaving group as a compromise between nucleophilicity for formation of the transfer reagent and reactivity with various amines. The transfer reagent **158** was synthesised in two steps from sulfinamide **151** through sulfonimidoyl fluoride **157** in good yield. **158** was reactive towards a wide range of amines including primary, secondary and electron deficient amines.

Further functionalisation of the trifluoromethyl sulfonimidamides was demonstrated through deprotection of the dimethoxybenzyl group and alkylation of the imine nitrogen. The transfer

reagent was also applicable to flow chemistry conditions resulting in trifluoromethyl sulfonimidamide **156** in good yield.

The transfer reagent was unreactive towards some carbon nucleophiles including Grignard reagents and zincates however trifluoromethyl sulfoximine **171** was synthesised using methyl lithium. Although the transfer reagent was limited in its applicability to sulfoximine formation, further reaction optimisation using Lewis acids could increase their reactivity towards a more diverse range of carbon nucleophiles.

The transfer reagent was proven to be more stable than the corresponding sulfonimidoyl fluoride **157** through chemical stability tests. **158** was stable to both acidic and neutral conditions unlike sulfonimidoyl fluoride and was also more stable under basic conditions than **157**. Therefore **158** represents a useful bench-stable reagent for the synthesis of trifluoromethyl sulfonimidamides which can be prepared on a large scale for long-term storage.



*Scheme 6.17. Summary of reactivity of transfer reagent **158** towards N and C nucleophiles.*

Chapter 7. Adenine-Based PROTACs for Selective Degradation of Ribonucleotide Reductase

This chapter describes a project that was undertaken in collaboration with Vincenzo D'Angiolella in the Department of Oncology.

7.1. Background – Ribonucleotide Reductase

Ribonucleotide diphosphate reductase (RNR) catalyses the formation of deoxyribonucleotides from ribonucleotides by removing the 2'-hydroxyl group of the ribose ring of nucleotide diphosphates (NDPs) and therefore catalyses the de-novo synthesis of deoxyribonucleotides (dNDPs) that are essential for DNA synthesis.[146,147] As a result, RNR represents an interesting target for cancer therapeutics because DNA replication mutation errors are major contributors to the onset of many cancers.[148] RNR is composed of two identical large subunits (RRM1, RNR1, RR1 or R1) and two identical small subunits (RRM2, RNR2, RR2 or R2).[149–151] The tetramer complex is necessary for functional catalytic activity (Figure 7.1). All three classes of RNR (I, II and III) show the same basic catalytic mechanism in which a thiyl radical in the active site abstracts the 3' hydrogen atom.

Class I RNR's reduce ribonucleoside 5'-diphosphates (NDPs) to deoxyribonucleoside 5'-diphosphates (dNDPs) while classes II and III reduce ribonucleoside 5'-triphosphates (NTPs) to deoxyribonucleoside 5'-triphosphates (dNTPs). An allosteric effector binds to the specificity site (S-site) to regulate the specificity of each four substrates.[151] The fully phosphorylated products, dATP, dGTP and dTTP and to a lesser extent dCTP,[152] act as allosteric effectors. Overall, the allosteric regulation of RNR results in a balanced supply of the four deoxynucleotides.

The RRM2 subunit has been shown to be targeted and degraded by Cyclin F, an E3 ubiquitin ligase while RRM1 is not regulated by proteolysis but through strong allosteric binding of dATP.[153]

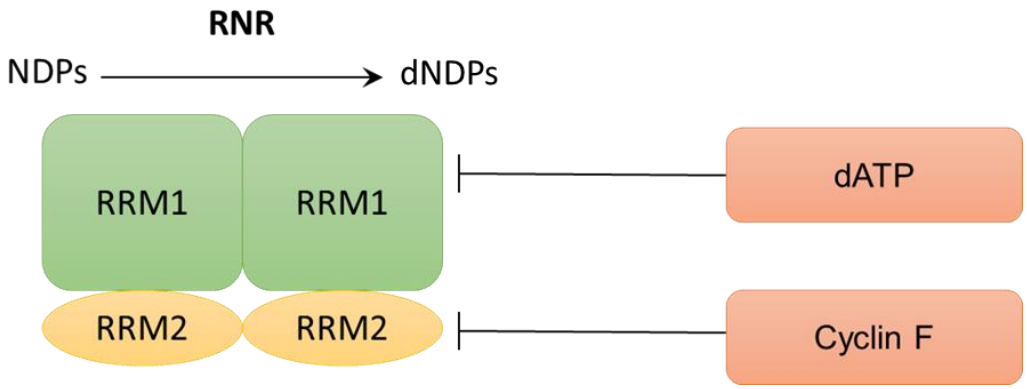


Figure 7.1. Regulation of dNTPs production by ribonucleotide diphosphate reductase (RNR).

7.2. Background – Use of PROTACs for Protein Degradation

An alternative strategy for targeting protein targets was reported by Crews and coworkers in 2001 through the development of proteolysis-targeting chimeras (PROTACs) which are heterobifunctional molecules containing two ligands connected by a linker; one ligand binds to the protein that is being targeted and another ligand recruits an E3 ubiquitin ligase (Figure 7.2).[154–156] This results in a ternary complex that positions the targeted protein in proximity for poly-ubiquitination and subsequent degradation by the proteosome.

PROTACs offer several advantages over traditional small-molecule inhibitors. Higher cellular potency can be achieved due to the catalytic mode of action. Highly selective degradation can be achieved with high quality ligands for the protein of interest.[157] PROTACs also have the potential for extended pharmacodynamic duration of action as once the target proteins are depleted through degradation, the PROTAC must only degrade slowly resynthesised protein.[158]

The rapid development in the application of PROTACs has been aided by the discovery of small-molecule ligands for the E3 ubiquitin ligases. High quality ligands have been developed for Von-Hippel Lindau (VHL) which is the substrate adapter for the Cullin E3 ligase complex that induces the degradation of its substrate HIF1α.[159–161] Cereblon (CRBN) is another E3 ubiquitin ligase which is a

substrate adapter for Cullin 4a E3 ligase complex.[162] The thalidomide drug and its analogues such as pomalidomide bind to CRBN and induce degradation of several proteins.[163,164]

Using high affinity ligands for a protein of interest, many PROTAC molecules have been developed to recruit E3 ubiquitin ligases. Different structural classes of protein have been degraded by PROTACS such as receptor tyrosine kinases and hormone receptors.[165] In the epigenetics field, bromodomains such as BRD4[166,167] and BRD9[168] have been successfully targeted by PROTAC compounds.

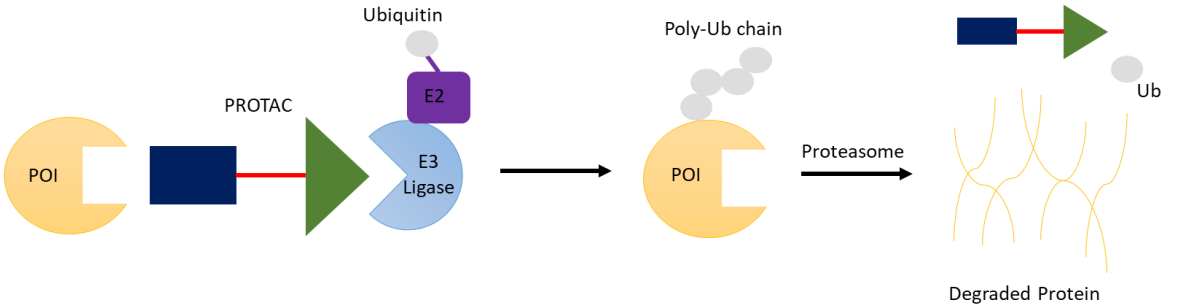


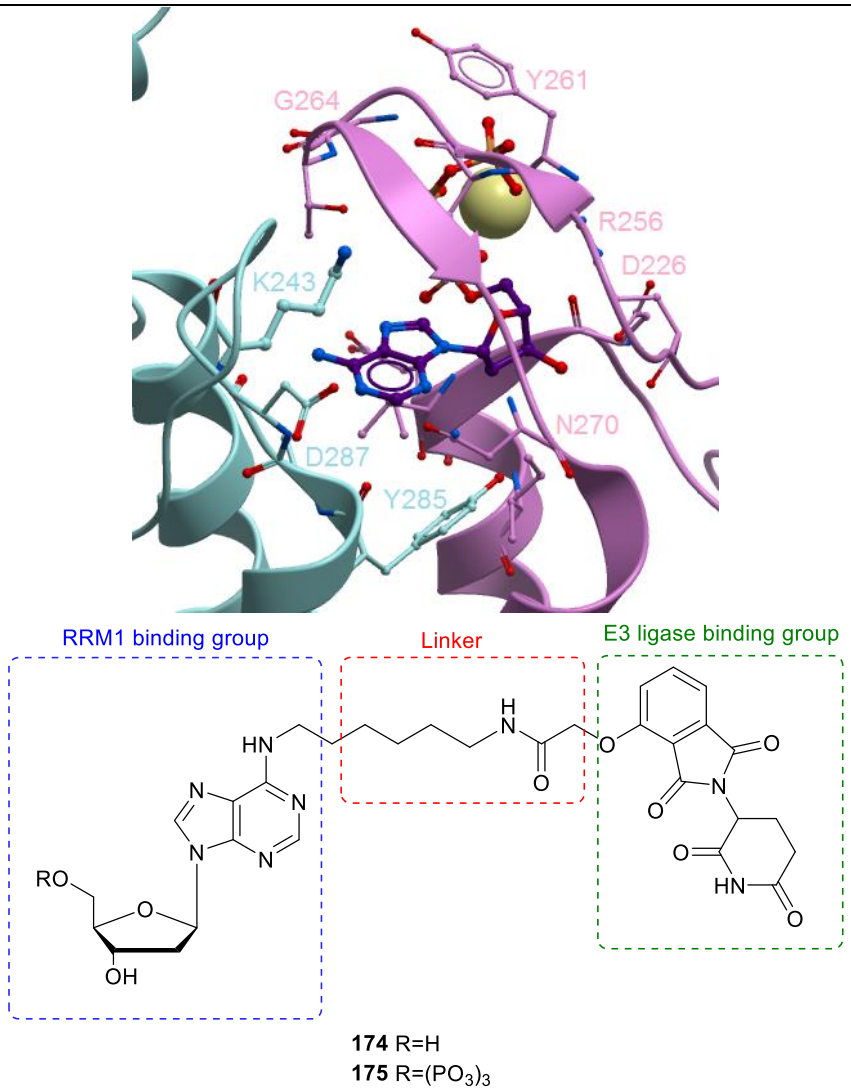
Figure 7.2. Protein degradation using a PROTAC that binds to protein of interest (POI) and recruits E3 ligase for polyubiquitination of the protein.

7.3. Design of Deoxyadenosine-Based PROTAC

The aim of this project was to design a deoxyadenosine-based PROTAC for the degradation of RRM1. Structural information from a crystal structure of human ribonucleotide reductase R1 subunit (RRM1) in complex with dATP (PDB ID 2WGH) revealed the key binding interactions (Figure 7.3). dATP binds between the two RRM1 subunits at the allosteric site through hydrogen bonding interactions between the aniline and ring nitrogens of the purine with D287 and between the 3' hydroxyl and D226 of the other subunit. The triphosphate group forms a salt bridging and hydrogen bonding network with K243, R256, G264 and with the magnesium ion.

Deoxyadenosine-based PROTAC **174** was designed comprising deoxyadenosine prodrug which could be phosphorylated to the nucleotide triphosphate **175** *in situ* and bind to RRM1 and the

pomalidomide-like scaffold as the E3 ligase cereblon binding moiety (Figure 7.3). The two ligands were conjugated through an aliphatic amide linker. The nature (hydrocarbon or PEG-based) and length (typically up to 20-carbon) of the linker is believed to be important for efficient recruitment of the E3 ligase so several compounds would need to be designed to maximise interactions with both the target protein and the E3 ligase.[169] As the 5' hydroxyl group was required for phosphorylation and the 3' hydroxyl was hindered by binding residues, the linker would be attached to the aniline nitrogen as the loss of one hydrogen bonding interactions may not be detrimental to binding.

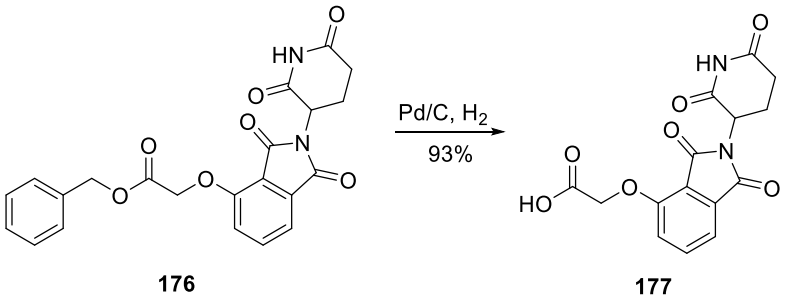


174 R=H
175 R=$(PO_3)_3$

*Figure 7.3. Crystal structure of dATP in the two subunits (blue and pink) of human ribonucleotide reductase R1 (RRM1) (above, PDB ID 2WGH) and structure of designed deoxyadenosine-based PROTAC **174** and triphosphate **175**.*

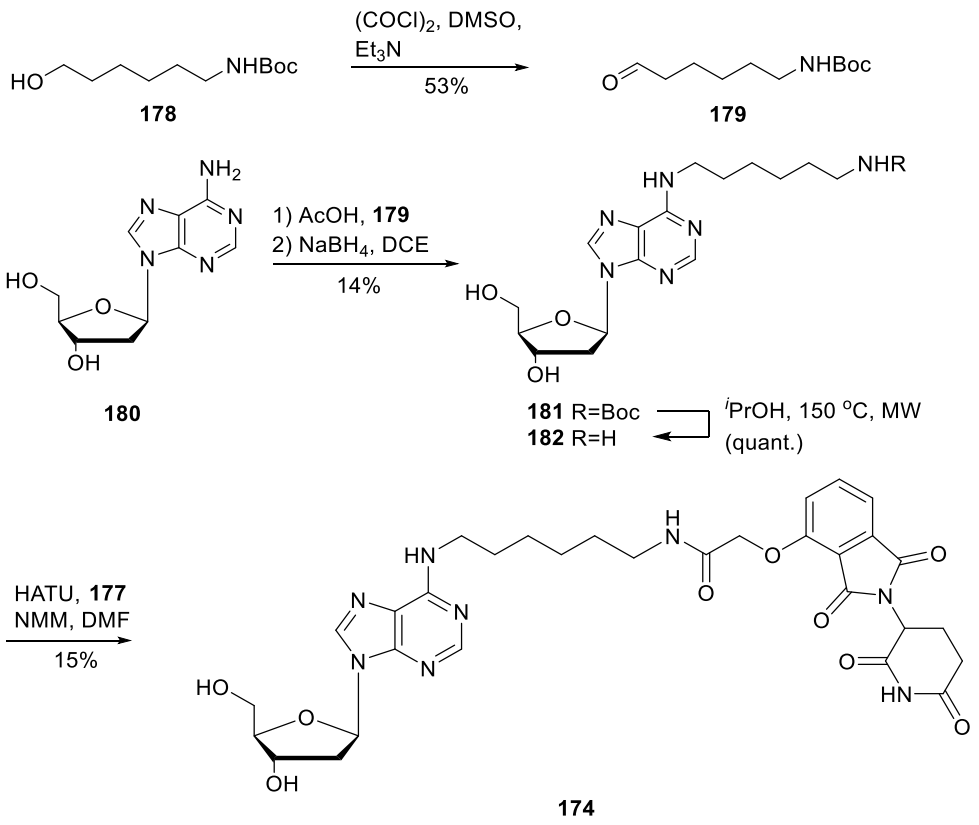
7.4. Synthesis of Adenine-Based PROTAC

The synthesis of the pomalidomide-like E3 ligase ligand required for protein degradation was achieved from **176** (previous steps by another colleague). Hydrogenation of benzyl ether **176** resulted in carboxylic acid **177** for subsequent amide coupling with the deoxyadenosine portion (Scheme 7.1).



*Scheme 7.1. Synthesis of carboxylic acid **177**.*

The synthesis of deoxyadenosine-PROTAC **174** was achieved starting from commercially available *tert*-butyl (6-hydroxyhexyl)carbamate **178** and deoxyadenosine **180** (Scheme 7.2). Swern oxidation of alcohol **178** afforded aldehyde **179**. Reductive amination with aniline of 2'-deoxyadenosine **180** and aldehyde **179** gave compound **181**. The yield was poor as the heterocyclic aniline was a poor nucleophile for the initial imine formation and the subsequent reduction of the stable imine required forcing conditions. Boc deprotection of **181** was attempted under acidic conditions such as trifluoroacetic acid and hydrochloric acid however both resulted in depurination. Successful Boc deprotection was achieved under neutral conditions through microwave heating at 150 °C in isopropanol to afford unprotected amine **182**. Amide coupling between **182** and **177** using HATU as a coupling reagent afforded the final product **174**.



*Scheme 7.2. Synthesis of deoxyadenosine-based PROTAC **174**.*

7.5. Degradation of RRM1 with Compound 174

PROTAC **174** was tested for its ability to degrade RRM1 using western blotting. Compound **174** was incubated with MCF7 cells at different concentrations from 10 nM to 100 µM. Compared to the DMSO control, the western blot showed a reduction in RRM1 in a dose dependent manner up to 10 µM. At a compound concentration of 100 µM, RRM1 protein reached the levels of the DMSO control which was likely due to the "hook effect". This occurs when excess unbound compound results in the formation of binary complexes which compete with and exceed the formation of ternary complexes. There was no reduction of RRM2B protein so the PROTAC was not inducing degradation of RRM2. In Hela cells, there is significant degradation of the RRM1 protein at 10 nM however at concentrations higher than 10 nM, the levels of RRM1 returned to that of the DMSO control which must be due to the "hook effect". The different potencies observed in the cell lines was likely due to the relative abundance of the RRM1 subunit.

As some degradation of the RRM1 subunit with PROTAC **174** was demonstrated, other compounds were designed to improve the formation of the ternary complex and subsequent degradation of RRM1.

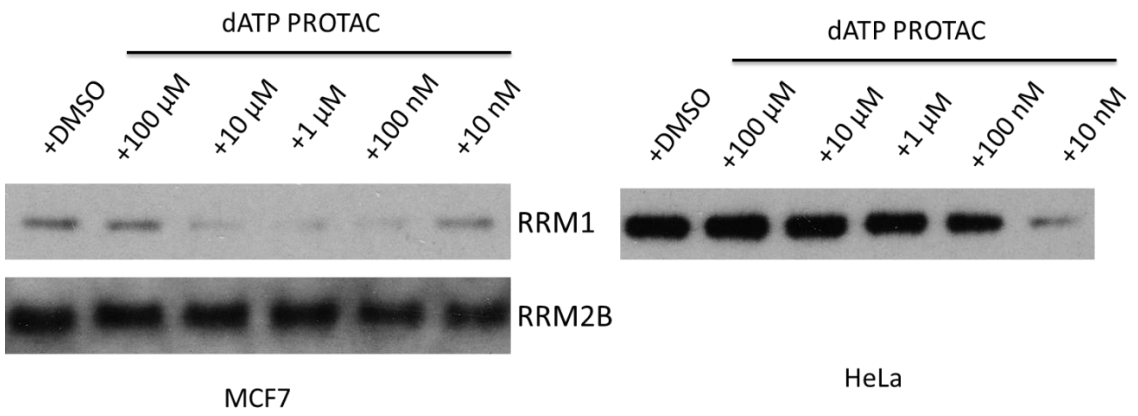


*Figure 7.4. Western blot of RRM1 and RRM2B after incubation of MCF7 and HeLa cells with **174**.*

7.6. Synthesis of a C-2 Substituted Deoxyadenosine-Based PROTAC

Given the biological results, it was thought that greater binding in the allosteric site would be achieved if the linker and pomalidomide-like moiety were added at the C-2 of the purine ring rather than the aniline nitrogen (Figure 7.5). The dATP molecule binds in a tight binding pocket and substitution of the aniline nitrogen may have hindered binding due to collisions with binding residues. The space filling model revealed that there was an opening between the two subunits at C-2 of the purine ring (indicated by the red arrow) which could be substituted with a linker to a pomalidomide-like group.

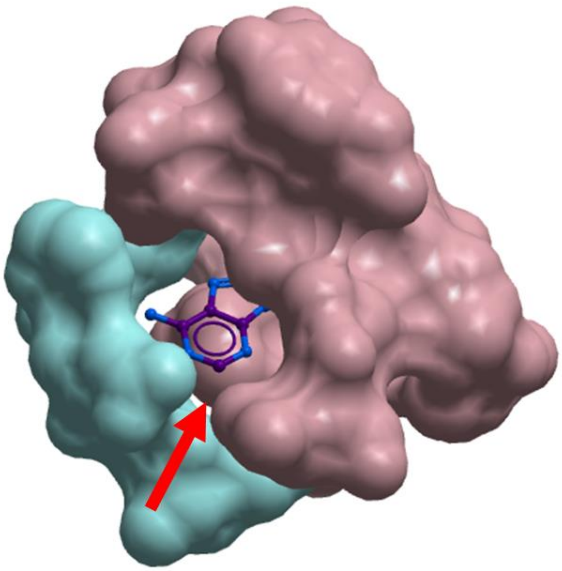


Figure 7.5. Space filling representation of the binding mode (PDB ID 2WGH).

C-2 substituted deoxyadenosine-based PROTAC **183** was proposed as the alkyne provided a straight vector out of the binding pocket and prevented collisions with binding residues (Figure 7.6). The synthesis was envisaged through a key Sonagashira reaction between compounds **184** and **185** to link the RRM1 binding group and pomalidomide-like scaffold.

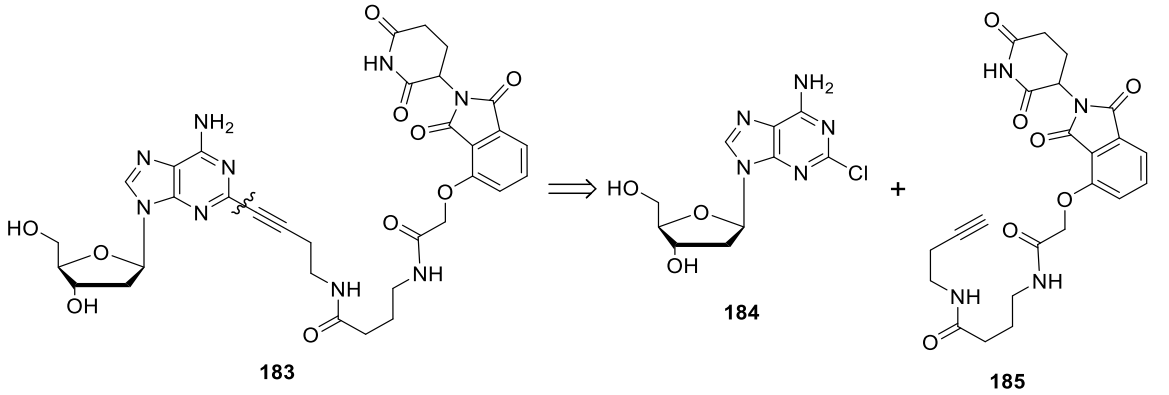
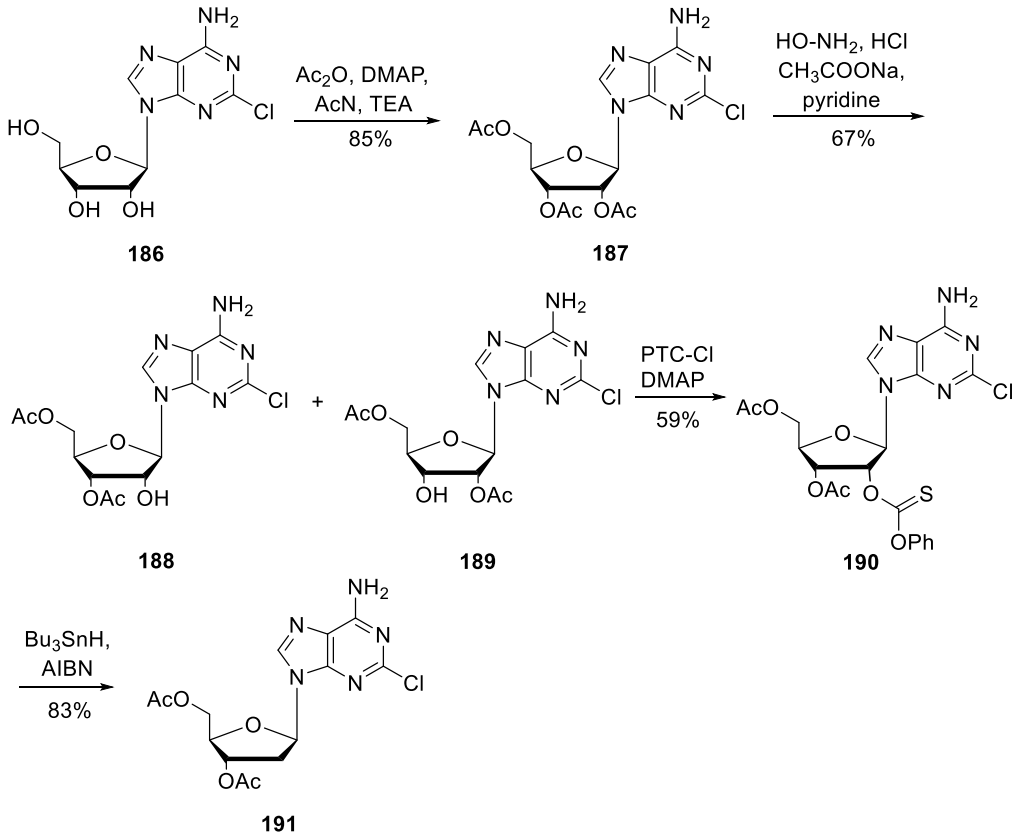


*Figure 7.6. Design of a C-2 alkyne deoxyadenosine-based PROTAC **183**.*

184 is cladribine, a clinical drug for the treatment of hairy cell leukemia and B-cell chronic lymphocytic leukemia,[170] so there have been a number of synthetic routes reported towards **184**. Xu *et al.* published the synthesis of compound **184** in five steps from cheap and commercially-

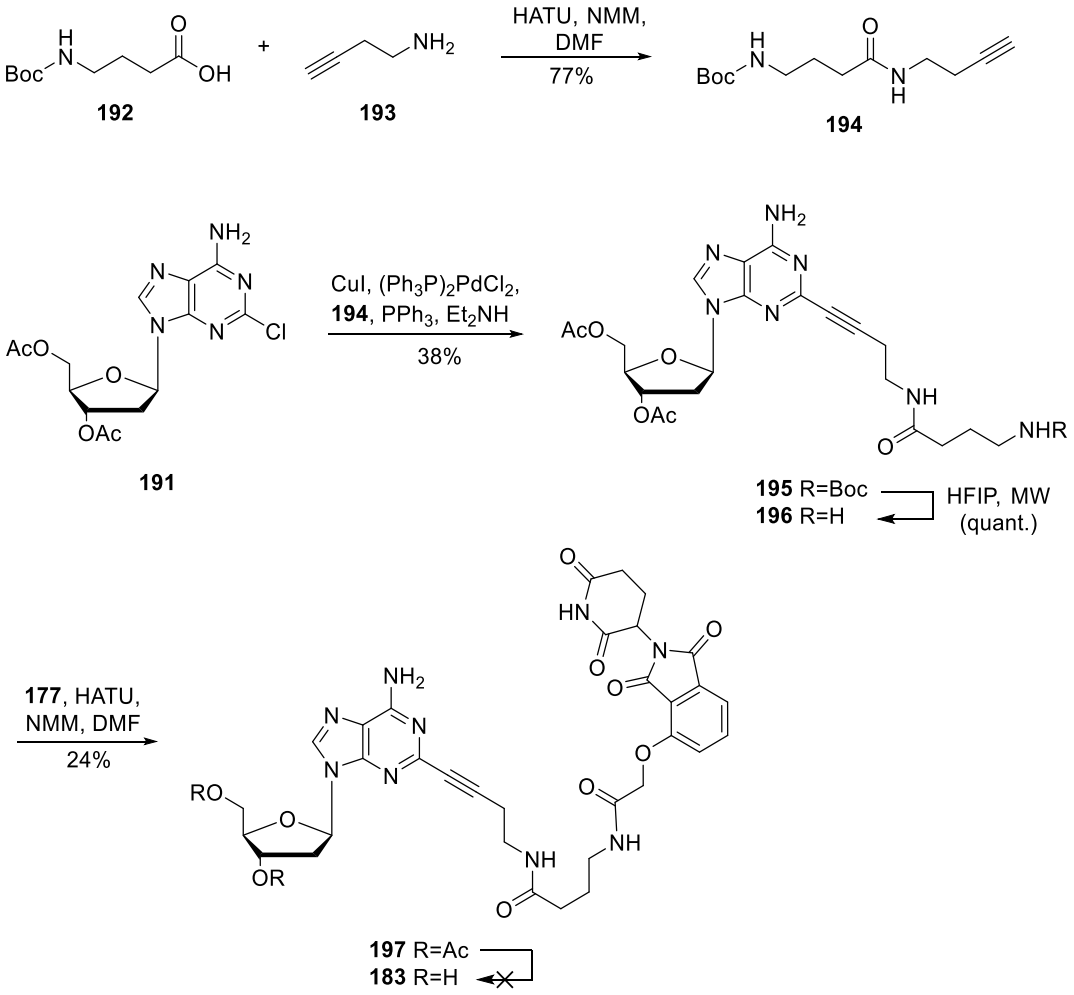
available chloroadenosine **186** through exhaustive acylation, followed by selective deacetylation at the 2' position and removal of the 2' hydroxyl group using a Barton-McCombie reaction.[171]

Acetylation of chloroadenosine **186** was achieved in 85% yield to give the triacetylated chloroadenosine **187** (Scheme 7.3). The deprotection of the 2'-OAc group was achieved using hydroxylamine and sodium acetate however some deacetylation at the 3' position was observed. The ratio of 2'-OH **188**:3'-OH **189** in the product was 3:1 by NMR which could not be separated by column chromatography. The mixture was therefore taken through to the next step by reaction with O-phenyl chlorothionoformate to give thioester **190** which could be separated from 3'-thioester isomer by column chromatography. Thioester **190** was used as a precursor for the Barton-McCombie deoxygenation selectively at the 2' position. This was achieved using tributyltin hydride and the radical initiator azobisisobutyronitrile (AIBN) resulting in deoxygenation of the 2' alcohol to afford **191** in good yield.



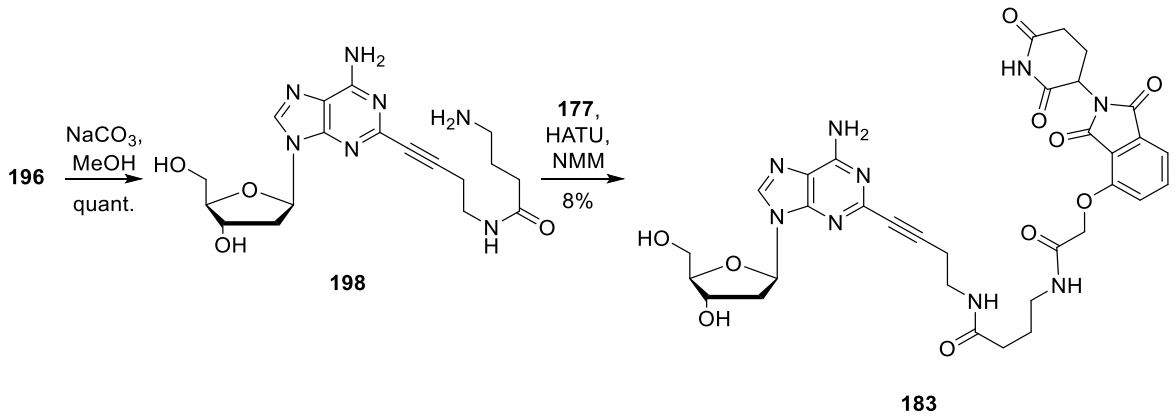
*Scheme 7.3. Synthesis of 2'-deoxygenated chloroadenosine **191**.*

Amide coupling between 4-(*tert*-Butoxycarbonylamino)butyric acid **192** and but-3-yn-amine **193** gave compound **194** to provide an aliphatic linker between the binding group and pomalidomide-like group (Scheme 7.4). Subsequent Sonagashira coupling between **191** and **194** was successful at forming **195** using dichlorobis(triphenylphosphine)palladium(II), diethylamine and copper iodide.[172] The yield was low due to unreacted starting material despite the use of an excess of **194**. The reaction also resulted in some decomposition products which were not possible to separate from the desired compound **195** so the crude mixture was used directly in the next step. As previously observed, Boc deprotection of the primary amine was unsuccessful using acidic conditions of trifluoroacetic acid due to depurination of the sugar. As basic conditions would result in deprotection of the acetyl protecting groups, Boc deprotection was attempted under neutral conditions through microwave heating in hexafluoroisopropanol (HFIP). Initial heating at 120 °C resulted in slow formation of amine **196** and upon prolonged heating resulted in decomposition products. Slow microwave heating at the lower temperature of 100 °C for 8 hours resulted in fewer side products and amine **196** was obtained in quantitative yield. The addition of the pomalidomide portion was achieved through HATU coupling between amine **196** and carboxylic acid **177** to give compound **197**. The final step to remove the acetyl groups proved challenging under basic conditions using ammonia in methanol or sodium methoxide due to ring opening of the pomalidomide-like portion.



*Scheme 7.4. Attempted synthesis of alkyne deoxyadenosine-based PROTAC **183**.*

As a result, it was decided to remove the acetyl groups prior to the addition of E3 ligase binding group as the primary amine would be the most nucleophilic for amide coupling. Deprotection of the acetyl groups was achieved under basic condition using sodium carbonate to afford compound **198** in quantitative yield (Scheme 7.5)[173] Amide coupling between amine **198** and carboxylic acid **177** afforded C-2 substituted deoxyadenosine PROTAC **183**. This compound is being tested in biological studies to demonstrate degradation of RRM1, but no conclusive results have been obtained at the time of writing this thesis.



*Scheme 7.5. Synthesis of C-2 deoxyadenosine PROTAC **183.***

7.7. Summary

Deoxyadenosine-based PROTAC **174** was designed to induce the selective degradation of RRM1, a cancer therapeutic target. The deoxyadenosine moiety would become phosphorylated and bind to RRM1, a subunit of ribonucleotide reductase, which is required for the synthesis of deoxyribonucleotides (dNTPs). The pomalidomide-like group would recruit an E3 ligase and cause the degradation of RRM1.

Two compounds were designed based on structural information; compound **174** in which the linker and pomalidomide-like group were added at the aniline nitrogen and compound **183** in which the E3 ligase binding group was substituted at C-2 of purine ring.

PROTAC **174** was synthesised via reductive amination of deoxyadenosine with aldehyde **179**, formed through Swern oxidation of alcohol **178**. Boc deprotection of **181** was achieved through microwave heating in isopropanol to give amine **182** which was coupled with carboxylic acid **177** to afford compound **174**. The ability of compound **174** to induce the selective degradation of RRM1 was confirmed through Western Blotting at low compound concentrations (10 nM) in MCF7 and HeLa cells.

PROTAC **183**, in which the linker is attached at C-2 of the purine ring, was designed for improved binding to RRM1 and to ensure the pomalidomide-like group is exposed for binding to the E3 ligase. Synthesis of the key intermediate **191** was achieved via Barton McCombie deoxygenation at the 2' position of chloroadenosine **186**. The alkyne linker **194** was attached via Sonogashira coupling with **191**. The final step towards compound **183** involved removal of all protecting groups prior to amide coupling with carboxylic acid **177**. Compound **183** will be tested for its ability to decrease levels of RRM1 through recruitment of E3 ligase.

Future work could explore different linker lengths and different E3 ligase binding moieties which could be important for efficient recruitment of the E3 ligase.

Chapter 8. Conclusion

Current small molecule KDM5 inhibitors generally bind in the 2-OG binding site through metal coordination and hydrogen bonding of the carboxylic acid or other bioisosteric replacements with key lysine and tyrosine residues. Selectivity over KDM4 has been difficult to achieve in the 8-pyridopyrimidinone-based inhibitors due to similarities in the 2-OG binding site. Poor cellular activity was also observed in this series which could be explained by high cellular levels of 2-OG that compete with the inhibitor for the binding site. This project developed a covalent inhibitor of KDM5B to reduce competition with the cosubstrate and improve selectivity over KDM4 and over other KDM5 isoforms through covalent binding to C480, a highly non-conserved residue.

Numerous compounds with cysteine-selective electrophilic warheads were synthesised via a multi-step synthetic route and subsequently profiled for activity against KDM5B in a time-dependent AlphaScreen assay in which IC_{50}'s were measured at different timepoints to determine kinetic parameters k_{inact} and K_i.

Piperazine analogues **61**-**69** were synthesised with different electrophilic warheads to fine-tune the covalent reactivity. Chloroacetamide **62**, acrylamide **61** and dimethylamino crotonamide **64** had the greatest k_{inact}/K_i so were the most covalently reactive. Covalent binding of the inhibitors was also confirmed through MS-labelling experiments and the protein-compound complex was subsequently subjected to protein digestion and MS analysis to determine the site of attachment. This was further confirmed through obtaining a co-crystal structure of piperazine acrylamide covalently bonded to C480. Although the piperazine analogues were potent in enzymatic assays, the compounds showed poor cell permeability.

Further compounds were therefore designed with the aim of improving their cell permeability which led to potent, covalent inhibitors of KDM5B in which the piperazine ring was replaced with methyl benzylamine, cyclopentyl benzylamine and tetrahydroisoquinolines. The most potent

compound **79** was identified through ranking based on their k_{inact}/K_i values. Chloroacetamide **79** also showed good selectivity over the other KDM families including KDM2, 3, 4 and 6. To test the hypothesis that the covalent inhibitors would be less competed by the co-substrate 2-OG, IC_{50}'s were determined at different concentrations of 2-OG up to 1 mM. Acrylamide **77** was slightly 2-OG competitive showing an 18-fold drop in IC_{50} from 0.5 μM to 1000 μM compared to the 500-fold drop with the published non-covalent pyridopyrimidinone **14** so the irreversible binding of acrylamide **77** significantly reduced competition by 2-OG for the binding site. Some cellular activity was observed in an immunofluorescence assay which showed that the compounds showed a global increase in H3K4me3 levels. The ability of the compounds to affect global levels of H3K4me3 in intact cells was also confirmed using ChIP-Seq experiments. A NanoBret assay also showed that the compounds engaged with KDM5B with IC_{50}'s between 10 and 20 μM. The lack of improved potency compared to the highly 2-OG competitive non-covalent inhibitor **14** was likely due to the lower cell permeability. To further confirm target engagement of the inhibitor in the cell, an alkyne clickable analogue **103** was synthesised for use in pull-down experiments.

In-gel fluorescence was successful when alkyne **103** was incubated with only KDM5B protein and subsequently clicked with an azido dye. This proved that the click reaction worked specifically between the clickable analogue bound to KDM5B and the dye. In-gel fluorescence in cell lysates, however, did not show KDM5B protein bands which may have been caused by background reactivity between the cellular components and the dye. Biotin pull-down was a more desirable approach as the samples are enriched via attachment to Streptavidin beads. No proteins bands relating to KDM5B were pulled down in MCF7 cell lysates and K562 cell lysates (lysed with strongly denaturing RIPA buffer). The click reaction was likely unsuccessful due to side reactions with cellular components.

Future work would attempt the click reaction between clickable analogue **103** and the biotin azide prior to incubation with cells to ensure the biotinylated compound is formed. Target engagement

with KDM5B would prove that the 8-pyridopyrimidinone covalent inhibitor **77** is a useful chemical tool for probing KDM5B biology. This approach could be extended to the development of covalent inhibitors that are selective for other KDM subfamilies.

In addition, a short project was carried out as part of an industrial placement in which a bench-stable transfer reagent **158** for the synthesis of CF_3-sulfonimidamides was developed. Optimisation of the leaving group ability led to tetrafluorophenol **158** which could be synthesised in two steps from sulfinamide **151** via the formation of sulfonimidoyl fluoride **157**. The transfer reagent was reactive to a diverse range of amines including primary and secondary amines as well as electron deficient amines such as aniline. The reagent could be easily deprotected at a later stage to give either the free imine or as a diversity point for further functionalisation. In addition, the reagent was reactive towards methyl lithium so has the potential for synthesis of CF_3-sulfoximines from carbon nucleophiles. Chemical stability tests were carried out which confirmed that transfer reagent **158** was significantly more stable than sulfonimidoyl fluoride **157** and therefore more suitable for long-term storage. This method was also applicable to flow chemistry conditions so has the potential to allow very efficient upscaling.

Further work would explore the synthesis of a more diverse range of CF_3-sulfoximines towards C-nucleophiles using Lewis acids to enhance the reactivity of the transfer reagent. This work could also be extended through the development of a transfer reagent for the synthesis of CF_2-sulfonimidamides **199** and CF-sulfonimidamides **200** (Figure 8.1). This would change the electronics of the sulfonimidamide through changes in the hydrogen bonding interactions with the protein target leading to interesting properties for drug development. The chirality around the sulfur atom could also be explored through reaction of the transfer reagent with optically pure amines or the addition of a chiral centre to the transfer reagent.

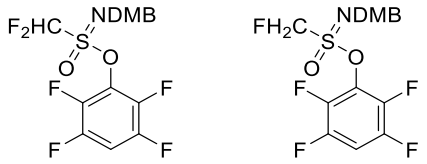


Figure 8.1. CF_2 and CF-sulfonimidamide transfer reagents.

Another approach to protein inhibition was reported in this thesis utilising the emerging PROTAC compounds. A PROTAC was developed for Ribonucleotide Reductase (RNR) as a strategy to degrade the RRM1 subunit through the design of deoxyadenosine-based PROTACs that bind to an allosteric site and recruit an E3 ligase for polyubiquitination and subsequent degradation.

The linker and E3 ligase binding group were attached at the aniline nitrogen in **174** and at C-2 of purine ring in **183**. Synthesis of **174** was achieved through reductive amination of deoxyadenosine **180** with aldehyde **179**, Boc deprotection and amide coupling with **177**. **183** was synthesised via deoxygenation of chloroadenosine **186** using Barton McCombie reaction to give **191**, Sonagashira coupling with alkyne **194** to give **195** and final amide coupling with **177**.

This work could be extended through the synthesis of deoxyadenosine-based PROTACs with different linker lengths. Encouraging results were obtained which showed compound **177** could induce degradation of RRM1 subunit at low compound concentrations. However, further biological studies are needed to determine the optimum position of substitution and linker type and length.

In this thesis is described three different medicinal chemistry projects that could have a significant impact on the field of oncology. A covalent inhibitor of KDM5B could prove useful for studying the role of this protein in various cancers and therefore provide validation as a drug target. The covalent inhibitors are promising starting points for drug development. Sulfonimidamides have been utilised as bioisosteric replacements of sulfonamides in drug discovery projects. Optimisation of the synthetic methodology to access this functionality could enable the discovery of new chemical entities against various diseases including cancer. The targeted degradation of RRM1 subunit of

RNR using PROTACs could prevent DNA synthesis, minimising the risk of mutation errors which can lead to cancer.

Experimental - Synthetic Procedures

General Experimental Details

All reactions involving moisture sensitive reagents were carried out under a nitrogen atmosphere using standard vacuum line techniques and dry solvents. An Elga DV 25 system was used for deionising water. Thin layer chromatography was performed on aluminium plates coated with 60 F_{254} silica gel. Plates were visualised using UV light (254 nm) or 1% aq. $KMnO_4$. Flash column chromatography was performed on a Biotage Isolera One flash column chromatography platform. Purification by HPLC was performed on a Waters SFO and 515 HPLC pump and Waters Binary Gradient 2545 device (5%-95% solvent A (18% water, 80% acetonitrile, 2% 0.5 M ammonium acetate pH 6.0) in solvent B (93% water, 5% acetonitrile, 2% 0.5 M ammonium acetate pH 6.0)). Detection was performed by a SQ Detector 2 and collection by a Waters Sample Manager 2767.

^{1}H and ^{13}C NMR spectra were obtained using Bruker NMR spectrometers (400.1MHz). The proton chemical shift values are reported in parts per million (ppm, δ scale) downfield from tetramethylsilane (TMS) and $CHCl_3$ (δ 7.26). The chemical shifts of the carbon atoms are reported in parts per million (ppm, δ scale) downfield from TMS and referenced to the carbon resonance of $CDCl_3$ (δ 77.16). The data are presented as chemical shift, multiplicity (s = singlet, d = doublet, t = triplet, q = quartet, quint = quintet, sext = sextet, sept = septet, dd – doublet of doublets, dt = doublet of triplets, m = multiplet and br = broad), coupling constant in hertz (Hz), and signal area integration in natural numbers.

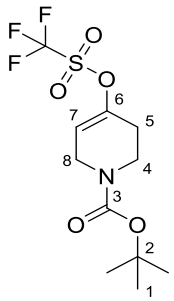
IR was recorded using a Thermo Scientific Nicolet iS5 FT-IR fitted with an iD7-ATR assessory. Low-resolution mass spectra were recorded on a Waters SQ Detector 2. High resolution mass spectrometry data was collected on an Agilent 6530 QTOF. Melting points were recorded using a Stuart SMP40 instrument.

LCMS was used as a measure of compound purity using either UV absorbance (Waters UV/visible Detector 2489), ELSD signal (Waters ELS Detector 2424) or ESI+ TIC (SQ Detector 2). Analytical LCMS

was performed on the following system: Kinetex 5µ EVO C18 100A 100 x 3.0 mm column using linear gradient of solvent A (93 % H_2O, 5 % Acetonitrile and 2 % of 0.5 M ammonium acetate pH 6.0) and solvent B (18 % H_2O, 80 % acetonitrile and 2 % ammonium acetate pH 6.0), eluting at a flow rate of 2 mL/min: 5 % B for 0.35 min, 5% B to 95% B for 1 min, 95% to 5% B for 0.1 min and 5% B for 0.8 min. Preparative LCMS was performed on the same system with a Kinetex 5u EVO C18 100A 150 x 21.2 mm column and a Waters 2767 Sample Manager. A linear gradient of solvent A and solvent B was used, eluting at a flow rate of 20 mL/min: 10% B over 2.5 min, 10% B to 90% B over 2.5 min, 90% B for 7 min and 90% to 10% B for 0.5 min and 10% B for 2.5 min. LRMS was recorded by LCMS using a Waters SQ Detector 2 and the data was acquired and processed using Waters FractionLynx software. HRMS was performed on a RapidFire 360 High Throughput MS system and processing was performed using Agilent MassHunter Workstation software.

Synthesis of KDM inhibitors

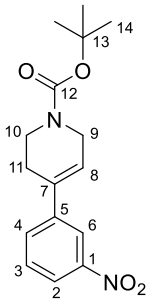
tert-butyl 4-(((trifluoromethyl)sulfonyl)oxy)-3,6-dihydropyridine-1(2H)-carboxylate, (**38**)



38 was synthesised using a literature procedure.[99] A solution of *tert*-butyl 4-oxopiperidine-1-carboxylate (1.859 g, 9.33 mmol) in THF (12 mL) was slowly added to a solution of LDA (5.60 mL, 11.20 mmol) in THF (12 mL) at -78 °C and stirred for 30 min. A solution of 1,1,1-trifluoro-N-phenyl-*N*-((trifluoromethyl)sulfonyl)methanesulfonamide (3.667 g, 10.26 mmol) in THF (12 mL) was added and stirred for 30 min. The cooling bath was removed, and the reaction mixture was slowly warmed to room temperature for 1.5 h. The reaction mixture was cooled to 0 °C and quenched with $NaHCO_3$ (30 mL) and extracted with Et_2O (200 mL). The organic layer was washed with 5% citric acid (40 mL),

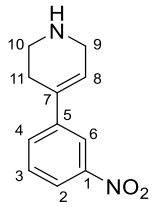
1M NaOH (3 x 35 mL), H_2O (50 mL) and brine (50 mL). The organic layer was dried over $MgSO_4$ and concentrated *in vacuo* to give **38** (3.09 g, quant.). The reaction mixture was taken on crude into the next step. ^{1}H NMR (400 MHz, $CDCl_3$) δ 5.76 (m, 1H, C*H*(7)), 4.04 (q, *J* = 3.1 Hz, 2H, C*H*(4)), 3.63 (t, *J* = 5.7 Hz, 2H, C*H*(8)), 2.44 (m, 2H, C*H*(5)), 1.47 (s, 9H, C*H*(1)).

tert-butyl 4-(3-nitrophenyl)-3,6-dihydropyridine-1(2H)-carboxylate, (**39**)



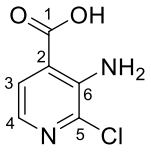
39 was synthesised using a literature procedure.[99] To a vial was added (3-nitrophenyl)boronic acid (1.310 g, 7.85 mmol), *tert*-butyl 4-(((trifluoromethyl)sulfonyl)oxy)-3,6-dihydropyridine-1(2H)-carboxylate (3.381 g, 10.21 mmol), $Pd(Ph_3P)_4$ (0.454 g, 0.393 mmol) and lithium chloride (0.666 g, 15.70 mmol) in 1,4-Dioxane (40 mL). Na_2CO_3 (9.81 mL, 19.63 mmol) was added and the solution heated to 80 °C for 3 h. The reaction mixture was diluted with EtOAc and washed with water, brine and dried over Na_2SO_4, filtered and concentrated *in vacuo* to give a brown oil. The crude product was adsorbed on silica and purified by column chromatography eluting with 0 – 10% EtOAc in Cyclohexane to give **39** (1.528 g, 64%) as a white solid. ^{1}H NMR (400 MHz, $CDCl_3$) δ 8.23 (t, *J* = 2.1 Hz, 1H, C*H*(6)), 8.11 (ddd, *J* = 8.2, 2.3, 1.0 Hz, 1H, C*H*(2)), 7.72 – 7.64 (m, 1H, C*H*(4)), 7.50 (t, *J* = 8.0 Hz, 1H, C*H*(3)), 6.19 (s, 1H, C*H*(8))), 4.12 (m, 2H, C*H*(9)), 3.67 (t, *J* = 5.7 Hz, 2H, C*H*(10)), 2.56 (m, 2H, C*H*(11)), 1.43 (s, 9H, C*H*(14)); LRMS (ESI$^+$) *m/z* 305.3 (M+H$^+$).

4-(3-nitrophenyl)-1,2,3,6-tetrahydropyridine, (**40**)



To a solution of **39** (100 mg, 0.329 mmol) in CH_2Cl_2 (1 mL) was added TFA (1 mL, 12.98 mmol). The reaction mixture was stirred at room temperature for 2 h. The solution was concentrated *in vacuo*, extracted with EtOAc (50 mL) and washed with $NaHCO_3$ (30 mL) and brine (30 mL). The organic layer was dried over Na_2SO_4, filtered and concentrated *in vacuo* to give **40** as a yellow oil (65 mg, 97%). ^{1}H NMR (400 MHz, $CDCl_3$) δ 8.23 (d, *J* = 2.0 Hz, 1H, C*H*(6)), 8.17 (ddd, *J* = 8.1, 2.2, 1.0 Hz, 1H, C*H*(2)), 7.78 – 7.65 (m, 1H, C*H*(4)), 7.55 (t, *J* = 8.0 Hz, 1H, C*H*(3)), 6.21 (d, *J* = 3.7 Hz, 1H, C*H*(8)), 3.90 – 3.72 (m, 2H, C*H*(9)), 3.42 (t, *J* = 6.0 Hz, 2H, C*H*(10)), 2.91 – 2.74 (m, 2H, C*H*(11)); LRMS (ESI^+) *m*/*z* 205.2 ($M+H^+$).

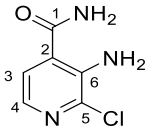
3-amino-2-chloroisonicotinic acid, (**42**)



The reaction was carried out following a literature procedure.[73] Sodium hydroxide (52 mL, 104 mmol) was added to a solution of methyl 3-amino-2-chloroisonicotinate (4.870 g, 26.1 mmol) in MeOH (45 mL)/Water (90 mL). The reaction mixture was stirred at room temperature for 1 h and acidified to pH=1 with concentrated hydrochloric acid. A white precipitate formed which was collected by filtration to give **42** as a white solid (4.463 g, 99%). Mp 258 – 261 °C; ν_{max}/cm^{-1} 3341 (N-H), 2417 (O-H), 1677 (C=O), 1571, 1408 (C-C), 1284 (C-N), 1224 (C-O); ^{1}H NMR (400 MHz, DMSO-d_6) 13.58 (br s, 1H, O*H*), 7.61 (d, *J* = 5.0 Hz, 1H, C*H*(4)), 7.58 (d, *J* = 5.0 Hz, 1H, C*H*(3)), 6.82 (br s, 2H, NH_2); ^{13}C NMR (101 MHz, DMSO) δ 168.4 (*C*(1)), 142.8 (*C*(6)), 138.4 (*C*(5)), 134.4 (*C*(4)), 124.2 (*C*(3)),

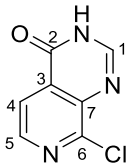
117.7 (*C*(2)); LRMS (ESI$^+$) *m/z* 172.9 (M+H$^+$); HRMS (ESI$^+$): calcd for $C_6H_6ClN_2O_2^+$ [M+H]$^+$ 173.0112, found 173.0104.

3-amino-2-chloroisonicotinamide, (**43**)



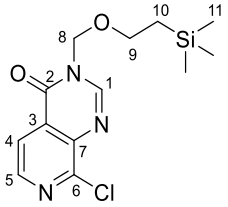
The reaction was carried out following a literature procedure.[73] DMF (0.050 mL, 0.70 mmol) was added to a suspension of 3-amino-2-chloroisonicotinic acid (2.425 g, 14 mmol) in thionyl chloride (30 mL) and the resulting suspension heated at 80 °C for 2 h. A clear orange solution formed which was cooled and then concentrated *in vacuo*. The resulting orange solid was dissolved in THF (15 mL) and added dropwise to ammonium hydroxide (29 mL, 737 mmol) at 0 °C to keep the internal temperature below 25 °C. The resulting suspension was warmed to room temperature and stirred at room temperature for 2 h. The suspension was extracted with EtOAc/ CH_2Cl_2 (13:1) (2 x 28 mL). The organic fraction was dried and concentrated *in vacuo* to give a yellow solid. The crude product was adsorbed on silica and purified by flash chromatography eluting with 0-20% EtOAc in Cyclohexane to give **43** as a white solid (1.988 g, 83%). Mp 180 – 183 °C; ν_{max}/cm^{-1} 3359, 3290 (N-H), 2417 (O-H), 1693 (C=O), 1597 (C-C), 1249 (C-N); ^{1}H NMR (400 MHz, DMSO-d_6) δ 8.17 (s, 1H, N*H*), 7.66 (s, 1H, N*H*), 7.61 (d, *J* = 5.1 Hz, 1H, C*H*(4)), 7.51 (d, *J* = 5.0 Hz, 1H, C*H*(3)), 6.75 (s, 2H, NH_2); ^{13}C NMR (101 MHz, DMSO) δ 168.8 (*C*(1)), 141.4 (*C*(6)), 137.9 (*C*(5)), 134.0 (*C*(4)), 121.7 (*C*(3)), 120.8 (*C*(2)); LRMS (ESI$^+$) m/z 171.9 (M$^+$); HRMS (ESI$^+$): calcd for $C_6H_7ClN_3O^+$ [M+H]$^+$ 172.0272, found 172.0268.

8-chloropyrido[3,4-d]pyrimidin-4(3H)-one, (**44**)



The reaction was carried out following a literature procedure.[73] A solution of 3-amino-2-chloroisonicotinamide (1.340 g, 7.8 mmol) in triethylorthoformate (34 mL, 203 mmol) was heated at 150 °C for 18 h. A yellow precipitate began to form after 1 h. The reaction mixture was cooled to room temperature. Water was added (50 mL) and the resulting suspension was heated at 60 °C and allowed to cool to room temperature slowly. The resulting precipitate was filtered, washing with water (3 x 5 mL). The precipitate was dried under vacuum to give **44** as a pale yellow solid (1.246 g, 88%). Mp 317 – 318 °C; ν_{max}/cm^{-1} 3442 (N-H), 1699 (C=O), 1600 (C-C); ^{1}H NMR (400 MHz, $CDCl_3$) δ 12.85 (s, 1H, N*H*), 8.43 (d, *J* = 5.1 Hz, 1H, C*H*(5)), 8.32 (s, 1H, C*H*(1)), 7.97 (d, *J* = 5.1, 1H, C*H*(4)); ^{13}C NMR (101 MHz, DMSO) δ 159.4 (*C*(2)), 149.6 (*C*(6)), 148.3 (*C*(1)), 144.7 (*C*(5)), 141.2 (*C*(7)), 130.4 (*C*(3)), 118.6 (*C*(4)); LRMS (ESI^+) *m/z* 182.2 ($M+H^+$); HRMS (ESI^+): calcd for $C_7H_5ClN_3O^+$ $[M+H]^+$ 182.0116, found 182.0116.

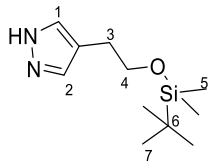
8-chloro-3-((2-(trimethylsilyl)ethoxy)methyl)pyrido[3,4-d]pyrimidin-4(3H)-one, (**45**)



The reaction was carried out following a literature procedure.[73] A suspension of 8-chloropyrido[3,4-d]pyrimidin-4(3H)-one **44** (1.233 g, 6.8 mmol) and potassium carbonate (1.877 g, 13.6 mmol) in DMF (45 mL) was stirred at room temperature for 30 min. (2-(chloromethoxy)ethyl)trimethylsilane (1.442 mL, 8.15 mmol) was added dropwise and the resulting mixture stirred at room temperature for 18 h. The reaction mixture was diluted with water (75 mL). A white precipitate formed which was filtered and washed with water to give **45** as an off-white solid (1.751 g, 83%). Mp 81 – 82 °C; ν_{max}/cm^{-1} 1697 (C=O), 1601 (C-C), 1078 (C-O); ^{1}H NMR (400 MHz, $CDCl_3$) δ 8.50 (d, *J* = 5.1, 1H, C*H*(5)), 8.33 (s, 1H, C*H*(1))), δ 8.06 (d, *J* = 5.1, 1H, C*H*(4)), 5.46 (s, 2H, C*H*(8)), 3.69 (m, 2H, C*H*(9)), 0.98 (m, 2H, C*H*(10)), 0.01 (s, 9H, C*H*(11)); ^{13}C NMR (101 MHz, $CDCl_3$) δ 159.6 (*C*(2)), 151.2 (*C*(6)), 148.1 (*C*(1)), 146.0 (*C*(5)), 140.7 (*C*(7)), 129.5 (*C*(3)), 119.0 (*C*(4)), 75.3

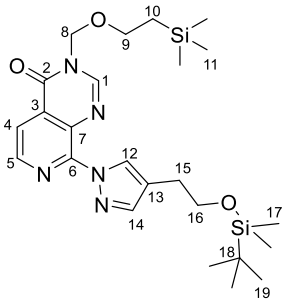
(*C*(8)), 68.2 (*C*(9)), 18.2 (*C*(10)), -1.3 (*C*(11)); LRMS (ESI$^+$) *m/z* 312.0 (M+H$^+$); HRMS (ESI$^+$): calcd for $C_{13}H_{19}ClN_3O_2Si^+$ [M+H]$^+$ 312.0930, found 312.0931.

4-(2-((*tert*-butyldimethylsilyl)oxy)ethyl)-1H-pyrazole (**47**)



A solution of 2-(1H-pyrazol-4-yl)ethan-1-ol (1 g, 8.92 mmol) in anhydrous DMF (50 mL) was cooled to 0 °C and imidazole (0.911 g, 13.4 mmol) was added in one portion. After 15 min, *tert*-butylchlorodimethylsilane (1.479 g, 9.81 mmol) was added. The reaction was warmed to room temperature, then stirred for 18 h. The solution was diluted with water (50 mL) and then extracted with Et_2O (75 mL). The organic layer was washed with water (50 mL) and brine (50 mL) and dried over Na_2SO_4. The filtrate was concentrated *in vacuo* (keeping the pressure above 450 mbar) to give **47** as a yellow oil (2.019 g, quant.) which was used without further purification. ν_{max}/cm^{-1} 3179 (N-H), 2952 (C-H), 1253 (C-N), 1094 (C-O); ^{1}H NMR (400 MHz, $CDCl_3$) δ 7.44 (s, 2H, C*H*(1+2)), 3.74 (t, *J* = 6.8 Hz, 2H, C*H*(4)), 2.70 (t, *J* = 6.8 Hz, 2H, C*H*(3)), 0.89 (s, 9H, C*H*(7)), -0.06 (s, 6H, C*H*(5)); LRMS (ESI$^+$) *m/z* 227.1 (M+H$^+$); HRMS (ESI$^+$): calcd for $C_{11}H_{23}N_2OSi^+$ [M+H]$^+$ 227.1574, found 227.1579.

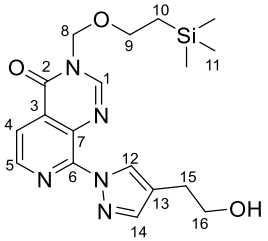
8-(4-(2-((*tert*-butyldimethylsilyl)oxy)ethyl)-1H-pyrazol-1-yl)-3-((2-(trimethylsilyl)ethoxy)methyl) pyrido[3,4-d]pyrimidin-4(3H)-one, (**48**)



The reaction was carried out following a literature procedure.[73] Cesium carbonate (2.720 g, 8.34 mmol) and **47** (1.888 g, 8.34 mmol) were added to a round bottom flask equipped with a stirrer bar

which was sealed, evacuated and flushed with nitrogen. Anhydrous AcN (3 mL) was added and the reaction mixture stirred for 20 min under nitrogen at room temperature. **45** (1.300 g, 4.17 mmol) was added, the vial resealed, evacuated and flushed with nitrogen. The reaction mixture was stirred at reflux for 18 h. Solids were removed by filtration and the reaction mixture was washed with CH_2Cl_2 (3 × 15 mL). The filtrate was concentrated *in vacuo* and purified by flash column chromatography eluting with 30% EtOAc in cyclohexane to give **48** as a pale yellow solid (1.713 g, 82%). Mp 81 – 84 °C; ν_{max}/cm^{-1} 2952 (C-H), 1689 (C=O), 1299 (C-N), 1248 (C-O); ^{1}H NMR (400 MHz, $CDCl_3$) δ 8.61 (d, *J* = 5.1 Hz, 1H, C*H*(5)), 8.59 (s, 1H, C*H*(12)), 8.28 (s, 1H, C*H*(1)), 8.04 (d, *J* = 5.1 Hz, 1H, C*H*(4)), 7.78 (s, 1H, C*H*(14)), 5.45 (s, 2H, C*H*(8)), 3.83 (t, *J* = 6.7 Hz, 2H, C*H*(16))), 3.75 – 3.62 (m, 2H, C*H*(9)), 2.79 (t, *J* = 6.7 Hz, 2H, C*H*(15)), 1.02 – 0.93 (m, 2H, C*H*(10)), 0.90 (s, 9H, C*H*(19)), 0.05 (s, 6H, C*H*(17)), -0.01 (s, 9H, C*H*(11)); ^{13}C NMR (101 MHz, $CDCl_3$) δ 159.7(*C*(2)) 148.3 (*C*(6)), 146.9 (*C*(1)), 145.6 (*C*(5)), 143.6 (*C*(14)), 134.6 (*C*(7)), 131.2 (*C*(12)), 130.3 (*C*(3)), 120.8 (*C*(13)), 117.9 (*C*(4), 75.1 (*C*(8)), 68.1 (*C*(9)), 63.7 (*C*(16)), 28.2 (*C*(15)), 26.1 (*C*(19)), 18.3 (*C*(10)), -1.3 (*C*(11)), -5.2 (*C*(17)); LRMS (ESI^+) *m/z* 502.2 ($M+H^+$); HRMS (ESI^+): calcd for $C_{24}H_{39}N_5O_3Si_2^+$ $[M+H]^+$ 502.2664, found 502.2668.

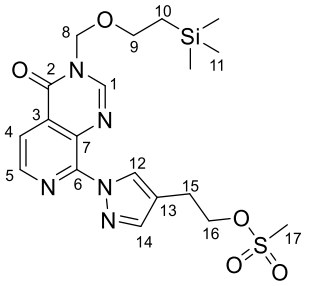
8-(4-(2-hydroxyethyl)-1H-pyrazol-1-yl)-3-((2-(trimethylsilyl)ethoxy)methyl)pyrido[3,4-d] pyrimidin-4(3H)-one, (49)



Reaction was carried out following a literature procedure.[73] 1N hydrochloric acid (17.5 mL, 17.5 mmol) was added to a solution of **48** (0.880 g, 1.75 mmol) in MeOH (18 mL) at 0 °C. The reaction was stirred at 0 °C for 1 h, then diluted with EtOAc (20 mL), washed with $NaHCO_3$ (20 mL), brine (20 mL), dried over $MgSO_4$ and concentrated *in vacuo* to give **49** as a white solid (0.680 g, quant.). Mp 125 – 128 °C; ν_{max}/cm^{-1} 3331 (O-H), 2952 (C-H), 1697 (C=O), 1610 (C-C), 1249 (C-N), 1072 (C-O); ^{1}H

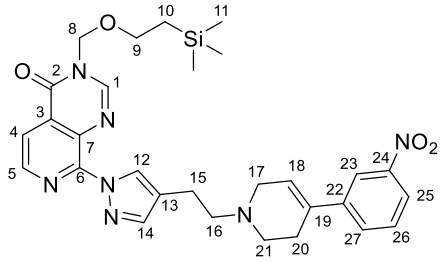
NMR (400 MHz, DMSO-d_6) δ 8.60 (d, *J* = 5.2 Hz, 1H, C*H*(5)), 8.59 (s, 1H, C*H*(1)), 8.38 (s, 1H, C*H*(12)), 8.04 (d, *J* = 5.1 Hz, 1H, C*H*(4)), 7.70 (s, 1H, C*H*(14)), 5.40 (s, 2H, C*H*(8)), 4.76 – 4.68 (m, 1H, O*H*), 3.70 – 3.57 (m, 4H, C*H*(9+16)), 2.72 – 2.63 (m, 2H, C*H*(15)), 0.95 – 0.87 (m, 2H, C*H*(10)), -0.04 (s, 9H, C*H*(11)); ^{13}C NMR (101 MHz, DMSO-d_6) δ 159.9 (*C*(2)), 150.0 (*C*(1)), 148.9 (*C*(6)), 145.7 (*C*(5)), 142.8 (*C*(14)), 135.9 (*C*(7)), 132.1 (*C*(12)), 130.8 (*C*(3)), 120.7 (*C*(13)), 119.0 (*C*(4)), 75.8 (*C*(8)), 67.3 (*C*(9)), 62.3 (*C*(16)), 28.4 (*C*(15)), 18.2 (*C*(10)), -0.5 (*C*(11)); LRMS (ESI$^+$) *m*/*z* 388.1 (M+H$^+$); HRMS (ESI$^+$): calcd for $C_{18}H_{26}N_5O_3Si^+$ [M+H]$^+$ 388.1799, found 388.1797.

2-(1-(4-oxo-3-((2-(trimethylsilyl)ethoxy)methyl)-3,4-dihydropyrido[3,4-d]pyrimidin-8-yl)-1H-pyrazol-4-yl)ethyl methanesulfonate, (**50**)



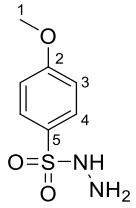
To a solution of **49** (0.256 g, 0.661 mmol) and triethylamine (0.184 mL, 1.321 mmol) in CH_2Cl_2 (8 mL) at 0 °C was added methanesulfonyl chloride (0.077 mL, 0.991 mmol) in one portion. Stirring was maintained at room temperature for 1 h. The solution was washed with $NaHCO_3$ (30 mL) and extracted with CH_2Cl_2 (2 x 30 mL). The combined organics were washed with brine (30 mL), dried over $MgSO_4$, filtered and concentrated *in vacuo* to give **50** as a yellow oil (0.308 g, quant.). This was taken on crude into the next step. ^{1}H NMR (400 MHz, $CDCl_3$) δ 8.67 (s, 1H, C*H*(1)), 8.64 (d, *J* = 5.1 Hz, 1H, C*H*(5)), 8.30 (s, 1H, C*H*(12)), 8.09 (d, *J* = 5.1 Hz, 1H, C*H*(4)), 7.80 (d, *J* = 0.8 Hz, 1H, C*H*(14)), 5.46 (s, 2H, C*H*(8)), 4.44 (t, *J* = 6.7 Hz, 2H, C*H*(16)), 3.74 – 3.63 (m, 2H, C*H*(9)), 3.07 (t, *J* = 6.6 Hz, 2H, C*H*(15)), 2.98 (s, 3H, C*H*(17)), 1.01 – 0.94 (m, 2H, C*H*(10)), 0.00 (s, 9H, C*H*(11)), LRMS (ESI$^+$) *m*/*z* 466.1 (M+H$^+$).

8-(4-(2-(4-(3-nitrophenyl)-3,6-dihydropyridin-1(2H)-yl)ethyl)-1H-pyrazol-1-yl)-3-((2-(trimethyl silyl)ethoxy)methyl)pyrido[3,4-d]pyrimidin-4(3H)-one, (**51**)



To a solution of **50** (0.636 g, 1.366 mmol) and 4-(3-nitrophenyl)-1,2,3,6-tetrahydropyridine **40** (0.363 g, 1.776 mmol) in AcN (20 mL), potassium carbonate (3.78 g, 27.3 mmol) and potassium iodide (0.907 g, 5.46 mmol) were added in one portion and stirring was maintained at 75 °C for 5 h. The reaction mixture was filtered to remove solids and washed with AcN. The filtrate was concentrated *in vacuo*. The crude product was purified by flash chromatography eluting with 0-10% MeOH in CH_2Cl_2 to give **51** as a yellow oil (0.200 g, 26%). ^{1}H NMR (400 MHz, $CDCl_3$) δ 8.63 (d, *J* = 5.1 Hz, 1H, C*H*(5)), 8.59 (s, 1H, C*H*(1)), 8.30 (s, 1H, C*H*(12)), 8.25 (m, 1H, C*H*(25)), 8.10 (m, 1H, C*H*(23)), 8.07 (d, *J* = 5.1 Hz, 1H, C*H*(4)), 7.81 (d, *J* = 0.8 Hz, 1H, C*H*(14)), 7.72 (dt, *J* = 8.1, 1.3 Hz, 1H, C*H*(26)), 7.50 (q, *J* = 7.7 Hz, 1H, C*H*(27)), 6.26 (m, 1H, C*H*(18)), 5.45 (s, 2H, C*H*(8)), 3.73 – 3.64 (m, 2H, C*H*(9)), 3.52 – 3.32 (m, 2H, C*H*(17)), 2.95 – 2.80 (m, 4H, C*H*(15,16)), 2.67 (s, 2H, C*H*(21)), 2.11 – 1.38 (m, 2H, C*H*(20)), 1.01 – 0.92 (m, 2H, C*H*(10)), -0.00 (s, 9H, C*H*(11)); LRMS (ESI$^+$) *m*/*z* 574.7 (M+H$^+$).

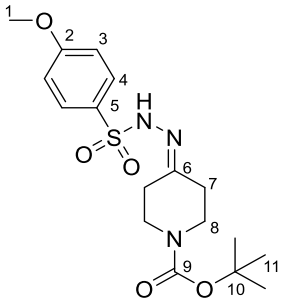
4-methoxybenzenesulfonohydrazide, (**54**)



Reaction carried out following a literature procedure.[100] To a solution of 4-methoxybenzenesulfonyl chloride (0.500 g, 2.420 mmol) in THF (12 mL) at 0 °C was added hydrazine hydrate (0.188 mL, 6.05 mmol) dropwise. The reaction mixture was stirred at 0 °C for 2 h. The mixture was diluted with EtOAc (100 mL), washed with water (75 mL), brine (75 mL), dried over

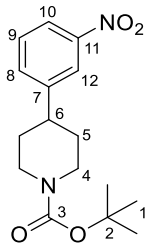
Na_2SO_4 and concentrated *in vacuo* to give **54** as a white solid (0.470 g, 96%). Mp 109 – 112; ν_{max}/cm^{-1} 3377, 3251, 1594 (N-H), 1324, 1154 (S=O), 1261, 1154 (C-O), 817 (C-H); ^{1}H NMR (400 MHz, DMSO-d_6) δ 8.23 – 8.16 (m, 1H, N*H*), 7.78 – 7.68 (m, 2H, C*H*(4)), 7.16 – 7.06 (m, 2H, C*H*(3)), 4.01 (d, *J* = 3.3 Hz, 2H, NH_2), 3.84 (s, 3H, C*H*(1)); ^{13}C NMR (101 MHz, DMSO) δ 162.4 (*C*(2)), 129.8 (*C*(5)), 129.6 (*C*(4)), 114.2 (*C*(3)), 55.6 (*C*(1)); LRMS (ESI$^+$) *m/z* 202.9 (M^+).

tert-butyl 4-(2-((4-methoxyphenyl)sulfonyl)hydrazono)piperidine-1-carboxylate, (**55**)



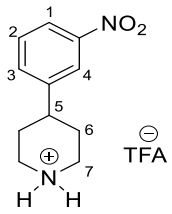
Reaction carried out following a literature procedure.[100] To a solution of 4-methoxybenzenesulfonohydrazide **54** (0.442 g, 2.183 mmol) in MeOH (5 mL) was added *tert*-butyl 4-oxopiperidine-1-carboxylate (0.435 g, 2.183 mmol). The solution was stirred at room temperature for 2 h. The reaction mixture was concentrated *in vacuo* to give **55** as a white solid (0.804 g, 96%). Mp 172 – 175; ν_{max}/cm^{-1} 3231, 1594 (N-H), 1697 (C=O), 1366, 1155 (S=O), 1240, 1094 (C-O), 1220 (C-N), 820 (C-H); ^{1}H NMR (400 MHz, DMSO-d_6) δ 10.16 (s, 1H, N*H*), 7.79 – 7.56 (m, 2H, C*H*(4)), 7.21 – 6.98 (m, 2H, C*H*(3)), 3.83 (s, 3H, C*H*(1)), 3.38 (m, 4H, C*H*(8)), 2.35 (m, 2H, C*H*(7)), 2.21 (m, 2H, C*H*(7)), 1.39 (s, 9H, C*H*(11)); ^{13}C NMR (101 MHz, DMSO) δ 162.5 (*C*(2)), 158.0 (*C*(6)), 153.8 (*C*(9)), 130.8 (*C*(5)), 129.7 (*C*(4)), 114.1 (*C*(3)), 79.0 (*C*(10)), 55.6 (*C*(1)), 43.5 (*C*(8)), 33.1 (*C*(7)), 28.0 (*C*(11)), 27.6 (*C*(7)); LRMS (ESI$^+$) *m/z* 384.1 ($M+H^+$); HRMS (ESI$^+$): calcd for $C_{17}H_{26}N_3O_5S^+$ $[M+H]^+$ 384.1588, found 384.1584.

tert-butyl 4-(3-nitrophenyl)piperidine-1-carboxylate, (**56**)



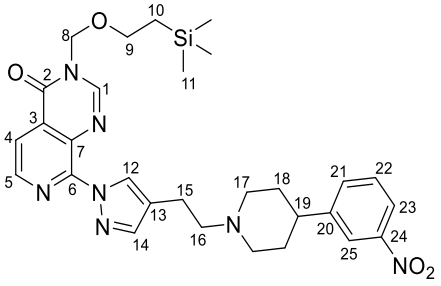
Reaction carried out following a literature procedure.[100] **55** (3.715 g, 9.69 mmol), (3-nitrophenyl)boronic acid (2.426 g, 14.4 mmol) and cesium carbonate (4.73 g, 14.53 mmol) was added to a dried round bottom flask *in vacuo* for 30 min. The vial was backfilled with nitrogen. 1,4-Dioxane (40 mL) was added and the reaction mixture was heated to 110 °C for 18 h. The reaction mixture was cooled to room temperature, quenched with $NaHCO_3$ (50 mL) and extracted with CH_2Cl_2 (50 mL). The organic layer was dried over $MgSO_4$ and concentrated *in vacuo*. The crude residue was adsorbed on silica and purified by flash chromatography eluting with 10-30% EtOAc in Cyclohexane to give **56** as a colourless oil (0.530 g, 18%). ν_{max}/cm^{-1} 1690 (C=O), 1533 (N-O), 1282, 1232, 1161 (C-N); ^{1}H NMR (400 MHz, $CDCl_3$) δ 8.10 (m, 2H, C*H*(10,12)), 7.63 – 7.42 (m, 2H, C*H*(8,9)), 4.31 (s, 2H, C*H*(6)), 2.95 – 2.75 (m, 3H, C*H*(4,6)), 1.89 (d, *J* = 13.0 Hz, 2H, C*H*(5)), 1.74 – 1.63 (m, 2H, C*H*(5)), 1.51 (s, 9H, C*H*(1)); LRMS (ESI$^+$) *m*/*z* 207.1 (M-Boc+H$^+$).

4-(3-nitrophenyl)piperidine TFA salt, (**57**)



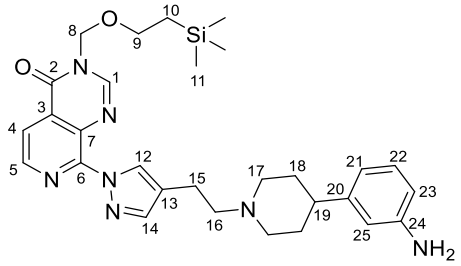
To a solution of **56** (0.530 g, 1.73 mmol) in CH_2Cl_2 (7.5 mL) was added trifluoroacetic acid (7.5 mL). The reaction mixture was stirred at room temperature for 2 h. The solution was concentrated *in vacuo* to give **57** as the TFA salt (0.554 g, quant.) which was taken on crude into the next step. ^{1}H NMR (400 MHz, $CDCl_3$) δ 8.27 – 8.00 (m, 2H, C*H*(1,4)), 7.74 – 7.41 (m, 2H, C*H*(2,3)), 3.66 (d, *J* = 13.0 Hz, 2H, C*H*(7)), 3.12 (q, *J* = 11.5 Hz, 2H, C*H*(7)), 2.94 (m, 1H, C*H*(5)), 2.36 – 1.89 (m, 4H, C*H*(6)).

8-(4-(2-(4-(3-nitrophenyl)piperidin-1-yl)ethyl)-1H-pyrazol-1-yl)-3-((2-(trimethylsilyl)ethoxy) methyl)pyrido[3,4-d]pyrimidin-4(3H)-one, (**58**)



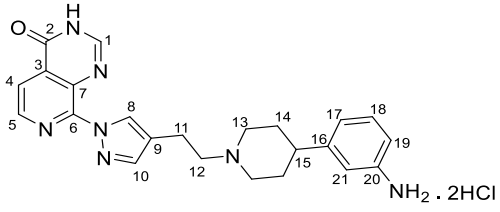
To a vial was added **50** (220 mg, 0.473 mmol), **57** (151 mg, 0.473 mmol), potassium iodide (314 mg, 1.89 mmol) and potassium carbonate (1.306 g, 9.45 mmol) in AcN (2 mL). The reaction mixture was heated to 75 °C for 18 h. The reaction mixture was diluted with EtOAc (75 mL) and washed with $NaHCO_3$ (50 mL) and brine (50 mL). The organic layer was dried over Na_2SO_4, filtered and concentrated *in vacuo*. The crude product was adsorbed on silica and purified by flash chromatography eluted with 0-10% MeOH in CH_2Cl_2 to give **58** as a yellow oil (138 mg, 51%). ν_{max}/cm^{-1} 2949 (C-H), 1693 (C=O), 1529 (N-O), 1102, 1078 (C-O), 1248 (C-N), 884, 836 (C-H); ^{1}H NMR (400 MHz, $CDCl_3$) δ 8.63 (d, *J* = 5.1 Hz, 1H, C*H*(5)), 8.57 (s, 1H, C*H*(1)), 8.31 (s, 1H, C*H*(12)), 8.17 – 8.03 (m, 3H, C*H*(4,23,25)), 7.80 (d, *J* = 0.7 Hz, 1H, C*H*(14)), 7.57 (dt, *J* = 7.7, 1.4 Hz, 1H, C*H*(22)), 7.47 (d, *J* = 7.9 Hz, 1H, C*H*(21)), 5.46 (s, 2H, C*H*(8)), 3.77 – 3.59 (m, 2H, C*H*(9)), 3.17 (d, *J* = 11.5 Hz, 2H, C*H*(17)), 2.83 (m, 2H, C*H*(15)), 2.77 – 2.59 (m, 3H, C*H*(16,19)), 2.18 (m, 2H, C*H*(17)), 2.01 – 1.76 (m, 4H, C*H*(18)), 1.09 – 0.86 (m, 2H, C*H*(10)), 0.00 (s, 9H, C*H*(11)); ^{13}C NMR (101 MHz, DMSO) δ 159.0 (*C*(2)), 149.2 (*C*(1)), 148.2 (*C*(24)), 148.1 (*C*(6)), 147.9 (*C*(20)), 144.8 (*C*(5)), 141.9 (*C*(14)), 135.1 (*C*(7)), 133.7 (*C*(21)), 131.1 (*C*(12)), 130.0 (*C*(3)), 129.9 (*C*(22)), 121.4, 121.2 (*C*(23, 25)), 120.4 (*C*(13)), 118.3 (*C*(4)), 75.0 (*C*(8)), 66.5 (*C*(9)), 58.5 (*C*(16)), 53.2 (*C*(17)), 41.0 (*C*(19)), 32.3 (*C*(18)), 21.2 (*C*(15)), 17.4 (*C*(10)), -1.4 (*C*(11)); LRMS (ESI$^+$) *m/z* 576.4 (M+H$^+$); HRMS (ESI$^+$): calcd for $C_{29}H_{38}N_7O_4Si^+$ $[M+H]^+$ 576.2749, found 576.2759.

8-(4-(2-(4-(3-aminophenyl)piperidin-1-yl)ethyl)-1H-pyrazol-1-yl)-3-((2-(trimethylsilyl)ethoxy) methyl)pyrido[3,4-d]pyrimidin-4(3H)-one, (**59**)



A solution of **58** (141 mg, 0.245 mmol), ammonium formate (62 mg, 0.980 mmol) and 5% palladium on carbon (104 mg, 0.049 mmol) in MeOH (1.2 mL) was stirred at room temperature for 18 h. The reaction mixture was filtered through Celite, washed with MeOH and concentrated *in vacuo* to give **59** as a brown solid (115 mg, 86%). ν_{max}/cm^{-1} 3348 (N-H), 2965 (C-H), 1691 (C=O), 1071 (C-O), 1249 (C-N), 884, 858 (C-H); ^{1}H NMR (400 MHz, $CDCl_3$) δ 8.69 (s, 1H, C*H*(12)), 8.64 (d, *J* = 5.1 Hz, 1H, C*H*(5)), 8.31 (s, 1H, C*H*(1)), 8.09 (d, *J* = 5.1 Hz, 1H, C*H*(4)), 7.78 (s, 1H, C*H*(14)), 7.09 (t, *J* = 7.7 Hz, 1H, C*H*(22)), 6.66 – 6.53 (m, 3H, C*H*(21,23,25)), 5.47 (s, 2H, C*H*(8)), 3.72 - 3.67 (m, 4H, C*H*(9+17)), 3.49 (m, 2H, C*H*(17)), 3.30 - 2.88 (m, 5H, C*H*(15,16,19), 2.66 - 2.50 (m, 2H, C*H*(18)), 1.97 (m, 2H, C*H*(18)), 1.04 – 0.93 (m, 2H, C*H*(10)), 0.01 (s, 9H, C*H*(11)); ^{13}C NMR (101 MHz, $CDCl_3$) δ 159.6 (*C*(2)), 148.0 (*C*(6)), 147.3 (*C*(1)), 146.9 (*C*(24)), 145.6 (*C*(5)), 142.6 (*C*(14)), 134.7 (*C*(7)), 131.5 (*C*(12)), 130.4 (*C*(3)), 129.7 (*C*(22)), 118.4 (*C*(4)), 117.4 (*C*(21)), 113.7, 113.5 (*C*(23, 25), 75.2 (*C*(8)), 68.2 (*C*(9)), 58.9 (*C*(16)), 54.1 (*C*(17)), 41.7 (*C*(19)), 31.6 (*C*(18)), 20.8 (*C*(15)), 18.2 (*C*(10)), -1.3 (*C*(11)); LRMS (ESI^+) m/z 546.3 ($M+H^+$); HRMS (ESI^+): calcd for $C_{29}H_{40}N_7O_2Si^+$ $[M+H]^+$ 546.3007, found 546.3006.

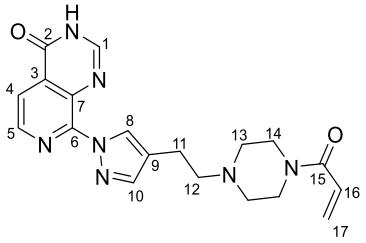
8-(4-(2-(4-(3-aminophenyl)piperidin-1-yl)ethyl)-1H-pyrazol-1-yl)pyrido[3,4-d]pyrimidin-4(3H)-one, 2HCl (**60**)



To a solution of **59** (110 mg, 0.202 mmol) in THF (2 mL) was added 6M HCl (2.0 mL, 12.09 mmol). The solution was heated at 50 °C for 3 h. The solution was concentrated *in vacuo* to give **60** as a

yellow solid (quant.). Mp 289 – 291 °C; ν_{max}/cm^{-1} 3346 (N-H), 1647 (C=O), 1233, 1150, 1069 (C-N), 870, 828 (C-H); ^{1}H NMR (400 MHz, DMSO-d_6) δ 10.81 (s, 1H, N*H*), 8.59 (d, *J* = 5.1 Hz, 1H, C*H*(5)), 8.51 (s, 1H, C*H*(8)), 8.30 (s, 1H, C*H*(1)), 8.03 (d, *J* = 5.1 Hz, 1H, C*H*(4)), 7.81 (s, 1H, C*H*(10)), 7.48 (t, *J* = 7.7 Hz, 1H, C*H*(18)), 7.38 – 7.16 (m, 3H, C*H*(17,19,20)), 3.70 – 3.52 (m, 2H, C*H*(13)), 3.42 – 3.27 (m, 2H, C*H*(12)), 3.22 – 3.05 (m, 4H, C*H*(11,13), 2.97 – 2.82 (m, 1H, C*H*(15)), 2.31 – 1.77 (m, 4H, C*H*(14)); ^{13}C NMR (101 MHz, DMSO-d_6) δ 159.4 (*C*(2)), 147.7 (*C*(1)), 147.4 (*C*(6)), 146.2 (*C*(20)), 144.3 (*C*(10)), 141.5 (*C*(10)), 135.5 (*C*(7)), 132.0 (*C*(16)), 131.5 (*C*(12)), 130.8 (*C*(3)), 130.0 (*C*(18)), 126.7 (*C*(17)), 121.7, 121.4 (*C*(19, 21)), 118.3 (*C*(4)), 117.6 (*C*(9)), 55.9 (*C*(12)), 51.8 (*C*(13)), 38.6 (*C*(15)), 29.6 (*C*(14)), 18.6 (*C*(11)); LRMS (ESI$^+$) *m/z* 416.2 (M+H$^+$); HRMS (ESI$^+$): calcd for $C_{23}H_{26}N_7O^+$ [M+H]$^+$ 416.2193, found 416.2180.

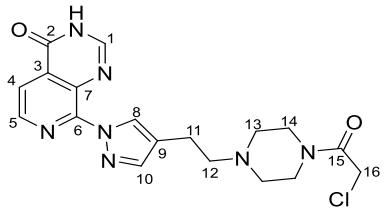
8-(4-(2-(4-acryloylpiperazin-1-yl)ethyl)-1H-pyrazol-1-yl)pyrido[3,4-d]pyrimidin-4(3H)-one, (**61**)



To a solution of **71** (150 mg, 0.377 mmol) in NMP (2 mL) was added PS-DIPEA (300 mg) and stirred for 5 min. The reaction mixture was cooled to 0 °C and acryloyl chloride (46 µL, 0.565 mmol) was added. The reaction mixture was warmed to room temperature and then stirred for 18 h. The solution was cooled to 0 °C and then more acryloyl chloride (56 µl, 0.692 mmol) was added. The reaction was warmed to room temperature and stirred for a further 6 h. The reaction mixture was filtered and washed with MeOH. The solution was concentrated *in vacuo* and then dried in a Genevac oven to give an orange solid. The crude product was adsorbed on silica and purified by flash chromatography on a KP-NH column eluting with 0-10% MeOH in CH_2Cl_2 to give **61** as a white solid (15 mg, 11%). Mp 150 – 152 °C; ν_{max}/cm^{-1} 3392 (N-H), 1697, 1608 (C=O), 1654 (C=C), 1250, 1156, 1072 (C-N); ^{1}H NMR (400 MHz, DMSO-d_6) δ 8.53 (d, *J* = 5.1 Hz, 1H, C*H*(5)), 8.42 (d, *J* = 8.4 Hz,

1H, C*H*(8)), 8.28 (s, 1H, C*H*(1)), 7.97 (d, *J* = 5.1 Hz, 1H, C*H*(4)), 7.70 (d, *J* = 8.4 Hz, 1H, C*H*(10)), 6.80 (dd, *J* = 16.7, 10.5 Hz, 1H, C*H*(16)), 6.10 (dd, *J* = 16.7, 2.4 Hz, 1H, C*H*(17)), 5.67 (dd, *J* = 10.5, 2.4 Hz, 1H, C*H*(17)), 3.62 – 3.50 (m, 4H, C*H*(14)), 2.74 – 2.62 (m, 2H, C*H*(11)), 2.61 – 2.51 (m, 2H, C*H*(12)), 2.44 (m, 4H, C*H*(13)); ^{13}C NMR (101 MHz, DMSO-d_6) δ 164.2 (*C*(15)), 160.1 (*C*(2)), 147.9 (*C*(1)), 147.7 (*C*(6)), 143.9 (*C*(5)), 136.0 (*C*(7)), 141.7 (*C*(10)), 131.1 (*C*(8)), 130.7 (*C*(3)), 128.3 (*C*(16)), 127.3 (*C*(17)), 120.4 (*C*(9)), 117.9 (*C*(4)), 58.4 (*C*(12)), 53.1 (*C*(13)), 45.1 (*C*(14)), 41.5 (*C*(14)), 21.2 (*C*(11)); LRMS (ESI$^+$) *m*/*z* 380.1 (M+H$^+$); HRMS (ESI$^+$): calcd for $C_{16}H_{20}N_7O^+$ [M+H]$^+$ 380.1829, found 380.1825.

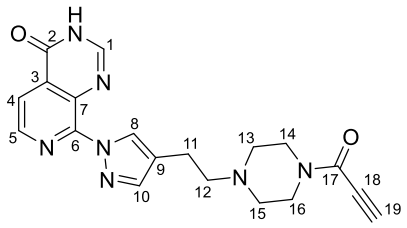
8-(4-(2-(4-(2-chloroacetyl)piperazin-1-yl)ethyl)-1H-pyrazol-1-yl)pyrido[3,4-d]pyrimidin-4(3H)-one, (62)



To a solution of **71** (100 mg, 0.251 mmol) in NMP (2.5 mL) was added PS-DIPEA (300 mg). The reaction mixture was cooled to 0 °C and 2-chloroacetyl chloride (30 µl, 0.377 mmol) was added. The reaction mixture was stirred at room temperature for 18 h. The solution was cooled to 0 °C and more 2-chloroacetyl chloride (30 µl, 0.377 mmol) was added and stirred for a further 6 h. The reaction mixture was filtered with MeOH, the filtrate was concentrated *in vacuo* and dried in a Genevac oven to remove excess NMP. The crude product was adsorbed on silica, purified by flash chromatography on a KP-NH column eluting with 10% MeOH in CH_2Cl_2 to give **62** as an off-white solid (32 mg, 32%). Mp 259 – 262 °C; ν_{max}/cm^{-1} 3378 (N-H), 1647, 1604 (C=O), 1240, 1213, 1159, 1059 (C-N), 739 (C-Cl); ^{1}H NMR (400 MHz, D_2O) δ 8.48 (d, *J* = 5.3 Hz, 1H, C*H*(5)), 8.24 (s, 1H), 8.20 (s, 1H), 8.05 (d, *J* = 5.3 Hz, 1H, C*H*(4)), 7.78 (s, 1H, C*H*(10)), 4.29 (s, 2H, C*H*(16)), 3.72 – 3.57 (m, 4H, C*H*(14)), 2.89 – 2.68 (m, 8H, C*H*(11,12,13)); ^{13}C NMR (101 MHz, D_2O) δ 167.8 (*C*(15)), 159.9 (*C*(2)), 147.6 (*C*(1,6)), 144.3 (*C*(5)), 142.5 (*C*(10)), 136.7 (*C*(7)), 131.9 (*C*(8)), 130.9 (*C*(3)), 119.4, 119.1

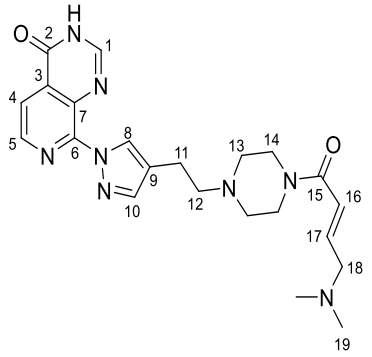
(*C*(4,9)), 57.3 (*C*(12)), 51.5, 51.2 (*C*(13)), 43.8 (*C*(14)), 41.0 (*C*(16)), 40.3 (*C*(14)), 19.3 (*C*(11)); LRMS (ESI$^+$) *m/z* 402.0 (M+H$^+$); HRMS (ESI$^+$): calcd for $C_{18}H_{21}ClN_7O_2^+$ [M+H]$^+$ 402.1440, found 402.1433.

8-(4-(2-(4-propioloylpiperazin-1-yl)ethyl)-1H-pyrazol-1-yl)pyrido[3,4-d]pyrimidin-4(3H)-one, (**63**)



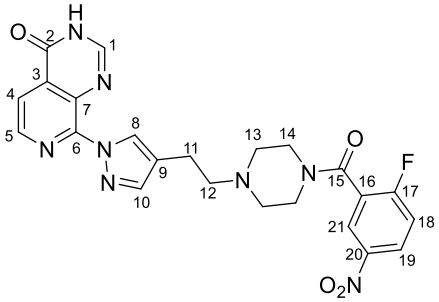
To a solution of propiolic acid (0.015 mL, 0.251 mmol) in DMA (2 mL) at 0 °C was added PS-DIPEA (300 mg), **71** (0.100 g, 0.251 mmol) and T3P (0.222 mL, 0.377 mmol). The reaction mixture was warmed to room temperature and stirred for 14 h. The reaction mixture was filtered and concentrated *in vacuo*. The crude product was adsorbed on silica and purified by flash chromatography on a KP-NH column in 0-20% MeOH in CH_2Cl_2 to give **63** as an off-white solid (0.037 g, 39%). Mp 256 – 259 °C; ν_{max}/cm^{-1} 3380 (N-H), 2102 (C≡C), 1697, 1610 (C=O), 1229, 1210, 1157, 1131 (C-N); ^{1}H NMR (400 MHz, DMSO-d_6) δ 8.53 (d, *J* = 5.1 Hz, 1H, C*H*(5)), 8.43 (s, 1H, C*H*(8)), 8.28 (s, 1H, C*H*(1)), 7.97 (d, *J* = 5.1 Hz, 1H, C*H*(4)), 7.71 (s, 1H, C*H*(10)), 4.55 (s, 1H, C*H*(19)), 3.70 (dd, *J* = 6.0, 4.1 Hz, 2H, C*H*(14,16), 3.51 (dd, *J* = 6.1, 4.2 Hz, 2H, C*H*(14,16)), 2.70 (t, *J* = 7.4 Hz, 2H, C*H*(11)), 2.62 – 2.54 (m, 2H, C*H*(12)), 2.49 – 2.31 (m, 4H, C*H*(13,15)); ^{13}C NMR (101 MHz, DMSO-d_6) δ 160.2 (*C*(2)), 151.0 (*C*(17)), 148.1 (*C*(1)), 147.7 (*C*(6)), 143.8 (*C*(5)), 141.6 (*C*(10)), 136.0 (*C*(7)), 131.2 (*C*(8)), 130.7 (*C*(3)), 120.3 (*C*(9)), 117.9 (*C*(4)), 82.4 (*C*(19)), 75.6 (*C*(18)), 58.3 (*C*(12)), 52.7 (*C*(13/15)), 51.9 (*C*(13/15)), 46.5 (*C*(14/16)), 41.0 (*C*(14/16)), 21.2 (*C*(11)); LRMS (ESI$^+$) *m/z* 378.3 (M+H$^+$); HRMS (ESI$^+$): calcd for $C_{19}H_{20}N_7O_2^+$ [M+H]$^+$ 378.1673, found 378.1679.

(*E*)-8-(4-(2-(4-(4-(dimethylamino)but-2-enoyl)piperazin-1-yl)ethyl)-1H-pyrazol-1-yl)pyrido[3,4-d]pyrimidin-4(3H)-one, (**64**)



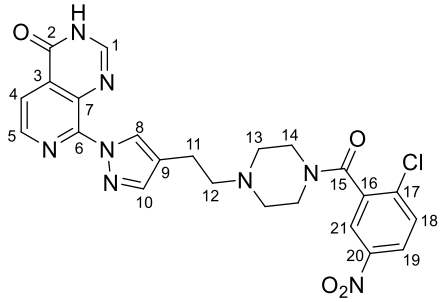
To a solution of **71** (100 mg, 0.251 mmol) and PS-DIPEA (300 mg) in DMA (2 mL) at 0 °C was added T3P (0.222 mL, 0.377 mmol) and (*E*)-4-(dimethylamino)but-2-enoic acid, HCl (42 mg, 0.251 mmol). The reaction mixture was warmed to room temperature and stirred overnight for 18 h. The reaction mixture was filtered, washed with MeOH and the filtrate was concentrated *in vacuo*. The crude product was adsorbed on silica and purified by flash chromatography eluting with 20% MeOH in CH_2Cl_2 on a KP-NH column to give **64** as an off-white solid (27 mg, 25%). Mp 184 – 186 °C; ν_{max}/cm^{-1} 3377 (N-H), 1697, 1606 (C=O), 1659 (C=C), 1239, 1214, 1160, 1134, 1022 (C-N); ^{1}H NMR (400 MHz, DMSO-d_6) δ 8.52 (d, *J* = 5.1 Hz, 1H, C*H*(5)), 8.43 (s, 1H, C*H*(8)), 8.28 (s, 1H, C*H*(4)), 7.96 (d, *J* = 5.1 Hz, 1H, C*H*(4)), 7.71 (s, 1H, C*H*(10)), 6.59 (m, 2H, C*H*(16+17), 3.54 (s, 4H, C*H*(14)), 3.08 – 2.97 (m, 2H, C*H*(18)), 2.70 (m, 2H, C*H*(11)), 2.57 (m, 2H, C*H*(12)), 2.44 (m, 4H, C*H*(13)), 2.14 (s, 6H, (*C*(19)); LRMS (ESI$^+$) m/z 437.3 (M+H$^+$); ^{13}C NMR (101 MHz, DMSO-d_6) δ 164.0 (*C*(15)), 160.4 (*C*(2))), 148.3 (*C*(1)), 147.7 (*C*(6)), 143.7 (*C*(5)), 142.0 (*C*(17)), 141.6 (*C*(10)), 136.1 (*C*(7)), 131.1 (*C*(8)), 130.6 (*C*(3)), 122.2 (*C*(16)), 120.3 (*C*(9)), 117.9 (*C*(4)), 60.0 (*C*(18)), 58.4 (*C*(12)), 53.1, 52.3 (*C*(13)), 45.1 (*C*(19)), 41.5 (*C*(14)), 21.2 (*C*(11)); LRMS (ESI$^+$) *m/z* 437.3 (M+H$^+$); HRMS (ESI$^+$): calcd for $C_{22}H_{29}N_8O_2^+$ [M+H]$^+$ 437.2408, found 437.2416.

8-(4-(2-(4-(2-fluoro-5-nitrobenzoyl)piperazin-1-yl)ethyl)-1H-pyrazol-1-yl)pyrido[3,4-d]pyrimidin-4(3H)-one, (**65**)



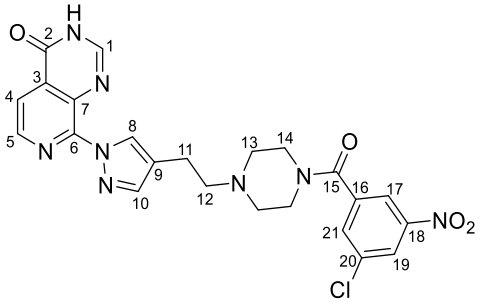
To a solution of **71** (100 mg, 0.251 mmol) and PS-DIPEA (300 mg) in DMA (1 mL) was added 2-fluoro-5-nitrobenzoic acid (51 mg, 0.276 mmol) and T3P (222 µL, 0.377 mmol) at 0 °C. The reaction mixture was stirred at room temperature for 18 h. The solid was filtered and washed with MeOH (30 mL). The solution was concentrated *in vacuo*. The crude product was adsorbed on silica and purified by flash chromatography on a KP-NH column eluting with 10% MeOH in CH_2Cl_2 to give **65** as an off-white solid (40 mg, 32%). Mp 270 – 272 °C; ν_{max}/cm^{-1} 3347 (N-H), 1717, 1626 (C=O), 1542 (N-O), 1237, 1223, 1133, 1098 (C-N); ^{1}H NMR (400 MHz, DMSO-d_6) δ 8.54 (d, *J* = 5.1 Hz, 1H, C*H*(5)), 8.42 (s, 1H, C*H*(8)), 8.37 (m, 1H, C*H*(19)), 8.32 (m, 1H, C*H*(21)), 8.28 (s, 1H, C*H*(1)), 7.97 (d, *J* = 5.1 Hz, 1H, C*H*(4)), 7.71 (s, 1H, C*H*(10)), 7.62 (t, *J* = 8.9 Hz, 1H, C*H*(18)), 3.69 (m, 2H, C*H*(14)), 3.27 (m, 2H, C*H*(14)), 2.70 (m, 2H, C*H*(11)), 2.58 (m, 4H, C*H*(12,13)), 2.43 (m, 2H, C*H*(13)); ^{13}C NMR (101 MHz, DMSO-d_6) δ 162.2, 161.6 (*C*(15)), 159.9 (*C*(2)), 159.7, 147.7 (*C*(1+6)), 144.3 (*C*(20)), 144.0 (*C*(5)), 141.7 (*C*(10)), 135.9 (*C*(7)), 131.1 (*C*(8)), 130.7 (*C*(3)), 127.1 (*C*(19)), 125.4 (*C*(16)), 124.9 (*C*(21)), 120.3 (*C*(9)), 117.9 (*C*(4)), 117.6 (*C*(18)), 58.3 (*C*(12)), 52.7, 52.0 (*C*(13)), 46.7, 41.6 (*C*(14)), 21.2 (*C*(11)); LRMS (ESI$^+$) *m/z* 493.2 (M+H$^+$); HRMS (ESI$^+$): calcd for $C_{23}H_{22}FN_8O_4^+$ [M+H]$^+$ 493.1743, found 493.1744.

8-(4-(2-(4-(2-chloro-5-nitrobenzoyl)piperazin-1-yl)ethyl)-1H-pyrazol-1-yl)pyrido[3,4-d]pyrimidin-4(3H)-one, (**66**)



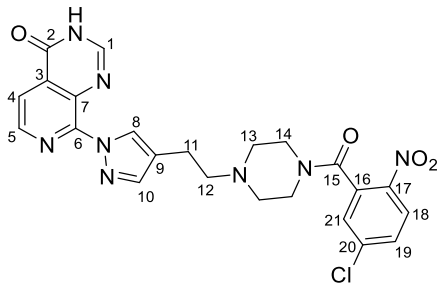
To a solution of **71** (80 mg, 0.246 mmol) and PS-DIPEA (0.300 g) in NMP (1.5 mL) at 0 °C was added 2-chloro-5-nitrobenzoyl chloride (60 mg, 0.270 mmol). The reaction mixture was stirred at room temperature for 18 h. The reaction mixture was filtered and washed with MeOH (30 mL). The solution was concentrated *in vacuo* and dried in a Genevac to remove NMP. The crude product was adsorbed on silica and purified by flash chromatography on a KP-NH column eluting with 11% MeOH in CH_2Cl_2. Collected fractions were concentrated *in vacuo* to give **66** as an off-white solid (0.030 g, 25%). Mp 157 – 160 °C; ν_{max}/cm^{-1} 3347 (N-H), 1685, 1608 (C=O), 1523 (N-O), 1241, 1215, 1164, 1128, 1053 (C-N); ^{1}H NMR (400 MHz, DMSO-d_6) δ 8.53 (d, *J* = 5.1 Hz, 1H, C*H*(5)), 8.43 (s, 1H, C*H*(8)), 8.30 – 8.22 (m, 3H, C*H*(1,19,21), 7.97 (d, *J* = 5.1 Hz, 1H, C*H*(4)), 7.88 – 7.81 (m, 1H, C*H*(18)), 7.71 (s, 1H, C*H*(10)), 3.64 (m, 2H, C*H*(14)), 3.19 (m, 2H, C*H*(14)), 2.70 (t, *J* = 7.3 Hz, 2H, C*H*(11)), 2.60 – 2.34 (m, 6H, C*H*(12,13)); ^{13}C NMR (101 MHz, DMSO) δ 163.4 (*C*(15)), 160.0 (*C*(2)), 147.9 (*C*(1)), 147.7 (*C*(6)), 146.6 (*C*(20)), 143.9 (*C*(5)), 141.6 (*C*(10)), 137.0 (*C*(17)), 136.1 (*C*(16)), 135.9 (*C*(7)), 131.1 (*C*(8,18)), 130.6 (*C*(3)), 125.2, 123.0 (*C*(19/21), 120.3 (*C*(9)), 117.9 (*C*(4)), 58.3 (*C*(12)), 52.6 (*C*(13)), 51.9 (*C*(13)), 46.3 (*C*(14)), 41.3 (*C*(14)), 21.2 (*C*(11)); LRMS (ESI$^+$) *m*/*z* 509.1 (M+H$^+$); HRMS (ESI$^+$): calcd for $C_{23}H_{22}ClN_8O_4^+$ $[M+H]^+$ 509.1447, found 509.1449.

8-(4-(2-(4-(3-chloro-5-nitrobenzoyl)piperazin-1-yl)ethyl)-1H-pyrazol-1-yl)pyrido[3,4-d]pyrimidin-4(3H)-one, (**67**)



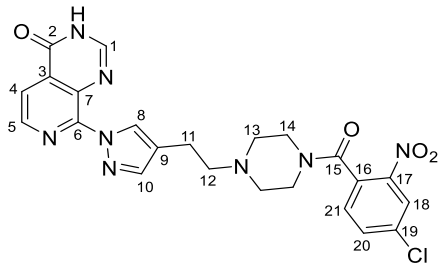
To a solution of 3-chloro-5-nitrobenzoic acid (51 mg, 0.254 mmol) and HATU (105 mg, 0.277 mmol) in DMA (2 mL) was added PS-DIPEA (300 mg). The reaction mixture was stirred at room temperature for 15 min and **71** (75 mg, 0.231 mmol) was added. The reaction mixture was stirred at room temperature for 16 h. The reaction mixture was filtered and washed with MeOH (30 mL). The filtrate was concentrated *in vacuo*. The crude solid was adsorbed on silica and purified by flash chromatography on KP-NH column eluting with 10% MeOH in CH_2Cl_2 to give **67** as an off-white solid (36 mg, 31%). Mp 237 – 239 °C; ν_{max}/cm^{-1} 1697, 1630 (C=O), 1544 (N-O), 1210, 1173, 1158, 1131, 1103 (C-N); ^{1}H NMR (400 MHz, DMSO-d_6) δ 12.81 (s, 1H, N*H*), 8.54 (d, *J* = 5.1 Hz, 1H, C*H*(5)), 8.42 (s, 1H, C*H*(8)), 8.35 (t, *J* = 2.1 Hz, 1H, C*H*(19)), 8.29 (s, 1H, C*H*(1)), 8.16 (t, *J* = 1.7 Hz, 1H, C*H*(17)), 7.98 (m, 2H, C*H*(4,21), 7.72 (s, 1H, C*H*(10)), 3.66 (m, 2H, C*H*(14)), 3.34 (m, 2H, C*H*(14)), 2.70 (m, 2H, C*H*(11)), 2.63 – 2.53 (m, 4H, C*H*(12,13), 2.44 (s, 2H, C*H*(13)); ^{13}C NMR (101 MHz, DMSO) δ 165.2 (*C*(15)), 159.8 (*C*(2)), 148.6 (*C*(18)), 147.6 (*C*(1,6)), 144.0 (*C*(5), 141.7 (*C*(10)), 139.1 (*C*(16)), 135.9 (*C*(7)), 134.4 (*C*(20)), 132.9 (*C*(21)), 131.1 (*C*(8)), 130.7 (*C*(3)), 124.2 (*C*(19)), 120.6 (*C*(17)), 120.3 (*C*(9)), 117.9 (*C*(4)), 58.3 (*C*(12)), 52.5, 51.9 (*C*(13)), 47.1, 41.8 (*C*(14)), 21.2 (*C*(11)); LRMS (ESI$^+$) *m*/*z* 509.1 (M+H$^+$); HRMS (ESI$^+$): calcd for $C_{23}H_{22}ClN_8O_4^+$ [M+H]$^+$ 509.1446, found 509.1444.

8-(4-(2-(4-(5-chloro-2-nitrobenzoyl)piperazin-1-yl)ethyl)-1H-pyrazol-1-yl)pyrido[3,4-d]pyrimidin-4(3H)-one, (**68**)



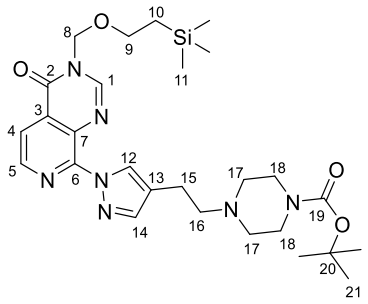
To a solution of 5-chloro-2-nitrobenzoic acid (56 mg, 0.277 mmol), HATU (131 mg, 0.346 mmol) in DMA (2 mL) was added PS-DIPEA (300 mg). The reaction mixture was stirred at room temperature for 15 min and **71** (75 mg, 0.231 mmol) was added. The reaction mixture was stirred at room temperature for 16 h. The reaction mixture was filtered, washed with MeOH (30 mL) and the filtrate was concentrated *in vacuo*. The crude product was adsorbed on silica and purified by flash chromatography eluting with 10% MeOH in CH_2Cl_2 to give **68** (26 mg, 22%) as an off-white solid. Mp 153 – 166 °C; ν_{max}/cm^{-1} 1701, 1638 (C=O), 1526 (N-O), 1211, 1160, 1131, 1101 (C-N); ^{1}H NMR (400 MHz, DMSO-d_6) δ 8.52 (d, *J* = 5.1 Hz, 1H, C*H*(5)), 8.44 (s, 1H, C*H*(8)), 8.27 (s, 1H, C*H*(1)), 8.22 (d, *J* = 8.8 Hz, 1H, C*H*(18)), 7.96 (d, *J* = 5.1 Hz, 1H, C*H*(4)), 7.77 (dd, *J* = 8.8, 2.3 Hz, 1H, C*H*(19)), 7.73 (d, *J* = 2.3 Hz, 1H, C*H*(21)), 7.71 (s, 1H, C*H*(10)), 3.65 – 3.60 (m, 2H, C*H*(14)), 3.25 – 3.19 (m, 2H, C*H*(14)), 2.70 (m, 2H, C*H*(11)), 2.59 (m, 4H, C*H*(12,13)), 2.47 – 2.31 (m, 2H, C*H*(13)); ^{13}C NMR (101 MHz, DMSO-d_6) δ 163.7 (*C*(15)), 160.4 (*C*(2)), 148.2 (*C*(1)), 147.7 (*C*(6)), 143.9 (*C*(17)), 143.8 (*C*(5)), 141.7 (*C*(10)), 139.8 (*C*(20)), 136.1 (*C*(7)), 134.2 (*C*(16)), 131.2 (*C*(8)), 130.7 (*C*(3)), 130.2 (*C*(19)), 127.9 (*C*(21)), 126.9 (*C*(18)), 120.3 (*C*(9)), 117.9 (*C*(4)), 58.4 (*C*(12)), 52.2, 51.7 (*C*(13)), 46.6 (*C*(14)), 41.4 (*C*(14)) 21.2 (*C*(11)); LRMS (ESI$^+$) *m/z* 509.1 (M+H$^+$); HRMS (ESI$^+$): calcd for $C_{23}H_{22}ClN_8O_4^+$ [M+H]$^+$ 509.1447, found 509.1444.

8-(4-(2-(4-(4-chloro-2-nitrobenzoyl)piperazin-1-yl)ethyl)-1H-pyrazol-1-yl)pyrido[3,4-d]pyrimidin-4(3H)-one, (**69**)



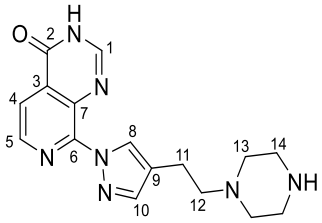
To a solution of 4-chloro-2-nitrobenzoic acid (46 mg, 0.231 mmol), HATU (131 mg, 0.346 mmol) in DMA (2 mL) was added PS-DIPEA (300 mg). The reaction mixture was stirred at room temperature for 15 min and **71** (0.075 g, 0.231 mmol) was added. The reaction mixture was stirred for 18 h. The reaction mixture was filtered, washed with MeOH (30 mL) and the filtrate concentrated *in vacuo*. The crude product was adsorbed in silica and eluted with 10% MeOH in CH_2Cl_2 to give **69** as a white solid (33 mg, 28%). Mp 273 – 276 °C; ν_{max}/cm^{-1} 1711, 1630 (C=O), 1560 (N-O), 1211, 1152, 1134, 1114 (C-N); ^{1}H NMR (400 MHz, DMSO-d_6) δ 8.53 (d, *J* = 5.1 Hz, 1H, C*H*(5)), 8.43 (s, 1H, C*H*(8)), 8.31 – 8.25 (m, 2H, C*H*(1,18), 7.97 (d, *J* = 5.1 Hz, 1H, C*H*(4)), 7.94 (dd, *J* = 8.2, 2.1 Hz, 1H, C*H*(20)), 7.71 (s, 1H, C*H*(10)), 7.59 (d, *J* = 8.2 Hz, 1H, C*H*(21)), 3.68 – 3.63 (m, 2H, C*H*(14)), 3.25 – 3.18 (m, 2H, C*H*(14)), 2.74 – 2.65 (m, 2H, C*H*(11)), 2.66 – 2.52 (m, 4H, C*H*(12,13)), 2.44 – 2.39 (m, 2H, C*H*(13)); ^{13}C NMR (101 MHz, DMSO-d_6) δ 164.3 (*C*(15)), 160.1 (*C*(2)), 147.9 (*C*(1)), 147.7 (*C*(6)), 146.2 (*C*(17)), 143.9 (*C*(5)), 141.7 (*C*(10)), 136.0 (*C*(7)), 134.7 (*C*(20)), 134.3 (*C*(19)), 131.2 (*C*(8)), 131.1 (*C*(16)), 130.7 (*C*(3)), 129.8 (*C*(21)), 124.8(*C*(18)), 120.3 (*C*(9)), 117.9 (*C*(4)), 58.4 (*C*(12)), 52.3, 51.8 (*C*(13)), 46.6, 41.5 (*C*(14)), 21.2 (*C*(11)); LRMS (ESI$^+$) *m*/*z* 509.1 (M+H$^+$); HRMS (ESI$^+$): calcd for $C_{23}H_{22}ClN_8O_4^+$ [M+H]$^+$ 509.1446, found 509.1444.

tert-butyl 4-(2-(1-(4-oxo-3-((2-(trimethylsilyl)ethoxy)methyl)-3,4-dihydropyrido[3,4-d]pyrimidin-8-yl)-1H-pyrazol-4-yl)ethyl)piperazine-1-carboxylate, (**70**)



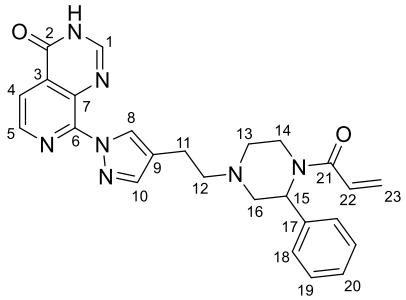
To a vial was added **50** (1.570 g, 3.37 mmol), *tert*-butyl piperazine-1-carboxylate (0.628 g, 3.37 mmol), potassium iodide (2.239 g, 13.49 mmol), potassium carbonate (9.32 g, 67.4 mmol) in AcN (17 mL). The reaction mixture was heated at 75 °C for 18 h. The reaction mixture was diluted with EtOAc (50 mL) and washed with $NaHCO_3$ (50 mL) and brine (50 mL). The organic layer was dried over Na_2SO_4, filtered and concentrated *in vacuo* to give an oil. The crude product was adsorbed on silica and purified by flash chromatography eluting with 0-10% MeOH in CH_2Cl_2 to give **70** as an off-white solid (1.382 g, 74%). Mp 70 – 75 °C; ν_{max}/cm^{-1} 1684 (C=O), 1170, 1076 (C-O), 1292, 1245, 1001 (C-N), 832 (C-H); ^{1}H NMR (400 MHz, $CDCl_3$) δ 8.62 (d, *J* = 5.1 Hz, 1H, C*H*(5)), 8.56 (d, *J* = 0.8 Hz, 1H, C*H*(1)), 8.30 (s, 1H, C*H*(12)), 8.06 (d, *J* = 5.1 Hz, 1H, C*H*(4)), 7.78 (d, *J* = 0.8 Hz, 1H, C*H*(14)), 5.46 (s, 2H, C*H*(8)), 3.72 – 3.64 (m, 2H, C*H*(9)), 3.47 (t, *J* = 5.1 Hz, 4H, C*H*(18)), 2.79 (t, *J* = 7.6 Hz, 2H, C*H*(15)), 2.65 (t, *J* = 7.7 Hz, 2H, C*H*(16)), 2.48 (m, 4H, C*H*(17)), 1.47 (s, 9H C*H*(21)), 1.18 – 0.84 (m, 2H, C*H*(10)), 0.00 (s, 9H, C*H*(11)); ^{13}C NMR (101 MHz, DMSO) δ 159.0 (*C*(2)), 153.8 (*C*(19)), 149.2 (C(1)), 148.1 (*C*(6)), 144.8 (*C*(5)), 141.9 (*C*(14)), 135.1 (*C*(7)), 131.1 (*C*(3)), 130.0 (*C*(12)), 120.6 (C(13)), 118.2 (*C*(4)), 78.7 (*C*(20)), 74.9 (*C*(8)), 66.4 (*C*(9)), 58.5 (*C*(16)), 52.4 (*C*(17)), 44.1 (*C*(18)) 28.1 (*C*(21)), 21.2 (*C*(15)), 17.4 (*C*(10), -1.3 (*C*(11)); LRMS (ESI^+) *m/z* 556.37 ($M+H^+$); HRMS (ESI^+): calcd for $C_{27}H_{42}N_7O_4Si^+$ $[M+H]^+$ 556.3062, found 556.3077.

8-(4-(2-(piperazin-1-yl)ethyl)-1H-pyrazol-1-yl)pyrido[3,4-d]pyrimidin-4(3H)-one, HCl (**71**)



To a solution of **70** (63 mg, 0.113 mmol) in THF (1 mL) was added 6M hydrochloric acid (1.134 mL, 6.80 mmol) and the solution was heated at 50 °C for 5 h. The solution was concentrated *in vacuo* to give **71** as a white solid (37 mg, quant.). Mp 241 – 245 °C; ν_{max}/cm^{-1} 3358 (N-H), 1728 (C=O), 1649 (N-H), 1232, 1208, 1150, 1079, 1010 (C-N), 862, 786 (C-H); ^{1}H NMR (400 MHz, DMSO-d_6) δ 12.18 (s, 1H, N*H*), 9.98 (s, 2H, NH_2), 8.57 (d, *J* = 5.1 Hz, 1H, C*H*(5)), 8.51 (s, 1H, C*H*(8)), 8.33 (s, 1H, C*H*(1)), 8.01 (d, *J* = 5.1 Hz, 1H, C*H*(4)), 7.81 (s, 1H, C*H*(10)), 3.86 – 3.68 (s, 2H, C*H*(13)), 3.65 – 3.52 (m, 2H, C*H*(14)), 3.49 – 3.23 (m, 6H, C*H*(12,13,14), 3.07 (m, 2H, C*H*(11)); ^{13}C NMR (101 MHz, DMSO-d_6) δ 159.4 (*C*(2)), 147.7 (*C*(1)), 147.3 (*C*(6)), 144.3 (*C*(5)), 141.5 (*C*(10)), 135.5 (*C*(7)), 131.6 (*C*(8)), 130.8 (*C*(3)), 118.3 (*C*(4)), 117.2 (*C*(9)), 55.4 (*C*(12)), 47.7 (*C*(13)), 39.6 (*C*(14)), 18.4 (C(11)); LRMS (ESI$^+$) *m*/*z* 326.1 (M+H$^+$); HRMS (ESI$^+$): calcd for $C_{16}H_{20}N_7O^+$ [M+H]$^+$ 326.1715, found 326.1724.

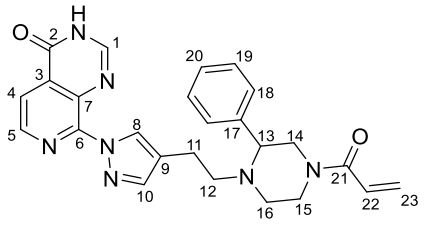
8-(4-(2-(4-acryloyl-3-phenylpiperazin-1-yl)ethyl)-1H-pyrazol-1-yl)pyrido[3,4-d]pyrimidin-4(3H)-one, (**72**)



To a solution of **86** (0.474 g, 0.750 mmol) was added 6M hydrochloric acid (7.50 mL, 45.0 mmol) and heated to 50 °C for 3 h. The solution was concentrated *in vacuo*. The crude product was loaded onto an SCX-2 column and washed with MeOH. The product was eluted by washing with 3.5N NH_3 in MeOH and the filtrate was concentrated *in vacuo* to give 8-(4-(2-(3-phenylpiperazin-1-yl)ethyl)-1H-pyrazol-1-yl)pyrido[3,4-d]pyrimidin-4(3H)-one (quant.). To a solution of 8-(4-(2-(3-

phenylpiperazin-1-yl)ethyl)-1H-pyrazol-1-yl)pyrido[3,4-d]pyrimidin-4(3H)-one (100 mg, 0.249 mmol) and PS-DIPEA (300 mg) in DMA (2 mL) at 0 °C was added acryloyl chloride (30 µL, 0.374 mmol). The reaction mixture was warmed to room temperature and stirred for 16 h. More acryloyl chloride (30 µL, 0.374 mmol) was added and the reaction mixture was stirred for a further 16 h. The reaction mixture was filtered, washed with MeOH (40 mL) and concentrated *in vacuo*. The crude product was dissolved in 1:1 MeOH:DMSO (1 mL) and purified by prep HPLC to give **72** as a white amorphous solid (10 mg, 9%). ν_{max}/cm^{-1} 3357 (N-H), 1702, 1637 (C=O), 1601, 1449 (C=C), 1215, 1159, 1019 (C-N), 964 (C=C-H), 826, 799 (C-H); ^{1}H NMR (400 MHz, DMSO-d_6) δ 8.55 (d, *J* = 5.1 Hz, 1H, C*H*(5)), 8.31 (s, 1H, C*H*(8)), 8.23 (s, 1H, C*H*(1)), 7.98 (d, *J* = 5.1 Hz, 1H, C*H*(4)), 7.63 (s, 1H, C*H*(10)), 7.33 (d, *J* = 7.7 Hz, 2H, C*H*(18)), 7.21 (t, *J* = 7.6 Hz, 2H, C*H*(19)), 7.09 (t, *J* = 7.3 Hz, 1H, C*H*(20)), 6.86 (dd, *J* = 16.6, 10.5 Hz, 1H, C*H*(22)), 6.18 (dd, *J* = 16.6, 2.4 Hz, 1H, C*H*(23)), 5.72 (d, *J* = 10.8 Hz, 1H, C*H*(23)), 3.58 (d, *J* = 12.0 Hz, 1H, C*H*(15)), 2.95 (d, *J* = 11.1 Hz, 1H), 2.76 – 2.50 (m, 4H, C*H*(11,12)), 2.37 (m, 1H, C*H*(16)); ^{13}C NMR (101 MHz, DMSO) δ 159.9 (*C*(2)), 149.1 (*C*(6)), 147.7 (*C*(1)), 144.0 (*C*(5)), 141.7 (*C*(10)), 136.4 (*C*(7)), 131.3 (*C*(8)), 130.6 (*C*(3)), 128.3-127.9 (*C*(19,22,23)), 127.6 (*C*(18)), 126.5 (*C*(20), 120.3 (*C*(9)), 117.8 (*C*(4)), 72.5, 63.1, 58.3 (*C*(12)), 30.7 (*C*(14)), 21.0 (*C*(11)); LRMS (ESI$^+$) *m/z* 456.7 (M+H$^+$); HRMS (ESI$^+$): calcd for $C_{25}H_{26}N_7O_2^+$ [M+H]$^+$ 456.2142, found 456.2143.

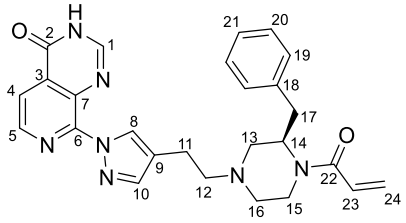
8-(4-(2-(4-acryloyl-2-phenylpiperazin-1-yl)ethyl)-1H-pyrazol-1-yl)pyrido[3,4-d]pyrimidin-4(3H)-one, (**73**)



To a solution of **87** (0.205 g, 0.324 mmol) in THF (3 mL) was added 6M hydrochloric acid (3 mL, 19.5 mmol). The reaction mixture was heated to 50 °C for 3 h. The crude product was loaded onto an SCX-2 column and washed with MeOH. The product was eluted by washing with 3.5N NH_3 in MeOH. The filtrate was concentrated *in vacuo* to give 8-(4-(2-(2-phenylpiperazin-1-yl)ethyl)-1H-pyrazol-1-

yl)pyrido[3,4-d]pyrimidin-4(3H)-one (quant.). A solution of 8-(4-(2-(2-phenylpiperazin-1-yl)ethyl)-1H-pyrazol-1-yl)pyrido[3,4-d]pyrimidin-4(3H)-one (86 mg, 0.214 mmol) and PS-DIPEA (300 mg) in DMA (2 mL) was stirred for 15 min. The reaction mixture was cooled to 0 °C and then acryloyl chloride (26 µL, 0.321 mmol) was added. The reaction mixture was warmed to room temperature and stirred for 16 h. More acryloyl chloride (12 µL, 0.154 mmol) was added and the reaction mixture was stirred at room temperature for 16 h. The reaction mixture was filtered, washed with MeOH (50 mL) and concentrated *in vacuo*. The crude product was dissolved in MeOH:DMSO (1 mL) and purified by prep HPLC to give **73** (7 mg, 7%) as a white solid. Mp 160 – 162 °C; ν_{max}/cm^{-1} 3303 (N-H), 1702, 1646 (C=O), 1607, 1550, 1460 (C=C), 1159, 1126, 1096 (C-N), 967 (C=C-H), 740 (C-H); ^{1}H NMR (400 MHz, DMSO-d_6) δ 8.49 (d, *J* = 5.1 Hz, 1H, C*H*(5)), 8.27 (s, 1H, C*H*(8)), 8.24 (s, 1H, C*H*(1)), 7.94 (d, *J* = 5.1 Hz, 1H, C*H*(4)), 7.49 (s, 1H, C*H*(10)), 7.40 – 7.20 (m, 5H, C*H*(18,19,20)), 6.83 (m, 1H, C*H*(22)), 6.12 (m, 1H, C*H*(22)), 5.68 (m, 1H, C*H*(22)), 4.50 – 3.85 (m, 3H, C*H*(13,14)), 3.26 – 2.87 (m, 2H, C*H*(15/16)), 2.71 – 2.56 (m, 4H, C*H*(11,12)), 2.21 (m, 2H, C*H*(15/16)); ^{13}C NMR (101 MHz, DMSO) δ 161.5 (C(2)), 143.4 (*C*(5)), 141.3 (*C*(10)), 136.2 (*C*(7)), 131.0 (*C*(8)), 130.5 (*C*(3)), 128.5, 127.7, 127.5 (*C*(18,19,20)), 127.4 (*C*(22)), 120.5, 120.0 (*C*(9)), 117.9 (*C*(4)), 54.5, 40.4, 40.1 (*C*(14)), 20.4 (*C*(11)); LRMS (ESI$^+$) *m/z* 456.4 (M+H$^+$); HRMS (ESI$^+$): calcd for $C_{25}H_{26}N_7O_2^+$ [M+H]$^+$ 456.2142, found 456.2145.

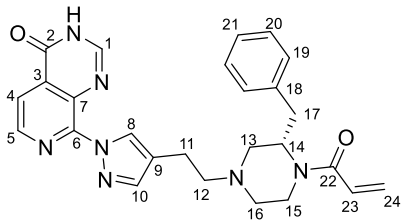
(*R*)-8-(4-(2-(4-acryloyl-3-benzylpiperazin-1-yl)ethyl)-1H-pyrazol-1-yl)pyrido[3,4-d]pyrimidin-4(3H)-one, (**74**)



To a solution of **88** (0.460 g, 0.712 mmol) in THF (6 mL) was added 6M hydrochloric acid (7.12 mL, 42.7 mmol). The reaction mixture was heated to 50 °C for 3 h and then concentrated *in vacuo*. The crude product was loaded onto an SCX-2 column and washed with MeOH. The product was eluted by washing with 3.5N NH_3 in MeOH. The filtrate was concentrated *in vacuo* to give (*R*)-8-(4-(2-(3-

benzylpiperazin-1-yl)ethyl)-1H-pyrazol-1-yl)pyrido[3,4-d]pyrimidin-4(3H)-one, 2HCl (quant.). A solution of (*R*)-8-(4-(2-(3-benzylpiperazin-1-yl)ethyl)-1H-pyrazol-1-yl)pyrido[3,4-d]pyrimidin-4(3H)-one, 2HCl (100 mg, 0.205 mmol) and PS-DIPEA (300 mg) in DMA (2 mL) was stirred for 15 min. The reaction mixture was cooled to 0 °C and then acryloyl chloride (25 µL, 0.307 mmol) was added. The reaction mixture was warmed to room temperature and stirred for 16 h. More acryloyl chloride (12 µL, 0.154 mmol) was added and the reaction mixture was stirred at room temperature for 16 h. The reaction mixture was filtered, washed with MeOH (50 mL) and concentrated *in vacuo*. The crude solid was dissolved in MeOH:DMSO (1 mL) and purified by prep HPLC to give **74** (7 mg, 7%) as a white solid. ν_{max}/cm^{-1} 3362 (N-H), 1676, 1637 (C=O), 1603, 1551 (C=C), 1215, 1010 (C-N), 968 (C=C-H); ^{1}H NMR (400 MHz, DMSO-d_6) δ 8.51 (m, 2H, C*H*(5,8)), 8.26 (s, 1H, C*H*(1)), 7.96 (d, *J* = 5.1 Hz, 1H, C*H*(4)), 7.75 (s, 1H, C*H*(10)), 7.28 – 7.20 (m, 2H, C*H*(19)), 7.16 (m, 3H, C*H*(20,21)), 6.47 – 6.01 (m, 1H, C*H*(23)), 5.90 – 5.36 (m, 2H, C*H*(24)), 4.36 – 4.13 (m, 2H, C*H*(14,17)), 3.17 – 2.80 (m, 5H, C*H*(13, 15, 16, 17)), 2.84 – 2.46 (m, 4H, C*H*(11, 12)), 2.11 – 1.92 (m, 3H, C*H*(13,16)); ^{13}C NMR (101 MHz, DMSO) δ 172.1 (*C*O (acetate)), 164.8 (*C*(22)), 160.7 (*C*(2)), 148.6 (*C*(1)), 147.6 (*C*(6)), 143.6 (*C*(5)), 141.7 (*C*(10)), 138.6 (*C*(18)), 136.1 (*C*(7)), 131.3 (*C*(8)), 130.6 (*C*(3)), 129.4 (*C*(20)), 128.4 (*C*(23)), 128.3 (*C*(19)), 127.2 (*C*(24)), 126.3 (*C*(21)), 120.4 (*C*(9)), 117.9 (*C*(4)), 58.4 (*C*(12)), 55.7 (C(13)), 54.7 (*C*(14)), 53.2, 52.7 (*C*(15,16)), 36.7 (*C*(17)), 21.2 (*C*(11)), 21.2 (*C*H$_3$ (acetate); LRMS (ESI$^+$) *m/z* 470.4 (M+H$^+$); HRMS (ESI$^+$): calcd for $C_{26}H_{28}N_7O_2^+$ [M+H]$^+$ 470.2299, found 470.2296.

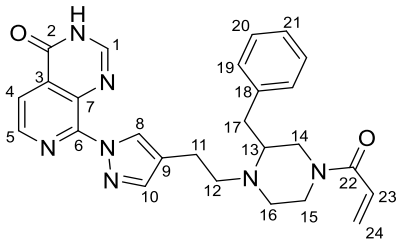
(*S*)-8-(4-(2-(4-acryloyl-3-benzylpiperazin-1-yl)ethyl)-1H-pyrazol-1-yl)pyrido[3,4-d]pyrimidin-4(3H)-one, (**75**)



To a solution of **89** (0.498 g, 0.771 mmol) in THF (7.71 mL) was added 6M hydrochloric acid (7.71 mL, 46.3 mmol). The reaction mixture was heated to 50 °C and then concentrated *in vacuo* to give

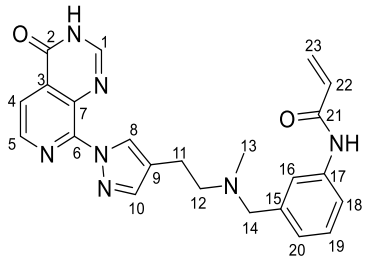
an off-white solid. The crude product was loaded onto an SCX-2 column and washed with MeOH. The product was eluted by washing with 3.5N NH_3 in MeOH. The filtrate was concentrated *in vacuo* to give (*S*)-8-(4-(2-(3-benzylpiperazin-1-yl)ethyl)-1H-pyrazol-1-yl)pyrido[3,4-d]pyrimidin-4(3H)-one (quant.). A solution of (*S*)-8-(4-(2-(3-benzylpiperazin-1-yl)ethyl)-1H-pyrazol-1-yl)pyrido[3,4-d]pyrimidin-4(3H)-one, 2HCl (100 mg, 0.205 mmol) and PS-DIPEA (300 mg) in DMA (2 mL) was stirred for 15 min. The reaction mixture was cooled to 0 °C and acryloyl chloride (25 µL, 0.307 mmol) was added. The reaction mixture was warmed to room temperature and stirred for 16 h. More acryloyl chloride (12 µL, 0.154 mmol) was added and the reaction mixture was stirred at room temperature for 16 h. The reaction mixture was filtered, washed with MeOH (50 mL) and concentrated *in vacuo*. The crude product was dissolved in MeOH:DMSO (1 mL) and purified by prep-HPLC to give **75** (7 mg, 8%) as a white solid. ν_{max}/cm^{-1} 3386 (N-H), 1701, 1637 (C=O), 1603, 1551 (C=C), 1216, 1061, 1011 (C-N), 968 (C=C-H); ^{1}H NMR (400 MHz, DMSO-d_6) δ 8.52 (d, *J* = 5.1 Hz, 1H, C*H*(5)), 8.49 (d, *J* = 0.8 Hz, 1H, C*H*(8)), 8.21 (s, 1H, C*H*(1)), 7.73 (s, 1H, C*H*(10)), 7.29 – 7.20 (m, 2H, C*H*(19)), 7.16 (tt, *J* = 6.4, 1.4 Hz, 3H, C*H*(20,21)), 6.52 (m, 1H, C*H*(23)), 5.92 (m, 1H, C*H*(24)), 5.52 (m, 1H, CH(24)), 4.15 (m, 1H, C*H*(14)), 3.11 – 2.99 (m, 5H, C*H*(15,16,17)), 2.84 (m, 1H, C*H*(13)), *2*.73 (t, *J* = 7.1 Hz, 2H, C*H*(11)), 2.68 – 2.47 (m, 2H, C*H*(12)), 2.04 (m, 2H, C*H*(13,16)); ^{13}C NMR (101 MHz, DMSO) δ 160.3 (*C*(2)), 148.2 (*C*(1)), 147.7 (*C*(6)), 143.7 (*C*(5)), 141.7 (*C*(10)), 136.3 (*C*(7)), 131.2 (*C*(8)), 130.6 (*C*(3)), 129.4 (C(20)), 128.3 (*C*(23)), 128.2 (*C*(19)), 126.3 (*C*(21)), 120.4 (*C*(9)), 117.8 (*C*(4)), 58.4 (*C*(12)), 21.2 (*C*(11)); LRMS (ESI$^+$) *m/z* 470.4 (M+H$^+$); HRMS (ESI$^+$): calcd for $C_{26}H_{27}N_7O_2^+$ [M+H]$^+$ 470.2299, found 470.2298.

8-(4-(2-(4-acryloyl-2-benzylpiperazin-1-yl)ethyl)-1H-pyrazol-1-yl)pyrido[3,4-d]pyrimidin-4(3H)-one, (76)



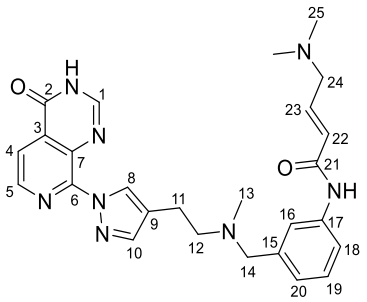
To a solution of **90** (0.146 g, 0.226 mmol) in THF (2 mL) was added 6M hydrochloric acid (2.260 mL, 13.56 mmol). The reaction mixture was heated to 50 °C for 3 h. The crude product was loaded onto an SCX-2 column and washed with MeOH. The product was eluted by washing with 3.5N NH_3 in MeOH. The filtrate was concentrated *in vacuo* to give 8-(4-(2-(2-benzylpiperazin-1-yl)ethyl)-1H-pyrazol-1-yl)pyrido[3,4-d]pyrimidin-4(3H)-one (0.086 g, 92%) which was taken on crude into the next step. To a solution of 8-(4-(2-(2-benzylpiperazin-1-yl)ethyl)-1H-pyrazol-1-yl)pyrido[3,4-d]pyrimidin-4(3H)-one (86 mg, 0.207 mmol) in DMA (2 mL) was added PS-DIPEA (300 mg). The reaction mixture was cooled to 0 °C, acryloyl chloride (25 µL, 0.310 mmol) was added and slowly warmed to room temperature. The reaction mixture was stirred for 16 h, filtered and concentrated *in vacuo*. The crude product was purified by prep HPLC to give **76** as a white solid (13 mg, 13%). Mp 161 – 163 °C; ν_{max}/cm^{-1} 1701, 1643 (C=O), 1603, 1550, 1492 (C=C), 1219, 1155, 1059 (C-N), 976, 915 (C=C-H), 740, 702 (C-H); ^{1}H NMR (400 MHz, DMSO-d_6) δ 8.55 (d, *J* = 5.1 Hz, 1H, C*H*(5)), 8.43 (s, 1H, C*H*(8)), 8.27 (s, 1H, C*H*(1)), 7.98 (d, *J* = 5.1 Hz, 1H, C*H*(4)), 7.72 (s, 1H, C*H*(10)), 7.33 – 7.14 (m, 5H, C*H*(19,20,21)), 6.84 (dd, *J* = 16.8, 10.6 Hz, 1H, C*H*(23)), 6.15 (dd, *J* = m, 1H, C*H*(24)), 5.67 (m, 1H, C*H*(24)), 3.65 (m, 1H, C*H*(14)), 3.55 (s, 1H, C*H*(14)), 3.49 – 3.29 (m, 3H, C*H*(13,16)), 3.04 – 2.76 (m, 8H, C*H*(11,12,15,17)); ^{13}C NMR (101 MHz, DMSO) δ 164.5 (*C*(22)), 160.0 (*C*(2,6)), 147.7 (*C*(1)), 144.1 (*C*(5)), 142.1 (*C*(10)), 139.4 (*C*(18)), 135.9 (C(7)), 131.3 (*C*(8)), 130.7 (*C*(3)), 128.5 (*C*(23)), 127.7 (*C*(24)), 129.6, 128.6, 126.3 (*C*(19,20,21)), 120.5 (*C*(9)), 117.9 (*C*(4)), 65.0 (*C*(13)), 60.1 (*C*(12)), 54.1, 48.7 (*C*(15), 45.0, 43.9 (*C*(14,16)), 32.4 (*C*(17)), 21.3 (*C*(11)); LRMS (ESI$^+$) *m/z* 470.1 (M+H$^+$); HRMS (ESI$^+$): calcd for $C_{26}H_{28}N_7O_2^+$ $[M+H]^+$ 470.2299, found 470.2307.

N-(3-((methyl(2-(1-(4-oxo-3,4-dihydropyrido[3,4-d]pyrimidin-8-yl)-1H-pyrazol-4-yl)ethyl)amino) methyl)phenyl)acrylamide, (**77**)



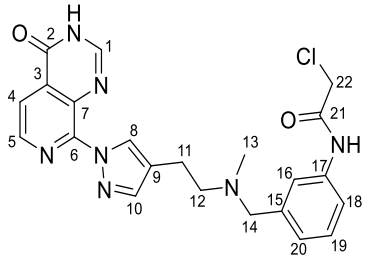
To a solution of **92** (179 mg, 0.354 mmol) in THF (4 mL) was added 6M hydrochloric acid (4 mL, 24.00 mmol). The reaction mixture was heated to 50 °C for 3 h. The reaction mixture was concentrated *in vacuo* to give 8-(4-(2-((3-aminobenzyl)(methyl)amino)ethyl)-1H-pyrazol-1-yl)pyrido[3,4-d]pyrimidin-4(3H)-one as the HCl salt (quant.). To a solution of 8-(4-(2-((3-aminobenzyl)(methyl)amino)ethyl)-1H-pyrazol-1-yl)pyrido[3,4-d]pyrimidin-4(3H)-one, HCl (75 mg, 0.200 mmol) and PS-DIPEA (300 mg) in DMA (2 mL) at 0 °C was added acryloyl chloride (24 µL, 0.300 mmol). The reaction mixture was warmed to room temperature and stirred for 3 h. The reaction mixture was filtered, washed with MeOH (40 mL) and concentrated *in vacuo*. The crude product was adsorbed on silica and purified by flash chromatography, eluting with 25% MeOH in CH_2Cl_2 to give **77** (12 mg, 14%) as a white solid. ν_{max}/cm^{-1} 1676 (C=O), 1608, 1490 (C=C), 1211, 1161, 1051 (C-N), 971 (C=C-H), 827, 798 (C-H); ^{1}H NMR (400 MHz, DMSO-d_6) δ 10.08 (s, 1H, N*H*), 8.52 (d, *J* = 5.1 Hz, 1H, C*H*(5)), 8.40 (s, 1H, C*H*(8)), 8.26 (s, 1H, C*H*(1)), 7.96 (d, *J* = 5.1 Hz, 1H, C*H*(4)), 7.69 (s, 1H, C*H*(10)), 7.64 – 7.55 (m, 2H, C*H*(16,18)), 7.24 (t, *J* = 7.8 Hz, 1H, C*H*(19)), 7.01 (d, *J* = 7.5 Hz, 1H, C*H*(20)), 6.40 (dd, *J* = 17.0, 10.1 Hz, 1H, C*H*(22)), 6.21 (dd, *J* = 17.0, 2.1 Hz, 1H, C*H*(23)), 5.72 (dd, *J* = 10.1, 2.1 Hz, 1H, C*H*(23)), 3.52 (s, 2H, C*H*(14)), 2.77 – 2.69 (m, 2H, C*H*(11)), 2.66 – 2.58 (m, 2H, C*H*(12)), 2.20 (s, 3H, C*H*(13)); ^{13}C NMR (101 MHz, DMSO) δ 163.0 (*C*(21)), 160.3 (*C*(2)), 148.1 (*C*(1)), 147.7 (*C*(6)), 143.7 (*C*(5)), 141.6 (*C*(10)), 139.8 (*C*(17)), 138.9 (*C*(15)), 136.0 (*C*(7)), 131.9 (*C*(22)), 131.1 (*C*(8)), 130.6 (*C*(3)), 128.5 (*C*(19)), 126.7 (*C*(23)), 123.9 (*C*(20)), 120.4 (*C*(9)), 119.5 (*C*(16)), 117.9 (*C*(4,18)), 61.5 (*C*(14)), 57.8 (*C*(12)), 41.7 (*C*(13)), 21.7 (*C*(11)); LRMS (ESI$^+$) *m/z* 430.2 (M+H$^+$); HRMS (ESI$^+$): calcd for $C_{23}H_{24}N_7O_2^+$ [M+H]$^+$ 430.1986, found 430.1986.

(*E*)-4-(dimethylamino)-N-(3-((methyl(2-(1-(4-oxo-3,4-dihydropyrido[3,4-d]pyrimidin-8-yl)-1H-pyrazol-4-yl)ethyl)amino)methyl)phenyl)but-2-enamide, (**78**)



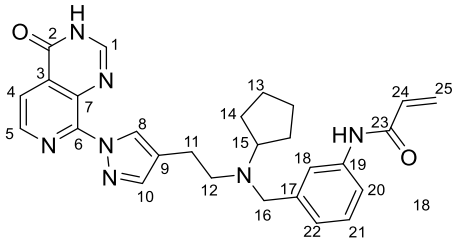
To a solution of 8-(4-(2-((3-aminobenzyl)(methyl)amino)ethyl)-1H-pyrazol-1-yl)pyrido[3,4-d]pyrimidin-4(3H)-one, HCl (100 mg, 0.266 mmol), PS-DIPEA (300 mg) and (*E*)-4-(dimethylamino)but-2-enoic acid, HCl (44 mg, 0.266 mmol) in DMA (2 mL) at 0 °C was added T3P (235 µL, 0.400 mmol). The reaction mixture was warmed to room temperature and stirred for 16 h. The reaction mixture was filtered, washed with MeOH (50 mL) and concentrated *in vacuo* to give a brown oil. The crude product was adsorbed on silica and added to a 11g KP-NH column eluting with 0-30% MeOH in CH_2Cl_2 to give **78** (39 mg, 30%) as a white solid. Mp 128 – 130 °C; ν_{max}/cm^{-1} 1688 (C=O), 1611, 1551, 1490, 1456 (C=C), 1158, 1038 (C-N); 912 (C=CH) 858, 826 (C-H); ^{1}H NMR (400 MHz, DMSO-d_6) δ 9.99 (s, 1H, N*H*), 8.48 (d, *J* = 5.1 Hz, 1H, C*H*(5)), 8.42 (s, 1H, C*H*(8)), 8.25 (s, 1H, C*H*(1)), 7.94 (d, *J* = 5.1 Hz, 1H, C*H*(4)), 7.68 (s, 1H, C*H*(10)), 7.61 (d, *J* = 1.9 Hz, 1H, C*H*(16)), 7.55 (dd, *J* = 8.1, 2.0 Hz, 1H, C*H*(18)), 7.23 (t, *J* = 7.8 Hz, 1H, C*H*(19)), 6.99 (d, *J* = 7.6 Hz, 1H, C*H*(20)), 6.68 (dt, *J* = 15.4, 5.9 Hz, 1H, C*H*(23)), 6.22 (dt, *J* = 15.3, 1.7 Hz, 1H, C*H*(22)), 3.51 (s, 2H, C*H*(14)), 3.03 (dd, *J* = 5.9, 1.6 Hz, 2H, C*H*(24)), 2.73 (m, 2H, C*H*(11)), 2.62 (m, 2H, C*H*(12)), 2.19 (s, 3H, C*H*(13)), 2.16 (s, 6H, C*H*(25)); ^{13}C NMR (101 MHz, DMSO) δ 163.1 (*C*(21)), 159.8 (*C*(2)), 148.5 (*C*(1)), 147.5 (*C*(6)), 144.0 (*C*(5)), 141.6 (*C*(10)), 141.1 (*C*(23)), 139.7 (*C*(17)), 139.1 (*C*(15)), 135.8 (*C*(7)) 131.1 (*C*(8)), 130.7 (*C*(3)), 128.4 (*C*(19)), 126.0 (*C*(22)), 123.7 (*C*(20)), 120.5 (*C*(9)), 119.5 (*C*(16)), 117.8 (*C*(4,18), 61.5 (*C*(14)), 59.7 (*C*(24)), 57.7 (*C*(12)), 45.1 (*C*(25)), 41.7 (*C*(13)), 21.7 (*C*(11)); LRMS (ESI^+) *m*/*z* 487.6 ($M+H^+$); HRMS (ESI^+): calcd for $C_{26}H_{31}N_8O_2^+$ $[M+H]^+$ 487.2565, found 487.2569.

2-chloro-N-(3-((methyl(2-(1-(4-oxo-3,4-dihydropyrido[3,4-d]pyrimidin-8-yl)-1H-pyrazol-4-yl)ethyl)amino)methyl)phenyl)acetamide, (**79**)



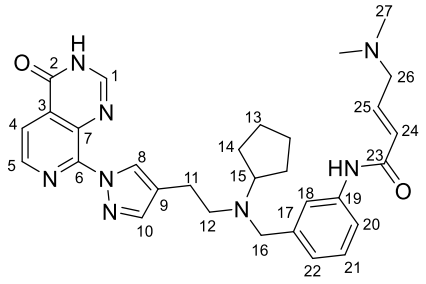
To a solution of 8-(4-(2-((3-aminobenzyl)(methyl)amino)ethyl)-1H-pyrazol-1-yl)pyrido[3,4-d]pyrimidin-4(3H)-one, HCl (100 mg, 0.266 mmol) and PS-DIPEA (300 mg) in NMP (3 mL) at 0 °C was added 2-chloroacetyl chloride (23 µl, 0.293 mmol). The reaction mixture was slowly warmed to room temperature and stirred for 16 h. The reaction mixture was filtered, washed with MeOH (50 mL) and concentrated *in vacuo* to give a brown oil. The crude product was adsorbed on silica and added to a 11g KP-NH column eluting with 0-20% MeOH in CH_2Cl_2 to give **79** (45 mg, 37%) as a white solid. Mp 118 – 120 °C; ν_{max}/cm^{-1} 3013 (N-H), 1682 (C=O), 1596, 1549, 1491, 1443 (C=C), 1211, 1158, 1059 (C-N), 825, 800 (C-H), 741 (C-Cl); ^{1}H NMR (400 MHz, DMSO-d_6) δ 10.26 (s, 1H, N*H*), 8.55 (d, *J* = 5.2 Hz, 1H, C*H*(5)), 8.38 (s, 1H, C*H*(8)), 8.26 (s, 1H, C*H*(1)), 7.98 (d, *J* = 5.1 Hz, 1H, C*H*(4)), 7.69 (s, 1H, C*H*(10)), 7.55 (s, 1H, C*H*(16)), 7.48 (d, *J* = 8.3 Hz, 1H, C*H*(18)), 7.26 (t, *J* = 7.8 Hz, 1H, C*H*(19)), 7.03 (d, *J* = 7.6 Hz, 1H, C*H*(20)), 4.21 (s, 2H, C*H*(22)), 3.53 (s, 2H, C*H*(14)), 2.72 (d, *J* = 7.7 Hz, 2H), 2.63 (d, *J* = 7.8 Hz, 2H), 2.20 (s, 3H, C*H*(13)); ^{13}C NMR (101 MHz, DMSO) δ 164.5 (*C*(21)), 159.8 (*C*(2)), 148.0 (*C*(1)), 147.2 (*C*(6)), 144.1 (*C*(5)), 141.6 (*C*(10)), 138.4 (*C*(15,17), 135.9 (*C*(7)), 131.1 (*C*(8)), 130.8 (*C*(3)), 128.7 (*C*(19)), 124.5 (*C*(20)), 119.7 (*C*(16)), 118.1 (*C*(18)), 117.9 (*C*(4)), 61.1 (*C*(14)), 57.7 (*C*(12)), 43.6 (*C*(22)), 41.4 (*C*(13)), 21.5 (*C*(11)); LRMS (ESI$^+$) m/z 452.7 (M+H$^+$); HRMS (ESI$^+$): calcd for $C_{22}H_{23}ClN_7O_2^+$ $[M+H]^+$ 452.1596, found 452.1566.

N-(3-((cyclopentyl(2-(1-(4-oxo-3,4-dihydropyrido[3,4-d]pyrimidin-8-yl)-1H-pyrazol-4-yl)ethyl) amino)methyl)phenyl)acrylamide, (**80**)



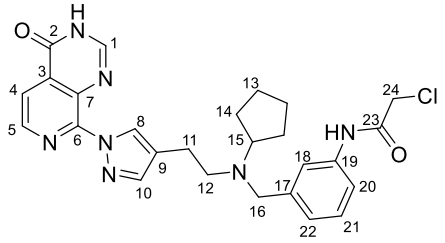
To a solution of **96** (90 mg, 0.354 mmol) in THF (4 mL) was added 6M hydrochloric acid (1.5 mL). The reaction mixture was heated to 50 °C for 3 h. The reaction mixture was concentrated *in vacuo* to give 8-(4-(2-((3-aminobenzyl)(cyclopentyl)amino)ethyl)-1H-pyrazol-1-yl)pyrido[3,4-d]pyrimidin-4(3H)-one as the HCl salt (quant.). To a solution of 8-(4-(2-((3-aminobenzyl)(cyclopentyl)amino)ethyl)-1H-pyrazol-1-yl)pyrido[3,4-d]pyrimidin-4(3H)-one, HCl (75 mg, 0.149 mmol) and PS-DIPEA (300 mg) in DMA (1.5 mL) at 0 °C was added acryloyl chloride (18 µL, 0.224 mmol). The reaction mixture was warmed to room temperature and stirred for 3 h. The reaction mixture was filtered, washed with MeOH (40 mL) and concentrated *in vacuo*. The crude product was adsorbed on silica and purified by flash chromatography, eluting with 10% MeOH in CH_2Cl_2 to give **80** (27 mg, 37%) as an off-white amorphous solid. ν_{max}/cm^{-1} 1665 (C=O), 1607, 1549, 1488 (C=C), 1210, 1157, 1060 (C-N), 966 (C=C-H), 826, 798 (C-H); ^{1}H NMR (400 MHz, DMSO-*d*6) δ 10.08 (s, 1H, N*H*), 8.51 (d, *J* = 5.1 Hz, 1H, C*H*(5)), 8.33 (s, 1H, C*H*(8)), 8.25 (s, 1H, C*H*(1)), 7.99 – 7.90 (d, *J* = 5.1 Hz, 1H, C*H*(4)), 7.68 – 7.54 (m, 3H, C*H*(10,18,20)), 7.24 (t, *J* = 7.8 Hz, 1H, CH(21)) 7.05 (d, *J* = 7.6 Hz, 1H, C*H*(22)), 6.51 – 6.35 (m, 1H, C*H*(24)), 6.21 (dd, *J* = 16.9, 2.1 Hz, 1H, C*H*(25)), 5.75 – 5.58 (m, 1H, C*H*(25)), 3.66 (s, 2H, C*H*(16)), 3.14 (m, 1H, C*H*(15)), 2.77 – 2.58 (m, 4H, C*H*(11+12)), 1.86 – 1.71 (m, 2H, C*H*(14)), 1.71 – 1.57 (m, 2H, C*H*(14)), 1.53 – 1.26 (m, 4H, C*H*(13)); ^{13}C NMR (101 MHz, DMSO) δ 163.0 (*C*(23)), 160.3 (*C*(2)), 148.1 (*C*(1)), 147.6 (*C*(6)), 143.7 (*C*(5)), 141.5 (*C*(10)), 141.5(*C*(19)), 138.9 (*C*(17)), 136.0 (*C*(7)), 131.9 (*C*(24)), 131.0 (*C*(8)), 130.6 (*C*(3)), 128.4 (*C*(21)), 126.7 (*C*(25)), 123.6 (*C*(22)), 120.5 (*C*(9)), 119.3 (*C*(18)), 117.8 (*C*(4)), 117.7(*C*(20)), 62.9 (*C*(15)), 55.4 (*C*(16)), 52.5 (*C*(12)), 29.0 (*C*(14)), 23.8 (*C*(13)), 21.3 (*C*(11)); LRMS (ESI$^+$) *m*/*z* 484.3 (M+H$^+$); HRMS (ESI$^+$): calcd for $C_{27}H_{30}N_7O_2^+$ [M+H]$^+$ 484.2455, found 484.2427.

(*E*)-N-(3-((cyclopentyl(2-(1-(4-oxo-3,4-dihydropyrido[3,4-d]pyrimidin-8-yl)-1H-pyrazol-4-yl)ethyl) amino)methyl)phenyl)-4-(dimethylamino)but-2-enamide, (**81**)



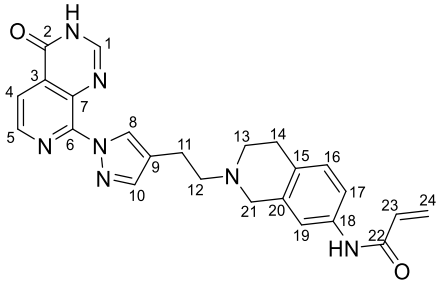
To a solution of 8-(4-(2-((3-aminobenzyl)(cyclopentyl)amino)ethyl)-1H-pyrazol-1-yl)pyrido[3,4-d]pyrimidin-4(3H)-one, HCl (0.075 g, 0.175 mmol), PS-DIPEA (300 mg) and (*E*)-4-(dimethylamino)but-2-enoic acid, HCl (0.029 g, 0.175 mmol) in DMA (2 mL) at 0 °C was added T3P (0.154 mL, 0.262 mmol). The reaction mixture was warmed to room temperature and stirred for 16 h. The reaction mixture was filtered, washed with MeOH (50 mL) and concentrated *in vacuo* to give a brown oil. The crude product was adsorbed on silica and purified by flash chromatography on a 11g KP-NH column eluting with 0-30% MeOH in CH_2Cl_2 to give **81** (0.008 g, 8%) as a yellow solid. Mp 110 – 112 °C; ν_{max}/cm^{-1} 1679, 1608 (C=O), 1549, 1488, 1437 (C=C), 1211, 1157, 1061, 1020 (C-N); 967 (C=CH) 858, 826 (C-H); ^{1}H NMR (400 MHz, DMSO-d_6) δ 9.99 (s, 1H, N*H*), 8.45 (d, *J* = 5.1 Hz, 1H, C*H*(5)), 8.36 (s, 1H, C*H*(8)), 8.23 (s, 1H, C*H*(1)), 7.92 (d, *J* = 5.1 Hz, 1H, C*H*(4)), 7.65 (d, *J* = 1.9 Hz, 1H, C*H*(18)), 7.60 (s, 1H, C*H*(10)), 7.56 (d, *J* = 7.9 Hz, 1H, C*H*(20)), 7.22 (t, *J* = 7.8 Hz, 1H), 7.03 (d, *J* = 7.7 Hz, 1H), 6.67 (dt, *J* = 15.4, 5.9 Hz, 1H), 6.22 (dt, *J* = 15.4, 1.7 Hz, 1H), 3.65 (s, 2H, C*H*(16)), 3.02 (dd, *J* = 6.0, 1.6 Hz, 2H, C*H*(26)), 2.72 – 2.57 (m, 4H, C*H*(11+12)), 2.16 (s, 6H, C*H*(27)), 2.15 (d, *J* = 13.9 Hz, 1H), 1.77 (d, *J* = 9.8 Hz, 3H, C*H*(14)), 1.60 (s, 3H, C*H*(13)), 1.56 – 1.32 (m, 2H, C*H*(13+14)); ^{13}C NMR (101 MHz, DMSO) δ 163.1, 143.0 (*C*(5)), 141.4 (*C*(10)), 141.3, 141.1, 139.1, 131.1 (*C*(8)), 130.5 (*C*(3)), 128.4 (*C*(21)), 126.8, 126.0 (*C*(24)), 123.4 (*C*(22)), 120.3 (*C*(9)), 119.2 (*C*(18)), 117.9 (*C*(4)), 117.5 (*C*(20)), 62.9 (*C*(15)), 59.7 (*C*(26)), 55.4 (*C*(16)), 52.4 (*C*(12)), 45.1 (*C*(27)), 29.0 (*C*(14)), 23.8 (*C*(13)), 21.3 (*C*(11)); LRMS (ESI^+) m/z 541.7 ($M+H^+$); HRMS (ESI^-): calcd for $C_{30}H_{37}N_8O_2^+$ $[M+H]^+$ 541.3034, found 541.3042.

2-chloro-N-(3-((cyclopentyl(2-(1-(4-oxo-3,4-dihydropyrido[3,4-d]pyrimidin-8-yl)-1H-pyrazol-4-yl)ethyl)amino)methyl)phenyl)acetamide, (**82**)



To a solution of 8-(4-(2-((3-aminobenzyl)(cyclopentyl)amino)ethyl)-1H-pyrazol-1-yl)pyrido[3,4-d]pyrimidin-4(3H)-one, HCl (74 mg, 0.172 mmol) and PS-DIPEA (300 mg) in NMP (1.5 mL) at 0 °C was added 2-chloroacetyl chloride (15 µL, 0.190 mmol). The reaction mixture was warmed to room temperature and stirred for 16 h. The reaction mixture was filtered, washed with MeOH (50 mL) and concentrated *in vacuo* to give a brown oil. The crude product was adsorbed on silica and purified by flash chromatography on a 11g KP-NH column eluting with 0-30% MeOH in CH_2Cl_2 to give an off-white solid. The solid was purified by prep HPLC to give **82** (6 mg, 7%) as an off-white amorphous solid. ν_{max}/cm^{-1} 1694 (C=O), 1552 (C=C), 1162, 1015 (C-N), 966 (C=C-H), 826, 798 (C-H) 656 (C-Cl); ^{1}H NMR (400 MHz, DMSO-d_6) δ 8.50 (d, *J* = 4.9 Hz, 1H, C*H*(5)), 8.33 (d, *J* = 7.2 Hz, 1H, C*H*(8)), 8.24 (s, 1H, C*H*(1)), 7.98 (d, *J* = 5.1 Hz, 1H, C*H*(4)), 7.67 – 7.53 (m, 2H, C*H*(10+18)), 7.52 – 7.43 (m, 1H, C*H*(20)), 7.24 (t, *J* = 7.4 Hz, 1H, C*H*(21)), 7.07 (d, *J* = 7.5 Hz, 1H, C*H*(22)), 4.20 (s, 2H, C*H*(24)), 3.65 (d, *J* = 3.8 Hz, 2H, C*H*(16)), 3.14 (dd, *J* = 13.6, 5.9 Hz, 1H, C*H*(15)), 2.76 – 2.56 (m, 4H, C*H*(11+12)), 1.90 (s, 3H), 1.81 – 1.73 (m, 2H, C*H*(14)), 1.60 (t, *J* = 7.3 Hz, 2H, C*H*(13)), 1.44 (ddt, *J* = 21.6, 16.8, 7.2 Hz, 4H, C*H*(13+14)); ^{13}C NMR (101 MHz, DMSO) δ 163.0 (*C*(23)), 160.3 (*C*(2)), 148.1 (*C*(1)), 147.6 (*C*(6)), 144.1 (*C*(5)), 141.9 (*C*(10)), 141.5 (*C*(19)), 138.9 (*C*(17)), 136.0 (*C*(7)), 131.9 (*C*(24)), 131.0 (*C*(8)), 130.6 (*C*(3)), 128.5 (*C*(21)), 126.7 (*C*(25)), 124.0 (*C*(22)), 120.5 (*C*(9)), 119.4 (*C*(18)), 117.8 (*C*(4)), 117.5 (*C*(20)), 62.9 (*C*(15)), 55.5 (*C*(16)), 52.5 (*C*(12)), 43.6 (C(24)), 29.1 (*C*(14)), 23.8 (*C*(13)), 21.1 (*C*(11)); LRMS (ESI$^+$) *m/z* 506.3 (M+H$^+$); HRMS (ESI$^+$): calcd for $C_{26}H_{29}ClN_7O_2^+$ [M+H]$^+$ 506.2066, found 506.2033.

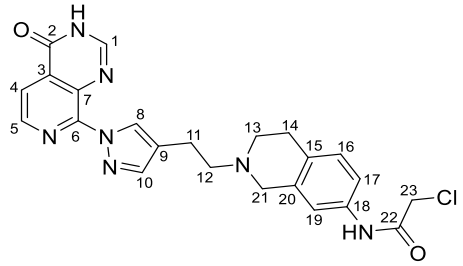
N-(2-(2-(1-(4-oxo-3,4-dihydropyrido[3,4-d]pyrimidin-8-yl)-1H-pyrazol-4-yl)ethyl)-1,2,3,4-tetrahydroisoquinolin-7-yl)acrylamide, (**83**)



A solution of **98** (42 mg, 0.108 mmol) in THF (1.5 mL) was added 6M hydrochloric acid (1.507 mL, 9.04 mmol). The reaction mixture was heated to 50 °C for 3 h. The reaction mixture was concentrated *in vacuo*. The crude product was loaded onto an SCX-2 column and washed with MeOH. The product was eluted by washing with 3.5N NH_3 in MeOH and the filtrate was concentrated *in vacuo* to give 8-(4-(2-(7-amino-3,4-dihydroisoquinolin-2(1H)-yl)ethyl)-1H-pyrazol-1-yl)pyrido[3,4-d]pyrimidin-4(3H)-one (quant.). A solution of 8-(4-(2-(7-amino-3,4-dihydroisoquinolin-2(1H)-yl)ethyl)-1H-pyrazol-1-yl)pyrido[3,4-d]pyrimidin-4(3H)-one (0.052 g, 0.134 mmol) and PS-DIPEA (150 mg) was cooled to 0 °C and acryloyl chloride (13 µl, 0.161 mmol) was added. The reaction mixture was warmed to room temperature and stirred for 14 h. The reaction mixture was filtered, washed with MeOH (50 mL) and concentrated *in vacuo*. The crude solid was dissolved in MeOH:DMSO (1 mL) was added and purified by prep HPLC to give **83** (7 mg, 12%) as a white solid. ν_{max}/cm^{-1} 3273 (N-H), 1636 (C=O), 1551, 1507, 1458 (C=C), 1215, 1015 (C-N), 967 (C=C-H); ^{1}H NMR (400 MHz, DMSO-d_6) δ 10.02 (s, 1H, N*H*), 8.52 (d, *J* = 5.1 Hz, 1H, C*H*(5)), 8.44 (s, 1H, C*H*(8)), 8.26 (s, 1H, C*H*(1)), 7.96 (d, *J* = 5.1 Hz, 1H, C*H*(4)), 7.73 (s, 1H, C*H*(10)), 7.42 (d, *J* = 2.2 Hz, 1H, C*H*(19)), 7.37 (dd, *J* = 8.2, 2.2 Hz, 1H, C*H*(17)), 7.04 (d, *J* = 8.3 Hz, 1H, C*H*(16)), 6.41 (dd, *J* = 17.0, 10.1 Hz, 1H, C*H*(23)), 6.23 (dd, *J* = 17.0, 2.1 Hz, 1H, C*H*(24)), 5.72 (dd, *J* = 10.1, 2.1 Hz, 1H, C*H*(24)), 3.64 – 3.59 (m, 2H, C*H*(21)), 2.84 – 2.68 (m, 8H, C*H*(11, 12, 13, 14)), 1.90 (s, 3H, CH_3(acetate)); ^{13}C NMR (101 MHz, DMSO) δ 163.0 (*C*(22)), 160.2 (*C*(2)), 148.0 (*C*(1)), 147.7 (*C*(6)), 143.9 (*C*(5)), 141.7 (*C*(10)), 136.5 (*C*(18)), 135.9 (*C*(7)), 135.2 (*C*(20)), 132.0 (*C*(23)), 131.1 (*C*(8)), 130.7 (*C*(3)), 129.6 (*C*(15)), 128.7 (*C*(16)), 126.6 (*C*(24)), 120.5 (*C*(9)), 117.9 (*C*(4)), 117.5, 117.2 (*C*(17,

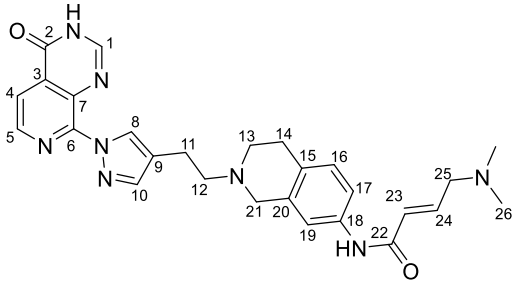
19), 58.4 (*C*(12)), 55.5 (*C*(21)), 50.5 (*C*(13)), 28.3 (*C*(14)), 21.6 (*C*(11)); LRMS (ESI$^+$) *m/z* 442.5 (M+H$^+$); HRMS (ESI$^+$): calcd for $C_{24}H_{24}N_7O_2^+$ [M+H]$^+$ 442.1986, found 442.1982.

2-chloro-N-(2-(2-(1-(4-oxo-3,4-dihydropyrido[3,4-d]pyrimidin-8-yl)-1H-pyrazol-4-yl)ethyl)-1,2,3,4-tetrahydroisoquinolin-7-yl)acetamide, (**84**)



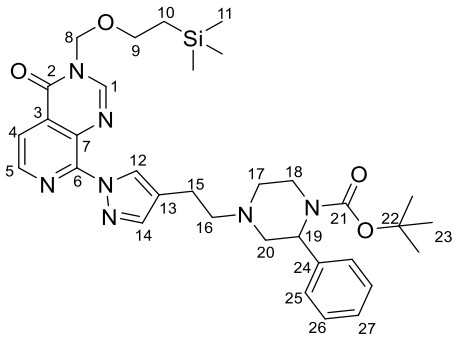
To a solution of 8-(4-(2-(7-amino-3,4-dihydroisoquinolin-2(1H)-yl)ethyl)-1H-pyrazol-1-yl)pyrido[3,4-d]pyrimidin-4(3H)-one, 2HCl (0.091 g, 0.235 mmol) and PS-DIPEA (300 mg) in NMP (2 mL) was added 2-chloroacetyl chloride (17 µL, 0.214 mmol) at 0 °C. The reaction mixture was warmed slowly to room temperature and stirred for 16 h. The reaction mixture was filtered, washed with MeOH (50 mL) and concentrated *in vacuo* to give a brown oil. The crude product was adsorbed on silica and purified by flash chromatography eluting with 0-30% MeOH in CH_2Cl_2 to give an off-white solid. The solid was purified by prep HPLC to give **84** (0.013 g, 13%). Mp 225-227 °C; ν_{max}/cm^{-1} 1677 (C=O), 1605, 1548, 1507 (C=C), 1212, 1159, 1060 (C-N), 825, 801 (C-H); ^{1}H NMR (400 MHz, DMSO-d_6) δ 10.19 (s, 1H, N*H*), 8.54 (d, *J* = 5.1 Hz, 1H, C*H*(5)), 8.43 (s, 1H, C*H*(8)), 8.25 (s, 1H, C*H*(1)), 7.97 (d, *J* = 5.1 Hz, 1H, C*H*(4)), 7.73 (s, 1H, C*H*(10)), 7.37 – 7.21 (m, 2H, C*H*(17,19)), 7.06 (d, *J* = 8.2 Hz, 1H, C*H*(16)), 4.21 (s, 2H, C*H*(23)), 3.70 - 3.20 (m, 2H, C*H*(21)), 2.84 – 2.67 (m, 8H, C*H*(11,12,13,14)), 1.90 (s, 3H, CH_3(acetate salt)); ^{13}C NMR (101 MHz, DMSO) δ 164.5 (*C*(22)), 160.2 (*C*(2)), 148.0 (*C*(1)), 147.7 (*C*(6)), 144.1 (*C*(5)), 141.8 (*C*(10)), 136.5 (*C*(18)), 136.0 (*C*(7)), 135.2 (*C*(20)), 132.0 (*C*(23)), 131.1 (*C*(8)), 130.7 (*C*(3)), 129.6 (*C*(15)), 128.9 (*C*(16)), 126.6 (*C*(24)), 120.5 (*C*(9)), 118.0 (*C*(4)), 117.3 (*C*(16)), 117.2 (*C*(17, 19), 58.4 (*C*(12)), 55.5 (*C*(21)), 50.3 (*C*(13)), 43.6 (C(23)), 26.4 (*C*(14)), 21.6 (*C*(11)); LRMS (ESI$^+$) *m/z* 464.2 (M+H$^+$); HRMS (ESI$^+$): calcd for $C_{23}H_{23}ClN_7O_2^+$ [M+H]$^+$ 464.1596, found 464.1567.

(*E*)-4-(dimethylamino)-N-(2-(2-(1-(4-oxo-3,4-dihydropyrido[3,4-d]pyrimidin-8-yl)-1H-pyrazol-4-yl)ethyl)-1,2,3,4-tetrahydroisoquinolin-7-yl)but-2-enamide, (**85**)



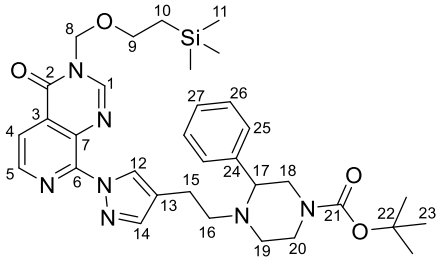
To a solution of 8-(4-(2-(7-amino-3,4-dihydroisoquinolin-2(1H)-yl)ethyl)-1H-pyrazol-1-yl)pyrido[3,4-d]pyrimidin-4(3H)-one, 2HCl, (*E*)-4-(dimethylamino)but-2-enoic acid, HCl (0.044 g, 0.266 mmol) and PS-DIPEA (300 mg) in DMA (2 mL) was added T3P (0.235 mL, 0.399 mmol) at 0 °C. The reaction mixture was warmed to room temperature and stirred for 16 h. The reaction mixture was filtered, washed with MeOH (50 mL) and concentrated *in vacuo* to give a brown oil. The crude product was adsorbed on silica and purified by flash chromatography eluting with 0-30% MeOH in CH_2Cl_2 to give a brown oil. The compound was dissolved in DMSO and purified by prep-HPLC to give **85** (5.5 mg, 4%) as a yellow amorphous solid. ν_{max}/cm^{-1} 3057 (N-H), 1685 (C=O), 1604, 1551, 1506 (C=C), 1217, 1160, 1061 (C-N); ^{1}H NMR (400 MHz, DMSO-d_6) δ 9.94 (s, 1H, N*H*), 8.49 (d, *J* = 3.9 Hz, 1H, C*H*(8)), 8.46 (d, *J* = 5.1 Hz, 1H, C*H*(5)), 8.25 (s, 1H, C*H*(1)), 7.91 (d, *J* = 5.1 Hz, 1H, C*H*(4)), 7.70 (d, *J* = 3.0 Hz, 1H, C*H*(9)), 7.43 – 7.32 (m, 2H, C*H*(17,19)), 7.03 (d, *J* = 8.3 Hz, 1H, C*H*(16)), 6.77 – 6.64 (m, 1H, C*H*(23)), 6.38 – 6.21 (m, 1H, C*H*(24)), 3.61 (s, 2H, C*H*(21)), 3.04 (d, *J* = 5.4 Hz, 2H, C*H*(25)), 2.83 – 2.62 (m, 8H, C*H*(11,12,13,14), 2.16 (s, acetate), 1.89 (s, 6H, C*H*(26)); ^{13}C NMR (101 MHz, $CDCl_3$) δ 150.1 (*C*(1)), 146.2 (*C*(6)), 142.9 (*C*(5)), 141.5 (*C*(10)), 135.1 (*C*(7)), 131.2 (C(8)), 130.5 (*C*(3)), 128.7 (*C*(16)), 121.4, 120.4 (*C*(9)), 118.0 (*C*(4)), 117.3 (*C*(17,19)), 112.8, 111.3, 59.8 (*C*(25)), 58.7 (*C*(12)), 57.2 (*C*(13)), 55.7 (*C*(21)), 51.1 (*C*(13)), 45.2 (*C*(26)), 27.9 (*C*(14)), 21.6 (*C*(11)), 21.3 (*C*(26)); LRMS (ESI^+) *m/z* 499.6 ($M+H^+$); HRMS (ESI^+): calcd for $C_{27}H_{31}N_8O_2^+$ $[M+H]^+$ 499.2565, found 499.2535.

tert-butyl 4-(2-(1-(4-oxo-3-((2-(trimethylsilyl)ethoxy)methyl)-3,4-dihydropyrido[3,4-d]pyrimidin-8-yl)-1H-pyrazol-4-yl)ethyl)-2-phenylpiperazine-1-carboxylate, (**86**)



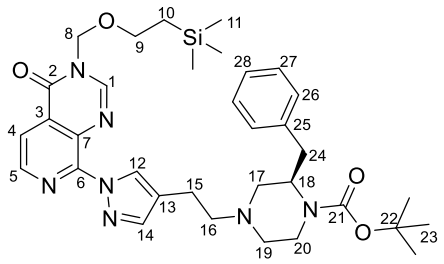
To a solution of **50** (0.546 g, 1.17 mmol), potassium iodide (0.779 g, 4.69 mmol) and potassium carbonate (3.24 g, 23.5 mmol) in AcN (12 mL) was added *tert*-butyl 2-phenylpiperazine-1-carboxylate (0.308 g, 1.17 mmol). The reaction mixture was stirred at 75 °C for 16 h. $NaHCO_3$ (60 mL) was added and back-extracted with EtOAc (2 x 75 mL). The combined organic extracts were washed with brine (75 mL). The organic layer was dried over Na_2SO_4, filtered and concentrated *in vacuo*. The crude product was adsorbed on silica and purified by flash chromatography eluting with 3% MeOH in CH_2Cl_2 to give **86** (0.530 g, 72%) as a yellow oil. ν_{max}/cm^{-1} 3421 (N-H), 1689, 1608 (C=O), 1249 (C-O), 1167, 1149, 1079 (C-N); 860, 836 (C-H); ^{1}H NMR (400 MHz, $CDCl_3$) δ 8.62 (d, *J* = 5.1 Hz, 1H, C*H*(5)), 8.50 (s, 1H, C*H*(12)), 8.21 (s, 1H, C*H*(1)), 8.06 (d, *J* = 5.1 Hz, 1H, C*H*(4)), 7.83 – 7.59 (s, 1H, C*H*(14)), 7.43 (dd, *J* = 8.0, 1.4 Hz, 2H, C*H*(25)), 7.22 (m, 2H, C*H*(26)), 7.16 – 7.03 (m, 1H, C*H*(27)), 5.56 – 5.39 (s, 2H, C*H*(8)), 3.94 (d, *J* = 13.3 Hz, 1H, C*H*(18)), 3.77 – 3.60 (m, 2H, C*H*(9)), 3.43 (dt, *J* = 11.8, 1.8 Hz, 1H, C*H*(20)), 3.05 (m, 1H, C*H*(18)), 2.93 – 2.71 (m, 3H, C*H*(15+17)), 2.71 – 2.56 (m, 2H, C*H*(16)), 2.48 (dd, *J* = 11.7, 4.3 Hz, 1H, C*H*(20)), 2.29 – 2.12 (m, 1H, *C*(17)), 1.47 (s, 9H, C*H*(23)) 1.01 – 0.92 (m, 2H, C*H*(10)), 0.00 (s, 9H, C*H*(11)); ^{13}C NMR (101 MHz, $CDCl_3$) δ 159.6 (*C*(2)), 155.1 (*C*(21)), 148.2 (*C*(6)), 147.0 (*C*(1)), 145.6 (*C*(5)), 143.2 (*C*(14)), 140.6 (*C*(24)), 134.6 (*C*(7)), 131.1 (*C*(12)), 130.3 (*C*(3)), 128.3 (*C*(26)), 127.5 (*C*(25)), 126.8 (*C*(27)), 121.6 (*C*(13)), 118.0 (*C*(4)), 80.1 (*C*(22)), 75.1 (*C*(8)), 68.1 (*C*(9)), 59.2 (*C*(16)), 55.5 (*C*(20)), 53.5, 53.4 (*C*(17, 19), 40.1 (*C*(18)), 28.6 (*C*(23)), 22.0 (*C*(15)), 18.1 (*C*(10)), -1.3 (*C*(11)); LRMS (ESI$^+$) *m/z* 402.5 (M-SEM-BOC+H$^+$); HRMS (ESI$^+$): calcd for $C_{22}H_{24}N_7O^+$ [M-SEM-BOC+H]$^+$ 402.2037, found 402.2036.

tert-butyl 4-(2-(1-(4-oxo-3-((2-(trimethylsilyl)ethoxy)methyl)-3,4-dihydropyrido[3,4-d]pyrimidin-8-yl)-1H-pyrazol-4-yl)ethyl)-3-phenylpiperazine-1-carboxylate, (**87**)



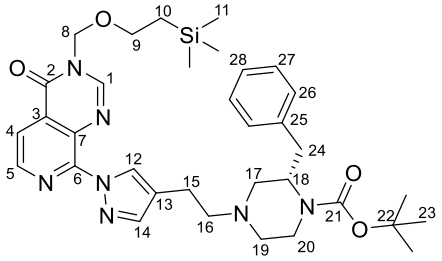
A solution of **50** (0.602 g, 1.293 mmol), *tert*-butyl 3-phenylpiperazine-1-carboxylate (0.339 g, 1.293 mmol), potassium carbonate (3.57 g, 25.9 mmol) and potassium iodide (0.859 g, 5.17 mmol) in AcN (13 mL) was heated to 75 °C for 16 h. $NaHCO_3$ (60 mL) was added and back-extracted with EtOAc (2 x 75 mL). The combined organic extracts were washed with brine (75 mL). The organic layer was dried over Na_2SO_4, filtered and concentrated *in vacuo*. The crude product was adsorbed on silica and purified by flash chromatography eluting with 3% MeOH in CH_2Cl_2 to give **87** (0.215 g, 26%) as a yellow oil. ^{1}H NMR (400 MHz, $CDCl_3$) δ 8.59 (d, *J* = 5.1 Hz, 1H, C*H*(5)), 8.38 (s, 1H, C*H*(12)), 8.26 (s, 1H, C*H*(1)), 8.03 (d, *J* = 5.1 Hz, 1H, C*H*(4)), 7.59 (s, 1H, C*H*(14)), 7.36 – 7.27 (m, 4H, C*H*(25,26)), 7.25 – 7.18 (m, 1H, C*H*(27)), 5.44 (s, 2H, C*H*(8)), 3.72 – 3.61 (m, 2H, C*H*(9)), 3.24 – 3.11 (m, 2H, C*H*(17+19)), 3.05 (t, *J* = 12.5 Hz, 1H, C*H*(18)), 2.88 – 2.58 (m, 4H, C*H*(15,16,18)), 2.35 – 2.19 (m, 2H, C*H*(16+19), 1.75 (s, 1H), 1.45 (s, 9H, C*H*(23)), 1.01 – 0.92 (m, 2H, C*H*(10)), -0.01 (s, 9H, C*H*(11)); ^{13}C NMR (101 MHz, $CDCl_3$) δ 159.6 (*C*(2)), 154.6 (*C*(21)), 148.3 (*C*(6)), 147.0 (*C*(1)), 145.6 (*C*(5)), 143.4 (*C*(14)), 140.7 (*C*(24)), 134.6 (*C*(7)), 130.7 (*C*(12)), 130.3 (*C*(3)), 128.6 (*C*(25)), 128.1 (*C*(26)), 127.8 (*C*(27)), 121.5 (*C*(13)), 118.0 (*C*(4)), 79.9 (*C*(22)), 75.1 (*C*(8)), 68.1 (*C*(9)), 67.1 (*C*(17)), 55.0 (*C*(16,18)), 51.5 (*C*(19)), 46.2 (*C*(20)), 28.6 (*C*(23)), 21.4 (*C*(15)) 18.1 (*C*(10)), -1.3 (*C*(11)); LRMS (ESI^+) *m/z* 632.3 ($M+H^+$); HRMS (ESI^+): calcd for $C_{33}H_{46}N_7O_4Si^+$ $[M+H]^+$ 632.3375, found 632.3353.

tert-butyl-(*R*)-2-benzyl-4-(2-(1-(4-oxo-3-((2-(trimethylsilyl)ethoxy)methyl)-3,4-dihydropyrido[3,4-d]pyrimidin-8-yl)-1H-pyrazol-4-yl)ethyl)piperazine-1-carboxylate, (**88**)



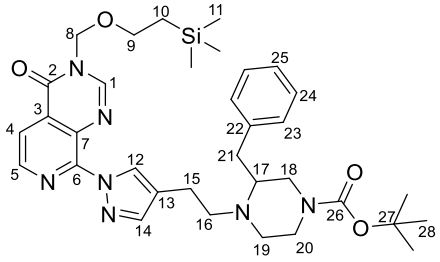
A solution of **50** (0.546 g, 1.17 mmol), *tert*-butyl (*R*)-2-benzylpiperazine-1-carboxylate (0.324 g, 1.17 mmol), potassium carbonate (3.24 g, 23.5 mmol) and potassium iodide (0.779 g, 4.69 mmol) in AcN (12 mL) was heated to 75 °C for 16 h. The reaction mixture was quenched with $NaHCO_3$ (75 mL) and extracted with EtOAc (3 x 75 mL). The combined organic extracts were washed with brine (50 mL), dried over Na_2SO_4, filtered and concentrated *in vacuo*. The crude product was adsorbed on silica and purified by flash chromatography eluting with 0-10% MeOH in CH_2Cl_2 to give **88** (0.500 g, 66%) as a yellow oil. ν_{max}/cm^{-1} 1688, 1608 (C=O), 1553, 1496, 1464 (C=C), 1249 (C-O), 1168, 1111, 1077 (C-N), 729, 698 (C-H); ^1H NMR (400 MHz, $CDCl_3$) δ 8.65 (s, 1H, C*H*(12)), 8.62 (d, *J* = 5.1 Hz, 1H, C*H*(5)), 8.24 (s, 1H, C*H*(1)), 8.05 (d, *J* = 5.1 Hz, 1H, C*H*(4)), 7.81 (s, 1H, C*H*(14)), 7.28 - 7.24 (m, 2H, C*H*(27)), 7.23 – 7.15 (m, 3H, C*H*(26+28)), 5.41 (d, *J* = 1.3 Hz, 2H, C*H*(8)), 4.10 (m, 2H), 3.72 – 3.62 (m, 2H, C*H*(9)), 3.23 (td, *J* = 12.7, 3.3 Hz, 1H, C*H*(20)), 3.08 (d, *J* = 9.9 Hz, 1H, C*H*(24)), 2.97 – 2.88 (m, 2H, C*H*(19+24), 2.79 – 2.71 (m, 3H, C*H*(15+17)), 2.62 (d, *J* = 23.6 Hz, 2H, C*H*(16)), 2.19 – 1.99 (m, 2H, C*H*(17+19), 1.39 (s, 9H, C*H*(23)), 1.01 – 0.89 (m, 2H, C*H*(10)), -0.00 (s, 9H, C*H*(23)); ^{13}C NMR (101 MHz, $CDCl_3$) δ 159.6 (*C*(2)), 154.8 (*C*(21)), 148.3 (*C*(6)), 147.1 (*C*(1)), 145.6 (*C*(5)), 143.3 (*C*(14)), 139.5 (*C*(25)), 134.6 (*C*(7)), 131.0 (*C*(12)), 130.4 (*C*(3)), 129.5 (*C*(26)), 128.5 (*C*(27)), 126.3 (*C*(28)), 121.9 (*C*(13)), 118.0 (*C*(4)), 79.7 (*C*(22)), 75.0 (*C*(8)), 68.1 (*C*(9)), 59.1 (*C*(16)), 54.3 (*C*(17)), 53.4 (*C*(19)), 39.4 (*C*(20)), 36.3 (*C*(24)), 28.4 (*C*(23)), 22.1 (*C*(15)), 18.1 (*C*(10)), -1.3 (*C*(11)); LRMS (ESI^+) *m*/*z* 646.4 ($M+H^+$).

tert-butyl (S)-2-benzyl-4-(2-(1-(4-oxo-3-((2-(trimethylsilyl)ethoxy)methyl)-3,4-dihydropyrido[3,4-d]pyrimidin-8-yl)-1H-pyrazol-4-yl)ethyl)piperazine-1-carboxylate, (**89**)



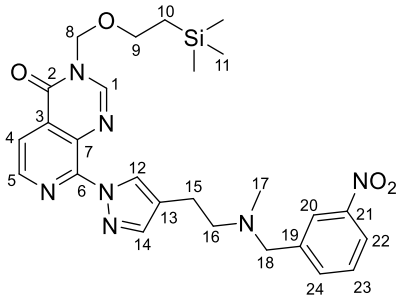
A solution of **50** (1 g, 1.611 mmol), *tert*-butyl (*S*)-2-benzylpiperazine-1-carboxylate (0.445 g, 1.611 mmol), potassium iodide (1.070 g, 6.44 mmol) and potassium carbonate (4.45 g, 32.2 mmol) in AcN (15 mL) was heated to 75 °C for 16 h. The reaction mixture was quenched with $NaHCO_3$ (75 mL) and extracted with EtOAc (3 x 75 mL). The combined organic extracts were washed with brine (50 mL), dried over Na_2SO_4, filtered and concentrated *in vacuo*. The crude product was adsorbed on silica and washed with purified by flash chromatography eluting with 0-5% MeOH in CH_2Cl_2 to give **89** (0.533 g, 51%) as a yellow oil; ^{1}H NMR (400 MHz, $CDCl_3$) δ 8.64 (s, 1H, C*H*(12)), 8.61 (d, *J* = 5.1 Hz, 1H, C*H*(5)), 8.23 (s, 1H, C*H*(1)), 8.04 (d, *J* = 5.1 Hz, 1H, C*H*(4)), 7.80 (s, 1H, C*H*(14)), 7.25 – 7.22 (m, 2H, C*H*(27)), 7.17 (dd, *J* = 7.5, 5.1 Hz, 3H, C*H*(26,28)), 5.40 (s, 2H, C*H*(8)), 4.23 (m, 1H, C*H*(18)), 3.95 (s, 1H), 3.70 – 3.61 (m, 2H, *C*(9)), 3.22 (td, *J* = 12.7, 3.4 Hz, 1H, C*H*(20)), 3.08 (m, 1H, C*H*(24)), 2.97 – 2.84 (m, 2H, C*H*(19+24)), 2.79 – 2.69 (m, 3H, C*H*(15+17)), 2.70 – 2.47 (m, 2H, C*H*(16)), 2.14 – 1.98 (m, 2H, C*H*(17+19)), 1.38 (s, 9H, C*H*(23)), 0.99 – 0.90 (m, 2H, C*H*(10)), -0.01 (s, 9H, C*H*(11)); ^{13}C NMR (101 MHz, $CDCl_3$) δ 159.6 (*C*(2)), 154.8 (*C*(21)), 148.2 (*C*(6)), 147.1 (*C*(1)), 145.6 (*C*(5)), 143.3 (*C*(14)), 139.5 (*C*(25)), 134.6 (*C*(7)), 131.0 (*C*(12)), 130.4 (*C*(3)), 129.5 (*C*(26)), 128.5 (*C*(27)), 126.3 (*C*(28)), 121.9 (*C*(13)), 118.0 (*C*(4)), 79.7 (*C*(22)), 75.0 (*C*(8)), 68.0 (*C*(9)), 59.0 (*C*(16)), 54.3 (*C*(17)), 53.4 (*C*(19)), 39.5 (*C*(20)), 36.3 (*C*(24)), 22.1 (*C*(15)), 18.1 (*C*(10)), -1.3 (*C*(11)); LRMS (ESI^+) *m/z* 646.4 ($M+H^+$).

tert-butyl 3-benzyl-4-(2-(1-(4-oxo-3-((2-(trimethylsilyl)ethoxy)methyl)-3,4-dihydropyrido[3,4-d] pyrimidin-8-yl)-1H-pyrazol-4-yl)ethyl)piperazine-1-carboxylate, (**90**)



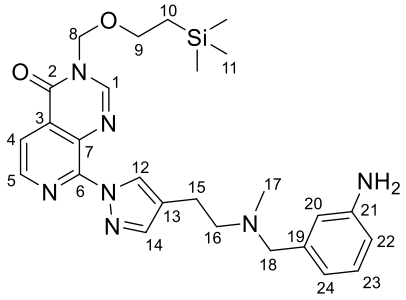
A solution of **50** (0.601 g, 1.29 mmol), *tert*-butyl 3-benzylpiperazine-1-carboxylate (0.357 g, 1.29 mmol), potassium carbonate (3.57 g, 25.8 mmol) and potassium iodide (0.857 g, 5.16 mmol) in AcN (13 mL) was heated to 75 °C for 16 h. $NaHCO_3$ (60 mL) was added and back extracted with EtOAc (2 x 75 mL). The combined organic extracts were washed with brine (75 mL). The organic layer was dried over Na_2SO_4, filtered and concentrated *in vacuo*. The crude product was adsorbed on silica and purified by flash chromatography eluting with 5% MeOH in CH_2Cl_2 to give **90** (0.192 g, 23%) as a yellow oil. ν_{max}/cm^{-1} 1689 (C=O), 1608, 1553, 1453 (C=C), 1169, 1121, 1079 (C-N), 883 (C=C-H), 745, 701 (C-H); ^{1}H NMR (400 MHz, $CDCl_3$) δ 8.61 (d, *J* = 5.1 Hz, 1H, C*H*(5)), 8.57 (s, 1H, C*H*(12)), 8.28 (s, 1H, C*H*(1)), 8.05 (d, *J* = 5.1 Hz, 1H, C*H*(4)), 7.77 (s, 1H, C*H*(14)), 7.35 – 7.27 (m, 2H, C*H*(24)), 7.19 (m, 3H, C*H*(23,25)), 5.45 (s, 2H, C*H*(8)), 3.73 – 3.63 (m, 3H, C*H*(9,20)), 3.44 – 3.11 (s, 3H, C*H*(18, 20)), 2.99 – 2.77 (m, 7H, C*H*(15,16,17,19,21)), 2.70 – 2.54 (m, 2H, C*H*(19, 21)), 1.44 (s, 9H, C*H*(11)), 1.01 – 0.92 (m, 2H, C*H*(10)), -0.01 (s, 9H, C*H*(28)); ^{13}C NMR (101 MHz, $CDCl_3$) δ 159.6 (*C*(2)), 155.1 (*C*(26)), 148.2 (*C*(6)), 147.1 (*C*(1)), 145.6 (*C*(5)), 143.3 (*C*(14)), 139.4 (*C*(22)), 134.7 (*C*(7)), 130.9 (*C*(12)), 130.4 (*C*(3)), 129.5 (*C*(23)), 128.6 (*C*(24)), 126.3 (*C*(25)), 121.5 (*C*(13)), 118.1 (*C*(4)), 79.9 (*C*(27)), 75.1 1 (*C*(8)), 68.1 (*C*(9)), 60.5 (*C*(17)), 55.1 (*C*(16)), 47.2 (C(19)), 46.2 (*C*(18)), 43.1 (*C*(20)), 31.0 (*C*(21)), 28.5 (*C*(28)), 22.1 (*C*(15)), 18.1 (*C*(10)), -1.3 (C(11)); LRMS (ESI$^+$) *m/z* 646.3 (M+H$^+$); HRMS (ESI$^+$): calcd for $C_{34}H_{48}N_7O_4Si^+$ [M+H]$^+$ 646.3532, found 646.3527.

8-(4-(2-(methyl(3-nitrobenzyl)amino)ethyl)-1H-pyrazol-1-yl)-3-((2-(trimethylsilyl)ethoxy)methyl) pyrido[3,4-d]pyrimidin-4(3H)-one, (**91**)



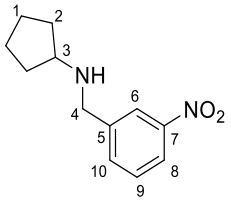
To a solution of **50** (1 g, 2.148 mmol), potassium iodide (1.426 g, 8.59 mmol) and potassium carbonate (5.94 g, 43.0 mmol) in AcN (21 mL) was added *N*-methyl-1-(3-nitrophenyl)methanamine (0.357 g, 2.148 mmol). The reaction mixture was stirred at 75 °C for 16 h. $NaHCO_3$ (60 mL) was added and back-extracted with EtOAc (2 x 75 mL). The combined organic extracts were washed with brine (75 mL). The organic layer was dried over Na_2SO_4, filtered and concentrated *in vacuo*. The crude product was adsorbed on silica and purified by flash chromatography eluting with 10% MeOH in CH_2Cl_2 to give **91** (0.985 g, 86%) as a yellow oil. ν_{max}/cm^{-1} 3311 (N-H), 1645 (C=O), 1538, 1363 (N-O), 1166, 1127, 1108 (C-N), 1570, 1464, 1441 (C=C), 787 (C-H); ^{1}H NMR (400 MHz, $CDCl_3$) δ 8.63 (d, *J* = 5.1 Hz, 1H, C*H*(5)), 8.56 (s, 1H, C*H*(12)), 8.29 (s, 1H, C*H*(1)), 8.20 (s, 1H, C*H*(20)), 8.08 (m, 2H, C*H*(4+22), 7.67 (d, *J* = 7.6 Hz, 1H, C*H*(24)), 7.46 (t, *J* = 7.9 Hz, 1H, C*H*(23)), 5.47 (s, 2H, C*H*(8)), 3.74 – 3.63 (m, 4H, C*H*(9+18)), 2.81 (t, *J* = 7.3 Hz, 2H, C*H*(15)), 2.76 – 2.68 (m, 2H, C*H*(16)), 2.31 (s, 3H, C*H*(17)), 1.02 – 0.93 (m, 2H, C*H*(10)), 0.00 (s, 9H, C*H*(11)); ^{13}C NMR (101 MHz, $CDCl_3$) δ 159.6 (C(2)), 147.1 (*C*(1)), 145.6 (*C*(5)), 143.3 (*C*(14)), 135.1 (*C*(24)), 134.7 (*C*(7)), 130.8 (*C*(12)), 129.3 (*C*(23)), 123.7 (*C*(20)), 122.3 (*C*(22)), 121.6 (*C*(13)), 118.1 (C(4)), 75.1 (*C*(8)), 68.1 (*C*(9)), 61.7 (*C*(18)), 58.3 (*C*(16)), 42.2 (*C*(17)), 22.7 (*C*(15)), 18.2 (*C*(10)), -1.3 (*C*(11)); LRMS (ESI^+) *m/z* 536.3 ($M+H^+$); HRMS (ESI^+): calcd for $C_{26}H_{34}N_7O_4Si^+$ $[M+H]^+$ 536.2436, found 536.2450.

8-(4-(2-((3-aminobenzyl)(methyl)amino)ethyl)-1H-pyrazol-1-yl)-3-((2-(trimethylsilyl)ethoxy) methyl)pyrido[3,4-d]pyrimidin-4(3H)-one, (**92**)



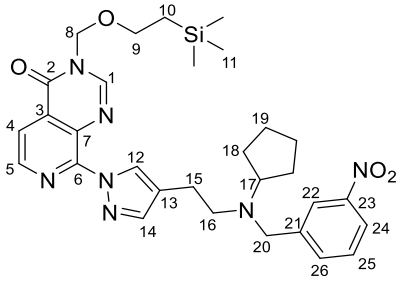
To a vial was added **91** (221 mg, 0.413 mmol) in 2-Propanol (1.5 ml) and Water (0.5 ml). Iron (138 mg, 2.475 mmol) and ammonium chloride (883 mg, 16.50 mmol) was added. The reaction mixture was heated to 50 °C for 4 h. The reaction mixture was filtered through Celite and washed with MeOH (50 mL). The filtrate was concentrated *in vacuo* to give a brown solid. The crude product was loaded onto an SCX-2 column and washed with MeOH. The product was eluted by washing with 3.5N NH_3 in MeOH and the solution was concentrated *in vacuo* to give **92** (179 mg, 86%) as a yellow amorphous solid. ν_{max}/cm^{-1} 3419 (N-H), 1693 (C=O), 1608, 1553, (C=C), 1198, 1024 (C-N), 802 (C-H); ^{1}H NMR (400 MHz, $CDCl_3$) δ 8.62 (d, *J* = 5.2 Hz, 1H, C*H*(5)), 8.55 (s, 1H, C*H*(12)), 8.29 (s, 1H, *C*(1)), 8.05 (d, *J* = 5.1 Hz, 1H, C*H*(4)), 7.76 (s, 1H, C*H*(14)), 7.07 (t, *J* = 7.7 Hz, 1H, C*H*(23)), 6.72 – 6.64 (m, 2H, C*H*(20+24)), 6.60 – 6.52 (m, 1H, C*H*(22)), 5.46 (s, 2H, C*H*(8)), 3.73 – 3.64 (m, 2H, C*H*(9)), 3.50 (s, 2H, C*H*(18)), 2.80 (t, *J* = 7.4 Hz, 2H, C*H*(15)), 2.69 (t, *J* = 7.4 Hz, 2H, C*H*(16)), 2.30 (s, 3H, C*H*(17)), 1.02 – 0.93 (m, 2H, C*H*(10)), 0.00 (s, 9H, C*H*(11))); ^{13}C NMR (101 MHz, $CDCl_3$) δ 159.7 (*C*(2)), 148.4 (*C*(6)), 147.1 (*C*(1)), 146.6 (*C*(21)), 145.6 (*C*(5)), 143.5 (*C*(14)), 140.2 (*C*(19)), 134.7 (*C*(7)), 130.9 (*C*(12)), 130.4 (*C*(3)), 129.2 (*C*(23)), 121.9 (*C*(13)), 119.4 (*C*(24)), 118.0 (*C*(4)), 115.7 (*C*(20)), 114.0 (*C*(22)), 75.1 (*C*(8)), 68.1 (*C*(9)), 62.4 (*C*(18)), 58.0 (*C*(16)), 42.2 (*C*(17)), 22.5 (*C*(15)), 18.2 (*C*(10)), -1.3 (*C*(11)).; LRMS (ESI^+) *m/z* 506.3 ($M+H^+$); HRMS (ESI^+): calcd for $C_{26}H_{36}N_7O_2Si^+$ $[M+H]^+$ 506.2694, found 506.2710.

N-(3-nitrobenzyl)cyclopentanamine, (**94**)



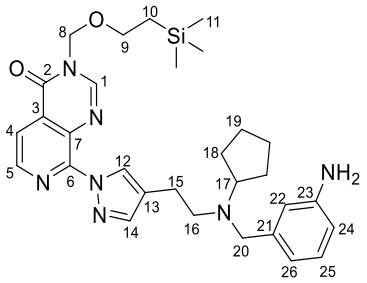
To a solution of 3-nitrobenzaldehyde (0.500 g, 3.31 mmol) in DCE (20 mL) was added cyclopentanamine (0.424 mL, 4.30 mmol). The solution was stirred at room temperature for 6 h and sodium triacetoxyborohydride (1.402 g, 6.62 mmol) was added and was stirred for 16 h. The reaction mixture was quenched with water (35 mL) and extracted with CH_2Cl_2 (3 x 30 mL). The combined extracts were dried over Na_2SO_4, filtered and concentrated *in vacuo* to give a yellow oil. The crude oil was loaded in MeOH on an SCX-2 column. The column was washed with MeOH and the product eluted with 3.5N NH_3 in MeOH to give **94** (0.718 g, 99%) as a yellow oil. ν_{max}/cm^{-1} 1523, 1345 (N-O), 1093 (C-N), 803 (C-H); ^{1}H NMR (400 MHz, $CDCl_3$) δ 8.21 (s, 1H, C*H*(6)), 8.10 (ddd, *J* = 8.2, 2.4, 1.1 Hz, 1H, C*H*(8)), 7.68 (dt, *J* = 7.6, 1.3 Hz, 1H, C*H*(10)), 7.48 (t, *J* = 7.9 Hz, 1H, C*H*(9)), 3.87 (s, 2H, C*H*(4)), 3.12 (p, *J* = 6.6 Hz, 1H, C*H*(3)), 1.92 – 1.78 (m, 2H, C*H*(2)), 1.79 – 1.62 (m, 2H, C*H*(1)), 1.62 – 1.50 (m, 2H, C*H*(1)), 1.45 – 1.31 (m, 2H, C*H*(2)); ^{13}C NMR (101 MHz, $CDCl_3$) δ 148.5 (*C*(7)), 143.3 (*C*(5)), 134.4 (*C*(10)), 129.3 (*C*(9)), 123.1 (*C*(6)), 122.1 (*C*(8)), 59.6 (*C*(3)), 52.0 (*C*(4)), 33.4 (*C*(2)), 24.2 (*C*(1)); LRMS (ESI$^+$) *m/z* 221.5 (M+H$^+$); HRMS (ESI$^+$): calcd for $C_{12}H_{17}N_2O_2^+$ [M+H]$^+$ 221.1285, found 221.1283.

8-(4-(2-(cyclopentyl(3-nitrobenzyl)amino)ethyl)-1H-pyrazol-1-yl)-3-((2-(trimethylsilyl)ethoxy) methyl)pyrido[3,4-d]pyrimidin-4(3H)-one, (**95**)



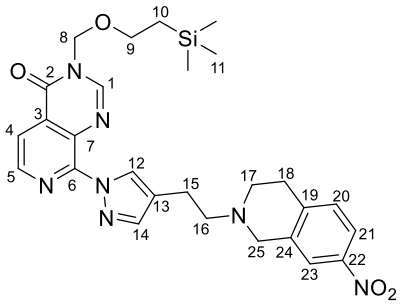
To a solution of **50** (1.592 g, 3.42 mmol), potassium iodide (2.270 g, 13.67 mmol) and potassium carbonate (9.45 g, 68.4 mmol) in AcN (34 mL) was added **94** (0.753 g, 3.42 mmol). The reaction mixture was stirred at 75 °C overnight for 44 h. $NaHCO_3$ (60 mL) was added and back-extracted with EtOAc (2 x 75 mL). The combined organic extracts were washed with brine (75 mL). The organic layer was dried over Na_2SO_4, filtered and concentrated *in vacuo*. The crude product was adsorbed on silica and purified by flash chromatography eluting with 10% MeOH in CH_2Cl_2 to give **95** (0.602 g, 30%) as a yellow oil. ν_{max}/cm^{-1} 3419 (N-H), 1693 (C=O), 1609, 1554 (C=C), 1365 (N-O), 1249 (C-O), 1171, 1080 (C-N); ^{1}H NMR (400 MHz, DMSO-*d*6) δ 8.59 (d, *J* = 5.1 Hz, 1H, C*H*(5)), 8.54 (s, 1H, C*H*(1)), 8.32 (s, 1H, C*H*(12)), 8.21 – 8.16 (m, 1H, C*H*(22)), 8.08 – 8.00 (m, 2H, C*H*(4+24)), 7.80 (d, *J* = 7.6 Hz, 1H, C*H*(26)), 7.64 (s, 1H, C*H*(14)), 7.58 (t, *J* = 7.9 Hz, 1H, C*H*(25)), 5.40 (s, 2H, C*H*(8)), 3.81 (s, 2H, C*H*(20)), 3.70 – 3.59 (m, 2H, C*H*(9)), 3.25 – 3.14 (m, 1H, C*H*(17)), 2.78 – 2.70 (m, 2H, C*H*(16)), 2.69 – 2.63 (m, 2H, C*H*(15)), 1.78 (d, *J* = 10.3 Hz, 2H, C*H*(18)), 1.51 – 1.40 (m, 6H, C*H*(18+19)), 0.94 – 0.85 (m, 2H, C*H*(10)), -0.04 (s, 9H, C*H*(11)); ^{13}C NMR (101 MHz, DMSO) δ 159.0 (*C*(2)), 149.1 (*C*(1)), 148.0 (*C*(6)), 147.8 (*C*(23)), 144.8 (*C*(5)), 141.8 (*C*(14)), 135.0 (*C*(26)), 134.8 (*C*(7)), 131.1 (*C*(12)), 129.9 (*C*(3)), 129.5 (*C*(25)), 122.5 (*C*(22)), 121.5 (*C*(24)), 120.6 (*C*(13)), 118.1 (*C*(4)), 74.9 (*C*(8)), 66.4 (*C*(9)), 63.1 (*C*(17)), 54.3 (*C*(20)), 52.7 (*C*(16)), 28.9 (*C*(18)), 23.7 (*C*(19)), 21.6 (*C*(15)), 17.4 (*C*(10)), -1.3 (*C*(11)); LRMS (ESI$^+$) *m*/*z* 590.4 (M+H$^+$); HRMS (ESI$^+$): calcd for $C_{30}H_{40}N_7O_4Si^+$ [M+H]$^+$ 590.2906, found 590.2908.

8-(4-(2-((3-aminobenzyl)(cyclopentyl)amino)ethyl)-1H-pyrazol-1-yl)-3-((2-(trimethylsilyl)ethoxy) methyl)pyrido[3,4-d]pyrimidin-4(3H)-one, (96)



To a solution of **95** (114 mg, 0.193 mmol) in 2-Propanol (1 mL) and Water (0.5 mL) was added iron (65 mg, 1.160 mmol), ammonium chloride (414 mg, 7.73 mmol) and formic acid (7.41 µl, 0.193 mmol). The reaction mixture was heated to 50 °C for 5 h. The reaction mixture was filtered through celite and washed with MeOH (40 mL) to give a brown solid. The crude product was loaded onto an SCX-2 column and washed with MeOH. The product was eluted by washing with 3.5N NH_3 in MeOH. and the solution was concentrated *in vacuo* to give **96** (89 mg, 82%) as a yellow oil. ν_{max}/cm^{-1} 3419 (N-H), 1693 (C=O), 1608, 1490 (C=C), 1248 (C-O), 1024 (C-N) 884, 803 (C-H); ^{1}H NMR (400 MHz, $CDCl_3$) δ 8.61 (d, *J* = 5.1 Hz, 1H, C*H*(5)), 8.47 (s, 1H, C*H*(1)), 8.29 (s, 1H, C*H*(12)), 8.05 (d, *J* = 5.1 Hz, 1H, C*H*(4)), 7.70 (s, 1H, C*H*(14)), 7.07 (t, *J* = 7.8 Hz, 1H, C*H*(25)), 6.74 (d, *J* = 7.2 Hz, 2H, C*H*(22+26), 6.55 (d, *J* = 8.1 Hz, 1H, C*H*(24)), 5.46 (s, 2H, C*H*(8)), 3.77 – 3.63 (m, 6H, C*H*(9+20)+N*H*$_2$), 3.25 – 3.20 (m, 1H, C*H*(17)), 2.83 – 2.78 (m, 2H, C*H*(16)), 2.74 – 2.69 (m, 2H, C*H*(15)), 1.89 – 1.81 (m, 4H, C*H*(18)), 1.56 – 1.51 (m, 4H, C*H*(19)), 1.02 – 0.89 (m, 2H, C*H*(10)), 0.00 (s, 9H, C*H*(11)); ^{13}C NMR (101 MHz, DMSO) δ 159.0 (*C*(20)), 149.2 (*C*(1)), 148.4 (*C*(23)), 148.1 (*C*(6)), 144.8 (*C*(5)), 141.8 (*C*(14)), 141.1 (*C*(21)), 135.1 (*C*(7)), 130.9 (*C*(12)), 129.9 (*C*(3)), 128.5 (*C*(25)), 120.9 (*C*(13)), 118.2 (*C*(4)), 116.2 (*C*(26)), 114.1 (*C*(22)), 112.4 (*C*(24)), 75.0 (*C*(8)), 66.4 (*C*(9)), 62.6 (*C*(17)), 55.7 (*C*(20)), 52.1 (*C*(16)), 28.9 (*C*(18)), 23.8 (*C*(19)), 21.1 (*C*(15)), 17.4 (*C*(10)), -1.3 (*C*(11)); LRMS (ESI$^+$) *m*/*z* 560.4 (M+H$^+$); HRMS (ESI$^+$): calcd for $C_{30}H_{42}N_7O_2Si^+$ [M+H]$^+$ 560.3164, found 560.3147.

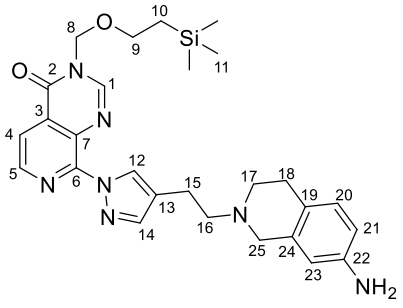
8-(4-(2-(7-nitro-3,4-dihydroisoquinolin-2(1H)-yl)ethyl)-1H-pyrazol-1-yl)-3-((2-(trimethylsilyl) ethoxy)methyl)pyrido[3,4-d]pyrimidin-4(3H)-one, (**97**)



To a solution of **50** (0.546 g, 1.17 mmol), potassium iodide (0.779 g, 4.69 mmol) and potassium carbonate (3.24 g, 23.5 mmol) in AcN (12 mL) was added 7-nitro-1,2,3,4-tetrahydroisoquinoline

(0.209 g, 1.173 mmol). The reaction mixture was stirred at 75 °C for 16 h. $NaHCO_3$ (60 mL) was added and back-extracted with EtOAc (2 x 75 mL). The combined organic extracts were washed with brine (75 mL). The organic layer was dried over Na_2SO_4, filtered and concentrated *in vacuo*. The crude product was adsorbed on silica and purified by flash chromatography eluting with 10% MeOH in CH_2Cl_2 to give **97** (0.397g, 62%) as a yellow oil. ν_{max}/cm^{-1} 1695 (C=O), 1608, 1465 (C=C), 1260 (C-O), 1522, 1343 (N-O), 1195, 1081 (C-N) 801 (C-H); ^{1}H NMR (400 MHz, $CDCl_3$) δ 8.60 (d, *J* = 5.1 Hz, 1H, C*H*(5)) 8.58 (s, 1H, C*H*(12)), 8.26 (s, 1H, C*H*(1)), 8.05 (d, *J* = 5.1 Hz, 1H, C*H*(4)), 7.97 (dd, *J* = 8.4, 2.5 Hz, 1H, C*H*(21)), 7.92 (d, *J* = 2.3 Hz, 1H, C*H*(23)), 7.80 (s, 1H, C*H*(14)), 7.25 (d, *J* = 8.4 Hz, 1H, C*H*(20)), 5.44 (s, 2H, C*H*(8)), 3.79 (s, 2H, C*H*(25)), 3.70 – 3.54 (m, 2H, C*H*(9)), 3.01 (t, *J* = 5.9 Hz, 2H, C*H*(18)), 2.87 (m, 6H, C*H*(15,16,17)), 1.08 – 0.88 (m, 2H, C*H*(10)), -0.01 (s, 9H, C*H*(11)); ^{13}C NMR (101 MHz, $CDCl_3$) δ 159.6 (*C*(2)), 148.2 (*C*(6)), 147.1 (*C*(1)), 146.2 (*C*(22)), 145.6 (*C*(5)), 143.2 (*C*(14)), 142.6 (*C*(19)), 136.5 (*C*(24)), 134.7 (*C*(7)), 130.8 (*C*(12)), 130.4 (*C*(3)), 129.7 (*C*(20)), 121.9 (*C*(23)), 121.4 (*C*(13)), 121.3 (*C*(21)), 118.1 (*C*(4)), 75.1 (*C*(8)), 68.1 (*C*(9)), 58.7 (*C*(16)), 55.7 (*C*(25)), 50.3 (*C*(17)), 29.6 (*C*(18)), 22.5 (*C*(15)), 18.1 (C(10)), -1.3 (*C*(11)); LRMS (ESI$^+$) *m*/*z* 548.3 (M+H$^+$); HRMS (ESI$^+$): calcd for $C_{27}H_{34}N_7O_4Si^+$ $[M+H]^+$ 548.2436, found 548.2444.

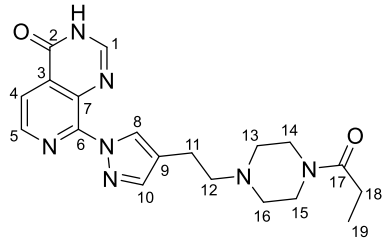
8-(4-(2-(7-amino-3,4-dihydroisoquinolin-2(1H)-yl)ethyl)-1H-pyrazol-1-yl)-3-((2-(trimethylsilyl) ethoxy)methyl)pyrido[3,4-d]pyrimidin-4(3H)-one, (**98**)



To a solution of **97** (0.357 g, 0.652 mmol) in 2-Propanol (2 mL) and Water (1 mL) was added iron (0.218 g, 3.91 mmol), ammonium chloride (1.395 g, 26.1 mmol) and formic acid (0.025 mL, 0.652 mmol). The reaction mixture was heated to 50 °C for 3 h. The reaction mixture was filtered through celite and washed with MeOH (300 mL). The filtrate was concentrated *in vacuo*. The crude product

was loaded onto an SCX-2 column and washed with MeOH. The product was eluted by washing with 3.5N NH_3 in MeOH and the filtrate was concentrated *in vacuo* to give **98** (0.202 g, 60%) as a yellow amorphous solid. ν_{max}/cm^{-1} 3349 (N-H), 1694 (C=O), 1609, 1554, 1512, (C=C), 1249 (C-O), 1198, 1072, 1036 (C-N); ^{1}H NMR (400 MHz, $CDCl_3$) δ 8.63 (d, *J* = 5.1 Hz, 1H, C*H*(5)), 8.60 (s, 1H, C*H*(12)), 8.29 (s, 1H, C*H*(1)), 8.06 (d, *J* = 5.1 Hz, 1H, C*H*(4)), 7.81 (s, 1H, C*H*(14)), 6.69 (d, *J* = 7.6 Hz, 1H), 6.63 (dd, *J* = 7.9, 1.4 Hz, 1H), 6.56 (t, *J* = 7.3 Hz, 1H), 6.51 (d, *J* = 7.4 Hz, 1H), 5.46 (s, 2H, C*H*(8)), 3.74 – 3.65 (m, 2H, C*H*(25)), 3.53 (t, *J* = 7.7 Hz, 2H, C*H*(9)), 3.39 (m, 4H, C*H*(17,18)), 2.93 – 2.85 (m, 4H, C*H*(15,16)), 1.02 – 0.92 (m, 2H, C*H*(10)), 0.00 (s, 9H, C*H*(11)); ^{13}C NMR (101 MHz, $CDCl_3$) δ 159.6 (*C*(2)), 148.2 (*C*(6)), 147.1 (*C*(1)), 145.6 (*C*(5)), 143.2 (*C*(14)), 134.7, 134.6 (*C*(7,24)), 134.1 (*C*(19)), 131.0 (*C*(12)), 130.4 (*C*(3)), 121.2 (*C*(13)), 119.4 (*C*(20)), 118.1 (*C*(4)), 117.6, 114.4 (*C*(21)), 111.3 (*C*(23)), 75.1 (*C*(8)), 68.1 (*C*(9)), 60.5 (*C*(16)), 52.6 (*C*(25)), 48.5 (*C*(17)), 41.0 (*C*(18)), 21.2 (*C*(15)), 18.2 (*C*(9)), -1.3 (*C*(11)); LRMS (ESI^+) *m/z* 518.3 ($M+H^+$); HRMS (ESI^+): calcd for $C_{27}H_{35}N_7O_2SiK^+$ $[M+K]^+$ 556.2253, found 556.2244.

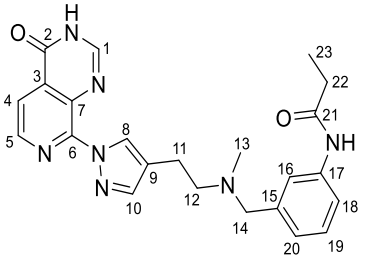
8-(4-(2-(4-propionylpiperazin-1-yl)ethyl)-1H-pyrazol-1-yl)pyrido[3,4-d]pyrimidin-4(3H)-one, (**99**)



To a solution of **71** (0.100 g, 0.307 mmol) and PS-DIPEA (300 mg) in NMP (2 mL) at 0 °C was added propionyl chloride (0.030 mL, 0.338 mmol). The reaction mixture was slowly warmed to room temperature and then stirred for 16 h. The reaction mixture was filtered, concentrated *in vacuo* and dried in Genevac. The crude product was adsorbed on silica, added to a 10 g KP-NH column and purified by flash chromatography eluting with 0-15% MeOH in CH_2Cl_2 to give **99** as a white solid (0.058 g, 50%). Mp 191 – 193 °C; ν_{max}/cm^{-1} 1698, 1639 (C=O), 1599, 1549 (C=C), 1215, 1157, 1132 (C-N); ^{1}H NMR (400 MHz, DMSO-d_6) δ 8.54 (d, *J* = 5.1 Hz, 1H, C*H*(5)), 8.41 (s, 1H, C*H*(8)), 8.26 (s, 1H,

C*H*(1)), 7.97 (d, *J* = 5.1 Hz, 1H, C*H*(4)), 7.71 (s, 1H, C*H*(10)), 3.49 – 3.41 (m, 4H, C*H*(14,15)), 2.69 (t, *J* = 7.5 Hz, 2H, *CH*(11)), 2.55 (t, *J* = 7.5 Hz, 2H, C*H*(12)), 2.46 – 2.36 (m, 4H, C*H*(13,16)), 2.29 (q, *J* = 7.4 Hz, 2H, C*H*(18)), 0.97 (t, *J* = 7.4 Hz, 3H, C*H*(19)); ^{13}C NMR (101 MHz, DMSO) δ 171.6 (*C*(17)), 160.0 (*C*(2)), 147.8 (*C*(1)), 147.7 (*C*(6)), 144.2 (*C*(5)), 141.9 (*C*(10)), 135.9 (*C*(7)), 131.3 (*C*(8)), 130.8 (*C*(3)), 120.6 (*C*(9)), 118.1 (*C*(4)), 58.6 (*C*(12)), 53.0, 52.5 (*C*(13, 16)), 44.9 41.2, (*C*(14, 15), 25.7 (*C*(18)), 21.3 (*C*(11)), 9.6 (*C*(19)); LRMS (ESI$^+$) *m/z* 382.6 (M+H$^+$); HRMS (ESI$^+$): calcd for $C_{19}H_{24}N_7O_2^+$ [M+H]$^+$ 382.1986, found 382.1985.

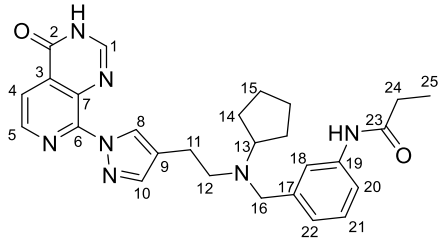
(*E*)-4-(dimethylamino)-*N*-(3-((methyl(2-(1-(4-oxo-3,4-dihydropyrido[3,4-d]pyrimidin-8-yl)-1H-pyrazol-4-yl)ethyl)amino)methyl)phenyl)but-2-enamide, (**100**)



To a solution of 8-(4-(2-((3-aminobenzyl)(methyl)amino)ethyl)-1H-pyrazol-1-yl)pyrido[3,4-d]pyrimidin-4(3H)-one, HCl (100 mg, 0.266 mmol) and PS-DIPEA (300 mg) in NMP (2 mL) at 0 °C was added propionyl chloride (26 µL, 0.293 mmol). The reaction mixture was warmed to room temperature and then stirred for 16 h. The reaction mixture was filtered, concentrated *in vacuo* and dried in a Genevac. The crude product was adsorbed on silica, added to a 28g KP-NH column and purified by flash chromatography eluting with 0-25% MeOH in CH_2Cl_2 to give **100** (0.025 g, 22%) as a white solid. Mp 138 – 140 °C; ν_{max}/cm^{-1} 1685 (C=O), 1596, 1549, 1458 (C=C), 1210, 1157, 1058 (C-N), 826, 800 (C-H); ^{1}H NMR (400 MHz, DMSO-d_6) δ 9.79 (s, 1H, N*H*), 8.55 (d, *J* = 5.1 Hz, 1H, C*H*(5)), 8.39 (s, 1H, C*H*(8)), 8.27 (s, 1H, C*H*(1)), 7.97 (d, *J* = 5.1 Hz, 1H, C*H*(4)), 7.69 (s, 1H, C*H*(10)), 7.54 (d, *J* = 1.8 Hz, 1H, C*H*(16)), 7.49 (dt, *J* = 8.2, 1.5 Hz, 1H, C*H*(18)), 7.20 (t, *J* = 7.8 Hz, 1H, C*H*(19)), 6.95 (dt, *J* = 7.6, 1.2 Hz, 1H, C*H*(20)), 3.50 (s, 2H, C*H*(14)), 2.73 (t, *J* = 7.4 Hz, 2H, C*H*(11)), 2.61 (m, 2H, C*H*(12)), 2.27 (q, *J* = 7.6 Hz, 2H, C*H*(22)), 2.19 (s, 3H, C*H*(13)), 1.05 (t, *J* = 7.5 Hz, 3H, C*H*(23)); ^{13}C NMR (101

MHz, DMSO) δ 171.9 (*C*(21)), 159.8 (*C*(2)), 147.5 (*C*(1)), 144.0 (*C*(5)), 141.6 (*C*(10)), 139.6 (*C*(17)), 139.3 (*C*(15)), 135.8 (*C*(7)), 131.0 (*C*(8)), 130.7 (*C*(3)), 128.3 (*C*(19)), 123.3 (*C*(20)), 120.5 (*C*(9)), 119.3 (*C*(16)), 117.8 (*C*(4)), 117.5 (*C*(18)), 61.5 (*C*(14)), 57.8 (*C*(12)), 41.7 (*C*(13)), 29.5 (*C*(22)), 21.7 (*C*(11)), 9.6 (*C*(23)); LRMS (ESI$^+$) *m/z* 432.6 (M+H$^+$); HRMS (ESI$^+$): calcd for $C_{23}H_{26}N_7O_2^+$ [M+H]$^+$ 432.2143, found 432.2143.

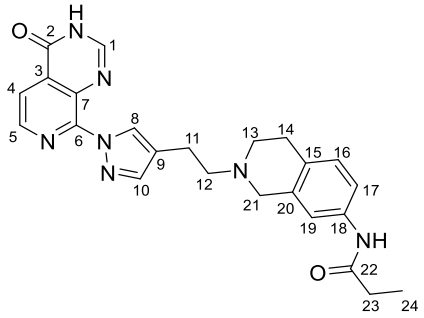
N-(3-((cyclopentyl(2-(1-(4-oxo-3,4-dihydropyrido[3,4-d]pyrimidin-8-yl)-1H-pyrazol-4-yl)ethyl) amino)methyl)phenyl)propionamide, (**101**)



To a solution of **96** (90 mg, 0.161 mmol) in THF (1.5 mL) was added 6M HCl (1.5 mL, 9.00 mmol). The reaction mixture was heated to 50 °C for 3 h. The reaction mixture was concentrated *in vacuo* to give 8-(4-(2-((3-aminobenzyl)(cyclopentyl)amino)ethyl)-1H-pyrazol-1-yl)pyrido[3,4-d]pyrimidin-4(3H)-one, HCl (quant.). To a solution of 8-(4-(2-((3-aminobenzyl)(cyclopentyl)amino)ethyl)-1H-pyrazol-1-yl)pyrido[3,4-d]pyrimidin-4(3H)-one, HCl (100 mg, 0.215 mmol) in NMP (2 mL) was added PS-DIPEA (300 mg) and propionyl chloride (21 µL, 0.236 mmol) at 0 °C. The reaction mixture was warmed to room temperature and stirred for 6 h. The reaction mixture was filtered, concentrated *in vacuo* and dried in the Genevac. The crude product was adsorbed on silica, added to a 11g KP-NH column and purified by flash chromatography eluting with 0-20% MeOH in CH_2Cl_2 to give **101** (38 mg, 37%) as an off-white solid. Mp 148 – 150 °C; ν_{max}/cm^{-1} 1701, 1663 (C=O), 1596, 1487, 1459 (C=C), 1210, 1157, 1060 (C-N), 826, 800 (C-H); ^{1}H NMR (400 MHz, DMSO-d_6) δ 9.79 (s, 1H, N*H*), 8.52 (d, *J* = 5.1 Hz, 1H, C*H*(5)), 8.31 (s, 1H, C*H*(8)), 8.24 (s, 1H, C*H*(1)), 7.96 (d, *J* = 5.1 Hz, 1H, C*H*(4)), 7.62 (s, 1H, C*H*(10)), 7.57 (t, *J* = 1.9 Hz, 1H, C*H*(18)), 7.49 (dd, *J* = 8.1, 2.1 Hz, 1H, C*H*(20)), 7.19 (t, *J* = 7.8 Hz, 1H, C*H*(21)), 6.99 (dt, *J* = 7.6, 1.3 Hz, 1H, C*H*(22)), 3.63 (s, 2H, C*H*(16)), 3.19 – 3.06 (m, 1H, C*H*(13)), 2.73 – 2.56 (m, 4H, C*H*(11,12)), 2.26 (q, *J* = 7.6 Hz, 2H, C*H*(24)), 1.82 – 1.71 (m, 2H, C*H*(14)), 1.66 –

1.53 (m, 2H, C*H*(15)), 1.52 – 1.35 (m, 4H, C*H*(14,15)), 1.03 (t, *J* = 7.6 Hz, 3H, C*H*(25)); ^{13}C NMR (101 MHz, DMSO) δ 172.0 (*C*(23)), 160.0 (*C*(2)), 147.6 (*C*(1)), 144.0 (*C*(5)), 141.6 (*C*(10)), 141.3 (*C*(19)), 139.3 (*C*(17)), 135.8 (*C*(7)), 131.0 (*C*(8)), 130.7 (*C*(3)), 128.3 (*C*(21)), 123.1 (*C*(22)), 120.6 (*C*(9)), 119.1 (*C*(18)), 117.9 (*C*(4)), 117.4 (*C*(20)), 62.9 (*C*(13)), 55.5 (*C*(16)), 52.4 (*C*(12)), 29.5 (*C*(24)), 29.1 (*C*(14)), 23.8 (*C*(15)), 21.2 (*C*(11)), 9.7 (*C*(25)); LRMS (ESI$^+$) *m*/*z* 486.7 (M+H$^+$); HRMS (ESI$^+$): calcd for $C_{27}H_{32}N_7O_2^+$ [M+H]$^+$ 486.2612, found 486.2619.

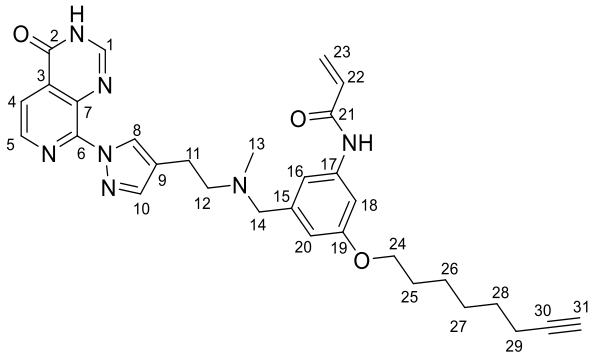
N-(2-(2-(1-(4-oxo-3,4-dihydropyrido[3,4-d]pyrimidin-8-yl)-1H-pyrazol-4-yl)ethyl)-1,2,3,4-tetrahydroisoquinolin-7-yl)propionamide, (**102**)



To a solution of 8-(4-(2-(7-amino-3,4-dihydroisoquinolin-2(1H)-yl)ethyl)-1H-pyrazol-1-yl)pyrido[3,4-d]pyrimidin-4(3H)-one (75 mg, 0.194 mmol) in NMP (2 mL) was added PS-DIPEA (225 mg) and propionyl chloride (19 µL, 0.213 mmol) at 0 °C. The reaction mixture was warmed to room temperature and stirred for 5 h. The reaction mixture was filtered, concentrated *in vacuo* and dried in the Genevac. The crude product was adsorbed on silica, added to a 11g KP-NH column and purified by flash chromatography eluting with 0-20% MeOH in CH_2Cl_2 to give **102** (31 mg, 36%) as an orange solid. ν_{max}/cm^{-1} 1701 (C=O), 1597, 1502, 1459 (C=C), 1212, 1158, 1059 (C-N); ^{1}H NMR (400 MHz, DMSO-d_6) δ 9.72 (s, 1H, N*H*), 8.53 (d, *J* = 5.1 Hz, 1H, C*H*(5)), 8.43 (s, 1H, C*H*(8)), 8.25 (s, 1H, C*H*(1)), 7.96 (d, *J* = 5.1 Hz, 1H, C*H*(4)), 7.73 (s, 1H, C*H*(10)), 7.34 (d, *J* = 2.1 Hz, 1H, C*H*(19)), 7.28 (dd, *J* = 8.2, 2.1 Hz, 1H, C*H*(17)), 7.00 (d, *J* = 8.3 Hz, 1H, C*H*(16)), 3.59 (s, 2H, C*H*(21)), 2.88 – 2.61 (m, 8H, C*H*(11, 12, 13, 14)), 2.28 (q, *J* = 7.5 Hz, 2H, C*H*(23)), 1.06 (t, *J* = 7.5 Hz, 3H, C*H*(24)); ^{13}C NMR (101 MHz, DMSO) δ 171.8 (*C*(22)), 160.0 (*C*(2)), 147.7 (*C*(1,6)), 144.0 (*C*(5)), 141.8 (*C*(10)), 136.9 (*C*(18)), 135.9 (*C*(7)), 135.1 (*C*(20)), 131.1 (*C*(8)), 130.7 (*C*(3)), 128.9 (*C*(15)), 128.6 (*C*(16)), 120.6 (*C*(9)), 117.9

(*C*(4)), 117.3 (*C*(17)), 116.9 (*C*(19)), 58.4 (*C*(12)), 55.5 (*C*(21)), 50.5 (*C*(13)), 29.5 (*C*(23)), 28.2 (*C*(14)), 21.6 (*C*(11)), 9.8 (*C*(24)); LRMS (ESI^+) *m/z* 444.6 ($M+H^+$); HRMS (ESI^+): calcd for $C_{24}H_{26}N_7O_2^+$ $[M+H]^+$ 444.2143, found 444.2144.

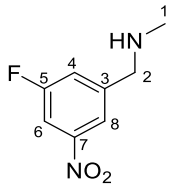
N-(3-((methyl(2-(1-(4-oxo-3,4-dihydropyrido[3,4-d]pyrimidin-8-yl)-1H-pyrazol-4-yl)ethyl)amino) methyl)-5-(oct-7-yn-1-yloxy)phenyl)acrylamide, (**103**)



To a solution of **123** (315 mg, 0.500 mmol) in THF (5 mL) was added 4M HCl (5 mL, 20.0 mmol). The reaction mixture was heated to 50 °C and stirred for 3 h. The reaction mixture was concentrated in vacuo. The crude product was loaded onto a 1 g SCX cartridge. The cartridge was washed with MeOH (10 mL) and the fractions discarded. The cartridge was washed with 3.5N NH_3 in MeOH (20 mL) and the collected fractions were concentrated *in vacuo* to give 8-(4-(2-((3-amino-5-(oct-7-yn-1-yloxy)benzyl)(methyl)amino)ethyl)-1H-pyrazol-1-yl)pyrido[3,4-d]pyrimidin-4(3H)-one (250 mg, quant.). To a solution of 8-(4-(2-((3-amino-5-(oct-7-yn-1-yloxy)benzyl)(methyl)amino)ethyl)-1H-pyrazol-1-yl)pyrido[3,4-d]pyrimidin-4(3H)-one (18 mg, 0.036 mmol) and PS-DIPEA (60 mg) in NMP (360 µl) at 0 °C was added acryloyl chloride (4 µl, 0.054 mmol). The reaction mixture was warmed to room temperature and stirred for 16 h. The reaction mixture was filtered, washed with MeOH, concentrated *in vacuo* and dried in the Genevac. The crude product was purified by prep HPLC to give **103** (2.6 mg, 13%) as an amorphous yellow solid. ^1H NMR (400 MHz, DMSO-d_6) δ 8.49 (d, *J* = 0.8 Hz, 1H, C*H*(8)), 8.38 (d, *J* = 5.1 Hz, 1H, C*H*(5)), 8.25 (s, 1H, C*H*(1)), 7.88 (d, *J* = 5.1, 1H, C*H*(4)), 7.65 (d, *J* = 0.7 Hz, 1H, C*H*(10)), 7.30 (d, *J* = 2.3 Hz, 1H, C*H*(18)), 7.09 (s, 1H, C*H*(16)), 6.57 (d, *J* = 1.9 Hz, 1H, C*H*(20)), 6.39 (dd, *J* = 17.0, 10.1 Hz, 1H, C*H*(22)), 6.21 (dd, *J* = 17.0, 2.1 Hz, 1H), 5.72 (dd, *J* = 10.1,

2.1 Hz, 1H, C*H*(23)), 3.84 (t, *J* = 6.4 Hz, 2H, C*H*(24)), 3.47 (s, 2H, C*H*(14)), 2.75 – 2.70 (m, 3H, C*H*(11+31)), 2.62 (d, *J* = 7.5 Hz, 2H, C*H*(12)), 2.20 (s, 3H, C*H*(13)), 2.14 (td, *J* = 6.8, 2.6 Hz, 2H, C*H*(29)), 1.87 (s, 9H, CH_3 (acetate salt)), 1.72 – 1.53 (m, 2H), 1.50 – 1.28 (m, 10H); ^{13}C NMR (101 MHz, DMSO) δ 172.4, 163.6 (*C*(2)), 163.1 (*C*(21)), 158.8, 153.3, 152.3, 147.4 (*C*(6)), 141.9 (*C*(5)), 141.2 (*C*(10)), 141.1 (*C*(15)), 139.9, 137.3 (*C*(7)), 131.9 (*C*(22)), 131.2 (*C*(8)), 130.3 (*C*(3)), 126.8 (*C*(23)), 120.1 (*C*(9)), 118.0 (*C*(4)), 111.7 (*C*(16)), 109.6 (*C*(20)), 104.2 (*C*(18)), 84.6 (*C*(30)), 71.2 (*C*(31)), 67.2 (*C*(24)), 61.5 (*C*(14)), 57.8 (*C*(12)), 41.8 (*C*(13)), 28.6 (*C*(25)), 27.9 (*C*(28,29)), 25.0 (*C*(27)), 21.8 (NH_4OAc), 21.7 (*C*(11)), 17.6 (*C*(29)); LRMS (ESI$^+$) *m/z* 554.6 (M+H$^+$); HRMS (ESI$^+$): calcd for $C_{31}H_{36}N_7O_3^+$ $[M+H]^+$ 554.2874, found 554.2871.

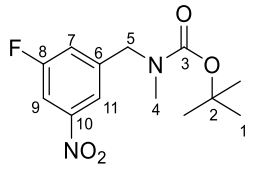
1-(3-fluoro-5-nitrophenyl)-N-methylmethanamine, (105)



To a solution of 3-fluoro-5-nitrobenzaldehyde (2.542 g, 15.0 mmol) in DCE (150 mL) was added methanamine (9.77 mL, 19.5 mmol) at room temperature and the solution was stirred for 6 h. sodium triacetoxyhydroborate (6.37 g, 30.1 mmol) was added and stirred at room temperature for 16 h. More sodium triacetoxyhydroborate (6.37 g, 30.1 mmol) was added and stirred for a further 6 h. The reaction mixture was quenched with $NaHCO_3$ (150 mL) and extracted with CH_2Cl_2 (5 x 100 mL). The combined organic extracts were washed with brine (75 mL), dried over Na_2SO_4, filtered and concentrated *in vacuo*. The crude product was adsorbed on silica and purified by flash chromatography eluting with 0-6% MeOH in CH_2Cl_2 to give **105** (1.851 g, 67%) as a yellow oil. ν_{max}/cm^{-1} 3098 (N-H), 1626, 1595, 1446 (C=C), 1529, 1348 (N-O), 1130, 1104, (C-N), 1080 (C-F); ^{1}H NMR (400 MHz, $CDCl_3$) δ 8.02 (ddd, *J* = 2.1, 1.4, 0.7 Hz, 1H, C*H*(8)), 7.79 (dt, *J* = 8.2, 2.3 Hz, 1H, C*H*(6)), 7.44 (dddt, *J* = 8.7, 2.2, 1.4, 0.7 Hz, 1H, C*H*(4)), 3.88 – 3.83 (m, 2H, C*H*(2)), 2.46 (s, 3H, C*H*(1)); ^{13}C NMR (101 MHz, $CDCl_3$) δ 163.8, 161.3 (*C*(5)), 149.2 (*C*(7)), 145.2, 145.1 (*C*(3)), 121.4, 121.2 (*C*(4)),

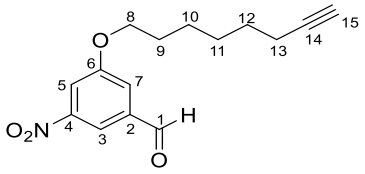
118.7 (*C*(8)), 110.0, 109.7 (*C*(6)), 54.9 (*C*(2)), 36.1(*C*(1)); LRMS (ESI$^+$) *m/z* 185.2 (M+H$^+$); HRMS (ESI$^+$): calcd for $C_8H_{10}FN_2O_2^+$ [M+H]$^+$ 185.0721, found 185.0718.

tert-butyl (3-fluoro-5-nitrobenzyl)(methyl)carbamate, (**106**)



To a solution of **105** (0.300 g, 1.63 mmol) in THF (16 mL) at 0 °C was added 4-(dimethylamino)pyridine (0.199 g, 1.63 mmol) and di-*tert*-butyl dicarbonate (0.427 g, 1.955 mmol). The reaction mixture was stirred at room temperature for 3 h. Water (25 mL) was added and the mixture was extracted with EtOAc (3 x 50 mL). The combined extracts were washed with brine (25 mL), dried over Na_2SO_4, filtered and concentrated *in vacuo*. The crude product was adsorbed on silica and purified by flash chromatography eluting with 0-20% EtOAc in cyclohexane to give **106** (0.327 g, 71%) as a colourless oil. ν_{max}/cm^{-1} 1687 (C=O), 1626, 1596, 1447 (C=C), 1536, 1348 (N-O), 1274, 1249, 1226 (C-O), 1142 (C-N), 1081 (C-F); ^{1}H NMR (400 MHz, $CDCl_3$) δ 7.91 (s, 1H, C*H*(11)), 7.83 (dt, *J* = 8.2, 2.3 Hz, 1H, C*H*(9)), 7.29 (d, *J* = 8.3 Hz, 1H, C*H*(7)), 4.50 (s, 2H, C*H*(5)), 2.89 (s, 3H, C*H*(4)), 1.48 (d, *J* = 9.0 Hz, 9H, C*H*(1)); ^{13}C NMR (101 MHz, $CDCl_3$) δ 163.9 (*C*(8)), 161.4 (*C*(3)), 149.4 (*C*(10)), 143.1, 143.0 (*C*(6)), 120.6 (*C*(7)), 118.1 (*C*(11)), 110.4, 110.1 (*C*(9)), 80.7 (*C*(2)), 52.2, 51.6 (*C*(5)), 34.7 (*C*(4)), 28.5 (*C*(1)); LRMS (ESI$^+$) *m/z* 285.4 (M+H$^+$); HRMS (ESI$^+$): calcd for $C_{13}H_{17}FN_2O_4Na^+$ [M+Na]$^+$ 307.1065, found 307.1068.

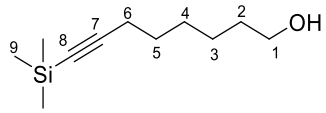
3-nitro-5-(oct-7-yn-1-yloxy)benzaldehyde, (**107**)



To a vial was added 3-hydroxy-5-nitrobenzaldehyde (0.291 g, 1.74 mmol) and potassium carbonate (0.289 g, 2.09 mmol) in DMF (17 mL). The reaction mixture was stirred at room temperature for 30

min. oct-7-yn-1-yl methanesulfonate **113** (1.067 g, 5.22 mmol) was added and the reaction mixture was heated at 80 °C for 16 h. The reaction mixture was diluted with EtOAc (75 mL) and washed with water (50 mL). The aqueous layer was back-extracted with EtOAc (2 x 50 mL). The combined organic extracts were dried over Na_2SO_4, filtered and concentrated *in vacuo*. The crude product was adsorbed on silica and purified by flash chromatography eluting with 0-10% EtOAc in cyclohexane to give **107** (0.385 g, 80%) as a yellow oil. ν_{max}/cm^{-1} 3286 (C≡C-H), 1465 (C=C), 1347 (N-O), 1248 (C-O), 1169 (C-N); ^{1}H NMR (400 MHz, $CDCl_3$) δ 10.03 (s, 1H, C*H*(1)), 8.26 (t, *J* = 1.6 Hz, 1H, C*H*(3)), 7.96 (t, *J* = 2.3 Hz, 1H, C*H*(5)), 7.69 (dd, *J* = 2.6, 1.2 Hz, 1H, C*H*(7)), 4.10 (t, *J* = 6.4 Hz, 2H, C*H*(8)), 2.21 (td, *J* = 6.8, 2.6 Hz, 2H, C*H*(13)), 1.94 (t, *J* = 2.7 Hz, 1H, C*H*(15)), 1.92 – 1.80 (m, 2H, C*H*(9)), 1.65 – 1.44 (m, 6H, C*H*(10,11,12)); ^{13}C NMR (101 MHz, $CDCl_3$) δ 189.8 (*C*(1)), 160.5 (*C*(6)), 149.8 (*C*(4)), 138.3 (*C*(2)), 119.8 (*C*(7)), 117.0 (*C*(3)), 115.1 (*C*(5)), 84.5 (*C*(14)), 69.4 (*C*(8)), 68.5 (*C*(15)), 28.9 (*C*(9)), 28.5 (*C*(12)), 28.4 (*C*(11)), 25.5 (*C*(10)), 18.4 (*C*(13)); LRMS (ESI$^-$) *m/z* 274.1 (M-H$^+$); HRMS (ESI$^+$): calcd for $C_{15}H_{18}NO_4^+$ [M+H]$^+$ 276.1230, found 276.1235.

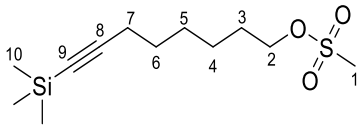
8-(trimethylsilyl)oct-7-yn-1-ol, (**110**)



To a solution of oct-7-yn-1-ol **109** (0.562 mL, 3.96 mmol) in THF (26.4 mL) at -78 °C was added ^{n}BuLi in hexane (5.45 mL, 8.72 mmol). The reaction mixture was stirred at -78 °C for 1 h and chlorotrimethylsilane (1.772 mL, 13.9 mmol) was added dropwise. The solution was warmed to room temperature and stirred for 16 h. 1N HCl (25 mL) was added and the solution was stirred for 30 minutes. The mixture was diluted with EtOAc (100 mL) and extracted. The aqueous layer was back-extracted with EtOAc (3 x 50 mL). The combined organic extracts were washed with saturated $NaHCO_3$ (75 mL) and brine (75 mL) and dried over Na_2SO_4, filtered and concentrated *in vacuo*. The crude product was adsorbed on silica and purified by flash chromatography eluting with 0-20% EtOAc in Cyclohexane to give **110** (0.420 g, 53%) as a colourless oil. ν_{max}/cm^{-1} 3329 (O-H), 2174 (C≡C),

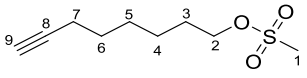
1248 (C-O); ^{1}H NMR (400 MHz, $CDCl_3$) δ 3.68 – 3.59 (m, 2H, C*H*(1)), 2.22 (t, *J* = 7.0 Hz, 2H, C*H*(6)), 1.63 – 1.47 (m, 4H, C*H*(2, 5)), 1.40 (m, 4H, C*H*(3, 4)), 1.26 (s, 1H,O*H*), 0.14 (s, 9H, C*H*(9)); ^{13}C NMR (101 MHz, $CDCl_3$) δ 107.7 (*C*(8)), 84.6 (*C*(7)), 63.1 (*C*(1)), 32.7 (*C*(2)), 28.7 (*C*(4, 5), 25.3 (*C*(3)), 19.9 (*C*(6)), 0.3 (*C*(9)); HRMS (ESI^+): calcd for $C_{11}H_{23}OSi^+$ $[M+H]^+$ 199.1513, found 199.1511.

8-(trimethylsilyl)oct-7-yn-1-yl methanesulfonate, (**112**)



To a solution of **110** (0.300 g, 1.51 mmol) in THF (15 mL) at 0 °C was added triethylamine (0.422 mL, 3.02 mmol). The reaction mixture was stirred for 10 min at 0 °C and methanesulfonyl chloride (0.176 mL, 2.27 mmol) was added. The reaction mixture was warmed to room temperature and stirred for 4 h. $NaHCO_3$ (50 mL) was added and extracted with EtOAc (3 x 25 mL). The combined organic extracts were washed with brine (20 mL), dried over Na_2SO_4, filtered and concentrated *in vacuo* to give **112** (0.400 g, 96%) as an oil. ν_{max}/cm^{-1} 2172 (C≡C), 1248, 1172 (C-O); ^{1}H NMR (400 MHz, DMSO-d_6) δ 4.18 (t, *J* = 6.5 Hz, 2H, C*H*(2)), 3.15 (s, 3H, C*H*(1)), 2.21 (t, *J* = 6.9 Hz, 2H, C*H*(7)), 1.65 (p, *J* = 6.8 Hz, 2H, C*H*(3)), 1.44 (m, 2H, C*H*(6)), 1.35 (m, 4H, C*H*(4,5)), 0.11 (s, 9H, C*H*(10)); ^{13}C NMR (101 MHz, DMSO) δ 108.0 (*C*(9)), 84.2 (*C*(8)), 70.3 (*C*(2)), 36.5 (*C*(1)), 28.4 (*C*(3)), 27.7 (*C*(6)), 27.6 (*C*(5)), 24.3 (*C*(4)), 19.0 (*C*(7)), 0.2 (*C*(1)).

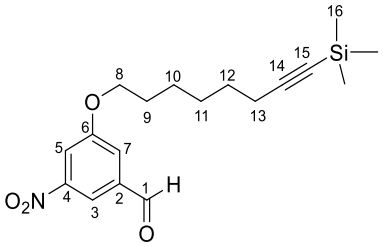
oct-7-yn-1-yl methanesulfonate, (**113**)



To a solution of oct-7-yn-1-ol (0.300 g, 2.38 mmol) in THF (24 mL) at 0 °C was added triethylamine (0.663 mL, 4.75 mmol). The reaction mixture was stirred at 0 °C for 15 min and methanesulfonyl chloride (0.276 mL, 3.57 mmol) was added. The reaction mixture was warmed to room temperature and stirred for 4 h. $NaHCO_3$ (30 mL) was added and back-extracted with EtOAc (3 x 25 mL). The combined organic extracts were washed with water (20 mL) and brine (20 mL), dried over Na_2SO_4,

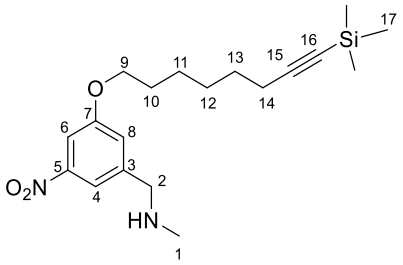
filtered and concentrated *in vacuo* to give **113** (0.398 g, 82%). ν_{max}/cm^{-1} 1169 (C-O); ^{1}H NMR (400 MHz, $CDCl_3$) δ 4.23 (t, *J* = 6.5 Hz, 2H, C*H*(2)), 3.00 (s, 3H, C*H*(1)), 2.20 (td, *J* = 6.9, 2.6 Hz, 2H, C*H*(7)), 1.94 (t, *J* = 2.6 Hz, 1H, C*H*(9)), 1.82 – 1.70 (m, 2H, C*H*(3)), 1.57 – 1.50 (m, 2H, C*H*(6)), 1.53 – 1.34 (m, 4H, C*H*(4, 5)); ^{13}C NMR (101 MHz, $CDCl_3$) δ 84.4 (*C*(9)), 70.1 (*C*(2)), 68.5 (*C*(9)), 37.5 (*C*(1)), 29.1 (*C*(3)), 28.3 (*C*(6)), 28.2 (*C*(5)), 25.1 (*C*(4)), 18.4 (*C*(7)).

3-nitro-5-((8-(trimethylsilyl)oct-7-yn-1-yl)oxy)benzaldehyde, (**118**)



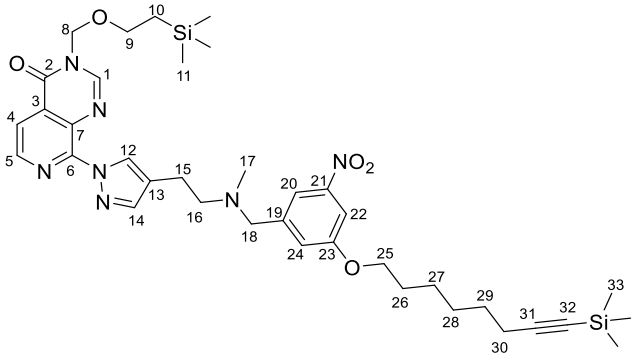
To a vial was added 3-hydroxy-5-nitrobenzaldehyde (0.166 g, 0.995 mmol) and potassium carbonate (0.206 g, 1.49 mmol) in DMF (9.95 mL). The reaction mixture was stirred at room temperature for 30 min. 8-(trimethylsilyl)oct-7-yn-1-yl methanesulfonate **112** (0.330 g, 1.19 mmol) was added and the reaction mixture was heated at 80 °C for 48 h. The reaction mixture was concentrated *in vacuo*. The crude product was adsorbed on silica and purified by flash chromatography eluting with 10-60% EtOAc in Cyclohexane to give **118** (0.122 g, 35%) as a colourless oil. ν_{max}/cm^{-1} 2172 (C≡C), 1465 (C=C), 1351 (N-O), 1248 (C-O), 1172 (C-N); ^{1}H NMR (400 MHz, $CDCl_3$) δ 10.03 (s, 1H, C*H*O), 8.27 (dd, *J* = 2.0, 1.2 Hz, 1H, C*H*(3)), 7.97 (t, *J* = 2.3 Hz, 1H, C*H*(5)), 7.70 (dd, *J* = 2.5, 1.2 Hz, 1H, C*H*(7)), 4.10 (td, *J* = 6.4, 1.3 Hz, 2H, C*H*(8)), 2.29 – 2.17 (m, 2H, C*H*(13)), 1.97 – 1.80 (m, 2H, C*H*(9)), 1.62 – 1.44 (m, 6H, C*H*(10,11, 12)), 0.13 (s, 9H, C*H*(16)); ^{13}C NMR (101 MHz, $CDCl_3$) δ 189.8 (*C*(1)), 160.5 (*C*(6)), 149.8 (*C*(4)), 138.3 (*C*(2)), 119.8 (*C*(7)), 117.0 (*C*(3)), 115.1 (*C*(5)), 107.4 (*C*(15)), 84.6 (*C*(14)), 69.4 (*C*(8)), 28.9 (*C*(9)), 28.5 (*C*(12)), 28.4 (*C*(11)), 25.5 (*C*(10)), 19.9 (*C*(13)), 0.3 (*C*(16)); LRMS (ESI^+) *m/z* 348.5 ($M+H^+$); HRMS (ESI^+): calcd for $C_{18}H_{26}NO_4Si^+$ $[M+H]^+$ 348.1626, found 348.1625.

N-methyl-1-(3-nitro-5-((8-(trimethylsilyl)oct-7-yn-1-yl)oxy)phenyl)methanamine, (**119**)



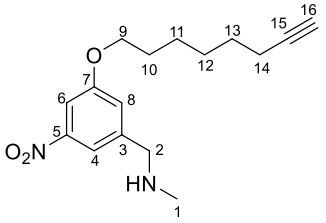
To a solution of **118** (0.109 g, 0.314 mmol) in DCE (3.14 mL) was added acetic acid (5 µl, 0.094 mmol) and methanamine (0.204 mL, 0.408 mmol). The reaction mixture was stirred at room temperature for 2 h. Sodium triacetoxyhydroborate (0.133 g, 0.627 mmol) was added and the reaction mixture was stirred for 16 h. The reaction mixture was quenched with $NaHCO_3$ (50 mL) and extracted with EtOAc (3 x 25 mL). The combined organic extracts were washed with brine (20 mL), dried over Na_2SO_4, filtered and concentrated *in vacuo*. The crude product was adsorbed on silica and purified by flash chromatography eluting with 0-5% MeOH in CH_2Cl_2 to give **119** (0.083g, 73%) as a yellow oil. ν_{max}/cm^{-1} 3309 (C≡C-H), 1624, 1581 (C=C), 1532, 1348 (N-O), 1280, 1248 (C-O), 1159, 1095, 1025 (C-N); ^{1}H NMR (400 MHz, $CDCl_3$) δ 7.78 (t, *J* = 1.8 Hz, 1H, C*H*(4)), 7.60 (t, *J* = 2.3 Hz, 1H, C*H*(6)), 7.21 (dd, *J* = 2.4, 1.4 Hz, 1H, C*H*(8)), 4.03 (t, *J* = 6.5 Hz, 2H, C*H*(9)), 3.80 (s, 2H, C*H*(2)), 2.46 (s, 3H, C*H*(1)), 2.24 (t, *J* = 6.9 Hz, 2H, C*H*(14)), 1.82 (t, *J* = 7.0 Hz, 2H, C*H*(10)), 1.62 – 1.44 (m, 6H, C*H*(11, 12, 13)), 0.14 (s, 9H, C*H*(17)); ^{13}C NMR (101 MHz, $CDCl_3$) δ 159.9 (*C*(7)), 149.4 (*C*(5)), 143.5 (*C*(3)), 121.1 (*C*(8)), 119.5, 115.3 (*C*(4)), 107.9 (*C*(16)) 107.5 (C(6)), 84.7 (*C*(15)), 68.7 (*C*(9)), 55.4 (*C*(2)), 36.2 (*C*(1)), 29.1 (*C*(10)), 28.6 (*C*(12,13)), 25.6 (*C*(11)), 19.9 (*C*(14)), 0.31 (*C*(17)); LRMS (ESI^+) *m*/*z* 363.6 ($M+H^+$); HRMS (ESI^+): calcd for $C_{19}H_{31}N_2O_3Si^+$ $[M+H]^+$ 363.2099, found 363.2103.

8-(4-(2-(methyl(3-nitro-5-((8-(trimethylsilyl)oct-7-yn-1-yl)oxy)benzyl)amino)ethyl)-1H-pyrazol-1-yl)-3-((2-(trimethylsilyl)ethoxy)methyl)pyrido[3,4-d]pyrimidin-4(3H)-one, (**120**)



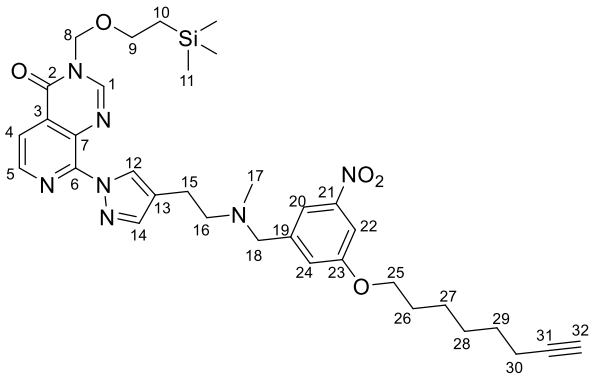
To a solution of **50** (98 mg, 0.210 mmol), potassium iodide (139 mg, 0.839 mmol) and potassium carbonate (0.579 g, 4.19 mmol) in AcN (2 mL) was added **119** (76 mg, 0.210 mmol). The reaction mixture was stirred at 75 °C for 16 h. $NaHCO_3$ (60 mL) was added and back-extracted with EtOAc (2 x 75 mL). The combined organic extracts were washed with brine (75 mL). The organic layer was dried over Na_2SO_4, filtered and concentrated *in vacuo*. The crude product was adsorbed on silica and purified by flash chromatography eluting with 10% MeOH in CH_2Cl_2 to give **120** (40 mg, 26%) as a yellow oil. ν_{max}/cm^{-1} 3299 (N-H), 1622 (C=O), 1529, 1346 (N-O), 1278 (C-O), 1157, 1052 (C-N) 868, 785 (C-H); ^{1}H NMR (400 MHz, $CDCl_3$) δ 8.60 (d, *J* = 5.2 Hz, 1H, C*H*(5)), 8.55 (d, *J* = 0.8 Hz, 1H, C*H*(12)), 8.28 (s, 1H, C*H*(1)), 8.04 (d, *J* = 5.1 Hz, 1H, C*H*(4)), 7.79 – 7.76 (s, 1H, C*H*(20)), 7.75 (d, *J* = 0.7 Hz, 1H, C*H*(14)), 7.55 (s, 1H, C*H*(22)), 7.19 (dd, *J* = 2.5, 1.3 Hz, 1H, C*H*(24)), 5.45 (s, 2H, C*H*(8)), 3.97 (t, *J* = 6.4 Hz, 2H, C*H*(25)), 3.73 – 3.63 (m, 2H, C*H*(9)), 3.58 (s, 2H, C*H*(18)), 2.79 (m, 2H, C*H*(15)), 2.75 – 2.65 (m, 2H, C*H*(16)), 2.28 (s, 3H, C*H*(17)), 2.22 (t, *J* = 7.0 Hz, 2H, C*H*(30)), 1.81 – 1.73 (m, 3H, C*H*(26)), 1.53 (m, 2H, C*H*(29)), 1.45 (m, 4H, C*H*(27, 28)), 1.01 – 0.92 (m, 2H, C*H*(10)), 0.12 (s, 9H, C*H*(33)), -0.01 (s, 9H, C*H*(11)); ^{13}C NMR (101 MHz, $CDCl_3$) δ 159.7 (*C*(23)), 159.6 (*C*(2)), 149.3 (*C*(21)), 148.2 (*C*(6)), 147.1 (*C*(1)), 145.5 (*C*(5)), 143.2 (*C*(14)), 142.7 (*C*(19)), 134.6 (*C*(7)), 130.8 (*C*(12)), 130.4 (*C*(3)), 121.7 (*C*(24)), 121.6 (*C*(13)), 118.0 (*C*(4)), 115.9 (*C*(20)), 107.5 (*C*(22, 32)), 84.6 (*C*(31)), 75.1 (*C*(8)), 68.7 (*C*(25)), 68.0 (*C*(9)), 61.8 (*C*(18)), 58.3 (*C*(16)), 53.53, 42.2 (*C*(17)), 29.0 (*C*(26)), 28.5 (*C*(28, 29)), 25.6 (*C*(27)), 22.6 (*C*(15)), 19.9 (*C*(30)), 18.1 (*C*(10)), 0.3 (*C*(33)), -1.3 (*C*(11)); HRMS (ESI$^+$): calcd for $C_{37}H_{54}N_7O_5Si_2^+$ $[M+H\text{-}TMS]^+$ 660.3324, found 660.3332.

N-methyl-1-(3-nitro-5-(oct-7-yn-1-yloxy)phenyl)methanamine, (**121**)



To a solution of **107** (0.385 g, 1.398 mmol) in DCE (13.98 mL) was added methanamine (1.049 mL, 2.10 mmol) and acetic acid (0.024 mL, 0.420 mmol). The reaction mixture was stirred at room temperature for 1 h. Sodium triacetoxyhydroborate (0.889 g, 4.20 mmol) was added and the reaction mixture stirred at room temperature for 14 h. The reaction mixture was quenched with $NaHCO_3$ (50 mL) and extracted with EtOAc (3 x 50 mL). The combined organic extracts were washed with water (50 mL) and brine (20 mL), dried over Na_2SO_4, filtered and concentrated *in vacuo*. The crude product was adsorbed on silica and purified by flash chromatography eluting with 0-5% MeOH in CH_2Cl_2 to give **121** (0.285 g, 70%) as a yellow oil. ν_{max}/cm^{-1} 3299 (C≡C-H), 1623, 1581 (C=C), 1531, 1348 (N-O), 1280 (C-O), 1161, 1096, 1035 (C-N); ^{1}H NMR (400 MHz, $CDCl_3$) δ 7.77 (t, *J* = 1.7 Hz, 1H, C*H*(4)), 7.59 (t, *J* = 2.3 Hz, 1H, C*H*(6)), 7.21 (t, *J* = 1.8 Hz, 1H, C*H*(8)), 4.02 (t, *J* = 6.4 Hz, 2H, C*H*(9)), 3.80 (s, 2H, C*H*(2)), 2.45 (s, 3H, C*H*(1)), 2.21 (td, *J* = 6.9, 2.7 Hz, 2H, C*H*(14)), 1.95 (t, *J* = 2.6 Hz, 1H, C*H*(16)), 1.81 (m, 2H, C*H*(10)), 1.64 – 1.50 (m, 2H, C*H*(12)), 1.49 (m, 4H, C*H*(11,13)); ^{13}C NMR (101 MHz, $CDCl_3$) δ 159.8 (*C*(7)), 149.3 (*C*(5)), 143.4 (*C*(3)), 121.1 (*C*(8)), 115.3 (*C*(4)), 107.5 (*C*(6)), 84.6 (*C*(15)), 68.7 (*C*(16)), 68.4 (*C*(9)), 55.4 (*C*(2)), 36.1 (*C*(1)), 29.0 (*C*(10)), 28.5 (*C*(13), 28.4 (*C*(12)), 25.6 (*C*(11)), 18.5 (*C*(14)); LRMS (ESI$^+$) *m/z* 291.5 (M+H$^+$); HRMS (ESI$^+$): calcd for $C_{16}H_{23}N_2O_3^+$ [M+H]$^+$ 291.1703, found 291.1707.

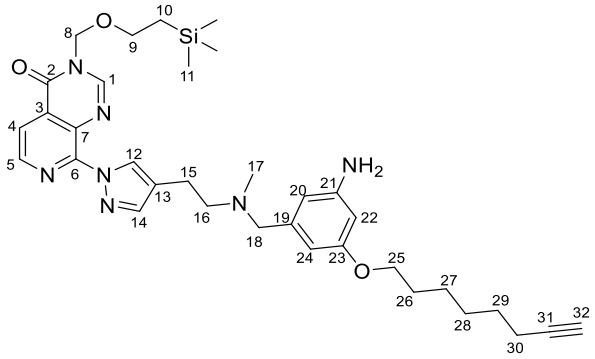
8-(4-(2-(methyl(3-nitro-5-(oct-7-yn-1-yloxy)benzyl)amino)ethyl)-1H-pyrazol-1-yl)-3-((2-(trimethylsilyl)ethoxy)methyl)pyrido[3,4-d]pyrimidin-4(3H)-one, (**122**)



To a solution of **50** (0.414 g, 0.889 mmol), potassium iodide (0.590 g, 3.55 mmol) and potassium carbonate (2.456 g, 17.77 mmol) in AcN (9 mL) was added **121** (0.258 g, 0.889 mmol) in AcN (9 mL). The reaction mixture was heated to 80 °C and stirred for 16 h. The reaction mixture was cooled to room temperature and quenched with $NaHCO_3$ (30 mL) and extracted with EtOAc (3 x 50 mL). The combined organic extracts were washed with brine (50 mL), dried over Na_2SO_4, filtered and concentrated *in vacuo*. The crude product was adsorbed on silica and purified by flash chromatography eluting with 0-10% MeOH in CH_2Cl_2 to give **122** (0.321 g, 55%) as a yellow oil. ν_{max}/cm^{-1} 3301 (N-H), 1690 (C=O), 1607, 1593, 1552 (C=C), 1530, 1347 (N-O), 1247, 1196 (C-O), 1152, 1070 (C-N) 857, 786 (C-H); ^{1}H NMR (400 MHz, $CDCl_3$) δ 8.62 (d, *J* = 5.1 Hz, 1H, C*H*(5)), 8.56 (d, *J* = 0.8 Hz, 1H, C*H*(12)), 8.30 (d, *J* = 7.2 Hz, 1H, C*H*(1)), 8.06 (d, *J* = 5.1 Hz, 1H, C*H*(4)), 7.79 (t, *J* = 1.7 Hz, 1H, C*H*(20)), 7.76 (d, *J* = 0.7 Hz, 1H, C*H*(12)), 7.57 (t, *J* = 2.3 Hz, 1H, C*H*(22)), 7.22 – 7.20 (m, 1H, C*H*(24)), 5.46 (s, 2H, C*H*(8)), 3.98 (t, *J* = 6.4 Hz, 2H, C*H*(25)), 3.74 – 3.65 (m, 2H, C*H*(9)), 3.60 (s, 2H, C*H*(18)), 2.85 – 2.76 (m, 2H, C*H*(15)), 2.75 – 2.67 (m, 2H, C*H*(16)), 2.30 (s, 3H, C*H*(17)), 2.22 – 2.11 (m, 2H, C*H*(30)), 1.95 (t, *J* = 2.6 Hz, 1H, C*H*(32)), 1.82 – 1.74 (m, 2H, C*H*(26)), 1.55 – 1.42 (m, 6H, C*H*(27, 28, 29)), 1.02 – 0.93 (m, 2H, C*H*(10)), 0.00 (s, 9H, C*H*(11)); ^{13}C NMR (101 MHz, $CDCl_3$) δ 159.7 (*C*(23)), 159.7 (*C*(2)), 149.3 (*C*(21)), 148.3 (*C*(6)), 147.1 (*C*(1)), 145.6 (*C*(5)), 143.2 (*C*(14)), 142.7 (*C*(19)), 134.7 (*C*(7)), 130.8 (*C*(12)), 130.4 (*C*(3)), 121.8 (*C*(24)), 121.7 (*C*(13)), 118.1 (*C*(4)), 115.9 (*C*(20)), 107.6 (*C*(22)), 84.6 (*C*(31)), 75.1 (*C*(8)), 68.7 (*C*(25)), 68.5 (*C*(32)), 68.1 (*C*(9)), 61.8 (*C*(18)), 58.3 (*C*(16)), 42.2 (*C*(17)), 29.0 (*C*(26)), 28.5 (*C*(28)), 28.4 (*C*(29)), 25.6 (*C*(27)), 22.7 (*C*(15)), 18.5

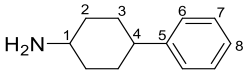
(*C*(30)), 18.2 (*C*(10)), -1.28 (*C*(11)); LRMS (ESI$^+$) *m/z* 660.9 (M+H$^+$); HRMS (ESI$^+$): calcd for $C_{34}H_{46}N_7O_5Si^+$ [M+H]$^+$ 660.3324, found 660.3326.

8-(4-(2-((3-amino-5-(oct-7-yn-1-yloxy)benzyl)(methyl)amino)ethyl)-1H-pyrazol-1-yl)-3-((2-(trimethylsilyl)ethoxy)methyl)pyrido[3,4-d]pyrimidin-4(3H)-one, (**123**)



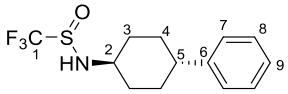
To a solution of **122** (315 mg, 0.477 mmol) in 2-Propanol (3 mL) and Water (1.5 mL) was added iron (160 mg, 2.86 mmol), ammonium chloride (1.021 g, 19.1 mmol) and formic acid (18 µl, 0.477 mmol). The reaction mixture was heated to 60 °C and stirred for 4 h. The reaction mixture was filtered through celite, washed with MeOH (100 mL) and the filtrate was concentrated *in vacuo*. The crude product was loaded onto an SCX-2 cartridge, washed with MeOH and the collected fractions were discarded. The cartridge was washed with 3.5N NH_3 in MeOH and the collected fractions were concentrated *in vacuo* to give **123** (202 mg, 67%) as a brown solid which was taken on crude into the next step. ν_{max}/cm^{-1} 3355 (N-H), 1694 (C=O), 1608, 1554 (C=C), 1249, 1188 (C-O), 1152, 1072 (C-N) 859, 804 (C-H); ^{1}H NMR (400 MHz, DMSO-d_6) δ 10.13 (s, 1H, N*H*), 8.62 (d, *J* = 5.1 Hz, 1H, C*H*(5)), 8.58 (s, 1H, C*H*(1)), 8.43 (s, 1H, C*H*(12)), 8.08 (d, *J* = 5.1 Hz, 1H, C*H*(4)), 7.75 (s, 1H, C*H*(14)), 6.41 – 6.13 (m, 3H, C*H*(20,22,24)), 5.41 (s, 2H, C*H*(8)), 4.02 (s, 1H), 3.84 (s, 2H, C*H*(25)), 3.66 (dd, *J* = 8.7, 7.5 Hz, 2H, C*H*(9)), 3.14 – 2.95 (m, 2H, C*H*(15)), 2.78 – 2.60 (m, 3H, C*H*(16,32)), 2.14 (td, *J* = 6.8, 2.7 Hz, 2H, C*H*(30)), 1.43 (d, *J* = 6.5 Hz, 1H), 1.65 (m, 2H, C*H*(26)), 1.54 – 1.35 (m, 6H, C*H*(27, 28, 29)), 0.94 – 0.84 (m, 2H, C*H*(10)), -0.03 (s, 9H, C*H*(11)); LRMS (ESI$^+$) *m/z* 630.8 (M+H$^+$).

4-phenylcyclohexan-1-amine, (**133**)



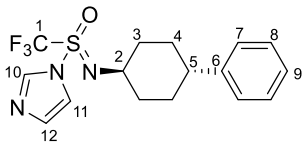
To a solution of 4-phenylcyclohexanone (4.8 g, 27.5 mmol) in MeOH (140 mL) under nitrogen at room temperature was added ammonium formate (17.3 g, 274 mmol) followed by the portionwise addition of sodium cyanoborohydride (1.774 g, 28.2 mmol). The reaction mixture was stirred at room temperature for 2 h. The solution was concentrated *in vacuo* and the residue was dissolved in CH_2Cl_2 (100 mL) and washed with 1M NaOH (2x100 mL). The organic layer was dried over $MgSO_4$, filtered and concentrated *in vacuo*. The crude product was purified by flash chromatography (0-10% 7M NH_3 in MeOH/CH_2Cl_2) to afford **133** (2.629 g, 54%). The product was taken on as a mixture of diastereomers into the next step.

1,1,1-trifluoro-*N*-((1r,4r)-4-phenylcyclohexyl)methanesulfinamide, (**134**)



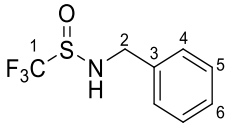
To a solution of sodium trifluoromethanesulfonate (1.425 g, 9.13 mmol) in EtOAc (10 mL) was added at room temperature, phosphoryl chloride (0.426 mL, 4.57 mmol). The resulting mixture was stirred for 5 min, then **133** (800 mg, 4.56 mmol) was added dropwise and the reaction mixture was stirred for an additional 30 min. The reaction mixture was washed with brine (20 mL) and extracted with ether (20 mL). The combined organic extracts were dried over $MgSO_4$, filtered and concentrated *in vacuo*. The crude product was purified by column chromatography (80 g silica) 0-10% EtOAc in heptane to yield **134** (308 mg, 23%) as a white solid; ^{1}H NMR (400 MHz, $CDCl_3$) δ 7.27 - 7.33 (m, 2H), 7.17 - 7.23 (m, 3H), 4.11 - 4.32 (m, 1H, N*H*), 3.40 - 3.50 (m, 1H, C*H*(2)), 2.46 - 2.62 (m, 1H), 2.16 - 2.24 (m, 2H), 1.87 - 2.04 (m, 2H), 1.56 - 1.65 (m, 1H), 1.42 - 1.53 (m, 1 H); ^{19}F NMR (377 MHz, $CDCl_3$) δ -78.45 (s, 1F); ^{13}C NMR (101 MHz, $CDCl_3$) δ 145.8 (*C*(6)), 128.5 (*C*(8)), 126.7 (*C*(7)), 126.3 (*C*(9)), 125.2 (*C*(1)), 121.9 (*C*(1)), 54.5 (*C*(2)), 43.1 (*C*(5)), 35.4 (*C*(3)), 32.8 (*C*(4)); LRMS (ESI^-) *m/z* 290.0 ($M-H^-$); HRMS (ESI^+): calcd for $C_{13}H_{17}F_3NOS^+$ $[M+H]^+$ 292.0983, found 292.0983.

1-(*N*-((1r,4r)-4-phenylcyclohexyl)-*S*-(trifluoromethyl)sulfonimidoyl)-1*H*-imidazole, (**135**)



To a solution of **134** (200 mg, 0.686 mmol) and *N*-chlorosuccinimide (101 mg, 0.755 mmol) in AcN (2 mL) at 0 °C was added tetrabutylammonium fluoride (1M in THF) (0.755 mL, 0.755 mmol). The reaction mixture was stirred for 30 min and concentrated *in vacuo*. Imidazole (280 mg, 4.119 mmol) and AcN (3.5 mL) was added and the reaction mixture was stirred at room temperature for 16 h. The reaction mixture was concentrated *in vacuo* and purified by flash chromatography eluting with 0-30% EtOAc in heptane to give **135** (64 mg, 26%); ^{1}H NMR (400 MHz, $CDCl_3$) δ 7.95 (s, 1H, C*H*(10)), 7.26 - 7.32 (m, 3H, C*H*(8,11)), 7.15 - 7.23 (m, 4H, C*H*(7,9,12)), 3.65 (tt, *J* = 11.4, 4.1 Hz, 1H, C*H*(2)), 2.52 (tt, *J* = 12.1, 3.6 Hz, 1H, C*H*(5)), 2.05 - 2.22 (m, 2H, C*H*(3/4)), 1.91 - 2.02 (m, 2H, C*H*(3/4)), 1.48 - 1.75 (m, 4H, C*H*(3/4)); ^{13}C NMR (101 MHz, $CDCl_3$) δ 146.1 (*C*(6)), 131.4 (*C*(12)), 128.4 (*C*(8)), 126.7 (*C*(7)), 126.2 (*C*(9)), 119.2 (*C*(1)), 55.4 (*C*(2)), 43.0 (*C*(5)), 36.1 (*C*(3)), 32.8 (*C*(4)); LRMS (ESI^+) *m*/*z* 358.2 ($M+H^+$); HRMS (ESI^-): calcd for $C_{16}H_{17}F_3N_3OS^-$ $[M-H]^-$ 356.1044, found 356.1042.

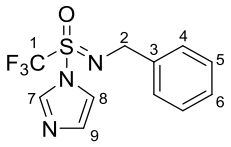
N-benzyl-1,1,1-trifluoromethanesulfinamide, (**138**)



To a 250 mL round bottom flask at 0 °C was added a solution of trifluoromethane sulfonyl chloride (1 mL, 9.39 mmol) in CH_2Cl_2 (30 mL) and a solution of triphenylphosphine (2.464 g, 9.39 mmol), benzylamine (1.026 mL, 9.39 mmol) and triethylamine (2.611 mL, 18.8 mmol) in CH_2Cl_2 (30 mL) using syringe pump at the same rate over 1 h. The solution was concentrated *in vacuo*. The crude product was purified by flash chromatography eluting with 0-20% EtOAc in heptane to give **138** (859 mg, 41%) as a colourless oil; ^{1}H NMR (400 MHz, $CDCl_3$) δ 7.29 - 7.51 (m, 5H, C*H*(4,5,6)), 4.45 - 4.64 (m, 2H, C*H*(2)+N*H*), 4.22 - 4.40 (m, 1H, C*H*(2)); ^{13}C NMR (101 MHz, $CDCl_3$) δ 136.5 (*C*(3))), 129.0,

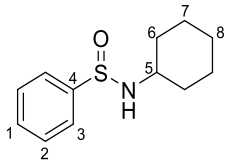
128.4, 128.1 (*C*(4,5,6), 125.4, 122.0 (*C*(1)), 46.5 (*C*(2)); LRMS (ESI^-) *m/z* 221.9 ($M\text{-}H^-$); HRMS (ESI^+): calcd for $C_8H_9F_3NOS^+$ $[M+H]^+$ 224.0357, found 224.0354.

1-(*N*-benzyl-S-(trifluoromethyl)sulfonimidoyl)-1*H*-imidazole, (**139**)



To a solution of **138** (300 mg, 1.344 mmol) and *N*-chlorosuccinimide (197 mg, 1.478 mmol) in AcN (7 mL) at 0 °C was added tetrabutylammonium fluoride (1M in THF) (1.478 mL, 1.478 mmol). The reaction mixture was stirred for 1 h and the solution concentrated *in vacuo*. Imidazole (549 mg, 8.06 mmol) and AcN (7 mL) was added and the reaction mixture stirred at room temperature for 3 h. The reaction mixture was concentrated *in vacuo*. The crude product was purified by flash chromatography eluting with 0-30% EtOAc in heptane to give **139** (112 mg, 29%) as a colourless oil; ^1H NMR (400 MHz, $CDCl_3$) δ 7.82 (s, 1H, C*H*(7)), 7.28 - 7.38 (m, 5H, C*H*(4,5,6), 7.17 (s, 1H, C*H*(8)), 7.13 (s, 1H, C*H*(9)), 4.56 (d, *J* = 19.1 Hz, 2H, C*H*(2)); ^{13}C NMR (101 MHz, $CDCl_3$) δ 138.2 (*C*(7)), 137.3 (*C*(3)), 131.5 (*C*(9)), 128.8, 127.9, 127.3 (*C*(4,5,6)), 123.6, 120.4, 117.2, 114.0 (*C*(1)), 118.9 (*C*(8)), 46.7 (*C*(2)); LRMS (ESI^+) *m/z* 290.1 ($M+H^+$); HRMS (ESI^-): calcd for $C_{11}H_9F_3N_3OS^-$ $[M-H]^-$ 288.0419, found 288.0421.

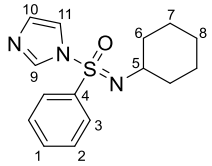
N-cyclohexylbenzenesulfinamide, (**142**)



To a solution of benzene sulfonyl chloride (1.083 mL, 8.49 mmol) and triethylamine (11.8 mL, 84.9 mmol) in CH_2Cl_2 (40 mL) at 0 °C was added a solution of triphenylphosphine (2.226 g, 8.49 mmol) and cyclohexylamine (0.971 mL, 8.49 mmol) in CH_2Cl_2 (10 mL) by syringe pump over 1 h. The

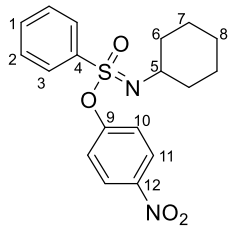
reaction mixture was concentrated *in vacuo*. The crude product was purified by flash chromatography eluting with 0-20% EtOAc in heptane to give **142** (1.252 g, 66%) as a white solid; ^{1}H NMR (400 MHz, $CDCl_3$) δ 7.64 - 7.74 (m, 2H, C*H*(3)), 7.40 - 7.60 (m, 3H, C*H*(1,2)), 3.89 (br d, *J* = 5.9 Hz, 1 H, N*H*), 3.16 - 3.39 (m, 1 H, C*H*(5)), 2.06 - 2.22 (m, 1 H, C*H*(6)), 1.85 - 1.53 (m, 4H, C*H*(6, 7)), 1.35 – 1.10 (m, 5H, C*H*(6, 7, 8); ^{13}C NMR (101 MHz, $CDCl_3$) δ 145.5 (*C*(4)), 130.7 (*C*(1)), 128.7 (*C*(2)), 125.7 (*C*(3)), 53.1 (*C*(5)), 35.2, 34.9 (*C*(6)), 25.4, 24.8, 24.7 (*C*(7,8)); LRMS (ESI$^+$) *m/z* 224.1 (M+H$^+$); HRMS (ESI$^+$): calcd for $C_{12}H_{18}NOS^+$ [M+H]$^+$ 224.1109, found 224.1111.

1-(*N*-cyclohexylphenylsulfonimidoyl)-1H-imidazole, (**143**)



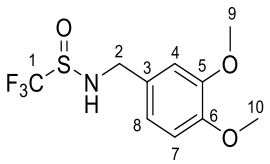
To a solution of **142** (200 mg, 0.895 mmol) and *N*-chlorosuccinimide (132 mg, 0.985 mmol) in AcN (5 mL) at 0 °C was tetrabutylammonium fluoride (1M in THF) (0.985 mL, 0.985 mmol). The reaction mixture was stirred for 1 h and the solution concentrated *in vacuo*. Imidazole (366 mg, 5.37 mmol) and AcN (2 mL) were added and the reaction mixture stirred at 60 °C for 30 h. The reaction mixture was concentrated *in vacuo* and the crude product was purified by column chromatography eluting with 0-50% EtOAc in heptane to give **143** (75 mg, 29%) as a white solid. ^{1}H NMR (400 MHz, $CDCl_3$) δ 7.96 - 8.03 (m, 2H, Ar*H*), 7.93 (t, *J* = 1.0 Hz, 1H, C*H*(9)), 7.52 - 7.60 (m, 1H, Ar*H*), 7.44 - 7.52 (m, 2H, Ar*H*), 7.19 - 7.27 (m, 1H, C*H*(11)), 7.04 (s, 1H, C*H*(10)), 3.44 - 3.53 (m, 1H, C*H*(5)), 1.94 - 2.01 (m, 1H, C*H*(6)), 1.70 - 1.89 (m, 3H, C*H*(6)), 1.41 - 1.60 (m, 2H, C*H*(7)), 1.12 - 1.37 (m, 4H, C*H*(7+8)); LRMS (ESI$^+$) *m/z* 290.2 (M+H$^+$); HRMS (ESI$^+$): calcd for $C_{15}H_{19}N_3OS^+$ [M+H]$^+$ 289.1249, found 289.1249.

4-nitrophenyl N-cyclohexylbenzenesulfonimidate



To a solution of **142** and *N*-chlorosuccinimide (66 mg, 0.493 mmol) in AcN (2 mL) was added tetrabutylammonium fluoride (1M in THF) (0.493 mL, 0.493 mmol) at 0 °C. The reaction mixture was stirred at room temperature for 30 min. The solution was concentrated *in vacuo* and 4-nitrophenol (249 mg, 1.791 mmol) and AcN (2 mL) were added. The reaction mixture was heated at reflux for 16 h. The reaction mixture was concentrated *in vacuo* and the crude product was purified by flash chromatography eluting with 0-20% EtOAc in heptane to give 4-nitrophenyl N-cyclohexylbenzenesulfonimidate (55 mg, 34%) as a colourless oil; ^{1}H NMR (400 MHz, $CDCl_3$) δ 8.12 (m, 2H, C*H*(11)), 7.94 (m, 2H, C*H*(3)), 7.57 - 7.65 (m, 1H, C*H*(1)), 7.43 - 7.54 (m, 2H, C*H*(2)), 7.12 - 7.01 (m, 2H, C*H*(10)), 3.85 - 3.76 (m, 1 H, C*H*(5)), 2.04 – 1.86 (m, 2H, C*H*(6)), 1.84 - 1.73 (m, 2H, C*H*(7)), 1.65 - 1.57 (m, 1H, C*H*(8)), 1.52 - 1.45 (m, 2H, C*H*(6)) 1.43 - 1.33 (m, 2 H, C*H*(7)); ^{13}C NMR (101 MHz, $CDCl_3$) δ 156.6 (*C*(12)), 145.1 (*C*(9)), 137.5 (*C*(4)), 133.5 (*C*(1)), 129.0 (*C*(2)), 128.0 (*C*(3)), 125.1 (*C*(11)), 122.9 (*C*(10)), 53.9 (*C*(5)), 36.0, 35.8, 25.6 (*C*(8)), 24.9; LRMS (ESI$^+$) m/z 361.2 ($M+H^+$).

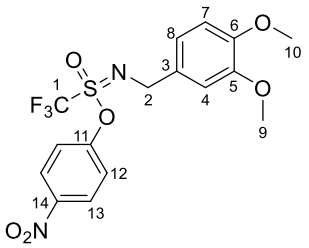
N-(3,4-dimethoxybenzyl)-1,1,1-trifluoromethanesulfinamide, (**151**)



To a 250 mL round bottom flask at 0 °C was added a solution of trifluorosulfonyl chloride **149** (1.059 mL, 9.95 mmol) in CH_2Cl_2 (30 mL) and a solution of triphenylphosphine (2.609 g, 9.95 mmol), triethylamine (2.766 mL, 19.9 mmol) and 3,4-dimethoxybenzylamine (1.5 mL, 9.95 mmol) in CH_2Cl_2 (30 mL) using a syringe pump at the same rate over an hour. The reaction mixture was concentrated

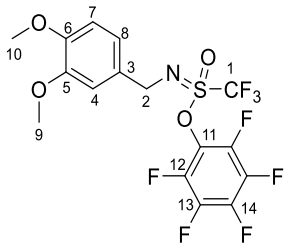
in vacuo and purified by flash chromatography eluting with 0-30% EtOAc in heptane to give **151** (1.338 g, 47%); ^{1}H NMR (400 MHz, $CDCl_3$) δ 6.54 - 6.94 (m, 3H) 4.53 - 4.67 (m, 1H) 4.39 - 4.51 (m, 1H) 4.18 - 4.32 (m, 1H) 3.88 (s, 6H); ^{13}C NMR (101 MHz, $CDCl_3$) δ 149.4, 149.1 (*C*(9,10)), 129.0 (C), 120.6 (*C*(8)), 128.7, 125.4, 122.1, 118.7 (*C*(1)), 111.3 (*C*(4,7)), 55.9 (*C*(9,10)), 46.3 (*C*(2)); LRMS (ESI^-) *m/z* 282.0 ($M\text{-}H^-$); HRMS (ESI^+): calcd for $C_{10}H_{16}F_3N_2O_3S^+$ $[M+NH_4]^+$ 301.0834, found 301.0836.

4-nitrophenyl-*N*-(3,4-dimethoxybenzyl)trifluoromethanesulfonimidate, (**152**)



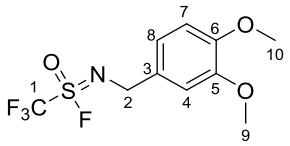
To a solution of 4-nitrophenol (491 mg, 3.53 mmol) in THF (15 mL) was added KO^{t}Bu (1M in THF) (3.53 mL, 3.53 mmol). The reaction mixture was stirred at room temperature for 20 min. The reaction mixture was concentrated *in vacuo* to give the potassium salt. To a solution of the sulfinamide **151** (500 mg, 1.765 mmol) and *N*-chlorosuccinimide (259 mg, 1.94 mmol) in AcN (8 mL) at 0 °C was added tetrabutylammonium fluoride (1M in THF) (1.942 mL, 1.94 mmol). The reaction mixture was stirred for 30 min and concentrated *in vacuo*. AcN (8 mL) was added and the solution was added to the potassium salt and stirred at room temperature for 2 h. The reaction mixture was concentrated *in vacuo*. The crude product was purified by flash chromatography eluting with 0-20% EtOAc in heptane to give **152** (498 mg, 67%); ^{1}H NMR (400 MHz, $CDCl_3$) δ 8.18 - 8.22 (m, 2H, C*H*(13)), 7.22 (d, *J*=9.4 Hz, 2H, C*H*(12)), 6.75 (s, 3H, C*H*(4, 7, 8)), 4.46 (d, *J*=3.7 Hz, 2H, C*H*(2)), 3.88 (s, 3H, C*H*(9/10)), 3.84 (s, 3H, C*H*(9/10)); ^{19}F NMR (377 MHz, $CDCl_3$) δ -73.93 (s, 3F); ^{13}C NMR (101 MHz, $CDCl_3$) δ 153.3 (*C*(11)), 149.1, 148.7 (*C*(5,6)), 146.3 (*C*(14)), 130.8 (*C*(3)), 125.4 (*C*(13)), 123.9 (*C*(12)), 119.7 (*C*(8)), 123.2, 120.7, 117.5, 114.3 (*C*(1)), 111.0, 110.9 (*C*(4,7)), 56.0, 55.8 (*C*(9,10)), 47.8 (*C*(2)); LRMS (ESI^-) *m/z* 419.0 ($M\text{-}H^-$); HRMS (ESI^-): calcd for $C_{16}H_{14}F_3N_2O_6S^-$ $[M\text{-}H]^-$ 419.0525, found 419.0527.

perfluorophenyl *N*-(3,4-dimethoxybenzyl)trifluoromethanesulfonimidate, (**155**)



To a solution of pentafluorophenol (1.222 g, 6.639 mmol) in THF (30 mL) was added 1M KO^{t}Bu in THF (5.975 mL, 5.975 mmol). The reaction mixture was stirred at room temperature for 20 min and concentrated *in vacuo* to give the potassium salt. A solution of **151** (200 mg, 0.664 mmol) in AcN (4 mL) was added the potassium salt and was stirred at room temperature for 14 h. The reaction mixture was concentrated *in vacuo*, diluted with CH_2Cl_2 and filtered. The filtrate was concentrated *in vacuo* and purified by flash chromatography eluting with 0-6% EtOAc in heptane to give **155** (244 mg, 67%). ^{1}H NMR (400 MHz, $CDCl_3$) δ 6.72 - 6.81 (m, 3H, C*H*(4,7,8)) 4.41 - 4.60 (m, 2H, C*H*(2)) 3.88 (s, 3H, C*H*(9/10)) 3.87 (s, 3H, C*H*(9/10)); ^{13}C NMR (101 MHz, $CDCl_3$) δ 149.1, 148.7 (*C*(5/6)), 143.0, 141.6, 140.6, 139.0, 136.5 (*C*()), 130.3 (*C*(3)), 123.5, 120.3, 117.1, 113.9 (*C*(1)), 119.5 (*C*(8)) 111.0, 110.4 (*C*(4/7)) 55.9, 55.8 (*C*(9/10)) 47.2 (*C*(2)); ^{19}F NMR (377 MHz, $CDCl_3$) δ -73.93, -151.3, -155.4, -161.0; LRMS (ESI$^-$) *m/z* 463.9 (M-H$^-$); HRMS (ESI$^-$): calcd for $C_{16}H_{10}F_8NO_4S^-$ [M-H]$^-$ 464.0203, found 464.0213.

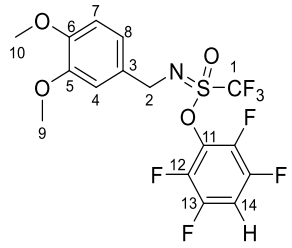
N-(3,4-dimethoxybenzyl)-1,1,1-trifluoromethanesulfonimidoyl fluoride, (**157**)



To a solution of **151** (3.451 g, 12.183 mmol) and *N*-chlorosuccinimide (1.789 g, 13.401 mmol) in AcN (82 mL) at 0 °C was added tetrabutylammonium fluoride (1M in THF) (13.4 mL, 13.401 mmol). The reaction mixture was stirred for 30 min and concentrated *in vacuo*. The crude product was purified by flash chromatography eluting with 0-5% EtOAc in heptane to give **157** (3.246 g, 88%) as a

colourless oil; ^{1}H NMR (400 MHz, $CDCl_3$) δ 6.85 (m, 3H, C*H*(4,7,8)), 4.57 (d, *J* = 9.0 Hz, 2H, C*H*(2)), 3.89 (s, 3H, C*H*(9/10)), 3.88 (s, 3H, C*H*(9/10)); ^{19}F NMR (377 MHz, $CDCl_3$) δ 64.43 (dtd, *J* = 33.8, 17.0, 17.0, 8.5 Hz, 1F) -73.09 (d, *J* = 17.1 Hz, 3F); ^{13}C NMR (101 MHz, $CDCl_3$) δ 149.1, 148.7 (*C*(5,6)), 129.7 (*C*(3)), 118.1 (dd, *J* = 323.2, 70.7 Hz, 1C, *C*(1)), 111.1, 110.5 (*C*(4,7)), 55.9, 55.8 (*C*(9,10)), 47.4, 47.3 (*C*(2)).

2,3,5,6-tetrafluorophenyl *N*-(3,4-dimethoxybenzyl)trifluoromethanesulfonimidate, (**158**)



The reaction mixture was split into 5 vials. To a solution of 2,3,5,6-tetrafluorophenol (13.3 g, 80.2 mmol) in THF (500 mL) was added KO^{t}Bu (1M in THF) (70 mL, 69.7 mmol). The reaction mixture was stirred at room temperature for 30 min. The reaction mixture was concentrated *in vacuo* to give the potassium salt. A solution of **157** (3 g, 9.96 mmol) in AcN (50 mL) was added to the potassium salt and the reaction mixture was stirred at room temperature for 14 h. The reaction mixture was concentrated *in vacuo*. The crude product was dissolved in CH_2Cl_2, filtered and the filtrate was concentrated *in vacuo*. The crude product was purified by flash chromatography eluting with 0-10% EtOAc in heptane to give **158** (3.008 g, 68%); Mp 73 – 77 °C; ^{1}H NMR (400 MHz, $CDCl_3$) δ 7.03 – 6.94 (m, 1H, C*H*(14)), 6.80 - 6.74 (m, 3H, C*H*(4,7,8)), 4.60 - 4.45 (m, 2H, C*H*(2)), 3.87 (s, 3H, C*H*(9/10)), 3.85 (s, 3H, C*H*(9/10)); ^{19}F NMR (377 MHz, $CDCl_3$) δ -73.5 (s, 3F), -137.7 (d, *J* = 15.1 Hz, 2F), -151.6 (d, *J* = 37.7 Hz, 2F); ^{13}C NMR (101 MHz, $CDCl_3$) δ 149.0, 148.5 (*C*(5,6)), 145.9 (*C*(13)), 141.1 (*C*(12)), 139.8 (11)), 130.45 (*C*(3)), 118.7 (q, *J* = 323.2, 1C, *C*(1)), 119.5 (*C*(8)), 111.0, 110.3 (*C*(4,7)), 104.5 (*C*(14)), 55.9, 55.7 (*C*(9,10)) 47.1 (*C*(2)); LRMS (ESI$^-$) *m/z* 446.1 (M-H$^-$); HRMS (ESI$^-$): calcd for $C_{16}H_{12}F_7NO_4S^-$ [M-H]$^-$ 446.0297, found 446.0300.

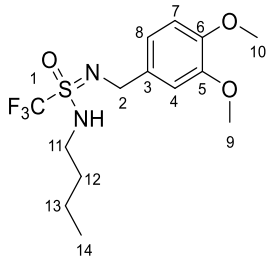
General Procedures for Sulfonimidamides

General Procedures. *Procedure A*; To a solution of transfer reagent **158** (1 equiv.) in DMF (0.1 M) was added amine (2 equiv.). The reaction was stirred at room temperature. After completion, the reaction mixture was concentrated *in vacuo* and then purified by flash chromatography to afford the product.

Procedure B; To a solution of transfer reagent **158** (1 equiv.) in DMF (0.1 M) was added amine (2 equiv.). The reaction was stirred at 50 °C. After completion, the reaction mixture was concentrated *in vacuo* and then purified by flash chromatography to afford the product.

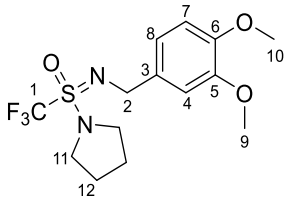
Synthesis of Sulfonimidamides

N-butyl-*N*'-(3,4-dimethoxybenzyl)-1,1,1-trifluoromethanesulfonimidamide, (**153**)



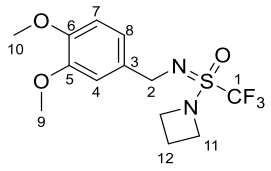
Prepared following Procedure A using **158** (250 mg, 0.559 mmol) and butylamine (110 µL, 1.12 mmol) and stirring at room temperature for 1 h. Column chromatography (25 g silica, 0-15% EtOAc in heptane) yielded **153** (157 mg, 79%) as a colourless oil; ^{1}H NMR (400 MHz, $CDCl_3$) δ 6.78 - 6.94 (m, 3H, C*H*(4,7,8)), 4.41 - 4.52 (br s, 1H, N*H*), 4.29 - 4.41 (m, 2H, C*H*(2)), 3.90 (s, 3H, C*H*(9/10)), 3.88 (s, 3H, C*H*(9/10)), 3.12 - 3.30 (m, 2H, C*H*(11)), 1.55 (m, 2H, C*H*(12)), 1.30 - 1.44 (m, 2H, C*H*(13)), 0.92 (t, *J* = 7.5 Hz, 3H, C*H*(14)); ^{19}F NMR (377 MHz, $CDCl_3$) δ -75.2 (s); ^{13}C NMR (101 MHz, $CDCl_3$) δ 149.2, 148.4 (*C*(5,6)) 131.3 (*C*(3)), 119.6 (*C*(8)), 120.5 (q, *J* = 328.3 Hz, 1C, *C*(1)), 111.2, 110.8 (*C*(4,7)) 56.0, 55.8 (*C*(9/10)), 46.4 (*C*(2)), 43.4 (*C*(11)), 33.0 (*C*(12)), 19.7 (*C*(13)), 13.6 (*C*(14)); LRMS (ESI^-) *m/z* 353.1 ($M\text{-}H^-$); HRMS (ESI^-): calcd for $C_{14}H_{20}F_3N_2O_3S^-$ $[M\text{-}H]^-$ 353.1147, found 353.1146.

1-(*N*-(3,4-dimethoxybenzyl)-*S*-(trifluoromethyl)sulfonimidoyl)pyrrolidine, (**156**)



Prepared following Procedure A using **158** (250 mg, 0.559 mmol) and pyrrolidine (0.093 mL, 1.118 mmol) and stirring at room temperature for 1 h. Column chromatography (25 g silica, 0-20% EtOAc in heptane) yielded **156** (163 mg, 83%) as a colourless oil; ^{1}H NMR (400 MHz, $CDCl_3$) δ 6.95 (m, 1H, C*H*(4)), 6.97 - 6.92 (m, 1H, C*H*(8)), 6.83 - 6.80 (m, 1H, C*H*(7)), 4.43 - 4.24 (m, 2H, C*H*(2)), 3.88 (s, 3H, C*H*(9/10)), 3.86 (s, 3H, C*H*(9/10)), 3.58 - 3.28 (m, 4H, C*H*(11)), 1.93 (m, 4H C*H*(12)); ^{19}F NMR (377 MHz, $CDCl_3$) δ -72.5 (s); ^{13}C NMR (101 MHz, $CDCl_3$) δ 148.9, 148.0 (*C*(5,6)), 132.7 (*C*(3)), 121.1 (q, *J* = 329.3 Hz, 1C, *C*(1)), 119.2 (C(8)), 111.0, 110.7 (*C*(4,7)), 56.0, 55.8 (*C*(9,10)), 48.8 (*C*(11)), 45.5 (*C*(2)), 25.9 (*C*(12)); LRMS (ESI^-) *m/z* 353.1 ($M+H^+$); HRMS (ESI^-): calcd for $C_{14}H_{18}F_3N_2O_3S^-$ $[M-H]^-$ 351.0990, found 351.1006.

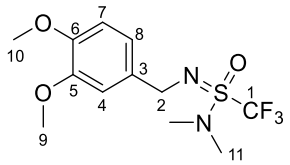
1-(*N*-(3,4-dimethoxybenzyl)-*S*-(trifluoromethyl)sulfonimidoyl)azetidine, (**159**)



Prepared following Procedure A using **158** (200 mg, 0.447 mmol) and azetidine (0.060 mL, 0.894 mmol) and stirring at room temperature for 1 h. Column chromatography (25 g silica, 0-20% EtOAc in heptane) yielded **159** (126 mg, 83%) as a colourless oil; ^{1}H NMR (400 MHz, $CDCl_3$) δ 6.93 (m, 1H, C*H*(4)), 6.92 - 6.88 (m, 1H, C*H*(8)), 6.84 - 6.81 (m, 1H, C*H*(7)), 4.35 (d, *J*=8.1 Hz, 2H, C*H*(2)), 4.11 (m, 4H, C*H*(11)), 3.89 (s, 3H, C*H*(9/10)), 3.87 (s, 3H, C*H*(9/10)), 2.33 - 2.24 (m, 2H, C*H*(12)); ^{13}C NMR (101 MHz, $CDCl_3$) δ 148.9, 148.0 (*C*(5,6)), 132.8 (*C*(3)), 120.9 (q, *J* = 329.3 Hz, 1C, *C*(1)), 119.2 (*C*(8)), 111.0 (*C*(7)), 110.7 (*C*(4)), 56.0, 55.8 (*C*(9,10)), 52.1 (*C*(11)), 45.7 (*C*(2)), 15.0 (*C*(12)); ^{19}F NMR (377 MHz,

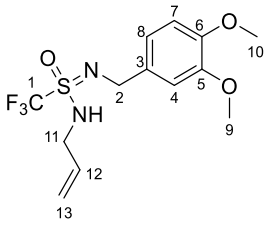
$CDCl_3$) δ -72.56 (s); LRMS (ESI^-) *m/z* 337.1 ($M\text{-}H^-$); HRMS (ESI^-): calcd for $C_{13}H_{16}F_3N_2O_3S^-$ $[M\text{-}H]^-$ 337.0834, found 337.0831.

N'-(3,4-dimethoxybenzyl)-1,1,1-trifluoro-*N*,*N*-dimethylmethanesulfonimidamide, (**160**)



Prepared following Procedure B using **158** (200 mg, 0.447 mmol) and dimethylamine (2M in THF) (0.447 mL, 0.894 mmol) and stirring at 50 °C for 21 h. Column chromatography (25 g silica, 0-20% EtOAc in heptane) yielded **160** (100 mg, 69%) as a colourless oil; ^1H NMR (400 MHz, $CDCl_3$) δ 6.92 - 6.97 (m, 1H, C*H*(4)), 6.86 - 6.91 (m, 1H, C*H*(8)), 6.78 - 6.86 (m, 1H, C*H*(7)) 4.17 - 4.40 (m, 2H, C*H*(2)) 3.88 (s, 3H, C*H*(9/10)), 3.87 (s, 3H, C*H*(9/10)), 3.01 – 2.98 (m, 6H, C*H*(11)); ^{19}F NMR (377 MHz, $CDCl_3$) δ -72.81 (s); ^{13}C NMR (101 MHz, $CDCl_3$) δ 148.9, 148.0 (*C*(5,6)), 132.5 (*C*(3)), 120.7 (q, *J*=327.2 Hz, 1C, *C*(1)), 119.3 (*C*(8)), 111.0, 110.7 (*C*(4,7)), 56.0, 55.8 (*C*(9,10)), 45.2 (*C*(2)), 38.4 (*C*(11)); LRMS (ESI^+) *m/z* 327.1 ($M+H^+$); HRMS (ESI^-): calcd for $C_{12}H_{16}F_3N_2O_3S^-$ $[M\text{-}H]^-$ 325.0834, found 325.0837.

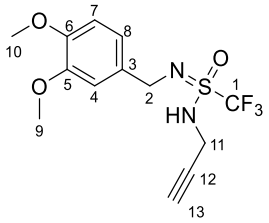
N-allyl-*N*'-(3,4-dimethoxybenzyl)-1,1,1-trifluoromethanesulfonimidamide, (**161**)



Prepared following Procedure A using **158** (250 mg, 0.559 mmol) and allylamine (0.084 mL, 1.118 mmol) and stirring at room temperature for 17 h. Column chromatography (25 g silica, 0-20% EtOAc in heptane) yielded **161** (154 mg, 81%) as a colourless oil; ^1H NMR (400 MHz, $CDCl_3$) δ 6.89 – 6.82 (m, 3H, C*H*(4,7,8)), 5.82 - 5.92 (m, 1H, C*H*(12)), 5.27 (dd, *J* = 17.1, 1.2 Hz, 1H, C*H*(13_t)), 5.15 (dd, *J* =

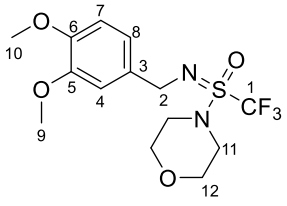
10.4, 1.4 Hz, 1H, C*H*(13$_c$)), 4.71 (s, 1H, N*H*), 4.34 (d, *J* = 6.9 Hz, 2H, C*H*(2)), 3.89 (s, 3H, C*H*(9/10)), 3.88 (s, 3H, C*H*(9/10)), 3.85 - 3.82 (m, 2H, C*H*(11)); ^{13}C NMR (101 MHz, $CDCl_3$) δ 149.2, 148.6 (*C*(5,6)), 134.4 (*C*(12)), 130.6 (*C*(3)), 120.4 (q, *J*=327.2 Hz, 1C, *C*(1)), 119.7 (*C*(8)), 116.7 (*C*(13)), 111.2, 110.8 (*C*(4,7), 56.0, 55.9 (*C*(9/10)), 46.7 (*C*(2)), 45.6 (*C*(11)); ^{19}F NMR (377 MHz, $CDCl_3$) δ -75.43 (F), LRMS (ESI^+) *m/z* 337.1 ($M+H^+$); HRMS (ESI^-): calcd for $C_{13}H_{16}F_3N_2O_3S^-$ $[M-H]^-$ 337.0834, found 337.0838.

N'-(3,4-dimethoxybenzyl)-1,1,1-trifluoro-*N*-(prop-2-yn-1-yl)methanesulfonimidamide, (**162**)



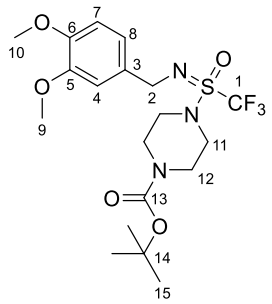
Prepared following Procedure B using **158** (200 mg, 0.447 mmol) and propargyl amine (0.057 mL, 0.894 mmol) and stirring at 50 °C for 21 h. Column chromatography (25 g silica, 0-20% EtOAc in heptane) yielded **162** (109 mg, 72%) as a colourless oil; ^{1}H NMR (400 MHz, $CDCl_3$) δ 6.89 – 6.81 (d, *J* = 14.7 Hz, 3H, C*H*(4,7,8)), 4.95 - 5.03 (m, 1H), 4.36 (d, *J* = 9.7 Hz, 2H, C*H*(2)), 3.92 - 4.12 (m, 2H, C*H*(11)), 3.88 (s, 3H, C*H*(9/10)), 3.87 (s, 3H, C*H*(9/10)), 2.28 (t, *J* = 2.5 Hz, 1H, C*H*(13)); ^{19}F NMR (377 MHz, $CDCl_3$) δ -75.68 (s); ^{13}C NMR (101 MHz, $CDCl_3$) δ 149.3, 148.9 (*C*(5,6)), 129.4 (C), 120.1 (q, *J* = 328.3 Hz, 1C, *C*(1)), 120.1 (*C*(8)), 111.2, 111.0 (*C*(4,6)), 80.2 (*C*(12)), 71.9 (*C*(13)), 56.0, 55.9 (*C*(9,10)), 47.4 (*C*(2)), 32.1 (*C*(11)); LRMS (ESI^-) *m/z* 335.0 ($M-H^-$); HRMS (ESI^-): calcd for $C_{13}H_{14}F_3N_2O_3S^-$ $[M-H]^-$ 335.0677, found 335.0684.

4-(*N*-(3,4-dimethoxybenzyl)-*S*-(trifluoromethyl)sulfonimidoyl)morpholine, (**163**)



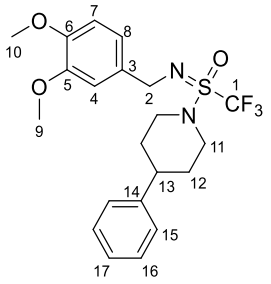
Prepared following Procedure B using **158** (200 mg, 0.447 mmol) and morpholine (0.078 mL, 0.894 mmol) and stirring at 50 °C for 27 h. Column chromatography (25 g silica, 0-20% EtOAc in heptane) yielded **163** (112 mg, 68%) as a colourless oil; ^{1}H NMR (400 MHz, $CDCl_3$) δ 6.93 (d, *J* = 2.0 Hz, 1H, C*H*(4)), 6.87 - 6.91 (m, 1H, C*H*(8)), 6.80 - 6.84 (m, 1H, C*H*(7)), 4.33 (d, *J* = 15.6 Hz, 2H, C*H*(2)), 3.88 (s, 3H, C*H*(9/10)) 3.87 (s, 3H, C*H*(9/10)), 3.66 - 3.63 (m, 4H, C*H*(12)), 3.49 - 3.34 (m, 4H, C*H*(11)); ^{19}F NMR (377 MHz, $CDCl_3$) δ -73.46 (s); ^{13}C NMR (101 MHz, $CDCl_3$) δ 149.0, 148.2 (*C*(5,6)), 132.2 (*C*(3)), 120.4 (q, *J* = 327.2 Hz, 1C, *C*(1)), 119.4 (*C*(8)) 111.1, 110.8 (*C*(4,7)), 66.5 (*C*(12)), 56.0, 55.9 (*C*(9,10)), 46.9 (*C*(11)), 45.4 (*C*(2)); LRMS (ESI^-) *m/z* 367.2 ($M\text{-}H^-$); HRMS (ESI^-): calcd for $C_{14}H_{18}F_3N_2O_4S^-$ $[M\text{-}H]^-$ 367.0939, found 367.0919.

tert-butyl-4-(N-(3,4-dimethoxybenzyl)-*S*-(trifluoromethyl)sulfonimidoyl)piperazine-1-carboxylate, (164)



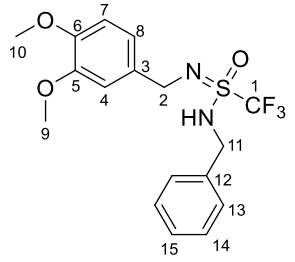
Prepared following Procedure B using **158** (200 mg, 0.447 mmol) and 1-(*tert*-butoxycarbonyl)piperazine (167 mg, 0.894 mmol) and stirring at 50 °C for 40 h. Column chromatography (25 g silica, 0-20% EtOAc in heptane) yielded **164** (101 mg, 48%) as a colourless oil; ^{1}H NMR (400 MHz, $CDCl_3$) δ 6.93 - 6.91 (m, 1H, C*H*(4)), 6.90 - 6.87 (m, 1H, C*H*(8)), 6.84 - 6.81 (m, 1H, C*H*(7)), 4.40 - 4.26 (m, 2H, C*H*(2)), 3.88 (s, 3H, C*H*(9/10)), 3.87 (s, 3H, C*H*(9/10)), 3.28 - 3.51 (s, 8H, C*H*(11,12)), 1.46 (s, 9H, C*H*(15)); ^{19}F NMR (377 MHz, $CDCl_3$) δ -73.8 (s); ^{13}C NMR (101 MHz, $CDCl_3$) δ 154.2 (*C*(13)), 149.0, 148.1 (*C*(5,6)), 132.1 (*C*(3)), 120.4 (q, *J* = 327.2 Hz, 1C, *C*(1)), 119.3 (*C*(8)), 111.0, 110.8 (*C*(4,7)), 80.6 (*C*(14)), 55.9 (*C*(9,10)), 46.7 (*C*(12)), 45.4 (*C*(2)), 28.3 (*C*(15)); LRMS (ESI^-) *m/z* 466.1 ($M\text{-}H^-$); HRMS (ESI^-): calcd for $C_{19}H_{27}F_3N_3O_5S^-$ $[M\text{-}H]^-$ 466.1624, found 466.1615.

1-(*N*-(3,4-dimethoxybenzyl)-*S*-(trifluoromethyl)sulfonimidoyl)-4-phenylpiperidine, (**165**)



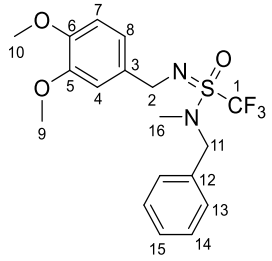
Prepared following Procedure B using **158** (200 mg, 0.447 mmol) and 4-phenylpiperidine (144 mg, 0.894 mmol) and stirring at 50 °C for 4 h. Column chromatography (25 g silica, 0-15% EtOAc in heptane) yielded **165** (170 mg, 86%) as a colourless oil; ^{1}H NMR (400 MHz, $CDCl_3$) δ 7.35 - 7.29 (m, 2H, C*H*(16)), 7.25 - 7.20 (m, 1H, C*H*(17)), 7.18 - 7.15 (m, 2H, C*H*(15)), 6.98 - 6.96 (m, 1H, C*H*(4)), 6.94 - 6.90 (m, 1H, C*H*(8)), 6.84 - 6.81 (m, 1H, C*H*(7)), 4.35 (d, *J*=15.8 Hz, 2H, C*H*(2)), 4.15 - 4.02 (m, 2H, C*H*(11)), 3.89 (s, 3H, C*H*(9/10)) 3.86 (s, 3H, C*H*(9/10)), 3.03 (br t, *J* = 12.3 Hz, 2H, C*H*(11)), 2.63 (tt, *J* = 12.2, 3.5 Hz, 1H, C*H*(13)), 1.95 – 1.80 (m, 2H, C*H*(12)), 1.72 (qd, *J* = 12.7, 4.3 Hz, 1H, C*H*(12)), 1.60 - 1.49 (m, 1H, C*H*(12)); ^{13}C NMR (101 MHz, $CDCl_3$) δ 149.0, 148.1 (*C*(5,6)), 144.6 (C(14)), 132.5 (*C*(3)), 128.6 (*C*(16)), 126.7, 126.6 (*C*(15,17)), 120.5 (q, *J*=326.2 Hz, 1C, *C*(1)), 119.4 (*C*(8)), 111.1, 110.9 (*C*(4,7)), 55.9, 55.8 (*C*(9,10)), 47.7, 47.5 (*C*(11)), 45.4 (*C*(2)), 41.9 (*C*(13)), 33.2, 32.9 (*C*(12)); ^{19}F NMR (377 MHz, $CDCl_3$) δ -73.9 (s); LRMS (ESI^+) *m/z* 443.1 ($M+H^+$); HRMS (ESI^-): calcd for $C_{21}H_{24}F_3N_2O_3S^-$ $[M-H]^-$ 441.1460, found 441.1439.

N-benzyl-*N*'-(3,4-dimethoxybenzyl)-1,1,1-trifluoromethanesulfonimidamide, (**166**)



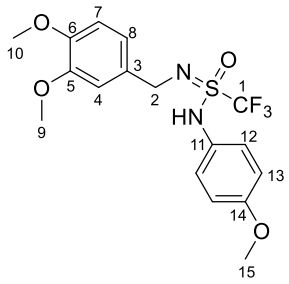
Prepared following Procedure B using **158** (200 mg, 0.447 mmol) and benzylamine (0.098 mL, 0.894 mmol) and stirring at room temperature for 22 h. Column chromatography (25 g silica, 0-20% EtOAc in heptane) yielded **166** (133 mg, 77%) as a colourless oil; ^{1}H NMR (400 MHz, $CDCl_3$) δ 7.35 - 7.24 (m, 5H, C*H*(13,14,15)), 6.77 - 6.87 (m, 3H, C*H*(4,7,8)) 4.42 - 4.25 (m, 4H, C*H*(2,11)), 3.86 (s, 3H, C*H*(9/10)), 3.83 (s, 3H, C*H*(9/10)); ^{19}F NMR (377 MHz, $CDCl_3$) δ -75.16 (s); ^{13}C NMR (101 MHz, $CDCl_3$) δ 149.2, 148.7 (*C*(5,6)), 138.1 (*C*(12)), 130.4 (*C*(3)), 128.7, 127.6, 127.4 (*C*(13,14,15)), 120.5 (q, *J* = 327.2 Hz, 1C, *C*(1)), 119.8 (*C*(8)), 111.2, 110.9 (*C*(4,7)), 56.0, 55.8 (*C*(9,10)), 46.9 (*C*(2,11)); LRMS (ESI$^-$) *m/z* 387.1 (M-H$^-$); HRMS (ESI$^-$): calcd for $C_{17}H_{19}F_3N_2O_3S^-$ [M-H]$^-$ 387.0990, found 387.0995.

N-benzyl-*N*'-(3,4-dimethoxybenzyl)-1,1,1-trifluoro-N-methylmethanesulfonimidamide, (**167**)



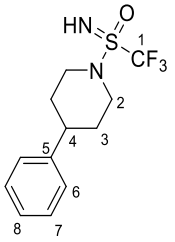
Prepared following Procedure B using **158** (200 mg, 0.447 mmol) and *N*-methylbenzylamine (0.115 mL, 0.939 g/mL, 0.894 mmol) and stirring at 50 °C for 48 h. Column chromatography (25 g silica, 0-15% EtOAc in heptane) yielded **167** (88 mg, 49%) and **158** (50 mg, 25%) as a colourless oil; ^{1}H NMR (400 MHz, $CDCl_3$) δ 7.41 - 7.28 (m, 5H, C*H*(13,14,15)), 6.93 - 6.91 (m, 1H, C*H*(4)), 6.89 - 6.86 (m, 1H, C*H*(8)), 6.80 - 6.77 (m, 1H, C*H*(7)), 4.66 - 4.61 (m, 1H, C*H*(11)) 4.44 - 4.28 (m, 3H, C*H*(2,11)), 3.85 (s, 3H, C*H*(9/10)), 3.83 (s, 3H, C*H*(9/10)), 2.84 (s, 3H, C*H*(16)); ^{19}F NMR (377 MHz, $CDCl_3$) δ -73.15 (s); ^{13}C NMR (101 MHz, $CDCl_3$) δ 148.9, 148.0 (*C*(5,6)), 135.4 (*C*(12)), 132.4 (*C*(3)), 128.8, 128.2, 128.1 (*C*(13,14,15)), 120.8 (q, *J*=328.3 Hz, 1C, (*C*(1)), 119.3 (*C*(8)), 111.0, 110.7 (*C*(4,7)), 55.9, 55.8 (*C*(9,10)), 54.8 (*C*(11)), 45.4 (*C*(2)), 35.0 (*C*(16)); LRMS (ESI$^+$) *m/z* 403.2 (M+H$^+$); HRMS (ESI$^-$): calcd for $C_{18}H_{20}F_3N_2O_3S^-$ [M-H]$^-$ 401.1147, found 401.1147.

N'-(3,4-dimethoxybenzyl)-1,1,1-trifluoro-*N*-(4-methoxyphenyl)methanesulfonimidamide, (**168**)



Prepared following Procedure B using **158** (200 mg, 0.447 mmol) and *p*-anisidine (0.110 g, 0.894 mmol) and stirring at 50 °C for 6 days. Column chromatography (25 g silica, 0-20% EtOAc in heptane) yielded **168** (32 mg, 18%) and **158** (127 mg, 64%) as a colourless oil; ^{1}H NMR (400 MHz, $CDCl_3$) δ 7.07 - 7.04 (m, 2H), 6.82 - 6.77 (m, 4H), 6.72 - 6.70 (m, 1H), 4.37 (d, *J* = 4.4 Hz, 2H), 3.86 (s, 3H) 3.79 (s, 3H), 3.77 (s, 3H); ^{19}F NMR (377 MHz, $CDCl_3$) δ -75.12 (s); ^{13}C NMR (101 MHz, $CDCl_3$) δ 156.2 (*C*(14)), 149.2 (*C*(5,6)), 132.87 (*C*(3)), 128.2 (*C*(11)), 120.3 (q, *J* = 323.3 Hz, 1C, *C*(1)), 124.8 (*C*(12)), 120.5 (*C*(8)), 114.6 (*C*(13)), 111.2, 111.0 (*C*(4,7)), 56.0 (*C*(15)), 55.9, 55.5 (*C*(9,10)), 48.4 (*C*(2)); LRMS (ESI^-) *m/z* 403.1 ($M\text{-}H^-$); HRMS (ESI^-): calcd for $C_{17}H_{18}F_3N_2O_4S^-$ $[M\text{-}H]^-$ 403.0940, found 403.0944.

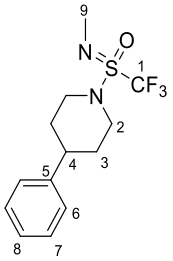
4-phenyl-1-(*S*-(trifluoromethyl)sulfonimidoyl)piperidine, (**169**)



To a solution of **165** (100 mg, 0.226 mmol) in AcN (2 mL) and distilled water (1 mL) at 0 °C was added ceric ammonium nitrate (310 mg, 0.565 mmol). The reaction mixture was stirred for 30 min and diluted with water (20 mL) and extracted with EtOAc (3 x 15 mL). The combined organic extracts were dried over $MgSO_4$, filtered and concentrated *in vacuo*. The crude product was purified by flash chromatography eluting with 0-15% EtOAc in heptane to give **169** (48 mg, 73%) as a colourless oil; ^{1}H NMR (400 MHz, $CDCl_3$) δ 7.35 – 7.30 (m, 2H, C*H*(7)), 7.27 - 7.18 (m, 3H, C*H*(6,8)), 4.29 - 4.16 (m,

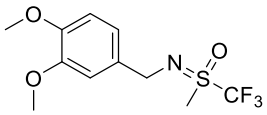
2H, C*H*(2)), 3.15 – 2.98 (m, 3H, C*H*(2)+N*H*), 2.73 - 2.64 (m, 1H, C*H*(4)), 1.99 – 1.92 (m, 2H, C*H*(3)), 1.85 - 1.73 (m, 2H, C*H*(3)); ^{13}C NMR (101 MHz, $CDCl_3$) δ 144.5 (*C*(5)), 128.7 (*C*(7)), 126.7, 126.7 (*C*(6,8)), 121.0 (q, *J*=328.2 Hz, 1C, *C*(1)), 48.0, 47.1 (*C*(2)), 41.9 (*C*(4)), 33.2, 33.1 (*C*(3)); ^{19}F NMR (377 MHz, $CDCl_3$) δ -75.4 (s); LRMS (ESI^+) *m/z* 293.2 ($M+H^+$); HRMS (ESI^-): calcd for $C_{12}H_{14}F_3N_2OS^-$ $[M-H]^-$ 291.0779, found 291.0784.

1-(*N*-methyl-*S*-(trifluoromethyl)sulfonimidoyl)-4-phenylpiperidine, (**170**)



To a solution of **169** (65 mg, 0.222 mmol) in THF (1.48 mL) was added NaH (60% dispersion in mineral oil) (26.7 mg, 0.667 mmol) at 0 °C. The reaction mixture was stirred for 30 min. MeI (0.138 mL, 2.224 mmol) was added and the solution was stirred at room temperature for 20 h. The reaction mixture was diluted with CH_2Cl_2 (10 mL) and washed with water. The aqueous layer was back-extracted with CH_2Cl_2 (3 x 10 mL). The combined organic extracts were dried over $MgSO_4$, filtered and concentrated *in vacuo*. The crude product was purified by flash chromatography eluting with 0-15% EtOAc in heptane to give **170** (34 mg, 74%); ^{1}H NMR (400 MHz, $CDCl_3$) δ 7.35 – 7.30 (m, 2H, C*H*(7)), 7.25 - 7.19 (m, 3H, C*H*(6,8)) 4.14 – 4.04 (m, 2H, C*H*(2)), 3.13 – 3.04 (br t, *J* = 12.3 Hz, 2H, C*H*(2)), 2.88 (s, 3H, C*H*(9)), 2.72 – 2.68 (m, 1H, C*H*(4)), 1.99 - 1.92 (m, 2H, C*H*(3)), 1.85 - 1.71 (m, 2H, C*H*(3)); ^{13}C NMR (101 MHz, $CDCl_3$) δ 144.6 (*C*(5)), 128.7 (*C*(7)), 126.7, 126.7 (C(6,8)), 120.5 (q, *J* = 326.2 Hz, 1C, (*C*(1)), 47.6, 47.3 (*C*(2)), 42.0 (C), 33.3, 33.1 (*C*(3)), 27.9 (*C*(9)); ^{19}F NMR (377 MHz, $CDCl_3$) δ -73.61 (s); LRMS (ESI^+) *m/z* 307.1 ($M+H^+$); HRMS (ESI^+): calcd for $C_{13}H_{18}F_3N_2OS^+$ $[M+H]^+$ 307.1092, found 307.1095.

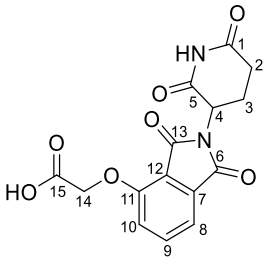
((3,4-dimethoxybenzyl)imino)(methyl)(trifluoromethyl)- λ^6-sulfanone, (**171**)



To a solution of **158** in THF (1 mL) at -78 °C was added methyl lithium (1.6M in THF) (0.14 mL, 0.224 mmol). The reaction mixture was stirred for 15 min. The reaction mixture was washed with saturated ammonium chloride (20 mL) and extracted with CH_2Cl_2 (3 x 15 mL). The combined organics were dried over $MgSO_4$, filtered, concentrated *in vacuo*. The crude product was purified by flash chromatography eluting with 0-20% EtOAc in heptane to **171** (20 mg, 60%); ^{1}H NMR (400 MHz, $CDCl_3$) δ 6.90 - 6.81 (m, 3H, C*H*(4,7,8)), 4.45 - 4.38 (m, 1H, C*H*(2)), 4.24 - 4.17 (m, 1H, C*H*(2)), 3.89 (s, 3H, C*H*(9/10)), 3.87 (s, 3H, C*H*(9/10)), 3.09 (d, *J* = 0.7 Hz, 3H, C*H*(11)); ^{19}F NMR (377 MHz, $CDCl_3$) δ -74.71 (s); ^{13}C NMR (101 MHz, $CDCl_3$) δ 149.0, 148.2 (*C*(5,6)), 132.1 (*C*(3)), 121.4 (q, *J*=341.4 Hz, 1C, (*C*(1))), 119.7 (*C*(8)), 111.1, 110.9 (*C*(4,7)), 56.0, 55.8 (*C*(9,10)), 46.7 (*C*(2)), 37.7 (*C*(11)); LRMS (ESI^+) *m/z* 298.1 ($M+H^+$); HRMS (ESI^-): calcd for $C_{11}H_{13}F_3NO_3S^-$ $[M-H]^-$ 296.0568, found 296.0556.

Synthesis of PROTAC compounds

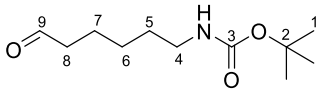
2-((2-(2,6-dioxopiperidin-3-yl)-1,3-dioxoisoindolin-4-yl)oxy)acetic acid, (**177**)



To a solution of **176** (556 mg, 1.32 mmol) in EtOAc:CH_2Cl_2 5:2 (12 mL) was added Palladium on carbon 10% w/w (560 mg, 0.527 mmol) followed by an atmosphere of hydrogen. The reaction mixture was stirred for 3 h. The mixture was diluted with 5 mL MeOH and heated to reflux. The reaction mixture was filtered through Celite and washed with hot methanol (50 mL). The filtrate was concentrated *in vacuo* to give **177** (405 mg, 93%). Mp 166 – 168 °C; ν_{max}/cm^{-1} 3224 (N-H), 1694,

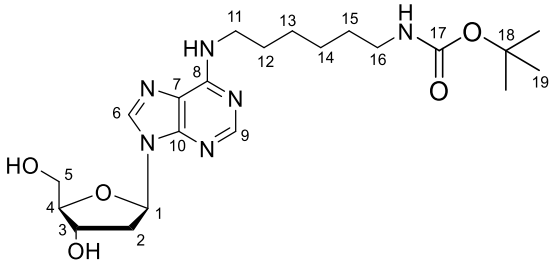
1613 (C=O), 1484 (C=C), 1193 (C-N), 1121 (C-O); ^{1}H NMR (400 MHz, DMSO-d_6) δ 11.12 (s, 1H), 7.77 (dd, *J* = 8.5, 7.2 Hz, 1H, C*H*(9)), 7.45 (d, *J* = 7.2 Hz, 1H, C*H*(8)), 7.36 (d, *J* = 8.6 Hz, 1H, C*H*(10)), 5.10 (dd, *J* = 12.9, 5.4 Hz, 1H, C*H*(4)), 4.91 (s, 2H, C*H*(14)), 2.89 (ddd, *J* = 17.2, 14.0, 5.4 Hz, 1H, C*H*(2)), 2.63 – 2.47 (m, 2H, C*H*(2+3)), 2.12 – 1.97 (m, 1H, C*H*(3)); ^{13}C NMR (101 MHz, DMSO) δ 172.9 (*C*(1)), 170.0 (*C*(5)), 169.6 (*C*(15)), 166.8 (*C*(6)), 165.3 (*C*(13)) 155.4 (*C*(11)), 136.7 (*C*(9)), 133.2 (*C*(7)), 119.9 (*C*(10)), 116.2 (*C*(12)), 115.6 (*C*(8)), 65.4 (*C*(14)), 48.8 (*C*(4)), 31.0 (*C*(2)), 22.0 (*C*(3)); LRMS (ESI$^+$) *m/z* 333.5 (M+H$^+$); HRMS (ESI$^+$): calcd for $C_{15}H_{13}N_2O_7^+$ [M+H]$^+$ 333.0717, found 333.0720.

tert-butyl (6-oxohexyl)carbamate, (**179**)



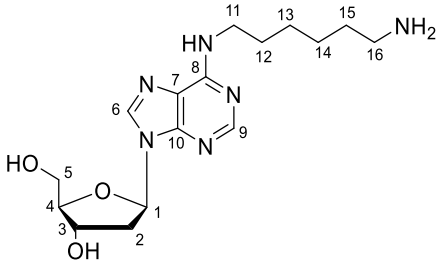
A solution of oxalyl dichloride (0.350 g, 2.76 mmol) in CH_2Cl_2 (20 mL) at -78 °C was treated with (methylsulfinyl)methane (0.449 g, 5.75 mmol) and stirred for 5 min. A solution of *tert*-butyl (6-hydroxyhexyl)carbamate **178** (0.5 g, 2.301 mmol) in CH_2Cl_2 (10 mL) was added, stirred for 15 min and triethylamine (1.604 mL, 11.50 mmol) was added. The reaction mixture was warmed to room temperature and stirred for 1 h. The reaction mixture was partitioned between water (30 mL) and CH_2Cl_2 (75 mL). The organic layer was washed with brine (30 mL), dried over Na_2SO_4, filtered and concentrated *in vacuo*. The crude product was adsorbed on silica and purified by flash chromatography eluting with 0-20% EtOAc in cyclohexane to give **179** (0.260 g, 53%) as a colourless oil. ν_{max}/cm^{-1} 3351 (N-H), 1686 (C=O), 1248, 1164 (C-N); ^{1}H NMR (400 MHz, $CDCl_3$) δ 9.76 (t, *J* = 1.7 Hz, 1H, C*H*(9)), 4.52 (m, 1H, N*H*), 3.11 (q, *J* = 6.7 Hz, 2H, C*H*(4)), 2.43 (td, *J* = 7.3, 1.7 Hz, 2H, C*H*(8)), 1.69 – 1.56 (m, 2H, C*H*(7)), 1.49 (m, 3H, C*H*(5)), 1.43 (s, 9H, C*H*(1)), 1.38 – 1.29 (m, 2H, C*H*(6)); ^{13}C NMR (101 MHz, $CDCl_3$) δ 202.6 (*C*(9)), 156.1 (*C*(2)), 79.3 (*C*(2)), 43.9 (*C*(8)), 40.5 (*C*(4)), 30.0 (*C*(5)), 28.6 (*C*(1)), 26.4 (*C*(6)), 21.8 (*C*(7)); LRMS (ESI$^+$) *m/z* 216.5 (M+H$^+$).

tert-butyl (6-((9-((2*R*,4*S*,5*R*)-4-hydroxy-5-(hydroxymethyl)tetrahydrofuran-2-yl)-9H-purin-6-yl) amino)hexyl)carbamate, (**181**)



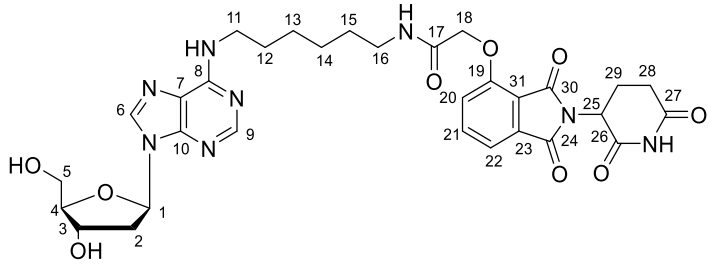
To a solution of 2'-deoxyadenosine **180** (0.767 g, 3.05 mmol), *tert*-butyl (6-oxohexyl)carbamate **179** (1.972g, 9.16 mmol) in MeOH (30 mL) was added acetic acid (0.524 mL, 9.16 mmol). The reaction mixture was heated to reflux for 16 h. The reaction mixture was cooled and quenched with $NaHCO_3$ (50 mL) and extracted with EtOAc (2 x 75 mL). The combined organic extracts were washed with brine (50mL), dried over Na_2SO_4, filtered and concentrated *in vacuo*. To a solution of imine in DCE (18 mL) was added $NaBH_4$ (0.578 g, 15.27 mmol) at 0 °C. The reaction mixture was heated to 50 °C and stirred for 18 h. The reaction mixture was quenched with $NaHCO_3$ (50 mL) and extracted with EtOAc (2 x 75 mL). The combined organic extracts were washed with brine (50mL), dried over Na_2SO_4, filtered and concentrated *in vacuo*. The crude product was adsorbed on silica and purified by flash chromatography eluting with 0-8% MeOH in CH_2Cl_2 to give **181** (0.179 g, 13%) as a white solid. ν_{max}/cm^{-1} 3317 (O-H), 1686 (C=O), 1622 (C=N), 1247, 1164 (C-N) 1098 (C-O); ^{1}H NMR (400 MHz, $CDCl_3$) δ 8.31 (d, *J* = 8.7 Hz, 1H, C*H*(6)), 8.19 (s, 1H, C*H*(9)), 7.77 (s, 1H, N*H*), 6.36 – 6.31 (m, 1H, C*H*(1)), 6.11 (s, 1H, N*H*), 4.78 (d, *J* = 5.0 Hz, 1H, C*H*(3)), 4.57 (t, *J* = 5.9 Hz, 1H), 4.22 (m, 1H, C*H*(4)), 3.97 (dd, *J* = 12.9, 1.7 Hz, 1H, C*H*(5)), 3.76 (d, *J* = 29.1 Hz, 1H, C*H*(5)), 3.66 – 3.58 (m, 2H), 3.08 (dtt, *J* = 13.4, 9.5, 4.4 Hz, 3H), 2.30 (dd, *J* = 13.4, 5.6 Hz, 1H, C*H*(2)), 2.02 (d, *J* = 16.3 Hz, 2H), 1.66 (q, *J* = 7.3 Hz, 2H, C*H*(12)), 1.53 – 1.35 (m, 2H, C*H*(15)), 1.43 (s, 9H, C*H*(19)), 1.35 (s, 4H, C*H*(13,14)); ^{13}C NMR (101 MHz, $CDCl_3$) δ 156.2 (*C*(17)), 155.4 (*C*(8)), 152.7 (*C*(9)), 147.4 (*C*(10)), 139.5 (*C*(6)), 121.5 (*C*(7)), 89.9 (*C*(4)), 88.0 (*C*(1)), 79.2 (*C*(18)), 73.5 (*C*(3)), 63.6 (*C*(5)), 41.0 (*C*(2)), 40.6 (*C*(11+16)), 30.1 (*C*(15)), 29.6 (*C*(12)), 28.6 (*C*(19)), 26.6, 26.5 (*C*(13+14); LRMS (ESI$^+$) *m/z* 451.7 ($M+H^+$); HRMS (ESI$^+$): calcd for $C_{21}H_{35}N_6O_5^+$ $[M+H]^+$ 451.2669, found 451.2662.

(2*R*,3S,5R)-5-(6-((6-aminohexyl)amino)-9H-purin-9-yl)-2-(hydroxymethyl)tetrahydrofuran-3-ol, (**182**)



To a microwave vial was added **181** (113 mg, 0.251 mmol) in 1,1,1,3,3,3-hexafluoropropan-2-ol (2 mL). The vial was heated in the MW at 150 °C for 2 h. The reaction mixture was concentrated *in vacuo* to give **182** (87 mg, quant.). The reaction was taken on crude into the next step. ^{1}H NMR (400 MHz, DMSO-d_6) δ 8.32 (s, 1H, C*H*(6)), 8.19 (s, 1H, C*H*(9)), 7.84 (s, 1H, N*H*), 6.35 (dd, *J* = 7.9, 6.1 Hz, 1H, C*H*(1)), 4.42 (dt, *J* = 5.6, 2.7 Hz, 1H, C*H*(3)), 3.89 (td, *J* = 4.2, 2.4 Hz, 1H, C*H*(4)), 3.63 (dd, *J* = 11.9, 4.3 Hz, 1H, C*H*(5)), 3.53 (dd, *J* = 11.9, 4.2 Hz, 1H, C*H*(5)), 3.44 (m, 2H, C*H*(11)), 2.92 – 2.86 (m, 1H), 2.78 – 2.67 (m, 1H), 2.49 (m, 2H, C*H*(16)), 2.26 (ddd, *J* = 13.1, 6.1, 2.9 Hz, 1H, C*H*(2)), 1.63 – 1.54 (m, 2H, C*H*(12)), 1.33 – 1.28 (m, 6H, C*H*(13,14,15)); LRMS (ESI$^+$) *m*/*z* 351.7 (M+H$^+$).

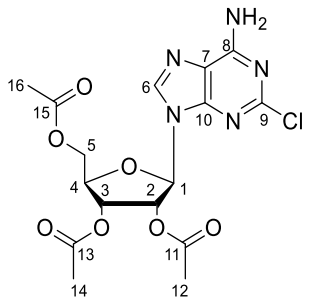
2-((2-(2,6-dioxopiperidin-3-yl)-1,3-dioxoisoindolin-4-yl)oxy)-*N*-(6-((9-((2*R*,4*S*,5*R*)-4-hydroxy-5-(hydroxymethyl)tetrahydrofuran-2-yl)-9H-purin-6-yl)amino)hexyl)acetamide, (**174**)



To a solution of **177** (30 mg, 0.089 mmol) and HATU (42 mg, 0.111 mmol) in DMF (0.5 mL) was added *N*-methylmorpholine (33 µl, 0.297 mmol). The solution was stirred at room temperature for 30 min. A solution of **182** (26 mg, 0.074 mmol) in DMF (0.5 mL) was added and the solution was stirred at room temperature for 18 h. The reaction mixture was diluted with EtOAc (4 mL) and washed with water (40 mL). The aqueous layer was back-extracted with EtOAc (2 x 40 mL). The combined organic extracts were dried over Na_2SO_4, filtered and concentrated *in vacuo*. The crude

product was adsorbed on silica and purified by flash chromatography eluting with 0-10% MeOH to CH_2Cl_2 to give **174** (7 mg, 14%). ν_{max}/cm^{-1} 3200 (O-H), 1725, 1697, 1648 (C=O), 1597, 1560 (C=C), 1619 (C=N), 1263, 1177, 1045 (C-N) 1235, 1124, 1091 (C-O); ^{1}H NMR (400 MHz, DMSO-d_6) δ 11.11 (s, 1H, N*H*), 8.31 (s, 1H, C*H*(6)), 8.16 (d, *J* = 15.0 Hz, 1H, C*H*(9)), 7.93 (t, *J* = 5.7 Hz, 1H, N*H*), 7.84 – 7.75 (m, 2H, C*H*(21), N*H*), 7.48 (d, *J* = 7.2 Hz, 1H, C*H*(22)), 7.38 (d, *J* = 8.5 Hz, 1H, C*H*(20)), 6.34 (dd, *J* = 7.9, 6.0 Hz, 1H, C*H*(1)), 5.30 (s, 1H, OH), 5.24 (s, 1H, OH), 5.11 (dd, *J* = 12.9, 5.4 Hz, 1H, C*H*(25)), 4.76 (s, 2H, C*H*(18)), 4.40 (d, *J* = 4.6 Hz, 1H, C*H*(3)), 3.88 (td, *J* = 4.2, 2.4 Hz, 1H, C*H*(4)), 3.66 – 3.58 (m, 1H, C*H*(5)), 3.55 – 3.47 (m, 1H, C*H*(5)), 3.47 – 3.42 (m, 2H, C*H*(11)), 3.19 – 3.08 (m, 2H, C*H*(16)), 2.96 – 2.82 (m, 1H, C*H*(28)), 2.78 – 2.66 (m, 1H, C*H*(2)), 2.65 – 2.51 (m, 2H, C*H*(28,29)), 2.25 (ddd, *J* = 13.1, 6.1, 2.8 Hz, 1H, C*H*(2)), 2.11 – 1.98 (m, 1H, C*H*(29)), 1.57 (m, 2H, C*H*(12)), 1.43 (d, *J* = 7.8 Hz, 2H, C*H*(15)), 1.33 – 1.26 (m, 4H, C*H*(13,14)), 1.24 (d, *J* = 6.4 Hz, 1H); ^{13}C NMR (101 MHz, DMSO) δ 172.8 (*C*(27)), 166.6 (*C*(17)), 169.9, 166.7, 165.5 (*C*(24,26,30)), 155.1 (*C*(8,19)), 152.3 (*C*(9)), 147.7 (*C*(10)), 139.2 (*C*(6)), 136.9 (*C*(21)), 133.0 (*C*(23)), 120.4 (*C*(20)), 119.5 (C(7)), 116.8 (*C*(31)), 116.0 (*C*(22)), 88.0 (*C*(4)), 83.9 (*C*(1)), 71.0 (*C*(3)), 67.6 (*C*(18)), 61.9 (*C*(5)), 48.8 (*C*(25)), 39.7 (*C*(2,11)), 38.3 (*C*(16)), 30.9 (*C*(28)), 29.3 (C(12,15)), 26.1 (*C*(13,14)), 22.0 (*C*(29)); LRMS (ESI$^+$) m/z 665.9 (M+H$^+$);

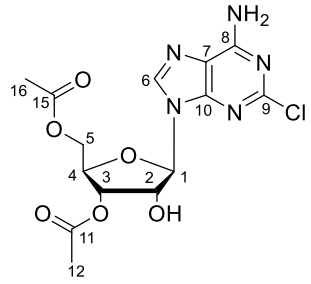
2’, 3’ 5’-O-triacetyl-2-chloroadenosine, (**187**)



187 was synthesised via literature procedure.[171] Acetic anhydride (1.908 mL, 20.22 mmol) was added to a suspension of 2-chloroadenosine **186** (2 g, 6.63 mmol), 4-(dimethylamino)pyridine (0.061 g, 0.497 mmol), triethylamine (3.7 mL, 26.5 mmol) in AcN (5 mL). The mixture was stirred and heated to 50 °C for 10 min. The reaction mixture was quenched with MeOH and concentrated

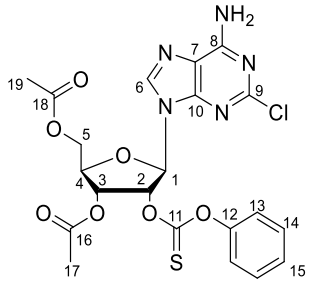
in vacuo. EtOAc (150 mL) was added and washed with water (5 x 75 mL). The combined organic extracts were dried over Na_2SO_4, filtered and concentrated *in vacuo*. The crude oil was triturated with EtOH (5 mL) and a white solid **187** (2.414 g, 85%) was collected. Mp 139 – 141 °C; ν_{max}/cm^{-1} 3401 (N-H), 1740, 1653 (C=O), 1599, 1568 (C=C), 1305 (C-N) 1212, 1170, 1095 (C-O), 558 (C-Cl); ^{1}H NMR (400 MHz, DMSO-d_6) δ 8.38 (s, 1H, C*H*(6)), 7.94 (s, 2H, NH_2), 6.15 (d, *J* = 5.5 Hz, 1H, C*H*(1)), 5.88 (t, *J* = 5.7 Hz, 1H, C*H*(2)), 5.62 – 5.54 (m, 1H, C*H*(3)), 4.41 – 4.33 (m, 2H, C*H*(4,5)), 4.28 – 4.22 (m, 1H, C*H*(5)), 2.12 (s, 3H), 2.05 (s, 3H), 2.02 (s, 3H); ^{13}C NMR (101 MHz, DMSO) δ 170.1 (*C*(15)), 169.5, 169.3 (C(11,13)), 156.9 (*C*(8)), 153.3 (*C*(9)), 150.1 (*C*(10)), 140.3 (*C*(6)), 118.2 (*C*(7)), 85.4 (*C*(1)), 79.5 (*C*(4)), 72.1 (*C*(2)), 69.9 (*C*(3)), 62.7 (*C*(5)), 20.5, 20.4, 20.2 (*C*(12,14,16); LRMS (ESI$^+$) *m/z* 428.3 (M+H$^+$); HRMS (ESI$^+$): calcd for $C_{16}H_{19}ClN_5O_7^+$ [M+H]$^+$ 428.0979, found 428.0968.

((2*R*,3*S*,4*R*,5*R*)-3-acetoxy-5-(6-amino-2-chloro-9H-purin-9-yl)-4-hydroxytetrahydrofuran-2-yl)methyl acetate, (**188**)



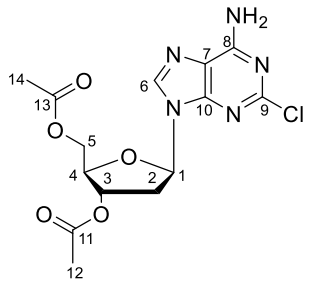
188 was synthesised via literature procedure.[171] A suspension of hydroxylamine hydrochloride (0.999 g, 14.4 mmol) and anhydrous sodium acetate (1.007 g, 12.3 mmol) in Pyridine (39 mL) was stirred at 0 °C for 30 min. **187** (5 g, 11.7 mmol) was added in one portion to the stirred solution. The mixture became clear at which time it was kept in the chiller at 0 °C for 22 h. The reaction mixture was concentrated *in vacuo*, azeotroping with toluene three times. The crude oil was purified by flash chromatography eluting with 0-4% MeOH in CH_2Cl_2. The collected fractions were concentrated *in vacuo* to give **188** (2.997 g, 67%) in a 3:1 ratio of product:impurity **189** (deacetylation on 3' position) and **187** (1.588 g, 32%). The mixture was taken on crude into the next step.

((2*R*,3*R*,4*R*,5*R*)-3-acetoxy-5-(6-amino-2-chloro-9H-purin-9-yl)-4-((phenoxycarbonothioyl)oxy) tetrahydrofuran-2-yl)methyl acetate, (**190**)



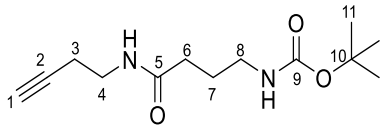
190 was synthesised via literature procedure.[171] To a solution of **188**/**189** (3:1) (2.006 g, 5.20 mmol), and 4-(dimethylamino)pyridine (1.379 g, 11.3 mmol) in AcN (25 mL) was added O-phenyl carbonochloridothioate (0.834 mL, 6.03 mmol). The reaction mixture was stirred at room temperature for 2 h. The reaction mixture was concentrated *in vacuo*. The crude oil was dissolved in EtOAc (30 mL) and washed with water (20 mL). The aqueous layer was back-extracted with EtOAc (2 x 30 mL). The combined organics were washed with 0.5N HCl (2 x 25 mL), brine (25 mL). The combined organic extracts were dried over Na_2SO_4, filtered and concentrated *in vacuo*. The crude product was purified by flash chromatography and eluted with 0-50% EtOAc in Cyclohexane to give **190** (1.6 g, 59%). Mp 70 – 71 °C; ν_{max}/cm^{-1} 3320 (N-H), 1745, 1640 (C=O), 1590 (C=C), 1345 (C-N) 1195, 1098 (C-O), 688 (C-Cl); ^{1}H NMR (400 MHz, DMSO-d_6) δ 8.41 (s, 1H, C*H*(6)), 7.97 (s, 2H), 7.47 (dd, *J* = 8.5, 7.3 Hz, 2H), 7.41 – 7.21 (m, 1H, C*H*(15)), 7.22 – 7.09 (m, 2H), 6.41 (d, *J* = 4.8 Hz, 1H, C*H*(1)), 6.37 (dd, *J* = 5.9, 4.8 Hz, 1H, C*H*(2)), 5.83 (t, *J* = 5.7 Hz, 1H, C*H*(4)), 4.52 – 4.36 (m, 2H, C*H*(3,5)), 4.29 (dd, *J* = 12.1, 5.2 Hz, 1H, C*H*(5)), 2.15 (s, 3H), 2.03 (s, 3H); ^{13}C NMR (101 MHz, DMSO) δ 193.2 (*C*(11)), 170.0, 169.4 (*C*(16,18)), 156.9, 153.4, 152.9 (*C*(12)), 150.0 (*C*(10)), 140.5 (*C*(6)), 129.9 (*C*(14)), 127.0 (*C*(15)), 121.5 (*C*(13)), 118.2 (*C*(7)), 85.2 (*C*(1)), 80.3 (*C*()), 79.5 (*C*(4)), 69.3 (*C*(3)), 62.5 (*C*(5)), 20.5, 20.5 (*C*(17,19)); LRMS (ESI$^+$) *m*/*z* 522.2 (M+H$^+$); HRMS (ESI$^+$): calcd for $C_{21}H_{21}ClN_5O_7S^+$ [M+H]$^+$ 522.0845, found 522.0852.

((2R,3S,5R)-3-acetoxy-5-(6-amino-2-chloro-9H-purin-9-yl)tetrahydrofuran-2-yl)methyl acetate, (**191**)



191 was synthesised via literature procedure.[171] A solution of **190** (1.525 g, 2.92 mmol), 2,2'-azobis(2-methylpropionitrile (0.029 g, 0.175 mmol), tributyltin hydride (1.706 mL, 6.34 mmol) in Toluene (5 mL) was heated to 100 °C for 3 h. The reaction mixture was concentrated *in vacuo*. The crude product was adsorbed on silica and purified by flash chromatography eluting with 0-100% EtOAc in Cyclohexane to give **191** (0.980 g, 83%) as a white solid. Mp 178 – 180 °C; ν_{max}/cm^{-1} 3320 (N-H), 1750, 1659 (C=O), 1598 (C=C), 1349, 1303 (C-N) 1203, 1169 (C-O), 635 (C-Cl); ^{1}H NMR (400 MHz, DMSO-d_6) δ 8.38 (s, 1H, C*H*(6)), 7.87 (s, 2H, NH_2), 6.29 (dd, *J* = 8.0, 6.2 Hz, 1H, C*H*(1)), 5.37 (dt, *J* = 6.5, 2.6 Hz, 1H, C*H*(3)), 4.46 – 3.94 (m, 3H, C*H*(4+5)), 3.04 (ddd, *J* = 14.4, 8.1, 6.5 Hz, 1H, C*H*(2)), 2.60 – 2.51 (m, 1H, C*H*(2)), 2.09 (s, 3H, C*H*(12)), 2.02 (s, 3H, C*H*(14)); ^{13}C NMR (101 MHz, DMSO) δ 170.2, 170.1 (*C*(11,13)), 156.9 (*C*(8)), 153.2 (*C*(9)), 150.2 (*C*(10)), 139.8 (*C*(6)), 118.2 (*C*(17)), 83.3 (*C*(1)), 81.7 (*C*(4)), 74.2 (*C*(3)), 63.5 (*C*(5)), 35.4 (*C*(2)), 20.8 (*C*(12)), 20.6 (*C*(14)); LRMS (ESI$^+$) *m/z* 370.2 (M+H$^+$); HRMS (ESI$^+$): calcd for $C_{14}H_{17}ClN_5O_5^+$ [M+H]$^+$ 370.0913, found 370.0922.

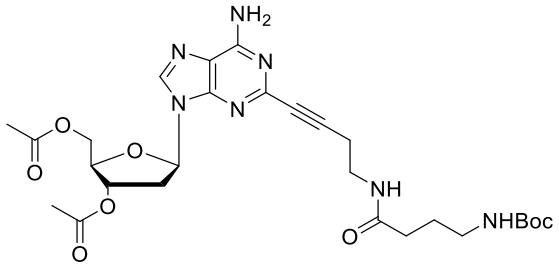
tert-butyl (4-(but-3-yn-1-ylamino)-4-oxobutyl)carbamate, (**194**)



To a solution of 4-((*tert*-butoxycarbonyl)amino)butanoic acid (4.81 g, 23.7 mmol) in DMA (100 mL) was added HATU (11.71 g, 30.8 mmol) and 4-methylmorpholine (10.4 ml, 95 mmol). The reaction mixture was stirred at room temperature for 30 min. But-3-yn-1-amine, HCl (2.5 g, 23.7 mmol) was

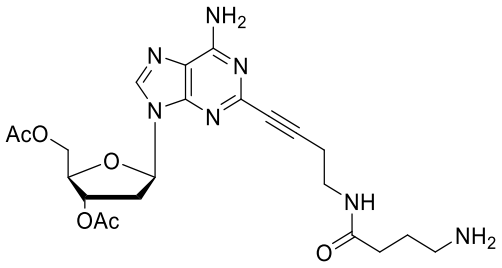
added and the reaction mixture was stirred for 16 h. The reaction mixture was extracted with EtOAc (200 mL) and washed with $NaHCO_3$ (100 mL) and 1N HCl (100 mL) and water (3 x 100 mL). The organic extract was dried over Na_2SO_4, filtered and concentrated *in vacuo*. The crude product was purified by flash chromatography eluting with 0-80% EtOAc in Cyclohexane to give **194** (4.253 g, 71%) as a white amorphous solid. ν_{max}/cm^{-1} 3338 (N-H), 3278 (C≡C-H), 1689, 1655 (C=O), 1365 (C-N) 1167 (C-O); ^{1}H NMR (400 MHz, DMSO-d_6) δ 7.97 (t, *J* = 5.7 Hz, 1H, N*H*), 6.79 (t, *J* = 5.8 Hz, 1H, N*H*), 3.13 (td, *J* = 7.1, 5.7 Hz, 2H, C*H*(4)), 2.93 – 2.83 (m, 2H, C*H*(8)), 2.80 (t, *J* = 2.6 Hz, 1H, C*H*(1)), 2.26 (td, *J* = 7.1, 2.7 Hz, 2H, C*H*(3)), 2.04 (t, *J* = 7.5 Hz, 2H, C*H*(6)), 1.63 – 1.51 (m, 2H, C*H*(7)), 1.37 (s, 9H, C*H*(11)); ^{13}C NMR (101 MHz, DMSO) δ 171.9 (*C*(5)), 155.6 (*C*(9)), 82.3 (*C*(2)), 77.4 (*C*(10)), 72.0 (*C*(1)), 39.5 (*C*(8)), 37.7 (*C*(4)), 32.8 (*C*(6)), 28.3 (*C*(11)), 25.8 (*C*(7)), 18.8 (*C*(3)); LRMS (ESI$^+$) *m/z* 255.5 (M+H$^+$); HRMS (ESI$^+$): calcd for $C_{13}H_{23}N_2O_3^+$ [M+H]$^+$ 255.1703, found 255.1704.

((2R,3S,5R)-3-acetoxy-5-(6-amino-2-(4-(4-((tert-butoxycarbonyl)amino)butanamido)but-1-yn-1-yl)-9H-purin-9-yl)tetrahydrofuran-2-yl)methyl acetate, (**195**)



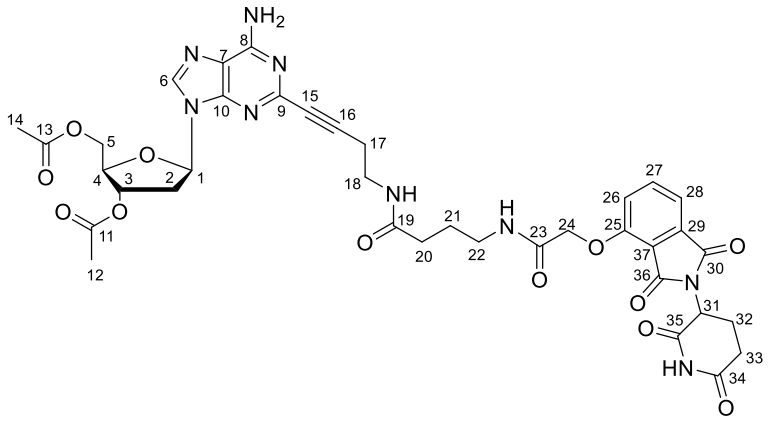
To a solution of **191** (0.100 g, 0.270 mmol), triphenylphosphine (0.018 g, 0.068 mmol), $PdCl_2(PPh_3)_2$ (0.025 g, 0.035 mmol), copper(I) iodide (6.70 mg, 0.035 mmol), **194** (0.083 g, 0.325 mmol) and diethylamine (2 mL) in DMF (1 mL). The reaction mixture was heated at 100 °C in the MW for 15 min. The reaction mixture was diluted with EtOAc (20 mL) and washed water (20 mL x 3). The combined organic extracts were dried over Na_2SO_4, filtered and concentrated *in vacuo*. The crude product was purified by flash chromatography eluting with 0-6% MeOH in CH_2Cl_2 to give **195** (0.060 g, 38%) which was taken on crude into the next step.

((2R,3S,5R)-3-acetoxy-5-(6-amino-2-(4-(4-aminobutanamido)but-1-yn-1-yl)-9H-purin-9-yl) tetrahydrofuran-2-yl)methyl acetate, (**196**)



A vial of **195** (130 mg, 0.221 mmol) in 1,1,1,3,3,3-hexafluoropropan-2-ol (1 mL) was heated in the microwave to 100 °C for 8 h. The reaction mixture was concentrated *in vacuo* to give **196** in quantitative yield which was taken on crude into the next step.

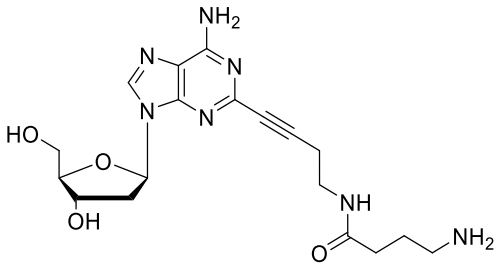
((2*R*,3*S*,5*R*)-3-acetoxy-5-(6-amino-2-(4-(4-(2-((2-(2,6-dioxopiperidin-3-yl)-1,3-dioxoisoindolin-4-yl)oxy)acetamido)butanamido)but-1-yn-1-yl)-9H-purin-9-yl)tetrahydrofuran-2-yl)methylacetate, (**197**)



To a solution of **177** (74 mg, 0.222 mmol) in DMF (2 mL) was added HATU (101 mg, 0.266 mmol) and 4-methylmorpholine (97 µL, 0.886 mmol). The reaction was stirred at room temperature for 15 min and **196** (108 mg, 0.222 mmol) and the reaction mixture was stirred at room temperature for 14 h. The reaction mixture was extracted with EtOAc (10 mL) and washed with water (20 mL). The aqueous layer was back-extracted with EtOAc (3 x 10 mL). The combined organic extracts were washed with brine, dried over Na_2SO_4, filtered and concentrated *in vacuo* to give **197** (42 mg, 24%) as a yellow solid. ν_{max}/cm^{-1} 3325 (N-H), 2253 (C≡C), 1705, 1639, 1590 (C=O), 1099, 1053 (C-N) 1201

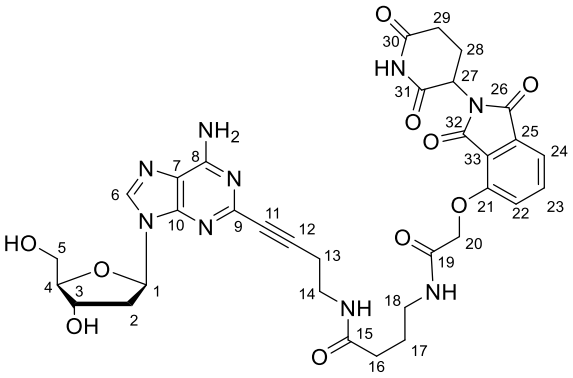
(C-O); ^{1}H NMR (400 MHz, DMSO-d_6) δ 11.12 (s, 1H, N*H*), 8.41 (s, 1H, C*H*(6)), 8.32 (t, *J* = 5.8 Hz, 1H, N*H*), 7.81 – 7.76 (m, 1H, C*H*(27)), 7.49 – 7.37 (m, 4H, C*H*(26, 28, NH_2)), 6.31 (dd, *J* = 8.4, 6.0 Hz, 1H, C*H*(1)), 5.34 (d, *J* = 5.8 Hz, 1H, C*H*(3)), 5.10 (dd, *J* = 12.8, 5.3 Hz, 1H, C*H*(31)), 4.82 (s, 2H, C*H*(24)), 4.33 – 4.15 (m, 3H, C*H*(4+5)), 3.38 (m, 2H, C*H*(18)), 3.04 (m, 1H, C*H*(2)), 2.93 – 2.82 (m, 1H, C*H*(33)), 2.64 – 2.51 (m, 5H, C*H*(2,17,32,33)), 2.10 – 1.97 (m, 7H, C*H*(12,14,32)); ^{13}C NMR (101 MHz, DMSO) δ 172.8 (*C*(34)), 170.2, 170.1 (*C*(11,13)), 169.9 (*C*(35)), 167.2 (*C*(23)), 166.7, 165.4 (*C*(30,36)), 155.8, 155.1 (*C*(8,25)), 149.4 (*C*(10)), 145.7 (*C*(9)), 139.8 (*C*(6)), 137.0 (*C*(27)), 133.1 (*C*(29)), 120.5 (*C*(26)), 118.5 (*C*(7)), 116.8 (*C*(37)), 116.0 (*C*(28)), 83.0 (*C*(1)), 82.8, 81.8 (*C*(15,16)), 81.6 (*C*(4)), 74.4 (*C*(3)), 67.6 (*C*(24)), 63.6 (*C*(5)), 48.8 (*C*(31)), 37.4 (*C*(18)), 35.5 (*C*(2)), 31.0 (*C*(33)), 22.0 (*C*(32)), 20.8 (*C*(12)), 20.6 (*C*(14)), 19.1 (*C*(17)); LRMS (ESI$^+$) *m/z* 717.7 (M-2Ac+H$^+$).

4-amino-*N*-(4-(6-amino-9-((2R,4S,5R)-4-hydroxy-5-(hydroxymethyl)tetrahydrofuran-2-yl)-9H-purin-2-yl)but-3-yn-1-yl)butanamide, (**198**)



198 was synthesised via a literature procedure.[173] To a solution of **196** (100 mg, 0.205 mmol) in MeOH (1 mL) was saturated solution of Na_2CO_3 until pH reached 8-9. The reaction was stirred at room temperature for 2 h. The reaction mixture was concentrated *in vacuo*. The crude product was adsorbed on an SCX-2 cartridge. The cartridge was washed with MeOH and the collected fractions were discarded. The cartridge was washed with NH_3 in MeOH and the collected fractions were concentrated *in vacuo* to give **198** (70 mg, 85%) which was taken on crude into the next step.

N-(4-(6-amino-9-((2R,4S,5R)-4-hydroxy-5-(hydroxymethyl)tetrahydrofuran-2-yl)-9H-purin-2-yl)but-3-yn-1-yl)-4-(2-((2-(2,6-dioxopiperidin-3-yl)-1,3-dioxoisoindolin-4-yl)oxy)acetamido) butanamide (**183**)



To a solution of **177** (60 mg, 0.181 mmol) in DMF (1 mL) was added HATU (86 mg, 0.227 mmol) and *N*-methylmorpholine (0.066 mL, 0.605 mmol). The reaction mixture was stirred for 30 min at room temperature. A solution of **198** (61 mg, 0.151 mmol) in DMF (0.5 mL) was added. The reaction mixture was stirred at room temperature for 16 h. The solution was concentrated *in vacuo*. The crude product was purified by prep LCMS to afford **183** (8 mg, 7%) as a yellow amorphous solid. ν_{max}/cm^{-1} 3201 (N-H), 2254 (C≡C), 1702, 1637 (C=O), 1261, 1094, 1054 (C-N) 1200 (C-O); ^{1}H NMR (400 MHz, DMSO-d_6) δ 8.37 (d, *J* = 3.3 Hz, 1H, C*H*(6)), 8.31 (t, *J* = 5.9 Hz, 1H, N*H*), 8.14 – 7.90 (m, 1H, N*H*), 7.79 (m, 1H, C*H*(23)), 7.52 – 7.30 (m, 4H, C*H*(22+24)), 6.30 (t, *J* = 6.9 Hz, 1H, C*H*(1)), 5.11 (m, 1H, C*H*(27)), 4.79 (s, 2H, C*H*(20)), 4.38 (s, 1H, C*H*(3)), 3.87 (dd, *J* = 4.6, 2.4 Hz, 1H, C*H*(4)), 3.66 – 3.46 (m, 2H, C*H*(5)), 3.38 (2H, C*H*(14)), 3.15 (q, *J* = 6.5 Hz, 2H, C*H*(18)), 2.99 – 2.77 (m, 1H, C*H*(29)), 2.72 – 2.54 (m, 5H, C*H*(2,13,28,29)), 2.41 – 2.21 (m, 1H, C*H*(2)), 2.16 – 1.99 (m, 3H, C*H*(16+28)), 1.83 – 1.54 (m, 2H, C*H*(17)); ^{13}C NMR (101 MHz, DMSO) δ 172.8 (*C*(30)), 171.9 (*C*(15)), 169.9 (*C*(31)), 167.2 (*C*(19)), 166.7, 165.4 (*C*(26, 32)), 155.8, 155.1 (*C*(8,21)), 149.0 (*C*(10)), 145.4 (*C*(9)), 140.0 (*C*(6)), 136.9 (*C*(23)), 133.0 (*C*(25)), 120.5 (*C*(22)), 118.6 (*C*(7)), 116.8 (*C*(33)), 116.0 (*C*(24)), 87.9 (*C*(4)), 83.6 (*C*(1)), 82.8, 81.8 (*C*(11,12)), 70.8 (*C*(3)), 67.6 (*C*(20)), 61.8 (*C*(5)), 48.8 (*C*(27)), 39.4 (*C*(2)), 37.6, 37.5 (*C*(14,18), 32.7 (*C*(16)), 30.9 (*C*(29)), 25.2 (*C*(17)), 22.0 (*C*(28)), 21.2 (NH_4OAc), 19.1 (*C*(13)); LRMS (ESI^-) *m/z* 716.5 ($M-H^-$); HRMS (ESI^-): calcd for $C_{33}H_{36}N_9O_{10}^+$ $[M+H]^+$ 718.2580, found 718.2588.

Experimental – Assays

AlphaScreen KDM5 assay

2-[4-(2-Hydroxyethyl)piperazin-1-yl]ethanesulfonic acid (HEPES) buffer was obtained from Life Technologies. The biotinylated peptide ligand substrate (H3(1−21)K4-Me_3-GGK Biotin) was sourced from Anaspec. Anti H3K4Me_2 antibody and AlphaScreen General IgG detection kit were obtained from Cell Signalling Technologies and PerkinElmer respectively. The assay buffer contained 50 mM HEPES pH 7.5, 0.1% BSA, 0.01% Tween-20. Ferrous ammonium sulphate was prepared fresh each day by diluting to 400 mM in 20 mM HCl and then to 1 mM in deionised water. 2-OG and L-Ascorbic acid were prepared each day by diluting with deionized water to 10 mM and 50 mM respectively. Compounds were dispensed using an ECHO-550 acoustic dispenser (Labcytes). Enzyme and substrate solutions were dispensed using a multidrop combi reagent dispenser (Thermo Scientific) fitted with a small tube dispensing cassette (Thermo Scientific). Antibody/Bead mix was dispensed manually using a multichannel pipette. KDM5 assay was carried out in a white 384-well proxiplate plus (PerkinElmer). Compounds were dissolved in 100% DMSO to a concentration of 10 mM and then dispensed using ECHO-550 acoustic dispenser to give a range of concentrations down each column from 100 µM to 0.006 µM with 11 points a 3 fold dilution factor. 100 nl of 2-PDCA (100 µM) was added to all wells of row A and P and 100 nl of DMSO was added to each well of row B and O. KDM5B was diluted to 4 nM in assay buffer. 5 µl of enzyme solution was added to each well of each Proxiplate at different timepoints (0-120 minutes) and then centrifuged at 2000 rpm for 10 s. Substrate solution was prepared in assay buffer (200 µM L-AA, 20 µM FAS, 0.2 µM H3K4Me_3 peptide, 10 µM 2-OG) and 5 µl was added to each well of each plate to initiate enzyme reaction. Plates were centrifuged at 2000 rpm for 10 s and incubated for 20 min at room temperature. The addition of 5 µl of assay buffer containing EDTA (30 mM) and NaCl (1.6 mM) to each well stopped the enzyme reactions. AlphaScreen detection reagent was prepared by diluting AlphaScreen streptavidin donor and protein A acceptor beads in assay buffer (0.08 mg/mL with respect to each

bead) containing anti-H3K4Me$_2$ antibody (1:750) and preincubated for 3 h. 5 µL of detection reagent was added to each well and then incubated in the dark and at room temperature overnight. After 16 hr, plates were read in a BMG Labtech plate reader equipped with an AlphaScreen 680 nm/570 nm optic module. Data were normalized to the no enzyme (2,4-PDCA) control and IC_{50} determined from nonlinear regression curve fitting using Graphpad Prism 5.0.

k_{inact}/K_i calculations

The K_i and k_{inact} were calculated through a least squares fit of the obtained IC_{50} at the different timepoints into equations 1 and 2 which was derived by Krippendorff *et al.*[93] S is the H3K4me3 peptide substrate concentration of 0.1 µM and K_M is the Michaelis-Menten constant for the substrate of 0.5 µM. XLFit software was used to compute the values of K_i and k_{inact}.

AlphaScreen KDM selectivity

AlphaScreen with the other KDM proteins (KDM2, KDM3, KDM4 and KDM6) was carried out as described above with a 2-hour pre-incubation time between the compounds and enzymes and with different substrates, cosubstrates and antibody concentrations.

	KDM2	KDM3	KDM4	KDM5	KDM6
Enzyme (nM)	KDM2A – 5 nM	KDM3A – 0.25 nM	KDM4A – 2 nM KDM4B – 2 nM KDM4C – 0.5 nM KDM4D – 2 nM	KDM5A – 4 nM KDM5B – 2 nM KDM5C – 2 nM KDM5D – 2 nM	KDM6B – 0.1 nM
OG	10 µM	5 µM	10 µM	5 µM	10 µM
L-Ascorbic acid	100 µM	100 µM	100 µM	100 µM	100 µM
Ferrous Ammonium Sulfate	1 µM	10 µM	1 µM	10 µM	10 µM
Peptide	0.1 µM	0.06 µM	0.03 µM	0.1 µM	0.06 µM
Substrate Incubation Time	30 min	5 min	10 min	20 min	10 min
Antibody	0.03 µg/mL	0.03 µg/mL	0.03 µg/mL	0.3 µg/mL	0.3 µg/mL

2-OG competition assays

2-OG competition assay were performed as described for the general KDM5B AlphaScreen method above, varying the 2-OG concentrations from a range of 0.5 µM to 1000 µM. Data were normalized to the no enzyme control and the IC_{50} determined from the nonlinear regression curve fit using GraphPad Prism 7.

RapidFire assays – Kinetics of covalent binding of acrylamide 61 and chloroacetamide 62

Chloroacetamide **62** and acrylamide **61** were diluted to 50 mM in DMSO and were diluted to 10 µM in buffer (50mM HEPES pH 7.5/0.1%BSA/0.01% Tween 20) and incubated with 0.33 µM KDM5B at room temperature. The samples were injected into a RapidFire RF360 high-throughput sampling robot connected to an Agilent 6530 Accurate-mass Quadrupole Time-of-Flight at various time points up to 90 min when the degree of modification had remained unchanged. The data was processed using Agilent MassHunter Workstation software. The deconvoluted protein mass peaks

were integrated and an average area calculated from the triplicates. The concentration of unmodified enzyme at each time point was determined by calculating the degree of modification. The concentration of substrate was considered constant as it is in large excess, so the reaction is first order.

RapidFire assays - Incubation of piperazine acrylamide 61 with JARID1C

Piperazine acrylamide **61** was diluted to 50 mM in DMSO and diluted to different concentrations (6.25-50 µM) in 50 mM MES buffer at pH 7.0. The compound solution was incubated at 1 µM KDM5C at room temperature at different time points. The samples were injected into the RapidFire and processed as previous compounds.

Elastase Digest

33 µM **61** and **62** were incubated with 0.33 µM KDM5B in 1 mL at room temperature for 4 h. 200 mM DTT in 0.1 M Tris buffer, pH 7.8 was added to a final concentration of 5 mM and the solution was vortexed and incubated for 60 min at room temperature. 200 mM iodoacetamide in 0.1 M Tris, pH 7.8 was added to a final concentration of 20 mM and the solution was vortexed and incubated for 60 min at room temperature. The sample was split into 200 µL aliquots and 600 µL MeOH, 150 µl $CHCl_3$ were added and vortexed. 450 µl MilliQ-H_2O was added and the sample was vortexed and centrifuged at max speed (14.8 RPM) for 1 min. The top layer was pipetted off and 450 µl MeOH was added, vortexed and centrifuged for 2 min at room temperature. The supernatant was removed and the protein pellet was resuspended in 50 µl 6M Urea in Tris buffer, pH 7.8 by vortexing and sonication. The solution was diluted with MilliQ-H_2O to a final concentration of Urea of 1M. 1 µl Elastase (1 in 50 regarding total protein concentration of sample) was added and the samples were incubated overnight at 37 °C. The digested protein was purified using a Water Sep-Pak C18

Plus (WAT020515) cartridge. The column was equilibrated with 5 mL of solution B (65% AcN, 35% MilliQ-H_2O, 0.1% TFA). 10 mL of solution A (98% MilliQ-H_20, 2% AcN, 0.1% TFA) was added to the column and the peptide digest sample was added to the 10 mL of solution of A and the solution was loaded on the column slowly. The column was washed with 10 mL of solution A. The purified samples were eluted with 2 x 600 µL solution B and dried down completely in a speed vac. The purified peptides were resuspended in 20 µL solution A and injected into an Orbitrap-MS for analysis of peptide fragments using PEAKS analysis.

RapidFire assays – Incubation of methyl benzylamines with KDM5B, KDM5C and KDM4B

Methyl benzylamines **77**-**79** were diluted to 10 mM in DMSO and diluted to 10 µM in buffer (50 mM MES buffer at pH 7.0). The compound solutions were incubated with 1 µM KDM5B/KDM5C/KDM4B for 2 hours at room temperature. The samples were injected into a RapidFire RF360 high-throughput sampling robot connected to an Agilent 6530 Accurate-mass Quadrupole Time-of-Flight. The data was processed using Agilent MassHunter Workstation software.

RapidFire assays – Incubation of clickable alkyne 103 with KDM5B

Clickable alkyne **103** was diluted to 10 mM in DMSO and diluted to 10 µM in buffer (50 mM MES buffer at pH 7.0). The compound solution was incubated with 1 µM KDM5B at 37 °C for 30 min. The samples were injected into a RapidFire RF360 high-throughput sampling robot connected to an Agilent 6530 Accurate-mass Quadrupole Time-of-Flight. The data was processed using Agilent MassHunter Workstation software and the deconvoluted protein peak was extracted from the chromatogram.

Immunofluorescence-based assay

The KDM5B overexpression immunofluorescence assay was carried out as previously described.[73] Cells were transfected with KDM5B. Four hours after transfection, the cells were treated with serial dilutions of compounds for 24 hours. The cells were fixed and stained with an anti-Flag antibody and an anti-H3K4me3 antibody. The secondary antibodies were labelled with Alexa Fluor 488. Image acquisition was performed using the Operatta High Content Imaging System and image analysis was performed with the Columbus software.

NanoBRET assay

HEK293 cells were transfected with Nanoluc luciferase fused KDM5B. 24 hours after transfection, the cells were resuspended in OptiMEM and seeded into 384-well plates with tracer (2 µM). Cells were treated with serial dilutions of compounds for 5 hours. Nano-Glo substrate and extracellular inhibitor were added and BRET signal was measured on the PHERAstar at 450 nm and 610 nm.

Pull-down assays – in-gel fluorescence with KDM5B protein

Clickable analogue **103** and non-clickable analogue **77** were prepared at 10 mM, 2 mM and 1 mM in DMSO. KDM5B (7.6 mg/mL) was diluted to 1.3 µM in lysis buffer and the compounds were incubated with the protein at 5 µM for 2 h at 37 °C with shaking. The lysis buffer was prepared as follows:

Component	Final Conc.	Stock Conc.	Dilution Factor	Volume of Stock (mL) for 100 mL	
NP-40	0.80%	10%	12.5	8	
Tris pH 7.5	50 mM	1 M	20	5	
Glycerol	5%	100%	20	5	**Total = 92.6 mL**
MgCl2	1.5 mM	1 M	666.7	0.15	
NaCl	100 mM	5 M	50	2	
NaF	25 mM	500 mM	20	5	
Na3VO4	1 mM	100 mM	100	1	
PMSF	1 mM	100 mM (EtOH)	100	1	**Add Fresh**
TCEP	1 mM	1 M	1000	0.1	
TLCK	10 µg/mL	5 mg/mL	500	0.2	
Cocktail			1000	0.1	

10% SDS in PBS was added to a final concentration of 1% SDS. The click mix was prepared in a 1:2:2:1 ratio of 10 mM azido dye in DMSO: 50 mM $CuSO_4$ in H_2O: 50 mM TCEP in H_2O: 10 mM TBTA in DMSO. No-$CuSO_4$ click mix was prepared in the same ratio and concentrations but 50 mM $CuSO_4$ was replaced with H_2O. Importantly, the azide, $CuSO_4$ and TCEP were incubated for 2 min prior to the addition of TBTA and the click mix was used immediately. The click mix was added to the samples to give final concentrations of 100 µM click reagent, 1 mM $CuSO_4$, 1mM TCEP and 100 µM TBTA. The samples were incubated at room temperature for 1 h with shaking. The click reaction was quenched with 5 mM EDTA from 500 mM stock. The protein was precipitated by adding 200 µL MeOH, followed by 50 µL $CHCl_3$ and vortexing. 100 µL water was added and vortexed. The samples were centrifuged at max speed at room temperature for 2 min and the top layer was removed. 1 mL MeOH was added and the samples were centrifuged at max speed at room temperature for 5 min. The wash with MeOH was repeated and the protein was air-dried and resuspended in 2% SDS in PBS to a concentration of 1 mg/mL in 200 µL. 4 µL sample loading buffer (20% DTT in (4 x lammeli buffer) was added to 10 µL sample and the samples were heated at 70 °C

for 7 min to denature the proteins. The samples (14 µL) as well as the ladder (3 µL-Bio-Rad Precision Plus Protein™ All Blue Prestained Protein Standards #1610373) were loaded on the gel and run under a voltage of 100 V for 10 min and 170 V for 50 min. The gel was fixed in a solution of 10% AcOH and 50% MeOH and imaged on Li-Cor.

The gel was stained to visualise all proteins through incubation of the gel with Coomassie Blue at room temperature for 45 min.

Pull-down assays – in-gel fluorescence in cell lysates

The MCF7 lysate concentration was determined using a calibration curve. Solutions of Bovine Serum Albumin (BSA) were prepared at different concentrations (4, 3.5, 3, 2.5, 2, 1.75, 1.5, 1.25, 1, 0.75, 0.5, 0 mg/mL) as a standard. The lysates were diluted 1 in 5, 1 in 10 and 1 in 20 in duplicate in lysis buffer. A mixture of reagent A and reagent S were prepared (1 mL DC Protein assay Reagent A (BioRad) + 20 µL DC Protein assay Reagent S (BioRad)). 5 µL of each sample was added to a well and 25 µL of mixture was added to each well. 200 µL Reagent B (DC Protein Assay Reagent B (BioRad)) was added to each well and the solutions were incubated at room temperature for 20 min. The plate was read on a TECAN using Magdellan software. The absorbance values were calculated to create a calibration curve from BSA to determine the lysate concentration. The cell lysates were diluted to a concentration of 2 mg/mL in 100 µL in lysis buffer. Clickable analogue **103** was prepared in 10 mM, 2 mM, 1 mM, 200 µM and 100 µM DMSO stock. 0.5 µL of compounds were added to the cell lysate to give final compound concentrations of 50 µM, 10 µM, 5 µM, 1 µM and 0.5 µM. The resulting samples were incubated with shaking for 2 h at 37 °C. The lysate was precipitated through the addition of 200 µL MeOH to each sample followed by 50 µL $CHCl_3$. 100 µL MilliQ-H_2O was added, vortexed and centrifuged at max speed for 2 min at room temperature. The top layer was pipetted off. 1 mL MeOH was added, vortexed and centrifuged at max speed at room temperature for 5 min. The supernatant was removed and the lysate was washed with MeOH another time. The resulting

lysate was air-dried and the samples were re-suspended to 2 mg/mL in lysis buffer (94 µL). The click reaction was carried out as previously described in a 1:2:2:1 ratio of 10 mM azido dye: 50 mM $CuSO_4$: 50 mM TCEP: 10 mM TBTA. 6 µL click mix was added to give the desired final concentration of click reagents. The samples were incubated at room temperature for 1 h with shaking. The reaction was quenched with 5 mM EDTA (500 mM EDTA). The lysate proteins were precipitated as described in previous step. The protein pellet was resuspended in 2% SDS in PBS to 1 mg/mL in 200 µL. 4 µL sample loading buffer (20% DTT in (4 x Lammeli buffer) was added to 10 µL samples. The samples were denatured through heating for 7 min at 70 °C and loaded onto a gel. The gel was run at a voltage of 100 V for 10 min and 170 V for 50 min. The gel was fixed with solution of 10% AcOH, 50% MeOH and imaged on Li-Cor reader.

Pull-down assays – Biotin pull-down in MCF7 cell lysates

The incubation of cell lysate with compound and click reaction were carried out as described with in-gel fluorescence except biotin azide was used in place of azido dye. The cell lysate pellet was diluted in 2% SDS in PBS (20 µL) and 2 µL 100mM DTT was added. The lysate was diluted further to 0.2% SDS in PBS (180 µL PBS). 20 µL was retained as an input sample. 15 µL beads (Dynabeads™ MyOne™ Streptavidin C1) were used for each sample (200 µg protein) and the beads were washed with 150 µL 0.2% SDS in PBS, placed in a magnetic bead rack and the supernatant was removed. The washes were repeated three times. The samples were incubated with the beads for 1 h at room temperature. The samples were placed in bead rack and supernatant was removed as an input for the gel. The incubated beads were washed 3 times with 150 µL 0.2% SDS in PBS. The beads were suspended in 16 µL 2 x SLB and heated at 100 °C for 10 min to elute proteins from beads. The supernatant was removed from beads. 4 µL (4 x SLB) was added to input 1 and 2 (12 µL) and all the samples were heated to 100 °C for 5 min. The samples were run on SDS-PAGE (10 min at 100 V and 1 h at 170 V). The gels were transferred to a nitrocellulose membrane through electro-Blotting (100

V for 30 min) using a transfer buffer (80 mL (Novex Tris-Glycine transfer buffer (x25)) + 10% MeOH in 2 L water). The membrane was incubated with blocking buffer (1.2 g Block Quick in 50 mL PBS-0.05% Tween) at room temperature for 1 h. The blocking buffer was removed and Streptavidin-IR dye was added to the blocking buffer in a 1:5000 dilution and incubated for 2 h at room temperature. The membrane was washed with PBS-Tween and the membrane was imaged on the Li-Cor.

Pull-down assays – Western blotting of MCF7 and K562 cell lysates

The samples were prepared for loading on the gel by denaturing the cell lysates (10 µL sample + 4 µL SLB) and heating samples for 7 minutes at 70 °C. The gel was transferred to the nitrocellulose membrane through electro-blotting (100 V for 30 min). The membrane was incubated at room temperature with blocking buffer for 45 min. 1 in 10000 dilution of Rabbit-Anti JARID1B was added to the blocking buffer and incubated overnight at 4 °C. The membrane was washed with PBS-Tween (0.05%) and incubated for 5 min at room temperature. The washes with PBS-Tween were repeated 3 times. The membrane was incubated with secondary antibody (Goat anti Rabbit-AlexaFluor680) for 1 hr at room temperature. Three washes with PBS-Tween (0.05%). Read on LiCor machine.

Pull-down assays – Biotin pull-down in k562 cell lysates

K562 cell lysate concentration was calculated as 1.8 mg/mL. 400 µg (~200 µL) lysate was used and 1 µL clickable analogue (1 mM in DMSO) was added. The sample was incubated at 37 °C for 1 h and the lysate pellet was precipitated with 2 volumes MeOH, 0.5 volumes $CHCl_3$ and 1 volume H_2O and centrifuged for 2 min at max speed. The top layer was removed, 1 mL MeOH was added and centrifuged at max speed for 5 min. The supernatant was removed and MeOH wash was repeated. The lysate concentration was adjusted to 1.8 mg/mL in 0.2% SDS in PBS. 10 µL was retained as an

input sample. Subsequent steps of the click reaction, protein precipitation and bead incubation were as previously described with MCF7 lysates.

Docking

Compounds were docked into protein crystal structures using the MolSoft ICM-Pro internal coordinate modelling (ICM) methodology.

Bibliography

[1] A. Portela, M. Esteller, *Nat Biotech* **2010**, *28*, 1057–1068.

[2] G. L. Gravina, C. Festuccia, F. Marampon, V. M. Popov, R. G. Pestell, B. M. Zani, V. Tombolini, *Mol. Cancer* **2010**, *9*, 305.

[3] W. S. Xu, R. B. Parmigiani, P. A. Marks, *Oncogene* **2007**, *26*, 5541–5552.

[4] C. H. Arrowsmith, C. Bountra, P. V Fish, K. Lee, M. Schapira, *Nat. Rev. Drug Discov.* **2012**, *11*, 384.

[5] V. G. Allfrey, A. E. Mirsky, *Science* **1964**, *144*, 559.

[6] Y. Shi, F. Lan, C. Matson, P. Mulligan, J. R. Whetstine, P. A. Cole, R. A. Casero, Y. Shi, *Cell* **2004**, *119*, 941–53.

[7] S. Chuikov, J. K. Kurash, J. R. Wilson, B. Xiao, N. Justin, G. S. Ivanov, K. McKinney, P. Tempst, C. Prives, S. J. Gamblin, et al., *Nature* **2004**, *432*, 353–360.

[8] B. D. Strahl, C. D. Allis, *Nature* **2000**, *403*, 41–45.

[9] S. M. Kooistra, K. Helin, *Nat Rev Mol Cell Biol* **2012**, *13*, 297–311.

[10] H. P. Mohammad, K. N. Smitheman, C. D. Kamat, D. Soong, K. E. Federowicz, G. S. Van Aller, J. L. Schneck, J. D. Carson, Y. Liu, M. Butticello, et al., *Cancer Cell* **2015**, *28*, 57–69.

[11] Y. C. Zheng, B. Yu, G. Z. Jiang, X. J. Feng, P. X. He, X. Y. Chu, W. Z. and H. M. Liu, *Curr. Top. Med. Chem.* **2016**, *16*, 2179–2188.

[12] M. Labelle, T. Boesen, Q. Khan, R. R. Vakiti, U. Sharma, Y. Yang, M. Mehrotra, N. Saraswat, F. Ullah, *Inhibitors of Histone Demethylases*, **2017**, US9650339B2.

[13] L. J. Walport, R. J. Hopkinson, C. J. Schofield, *Curr. Opin. Chem. Biol.* **2012**, *16*, 525–34.

[14] R. J. Klose, E. M. Kallin, Y. Zhang, *Nat Rev Genet* **2006**, *7*, 715–727.

[15] L. J. Walport, R. J. Hopkinson, M. Vollmar, S. K. Madden, C. Gileadi, U. Oppermann, C. J. Schofield, C. Johansson, *J. Biol. Chem.* **2014**, *289*, 18302–18313.

[16] J. Christensen, K. Agger, P. A. C. Cloos, D. Pasini, S. Rose, L. Sennels, J. Rappsilber, K. H. Hansen, A. E. Salcini, K. Helin, *Cell* **2007**, *128*, 1063–1076.

[17] S. Iwase, F. Lan, P. Bayliss, L. de la Torre-Ubieta, M. Huarte, H. H. Qi, J. R. Whetstine, A. Bonni, T. M. Roberts, Y. Shi, *Cell* **2007**, *128*, 1077–1088.

[18] K. Yamane, K. Tateishi, R. J. Klose, J. Fang, L. A. Fabrizio, H. Erdjument-Bromage, J. Taylor-Papadimitriou, P. Tempst, Y. Zhang, *Mol. Cell* **2007**, *25*, 801–812.

[19] K. Agger, P. A. C. Cloos, J. Christensen, D. Pasini, S. Rose, J. Rappsilber, I. Issaeva, E. Canaani, A. E. Salcini, K. Helin, *Nature* **2007**, *449*, 731.

[20] S. Hong, Y.-W. Cho, L.-R. Yu, H. Yu, T. D. Veenstra, K. Ge, *Proc. Natl. Acad. Sci.* **2007**, *104*, 18439–18444.

[21] Y. Tsukada, J. Fang, H. Erdjument-Bromage, M. E. Warren, C. H. Borchers, P. Tempst, Y. Zhang, *Nature* **2005**, *439*, 811.

[22] K. Yamane, C. Toumazou, Y. Tsukada, H. Erdjument-Bromage, P. Tempst, J. Wong, Y. Zhang, *Cell* **2006**, *125*, 483–495.

[23] C. Loenarz, W. Ge, M. L. Coleman, N. R. Rose, C. D. O. Cooper, R. J. Klose, P. J. Ratcliffe, C. J. Schofield, *Hum. Mol. Genet.* **2010**, *19*, 217–222.

[24] P. A. C. Cloos, J. Christensen, K. Agger, K. Helin, *Genes Dev.* **2008**, *22*, 1115–40.

[25] R. J. Klose, Y. Zhang, *Nat Rev Mol Cell Biol* **2007**, *8*, 307–318.

[26] P. A. C. Cloos, J. Christensen, K. Agger, A. Maiolica, J. Rappsilber, T. Antal, K. H. Hansen, K. Helin, *Nature* **2006**, *442*, 307.

[27] B. D. Fodor, S. Kubicek, M. Yonezawa, R. J. O'Sullivan, R. Sengupta, L. Perez-Burgos, S. Opravil, K. Mechtler, G. Schotta, T. Jenuwein, *Genes Dev.* **2006**, *20*, 1557–1562.

[28] J. R. Whetstine, A. Nottke, F. Lan, M. Huarte, S. Smolikov, Z. Chen, E. Spooner, E. Li, G. Zhang, M. Colaiacovo, et al., *Cell* **2006**, *125*, 467–481.

[29] M. Brauchle, Z. Yao, R. Arora, S. Thigale, I. Clay, B. Inverardi, J. Fletcher, P. Taslimi, M. G. Acker, B. Gerrits, et al., *PLoS One* **2013**, *8*, e60549.

[30] T. Lu, M. W. Jackson, B. Wang, M. Yang, M. R. Chance, M. Miyagi, A. V Gudkov, G. R. Stark, *Proc. Natl. Acad. Sci. U. S. A.* **2010**, *107*, 46–51.

[31] S. Solá, J. M. Xavier, D. M. Santos, M. M. Aranha, A. L. Morgado, K. Jepsen, C. M. P. Rodrigues, *PLoS One* **2011**, *6*, e18421.

[32] L. Walport, R. Hopkinson, R. Chowdhury, R. Schiller, W. Ge, A. Kawamura, C. Schofield, *Nat. Commun.* **2016**, *7*, 11974.

[33] D. Balciunas, H. Ronne, *Trends Biochem. Sci.* **2000**, *25*, 274–276.

[34] J. R. Horton, A. K. Upadhyay, H. H. Qi, X. Zhang, Y. Shi, X. Cheng, *Nat. Struct. Mol. Biol.* **2010**, *17*, 38–43.

[35] I. O. Torres, K. M. Kuchenbecker, C. I. Nnadi, R. J. Fletterick, M. J. S. Kelly, D. G. Fujimori, *Nat. Commun.* **2015**, *6*, 6204.

[36] L. M. Iyer, S. Abhiman, R. F. de Souza, L. Aravind, *Nucleic Acids Res.* **2010**, *38*, 5261–5279.

[37] S. Markolovic, T. M. Leissing, R. Chowdhury, S. E. Wilkins, X. Lu, C. J. Schofield, *Curr. Opin. Struct. Biol.* **2016**, *41*, 62–72.

[38] M. A. McDonough, C. Loenarz, R. Chowdhury, I. J. Clifton, C. J. Schofield, *Curr. Opin. Struct. Biol.* **2010**, *20*, 659–672.

[39] W. Aik, M. A. McDonough, A. Thalhammer, R. Chowdhury, C. J. Schofield, *Curr. Opin. Struct. Biol.* **2012**, *22*, 691–700.

[40] S. B. Hatch, C. Yapp, R. C. Montenegro, P. Savitsky, V. Gamble, A. Tumber, G. F. Ruda, V. Bavetsias, O. Fedorov, B. Atrash, et al., *Epigenetics Chromatin* **2017**, 1–17.

[41] T. Sengoku, S. Yokoyama, *Genes Dev.* **2011**, *25*, 2266–2277.

[42] L. Kruidenier, C. Chung, Z. Cheng, J. Liddle, K. Che, G. Joberty, M. Bantscheff, C. Bountra, A. Bridges, H. Diallo, et al., *Nature* **2012**, *488*, 404–8.

[43] N. R. Rose, E. C. Y. Woon, G. L. Kingham, O. N. F. King, J. Mecinović, I. J. Clifton, S. S. Ng, J. Talib-Hardy, U. Oppermann, M. A. McDonough, et al., *J. Med. Chem.* **2010**, *53*, 1810–1818.

[44] R. J. Hopkinson, A. Tumber, C. Yapp, R. Chowdhury, W. Aik, K. H. Che, X. S. Li, J. B. L. Kristensen, O. N. F. King, M. C. Chan, et al., *Chem. Sci.* **2013**, *4*, 3110–3117.

[45] D. Wilsker, L. Probst, H. M. Wain, L. Maltais, P. W. Tucker, E. Moran, *Genomics* **2005**, *86*, 242–51.

[46] J. Wysocka, T. Swigut, H. Xiao, T. A. Milne, S. Y. Kwon, J. Landry, M. Kauer, A. J. Tackett, B. T. Chait, P. Badenhorst, et al., *Nature* **2006**, *442*, 86–90.

[47] L. C. Young, D. W. McDonald, M. J. Hendzel, *J. Biol. Chem.* **2013**, *288*, 21376–21388.

[48] J. C. Black, A. L. Manning, C. Van Rechem, J. Kim, B. Ladd, J. Cho, C. M. Pineda, N. Murphy, D. L. Daniels, C. Montagna, et al., *Cell* **2013**, *154*, 541–555.

[49] L. C. Young, M. J. Hendzel, *Biochem. Cell Biol.* **2012**, *91*, 369–377.

[50] G. G. Wang, J. Song, Z. Wang, H. L. Dormann, F. Casadio, H. Li, J.-L. Luo, D. J. Patel, C. D. Allis, *Nature* **2009**, *459*, 847.

[51] X. Liang, J. Zeng, L. Wang, M. Fang, Q. Wang, M. Zhao, X. Xu, Z. Liu, W. Li, S. Liu, et al., *PLoS One* **2013**, *8*, e69784.

[52] Y.-C. Teng, C.-F. Lee, Y.-S. Li, Y.-R. Chen, P.-W. Hsiao, M.-Y. Chan, F.-M. Lin, H.-D. Huang, Y.-T. Chen, Y.-M. Jeng, et al., *Cancer Res.* **2013**, *73*, 4711 LP-4721.

[53] J. Zeng, Z. Ge, L. Wang, Q. Li, N. Wang, M. Björkholm, J. Jia, D. Xu, *Gastroenterology* **2010**, *138*, 981–992.

[54] A. Roesch, M. Fukunaga-Kalabis, E. C. Schmidt, S. E. Zabierowski, P. A. Brafford, A. Vultur, D. Basu, P. Gimotty, T. Vogt, M. Herlyn, *Cell* **2010**, *141*, 583–594.

[55] B. Angela, M. Bente, C. John, L. P. Juan, C. Lucienne, S. A. G., B. Joy, T. Joyce, *Int. J. Cancer* **2002**, *101*, 581–588.

[56] L. Wang, Y. Mao, G. Du, C. He, S. Han, *Tumor Biol.* **2015**, *36*, 2465–2472.

[57] B. Madsen, M. Tarsounas, J. M. Burchell, D. Hall, R. Poulsom, J. Taylor-Papadimitriou, *Chromosoma* **2003**, *112*, 124–132.

[58] Y. Xiang, Z. Zhu, G. Han, X. Ye, B. Xu, Z. Peng, Y. Ma, Y. Yu, H. Lin, A. P. Chen, et al., *Proc. Natl. Acad. Sci. U. S. A.* **2007**, *104*, 19226–19231.

[59] Z. Wang, F. Tang, G. Qi, S. Yuan, G. Zhang, B. Tang, S. He, *Am. J. Cancer Res.* **2015**, *5*, 87–100.

[60] M. H. Stewart, M. Albert, P. Sroczynska, V. A. Cruickshank, Y. Guo, D. J. Rossi, K. Helin, T. Enver, *Blood* **2015**, *125*, 2075–2078.

[61] B. Dai, Z. Hu, H. Huang, G. Zhu, Z. Xiao, W. Wan, P. Zhang, W. Jia, L. Zhang, *Biochem. Biophys. Res. Commun.* **2014**, *454*, 221–7.

[62] S. U. Schmitz, M. Albert, M. Malatesta, L. Morey, J. V Johansen, M. Bak, N. Tommerup, I. Abarrategui, K. Helin, *EMBO J.* **2011**, *30*, 4586–4600.

[63] M. Labelle, T. Boesen, Q. Khan, R. R. Vakiti, U. Sharma, Y. Yang, M. Mehrotra, N. Saraswat, F. Ullah, *Inhibitors of Histone Demethylases*, **2014**, Patent WO2014053491 A1.

[64] C. Johansson, S. Velupillai, A. Tumber, A. Szykowska, E. S. Hookway, R. P. Nowak, C. Strain-Damerell, C. Gileadi, M. Philpott, N. Burgess-Brown, et al., *Nat. Chem. Biol.* **2016**, *12*, 539.

[65] J. R. Horton, X. Liu, M. Gale, L. Wu, J. R. Shanks, X. Zhang, P. J. Webber, J. S. K. Bell, S. C. Kales,

B. T. Mott, et al., *Cell Chem. Biol.* **2016**, *23*, 769–781.

[66] Z. Nie, L. Shi, C. Lai, S. M. O'Connell, J. Xu, R. K. Stansfield, D. J. Hosfield, J. M. Veal, J. A. Stafford, *Bioorg. Med. Chem. Lett.* **2018**, *28*, 1490–1494.

[67] S. M. Westaway, A. G. S. Preston, M. D. Barker, F. Brown, J. A. Brown, M. Campbell, C. Chung, H. Diallo, C. Douault, G. Drewes, et al., *J. Med. Chem.* **2016**, *59*, 1357–1369.

[68] Y. K. Chen, T. Bonaldi, A. Cuomo, J. R. Del Rosario, D. J. Hosfield, T. Kanouni, S. Kao, C. Lai, N. A. Lobo, J. Matuszkiewicz, et al., *ACS Med. Chem. Lett.* **2017**, *8*, 869–874.

[69] J. R. Horton, X. Liu, L. Wu, K. Zhang, J. Shanks, X. Zhang, G. Rai, B. T. Mott, D. J. Jansen, S. C. Kales, et al., *J. Med. Chem.* **2018**, *61*, 3193–3208.

[70] A. Tumber, A. Nuzzi, E. S. Hookway, S. B. Hatch, S. Velupillai, C. Johansson, A. Kawamura, P. Savitsky, C. Yapp, A. Szykowska, et al., *Cell Chem. Biol.* **2018**, *24*, 371–380.

[71] S. M. Westaway, A. G. S. Preston, M. D. Barker, F. Brown, J. A. Brown, M. Campbell, C. Chung, G. Drewes, R. Eagle, N. Garton, et al., *J. Med. Chem.* **2016**, *59*, 1370–1387.

[72] K. Thirstrup, S. Christensen, H. A. Møller, A. Ritzén, A.-L. Bergström, T. N. Sager, H. S. Jensen, *Pharmacol. Res.* **2011**, *64*, 268–273.

[73] V. Bavetsias, R. M. Lanigan, G. F. Ruda, B. Atrash, M. G. McLaughlin, A. Tumber, N. Y. Mok, Y.-V. Le Bihan, S. Dempster, K. J. Boxall, et al., *J. Med. Chem.* **2016**, *59*, 1388–1409.

[74] B. Heinemann, J. M. Nielsen, H. R. Hudlebusch, M. J. Lees, D. V. Larsen, T. Boesen, M. Labelle, L.-O. Gerlach, P. Birk, K. Helin, *Nature* **2014**, *514*, E1.

[75] M. Vinogradova, V. S. Gehling, A. Gustafson, S. Arora, C. A. Tindell, C. Wilson, K. E. Williamson, G. D. Guler, P. Gangurde, W. Manieri, et al., *Nat Chem Biol* **2016**, *12*, 531–538.

[76] J. Liang, B. Zhang, S. Labadie, D. F. Ortwine, M. Vinogradova, J. R. Kiefer, V. S. Gehling, J.-C. Harmange, R. Cummings, T. Lai, et al., *Bioorg. Med. Chem. Lett.* **2016**, *26*, 4036–4041.

[77] S. S. Labadie, P. S. Dragovich, R. T. Cummings, G. Deshmukh, A. Gustafson, N. Han, J.-C. Harmange, J. R. Kiefer, Y. Li, J. Liang, et al., *Bioorg. Med. Chem. Lett.* **2016**, *26*, 4492–4496.

[78] J. Liang, S. Labadie, B. Zhang, D. F. Ortwine, S. Patel, M. Vinogradova, J. R. Kiefer, T. Mauer, V. S. Gehling, J.-C. Harmange, et al., *Bioorg. Med. Chem. Lett.* **2017**, *27*, 2974–2981.

[79] A. Kawamura, M. Münzel, T. Kojima, C. Yapp, B. Bhushan, Y. Goto, A. Tumber, T. Katoh, O. N. F. King, T. Passioura, et al., *Nat. Commun.* **2017**, *8*, 14773.

[80] J. Singh, R. C. Petter, T. A. Baillie, A. Whitty, *Nat Rev Drug Discov* **2011**, *10*, 307–317.

[81] T. D. Warner, J. A. Mitchell, *Proc. Natl. Acad. Sci.* **2002**, *99*, 13371 LP-13373.

[82] J. Gan, Q. Ruan, B. He, M. Zhu, W. C. Shyu, W. G. Humphreys, *Chem. Res. Toxicol.* **2009**, *22*, 690–698.

[83] D. Li, L. Ambrogio, T. Shimamura, S. Kubo, M. Takahashi, L. R. Chirieac, R. F. Padera, G. I. Shapiro, A. Baum, F. Himmelsbach, et al., *Oncogene* **2008**, *27*, 4702.

[84] T. A. Yap, L. Vidal, J. Adam, P. Stephens, J. Spicer, H. Shaw, J. Ang, G. Temple, S. Bell, M. Shahidi, et al., *J. Clin. Oncol.* **2010**, *28*, 3965–3972.

[85] M. N. Balak, Y. Gong, G. J. Riely, R. Somwar, A. R. Li, M. F. Zakowski, A. Chiang, G. Yang, O. Ouerfelli, M. G. Kris, et al., *Clin. Cancer Res.* **2006**, *12*, 6494 LP-6501.

[86] C.-H. Yun, K. E. Mengwasser, A. V Toms, M. S. Woo, H. Greulich, K.-K. Wong, M. Meyerson, M. J. Eck, *Proc. Natl. Acad. Sci.* **2008**, *105*, 2070 LP-2075.

[87] A. Lewandowicz, P. C. Tyler, G. B. Evans, R. H. Furneaux, V. L. Schramm, *J. Biol. Chem.* **2003**, *278*, 31465–31468.

[88] E. L. Kwak, R. Sordella, D. W. Bell, N. Godin-Heymann, R. A. Okimoto, B. W. Brannigan, P. L. Harris, D. R. Driscoll, P. Fidias, T. J. Lynch, et al., *Proc. Natl. Acad. Sci. U. S. A.* **2005**, *102*, 7665–7670.

[89] Q. Liu, Y. Sabnis, Z. Zhao, T. Zhang, S. J. Buhrlage, L. H. Jones, N. S. Gray, *Chem. Biol.* **2013**, *20*, 146–159.

[90] D. A. Shannon, E. Weerapana, *Curr. Opin. Chem. Biol.* **2015**, *24*, 18–26.

[91] D. A. Shannon, R. Banerjee, E. R. Webster, D. W. Bak, C. Wang, E. Weerapana, *J. Am. Chem. Soc.* **2014**, *136*, 3330–3333.

[92] J. S. Walsh, G. T. Miwa, *Annu. Rev. Pharmacol. Toxicol.* **2011**, *51*, 145–167.

[93] B.-F. Krippendorff, R. Neuhaus, P. Lienau, A. Reichel, W. Huisinga, *J. Biomol. Screen.* **2009**, *14*, 913–923.

[94] J. Engel, A. Richters, M. Getlik, S. Tomassi, M. Keul, M. Termathe, J. Lategahn, C. Becker, S. Mayer-Wrangowski, C. Grütter, et al., *J. Med. Chem.* **2015**, *58*, 6844–6863.

[95] P. A. Schwartz, P. Kuzmic, J. Solowiej, S. Bergqvist, B. Bolanos, C. Almaden, A. Nagata, K. Ryan, J. Feng, D. Dalvie, et al., *Proc. Natl. Acad. Sci.* **2014**, *111*, 173 LP-178.

[96] E. F. Ullman, H. Kirakossian, S. Singh, Z. P. Wu, B. R. Irvin, J. S. Pease, A. C. Switchenko, J. D. Irvine, A. Dafforn, C. N. Skold, *Proc. Natl. Acad. Sci. U. S. A.* **1994**, *91*, 5426–5430.

[97] A. Kawamura, A. Tumber, N. R. Rose, O. N. F. King, M. Daniel, U. Oppermann, T. D. Heightman, C. Schofield, *Anal. Biochem.* **2010**, *404*, 86–93.

[98] J. Sayegh, J. Cao, M. R. Zou, A. Morales, L. P. Blair, M. Norcia, D. Hoyer, A. J. Tackett, J. S. Merkel, Q. Yan, *J. Biol. Chem.* **2013**, *288*, 9408–9417.

[99] M. R. Marzabadi, J. Wetzel, J. E. Deleon, Y. Jiang, C.-A. Chen, K. Lu, B. Lagu, *Substituted Anilinic Piperidines as MCH Selective Antagonists*, **2003**, WO2003004027A1.

[100] D. M. Allwood, D. C. Blakemore, A. D. Brown, S. V Ley, *J. Org. Chem.* **2014**, *79*, 328–338.

[101] Z. Zhao, P. E. Bourne, *Drug Discov. Today* **2018**, *23*, 727–735.

[102] S. W. Goldstein, A. Bill, J. Dhuguru, O. Ghoneim, *J. Chem. Educ.* **2017**, *94*, 1388–1390.

[103] M. E. Flanagan, J. A. Abramite, D. P. Anderson, A. Aulabaugh, U. P. Dahal, A. M. Gilbert, C. Li, J. Montgomery, S. R. Oppenheimer, T. Ryder, et al., *J. Med. Chem.* **2014**, *57*, 10072–10079.

[104] R. Lonsdale, J. Burgess, N. Colclough, N. L. Davies, E. M. Lenz, A. L. Orton, R. A. Ward, *J. Chem. Inf. Model.* **2017**, *57*, 3124–3137.

[105] T. Machleidt, C. C. Woodroofe, M. K. Schwinn, J. Méndez, M. B. Robers, K. Zimmerman, P. Otto, D. L. Daniels, T. A. Kirkland, K. V Wood, *ACS Chem. Biol.* **2015**, *10*, 1797–1804.

[106] M. B. Robers, M. L. Dart, C. C. Woodroofe, C. A. Zimprich, T. A. Kirkland, T. Machleidt, K. R. Kupcho, S. Levin, J. R. Hartnett, K. Zimmerman, et al., *Nat. Commun.* **2015**, *6*, 10091.

[107] D. A. Orlando, M. W. Chen, V. E. Brown, S. Solanki, Y. J. Choi, E. R. Olson, C. C. Fritz, J. E.

Bradner, M. G. Guenther, *Cell Rep.* **2014**, *9*, 1163–1170.

[108] S. A. E., C. B. F., *ChemBioChem* **2003**, *5*, 41–47.

[109] N. Jessani, B. F. Cravatt, *Curr. Opin. Chem. Biol.* **2004**, *8*, 54–59.

[110] M. J. Evans, B. F. Cravatt, *Chem. Rev.* **2006**, *106*, 3279–3301.

[111] H. C. Kolb, K. B. Sharpless, *Drug Discov. Today* **2003**, *8*, 1128–1137.

[112] A. E. Speers, G. C. Adam, B. F. Cravatt, *J. Am. Chem. Soc.* **2003**, *125*, 4686–4687.

[113] A. E. Speers, B. F. Cravatt, *Chem. Biol.* **2004**, *11*, 535–546.

[114] Y. Liu, M. P. Patricelli, B. F. Cravatt, *Proc. Natl. Acad. Sci.* **1999**, *96*, 14694 LP-14699.

[115] D. Kidd, Y. Liu, B. F. Cravatt, *Biochemistry* **2001**, *40*, 4005–4015.

[116] M. P. Patricelli, D. K. Giang, L. M. Stamp, J. J. Burbaum, *Proteomics* **2001**, *1*, 1067–1071.

[117] D. Greenbaum, A. Baruch, L. Hayrapetian, Z. Darula, A. Burlingame, K. F. Medzihradszky, M. Bogyo, *Mol. Cell. Proteomics* **2002**, *1*, 60–68.

[118] N. Jessani, S. Niessen, B. Q. Wei, M. Nicolau, M. Humphrey, Y. Ji, W. Han, D.-Y. Noh, J. R. Yates III, S. S. Jeffrey, et al., *Nat. Methods* **2005**, *2*, 691.

[119] G. C. Adam, J. Burbaum, J. W. Kozarich, M. P. Patricelli, B. F. Cravatt, *J. Am. Chem. Soc.* **2004**, *126*, 1363–1368.

[120] E. S. Okerberg, J. Wu, B. Zhang, B. Samii, K. Blackford, D. T. Winn, K. R. Shreder, J. J. Burbaum, M. P. Patricelli, *Proc. Natl. Acad. Sci. U. S. A.* **2005**, *102*, 4996 LP-5001.

[121] M. Wright, C. Martínez-Lamenca, J. E. Leenaerts, P. E. Brennan, A. A. Trabanco, D. Oehlrich, *J. Org. Chem.* **2018**, *83*, 9510–9516.

[122] E. S. Levchenko, I. E. Sheinkman, A. V. Kirsanov, *Zh. Obs. Khim.* **1960**, *30*, 1941.

[123] E. S. Levchenko, N. Y. Derkach, A. V. Kirsanov, *Zh. Obs. Khim.* **1962**, *30*, 1208.

[124] D. Leca, A. Toussaint, C. Mareau, L. Fensterbank, E. Lacôte, M. Malacria, *Org. Lett.* **2004**, *6*, 3573–3575.

[125] S. Azzaro, M. D.-E. Murr, L. Fensterbank, E. Lacôte, M. Malacria, *Synlett* **2011**, *2011*, 849–851.

[126] P. H. Di Chenna, F. Robert-Peillard, P. Dauban, R. H. Dodd, *Org. Lett.* **2004**, *6*, 4503–4505.

[127] C. Worch, C. Bolm, *Synlett* **2009**, *2009*, 2425–2428.

[128] M. Steurer, C. Bolm, *J. Org. Chem.* **2010**, *75*, 3301–3310.

[129] J. Buendia, B. Darses, P. Dauban, *Angew. Chemie Int. Ed.* **2015**, *54*, 5697–5701.

[130] J. Buendia, G. Grelier, B. Darses, A. G. Jarvis, F. Taran, P. Dauban, *Angew. Chemie Int. Ed.* **2016**, *55*, 7530–7533.

[131] C. R. Johnson, E. U. Jonsson, C. C. Bacon, *J. Org. Chem.* **1979**, *44*, 2055–2061.

[132] C. Ballatore, D. M. Huryn, A. B. Smith, *ChemMedChem* **2013**, *8*, 385–395.

[133] P. F. W., W. Christin, S. M. A., S. A. L., B. Carsten, R. J. N. H., *Adv. Synth. Catal.* **2012**, *354*, 59–64.

[134] C. P. K., N. Tricia, T. Niranjan, G. Thavendran, K. H. G., A. P. I., *Angew. Chemie Int. Ed.* **2016**, *56*, 4100–4109.

[135] T. Biftu, T. A. Khan, *Treating Diabetes with Dipeptidyl Peptidase-IV Inhibitors*, **2014**, WO2014018355A1 and US20150175609A1.

[136] B. Bartels, C. Dolente, W. Guba, W. Haap, A. Kuglstatter, S. Ulrike Obst, J.-U. Peters, T. Rogers-Evans, Mark, Woltering, C. Schnider, R. Wermuth, *Pyridyl-Triazabicycles*, **2016**, WO2016012422A1.

[137] F. Izzo, M. Schäfer, R. Stockman, U. Lücking, *Chem. – A Eur. J.* **2017**, *23*, 15189–15193.

[138] T. Q. Davies, A. Hall, M. C. Willis, *Angew. Chemie Int. Ed.* **2017**, *56*, 14937–14941.

[139] E. P. Gillis, K. J. Eastman, M. D. Hill, D. J. Donnelly, N. A. Meanwell, *J. Med. Chem.* **2015**, *58*, 8315–8359.

[140] S. Noritake, N. Shibata, S. Nakamura, T. Toru, M. Shiro, *European J. Org. Chem.* **2008**, *2008*, 3465–3468.

[141] M. Härter, H. Beck, P. Ellinghaus, K. Berhoerster, S. Greschat, K. H. Thierauch, F. Suessmeier, *Heteroaromatische Verbindungen Zur Verwendung Als Hif-Inhibitoren*, **2010**, WO 20100 54763.

[142] C. S. Richards-Taylor, C. Martínez-Lamenca, J. E. Leenaerts, A. A. Trabanco, D. Oehlrich, *J. Org. Chem.* **2017**, *82*, 9898–9904.

[143] F. A. Abulwerdi, C. Liao, A. S. Mady, J. Gavin, C. Shen, T. Cierpicki, J. A. Stuckey, H. D. H. Showalter, Z. Nikolovska-Coleska, *J. Med. Chem.* **2014**, *57*, 4111–4133.

[144] L. Yan, D. C. G. Bertarelli, A. M. Hayallah, H. Meyer, K.-N. Klotz, C. E. Müller, *J. Med. Chem.* **2006**, *49*, 4384–4391.

[145] S. Caddick, J. D. Wilden, H. D. Bush, S. N. Wadman, D. B. Judd, *Org. Lett.* **2002**, *4*, 2549–2551.

[146] S. J. Elledge, Z. Zhou, J. B. Allen, *Trends Biochem. Sci.* **1992**, *17*, 119–123.

[147] J. L. Sneeden, L. A. Loeb, *J. Biol. Chem.* **2004**, *279*, 40723–40728.

[148] C. Tomasetti, L. Li, B. Vogelstein, *Science* **2017**, *355*, 1330 LP-1334.

[149] N. J. Parker, C. G. Begley, R. M. Fox, *Genomics* **1995**, *27*, 280–285.

[150] J. W. Fairman, S. R. Wijerathna, M. F. Ahmad, H. Xu, R. Nakano, S. Jha, J. Prendergast, R. M. Welin, S. Flodin, A. Roos, et al., *Nat. Struct. Mol. Biol.* **2011**, *18*, 316.

[151] P. Nordlund, P. Reichard, *Annu. Rev. Biochem.* **2006**, *75*, 681–706.

[152] R. Eliasson, E. Pontis, A. Jordan, P. Reichard, *J. Biol. Chem.* **1996**, *271*, 26582–26587.

[153] V. D'Angiolella, V. Donato, F. M. Forrester, Y.-T. Jeong, C. Pellacani, Y. Kudo, A. Saraf, L. Florens, M. P. Washburn, M. Pagano, *Cell* **2012**, *149*, 1023–1034.

[154] K. M. Sakamoto, K. B. Kim, A. Kumagai, F. Mercurio, C. M. Crews, R. J. Deshaies, *Proc. Natl. Acad. Sci.* **2001**, *98*, 8554 LP-8559.

[155] I. Churcher, *J. Med. Chem.* **2018**, *61*, 444–452.

[156] T. K. Neklesa, J. D. Winkler, C. M. Crews, *Pharmacol. Ther.* **2017**, *174*, 138–144.

[157] L. A. C., T. Momar, H. Doris, S. Jemilat, J.-F. Saul, K. Eunhwa, H. John, C. C. M., *Angew. Chemie*

Int. Ed. **2015**, *55*, 807–810.

[158] S. Björn, G. Manfred, D. Gunnar, S. Matthias, *Proteomics* **2008**, *9*, 205–209.

[159] R. J. Deshaies, C. A. P. Joazeiro, *Annu. Rev. Biochem.* **2009**, *78*, 399–434.

[160] D. L. Buckley, I. Van Molle, P. C. Gareiss, H. S. Tae, J. Michel, D. J. Noblin, W. L. Jorgensen, A. Ciulli, C. M. Crews, *J. Am. Chem. Soc.* **2012**, *134*, 4465–4468.

[161] C. Galdeano, M. S. Gadd, P. Soares, S. Scaffidi, I. Van Molle, I. Birced, S. Hewitt, D. M. Dias, A. Ciulli, *J. Med. Chem.* **2014**, *57*, 8657–8663.

[162] E. S. Fischer, K. Böhm, J. R. Lydeard, H. Yang, M. B. Stadler, S. Cavadini, J. Nagel, F. Serluca, V. Acker, G. M. Lingaraju, et al., *Nature* **2014**, *512*, 49.

[163] P. P. Chamberlain, A. Lopez-Girona, K. Miller, G. Carmel, B. Pagarigan, B. Chie-Leon, E. Rychak, L. G. Corral, Y. J. Ren, M. Wang, et al., *Nat. Struct. Mol. Biol.* **2014**, *21*, 803.

[164] J. Krönke, N. D. Udeshi, A. Narla, P. Grauman, S. N. Hurst, M. McConkey, T. Svinkina, D. Heckl, E. Comer, X. Li, et al., *Science* **2014**, *343*, 301 LP-305.

[165] G. M. Burslem, B. E. Smith, A. C. Lai, S. Jaime-Figueroa, D. C. McQuaid, D. P. Bondeson, M. Toure, H. Dong, Y. Qian, J. Wang, et al., *Cell Chem. Biol.* **2018**, *25*, 67–77.e3.

[166] J. Lu, Y. Qian, M. Altieri, H. Dong, J. Wang, K. Raina, J. Hines, J. D. Winkler, A. P. Crew, K. Coleman, et al., *Chem. Biol.* **2015**, *22*, 755–763.

[167] K. Raina, J. Lu, Y. Qian, M. Altieri, D. Gordon, A. M. K. Rossi, J. Wang, X. Chen, H. Dong, K. Siu, et al., *Proc. Natl. Acad. Sci.* **2016**, *113*, 7124 LP-7129.

[168] R. David, B. D. L., P. Joshiawa, B. G. L., S. Matthew, S. Hyuk-Soo, D. Shiva, W. Martin, D.-P. Sirano, A. S. A., et al., *Angew. Chemie Int. Ed.* **2017**, *56*, 5738–5743.

[169] K. Cyrus, M. Wehenkel, E.-Y. Choi, H.-J. Han, H. Lee, H. Swanson, K.-B. Kim, *Mol. Biosyst.* **2011**, *7*, 359–364.

[170] D. J. Inwards, P. A. Fishkin, B. R. LaPlant, M. T. Drake, P. J. Kurtin, D. A. Nikcevich, D. B. Wender, B. S. Lair, T. E. Witzig, *Ann. Oncol.* **2014**, *25*, 2020–2024.

[171] S. Xu, P. Yao, G. Chen, H. Wang, *Nucleos. Nucleot. Nucl.* **2011**, *30*, 353–359.

[172] D. Beattie, A. Brearley, Z. Brown, S. J. Charlton, B. Cox, R. A. Fairhurst, J. R. Fozard, P. Gedeck, P. Kirkham, K. Meja, et al., *Bioorg. Med. Chem. Lett.* **2010**, *20*, 1219–1224.

[173] R. Xia, L.-S. Chen, *Nucleos. Nucleot. Nucl.* **2015**, *34*, 729–735.

Appendix

Chemical stability tests with sulfonimidoyl fluoride **157**:

157 was subjected to the different conditions, injected into a HPLC and the proportion of the compounds was measured by their integrated areas.

	Days	Tetrafluorophenol	Sulfonamide **154**	**157**
0.1N HCl 37 °C	0			100
	1		5.56	94.44
	2		10.73	89.77
0.1N HCl 60 °C	0			N/A
	1	2.64	95.91	1.45
	2	2.61	97.39	
0.1N NaOH 37 °C	0		100	
	1		100	
	2		100	
0.1N NaOH 60 °C	0			N/A
	1		100	
	2		100	
pH 4 37 °C	0			100
	1		1.5	98.5
	2		2.8	97.2
pH 4 60 °C	0			N/A
	1	8.95	27.92	63.13
	2	11	43.43	45.47
pH 7.4 37 °C	0			100
	1		19.98	80.02
	2		34.35	65.65
pH 7.4 60 °C	0			N/A
	1	0.5	99.5	
	2	0.93	99.07	
MeOH 37 °C	0			100
	1		2.24	97.76
	2		1.03	98.97
MeOH 60 °C	0			N/A
	1		6.33	93.67
	2		9.56	90.44
DMSO 37 °C	0			100
	1			100
	2		1.15	98.85
DMSO 60 °C	0			N/A
	1		1.8	98.2
	2		2.78	97.22

Chemical stability tests with transfer reagent **158**:

158 was subjected to the different conditions, injected into a HPLC and the proportion of the compounds was measured by their integrated areas.

	Days	Tetrafluorophenol	Sulfonamide **154**	**158**
0.1N HCl 37 °C	0			100
	1			100
	2			100
0.1N HCl 60 °C	0			N/A
	1			100
	2			100
0.1N NaOH 37 °C	0	54.59	45.41	0
	1	45.62	45.38	0
	2	54.85	45.15	0
0.1N NaOH 60 °C	0			N/A
	1	48.49	41.51	0
	2	58.68	41.32	0
pH 4 37 °C	0			100
	1			100
	2			100
pH 4 60 °C	0			N/A
	1			100
	2			100
pH 7.4 37 °C	0			100
	1			100
	2			100
pH 7.4 60 °C	0			N/A
	1			100
	2			100
MeOH 37 °C	0			100
	1			100
	2			100
MeOH 60 °C	0			N/A
	1			100
	2			100
DMSO 37 °C	0			100
	1			100
	2			100
DMSO 60 °C	0			N/A
	1	3.02	1.3	95.68
	2	4.51	2.09	88.43